

Tsunenori Mine · Akira Fukuda ·  
Shigemi Ishida *Editors*

# Intelligent Transport Systems for Everyone's Mobility

 Springer

# Intelligent Transport Systems for Everyone's Mobility

Tsunenori Mine · Akira Fukuda ·  
Shigemi Ishida  
Editors

# Intelligent Transport Systems for Everyone's Mobility

 Springer

*Editors*

Tsunenori Mine  
Department of Advanced Information  
Technology  
Kyushu University  
Fukuoka, Japan

Akira Fukuda  
Department of Advanced Information  
Technology  
Kyushu University  
Fukuoka, Japan

Shigemi Ishida  
Department of Advanced Information  
Technology  
Kyushu University  
Fukuoka, Japan

ISBN 978-981-13-7433-3      ISBN 978-981-13-7434-0 (eBook)  
<https://doi.org/10.1007/978-981-13-7434-0>

Library of Congress Control Number: 2019936277

© Springer Nature Singapore Pte Ltd. 2019

This work is subject to copyright. All rights are reserved by the Publisher, whether the whole or part of the material is concerned, specifically the rights of translation, reprinting, reuse of illustrations, recitation, broadcasting, reproduction on microfilms or in any other physical way, and transmission or information storage and retrieval, electronic adaptation, computer software, or by similar or dissimilar methodology now known or hereafter developed.

The use of general descriptive names, registered names, trademarks, service marks, etc. in this publication does not imply, even in the absence of a specific statement, that such names are exempt from the relevant protective laws and regulations and therefore free for general use.

The publisher, the authors and the editors are safe to assume that the advice and information in this book are believed to be true and accurate at the date of publication. Neither the publisher nor the authors or the editors give a warranty, expressed or implied, with respect to the material contained herein or for any errors or omissions that may have been made. The publisher remains neutral with regard to jurisdictional claims in published maps and institutional affiliations.

This Springer imprint is published by the registered company Springer Nature Singapore Pte Ltd. The registered company address is: 152 Beach Road, #21-01/04 Gateway East, Singapore 189721, Singapore

# Preface

This book presents the latest, most interesting research efforts regarding intelligent transport system (ITS) technologies, from theory to practice. The book's main theme is "Mobility for everyone by ITS"; accordingly, it gathers a range of contributions on human-centered factors in the use or development of ITS technologies, infrastructures, and applications. Each of these contributions proposes a novel method for ITS and discusses the method on the basis of case studies conducted in the Asia-Pacific region.

The book consists of 26 chapters, which were selected from over 150 papers after strict reviews, and are roughly divided into four general categories: (1) Safe and Secure Society, (2) ITS-Based Smart Mobility, (3) Next-Generation Mobility, and (4) Infrastructure Technologies for Practical ITS. In these categories, several key topics are touched on with each other such as driver assistance and behavior analysis, traffic accident and congestion management, vehicle flow management at large events, automated or self-driving vehicles, V2X technologies, next-generation public transportation systems, and intelligent transportation systems made possible by big data analysis. In addition, important current and future ITS-related problems are discussed, taking into account many case studies that have been conducted in this regard.

Dr. Tsunenori Mine, Dr. Shigemi Ishida, and Dr. Akira Fukuda are grateful to the authors and reviewers for their great contributions to this work. The editors also acknowledge with their gratitude the editorial team of Springer-Verlag for their support and patience during the preparation of the manuscripts of this book.

Fukuoka, Japan  
February 2019

Tsunenori Mine  
Akira Fukuda  
Shigemi Ishida

# Contents

## Part I Safe and Secure Society

<b>The Unconscious Learning Effect on Driver Attention</b> . . . . .	3
Shuji Sudo and Toshio Ito	
<b>Inattentive Driving Effects on Eye Movement and Driving Behavior</b> . . . . .	15
He Xi and Kazunori Shidoji	
<b>Automatic Extraction of Passing Scene Through Signalized Intersection from Event Data Recorder During Night Time and also Daylight</b> . . . . .	31
Mikuni Motoi, Haruki Kawanaka, Md. Shoaib Bhuiyan and Koji Oguri	
<b>Collision Warning Strategies Using V2X: An Analysis of How Motorcycles and Bicycles Undergo Collisions</b> . . . . .	51
Tien-Pen Hsu, Wei-Lun Hsiao and Wan-Ching Ho	
<b>Assistive Devices for Safe Driving at a Crossing with No Traffic Lights Using 920 MHz Band</b> . . . . .	77
Shintaro Uno	
<b>Validation for Improving Reliability in Driver Arousal Method by Physiological Magnetic Stimulation</b> . . . . .	93
Yoshihide Hayashi, Masashi Tsukada, Tomoaki Nakano, Muneo Yamada and Kaneo Mohri	
<b>Study on Simultaneous-Action Discrimination System Using the Neural Network</b> . . . . .	109
Takahiko Murayama, Masato Ito, Hatsuo Yamasaki, Tomoaki Nakano and Muneo Yamada	

## Part II ITS-Based Smart Mobility

<b>Prediction of Travel Time over Unstable Intervals Between Adjacent Bus Stops Using Historical Travel Time in Both the Previous and Current Time Periods</b> . . . . .	131
Mansur As and Tsunenori Mine	
<b>Dynamic Arrival Time Estimation Model and Visualization Method for Bus Traffic</b> . . . . .	155
Kei Hiroi, Hitomi Imai and Nobuo Kawaguchi	
<b>Simulation for Passengers Convenience Using Actual Bus Traffic Data</b> . . . . .	175
Kei Hiroi, Takehiro Arai and Nobuo Kawaguchi	
<b>Adaptive Traffic Signal Control Methods Based on Deep Reinforcement Learning</b> . . . . .	195
Chia-Hao Wan and Ming-Chorng Hwang	
<b>Analysis of Quality/Quantity Trade-Off of Images Collected by On-Vehicle Fisheye Cameras for Super Resolution</b> . . . . .	211
Shintaro Ono, Teruhisa Takano, Hiroshi Kawasaki and Katsushi Ikeuchi	
<b>Architecture and Development of Agent-Based Unified Simulation Environment for ITS Services</b> . . . . .	227
Ryo Fujii, Takahiro Ando, Kenji Hisazumi, Tsunenori Mine, Tsuneo Nakanishi and Akira Fukuda	
<b>Traffic State Estimation Using Traffic Measurement from the Opposing Lane—Error Analysis Based on Fluctuation of Input Data</b> . . . . .	247
Katsuya Kawai, Atsushi Takenouchi, Masahiko Ikawa and Masao Kuwahara	
<b>Development of a Statistical Model to Predict Traffic Congestion in Winter Seasons in Nagaoka, Japan Using Publicly Available Data</b> . . . . .	265
Hiroaki Ikeuchi, Kiichiro Hatoyama, Ryota Kusakabe and Ikumi Kariya	
<b>Warning Notification of Potential Collisions for Comfort Intelligence on Autonomous Vehicles</b> . . . . .	279
Taishi Sawabe, Shohei Ota, Masayuki Kanbara, Norimichi Ukita, Tetsushi Ikeda, Luis Yoichi Morales Saiki, Atsushi Watanabe and Norihiro Hagita	

**Part III Next-Generation Mobility**

**Exploring System Characteristics of Autonomous Mobility On-Demand Systems Under Varying Travel Demand Patterns . . . . .** 299  
 Farid Javanshour, Hussein Dia and Gordon Duncan

**Strategies to Increase the Response Rate of Smartphone-Based Travel Surveys in Afghanistan: Exploring the Effects of Incentives and Female Survey Conductors . . . . .** 317  
 Qudratullah and Takuya Maruyama

**Sensing Information Dissemination Strategy for Collective Perception in VANET Based on the Relative Position of Vehicles and the Road Structure . . . . .** 337  
 Kaito Furukawa, Mineo Takai and Susumu Ishihara

**Increase of Traffic Efficiency by Mutual Concessions of Autonomous Driving Cars Using Deep Q-Network . . . . .** 357  
 Tomohisha Yamashita, Ichitaro Ogawa, Soichiro Yokoyama, Hidenori Kawamura, Akira Sakatoku, Tadashi Yanagihara, Tomohiko Ogishi and Hideaki Tanaka

**Floating Car Data-Based Real-Time Road Traffic Prediction System and Its Application in Macau Grand Prix Event . . . . .** 377  
 Ngoc-vai Chiang, Lap-mou Tam, Kin-hou Lai, Ka-in Wong and Wai-meng Si Tou

**Part IV Infrastructure Technologies for Practical ITS**

**Modeling Speed Profile of Two-Way Two-Lane Expressways in Japan . . . . .** 395  
 Makoto Kasai, Jian Xing and Shin-ichi Narushima

**Effect of the Moving-Light-Guide-System on Driving Behavior at Sag . . . . .** 407  
 Yuuta Tabira and Yasuhiro Shiomi

**Proposal of Acoustic Train Detection System for Crowdsensing . . . . .** 427  
 Koji Sato, Shigemi Ishida, Jumpei Kajimura, Shigeaki Tagashira and Akira Fukuda

**A Study for Social Benefit of VICS WIDE Service by Using Traffic Simulation in Tokyo . . . . .** 445  
 Shinya Adachi, Yasuhiko Iwasaki, Kazuhiko Mizushima and Hisatomo Hanabusa

**Explore User Behavior of the Taipei Bikesharing System via Electronic Payment Service Data . . . . .** 459  
 Chih-Lin Chung and Shu-Yuan Li



**Part I**  
**Safe and Secure Society**

# The Unconscious Learning Effect on Driver Attention



Shuji Sudo and Toshio Ito

**Abstract** The rate of traffic accidents caused by low driver awareness for the confirmation of surrounding safety is high. In this study, we improved driver safety confirmation by using the technique of unconscious learning and action. Here, we assumed that drivers will unconsciously learn an alarm pattern that sounds during dangerous scenarios when driving. In our experiment, we used a driving simulator and eye mark recorder. Subjects were drivers who do not check their environment fully. The experiment was conducted five times every few days. The alarm we used to encourage safety confirmation had a frequency of 250 Hz and an intermittent sound. This frequency is slightly higher than the noise of a car. The experiment interval was every three days or every week. In the first session, we checked the subjects' safety confirmation on a course with intersections where dangerous scenarios played out. After a few days, the subjects drove the course with the alarm sounding at the intersections, and ended up looking around at their surroundings when hearing the alarm. We told only some of the subjects the details and timing of the alarm. After this drive, we asked them whether the sound seemed noisy or not. This was repeated three times. Finally, the subjects drove another different course with intersections with dangerous scenarios. We then compared their safety confirmation between the first and last experiment, and found that the subjects looked at their surroundings better in the later experiment, than they did at first. The subjects found the alarm noisy the first time, but gradually grew used to it, so that it eventually stopped seeming noisy. From this result, we determined that the effect of unconscious learning with an alarm can change a driver's safety confirmation.

**Keywords** Human behavior · Alarm

---

S. Sudo · T. Ito (✉)  
Shibaura Institute of Technology, 307 Fukasaku, Minuma-ku, Saitama-City 337-8570, Japan  
e-mail: [tosu-ito@shibaura-it.ac.jp](mailto:tosu-ito@shibaura-it.ac.jp)

S. Sudo  
e-mail: [mf17039@shibaura-it.ac.jp](mailto:mf17039@shibaura-it.ac.jp)

© Springer Nature Singapore Pte Ltd. 2019  
T. Mine et al. (eds.), *Intelligent Transport Systems for Everyone's Mobility*, [https://doi.org/10.1007/978-981-13-7434-0\\_1](https://doi.org/10.1007/978-981-13-7434-0_1)

## 1 Introduction

In recent years, safety technology has been developed to reduce traffic accidents. The major cause of traffic accidents in Japan is a lack of surrounding safety confirmation by the driver [1]. These accidents increase with the automation of operation [2]. One of the technologies used to prevent this kind of accident is the Inter-Vehicles Distance Warning System (IVDWS). IVDWS warns the driver if there is a possibility of crashing with the vehicle in front. However, the alarm system of the IVDWS has a high frequency sound and is set to ring early, before a possible crash takes place. This makes the system prone to false alarm, which can be annoying for the driver, and can even result in them turning off the system as a whole.

In a previous study [3], the author considered the fact that the warning sound does not need to be at a high frequency. In cognitive psychology, the process of driving has three elements (Cognition, Judgment and Operation) [4]. IVDWS is included within the cognition element, because the system tells the driver about incoming danger. However, cerebral activity preceded the reported time of a conscious intention to act by about 0.3 ms [5]. Moreover, the author focused on unconscious human learning and human action [6]. Humans get some information by their ears and eyes and unconsciously select the information that is necessary (the Cocktail Party Effect) [7, 8]. Drivers unconsciously choose the necessary information in a vehicle with multiple competing sounds. Therefore, drivers learn that the sound can indicate danger. The author believes that a sound that is not high frequency can be used to inform the driver of danger. The current warning sound of the IVDWS is an intermittent sound of 1 to 4 kHz, chosen because humans feel a sense of urgency when they hear a high frequency and intermittent sound [9, 10]. However, in an emergency situation, the author considered the fact that drivers could psychologically react more calmly to a low frequency and gentle sound, than they would to a high frequency one. As such, the author conducted an experiment to test this idea using a driving simulator. The experiment scene was a pedestrian suddenly rushing out into the road in front of the driver's vehicle. The alarm sounds 1.8 s before collision with the pedestrian. The alarm used was an intermittent, 250 Hz sound, which is a slightly higher frequency than the load noise in the vehicle [11]. As a result, the drivers reacted more quickly than with the current alarm warning system. Moreover, the drivers found the gentle, low frequency alarm to be acceptable, and so will not turn it off even in the event of a false warning.

In this study, we adopted a gentle, low frequency alarm, which we will refer to as the "gentle alarm", as the sound for encouraging drivers to check the safety of their vehicle's surroundings. When the drivers suddenly hear an alarm sound, they will tend to look and check their surroundings, and at the same time, will unconsciously ask questions like "Why is the alarm sounding?" and "When does the alarm sound?" As a result, we hypothesized that drivers who learn about the alarm warning unconsciously will also look and check their surroundings unconsciously. This brings us to the aim of this study, which is to improve the behavior of drivers that do not tend to confirm the safety of their surroundings sufficiently while driving (Fig. 1).

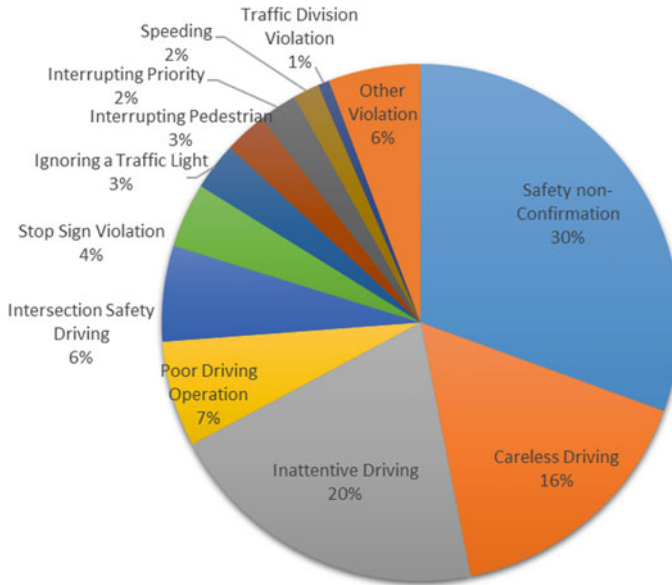


**Fig. 1** Japanese traffic accidents in 2016

## 2 Learning by Gentle Alarm

### 2.1 Experiment Scenario

The study we conducted was approved by the Research Ethics Committee of the Shibaura Institute of Technology. The subjects received an explanation of the experiments and signed a participation agreement. The subjects in the study were six university students who hold a driver's license. We used a swing-type, six-axis driving simulator with an eye mark recorder (nac: EMR-8B) to determine the eye position of the driver (and thus, determine where they are looking). The driving course was set to be a general road occupied by pedestrians and other vehicles. The subjects were told to drive while listening to classical music, namely Pachelbel Canon, playing in the background. This was in order to hide the presence and sound of the gentle alarm to some extent.

In this experiment, we grouped the subjects as shown in Table 1. Group A knew about the gentle alarm while Group B did not. At first, the subjects drove on a course (Course 1) without the use of any alarm. This was to determine the baseline performance of their awareness of the surrounding safety. At five specific intersections, the subjects experienced dangerous scenarios, such as the sudden appearance of a bicycle (Fig. 2). We also tracked the subjects' eye position to determine where they were looking while driving (Eye Track Result 1).

**Table 1** Group

Group	Group A	Group B
Gentle alarm	Known	Unknown
Number of subjects	2	4

**Fig. 2** Example of a dangerous scene

Three days later, the subjects drove on a different course (Course 2), but with the gentle alarm present. This drive saw an improvement in the subjects' behavior. They drove this course three times, once every three days. This was implemented based on Ebbinghaus's Forgetting Curve [12, 13], which shows the relationship between memory and time. This curve indicates that humans forget about 70% of things they have learned after three days. The gentle alarm used here was an intermittent sound of 250 Hz, which starts to sound when the turn signal is used. At the end of each of the three drives, the subjects filled out a questionnaire evaluating the gentle alarm.

Finally, the subjects drove back on Course 1 without the gentle alarm being present. On this drive, we tracked their eye position one more time, in order to determine where they were looking while driving (Eye Track Result 2), and then compared Eye Track Result 1 with Eye Track Result 2.

## 2.2 Experiment Result and Discussion

In this experiment, there were two criteria for evaluating whether the subjects sufficiently check their surroundings for safety confirmation. The first criterion was the place where the subject is looking. Here, we set four defined targets which were:

1. Back of the sidewalk
2. Back of the crosswalk
3. In front of the crosswalk
4. In front of the sidewalk

The second criterion was whether the subjects look to each target three or more times. We assumed that each time a subject looks at the above four places, they:

1. Grasp the traffic condition at the intersection
2. Look at their surroundings before turning left/right
3. Check for any dangerous threats

The experimental results are as shown in Table 2. The table shows the eye tracking results for one of the intersections with a dangerous scenario on the course (this intersection is as depicted in Fig. 2). Figures 3 and 4 show the results for the subjects in Group A and Group B, respectively. The boxes in Figs. 3 and 4 visualize the number of times the subjects looked and checked for safety at those boxes' positions which correspond to the four defined targets. A subject in Group A (No. i) looked only forward and did not checked the sidewalk in the first drive. However, in the final drive, the same subject checked the surroundings and thus, increased the value for surrounding safety. This shows that the gentle alarm is effective in increasing the subjects' awareness of the safety of their surroundings. A subject in Group B (No. iii) only looked at and checked the crosswalk in the first drive. However, in the final drive, the same subject looked at and checked the crosswalk and the sidewalk. This result is basically the same as with Group A.

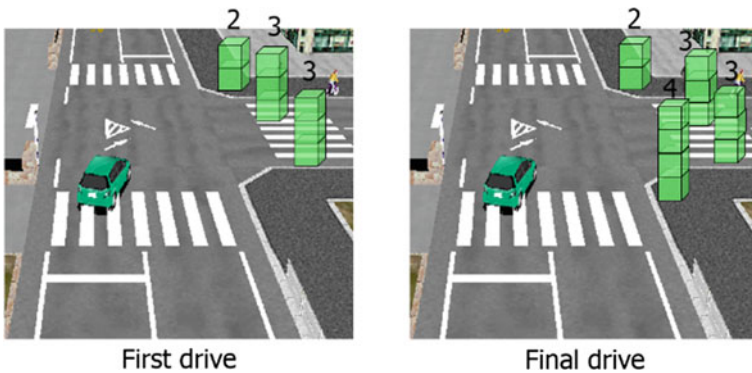


Fig. 3 Experiment result (Group A)

**Table 2** Experiment result for the subjects' eye movement (turning right at an intersection)

Subject		Eye track result 1						Eye track result 2				
Group	Subject no	Back of the sidewalk	Back of the crosswalk	In front of the crosswalk	In front of the sidewalk	Back of the sidewalk	Back of the crosswalk	In front of the crosswalk	In front of the sidewalk	Back of the crosswalk	In front of the crosswalk	In front of the sidewalk
Group A	i	2	3	3	0	2	3	3	3	3	3	4
	ii	2	2	2	0	2	3	3	3	3	3	1
Group B	iii	0	3	2	0	1	4	3	1	4	3	1
	iv	1	1	0	0	3	3	3	3	3	3	0
	v	2	3	1	1	2	3	3	2	3	3	1
	vi	1	2	0	0	1	3	3	1	3	3	1

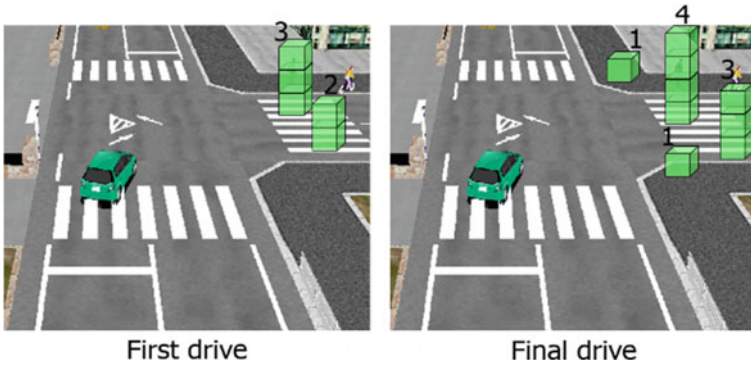


Fig. 4 Experiment result (Group B)

We also found that the subjects checked their surrounding for safety confirmation at the other four dangerous intersections in the course more in their final drive than in the first. Here, we used the t-test to show statistically that the unconscious learning phase is effective in these subjects. We did this by comparing the total value for the subjects' surrounding safety confirmation in the first and final drive in each scenario.

As for the result of the questionnaire, all of the subjects were happy with the low frequency sound of the gentle alarm. At first, the subjects in Group B were annoyed by the number of times the gentle alarm sounded but then, they got used to it. The subjects in Group B thought that the alarm warned them when they were approaching pedestrians or other vehicles. The subjects felt that even a low frequency sound was alarming, and therefore, led to awareness of surrounding safety confirmation.

In this experiment, the intermittent 250 Hz alarm sounded at road intersections when a driver is driving. This resulted in an improvement in driver awareness of the surrounding safety confirmation, without causing annoyance in the process.

However, there were two issues with this experiment.

1. Since the subjects drove on the same course (in the first and final drive) and the three-day experiment interval can be considered short, there is a possibility that the subjects performed better in the final drive because they were familiar with the course.
2. Since the subjects do not usually drive, the result of this experiment might be not correct.

In order to verify whether or not the above two issues affected the experiment, we conducted a new experiment, as described in Sect. 3.



### 3 Learning by Gentle Alarm or Getting Used to Driving

#### 3.1 Experiment Scenario

In this experiment, we examined the effect of learning by the gentle alarm and the effect of getting used to driving. The subjects comprised ten persons, all of whom differed from previous experiment. However, the experiment process was almost the same as previously.

At first, the subjects drove on the same course as in the previous experiment's first course, and experienced dangerous scenarios at five specific intersections.

Next, the subjects were divided into two groups, as in Table 3, with Group A to drive the next three courses (each differing from the others) with the gentle alarm present. Group B did the same, but without the presence of the gentle alarm. We set the experiment interval at one week. We instructed Group A, "If you hear the alarm sound, please look at your surroundings". The subjects in Group A then filled out a questionnaire evaluating the gentle alarm.

Finally, all of the subjects drove on a new course without the gentle alarm being present. We then compared the eye track result of the first drive with that of the final drive, in order to evaluate their performance in checking the surroundings for safety confirmation.

#### 3.2 Experiment Result and Discussion

The result of the subjects' eyes movement at one of the road intersections with a dangerous scenario is shown in Table 4. As the table shows, we were unable to acquire some of the results, as the subjects ran into pedestrians or bicycles at the intersection. Figures 5 and 6 show results for the subjects in Group A and Group B, respectively. The boxes in Figs. 5 and 6 visualize the number of times the subjects looked and checked for safety at those targets.

A subject in Group A (No. i) only looked forward and did no check his surroundings in the first drive. However, in the final drive, the same subject looked and checked his surrounding and, therefore, increased the value for surrounding safety confirmation. This result is the same as in the previous experiment.

A subject in Group B (No. vi) only looked forward and did not check his surroundings in the first drive. However, in the final drive, his frequency of looking

**Table 3** Group

Group	Group A	Group B
Gentle alarm	Sound	No alarm
Number of subjects	5	5

**Table 4** Experiment result of the subject’s eye movement

Subject		Eye Track Result 1				Eye Track Result 2			
Group	Subject No	Back of the sidewalk	Back of the crosswalk	In front of the crosswalk	In front of the sidewalk	Back of the sidewalk	Back of the crosswalk	In front of the crosswalk	In front of the sidewalk
Group A	i	3	2	0	0	1	3	3	0
	ii					2	2	2	0
	iii					2	4	3	0
	iv	4	3	2	1	3	3	3	2
	v	2	2	1	0	3	2	2	1
Group B	vi	1	1	0	0	0	3	2	0
	vii	1	1	0	0	1	2	1	0
	viii					2	3	2	0
	ix					0	3	3	2
	x	3	2	0	0	3	2	3	1

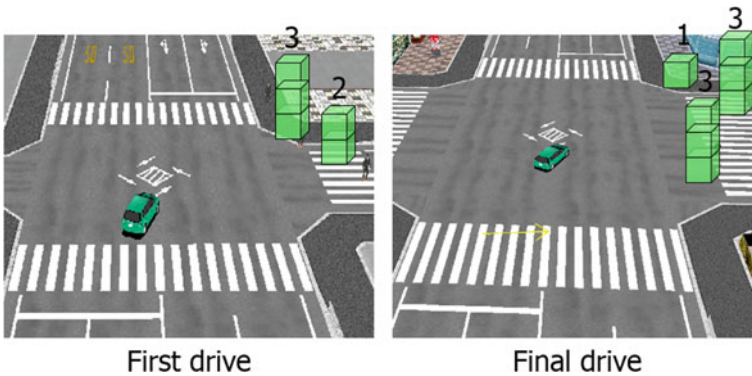


**Fig. 5** Experiment result (Group A)

and checking the surroundings increased. This indicates that the surrounding safety confirmation of the subjects had improved.

Five subjects (Nos. i, ii, iii, vi, vii) across both of the groups ran into pedestrians or bicycles in the first drive. However, in the final drive, only one subject (No. iii) in Group A ran into a bicycle, while three subjects in Group B ran into pedestrians. This suggests the possibility that in the first experiment, the gentle alarm was effective at increasing driver awareness of the surroundings, and that it was not caused by the two aforementioned issues. Nevertheless, we still cannot dismiss the idea that getting used to driving while participating in this experiment could have contributed to the subjects becoming more aware of their surroundings during the final drive. This is a matter to be investigated in future work.

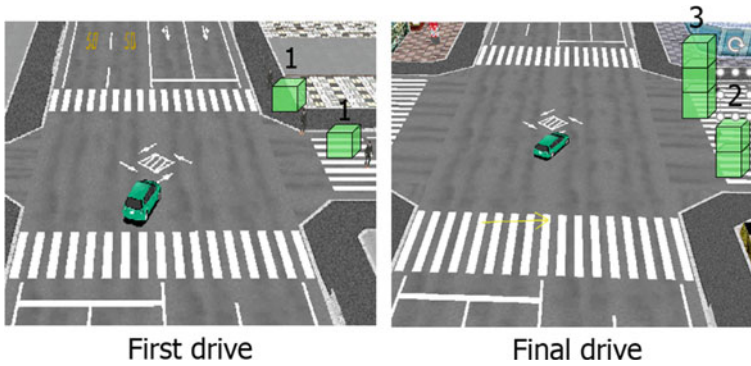


**Fig. 6** Experimental result (Group B)

As for the questionnaire results, the subjects in Group A did not find the gentle alarm noisy, and were not annoyed by it. The subjects felt that even a low frequency sound is alarming enough to lead them to a greater awareness of their surroundings.

## 4 Conclusion

In this study, we focused on unconscious human learning and human action. We alerted drivers who do not fully check their surroundings for safety via the use of the gentle alarm.

The drivers unconsciously learned the alarm pattern, which then caused them to look and check their surrounding better than they had prior to learning. In conclusion, we can say that the use of the gentle alarm succeeded in improving the drivers' awareness for surrounding safety confirmation in this study.

We made use of an eye mark recorder in the experiment to track the eye positions of the subjects and thus, were able to check whether or not they were aware of their surroundings for safety confirmation. The gentle alarm we used has an intermittent sound of 250 Hz, and the experiment interval was three days or one week. We found that the effect of unconscious learning was effective even if the subjects did not know about the presence of the gentle alarm beforehand. Furthermore, the subjects who knew about the alarm did not feel annoyed by its sound.

On the other hand, it may not have been solely the gentle alarm that was responsible for the improvement in the drivers' awareness of their surrounding safety confirmation; the effect of getting used to driving while participating in the experiment could also have contributed. However, we feel that the effectiveness of the gentle alarm was more prominent, although this is a matter to be investigated further.

In terms of future work, we are considering extending our research by altering the gentle alarm, and by investigating the effectiveness of unconscious learning when other scenarios and places are used. In addition, we are considering adding another

evaluation method besides just tracking eye movement, such as evaluating the drivers' behavior via a driving style check sheet.

## References

1. National Police Agency Traffic Bureau: 2016 Traffic Accidents and Road Traffic Act Violation Crackdown, p. 19 (2017)
2. Wasino, S.: Traffic Psychological Considerations on Causes of Traffic Accidents and a Prototype of a System to prevent from Rear-End Collisions, Information Processing Society of Japan, pp. 1–8 (2004)
3. Osawa, K., Yamazaki, K., Ito, T.: Study on Effective Method of Provision REAR-END Collision Warning System, Society of Automotive Engineers of the 2015 Autumn Meeting Academic Lecture Presentation Paper, pp. 1376–1379 (2015)
4. Renge, K.: Social Psychology of Traffic Behavior, Kitaoji Shobo, p. 9 (2005)
5. Libet, B.: Time of Conscious Intention To Act in Relation to Onset of Cerebral Activity (Readiness-Potential) (1983)
6. Maeno, T.: How to make a conscious robot: fundamental idea based on passive consciousness model. *Robot. Soc. Jpn.* **23**(1), 51–62 (2005)
7. Hakoda, Y., Tuduki, T., Kawabata, H., Hagiwara, S.: Cognitive Psychology: Brain, Modeling and Evidence, Yuhikaku, pp. 65–73 (2010)
8. Cherry, E.C.: Some experiments on recognition of speech, with one and with two ears. *J. Acoust. Soc. Am.*, 975–979 (1953)
9. Tsuchida, S.: Fundamental consideration on information transmission by sound. *Soundscape Assoc. Jpn. J. Soundscape Assoc. Jpn.* **2**, 15 (2000)
10. Matsuda, N., Akita, T., Koga, T.: Effects of Frequency of a Sound and Rumbling Cycle on Feeling Pressure, Architectural Institute of Japan, pp. 847–848 (2005)
11. Society of Automotive Engineers of Japan: Handbook of Society of Automotive Engineers volume 1st -Basics and Theory, pp. 326–327 (2004)
12. Ishida, A.: Theory and Exercises in Cognitive Psychology –Vision and Memory, Ohmasha, pp. 103–104 (2012)
13. Ichikawa, S., Nakagawa, M.: Mathematics and psychology—‘psychology understood by mathematics’ and ‘psychology understanding mathematics’. *Math. Soc. Jpn.* **53**(4), 410–421 (2001)

# Inattentive Driving Effects on Eye Movement and Driving Behavior



He Xi and Kazunori Shidoji

**Abstract** Many studies of Intelligent Transport Systems (ITS) have been conducted to reduce traffic accidents. Driver monitoring systems can detect dangerous driver behaviors and reduce traffic accidents through alarm and active safety systems. Data from the National Police Agency of Japan for 2017 show that the main cause of fatal traffic accidents is driver inattentiveness. Investigating eye movement characteristics and driving behavior during inattentive driving can reveal characteristics of inattentiveness. For this study, we designed a driving simulation experiment with subtasks while driving to assess the inattentive behavior of drivers. During the driving experiment, drivers were asked to drive normally, drive and answer arithmetic problems, or drive and answer questions about a map. Driver reaction times during emergency braking to a sudden appearance of a car at an intersection, sudden appearance of a pedestrian at a non-intersection, and steering performance on curved roads were assessed. In addition, we assessed gaze fixation time and driver eye movement velocity and direction. Inattentive driving resulted in a longer reaction time, more steering wheel operation, shorter fixation time, slower angular speed of eye movement, and lower frequency of left–right direction change.

**Keywords** Driving simulation · Eye movements · Inattentive driving · Mental calculation · Memory of maps · Reaction time · Steering performance

---

H. Xi

Graduate School of Integrated Frontier Sciences, Kyushu University, 744 Motooka, Nishi-ku, Fukuoka 819-0395, Japan  
e-mail: [hex@cog.inf.kyushu-u.ac.jp](mailto:hex@cog.inf.kyushu-u.ac.jp)

K. Shidoji (✉)

Faculty of Information Science and Electrical Engineering, Kyushu University, 744 Motooka, Nishi-ku, Fukuoka 819-0395, Japan  
e-mail: [shidoji@inf.kyushu-u.ac.jp](mailto:shidoji@inf.kyushu-u.ac.jp)

# 1 Introduction

Distraction is a general phenomenon in daily life. In some circumstances that require a driver's close attention to road conditions, distraction degrades safety and traffic flow [22], and occurs frequently at all ages [14]. To reduce traffic accidents caused by distractions, many studies have investigated distracted driving. Most studies specifically examine distracted driving caused by external factors such as mobile phones [4, 15, 16], in-vehicle information systems [2], passengers [3, 10, 19], and music and auditory materials [6, 7, 24].

There is one type of distraction that has nothing to do with external factors: inattentive driving [11]. This distraction is difficult to examine, but it is extremely dangerous and difficult to control. Based on National Police Agency of Japan data, careless driving (inattentive driving) is the most common reason reported for all fatal traffic accidents attributed to a violation of safe driving practices (Fig. 1). To reduce traffic accidents and to resolve traffic difficulties of all kinds, Intelligent Transport Systems (ITS) have become a mainstream field of study, especially to alleviate inattentive driving.

Because it is difficult to ascertain and control the timing of an inattentive state, subtasks while driving, such as mathematical operations, are generally used to study inattentive driving. When examiners ask participants verbal questions while driving, drivers blink more frequently, and their fixation time is reduced [23]. Harbluk et al. [5] used easy tasks and difficult arithmetic tasks to assess distracted driving, and found that the mean number of braking events with difficult tasks during driving was higher than that without a task. When driving while following other vehicles, brake reaction

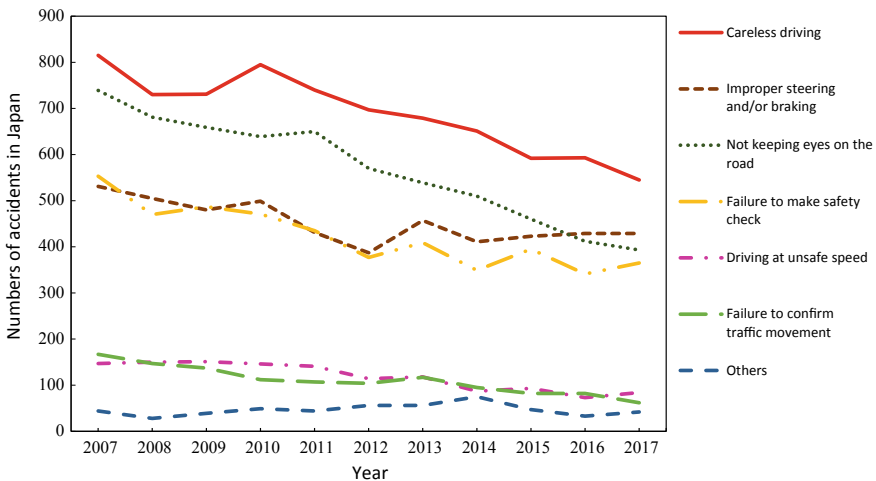


**Fig. 1** Annual fatal accidents in Japan data [17] by type of violation involving primary parties (based on the National Police Agency of Japan data)

times are longer if drivers are doing mental arithmetic [8]. If numerous vehicles are on the road and the driver is doing mental arithmetic while driving, then the frequency of eye fixation time is increased at the 0.1–1 s time interval, and eyes move more often. With few other vehicles on the road, the result is the opposite [1]. Louie and Mouloua [9] used mathematical problems that are commonly encountered in life (e.g., the total price of 2 boxes of \$3 turkey). Slower braking reactions occurred when a yellow traffic light appeared and during the sudden appearance of vehicles when distracted. Some studies have used subtasks such as memories. Akiyama et al. [1] used numerical memorization tasks, and Ross et al. [20] studied the effect of a verbal working memory load task on driving behavior. Driving performance deteriorated with increasing verbal working memory load in terms of the mean deviation in the lane change path, lane change initiation, and the percentage of correct lane changes.

Some studies have measured eye movement during distracted driving [13, 25]. Metz et al. [12] compared the visual attention in driving for two visual secondary tasks and found that drivers had a longer fixation in a driving simulation. Savage et al. [21] studied the effects of mobile phone conversations on eye movement during driving and found higher saccade peak velocities, increased blink frequencies, and a reduction in the spread of fixation along the horizontal axis. Wang et al. [27] designed an experiment with and without a mobile phone and found that compared to drivers without mobile phones, drivers with them had higher numbers of glance transitions and shorter on-road glance duration during distracted driving.

Drivers will often think or recall something during inattentive driving. Furthermore, an image might appear in the person's mind during recall. To ascertain the manner by which and the degree to which this process affects drivers, we designed two subtasks of mental arithmetic and map recall to simulate thinking and recall processes during driving.

An inattentive state has a significant impact on eye movement [26], and driving behavior has a direct relationship with traffic accidents. We examined the influence of mental arithmetic and map recall on driver behavior when a car or a pedestrian suddenly appeared in front of the vehicle. Driving behavior and eye movements were captured using the driving simulation and eye movement measurement apparatus. We measured brake reaction time, the number of steering wheel rotations, fixation time, angular eyeball speed, and the direction of focal point movement.

## 2 Methods

### 2.1 Participants

Thirteen participants (10 men, 3 women) from Kyushu University participated in this experiment. Participants were 22–29 years old, and each participant held a valid driver's license.

## 2.2 Equipment

**Hardware.** The simulator was controlled using a PC (Precision T1700; Dell Inc.). The image was displayed on a 27-inch liquid crystal monitor (T 270 W; Hyundai IBT Co. Ltd.) with a resolution of  $1,920 \times 1,080$  pixels. A simulated vehicle steering wheel, accelerator pedal, and brake pedal were used (Driving Force GT, Logicool; Logitech Corp.). An eye movement measurement apparatus (EMR-9; NAC Image Technology Inc.) was used to measure eye movements.

**Software.** The driving simulator control program was created using software (UC-win Road Ver. 6.00.02; Forum 8). Data related to brake operation, steering operation, and other vehicle parameters were measured using the UC-win Road Drive Log plugin, which we created in our laboratory. The system frame rate was about 50 fps in all experiments. Reaction time accuracy was about 20 ms. Eye movements were analyzed using software (EMR-dFactory; NAC Image Technology Inc.).

## 2.3 Design

To find driving behavior and eye movement differences between participants driving while doing a subtask and without doing a subtask, four types of roads were designed: S1, S2, C1, and C2. Roads S1 and S2 were straight lines with three intersections. Because the buildings on road S1 were taller and closer to the road, the view of the driver on road S1 was narrower than that on road S2. At the intersection, another vehicle might suddenly cross the vehicle path. At this point, we measured the driver's emergency braking reaction time. Roads C1 and C2 were curved roads: road C1 was more curved than road C2. The purpose of the curved roads was to study the direction change, the right and left fine adjustment, of the steering wheel. In this experiment, all participants drove six road combinations with a driving simulator. All road combinations comprised the four roads: S1, S2, C1, and C2 (Table 1). A three-second break was inserted between roads.

**Table 1** Road combinations of six types

Road combination number	Road combination order
1	S1—break—C2—break—C1
2	C2—break—S2—break—S1—break—S2
3	C1—break—S1—break—C2
4	S2—break—C1—break—S1
5	S1—break—S2—break—C2—break—S2
6	C2—break—S1—break—C2—break—S2



## 2.4 Tasks

**Main task.** Figure 2 presents some captured monitor screens. All participants were required to drive at up to 60 km/h. They were able to brake when any possibility of a road incident was presented.

**Subtasks.** The subtasks were for participants to do mental arithmetic and drive during map recall.

*Mental arithmetic.* With an increase in the difficulty level of arithmetic calculations, the brake reaction time increases gradually [29]. To prevent the calculations from being too simple to affect driving, six sets of mental arithmetic of double digit sums and subtractions were used in the six road combinations. The answers to mental arithmetic questions were 0–99 (Table 2). Participants had 3 s to answer each question before the next question was asked.

*Recall the map.* Six maps were used in the six road combinations. Each map had markings for seven locations, several roads, and north (Fig. 3). The map was displayed on the monitor for two and a half minutes before each driving test for the driver to memorize. The map then disappeared and driving started. While driving, the participant was asked map-information-related questions continuously. The questions were about directions and distances between several locations, location on the map, and the number of intersections between locations (Table 3). Participants had five seconds to answer before the next question was asked.

**Table 2** Examples of questions related to mental arithmetic

Number	Mental arithmetic
1	41 – 33 =
2	50 – 19 =
3	44 – 27 =
4	26 + 25 =
5	45 + 26 =
6	45 + 47 =
7	38 – 16 =
8	41 – 21 =
9	28 – 12 =
10	38 – 10 =
11	42 + 50 =
12	41 – 33 =
...	...



(a) Sudden car appearance at road S1



(b) Sudden car appearance at road S2



(c) Sudden appearance of pedestrian at road C1/C2

**Fig. 2** Three road incident situations

**Fig. 3** Example of maps in the map recall experiment

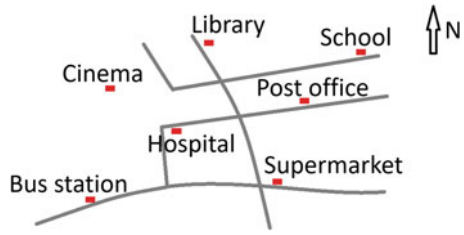


**Table 3** Examples of questions related to map recall

Number	Questions
1	Where is the westernmost location?
2	Where is the nearest place from the hospital?
3	Which direction is the post office from the library?
4	Which direction is the supermarket from the post office?
5	How many intersections from the library to the hospital?
6	What is the farthest place from school?
7	Which direction is the cinema from the school?
8	Where is the southernmost location?
9	How many intersections from the bus station to the supermarket?
10	Do you think the school is southeast of the hospital?
11	Do you think the library is the closest place from the post office?
12	Do you think the hospital is southwest of the cinema?
...	...

### 2.5 Procedure

The participants were divided into two groups. The first group started with the mental arithmetic subtask. A week later, they were asked to continue the experiment for the map recall subtask. The other group participated in the experiment in the opposite order, and each participant spent around forty minutes a day for the experiment.

On the first day after the experiment was explained, participants were asked for their consent to participate. After an eye movement measurement apparatus was applied, participants practiced using the driving simulator. No sudden incidents were presented during practice mode, which was intended for participants to become accustomed to the system and road combinations. The requirements below were given to the participants.

- The accelerator pedal should be pushed to the end, always maintaining driving speed at 60 km/h on smooth roads: 60 km/h was set as the maximum speed.
- The brake pedal must be pressed immediately when a pedestrian or vehicle suddenly enters the road.
- After pushing the brake pedal to allow a pedestrian or vehicle to pass, release the brake pedal and press the accelerator pedal to the end to continue the driving simulation.

The experiment started after completion of the process described above. First, we let participants drive through all six road combinations in the order of with-subtask—without-subtask—with-subtask—without-subtask—with-subtask—without-subtask. Second, we reversed the order of the with/without subtasks, and let participants drive through all road combinations. These two steps were to ensure that with-subtask and without-subtask situations had been met in all road combinations. We eliminated possible influences that the subtask order may have had on the experiment results.

We used R (3.5.0) software for statistical processing. Anovakun (4.7.0) was used for analysis of variance (ANOVA). Mendoza's Multisample Sphericity Test was used to test for the assumption of sphericity. The degrees of freedom were corrected using the Greenhouse–Geisser method if the assumption was not valid. Multiple comparisons were used when a significant difference was found using Shaffer's F-Modified Sequentially Rejective Bonferroni Procedure. Average values were used for without-subtask conditions because the without-tasks were conducted both days.

## 3 Results

### 3.1 Driving Behavior

**Reaction time of braking.** The reaction time was the time from the appearance of a vehicle or a pedestrian appearing on the screen to the time when the driver started to brake. Figure 4 shows the average of all participants' reaction times for the three types of incidents during driving with subtasks, mental arithmetic and map recall, and during driving without the subtasks. Data were calculated using two-factor ANOVA according to the incident and the subtask type. A significant difference was found for the main effects of an incident ( $F(2, 24) = 38.5888$ ,  $MSE = 0.0065$ ,  $\eta_p^2 = 0.7628$ ,  $p = 0.0000$ ) and for the subtask type ( $F(1.21, 14.54) = 10.4468$ ,  $MSE = 0.0285$ ,  $\eta_p^2 = 0.4654$ ,  $p = 0.0041$ ). Furthermore, a marginally significant effect was found for the interaction of those two factors ( $F(4, 48) = 2.5277$ ,  $MSE = 0.0032$ ,  $\eta_p^2 = 0.1740$ ,  $p = 0.0527$ ). For driving without a subtask, the reaction times of braking to the sudden appearance of a car on road S2 (0.657 s) and to the appearance of a pedestrian (0.701 s) were longer than that of the appearance of a car on road S1 (0.540 s). When driving with mental arithmetic, the reaction times of braking to the car appearance on road S2 (0.642 s) and the appearance of a pedestrian (0.668 s) were

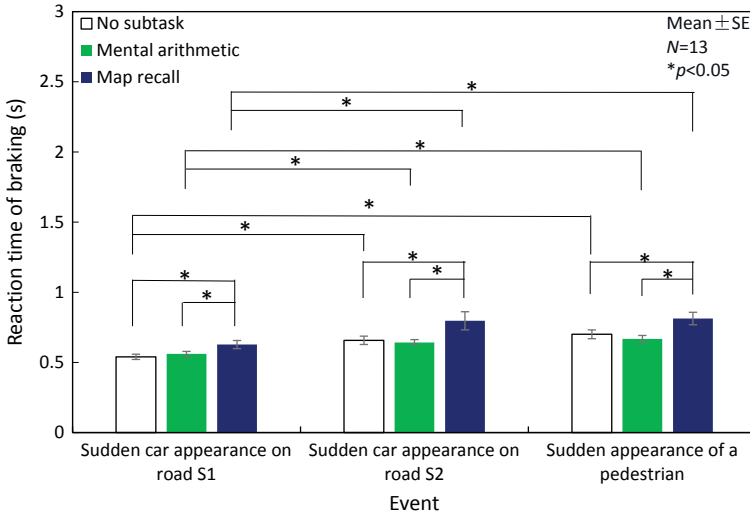
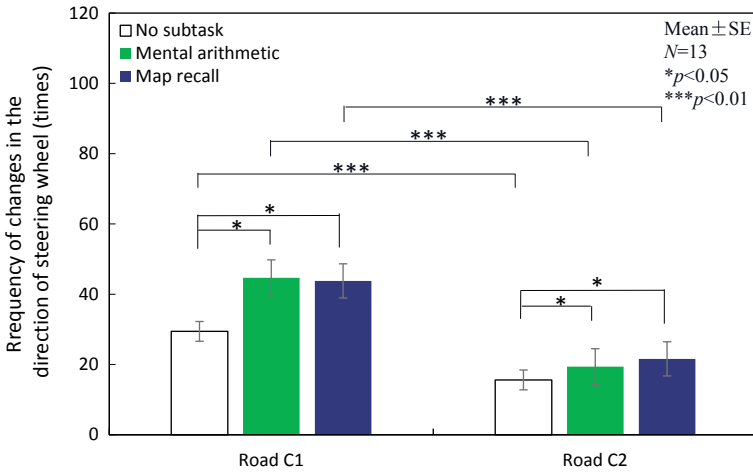


Fig. 4 Reaction time of braking for all incidents

longer than that to a car appearance on road S1 (0.561 s). When driving during map recall, the reaction time of braking to a car appearance on road S2 (0.797 s) and the reaction time of braking to the appearance of a pedestrian (0.813 s) were longer than that to a car appearance on road S1 (0.628 s). For the car appearance on road S1, the reaction time of braking when driving during map recall (0.628 s) was longer than that when driving with no subtask (0.540 s) or when driving with mental arithmetic (0.561 s). For the car appearance on road S2, the reaction time when driving during map recall (0.797 s) was longer than that when driving without a subtask (0.657 s) or with mental arithmetic (0.642 s). After the appearance of a pedestrian, the reaction time when driving during map recall (0.813 s) was significantly longer than that when driving without a subtask (0.701 s) or when driving with mental arithmetic (0.668 s).

**Frequency of steering wheel fine adjustment.** The number of times that the steering wheel was manipulated clockwise or counterclockwise to keep the car in the lane on a curved road. Figure 5 shows the average number of times that all participants were driving through roads C1 and C2. Data were calculated using two-factor ANOVA according to the type of road and subtask type. A significant difference was found for the main effect of roads ( $F(1, 12) = 69.1188, MSE = 117.6255, \eta_p^2 = 0.8521, p = 0.0000$ ) and for the subtask type ( $F(2, 24) = 21.8786, MSE = 38.5584, \eta_p^2 = 0.6458, p = 0.0000$ ). Furthermore, a significant difference was found for the interaction of those two factors ( $F(2, 24) = 13.4338, MSE = 16.9968, \eta_p^2 = 0.5282, p = 0.0001$ ). With regard to the type of road when driving without a subtask, the frequency of changes in the direction of the steering wheel on road C1 (29.4 times) was higher than that for road C2 (15.6 times). When driving while doing mental arithmetic, the



**Fig. 5** Frequency of rotating the steering wheel on roads C1 and C2

frequency of changes in the direction of the steering wheel on road C1 (29.4 times) was more than that for road C2 (19.4 times). When driving during map recall, the frequency of changes in the steering wheel direction on road C1 (43.8 times) was more than that on road C2 (21.6 times). Regarding the subtask type, when driving with mental arithmetic (44.7 times) and during map recall (43.8 times), the participants rotated the steering wheel more frequently than without a subtask (29.4 times) on road C1. For driving with mental arithmetic (19.4 times) and during map recall (21.6 times), the average number of times that participants rotated the steering wheel was more than that without the subtask (15.6 times) on road C2.

### 3.2 Eye Movement Characteristics

**Fixation time frequency distribution.** Figure 6 shows the average frequency distribution of different fixation times. Data were used with three-factor ANOVA according to the six types of road combinations, the subtask type, and the fixation time. A significant difference was found for the main effect of fixation time ( $F(15, 180) = 147.4924$ ,  $MSE = 85.9559$ ,  $\eta_p^2 = 0.9197$ ,  $p = 0.0000$ ). Furthermore, a significant difference ( $F(30, 360) = 1.7999$ ,  $MSE = 29.4200$ ,  $\eta_p^2 = 0.1304$ ,  $p = 0.0072$ ) was found for the interaction of the subtask type and fixation time. Compared to the without-subtask figure, the fixation time when driving with mental arithmetic had a lower frequency in the 0.5–0.7 s and 0.8–0.9 s time intervals; the fixation time when driving during map recall had a higher frequency in the 0.2–0.3 s time interval, but a lower frequency in the 0.7–0.8 s time interval. The frequency of the fixation time with map recall was higher than other tasks in the 0.2–0.3 s time interval.

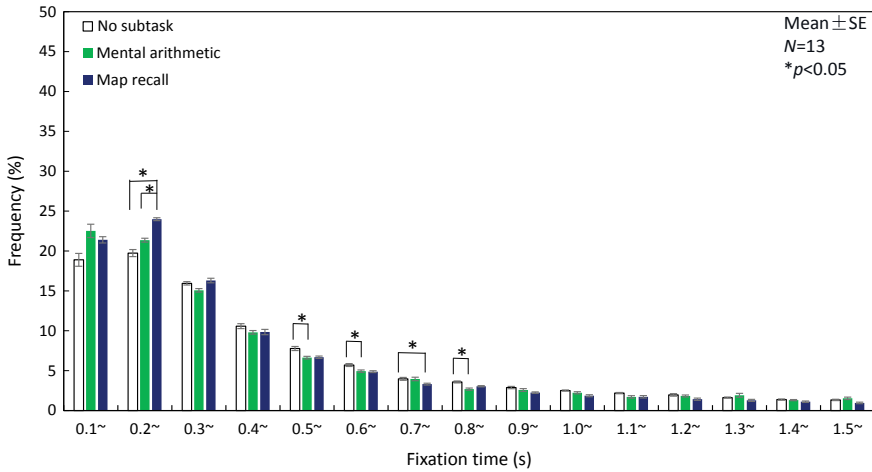


**Fig. 6** Fixation time frequency distribution

**Traveling speed frequency distribution.** Figure 7 shows the average frequency distribution of all participants’ angular eyeball speed. Data were calculated using three-factor ANOVA according to the six types of road combinations, the subtask type, and the angular eyeball speed. A significant difference was found for the main effect of the angular eyeball speed ( $F(1.14, 13.68) = 63.3727, MSE = 3087.5676, \eta_p^2 = 0.8408, p = 0.0000$ ). Furthermore, a significant difference was found ( $F(18, 216) = 2.9505, MSE = 87.0523, \eta_p^2 = 0.1974, p = 0.0001$ ) for the interaction of the subtask type and the angular eyeball speed. Compared to driving without a subtask, the angular eyeball speed with mental arithmetic was found to have a higher frequency in the 0–30 deg/s speed interval, but a lower frequency in the 150–180 deg/s speed interval. In the case of map recall, a higher frequency was found in the 0–30 deg/s speed interval, but a lower frequency was found in the 60–120 and 150–180 deg/s speed intervals. The frequency of traveling speed with mental arithmetic was higher in the 60–90 deg/s speed interval than that with map recall.

**Traveling direction frequency distribution.** Figure 8 shows the average frequency distribution of all participants’ eye movement directions. Data were calculated using three-factor ANOVA according to the six types of road combinations, the subtask type, and the fixation direction. A significant difference was found for main effects of the angular speed of fixation direction ( $F(1.27, 15.22) = 89.9521, MSE = 1537.8463, \eta_p^2 = 0.8823, p = 0.0000$ ). Furthermore, a significant difference was found ( $F(14, 168) = 5.0601, MSE = 41.3128, \eta_p^2 = 0.2966, p = 0.0000$ ) for the interaction of the subtask type and fixation direction. Compared to driving without a subtask, the fixation with mental arithmetic had a lower frequency in the left and right directions, but a higher frequency was found in the up/right, up, and down directions. Compared with no subtask and with map recall, a lower frequency was found in the left and right directions with map recall, but the frequency was higher in the up/right, down/left,

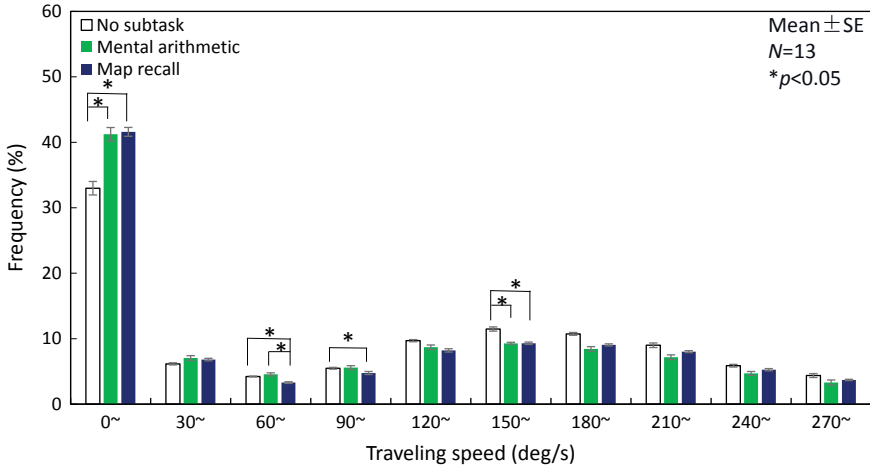


Fig. 7 Angular speed frequency distribution

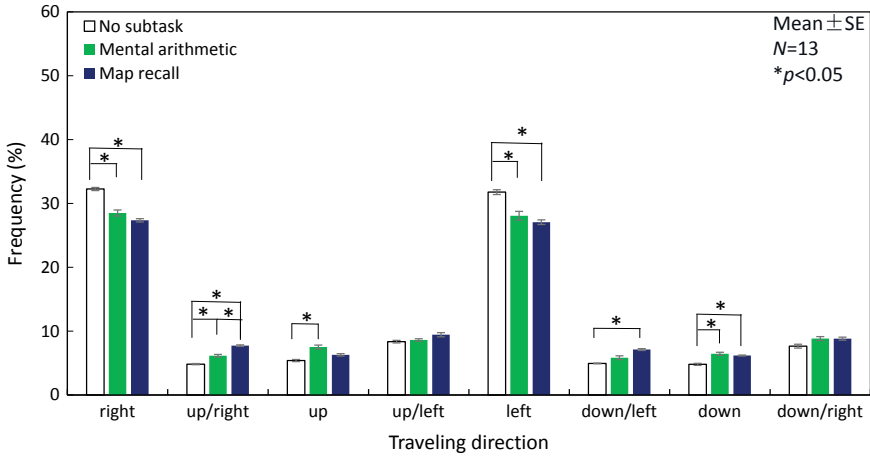


Fig. 8 Fixation direction frequency distribution

and down directions with map recall. For subtasks between driving with mental arithmetic and driving during map recall, the frequency of traveling direction was higher in the up/right direction.



## 4 Discussion

We investigated the influence of mental arithmetic and map recall on eye movement and driving performance. Each task weakened driving ability, increased driver burden, and altered eye movements.

Brake reaction times were longer for map recall than for driving without a subtask and driving with mental arithmetic in response to the sudden appearance of a car or pedestrian. When following a lead vehicle, memory tasks also increase brake reaction times [28]. Compared to driving with no subtask, no significant difference in reaction time was found with mental arithmetic during driving. This result demonstrates that mental arithmetic does not affect a driver's ability to brake, which differs from other results [8]. This result may be true because of the lower difficulty of mental arithmetic, such as ample time for thinking, which has a lower burden on participants. Map memory had a strong effect, and drivers needed more time to slow. Under the same subtask condition, brake reaction time was significantly different for different incidents.

For all subtasks, brake reaction times to a car appearance on road S2 and a pedestrian appearance were longer than that to a car appearance on road S1. The brake reaction time was shorter for narrow field of view intersections (Road S1). The brake reaction time from a pedestrian appearance was longer than that from a car appearance on road S1. One likely reason is that the participants did not anticipate pedestrians entering into the road. Because of the narrow field of view for intersections on road S1, participants may have had increased vigilance. In contrast, the wide field of view intersections on road S2 may have resulted in decreased vigilance. Although the participants could not estimate which intersections will have vehicles suddenly entering the intersection, they understood that vehicles could only enter at intersections. Pedestrians could enter the road at any point, which was unpredictable. Therefore, the overall reaction time was longer when pedestrians entered the road.

The number of times rotating the steering wheel was higher for driving with mental arithmetic and driving during map recall than for without-subtask driving. Therefore, both subtasks increased driver burden, reduced driver attention to road conditions, and increased actions for correct driving.

Furthermore, a significant difference was found between two different curved roads, which suggested that driving on a more curved road was more difficult and required more steering wheel maneuvers.

Eye movement was expressed as a frequency of distribution. Both subtasks decreased eye fixation time, and eyes had more movement during with-subtask driving, which suggests that thinking or recall will increase driver burden and make it difficult for a driver to fix on one point for long periods. However, the frequency of the fixation time when driving during map recall was higher than with the other subtasks in the 0.2–0.3 s time interval. The influence of map recall was stronger than that of mental arithmetic. Recarte and Nunes [18] showed that fixation time was longer during a spatial-imagery task. Therefore, an image-related task increases the maximum fixation time, but the frequency of a long fixation time was not high.

Angular eyeball speed was lower for driving with mental arithmetic and driving during map recall. When driving without a subtask, the distribution of angular eyeball speed was highest in the 0–30 deg/s speed interval, and subtasks further improved this distribution. A slower angular speed might increase the time to recognize pedestrians or vehicles entering an intersection, which may increase brake reaction times. Wakui and Hirata [26] showed a horizontal saccadic movement with a peak speed less than 40 deg/s and at time intervals of less than 0.2 s increased while driving in an inattentive state. Combining their results and ours, the frequency of fixation time in the 0.1–0.3 s interval and travel speed in the 0–40 deg/s interval may be an important indicator of the inattentive state.

Eye direction frequency was lower in the left/right directions and higher in the up/down directions for mental arithmetic and map recall, which indicates that thinking or recall required the eyes to move frequently in the up/down directions. The frequency of the traveling direction with map recall was higher than when driving with mental arithmetic in the up/right direction. Subtasks increased driver burden and reduced driver awareness in the left/right direction.

We found that map recall decreased driving ability, which suggests that mental images impair real ones. Mental arithmetic and map recall subtasks require numerical analysis and comparison, and eye movements are produced throughout the whole driving process. Whether eye movements at intersections differ from periods between intersections needs more investigation.

## References

1. Akiyama, T., Inagaki, T., Furukawa, H., Itoh, M.: Eye movement analysis for detecting driver's inattentiveness. *Hum. Interface Soc.* **1**, 345–350 (2005). (in Japanese)
2. Blanco, M., Biever, W.J., Gallagher, J.P., Dingus, T.A.: The impact of secondary task cognitive processing demand on driving performance. *Accid. Anal. Prev.* **38**, 895–906 (2006)
3. Chan, M., Nyazika, S., Singhal, A.: Effects of a front-seat passenger on driver attention: An electrophysiological approach. *Transp. Res. Part F Traffic Psychol. Behav.* **43**, 67–79 (2016)
4. Dula, C.S., Martin, B.A., Fox, R.T., Leonard, R.L.: Differing types of cellular phone conversations and dangerous driving. *Accid. Anal. Prev.* **43**, 187–193 (2011)
5. Harbluk, J.L., Noy, Y.I., Trbovich, P.L., Eizenman, M.: An on-road assessment of cognitive distraction: impacts on drivers' visual behavior and braking performance. *Accid. Anal. Prev.* **39**, 372–379 (2007)
6. Horrey, W.J., Lesch, M.F., Garabet, A., Simmons, L., Maikala, R.: Distraction and task engagement: How interesting and boring information impact driving performance and subjective and physiological responses. *Appl. Ergon.* **58**, 342–348 (2017)
7. Hughes, G.M., Rudin-Brown, C.M., Young, K.L.: A simulator study of the effects of singing on driving performance. *Accid. Anal. Prev.* **50**, 787–792 (2013)
8. Kawakita, E., Abe, K., Miyatake, H., Oguri, K.: Effect evaluation of mental calculation task on driver's physiological signals and pedal manipulation during driving after leading car using DS. IEICE Technical Report, ITS2007–87 (2008). (in Japanese)
9. Louie, J.F., Mouloua, M.: Predicting distracted driving: the role of individual differences in working memory. *Appl. Ergon.* **74**, 154–161 (2019). (in Progress)

10. Maciej, J., Nitsch, M., Vollrath, M.: Conversing while driving: the importance of visual information for conversation modulation. *Transp. Res. Part F Traffic Psychol. Behav.* **14**, 512–524 (2011)
11. Martens, M.H., Brouwer, R.F.T.: Measuring being lost in thought: an exploratory driving simulator study. *Transp. Res. Part F Traffic Psychol. Behav.* **20**, 17–28 (2013)
12. Metz, B., Schömig, N., Krüger, Hans-P: Attention during visual secondary tasks in driving: adaptation to the demands of the driving task. *Transp. Res. Part F Traffic Psychol. Behav.* **14**, 369–380 (2011)
13. Niezgodna, M., Tarnowski, A., Kruszewski, M., Kamiński, T.: Towards testing auditory-vocal interfaces and detecting distraction while driving: a comparison of eye-movement measures in the assessment of cognitive workload. *Transp. Res. Part F Traffic Psychol. Behav.* **32**, 23–34 (2015)
14. Northcutt-Pope, C., Bell, T.R., Stavrinou, D.: Mechanisms behind distracted driving behavior: the role of age and executive function in the engagement of distracted driving. *Accid. Anal. Prev.* **98**, 123–129 (2017)
15. Oviedo-Trespalacios, O., Haque, MdM, King, M., Washington, S.: Understanding the impacts of mobile phone distraction on driving performance: a systematic review. *Transp. Res. Part C Emerg. Technol.* **72**, 360–380 (2016)
16. Oviedo-Trespalacios, O., Haque, MdM, King, M., Demmel, S.: Driving behaviour while self-regulating mobile phone interactions: a human-machine system approach. *Accid. Anal. Prev.* **118**, 253–262 (2018)
17. Portal Site of official Statistics of Japan. <https://www.npa.go.jp/publications/statistics/koutsuu/H29siboumatome.pdf>. Last accessed 20 Aug 2018. (in Japanese)
18. Recarte, M.A., Nunes, L.M.: Effects of verbal and spatial-imagery tasks on eye fixations while driving. *J. Exp. Psychol. Appl.* **6**, 31–43 (2000)
19. Rhodes, N., Pivik, K., Sutton, M.: Risky driving among young male drivers: the effects of mood and passengers. *Transp. Res. Part F Traffic Psychol. Behav.* **28**, 65–76 (2015)
20. Ross, V., Jongen, E.M.M., Wang, W., Brijs, T., Brijs, K., Ruiter, R.A.C., Wets, G.: Investigating the influence of working memory capacity when driving behavior is combined with cognitive load: an LCT study of young novice drivers. *Accid. Anal. Prev.* **62**, 377–387 (2014)
21. Savage, S.W., Potter, D.D., Tatler, B.W.: Does preoccupation impair hazard perception? A simultaneous EEG and eye tracking study. *Transp. Res. Part F Traffic Psychol. Behav.* **17**, 52–62 (2013)
22. Stavrinou, D., Jones, J.L., Garner, A.A., Griffin, R., Franklin, C.A., Ball, D., Welburn, S.C., Ball, K.K., Sisiopiku, V.P., Fine, P.R.: Impact of distracted driving on safety and traffic flow. *Accid. Anal. Prev.* **61**, 63–70 (2013)
23. Takahashi, K., Nakayama, M., Shimizu, Y.: Eye-movements and pupillary changes during simulated driving. *J. Inst. Image Inf. Telev. Eng.* **54**, 1323–1329 (2000). (in Japanese)
24. Ünal, Ayça B., de Waard, D., Epstude, K., Steg, L.: Driving with music: effects on arousal and performance. *Transp. Res. Part F Traffic Psychol. Behav.* **21**, 52–65 (2013)
25. Victor, T.W., Harbluk, J.L., Engström, J.A.: Sensitivity of eye-movement measures to in-vehicle task difficulty. *Transp. Res. Part F Traffic Psychol. Behav.* **8**, 167–190 (2005)
26. Wakui, H., Hirata, Y.: Detection of reduced arousal by saccadic eye movements. *Trans. Jpn. Soc. Med. Biol. Eng.* **51**, 328–341 (2013). (in Japanese)
27. Wang, Y., Bao, S., Du, W., Ye, Z., Sayer, J.R.: Examining drivers' eye glance patterns during distracted driving: insights from scanning randomness and glance transition matrix. *J. Saf. Res.* **63**, 149–155 (2017)
28. Watson, J.M., Memmott, M.G., Moffitt, C.C., Coleman, J., Turrill, J., Fernández, Á., Strayer, D.L.: On working memory and a productivity illusion in distracted driving. *J. Appl. Res. Mem. Cogn.* **5**, 445–453 (2016)
29. Yan, W., Xiang, W., Wong, S.C., Yan, X., Li, Y.C., Hao, W.: Effects of hands-free cellular phone conversational cognitive tasks on driving stability based on driving simulation experiment. *Transp. Res. Part F Traffic Psychol. Behav.* **58**, 264–281 (2018)

# Automatic Extraction of Passing Scene Through Signalized Intersection from Event Data Recorder During Night Time and also Daylight



Mikuni Motoi, Haruki Kawanaka, Md. Shoaib Bhuiyan and Koji Oguri

**Abstract** Data from event data recorders (EDR) are used for driver education and safety in Japan. Thus, dangerous driving behaviors of individuals such as failure to stop at a red light are found out and are shown to the drivers from the video images of EDR. In order to detect ‘the failure to stop at a red light’ automatically from event data recorder images, our method aims to extract passing scenes through a signalized intersection. To extract passing scenes through a signalized intersection, it is necessary to detect the positions of traffic light candidates in each frame. However, the detection of traffic lights may be affected by various lighting conditions according to weather and time. In this paper, we propose a method to automatically extract the scene passing through a signalized intersection considering lighting conditions from EDR. Experiments we conducted show that our proposed algorithm successfully extracts the passing scene through signalized intersection.

---

M. Motoi (✉) · H. Kawanaka · K. Oguri  
Graduate School of Information Science and Technology, Aichi Prefectural University,  
1522-3 Ibaragabasama, Nagakute, Aichi 480-1198, Japan  
e-mail: [m.motoi@bme.ist.aichi-pu.ac.jp](mailto:m.motoi@bme.ist.aichi-pu.ac.jp)

H. Kawanaka  
e-mail: [kawanaka@bme.ist.aichi-pu.ac.jp](mailto:kawanaka@bme.ist.aichi-pu.ac.jp)

K. Oguri  
e-mail: [oguri@bme.ist.aichi-pu.ac.jp](mailto:oguri@bme.ist.aichi-pu.ac.jp)

Md. S. Bhuiyan  
Faculty of Medical Engineering, Suzuka University of Medical Science, 1001-1 Kishioka,  
Suzuka, Mie 510-0293, Japan  
e-mail: [bhuiyan@suzuka-u.ac.jp](mailto:bhuiyan@suzuka-u.ac.jp)

## 1 Introduction

An event data recorder (EDR) which can record not only when traffic accidents have occurred but also throughout the driving is widely used nowadays. In Japan, for example, education of safety driving for professional drivers of transport companies is conducted using the video images thus obtained from EDR, which is equipped on the trucks they drive [1].

During the course of driver education and safety, the EDR is first installed into almost every truck, the video images are thus collected and managed in the video storage of the transport control office. Next, scenes of dangerous driving such as the failure to stop at a red light and the pedestrian interference are manually found out from the collected data by the human analyst. At this time, the analyst must find scenes of dangerous driving by visual observation of all the collected video data. After that, the professional driver looks back on his or her own behavior of dangerous driving from the found images approximately within a month. Individual driver can thus grasp his or her own undesirable driving behavior and can improve awareness of safe driving by taking advantage of own reflections.

To extract the scenes of dangerous driving behavior used for safe driving education, visual analysis of the total number of images is required. However, it is too difficult to manually find out the scenes of dangerous driving behavior, such as the failure to stop at a red light, from EDR's data which is usually for a very long duration. This problem is one main reason why the EDR is not used widely for driver education and safety. It is required to extract such scenes efficiently from the video images of EDR. In order to detect 'the failure to stop at a red light' automatically from EDR images, we propose a method to extract passing scenes through a signalized intersection. Finally, we demonstrated the effectiveness of our proposed method by conducting an experiment and evaluated the accuracy.

## 2 Definition of Extraction Subject

The failure to stop at a red light is judged when a vehicle enters the intersection when the traffic light is red, not otherwise. Therefore, it is important to know whether traffic signals are visible or not. Figure 1 shows the definition of a passing scene through a signalized intersection. The start point of the extraction period is defined as a frame in which the traffic signal has become visible and a stop line on the road does not exist. The final point of the extraction period is defined as a frame where the traffic signal has been shifted and disappeared.

By this definition, it is assumed that the traffic signal is visible in the image frames while one's own vehicle passes through the intersection. Thus, we detect traffic signals in order to extract a passing scene through an intersection and evaluate the color of the traffic light.

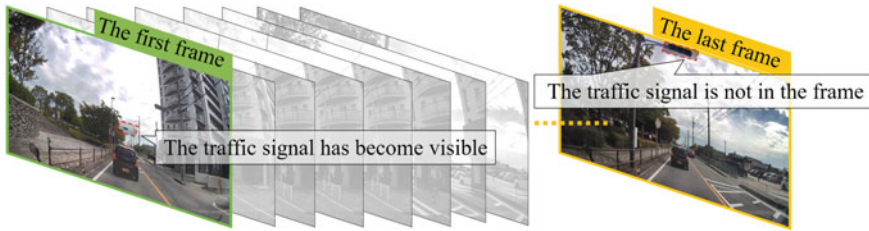


Fig. 1 Definition of a passing scene through a signalized intersection

### 3 Detection of Traffic Signal Candidates

#### 3.1 Previous Study to Detect Traffic Light

Color and shape of traffic signals varies from country and area. For example, traffic signals in USA are mostly arranged in vertical direction, while most traffic signals are arranged in horizontal direction in Japan. Comparing traffic lights, size and brightness, traffic lights of USA are often smaller, and brighter than those of Japan.

Appearance of traffic lights also differ with time. Figure 2a shows an example of a traffic light in the daytime. Figure 2b shows it in the night time. When comparing daytime images with night time images, the spreading and appearance of traffic lights are different. Because most of the EDR's camera has automatic gain control function, the lighting area of the traffic light in the night time gets overexposed and the traffic light color extends to surrounding area, making it difficult to distinguish whether an arrow signal is present or not and to recognize the direction of the arrow as shown in Fig. 2.

Using a high dynamic range (HDR) camera may be an alternative solution for handling the halation, and some methods to recognize traffic lights using a HDR camera have been proposed [2, 3]. For example, it is actually used as a camera for an autonomous driving and an automatic braking system. However, since the EDR is not for detecting objects but for recording video images, the EDR usually does



Fig. 2 Traffic lights of Japanese style

not consist of a HDR camera. Complex background in the image also makes traffic light recognition difficult. In daytime, objects such as advertising sign and billboards, which have similar color as traffic lights, easily add to false positive detections. In night time, surrounding neon signs and the tail lamps of preceding vehicles easily adds to false positive recognitions.

To solve problems mentioned above, many traffic light recognition methods have ever been proposed. In general, features used to detect a traffic light are often obtained from the standard of a traffic light. Researchers are frequently focused on the shape, aspect ratio, texture or size of detected objects. Circle and ellipse features are used to detect traffic lights [4–6], and radial symmetry transform is used to recognize a traffic light shape [7]. After detecting shape features, the object tracking is used to reduce false positive [8, 9]. In night time, traffic light recognition has been realized by color and shape features [10], especially spot shape feature has been used to recognize traffic lights [11, 12]. Although shape features such as circle, ellipse, spot and radial symmetry are useful for traffic light detection, these features are too simple. Therefore, they do not work well in images having complex background in daytime and lighting objects in night time.

Color features are used for traffic lights recognition [4–6, 8, 9, 13, 14], and selecting color space is important to obtain good recognition results. And, the multiple exposure is used for the halation problem [15]. However, in Japan, the traffic light color differs by a type of light source such as a lightemitting diode (LED) and an incandescent lamp. Additionally, in case of LED traffic lights, the traffic signals sometimes light out in the EDR's images because the traffic light is blinking at either 120 Hz or at 100 Hz in Japan. One other reason is the Japanese traffic regulations where a flashing red light means an instruction to temporarily stop. These make the extraction of passing scenes through signalized intersection more difficulty. Therefore, we also must detect blinking signals adaptively.

### ***3.2 Detection of Traffic Signal Candidates in the Daytime***

In each frame of the EDR video image, the position of the traffic signal candidate is detected using the Haar-like features and the Adaboost algorithm. The Adaboost which is used for visual object classification using the Haar-like features has been proposed by Viola & Jones for face and pedestrian detection [16]. And some researchers proposed a method to detect traffic signal areas in the frame image [17]. The method using the Adaboost has the advantage of being able to detect objects at a high speed with higher accuracy in various environments. As shown in Fig. 3, the traffic signal candidates are detected by the Adaboost with the Haar-like features.

For learning of the Adaboost classifier, some traffic light images are cut out from various video images recorded by EDRs. The training data consists of sample images of a traffic signal that we call 'positive image' which is scaled to the same size of another image that we call 'negative image' which is arbitrary image of the same size.

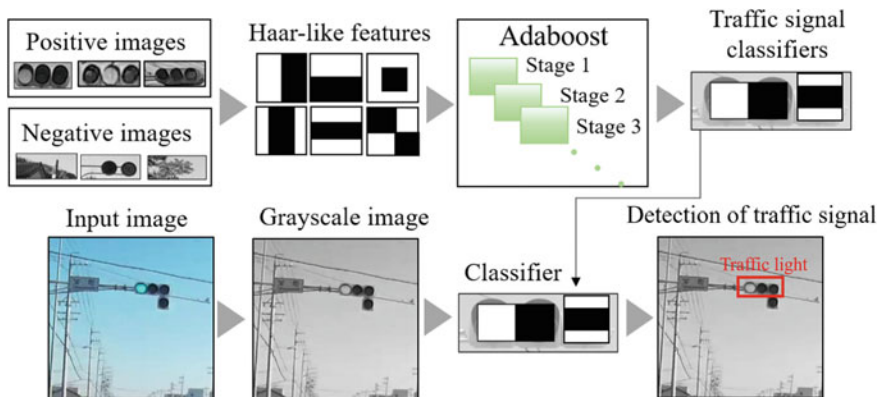


**Fig. 3** Detection of traffic signal candidates in the daytime

The traffic signal candidates are detected by applying the Adaboost algorithm based on the Haar-like features. However, false positives could not be filtered out because there are a few visual features that represent traffic lights in terms of the Haar-like features. In addition, when we detect the failure to stop at a red light automatically from the passing scene through signalized intersection extracted by our proposed method, recognition of the traffic light color is necessary. Thus, we are going to recognize traffic light color using color features of traffic signals and divide the traffic signal candidates into two groups, traffic lights and those other than traffic lights.

RGB components in original images may be affected by various illumination conditions such as RGB components that change nonlinearly according to surrounding light conditions, and it is hard to determine a specific color range for each color. Therefore, many researchers make conversion from RGB to HSV color spaces [18], HSI color spaces [19], La\*b\* color spaces [20] and YCbCr color spaces [17, 21]. In this paper, we use HSI color spaces [22] to analyze colors of traffic light. At first, the components of HSI space can be transformed from RGB spaces. A number of samples are extracted from several different images in order to determine the boundaries of HSI for green, yellow and red signals. Green, yellow and red pixels are selected manually in each samples. The analysis of distributions of hue, saturation, and intensity provides nine conditions. Therefore, we set up three segmentation formulations based on the following rules:

$$b_g(u, v) = \begin{cases} 1 & \text{if } \text{cond}(H_g) \cap \text{cond}(S_g) \cap \text{cond}(I_g) \\ 0 & \text{otherwise} \end{cases} \quad (1)$$

$$b_y(u, v) = \begin{cases} 1 & \text{if } \text{cond}(H_y) \cap \text{cond}(S_y) \cap \text{cond}(I_y) \\ 0 & \text{otherwise} \end{cases} \quad (2)$$



$$b_r(u, v) = \begin{cases} 1 & \text{if } \text{cond}(H_r) \cap \text{cond}(S_r) \cap \text{cond}(I_r) \\ 0 & \text{otherwise} \end{cases} \quad (3)$$

where, let  $H_g, H_y, H_r$  be hue of each color, and  $S_g, S_y, S_r$  be saturation of each color, and  $I_g, I_y, I_r$  be intensity of each color, and  $\text{cond}()$  be segmentation condition for extracting each color component of traffic light.

After three segmentation, we obtain three binary images  $b_g(u, v)$ ,  $b_y(u, v)$  and  $b_r(u, v)$  that describes the existence of green or yellow or red respectively. Figure 4 shows binary images of some sample images obtained by segmentation of HSI color space. Green components are extracted from  $b_g(u, v)$ , yellow components are extracted from  $b_y(u, v)$ , and red components are extracted from  $b_r(u, v)$ .

We use white pixels extracted as each color feature. However, it is not always possible to extract suitable pixels effectively as shown in Fig. 4. Because various environments easily affect the color of a traffic signal candidate, there are cases where white pixels were not extracted in intended area and where white pixels were extracted in an unintended area. Thus, a simple thresholding can not work well to narrow down the traffic signal candidates. Therefore, color information of traffic signals grabbed in various environments in advance are learned and used for recognition of the traffic light. We prepared a training dataset by manually extracting the traffic signal regions from various images of EDR and performed a machine learning technique for the color of the traffic signal. The algorithm is a multiclass classifier with the Random Forests [23] to distinguish them into four labels such as green light, red light, yellow light, and other than traffic lights. In order to effectively extract features and use information of the lighting position, we determine a specific area in which we extract features. Figure 5 shows the specific area on each binary image and features  $\eta_g, \eta_y$  and  $\eta_r$  extracted from the specific area. The specific area of  $b_g(u, v)$  is surrounded by a green rectangle, and the specific area of  $b_y(u, v)$  is surrounded by a yellow rectangle, and the specific area of  $b_r(u, v)$  is surrounded by a red rectangle. In addition, color features  $\eta_g, \eta_y$  and  $\eta_r$  are given by the following Eq. (4) for each specific area, and the green component ratio  $\eta_g$ , the yellow component ratio  $\eta_y$ , and the red component ratio  $\eta_r$  are obtained respectively by

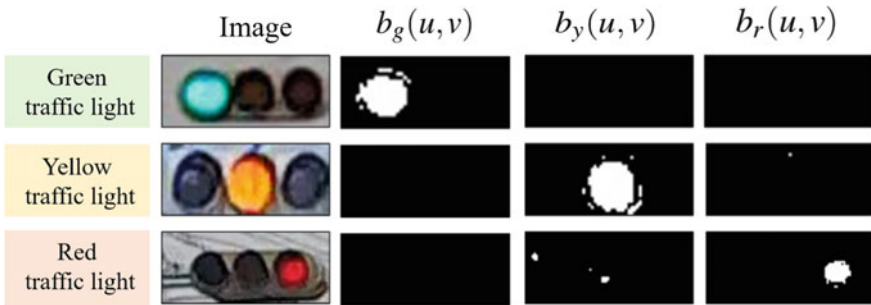
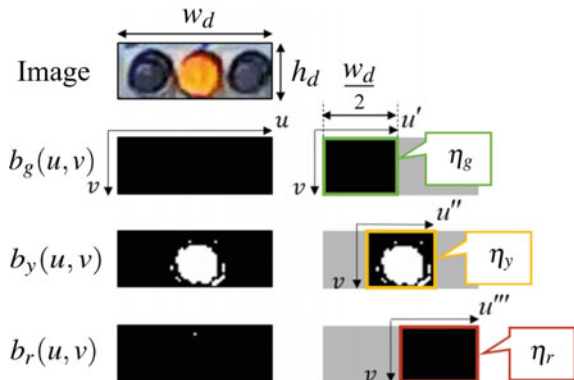


Fig. 4 Binary images obtained by segmentation of HSI color space

**Fig. 5** Specific area on each binary image and extracted features



$$\begin{bmatrix} \eta_g \\ \eta_y \\ \eta_r \end{bmatrix} = \begin{bmatrix} \frac{2}{w_d h_d} \sum_{u', v} b_g(u', v), \frac{2}{w_d h_d} \sum_{u'', v} b_y(u'', v), \frac{2}{w_d h_d} \sum_{u''', v} b_r(u''', v) \end{bmatrix}^T \quad (4)$$

where,  $w_d$  and  $h_d$  be the width and height of the traffic signal candidate. In this study, we use  $\eta_g$ ,  $\eta_y$ , and  $\eta_r$  as color features at Random Forest machine learning algorithm.

### 3.3 Detection of Traffic Signal Candidates in the Night time

The traffic lights usually have high brightness in the night time images. Therefore, all the spots of high brightness are extracted as traffic signal candidates by brightness segmentation. After a grabbed image as shown in Fig. 6 is gray-scaled, a binary image  $b(u, v)$  is derived by Eq. (5)

$$b(i, j) = \begin{cases} 1 & \text{if } f(u, v) \geq \alpha \\ 0 & \text{otherwise} \end{cases} \quad (5)$$

where, let  $f(u, v)$  be the brightness at pixel  $(u, v)$  of the grayscale image, and  $\alpha$  be a threshold (e.g.  $\alpha = 240$ ). Figure 7 shows an example of the binary image for the input image which is shown in Fig. 6.

After color segmentation, some scattered small blocks may be produced. In order to eliminate scattered small blocks of candidate regions and to preserve the connected regions more accurately, we apply expansion and contraction on the morphological operation known as opening process to the aforementioned binary image. This operation can connect nearby objects and smooth borders, but it does not significantly change its size, so it can remove noise effectively.

After noise reduction, there may be some regions which is not a traffic signal. So, we select appropriate regions by using shape features. When the car passes through

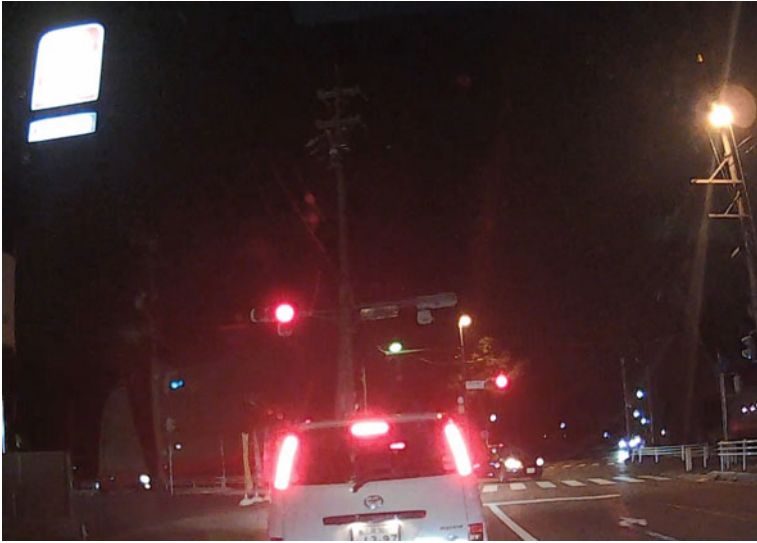


**Fig. 6** Input image contains several spots of high brightness



**Fig. 7** Binary image showing spots of high brightness

a signalized intersection, the traffic signals are located in front of the car. Therefore, it is assumed that the shape of a traffic light is approximately circular in the image. Thus, the regions that have irregular shapes should be filtered out. Here, circularity is defined as circular shape index  $C$  such as Eq. (6).

$$C = \frac{4\pi S}{L^2} \quad (6)$$

where, let  $S$  be an area of the traffic signal candidate, and  $L$  be a length around the spot of traffic signal candidate. If the shape is irregular and not circular then  $C$  becomes close to 0. So, it is extracted as a traffic light candidate when  $C \geq \beta$  (e.g.  $\beta = 0.8$ ). Figure 8 shows traffic signal candidates after the selection by circularity.

And then, the regions of traffic lights were extracted as rectangles for the machine learning which is the next step in processing. Rectangular regions, which satisfy two conditions consisted of the inclusion ratio (7) and the aspect ratio (8), are decided for the regions of traffic lights.

$$\frac{1}{w_n h_n} \sum_{u', v'} b(u', v') = \gamma \quad (7)$$

$$\frac{w_n}{h_n} = \delta \quad (8)$$

where, let  $w_n$  and  $h_n$  be the width and height of the rectangle. The parameters are set at  $\gamma = 0.31$  and  $\delta = 1.2$  empirically based on the training images for the machine



**Fig. 8** Spots of traffic signal candidates after selection by circularity



**Fig. 9** Rectangles of traffic signal candidate regions after screening based on rectangular conditions

learning. In addition, we decided that if an area of a rectangle is extremely large or small then the area should be eliminated. Figure 9 shows the candidates of traffic signals after screening based on rectangular conditions. The traffic signal candidates are now surrounded by red rectangles.

Any brightness circular region other than traffic lights such as street lamps and signboards, illumination of buildings would first be extracted as traffic signal candidates. Thus we are going to identify them using color features of traffic signals. Because a color of a traffic signal candidate is easily affected by various illuminations, a simple thresholding on each color channel can not work well to narrow down the traffic signal candidates. Therefore, color information of traffic signals grabbed in various environments in advance are learned and used for recognition of the traffic light. We again prepared a training dataset by manually extracting the traffic signal regions from various images of EDR and performed a machine learning technique for the color of the traffic signal. The algorithm is a multi-class classifier with the Random Forests algorithm to distinguish them into four labels such as green light, red light, yellow light, and other than traffic lights. Dominant component for a red, green and yellow light are extracted using color transform proposed by Ruta et al. [24]. A simple color enhancement is provided by a set of transformations given below in Eqs. (9), (10) and (11), and then the red-dominant component  $I_R(x)$ , the green-dominant component  $I_B(x)$  and the yellow-dominant component  $I_Y(x)$  are respectively obtained by

$$I_R(x(u, v)) = \frac{\min(x_R(u, v) - x_G(u, v), x_R(u, v) - x_B(u, v))}{s(u, v)} \quad (9)$$



**Fig. 10** Candidate regions after Traffic light classification

$$I_B(x(u, v)) = \frac{\min(x_G(u, v) - x_B(u, v), x_G(u, v) - x_R(u, v))}{s(u, v)} \quad (10)$$

$$I_Y(x(u, v)) = \frac{\min(x_R(u, v) - x_B(u, v), x_G(u, v) - x_B(u, v))}{s(u, v)} \quad (11)$$

where, let intensity values with RGB colors at each pixel  $(u, v)$  in the traffic candidate region be  $x(u, v) = [x_R(u, v), x_G(u, v), x_B(u, v)]$  and a summation of all the color components be  $s(u, v) = x_R(u, v) + x_G(u, v) + x_B(u, v)$ . In this study, we use  $\max(I_R(x))$ ,  $\max(I_B(x))$ ,  $\max(I_Y(x))$ ,  $\min(I_R(x))$ ,  $\min(I_B(x))$ ,  $\min(I_Y(x))$  as color features for each traffic candidate region using Random Forest machine learning algorithm. The traffic light classification result of the aforementioned sample is shown in Fig. 10. Traffic light candidate identified as a green traffic light is surrounded by green rectangle, and traffic signal candidates identified as other than traffic signal is surrounded by white rectangle.

## 4 Extraction of Passing Scenes Through a Signalized Intersection

It is assumed that some traffic light is visible in the frame image while one's own vehicle passes through the intersection. However, there are cases where brightness regions other than traffic lights are detected as traffic light candidates. Therefore, we determine the passing scenes through a signalized intersection or not on the

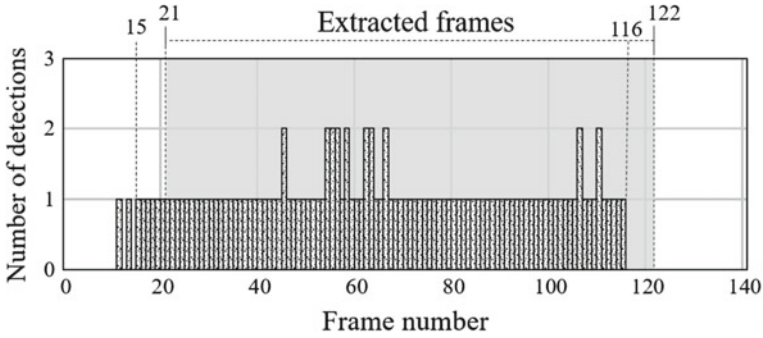


**Fig. 11** Example of extraction result of passing scenes through a signalized intersection

assumption that the traffic light should be continuously detected, and extract a scene under the conditions that the detection number of traffic signal candidates in each frame is one or more while traffic signal candidates are continuously detected over seven frames in test data. In this way, an extracted example is shown in Fig. 11. This Figure represents the number of detections of traffic light candidates for each frame.

## 5 Experiment

The experiments have been performed to evaluate the extraction accuracy of our proposed method. Detection of traffic light candidates for all frame and extraction of the passing scene through a signalized intersection were performed, then we evaluated the performance of our proposed method.

We applied the detection method of the traffic light in the daytime to the images captured between 5 AM and 7 PM, and applied the detection method of the traffic light in the night time to the images captured between 7 PM and 5 AM. We extracted the passing scenes through a signalized intersection from video images which were recorded by EDRs for a duration of about 330 min (daytime: about 180 min, night time: about 150 min) while three human drivers, both male and female. The total number of the passing scenes included in the video was 355 (daytime: 184, night time: 171). The frame rate of test videos is 30 fps and the size of each image frame was 1920 pixels by 1080 pixels. All the traffic lights that should be detected by the proposed method were restricted to horizontal signals and we excluded vertical traffic signals during this experiment.

In daytime images, we determined a narrow color range for each color because a low exposure image is used for color segmentation. Experimental parameters of Eqs. (1), (2), and (3) were given below in Eqs. (12–20).

$$\text{cond}(H_g) : 150 < H_g < 200 \quad (12)$$

$$\text{cond}(H_y) : 10 < H_y < 15 \quad (13)$$

$$\text{cond}(H_r) : 60 < H_r < 80 \quad (14)$$

$$\text{cond}(S_g) : 5 < H_r < 10 \quad (15)$$

$$\text{cond}(S_y) : S_y < 20 \quad (16)$$

$$\text{cond}(S_r) : S_r < 60 \quad (17)$$

$$\text{cond}(I_g) : 10 < I_g < 60 \quad (18)$$

$$\text{cond}(I_y) : 10 < I_y \quad (19)$$

$$\text{cond}(I_r) : 80 < I_r < 100 \quad (20)$$

In night time images, experimental parameters were as follows.  $\alpha = 240$ ,  $\beta = 0.8$ ,  $\gamma = 0.31$ ,  $\delta = 1.2$ , minimum rectangle area had 396 pixels, maximum rectangle area had 7664 pixels, and the number of continuous frames to be regarded as passing scene was set to 7.

We evaluated the extraction accuracy of our proposed method by precision (positive predictive value) and recall (sensitivity). Precision means the ratio of the scenes correctly extracted out of all the passing scenes through signalized intersection, while recall means the ratio of the scenes that is truly a passing scene through signalized intersection out of all the extracted scenes.

## 6 Results and Discussion

Table 1 shows extraction accuracy of passing scene through a signalized intersection. As of experimental result, 180 of 184 passing scenes through a signalized intersection were successfully extracted from the daytime images and the precision of our proposed method was 97.8% and the recall was 93.7%. 165 of 171 passing scenes through a signalized intersection were successfully extracted from the night time



**Table 1** Extraction accuracy of passing scene through a signalized intersection

Time zone	Precision	Recall
Daytime (184)	97.8% (180/184)	93.7% (180/192)
Night time (171)	96.5% (165/171)	85.2% (165/193)
Total (355)	97.2% (345/355)	89.6% (345/385)

**Table 2** Accuracy of traffic light recognition

Time zone	Color	Accuracy (%)	Precision (%)	Recall (%)
Daytime	Green	100.0	100.0	100.0
	Yellow	97.3	97.3	95.9
	Red	93.7	97.0	97.2
Night time	Green	98.9	99.0	97.9
	Yellow	93.1	91.0	91.9
	Red	93.2	96.0	87.9

images and the precision of our proposed method was 96.5% and the recall was 85.2%. Compared to the images captured at the daytime, the accuracy of the images captured at the night time was slightly lower. The extraction failure of passing scene through a signalized intersection were caused by undetected traffic signal candidates. The accuracy of traffic light recognition is shown in Table 2.

In daytime images, green traffic lights, yellow traffic lights, and red traffic lights showed high precision. Figure 12 shows results of some sample images correctly recognized as the green light, yellow light and red light respectively and binary images. Traffic lights affected by sunshine are recognized.

However, there are some false positives of yellow lights and red lights. The reason why the accuracy of the red signal and the yellow signal is lower than the green signal is the misidentification of the red light and the yellow light. Red traffic lights being recognized as yellow light have yellow component in a frame. As shown in Fig. 13, many white pixels were extracted as yellow component from  $b_r(u, v)$ . Contrary to this, many white pixels were extracted as red component from  $b_y(u, v)$ .

As regards night time images, green traffic lights, yellow traffic lights, and red traffic lights showed high precision as well as daytime images. However, the most important factors with lower precision compared to daytime images are misidentification between the red traffic light and the tail lamp. Furthermore, erroneous identification of yellow traffic lights and street lamps is also one of the main factors of erroneous extraction. The feature values of red traffic lights and tail lamps on  $\max(I_R(x))-\min(I_R(x))$  are shown in Fig. 14. And the feature values of yellow traffic lights and street lamps on  $\max(I_R(x))-\min(I_R(x))$  are shown in the Fig. 15. Figures 14 and 15 show that false positives are similar to a traffic light in terms of color features. False positives are also similar to the traffic lights even in terms of shape features. Figure 14 shows that color feature values of the traffic light with

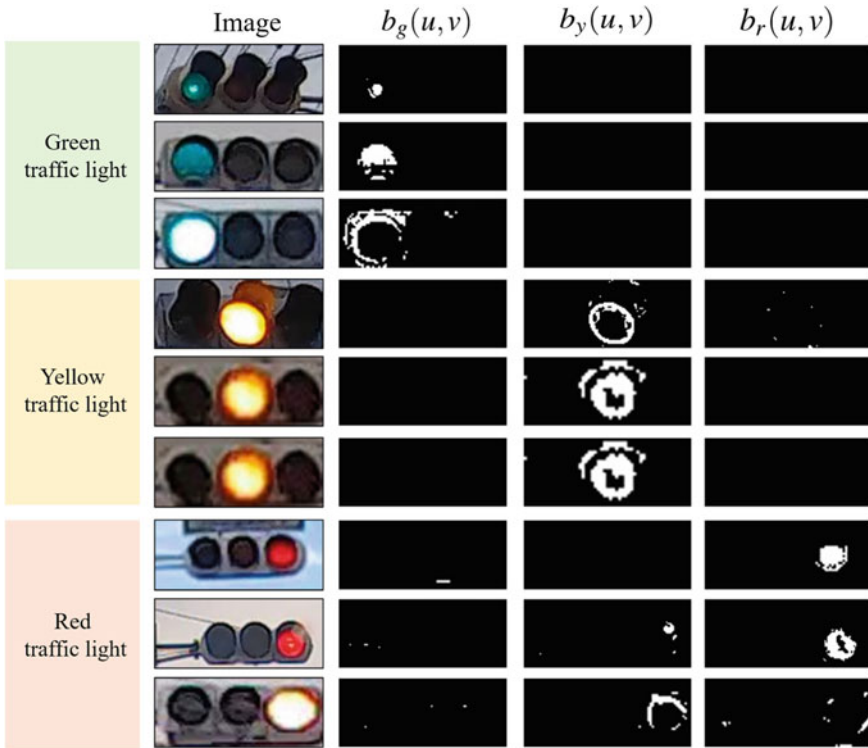


Fig. 12 Result of some sample images correctly recognized

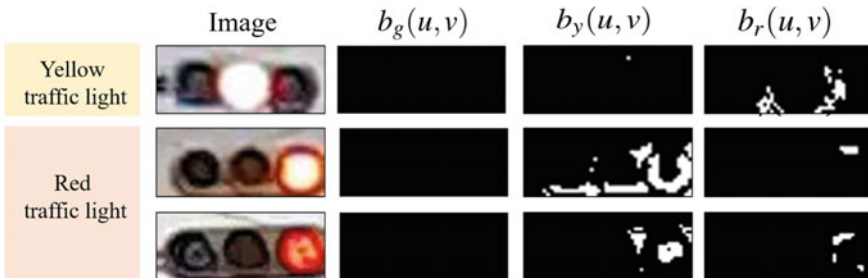


Fig. 13 Result of some samples of false recognition

arrows deviates from the range of the color feature values of the traffic light. This happens because the lighted portion of the traffic light images captured at night time overlap with the lighted portion of traffic lights with arrows. In experimental data, most traffic lights with arrows were undetected. It is necessary to discuss and implement a method to detect the traffic lights with arrows in the future.

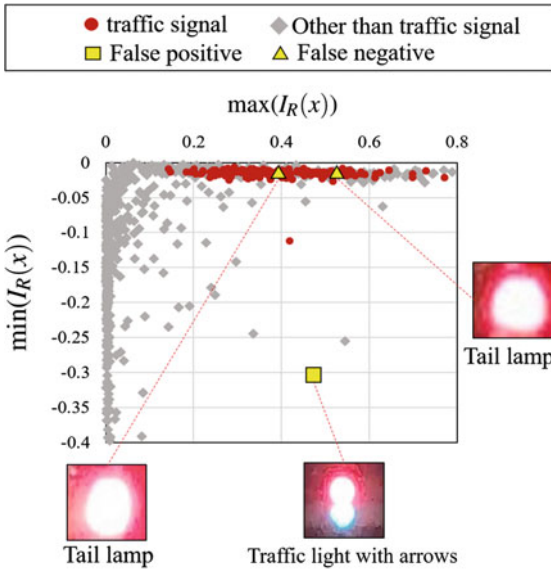


Fig. 14 Tail lamps erroneously detected as red traffic light

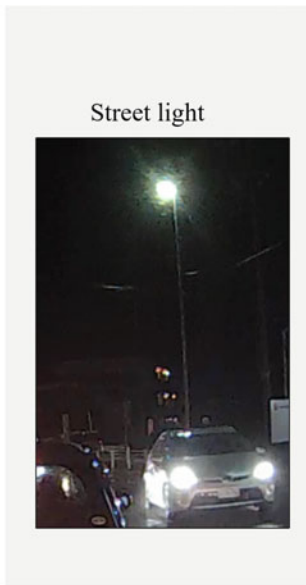
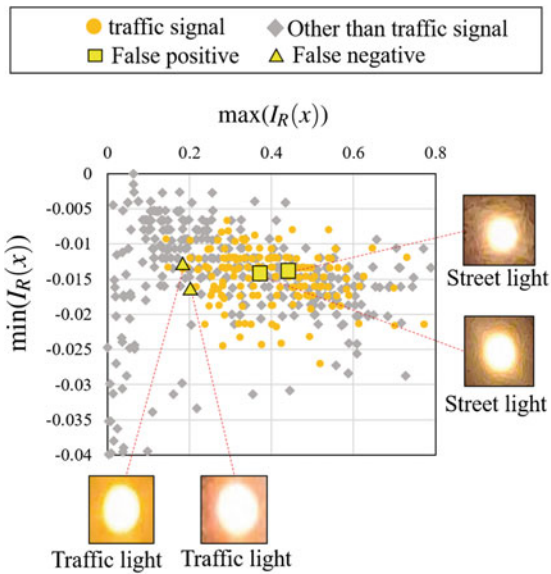


Fig. 15 Street lamps detected as yellow traffic light

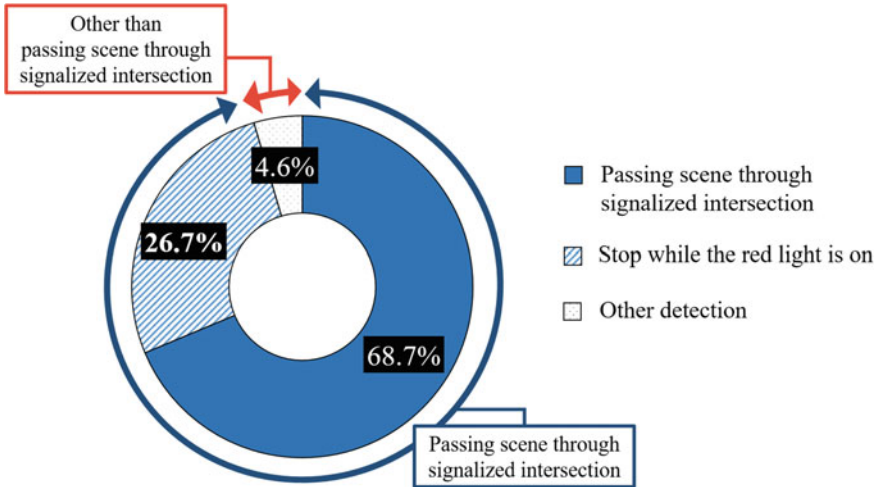


Fig. 16 The kind of extracted scene and the ration of factor of an error in the daytime images

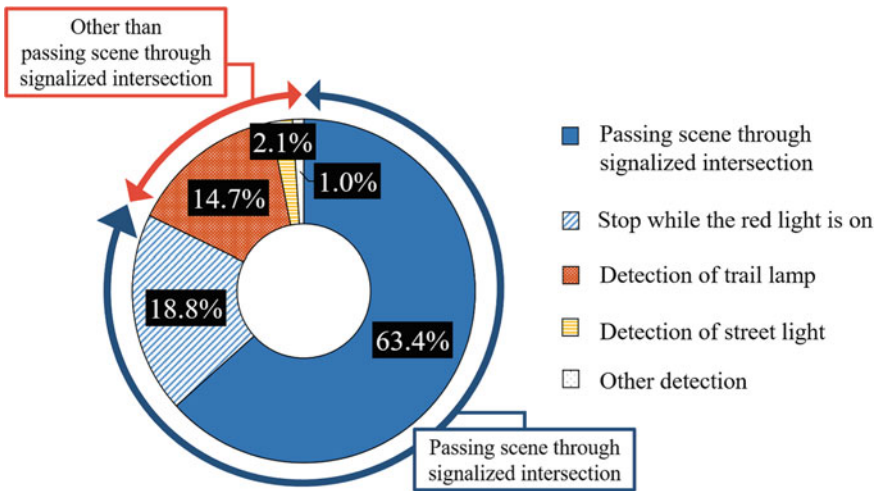


Fig. 17 The kind of extracted scene and the ration of factor of an error in the night time images

The kind of extracted scene and the ratio of factor of an error in daytime images is shown in Fig. 16. And the kind of extracted scene and the ratio of factor of an error in night time images is shown in Fig. 17. As shown Figs. 16 and 17, some scenes while the car is stopped for a long duration in front of red lights were also extracted as passing scenes through signalized intersection. In order to reduce such scenes, it is necessary to identify whether one’s own vehicle is stopping or passing through a

signalized intersection when the red light is on. If these identifications are realized, it will be possible to detect the failure of a vehicle to stop at a red light automatically from EDR data.

## 7 Conclusion

In order to detect the failure to stop at a red light automatically from EDR image frames, we proposed a method to extract passing scenes automatically through a signalized intersection. First, traffic light candidates are detected. We propose different methods for daytime and night time, because the detection of traffic lights may be affected by various lighting conditions according to weather and time. Next, passing scenes through signalized intersections were extracted. Experimental results showed that the proposed method had high extraction performance.

A future work might be to reduce misdetection of traffic light candidates and identifying whether one's own vehicle is stopping or passing through a signalized intersection while the red light is on.

## References

1. Takeda, K., Miyajima, C., Suzuki, T., Angkititrakul, P., Kurumida, K., Kuroyanagi, Y., Ishikawa, H., Terashima, R., Wakita, T., Oikawa, M., Komada, Y.: Self-coaching system based on recorded driving data: Learning from one's experiences. *IEEE Trans. Intell. Transp. Syst.* **13**(4), 1821–1831 (2012)
2. Omachi, M., Omachi, S.: Traffic light detection with color and edge information. In: 2nd IEEE International Conference on Computer Science and Information Technology, pp. 284–287 (2012)
3. Lindner, F., Kressel, U., Kaelberer, S.: Robust recognition of traffic signals. In: IEEE Intelligent Vehicles Symposium, pp. 49–53 (2004)
4. Omachi, M., Omachi, S.: Detection of traffic light using structural information. In: 10th International Conference on Signal Processing, pp. 809–893 (2010)
5. Diaz-Cabrera, M., Cerri, P.: Suspended traffic lights detection and distance estimation using color features. In: 15th International IEEE Conference on Intelligent Transportation System, pp. 1315–1320 (2012)
6. Chiang, C.C., Ho, M.C., Liao, H.S., Pratama, A.K., Syu, W.C.: Detecting and recognizing traffic lights by genetic approximate ellipse detection and spatial texture layouts. *Int. J. Innovative Comput. Inf. Control.* **7**(12), 6919–6934 (2011)
7. Sooksatra, S., Kondo, T.: Red traffic light detection using fast radial symmetry transform. In: 11th International Conference on Electrical Engineering/Electronics, Computer, Telecommunications and Information Technology, pp. 1–6 (2014)
8. Diaz-Cabrera, M., Cerri, P., Medici, P.: Robust real-time traffic light detection and distance estimation using a single camera. *Expert. Syst. Appl.* **42**(8), 3911–3923 (2015)
9. Lindner, F., Kressel, U., Kaelberer, S.: Robust recognition of traffic signals. In: IEEE Intelligent Vehicles Symposium, pp. 49–53 (2004)
10. Jang, C., Kim, C., Kim, D., Lee, M., Sunwoo, M.: Multiple exposure images based traffic light recognition. In: IEEE Intelligent Vehicles Symposium, pp. 1313–1318 (2014)

11. Charette, R., Nashashibi, F.: Real time visual traffic lights recognition based on spot light detection and adaptive traffic lights templates. In: IEEE Intelligent Vehicles Symposium, pp. 358–363 (2009)
12. Charette, R., Nashashibi, F.: Traffic light recognition using image processing compared to learning processes. In: IEEE/RSJ International Conference on Intelligent Robots and Systems, pp. 333–338 (2009)
13. Shen, Y., Ozguner, U., Redmill, K., Liu, J.: A robust video based traffic light detection algorithm for intelligent vehicles. In: IEEE Intelligent Vehicles Symposium, pp. 521–526 (2009)
14. Yu, C., Huang, C., Lang, Y.: Traffic light detection during day and night conditions by a camera. In: IEEE International Conference on Signal Processing, pp. 821–824 (2010)
15. Kim, H.K., Shin, Y.N., Kuk, S.G., Park, J.H., Jung, H.Y.: Night-time traffic light detection based on SVM with geometric moment features. *World Acad. Sci. Eng. Technol.* **7**(4), 454–457 (2013)
16. Viola, P., Jones, M.: Rapid object detection using a boosted cascade of simple features. In: IEEE Computer Society Conference on Computer Vision and Pattern Recognition, vol. 1, pp. 511–518 (2001)
17. Kim, H.K., Park, J.H., Jung, H.Y.: Effective traffic lights recognition method for real time driving assistance system in the daytime. *World Acad. Sci., Eng. Technol.* **59**, 311–314 (2011)
18. Gong, J., Jiang, Y., Xiong, G., Guan, C., Tao, G., Chen, H.: The recognition and tracking of traffic lights based on color segmentation and CAMSHIFT for intelligent vehicles. In: IEEE Intelligent Vehicles Symposium, pp. 431–435 (2010)
19. Wang, C., Jin, T., Yang, M., Wang, B.: Robust and real-time traffic light recognition in complex urban environments. *Int. J. Comput. Intell. Syst.* **4**(6), 1383–1390 (2011)
20. Said, A.F., Hazrati, M.K., Akhbari, F.: Real-time detection and classification of traffic light signals. In: IEEE Applied Imagery Pattern Recognition Workshop, pp. 1–5 (2016)
21. Cai, Z., Li, Y., Gu, M.: Real-time recognition system of traffic light in urban environment. In: IEEE Symposium on Computational Intelligence for Security and Defence Applications, pp. 1–6 (2012)
22. Gonzalez, R.C., Woods, R.E.: *Digital Image Processing*, 4th edn, Pearson (2018)
23. Breiman, L.: Random forests. *Mach. Learn.* **45**(1), 5–32 (2001)
24. Ruta, A., Li, Y., Liu, X.: Real-time traffic sign recognition from video by class-specific discriminative features. *Pattern Recognit.* **43**(11), 416–430 (2010)

# Collision Warning Strategies Using V2X: An Analysis of How Motorcycles and Bicycles Undergo Collisions



Tien-Pen Hsu, Wei-Lun Hsiao and Wan-Ching Ho

**Abstract** Connected vehicle technology which enables vehicles to communicate with nearby infrastructure and other vehicles is on the verge of revolutionizing transportation and vastly improving traffic safety. In recent years, many V2X systems have been tested worldwide in various complex traffic conditions. For example, in Taiwan, which typically can be characterized as a mixed flow heavy traffic environment that includes passenger cars, bicycles and motorcycles, developing such a V2X safety system becomes more complicated because these diverse vehicles have unique characteristics with regard to dynamics, size, driver behavior and directionality on roads, resulting in the complexity and variety of collision types. Insights into the crash patterns of motorcycles and bicycles are needed before developing a V2X collision warning system. For this reason, we analyzed the characteristics, accident types and features of various vehicle types using accident and traffic video data. We utilized accident statistics to identify critical collision patterns for each vehicle type. In addition, video data were collected to investigate the trajectories and driver behaviors with regard to each type of vehicle. We also performed comparisons of collision types and analyzed issues of system development for motorcycles and bicycles, the V2X power supply problem of non-motorized vehicles and potential challenges of issuing warnings in mixed flow traffic, etc.

**Keywords** Traffic safety · V2X · Collision warning system · Motorcycle · Bicycle

---

T.-P. Hsu (✉) · W.-L. Hsiao · W.-C. Ho  
Institute of Civil Engineering, National Taiwan University, Roosevelt Road Sec. 4, No.1, Taipei, Taiwan  
e-mail: [hsutp@ntu.edu.tw](mailto:hsutp@ntu.edu.tw)

W.-L. Hsiao  
e-mail: [b98501060@ntu.edu.tw](mailto:b98501060@ntu.edu.tw)

W.-C. Ho  
e-mail: [r05521525@ntu.edu.tw](mailto:r05521525@ntu.edu.tw)

## 1 Introduction

In Taiwan, traffic typically includes a high percentage of two wheeled vehicles such as motorcycles and bicycles. According to statistics on modal sharing in Taiwan in 2016, motorcycles accounted for 46%, almost twice that of passenger cars, of total traffic while buses and bicycles only made up 9% and 4% respectively, as shown in Fig. 1 [1]. These diverse vehicles form a special mixed flow traffic environment that must be better understood to increase traffic safety.

Annual modal shares of motorcycles, passenger cars and bicycles are shown in Fig. 2. From 2009 to 2016, the percentage of motorcycles and passenger cars held steady with an average annual growth rate of  $-0.27\%$  and  $0.17\%$  respectively, while bicycles made up only  $-4.33\%$ . Considering accidents per 100,000 population for each mode, as shown in Fig. 3, casualties involving passenger cars and bicycles per 100,000 population continued to increase at an average annual rate of  $6.91\%$  and  $5.44\%$ . On the other hand, those involving motorcycles rose between 2009 and 2014, before finally declining in 2015.

Traffic safety is a critical issue. In Taiwan, approximately six people out of 23.5 million die daily in traffic accidents. In addition to the human suffering, according to the Institute of Transportation of Ministry of Transportation and Communication (MOTC), the economic damage resulting from traffic accidents each year in Taiwan is estimated at \$16 billion, which accounts for  $3.1\%$  of the GDP.

Due to the fact that motorcycle riders and cyclists are very vulnerable on the road, scholars have been conducting related safety research and field trials on connected vehicle collision warning systems which have been proven to have potential to increase safety. Before these applications can be effectively utilized, collision or crash types must be clearly defined. Pre-crash scenarios help researchers understand how and why an accident occurred and how various vehicles withstood the accident.

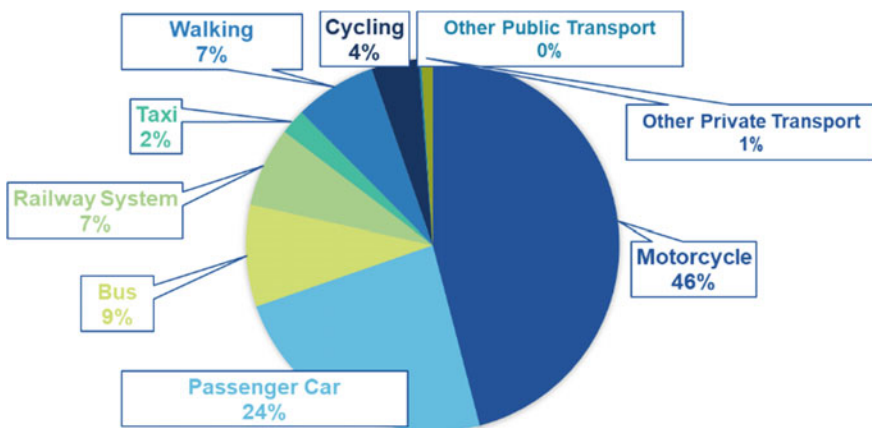


**Fig. 1** Modal share in Taiwan 2016



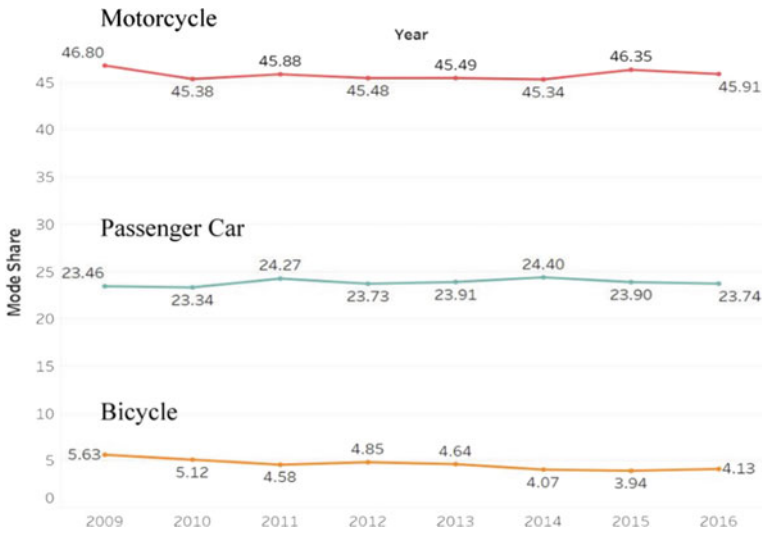


Fig. 2 Modal share of main transportation modes in Taiwan

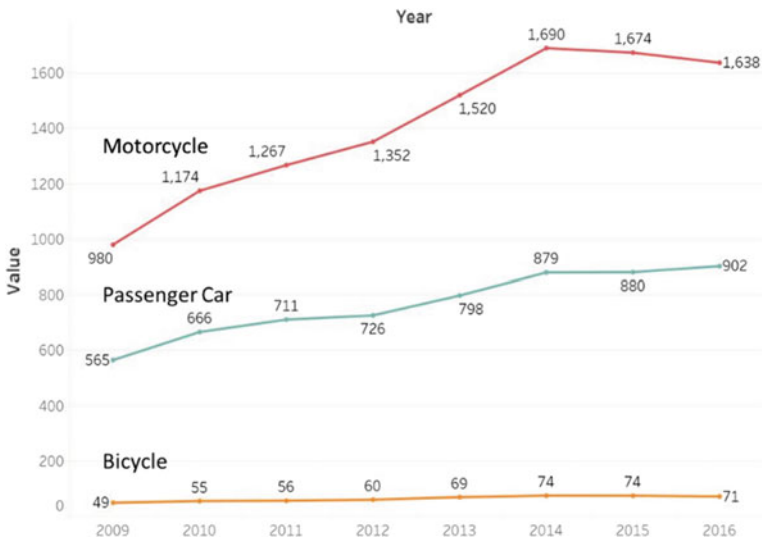


Fig. 3 Casualties per 100,000 population

In the U.S., several such crash typologies have been developed, such as “44-crashes” by General Motors and “pre-crash scenarios” by U.S. DOT [2]. However, the first has the shortcomings of limited data and difficulties replicating results when new data sources are introduced. The second excludes multi-vehicle and some low-frequency crash types and thus does not include all police-reported crashes [2]. Combining information from both crash types, Najm et al. found a new type consisting of 37 pre-crash scenarios involving at least one light vehicle which are then ranked by three qualities: crash frequency, functional years lost, and economic cost [2]. For heavy vehicles, they focused on a total of 37 pre-crash scenarios taken from the original 46. They also employed the same three aspects used to analyze the light vehicle crashes mentioned above [3]. Pre-crash scenarios were then used to assess potential safety applications in V2I and V2V communication systems [4, 5].

Although similar pre-crash scenarios may be effective for understanding numerous types of traffic conditions, the causes, types of crashes and frequencies may vary due to different traffic composition and road design. We will discuss these aspects as they relate to Taiwan’s mixed traffic environment, which consists of over 60% two-wheeled vehicles, including motorcycles and bicycles, and how to develop V2X collision warning systems for such a complex environment.

The purpose of this paper is to investigate the collision characteristics of motorcycles and bicycles in mixed flow traffic. We analyzed this data to determine the collision patterns for these two types of vehicles and how V2X technology might one day help to prevent crashes and save lives.

## 2 Overview of Accidents Involving Motorcycles and Bicycles

We collected crash statistics of total 31,293 records in Kaohsiung City in Taiwan from 2013 to 2015 and performed an analysis on involved vehicle types, severity, driver or rider’s age, and accident type to gain an overview of these crashes. Traffic accident data included A1 (fatal), A2 (injury) and A3 (property damage).

### 2.1 Analysis of Types of Vehicles Involved

Table 1 shows the breakdown of the involved vehicles by vehicle type. Passenger car drivers were most frequently at-fault, making up 50% of the total accident counts. This is particularly serious when we note that the modal share of passenger cars was only approximately 24% [6].

For motorcycle being an at-fault driver, the main victim vehicle type is motorcycle following by passenger car, the ratio between motorcycles and passenger cars was approximately 2:1. When cyclists were at fault, we found that they mainly had

**Table 1** Breakdown of the involved vehicles by vehicle type

		At-fault Driver				
		Motorcycle	Passenger Car	Bicycle	Heavy Vehicle	Pedestrian
	Motorcycle	47,487 25.05%	46,369 24.46%	2,373 1.25%	1,859 0.98%	1,237 0.65%
	Passenger Car	23,015 12.14%	48,560 25.61%	957 0.50%	5,287 2.79%	294 0.16%
Victim	Bicycle	2,910 1.53%	1,439 0.76%	111 0.06%	100 0.05%	21 0.01%
	Heavy Vehicle	794 0.42%	2,340 1.23%	38 0.02%	811 0.43%	17 0.01%
	Pedestrian	1,984 1.05%	1,436 0.76%	63 0.03%	77 0.04%	10 0.01%

collisions with motorcycle riders followed by passenger car drivers. The ratio of accidents between motorcycles and passenger cars was almost 2.5:1.

## 2.2 Severity Analysis

Figure 4 shows the statistics on the severity of motorcycle and bicycle accidents. For motorcycle involved accidents, the percentage of A1, A2 and A3 accidents were 0.3%, 91.8% and 7.9% respectively; for bicycle accidents, the percentage of each severity level was 0.6%, 94.5% and 4.9% respectively. Generally speaking, accidents involving bicycles entailed a higher severity of injuries than those involving motorcycles [1.1].

## 2.3 Statistics on Drivers' Ages

As seen in Fig. 5, the perpendicular line represents drivers who are 18-years old (the minimum age to get a driver's licence for cars and motorcycles in Taiwan). The peak age for motorcycle accidents was 19. Interestingly, we found a sudden drop until age 26, then a gradual decline. Therefore, compared to drivers of passenger cars, there were more underage motorcycle riders. Unlike motorcycle riders, for cyclists, there are two peaks in the curve. In the first, the highest peak of accidents occurs at age

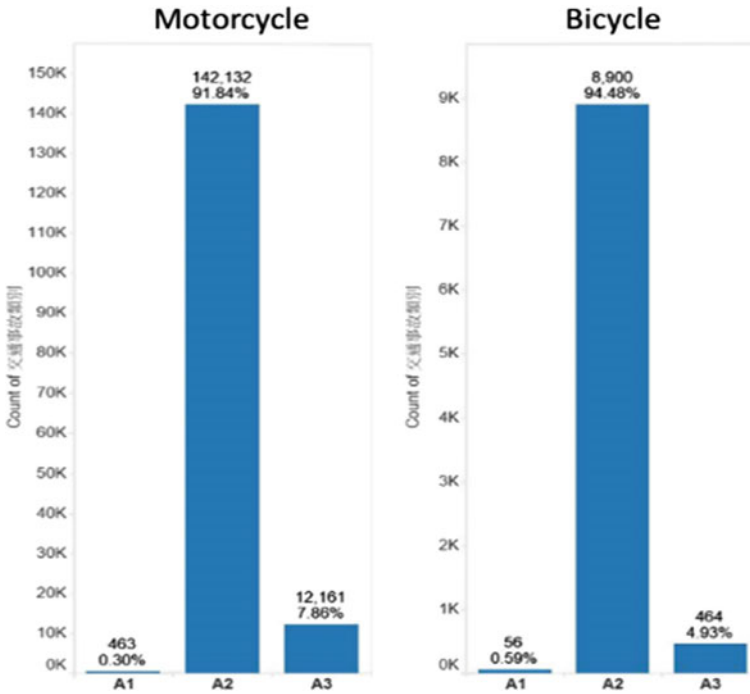


Fig. 4 Statistics on severity of motorcycle and bicycle accidents

14, After this age, the chance of causing an accident drops steeply until age 22, then it slowly increases until the second peak which is approximately at age 72 [6].

### 2.4 Statistics on Collision Type

Statistics on collision types at signalized intersections, non-signalized intersections and road section and a breakdown of at-fault and victims by vehicle types are shown in Tables 2, 3 and 4. Angled collisions were the most common type for all vehicles at both signalized and non-signalized intersections. Right angle collisions were the second most common which involved motorcycles and bicycles. Rear end collisions, were the most frequently occurring accidents between two passenger cars in signalized intersections. Angled collisions were also found to be most common for riders of two wheeled vehicles as they may be more likely to violate traffic laws by making unsafe turns. Generally, we found that rear end and sideswipe collisions frequently occurred in road sections between two different vehicle types. These two collision types happen because of speed differences when drivers of faster vehicles try to pass those that are slower. Sideswiping occurs most frequently either when motorcycle

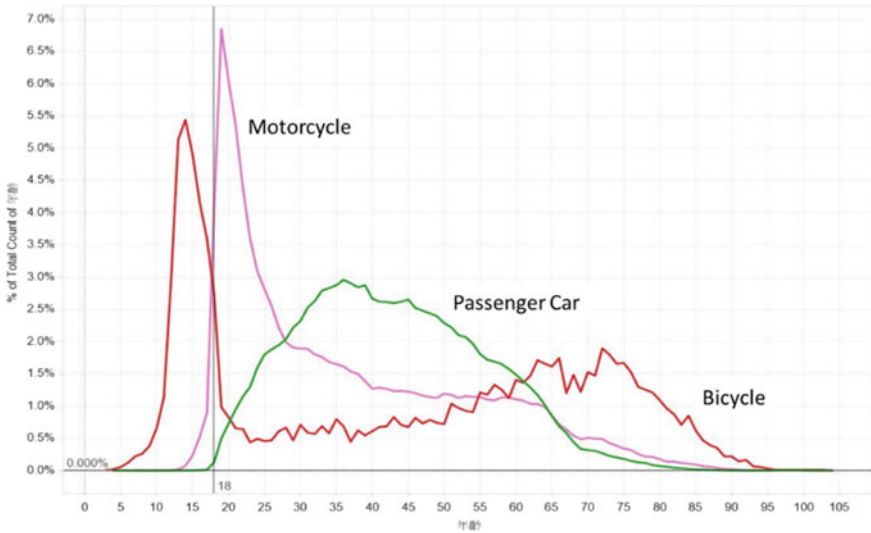


Fig. 5 Statistics on driver's or rider's age

riders attempt to weave in and out of fast moving traffic or when cyclists ride between rows of slow moving or stopped motor vehicles.

In the above analysis, we decided not to split angled collisions into right/left turn with through, right/left turn opposing through and so on due to the limited data. We provide detailed analysis later that includes diagrams of these types of accidents.

The collision type analysis above provides an overview on motorcycle and bicycle accidents. Now, we will look more closely at this phenomenon. Motorcycle riders and cyclists are particularly vulnerable to angled collisions, right angle collisions, rear end and sideswiping. Angled collisions can be further categorized in terms of the following scenarios. 1. If the involved vehicle was turning left, right or going straight 2. If the two involved vehicles were headed in the same direction, opposite directions or at an angle. 3. If the collision occurs on the roadway or at an intersection. Therefore, detailed collision type data should be collected in order to gain more insight into the most common collision types involving the most vulnerable motorists.

### 3 Analysis of Accidents Involving Motorcycles and Bicycles

In this section, we discuss detailed data and video accounts, particularly from Kaohsiung and Taipei City using an accident data base and videos of accidents.

**Table 2** Statistics on collision types in signalized intersections

At fault	Victim	Angled collisions	Right-angle	Rear end	Side-swipe	Head-on-sideswipe	Head on	Reversing collisions	Others	Self-inflicted	Involving a pedestrian	Total
Motorcycle	Motorcycle	35.95%	18.99%	14.38%	10.39%	1.52%	0.53%	0.01%	18.18%	0.04%	0.02%	100.00%
		6,467	3,416	2,586	1,869	273	96	1	3,270	7	3	17,988
	Passenger car	46.13%	12.79%	10.92%	9.39%	1.37%	0.24%	0.19%	18.89%	0.05%	0.03%	100.00%
Bicycle	Bicycle	32.31%	18.42%	15.06%	10.96%	1.32%	0.73%		21.05%		0.15%	100.00%
		221	126	103	75	9	5		144		1	684
	Motorcycle	63.53%	6.56%	2.59%	7.69%	2.08%	0.12%	0.98%	16.41%	0.01%	0.02%	100.00%
Passenger car	Motorcycle	13,400	1,384	547	1,621	439	25	207	3,461	3	4	21,091
	Passenger car	26.68%	3.46%	39.04%	14.06%	1.06%	0.20%	4.02%	11.40%	0.03%	0.06%	100.00%
	Bicycle	3,143	407	4,598	1,656	125	23	473	1,343	4	7	11,779
Bicycle	Bicycle	55.00%	11.21%	2.24%	4.48%	2.93%	0.34%	0.34%	23.45%			100.00%
		319	65	13	26	17	2	2	136			580
	Motorcycle	47.16%	18.62%	1.24%	5.14%	3.55%	1.42%		22.70%		0.18%	100.00%
Passenger car	Motorcycle	266	105	7	29	20	8		128		1	564
	Passenger car	53.24%	17.75%	1.37%	2.73%	4.10%	0.34%		20.48%			100.00%
	Bicycle	156	52	4	8	12	1		60			293
Bicycle	Bicycle	42.86%	14.29%		9.52%				33.33%			100.00%
		9	3		2				7			21

**Table 3** Statistics on collision types in unsignalized intersections

At fault	Victim	Angled collision	Right-angle	Rear end	Sideswipe	Head on-sideswipe	Head on	Reversing collision	Others	Self-inflicted	Involving a pedestrian	Total
Motorcycle	Motorcycle	41.64%	29.24%	4.76%	4.63%	2.28%	0.72%	0.02%	16.68%	0.03%	0.01%	100.00%
	Passenger car	4,474	3,142	511	498	245	77	2	1,792	3	1	10,745
		36.62%	36.26%	5.46%	4.05%	1.62%	0.50%	0.19%	0.02%	15.28%	0.02%	
Passenger car	Bicycle	1,917	1,898	286	212	85	26	10	800	1		5,235
	Motorcycle	36.24%	13.41%	12.94%	10.12%	1.18%	0.71%		25.41%			100.00%
		154	57	55	43	5	3		108			425
Bicycle	Motorcycle	54.42%	16.28%	1.41%	6.41%	1.56%	0.34%	2.33%	17.23%	0.02%		100.00%
	Passenger car	4,633	1,386	120	546	133	29	198	1,467	2		8,514
		28.16%	13.93%	17.15%	6.60%	1.97%	0.38%	17.29%	14.46%	0.05%	0.02%	100.00%
Bicycle	Passenger car	1,575	779	959	369	110	21	967	809	3	1	5,593
	Bicycle	47.35%	13.26%	1.52%	6.82%	2.65%		2.27%	25.76%		0.38%	100.00%
		125	35	4	18	7		6	68	1		264
Bicycle	Motorcycle	54.34%	16.18%	0.87%	5.35%	1.30%	0.87%		20.95%		0.14%	100.00%
	Passenger car	376	112	6	37	9	6		145		1	692
		44.73%	24.89%	2.53%	3.38%	1.27%	1.27%		21.94%			100.00%
Bicycle	Passenger car	106	59	6	8	3	3		52			237
	Bicycle	54.17%	12.50%	4.17%	12.50%				16.67%			100.00%
		13	3	1	3				4			24

Table 4 Statistics on collision types in road sections

At fault	Victim	Angled collision	Right-angle	Rear end	Sideswipe	Head on-sideswipe	Head on	Reversing collision	Others	Self-inflicted	Involving a pedestrian	Total
Motorcycle	Motorcycle	26.42%	0.56%	25.20%	17.80%	4.14%	3.20%	0.15%	22.43%	0.09%	0.01%	100.00%
	Passenger car	4,539	97	4,329	3,057	711	549	26	3,852	15	2	17,177
		20.88%	0.41%	27.79%	13.96%	3.73%	2.08%	1.12%	29.70%	0.23%	0.10%	100.00%
Bicycle	Bicycle	1,936	38	2,577	1,294	346	193	104	2,754	21	9	9,272
	Motorcycle	10.11%		42.43%	24.02%	1.69%	1.64%		19.93%	0.06%	0.12%	100.00%
		173		726	411	29	28		341	1	2	1,711
Passenger car	Motorcycle	41.04%	0.34%	4.43%	20.33%	2.26%	1.11%	5.55%	24.86%	0.06%	0.03%	100.00%
	Passenger car	6,243	51	674	3,092	344	169	844	3,781	9	5	15,212
		11.80%	0.16%	47.69%	11.23%	1.89%	0.37%	13.73%	12.99%	0.12%	0.03%	100.00%
Bicycle	Bicycle	3,454	48	13,961	3,288	552	109	4,018	3,802	34	9	29,275
	Motorcycle	22.74%	0.18%	7.58%	23.66%	1.85%	0.92%	4.44%	38.45%		0.18%	100.00%
		123	1	41	128	10	5	24	208	1	1	541
Passenger car	Motorcycle	47.86%	0.60%	2.98%	12.71%	5.66%	6.06%		24.03%		0.10%	100.00%
	Passenger car	482	6	30	128	57	61		242		1	1,007
		31.56%		9.81%	16.18%	6.10%	1.59%	0.27%	34.22%		0.27%	100.00%
Bicycle	Bicycle	119		37	61	23	6	1	129		1	377
	Motorcycle	22.00%		14.00%	26.00%	2.00%	2.00%		34.00%			100.00%
		11		7	13	1	1		17			50



### 3.1 Motorcycle Accident Analysis

Figure 6 shows the statistics on motorcycle accident types in Kaohsiung City in dangerous intersections. Angled collisions are separated into vehicles headed straight, turning right/left and left turn opposing through. The top three most common accident types for motorcycles are “through with right,” “right angle” and “left turn opposing through.” From the accident location analysis, shown in Fig. 7, approximately 60% of all collisions occur at intersections, and 42–45% of this type are angled collisions, while 12–23% of them are right angle collisions [7–9].

For example, Fig. 8 shows the crash trajectory of an accident in which the involved vehicles are turning right at the intersection, which was collected using real accident video. From the figure, it is clear that a car is turning right from the inner lane, and the car next to it is slowing down in response. However the motorcycle rider next to the car fails to see the car turning right on its left-hand side. Therefore, the motorcycle rider keeps going straight. On the other side, the driver that is turning right recognizes that the car on the right-hand side is slowing down and speeds up to pass through the intersection. However, the visibility of the motorcycle rider is blocked by the car, so it causes the two vehicles to collide. This is a common problem since many motorcycle riders tend to keep right on the road. Accidents occur when a car in the middle slows down; however, at the same time the driver who is turning and the motorcycle rider don’t see each other and maintain their original directions. Figure 9 illustrates another example of visibility problems regarding left turn opposing through. Visibility problems in non-signalized intersections cause right angle collisions to occur when cars are queuing and lane splitting motorcycles and bicycles collide with vehicles from adjacent approaches, as shown in Fig. 10.

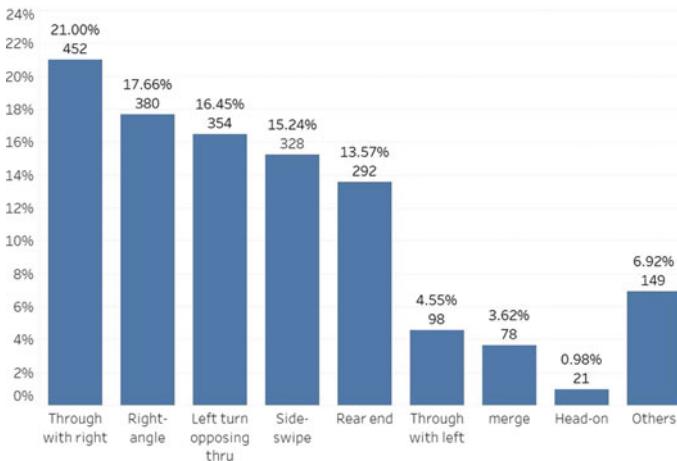


Fig. 6 Statistics on types of motorcycle accidents

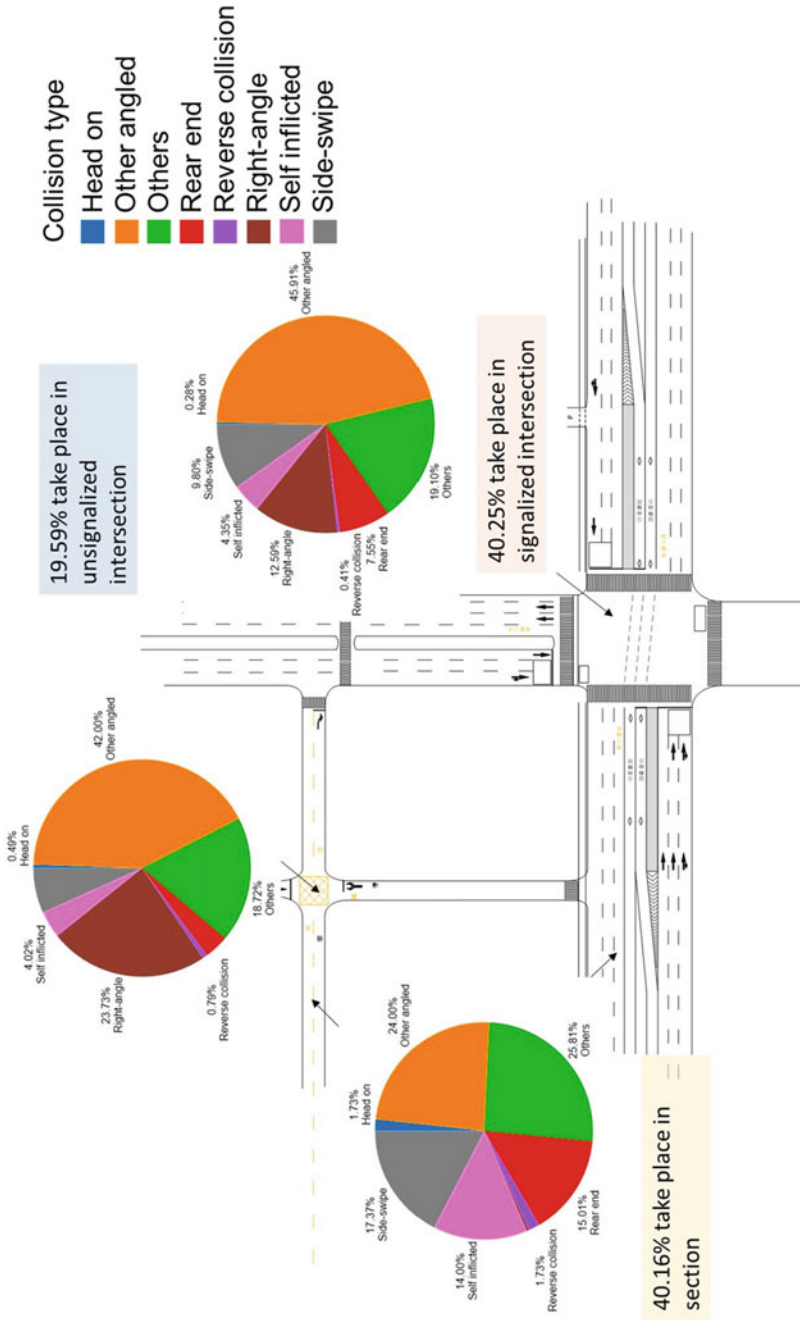


Fig. 7 Statistics on motorcycle accident locations and collision types

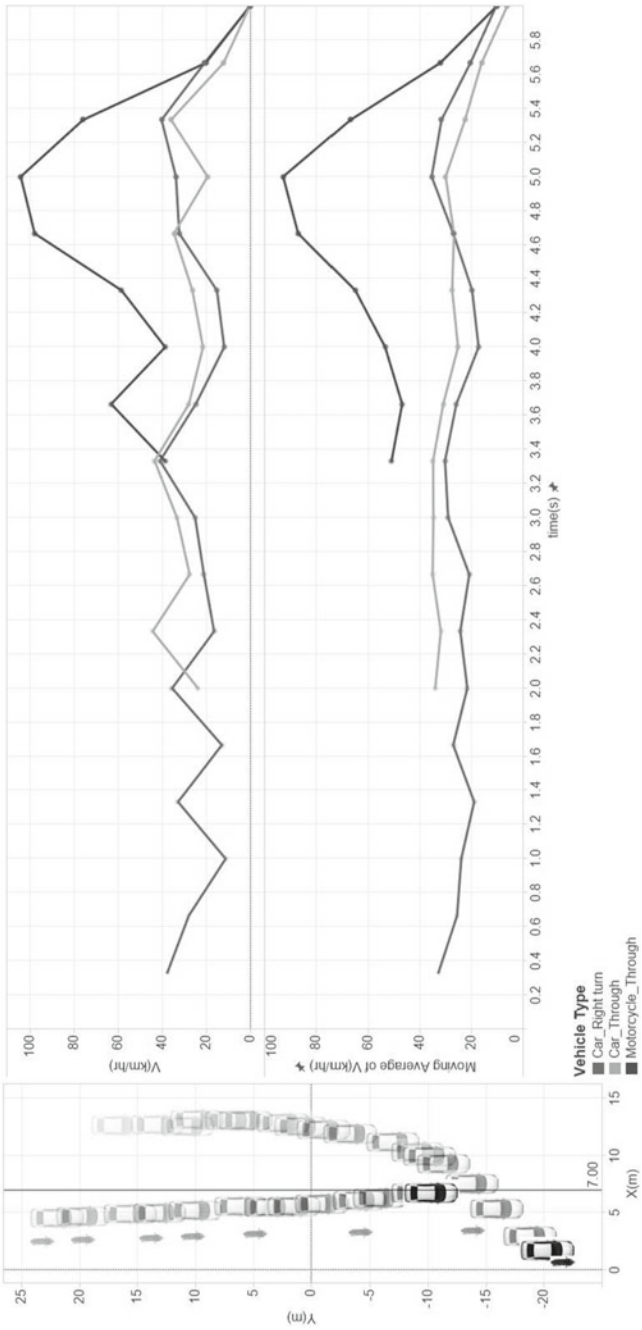
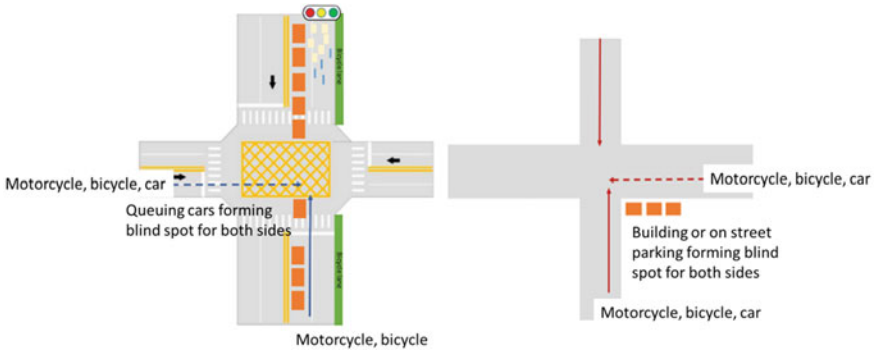


Fig. 8 Example of a through with right event



**Fig. 9** Example of a left turn opposing through event



**Fig. 10** Examples of right angle collisions caused by motorcycle riders and cyclists

In signalized intersections, the main contributing factor to right angle collisions is related to inter-green time.

The tendency of motorcycle riders to lane split greatly increases the incidences of sideswiped collisions. However, most of these involving bicycles occur when vehicles overtake them, while most sideswipe collisions involving motorcycles happen during lane splitting when a motorcycle rider attempts to overtake a car or when a car attempts to overtake a motorcycle.

### 3.2 Analysis of Accidents Involving Bicycles

Figure 11 shows the statistics on bicycle accident types in Taipei City. Compared to motorcycles, bicycles tend to be involved in more types of collisions because cyclists can ride either on the street, in the bicycle lane or on the sidewalk. Right angle collisions are by far the most prevalent, accounting for up to one fourth of all accidents, which is followed by sideswiping. From the accident location analysis shown in Fig. 12, approximately 60% of all collisions occur at intersections, and 33–37% of those are angled collisions, while 26–39% are right angle collisions.

The most frequent type of angled collision for cyclists is “through with left.” Interestingly, this is the least frequent type for motorcycles. It is most likely to occur at signalized intersections when a car turning left hits a cyclist crossing on the far side of the intersection, shown in Fig. 13. At non-signalized intersections, since cyclists tend to ride in the right-hand side of the street, more crashes happen when a cyclist turning left collides with a motorcycle rider or car going straight, as shown in Fig. 13, picture 2. There are some scenarios that exclusively affect cyclists because they can cross the street in two directions on a bicycle crossing and, furthermore, can either ride in the street or in the cross walk. These scenarios are shown in Fig. 13, i.e. “A” in picture 1, “B” in picture 3 and picture 4.

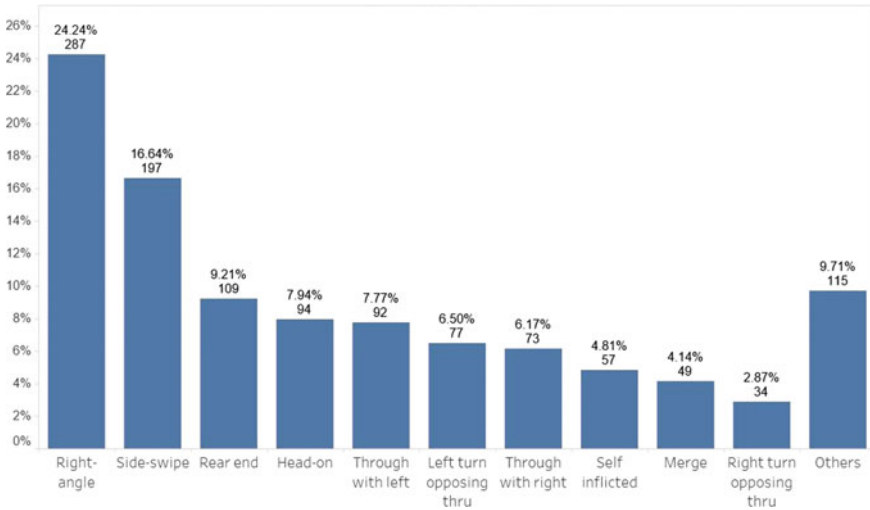


**Fig. 11** Statistics on types of bicycle accidents

## 4 Comparison of Motorcycle and Bicycle Accidents

Motorcycles and bicycles have different collision patterns because they have distinct operating speeds, acceleration performance, traffic laws and locations on the roads. These differences and corresponding collision types are summarized below:

1. Bicycles are slower than motorcycles, which increases the possibility of them becoming involved in “rear end” and “sideswipe” collisions. Both of these vehicles occupy the right lane, so they are more likely to be rear ended and sideswiped than cars, as illustrated in Table 4. Sideswipe type accidents occur with motorcycles during lane splitting either when the rider attempts to pass a car or a car attempts to pass the motorcycle rider, as shown in Table 4.
2. Motorcycles are involved in a higher percentage (7.6%) of “rear end” collisions at signalized intersections compared to bicycles (3.5%), as shown in Figs. 7 and 12.
3. Motorcycles and bicycles usually stay in the right lane. Cyclists will keep to the right regardless of which direction they are headed, which will increase the possibility of “through with left” accidents in non-signalized intersections, as shown in Figs. 6 and 11, in which 4.6% is all motorcycle-related accidents, and 7.8% is all bicycle-related accidents.
4. Because motorcycles and bicycles are smaller than other vehicles, they are difficult to see in traffic. When riders are in the right lane, “through with right” and “left turn opposing through” accidents are much more likely. Particularly when cars are lined up at a red light, the motorcycle rider may try to lane split and

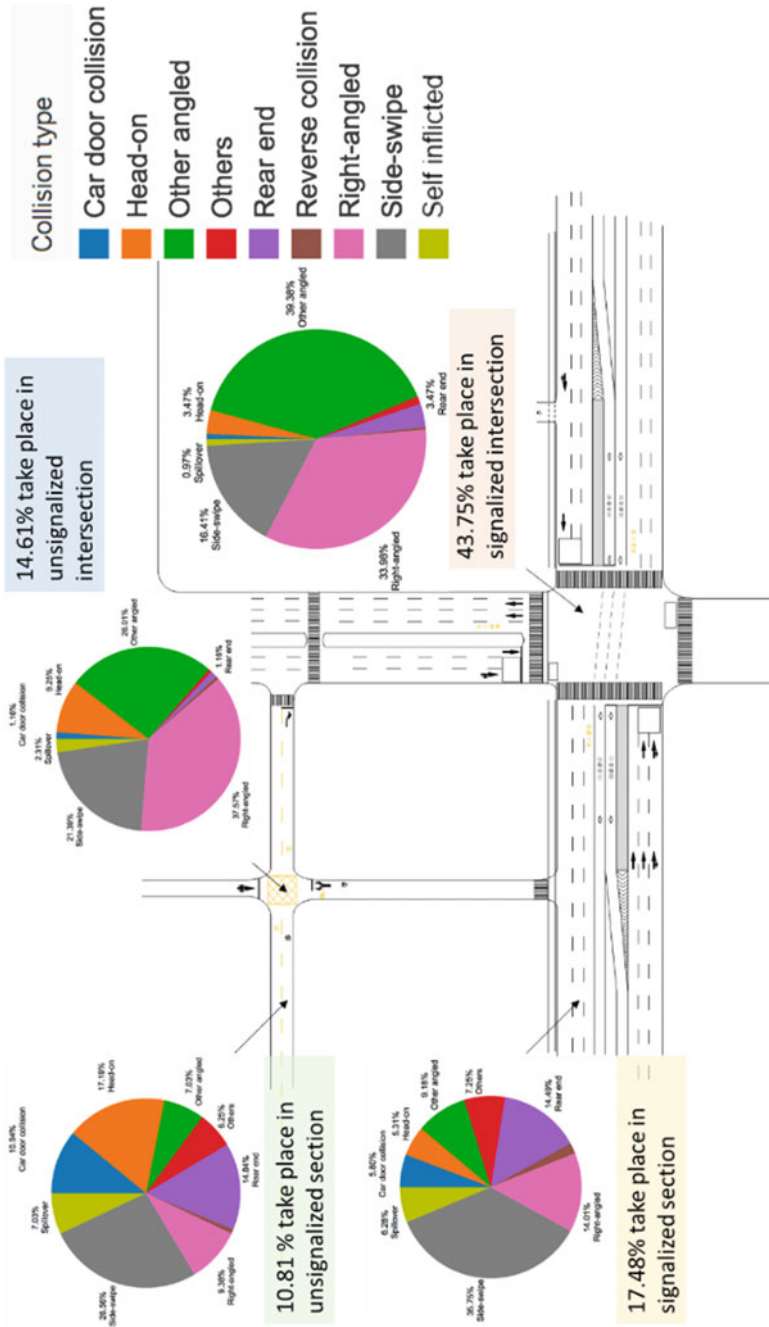
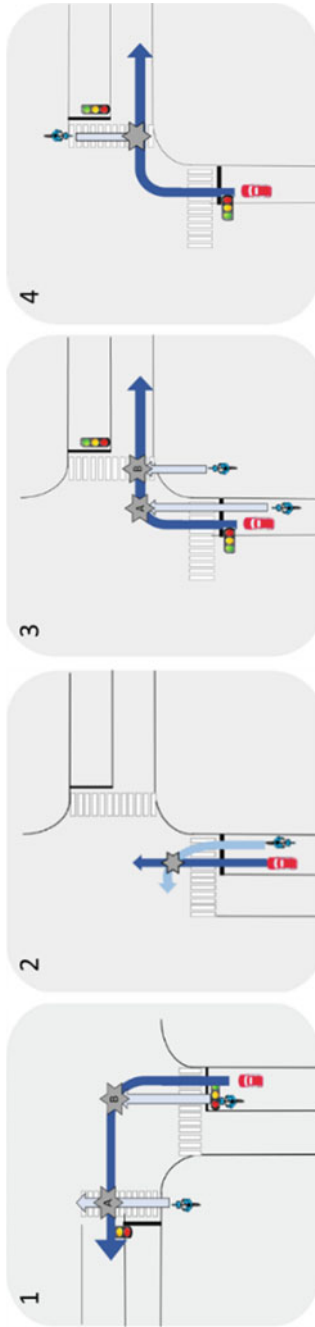


Fig. 12 Statistics on bicycle accident locations and collision types



**Fig. 13** Bicycle collision scenarios



cross the line of vehicles from the adjacent lane which would be likely to cause a “sideswipe” collision.

5. Unlike cars and motorcycles, bicycles don’t have bright headlights to warn other vehicles when they are approaching the intersection, which will also increase the risk of a “right angle collision” at a non-signalized intersection at night or in the early morning. This would increase the likelihood of having a “right or left turn into path” crash with merging vehicles.
6. Bicycle traffic laws fall somewhere between those for motor vehicles and pedestrians. When an intersection has no signal exclusively for cyclists, they should obey signals for motorized vehicles. However, if the signal timing-clearance time was designed with motorized vehicles in mind, it will be not be long enough for a bicycle. This situation may cause a “right angle collision” of a bicycle with a motor vehicle. On the other hand, because there are usually no laws regarding riding direction while a cyclist crosses an intersection, this situation may cause a “right turn opposing through” bicycle accident, a “through with left” collision in a crosswalk or a “right angle collision” in both the near side or far side of the pedestrian crossing.
7. Bicycles are slower and have more flexibility in changing direction than drivers of motorized vehicles; therefore, bicycle traffic is often more unpredictable compared to motorized vehicles. However, cyclists are faster than pedestrians and their trajectory is also unpredictable. Drivers will not have time to react and will collide with the bicycles.
8. Motorcycle riders and cyclists are more likely to violate traffic laws by riding in the wrong direction, especially on minor roads or small alleys, which makes their route of travel unpredictable for approaching vehicles.

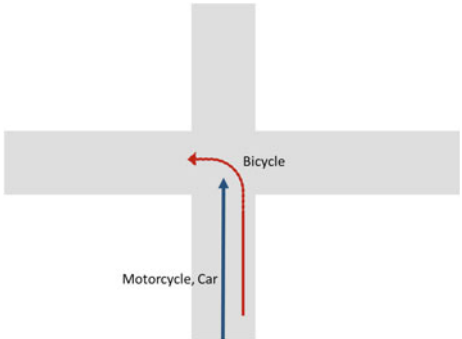
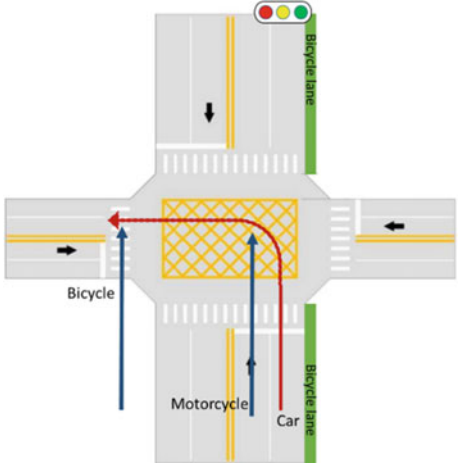
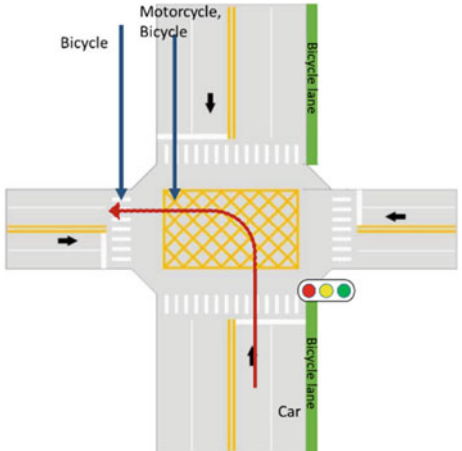
## 5 Motorcycle and Bicycle Crash Scenarios

According to the above analysis, we will discuss some common motorcycle and bicycle collision scenarios regarding the possible application of V2X technology for enhancing the safety that are illustrated in Table 5.

## 6 Conclusions and Suggestions

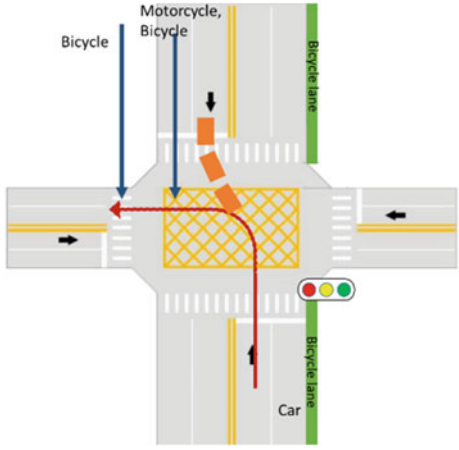
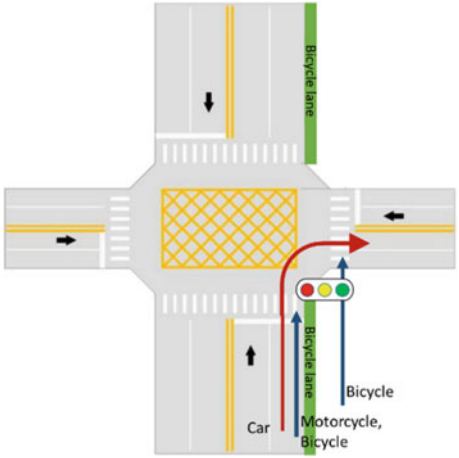
According to the statistical data, most accidents occur when motorcycle riders and cyclists collide with other motorcycles and passenger cars; therefore, both are more likely to be a victim rather than an at-fault driver. According to modal share, with the ratio of motorcycle riders and passenger cars being 2:1 on the road, most motorcycle accidents occur when a motorcycle collides with a passenger car, and most bicycle accidents occur when a cyclist collides with a motorcycle. In general, accidents involving cyclists have a higher death rate than motorcycle accidents. The most severe

**Table 5** Common Motorcycle and Bicycle Crash Scenarios

Collision type	Scenarios	Description
Left turn with through	 <p>The diagram shows a T-junction where a horizontal road crosses a vertical road. A blue arrow labeled 'Motorcycle, Car' points north on the vertical road. A red arrow labeled 'Bicycle' starts in the right lane of the vertical road and turns left across the path of the motorcycle or car.</p>	<p>Bicycle riders tend to be in the right lane. A cyclist turns left while in the right lane and hits a motorcycle to his or her left                      Location:                      Unsignalized intersection</p>
Left turn with through	 <p>The diagram shows a four-way signalized intersection with a central yellow cross-hatched area. A red arrow labeled 'Car' turns left from the right lane. A blue arrow labeled 'Motorcycle' and a green arrow labeled 'Bicycle' travel through the intersection. A red arrow also shows a cyclist turning left from the right lane. A traffic light is shown at the top with the red light illuminated.</p>	<p>A car turns left while in the right lane and hits a motorcycle to its left or a cyclist riding in a cross walk in the opposite direction                      Location:                      Signalized intersection</p>
Left turn opposing through	 <p>The diagram shows a four-way signalized intersection with a central yellow cross-hatched area. A red arrow labeled 'Car' turns left from the right lane. Blue arrows labeled 'Motorcycle, Bicycle' and a green arrow labeled 'Bicycle' travel through the intersection from the opposite direction. A traffic light is shown at the bottom with the red light illuminated.</p>	<p>Motorcycles and bicycles are smaller which makes them harder to see in traffic                      A car turns left and hits a motorcycle or bicycle coming from the opposite direction                      Location:                      Signalized intersection                      Non-signalized intersection</p>

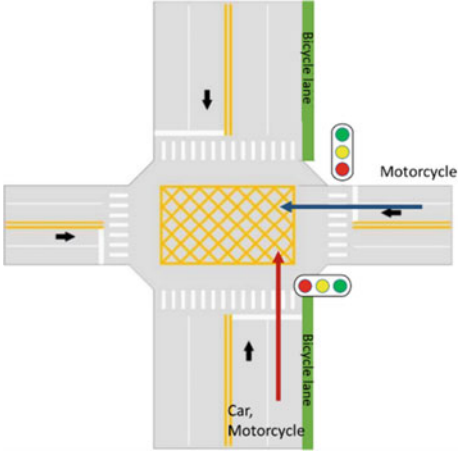
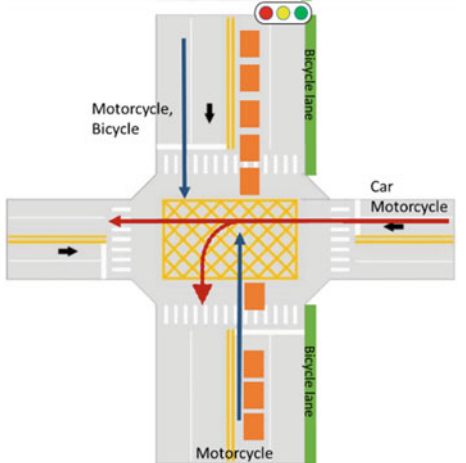
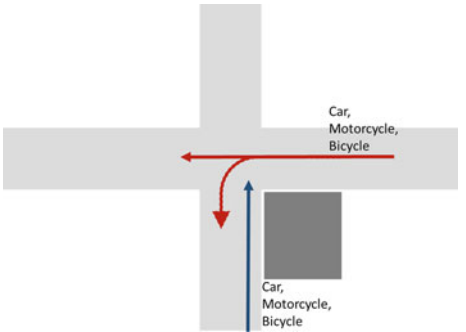
(continued)

**Table 5** (continued)

Collision type	Scenarios	Description
Left turn opposing through		<p>Cars that are lining up to turn left in the opposite direction form an obstruction between the cars turning left and the other vehicles headed in the opposite direction                      A car turns left and hits a motorcycle and a bicycle on the roadway or crosswalk                      Location:                      Signalized intersection</p>
Right turn with through		<p>A car turns right and hits a motorcycle and bicycle on its right. The conflict point could be on the roadway (slow traffic lane—the exclusive motorcycle lane) or at the crosswalk                      Location:                      Signalized intersection</p>

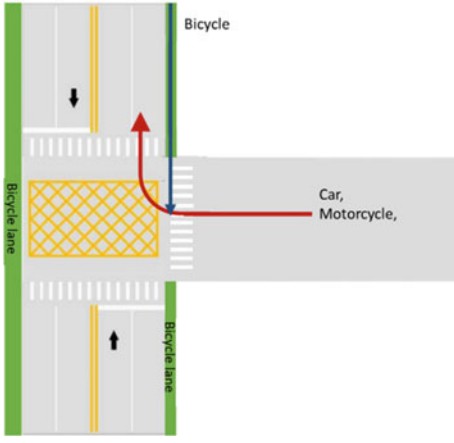
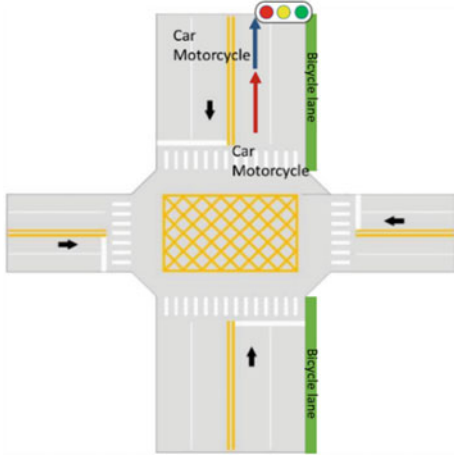
(continued)

**Table 5** (continued)

Collision type	Scenarios	Description
Right angle collision		<p>A car or motorcycle at the onset of yellow or the beginning of a red light fails to pass through the intersection and causes a right-angle collision on its right side                      Location:                      Signalized intersection</p>
Right angle collision		<p>Cars lining up to turn form an obstruction between vehicles on minor and major roads. A car going straight or turning left from a minor road, hits a motorcycle or bicycle from the adjacent approach                      Location:                      Unsignalized intersection with signalized intersection ahead</p>
Right angle collision		<p>Buildings on the corner or parked cars form an obstruction between two minor roads. A car going straight or turning left from a minor road, hits a motorcycle or bicycle from an adjacent road                      Location:                      Unsignalized intersection</p>

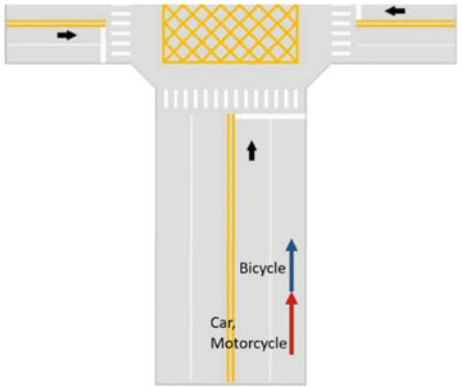
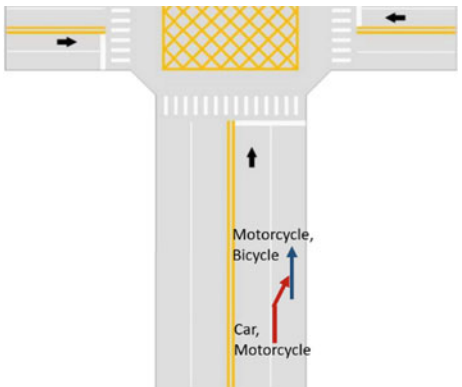
(continued)

**Table 5** (continued)

Collision type	Scenarios	Description
Right angle collision		<p>A car or motorcycle turns right from a minor road, hits a bicycle in the crosswalk from the right                      Location:                      Unsignalized intersection</p>
Rear end-in the intersection		<p>A car or motorcycle hits another car or motorcycle that is stopped while waiting for the light to change                      Location:                      Signalized intersection</p>

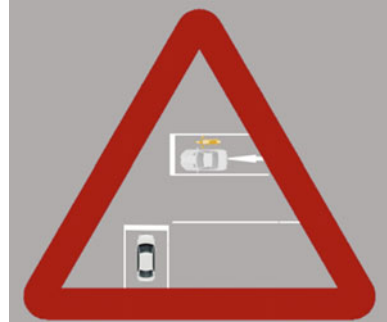
(continued)

**Table 5** (continued)

Collision type	Scenarios	Description
Rear end-in the intersection		<p>A car or motorcycle rear ends a bicycle when attempting to pass it                      Location:                      Section</p>
Sideswipe		<p>A car or motorcycle sideswipes a cyclist when attempting to pass it.. A motorcycle rider collides with other vehicles when lane filtering                      Location:                      Section</p>

type of motorcycle accidents are angled collisions, right angle, and sideswipes and, not surprisingly, these types are most severe for accidents involving bicycles. Right angle collisions are frequent for both motorcycles and bicycles. The lane splitting ability of motorcycle riders at high speed, their small size and speed difference from bicycles and other motor vehicles are the key factors that cause these accidents. The V2X system can be utilized to help drivers be aware of other vehicles, which is very beneficial in traffic situations in which motorcycles and bicycles are often obstructed by other vehicles. This technology includes displaying a warning message to the driver, as well as personal information via the on-board unit. It can also provide warning information to all approaching vehicles, as illustrated in Fig. 14.

**Fig. 14** Warning sign example (designed proposed in this study)



The efficacy of the V2X and warning system in mixed flow traffic with a high number of motorcycle riders and cyclists requires further study. For example, researchers must identify the warning threshold and how to filter out unnecessary warning messages. In other words, the drivers must be provided only with critical information and not be overwhelmed with extraneous data that might distract them and jeopardize their safety.

## References

1. Ministry of Transportation and Communication (MOTC): National Survey of Travel Mode Usage (2016)
2. Najm, W.G., Smith, D.L.: Definition of a pre-crash scenario typology for vehicle safety research. In Proceeding of the 20th International Technical Conference on the Enhanced Safety of Vehicles (2007)
3. Toma, S., Swanson, E., Smith, J. D., Najm, W.G.: Heavy truck pre-crash scenarios for safety applications based on vehicle-to-vehicle communications (No. DOT-VNTSC-NHTSA-11-14). United States. National Highway Traffic Safety Administration (2014)
4. Eccles, K., Gross, F., Liu, M., Council, F.: Crash data analyses for vehicle-to-infrastructure communications for safety applications (No. FHWA-HRT-11-040) (2012)
5. Najm, W.G., Ranganathan, R., Srinivasan, G., Smith, J.D., Toma, S., Swanson, E., Burgett, A.: Description of light-vehicle pre-crash scenarios for safety applications based on vehicle-to-vehicle communications (No. DOT-VNTSC-NHTSA-11-11). United States. National Highway Traffic Safety Administration (2013)
6. Hsu, T.P. et al.: Analysis on traffic accident. Research Report, Institute for Information Industry, Taiwan (2016)
7. Hsu, T.P. et al.: Accident-prone intersection safety improvement program in Kaohsiung 2013. Research Report of the Project by Transportation Bureau Kaohsiung City Government (2013)
8. Hsu, T.P. et al.: Accident-prone intersection safety improvement program in Kaohsiung 2014. Research Report of the Project by Transportation Bureau Kaohsiung City Government (2014)
9. Hsu, T.P. et al.: Accident-prone intersection safety improvement program in Kaohsiung 2015. Research Report of the Project by Transportation Bureau Kaohsiung City Government (2015)

# Assistive Devices for Safe Driving at a Crossing with No Traffic Lights Using 920 MHz Band



Shintaro Uno

**Abstract** V2I, a new system using 920 MHz band requiring lower power consumption and costs is introduced as an assistive device to reduce crashes at small-scale crossings without traffic lights. A prototype of this new V2I system was made.

**Keywords** V2I · 920 MHz · Safe driving

## 1 Introduction

In Japan, about one-third of the traffic accident cases occur at crossings [1]. Approx. 40% of them happen at small crossings without traffic lights [2], so, there is a critical need for preventing crashes at such crossings. Dedicated Short Range Communication (DSRC) with 5.8G band [3] and the 760 MHz band V2X system [4] whose PHY and MAC layer are based on IEEE802.11p [5] have already been developed using V2I system and V2V system to lessen crashes at crossings. In addition, Driving Safety Support System (DSSS) using optical beacon is also being developed [6].

However, these are targeting mainly large-scale crossings with traffic lights rather than small-scale crossings. Moreover, their power consumption and equipment costs are relatively high. To reduce crashes at minor crossings with no traffic lights, we propose a new V2I system using 920 MHz band of short-distance wireless whose power consumption and equipment costs are relatively low. 920 MHz band is included in the ISM band in Japan, and it is planned to be used for Home Energy Management System (HEMS) [7] and ZigBee IP [8]. The communication range of 920 MHz is longer than the other short-distance wireless such as ZigBee [9], and the diffraction is better.

In this chapter, we introduce a new V2I protocol that alerts the driver in a car approaching a crossing without traffic lights that another vehicle is approaching the crossing from different sides, utilizing the 920 MHz communication module. These

---

S. Uno (✉)

Faculty of Engineering, Aichi University of Technology, 50-2, Manori, Nishihassama-cho, Gamagori-City, Aichi 443-0047, Japan  
e-mail: [uno-shin@aut.ac.jp](mailto:uno-shin@aut.ac.jp)



drivers may receive the alert at points even a bit far from the crossing. Several field trials were conducted, and the effectiveness of this method was proved.

## 2 Related Work

In this section, several approaches to assist safe driving at crossings in Japan are discussed; such as DSSS, DSRC, 760 MHz and ASV. Moreover, trends in such approaches in the U.S. and Europe are also referred.

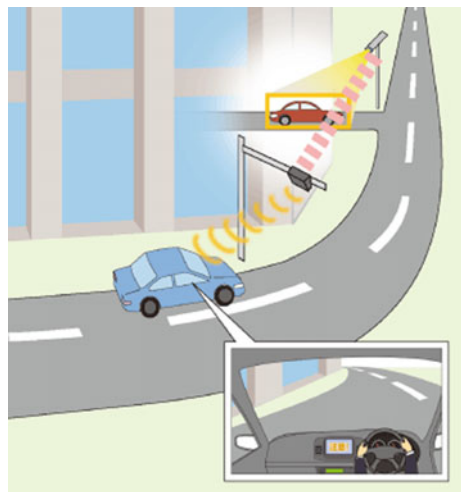
### 2.1 DSSS

DSSS shown in Fig. 1 [10] is used to expand the Vehicle Information and Communication Systems (VICS), with which a driver can recognize that another vehicle is approaching to the crossing by means of optical beacon. However, DSSS can only be applied to large-scale crossings.

### 2.2 DSRC

DSRC expands the functions of Electronic Toll Collection (ETC) in 5.8G band. Figure 2 shows a view of an experiment using vehicle-to-vehicle communication to avoid crashes at a crossing. The antenna installed on a vehicle is shown in Fig. 3

**Fig. 1** Avoidance of crashes at crossings with DSSS



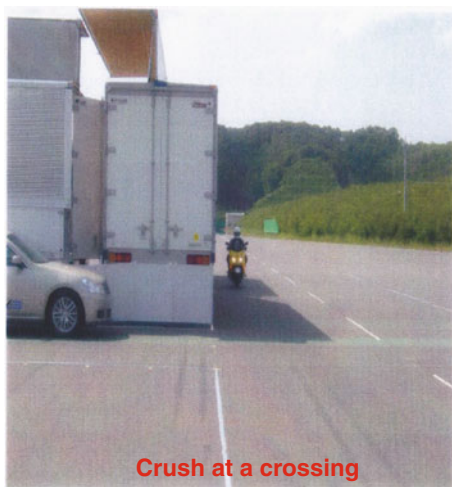


**Fig. 2** Experiment using vehicle-to-vehicle communication by DSRC to avoid crashes at a crossing



**Fig. 3** Antenna on a vehicle

[11]. Vehicle-to-vehicle communication is considered to be easily realized. However, it is not that effective at a crossing with poor visibility. A system using vehicle-to-infrastructure communication to avoid crashes at crossings is also being studied, which is applicable only for large-scale crossings.

### 2.3 760 MHz

The system supporting safe driving using 760 MHz was standardized as ARIB STD-T109 in Japan, and part of the system is already commercialized. A safe-driving assistance system using vehicle-to-vehicle communication is shown in Fig. 4 [12]. A system using vehicle-to-infrastructure communication in 760 MHz is also under development. Figure 5 shows an antenna for vehicle-to-infrastructure communication set at a large-scale crossing in Japan. There, relatively high equipment costs and power-consumption are required [13].

### 2.4 ASV

Advanced Safety Vehicle (ASV) [14] is a vehicle on which the equipment to avoid crashes using the millimeter-wave radar is installed. It is partly commercialized. This is quite effective against forward collisions, however, not able to cover all the crashes at a small-scale crossing with poor visibility.

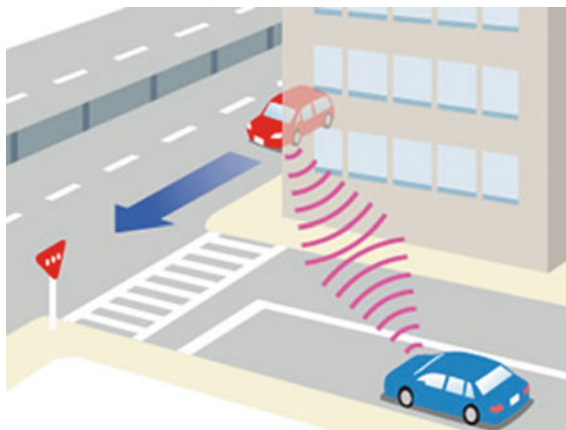


Fig. 4 Safe-driving assistance using vehicle-to-vehicle communication with 760 MHz



**Fig. 5** An antenna of vehicle-to-infrastructure communication with 760 MHz and a sensor

### ***2.5 Trends in the U.S. and Europe***

In the United States and Europe, the DSRC vehicle-to-infrastructure communication system and the vehicle-to-vehicle communication system using 5.9 GHz band are being examined for crashes at crossings. IEEE802.11p/1609.4 and ETSIES202663 are standardized in the United States and Europe, respectively. ARIB STD-T109 using 760 MHz band in Japan [15] is based on IEEE 802.11p. However, the frequency and channels used differ from the ones used in Japan.

## **3 920 MHz Communication Module**

As described above, 920 MHz has a lot of advantages such as the long-distance coverage and enough diffraction comparing with 2.4 GHz band. In Japan, while 920 MHz band is planned to be used for HEMS and ZigBee IP, it is hardly used for ITS. In this study, to decrease crashes at small-scale crossings with no traffic lights, we developed a new application protocol using 920 MHz communication module [16] whose PHY is 802.15.4d and MAC is based on IEEE 802.15.4 as shown in Fig. 6. The application software is realized on a PC connected to a 920 MHz module via the interface board shown in Fig. 7. The power consumption is under 120 mVA. The cost is cheaper than the module of DSRC.

**Fig. 6** 920 MHz communication module



**Fig. 7** Interface board



## 4 System Configuration and Protocol Flow

### 4.1 System Configuration

Figure 8 shows the system configuration of the vehicle equipment, roadside equipment, and control equipment. The vehicle equipment is set at the dash-board of a vehicle and some pieces of road equipment are set along the roads respectively. The control equipment is placed near the center of the crossing.

The basic flow is as follows.

1. Vehicle equipment of a car searches/finds a device set in the roadside equipment by comparing RSSI.
2. When the device with the highest RSSI was selected, the vehicle equipment sends data to that device, notifying the vehicle is approaching the crossing along the road.
3. The roadside equipment sends the data to the control equipment via some pieces of road equipment. The control equipment sends the crossing information to all the pieces of roadside equipment, notifying the vehicle is approaching the crossing from which road.

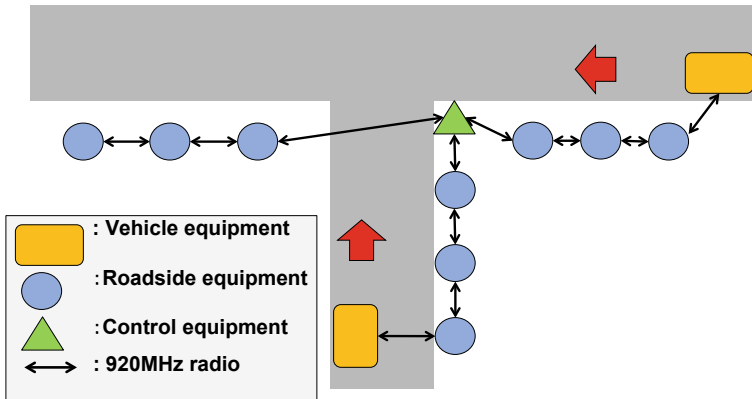


**Fig. 8** System configuration

4. The roadside equipment sends the crossing information to the vehicle equipment of vehicles approaching the crossing.
5. A view of an approaching vehicle pops up on the monitor of the vehicle equipment to tell each driver from which road other vehicle is coming.
6. When the vehicle passes the crossing and the vehicle equipment finds the roadside equipment set at the different road, the vehicle equipment sends the notification that the vehicle has left the crossing.
7. The data is sent to the control equipment, and it sends the crossing data with no information of the vehicle which has left the crossing.
8. The roadside equipment sends the data to the vehicle equipment, and the view is gone.

#### ***4.2 Protocol Flow of the Vehicle Equipment and the Roadside Equipment [17, 18]***

Protocol flow of the vehicle equipment and the roadside equipment are shown in Figs. 4 and 5 respectively. In Fig. 9, the interval of searching the device in the roadside equipment is set at 500 ms. When the vehicle equipment finds a certain device with the highest RSSI twice in a row, that device is the one to be selected. Since 920 MHz has enough diffraction, the vehicle equipment may find the device with the highest RSSI that is included in a piece of roadside equipment on different roads, not only the one closest to the vehicle. To avoid any error in finding the proper device, it is designed to find the one with the highest RSSI consecutively twice.

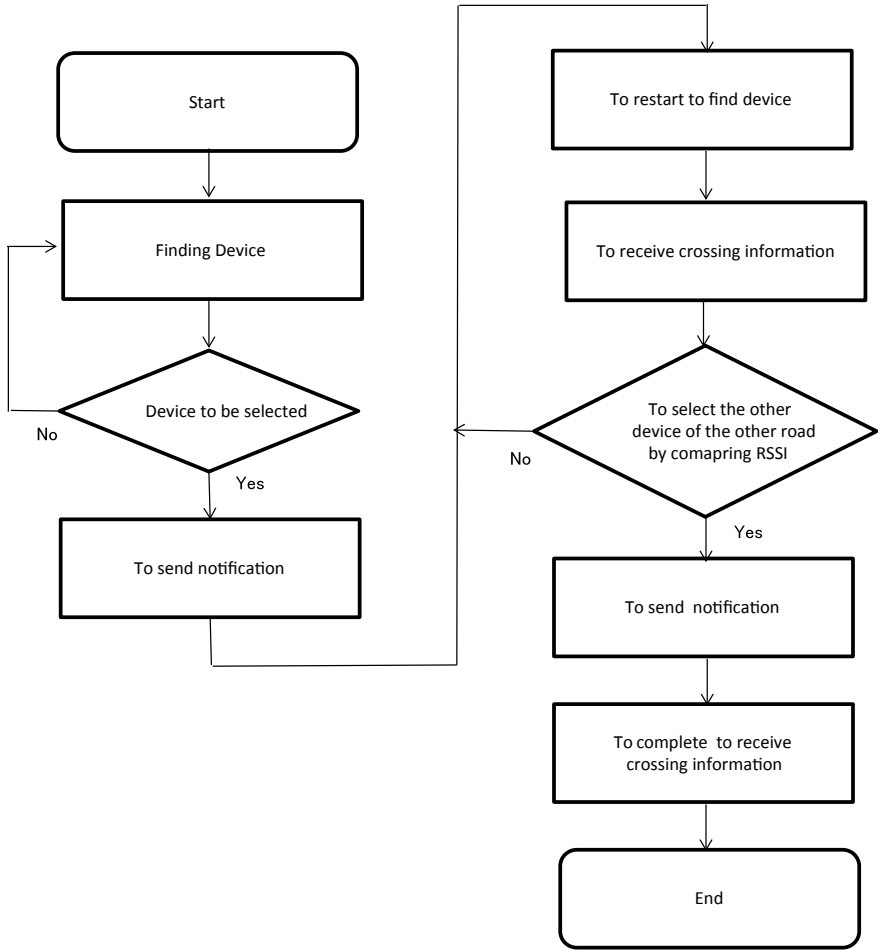


Fig. 9 Protocol flow of vehicle equipment

After selecting the device in the roadside equipment, the vehicle equipment sends the data of notification to the device in the roadside equipment and starts finding another device in the roadside equipment again. Figure 10 shows the protocol flow of the roadside equipment where the data is sent to the control equipment or to the vehicle equipment.

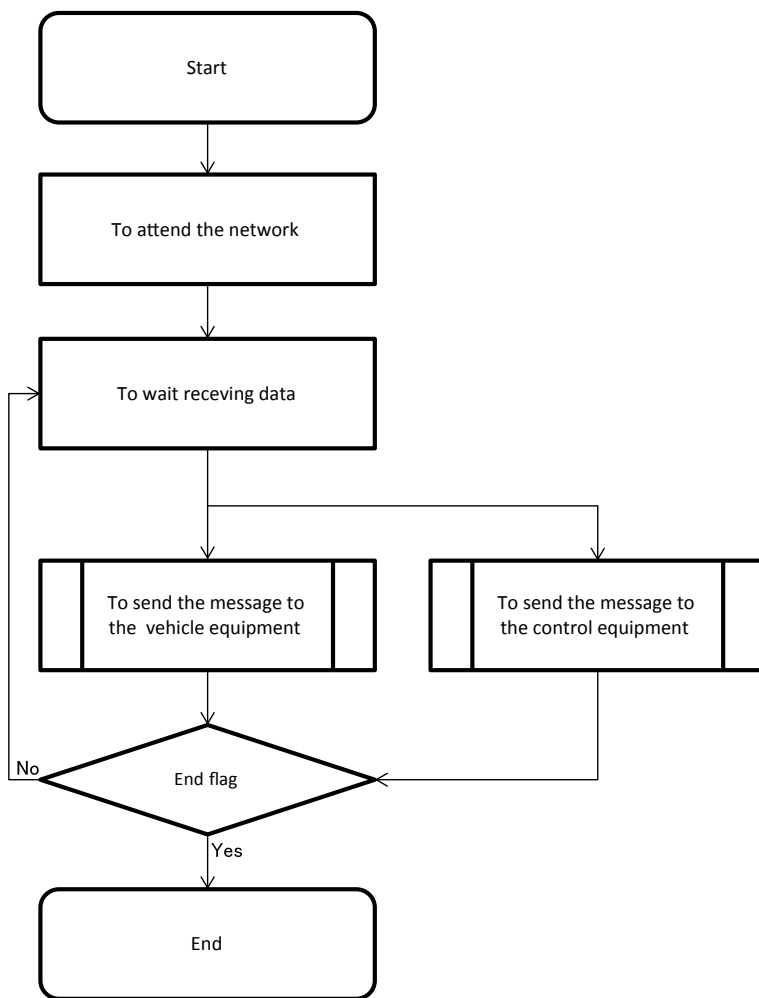


Fig. 10 Protocol flow of roadside equipment



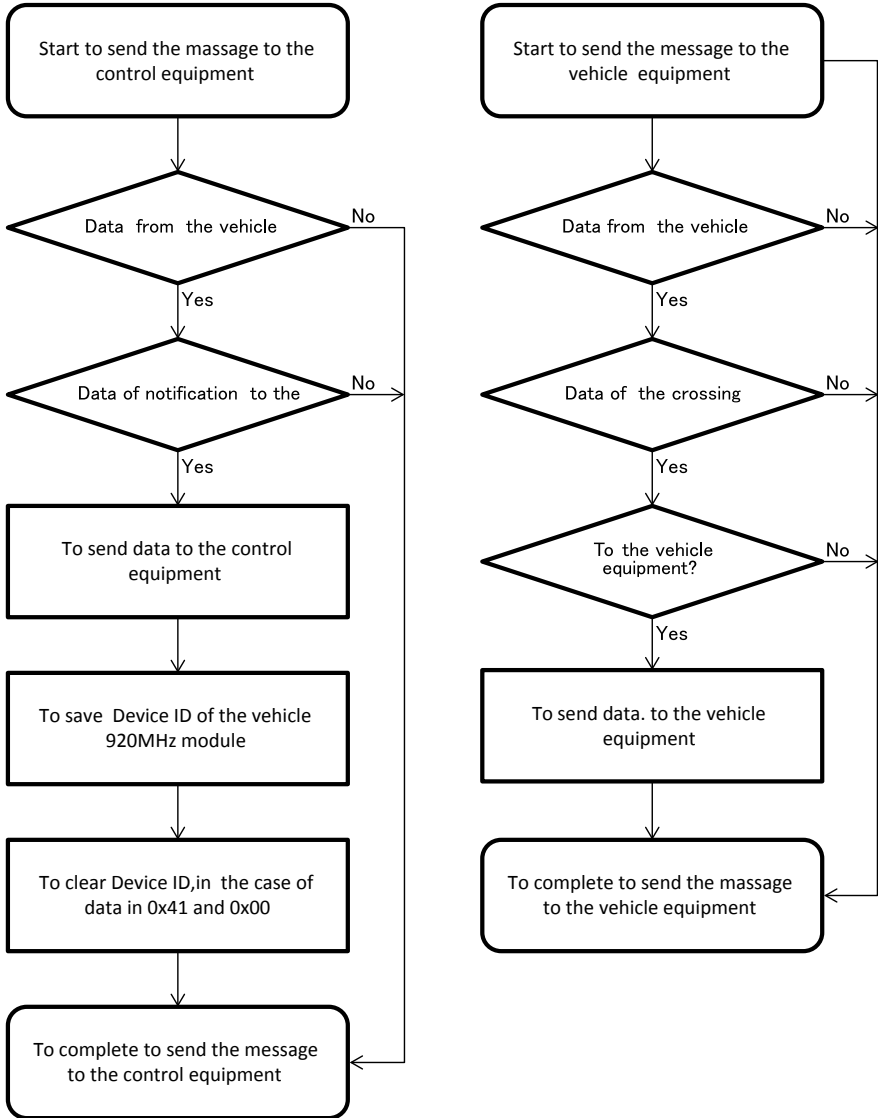


Fig. 10 (continued)

## 5 Miniaturization

Vehicle equipment and roadside equipment were miniaturized as shown in Figs. 11 and 12 using 8-bit microcomputer. The roadside equipment is installed in a water-proof case as shown in Fig. 12.



**Fig. 11** Miniaturization of vehicle equipment

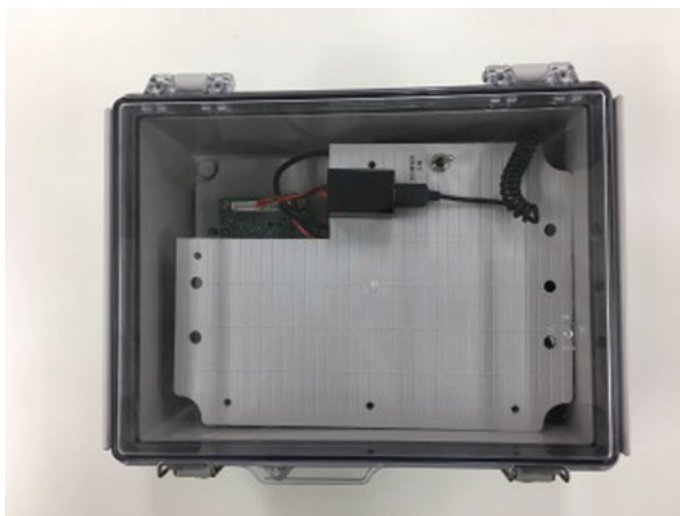


**Fig. 12** Miniaturization of roadside equipment

## 6 Field Trials and Evaluation

### 6.1 Field Trials

After developing the software based on the protocol flow in Figs. 9 and 10 using the 920 MHz communication module shown in Fig. 6, several field trials were conducted. The conditions of the field trials were as follows.

The spots where the field trials were held were two types of small crossings with no traffic lights. The control equipment was set near the center of the crossings, and three pieces of roadside equipment were set along the roads, respectively. Two vehicles approached each crossing from the different sides as shown in Fig. 8. The distance between the control equipment and the roadside equipment or between each piece of the roadside equipment was from 20 to 40 m. The height of the antenna was 1.0 m for the roadside equipment, and 0.8 m for the vehicle equipment. The speed of the vehicles was about 30 km/h. The transmission power of the 920 MHz communication module was 10 mW. The view of vehicle equipment is shown in Fig. 13.

The field trials were conducted three times. The results are shown in Table 1.

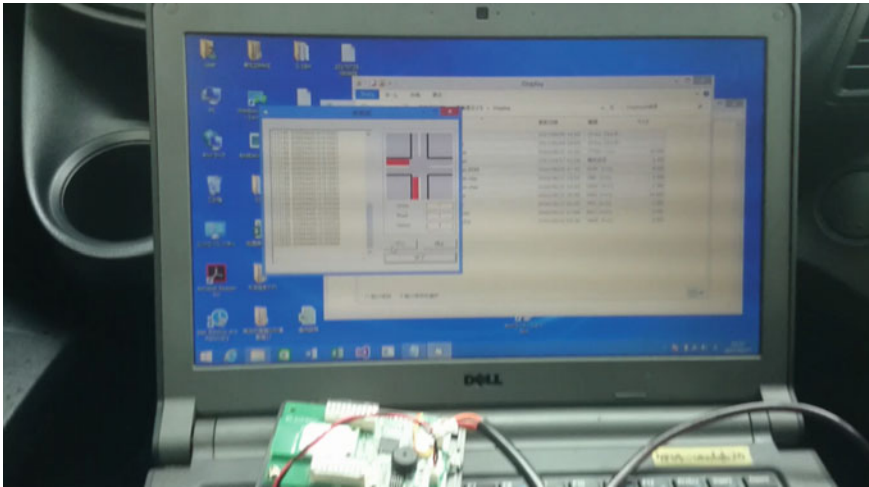


**Fig. 13** View of vehicle equipment

**Table 1** Results of field trials

	Number of trials	Number of success	Success rate (%)	System delay
Trial 1	13	12	92	299–688 ms
Trial 2	10	8	80	292–760 ms
Trial 3	25	24	92	–



**Fig. 14** View of roadside equipment

The definition of “Success” in Table 1 is as follows.

- Trial 1 and Trial 2: The on-board monitor displayed the approaching vehicle at 130–150 m before the crossing. The distance between each piece of the roadside equipment is 40 m.
  - Trial 3: The monitor displayed the approaching vehicle at 70 m before the crossing. The distance between each piece of the roadside equipment is 20 m.
  - Every trial: The display was gone after the vehicle had passed the crossing.
- Trial 3 was conducted with the miniaturized roadside equipment shown in Fig. 12 and the vehicle equipment shown in Fig. 11. Figure 14 shows the view of roadside equipment, and Fig. 15 shows the view of field Trial 3. The measured packet error rate was below  $10^{-2}$ .

## 6.2 Evaluation

According to the trial results, we confirmed that this method was effective at small-scale crossings with no traffic lights. In an un-successful case of Trial 1, the vehicle equipment sent data to the roadside equipment whose RSSI did not indicate at or higher the reference value of “−80 dBm.” So, the data could not reach the roadside equipment. In Trial 2, the vehicle equipment was made to send data only when the corresponding RSSI clears the reference value, by modifying the software. Transmis-



**Fig. 15** View of field Trial 3

sion power of roadside equipment can be selected from among 1, 5, 10 and 20 mW. It will not be easy for a vehicle equipment to find the roadside equipment far from the crossing if transmission power is lower than 10 mW. With the transmission power higher than 10 mW, on the other hand, a vehicle equipment will find the roadside equipment installed on other roads than the vehicle is running on. The optimum transmission power has not been verified yet, and further examinations should be carried out in the next step.

Two tests in Trial 2 were not successful. The obstacles such as parked vehicles near the roadside equipment seemed to have affected the radio condition. The same situation was observed in a test in Trial 3.

In the next step, therefore, we should examine the influence of obstacles by changing the height of antenna for the roadside equipment. Making the antenna higher than 1.5 m may improve the success rate of the system operation. In Japan, the system delay including communication delay and processing delay should be kept at or under 400 ms [19]. Retransmission performed under some unstable radio conditions may have caused system delays over 400 ms in trials 1 and 2. We should also examine how to minimize the system delay, even when some retransmission is necessary.

## 7 Conclusion and the Next Step

In this chapter, we propose a new V2I system based on 920 MHz to assist safe driving at small- scale un-signalized intersections, with lower equipment costs and power consumption. A prototype of this new system was made. Miniaturization of the vehicle equipment and roadside equipment was realized to conduct some field trials. The effectiveness of this system was proved at such crossings.

This system can co-exist with DSRC or 760 MHz system since the scale and type of respective targeted crossings are different. As described above, the influence of obstacles and retransmission delay should be thoroughly examined in the next step. Currently, this system using 920 MHz band seems not to be interfered by other systems such as HEMS, however, we should examine this in more detail in the next step.

## References

1. Traffic accident (2016). [http://www.ms-ins.com/special/rm\\_car/accidenta-data/](http://www.ms-ins.com/special/rm_car/accidenta-data/). Last accessed 25 July 2018
2. Ohhori, T.: ITARDA information, NO. 69, Tokyo (2007)
3. Kenny, J.B.: Dedicated short-range communications standards in the United States. *Proc. IEEE* **99**, 1162–1182 (2011)
4. Iwai, H.: Multipath Delay Profile Models for ITS in 700 MHz Band, VTC Fall 2011, IEEE, pp. 1–5 (2011)
5. Grau, G.P., et al.: Characterization of IEEE802.11p Radio channel for Vehicle-2-Vehicle communications using the CVIS platform. In: *Proceeding of the 7th International Symposium on CSNDSP 2010*, pp. 449–453 (2010)
6. UTMS. <http://www.utms.or.jp/english/index.html>. Last accessed 25 July 2018
7. Yoshikawa, T.: HEMS with resonant-type wireless power transmission. In: *IEEE MTT-S International IMWS 2011*, pp. 167–170 (2011)
8. Franceschinis, M.: On the performance of ZigBee Pro and ZigBee IP in IEEE 802.15.4 networks. In: *2013 IEEE 9th International Conference on WiMob*, pp. 83–88 (2013)
9. Zigbee (2018). <http://www.zigbee.org/>. Last accessed 25 July 2018
10. UTMS. <http://www.utms.or.jp/japanese/system/dsss.html>. Last accessed 25 July 2018
11. Ministry of Internal Affairs and Communications (2018) [http://www.soumu.go.jp/main\\_sosiki/joho\\_tsusin/policyports/chousa/its/pdf/081219\\_2\\_si2-2.pdf](http://www.soumu.go.jp/main_sosiki/joho_tsusin/policyports/chousa/its/pdf/081219_2_si2-2.pdf). Last accessed 25 July 2018
12. ITS-connect-pc (2018). [https://www.itsconnect-pc.org/about\\_its\\_connect/](https://www.itsconnect-pc.org/about_its_connect/). Last accessed 25 July 2018
13. Toyota (2018). <http://toyota.jp/technology/safety/itsconnect/>. Last accessed 25 July 2018
14. Ministry of Land, Infrastructure, Transport and Tourism (2018). <http://www.mlit.go.jp/jidosha/anzen/01asv/>. Last accessed 25 July 2018
15. Hirayama, Y., Sawada, M.: Technical trends and future outlook of V2X communication technologies. *J. IEICE* **98**(10), 860–863 (2015)
16. NEC (2018). <https://jpn.nec.com/embedded/products/nfc920/index.html>. Last Accessed 25 July 2018

17. Uno, S.: A study on assistance for safe driving at a crossing with no traffic lights using 920 MHz band. In: World ITS Congress 2017, AP-TP0813 (2017)
18. Takeuchi, S., Uno, S.: Development on assistance for safe driving at a crossing by using 920 MHz wireless. In: The 15th ITS Symposium 2017, 2-A-01 (2017)
19. Ministry of Internal Affairs and Communications, Mobile communication system committee. [http://www.soumu.go.jp/main\\_content/000121408](http://www.soumu.go.jp/main_content/000121408). Last accessed 25 July 2018

# Validation for Improving Reliability in Driver Arousal Method by Physiological Magnetic Stimulation



Yoshihide Hayashi, Masashi Tsukada, Tomoaki Nakano, Muneo Yamada  
and Kaneo Mohri

**Abstract** In recent years, the number of occurrences of traffic accidents tends to decrease. However, many traffic accidents caused by careless driving representative of drowsy driving are still reported. In accidents caused by drowsy driving, deceleration by brakes is not often performed immediately before a collision, so the impact at the time of a collision increases. Therefore, in order to reduce the fatalities caused by traffic accidents, it is essential to prevent drowsy of drivers while driving. So far, our research group has proposed a novel driver arousal method applying the principle of bioactivation, Magneto-protonics principle, and has been examining the effectiveness of the method. As a result, we obtained the result that drowsy driving is suppressed by applying a small extremely low frequency alternating magnetic field against the vehicle driver. In this study, we have newly verified and considered the sustain effect of drowsy driving suppression by magnetic stimulation and the influence of the experiment task which were not verified before. In addition, by further increasing the number of subjects, we tried to improve the reliability of the drowsy driving prevention effect by the proposed method.

---

Y. Hayashi (✉) · M. Tsukada

Division of Information Engineering, Graduate School of Science and Technology, Meijo University, 1-501, Shiogamaguchi, Tempaku-ku, Nagoya, Aichi 468-8502, Japan  
e-mail: [183426015@cmailg.meijo-u.ac.jp](mailto:183426015@cmailg.meijo-u.ac.jp)

M. Tsukada

e-mail: [173426016@c alumni.meijo-u.ac.jp](mailto:173426016@c alumni.meijo-u.ac.jp)

T. Nakano · M. Yamada

Faculty of Science and Technology, Department of Information Engineering, Meijo University, Nagoya, Japan  
e-mail: [tnakano@meijo-u.ac.jp](mailto:tnakano@meijo-u.ac.jp)

M. Yamada

e-mail: [myamada@meijo-u.ac.jp](mailto:myamada@meijo-u.ac.jp)

K. Mohri

Nagoya Industrial Science Research Institute, 1213, Shimada-Kuroishi, Tempaku-ku, Nagoya, Aichi 468-0028, Japan  
e-mail: [kaneo-mohri@fd5.so-net.ne.jp](mailto:kaneo-mohri@fd5.so-net.ne.jp)

© Springer Nature Singapore Pte Ltd. 2019

T. Mine et al. (eds.), *Intelligent Transport Systems for Everyone's Mobility*, [https://doi.org/10.1007/978-981-13-7434-0\\_6](https://doi.org/10.1007/978-981-13-7434-0_6)



**Keywords** Driver arousal method · Physiological magnetic stimulation · Magneto-protonics principle

## 1 Introduction

In recent years, the number of occurrences of traffic fatal accidents tends to decrease due to advancement of preventive safety technology and collision safety technology of automobile system [1–5]. However, many traffic accidents caused by accidental driving typified by drowsy driving are still reported. On August 25, 2017, extremely serious accident was occurred in which 16 people were killed or injured on the Tokushima Expressway [6]. In accidents caused by drowsy driving, deceleration by brakes is not often performed immediately before a collision, so the impact at the time of a collision increases. Therefore, there is a high possibility that damage will be enormous. Considering such circumstances, in order to reduce the fatalities caused by traffic accidents, it is essential to prevent drowsy of drivers while driving.

Under such circumstances, research on techniques for evaluating drowsiness and detecting drowsy driving has been actively conducted. There are methods using bioinformation such as blinking, pupil/eye movement, heartbeat, pulse wave and electroencephalogram [7–11], and vehicle information such as steering angle and speed [12, 13]. In addition, many researches using warning sounds, vibrations, fragrances, etc. [14–16] have been conducted as a method to prevent drowsy driving, and some systems combining drowsy driving detection technology and prevention technology are put to practical use [17, 18].

The drowsy prevention technology proposed so far directly stimulates visual, auditory and tactile sensation. However, in these sensory stimulus arousal methods, “sleep rebound phenomenon” is caused, in which sleepiness induced again after temporary forced awakening becomes deeper drowsiness [19]. In view of this, we focused on the principle of bioactivation, Magneto-protonics principle [20, 21], proposed a novel awakening method applying this principle and continuously verified its effectiveness [19, 22–33]. As a result [32], valid driver arousal effect was confirmed for 10 subjects.

In the previous verifications, the effect of fatigue, the sequential effect of magnetic stimulation and the remaining time of the arousal effect were unknown in the case of conducting the verification experiment several times on the same day. In order to avoid these effects, experiments that apply magnetic stimulation and experiments that do not apply magnetic stimulation were conducted separately each day.

Therefore, in this verification, we conducted experiments on the presence or absence of magnetic stimulation during the same day, and newly examined the effect of ordering, residual effect and fatigue by experimental tasks. In addition, additional verification was carried out by further increasing the number of subjects, and the reliability of the driver arousal effect by the physiological magnetic stimulation was improved.

## 2 Drowsy Driving Prevention Based on Magneto-Protonics Principle

Organisms have been producing the energy necessary for daily activities by consuming adenosine triphosphate (hereinafter called “ATP”) in the body. When driving a vehicle, the driver must repeat muscle contraction and consumes energy generated by decomposing ATP into ADP. ATP is replenished by conversion from ADP while sleeping. Adenosine is a sleeping substance that increases as ATP decreases, and it has the property of stimulating the sleeping nerve as well as suppressing the activity of the arousal nerve [34].

When this principle is applied to the living body, the ability to produce ATP, which is a bioenergetic substance, improves in the inner membrane of mitochondria by activating protons in cell water. In other words, by applying the magnetic stimulation based on the Magneto-protonics principle to the driver, the ability of ATP generation in cells is enhanced and it is possible to suppress the decrease in the arousal degree of the driver. For the detailed mechanism of the Magneto-protonics principle, see Mohri et al. [20, 21].

## 3 Magnetic Stimulation System

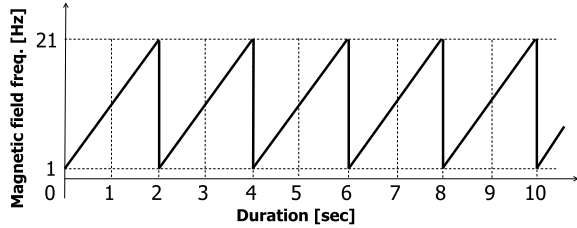
Verification experiments were conducted using a magnetic stimulation system with an electromagnetic coil (Helmholtz coil, size: 50 cm × 1.5 cm, direct current resistance: 56 Ω, number of turns: 50 turns) shown in Fig. 1, and an alternating current was supplied by the function generator (WF 1943 manufactured by NF Co.). Magnetic stimulation is applied to the driver from the electromagnetic coil disposed in the backrest portion of the driving simulator.

The magnetic field frequency was continuously and linearly swept from 1 to 21 Hz at 2 s intervals based on reference (Fig. 2) [32]. The magnetic field strength was set 600 mG at the center of the coil surface and 100 mG at 2 cm vertical from the center plane of the coil. We confirmed that the magnetic field frequency and the magnetic field strength are non-invasive to the human body from “ICNIRP Guidelines for limiting exposure to time-varying electric, magnetic, and electromagnetic fields (upto 300 GHz)” [35] defined by WHO-ICNIRP. This system enables a complete blind test on the presence or absence of magnetic stimulation.

**Fig. 1** Magnetic stimulation system with an electromagnetic coil



**Fig. 2** Output method of the magnetic field frequency



## 4 Evaluation Method of Arousal Degree by Electroencephalogram

### 4.1 Electroencephalogram Measurement Method

Electroencephalogram (hereinafter called “EEG”) was measured using Miniature DAQ Terminal intercross-410 manufactured by Intercross Co. (Fig. 3).

The probe electrode was attached to the parietal (C3, C4) and occipital region (O1, O2) according to electrodes of international 10–20 system [36], and the reference electrode was attached to the stable part of the right ear behind (Fig. 4). The sampling frequency was set to 1 kHz, and 50 Hz or more was cut off by a low-pass filter.

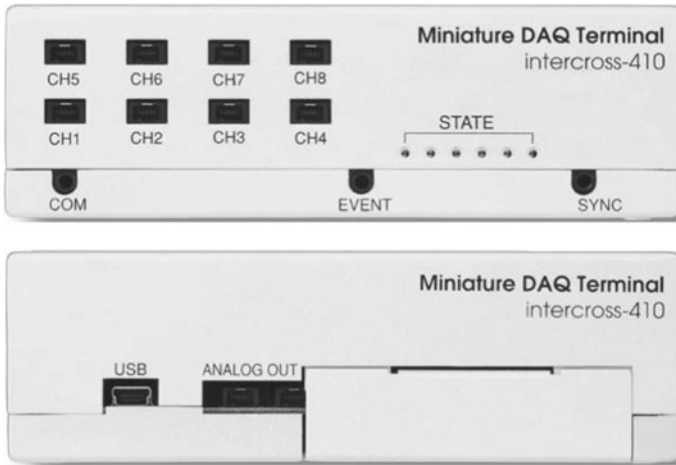
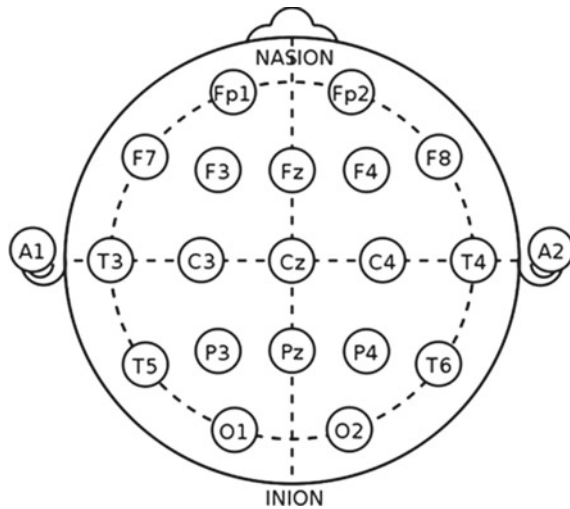


**Fig. 3** Miniature DAQ Terminal intercross-410 manufactured by Intercross Co

**Fig. 4** Electrode placement based on international 10–20 system



**4.2 Evaluation Method by EEG**

Partial Overall method [37] was adopted as an analysis method of EEG. The EEG was divided into four bands of 0.5 Hz to 4 Hz, 4 Hz to 8 Hz, 8 Hz to 13 Hz and 13 Hz to 30 Hz, and were defined as a  $\delta$  band, a  $\theta$  band, an  $\alpha$  band and a  $\beta$  band based on international 10–20 system [36], respectively. In this study,  $\alpha$  and  $\beta$  waves appearing during awakening were treated as “arousal EEG”, and  $\delta$  and  $\theta$  waves appearing during sleep were treated as “sleep EEG”. The PO values of each band were defined as  $\alpha_{po}$ ,  $\beta_{po}$ ,  $\delta_{po}$  and  $\theta_{po}$ , respectively. In order to evaluate the arousal degree by the ratio of

the arousal EEG to the sleep EEG, the arousal index (hereinafter called “AI”) (1) was calculated based on the PO value of the EEG.

$$AI = (\alpha_{po} + \beta_{po}) / (\delta_{po} + \theta_{po}) \quad (1)$$

The arousal index ratio (hereinafter called “AR”) (2) which is the ratio of the arousal index ( $AI_1$ ) for 3 min before driving to the arousal index ( $AI_2$ ) for 3 min after driving was calculated. The arousal effect was verified by the transition of the arousal index before and after the driving.

$$AR = AI_2 / AI_1 \quad (2)$$

For details on the evaluation of arousal degree based on EEG, see Mohri et al. [29, 30].

## 5 Verification of Influence on Arousal Degree by Conducting Experiment on the Same Day

In this verification, we examined the effects of fatigue by experimental tasks when subjects performed multiple experiments on the same day, the order effect of the presence or absence of magnetic stimulation and the remaining time of the arousal effect.

By conducting both experiments which apply magnetic stimulation twice in succession and experiment which does not apply it twice in succession, we examined the influence of fatigue by experimental task. In addition, we conducted experiments to replace the presence or absence of magnetic stimulation in the first and second experiments, and also verified the remaining effect and the order effect by experimental procedure.

### 5.1 Experimental Method

#### Experimental Conditions

The subjects were 10 men in their twenties who have a driver’s license. In addition, in order to unify the condition of subjects on the day of the experiment, the following conditions were set.

- Subjects get a sleep of 6 h or more the day before the experiment.
- Conduct an experiment 1 h after eating.
- Subjects did not take stimulants such as coffee, gum, and smoking on the day of the experiment.

- To eliminate the placebo effect, the experiments were carried out for subjects with a complete blind test that does not convey any information on the presence or absence of magnetic stimulation.

When the sleeping time on the day before the experiment is less than 4 h, the occurrence rate of the accident due to drowsy driving increases as sleeping time decreases. On the other hand, when the sleeping time was 6 h or more, the incidence of the accident did not change, so the sleeping time of the subject on the day before the experiment was set to 6 h or more [38]. In addition, in order to consider the induction of drowsiness due to satiety, the experiment start time was unified after 1 h after meals. Furthermore, since irritants such as coffee, gum, smoking etc., may affect the arousal degree, subjects were asked to refrain from taking intake. This study was conducted with the approval of the ethics review committee of Meijo University. Before the experiment, the contents of experiment were explained to the subject by document and verbally, and informed consent was got.

### **Experiment Procedure**

The following four experiments were conducted using a driving simulator.

- Experiment 1: Experiment that apply magnetic stimulation twice in succession were performed.
- Experiment 2: Experiment that does not apply magnetic stimulation twice in succession were performed.
- Experiment 3: Experiments that apply magnetic stimulation were performed in the first half, and experiments without magnetic stimulation were performed in the second half.
- Experiment 4: Experiments without magnetic stimulation were performed in the first half, and experiments that apply magnetic stimulation were performed in the second half

The above experiments were conducted in the following procedure.

1. Apply magnetic stimulation to the driver for 30 min before driving. In the case of not applying magnetic stimulation, setting the magnetic field intensity to 0.
2. Measure EEG for 3 min before driving ( $AI_1$ ).
3. Subjects drive a course simulating a night expressway for 20 min with magnetic stimulation. In the case of not applying magnetic stimulation, setting the magnetic field intensity to 0.
4. Measure EEG for 3 min after driving ( $AI_2$ ).
5. After a 30-minute break, a second experiment was conducted in experimental procedures 1 through 4.

Between the first half of the experiment and the second half of the experiment, we asked subjects to refrain from stimulant ingestion and nap. Based on reference [32], in order to obtain the arousal effect by magnetic stimulation, preliminary stimulation time is required about 30 min, so the magnetic stimulation time of 30 min was set in experimental procedure 1. For comparative evaluation of arousal effect, EEG was measured for 3 min before and after experimental procedure 3.

### 5.2 Experimental Result

Figure 5 shows the result of experiment 1 for 10 subjects. In this result, the AR of 9 out of 10 subjects was higher in the first half experiment than the second half experiment.

In addition, Fig. 6 shows the comparison result of the average values of the AR of 10 subjects in experiment 1. In this result, the AR in the second half of the experiment was 14.1% lower on average than the first half experiment. As a result of significant difference test by Wilcoxon signed-rank test, a significant difference was confirmed with a significance level of less than 5% ( $P = 0.0367$ ).

Figure 7 shows the result of experiment 2 for 10 subjects. In this result, the AR of all 10 subjects was higher in the first half experiment than the second half experiment.

In addition, Fig. 8 shows the comparison result of the average values of the AR of 10 subjects in experiment 2. In this result, the AR in the second half of the experiment was 20.1% lower on average than the first half experiment. As a result of significant difference test by Wilcoxon signed-rank test, a significant difference was confirmed with a significance level of less than 1% ( $P = 0.0051$ ).

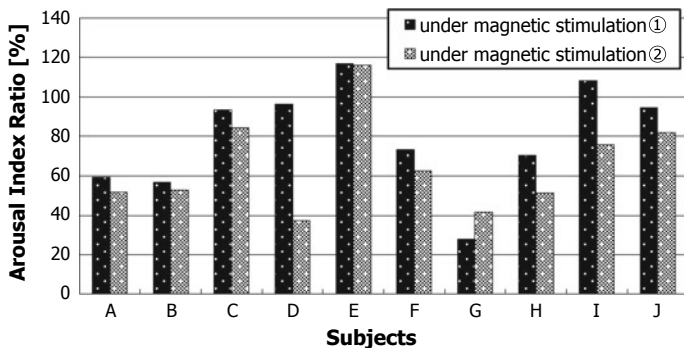
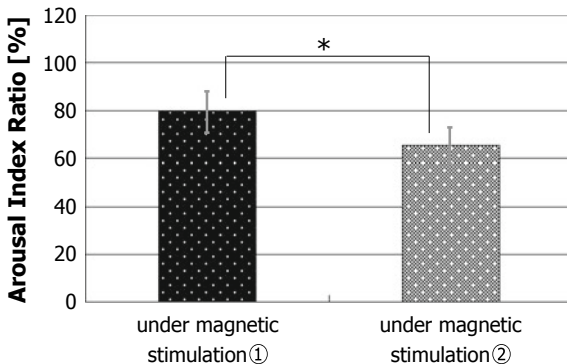


Fig. 5 AR of the 10 subjects in experiment 1

Fig. 6 Average AR of the 10 subjects in experiment 1



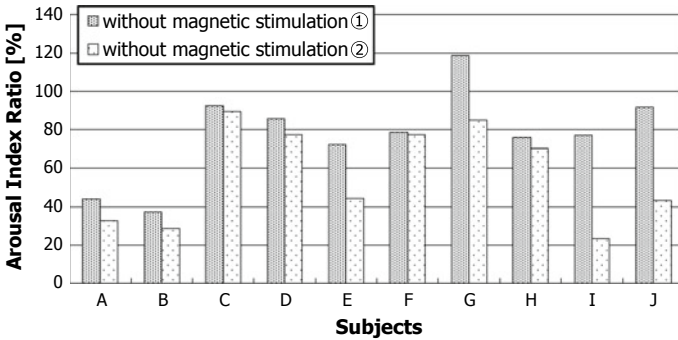


Fig. 7 AR of the 10 subjects in experiment 2

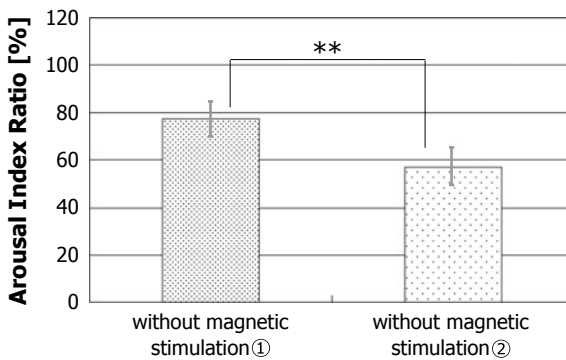


Fig. 8 Average AR of the 10 subjects in experiment 2

Figure 9 shows the result of experiment 3 for 10 subjects. In this result, the AR of all 10 subjects was higher in the experiment that applies the magnetic stimulation than the experiment which does not apply magnetic stimulation.

In addition, Fig. 10 shows the comparison result of the average values of the AR of 10 subjects in experiment 3. In this result, the AR in the second half of the experiment was 33.4% lower on average than the first half experiment. As a result of significant difference test by Wilcoxon signed-rank test, a significant difference was confirmed with a significance level of less than 1% ( $P = 0.0051$ ).

Figure 11 shows the result of experiment 4 for 10 subjects. In this result, the AR of 5 out of 10 subjects was higher in the experiment that applies the magnetic stimulation than the experiment which does not apply magnetic stimulation.

In addition, Fig. 12 shows the comparison result of the average values of the AR of 10 subjects in experiment 4. In this result, the AR in the second half of the experiment was 2.5% lower on average than the first half experiment. As a result of significant difference test by Wilcoxon signed-rank test, there is not a significant difference.



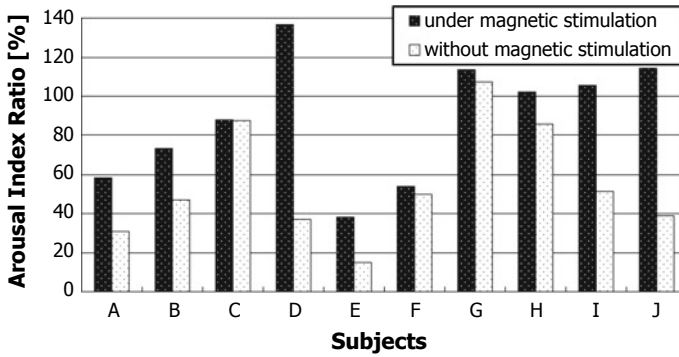


Fig. 9 AR of the 10 subjects in experiment 3

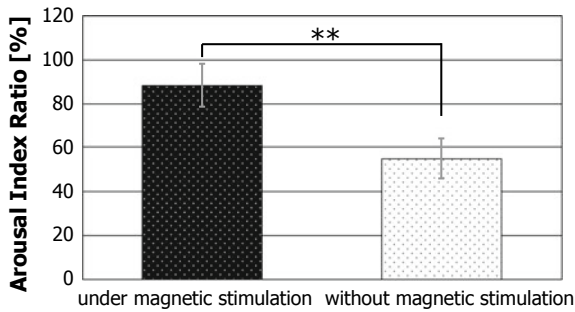


Fig. 10 Average of the 10 subjects in experiment 3

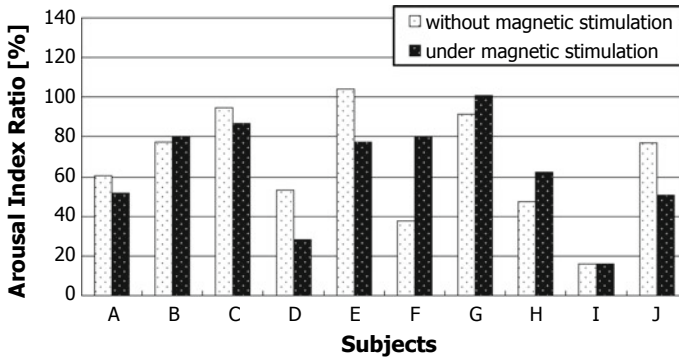
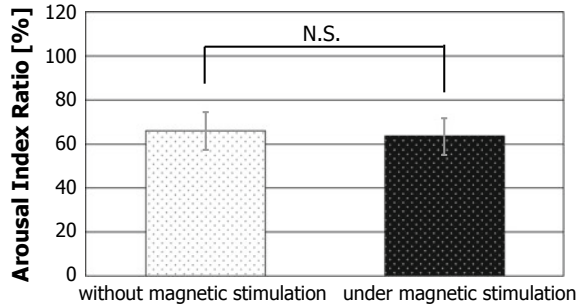


Fig. 11 AR of the 10 subjects in experiment 4

**Fig. 12** Average AR of the 10 subjects in experiment 4



### 5.3 Consideration

Based on the results of Experiment 1 and Experiment 2, it was confirmed that the average value of AR in the second experiment was significantly lower than AR in the first experiment, regardless of the presence or absence of magnetic stimulation. From these results, it was confirmed that when two experiments were conducted on the same day, the AR of the second half experiment decreased as a result of the fatigue caused by the experiment task in the first half. On the other hand, in Experiment 1, the average value of AR in the second experiment decreased by 20.1%, whereas in Experiment 2, the decrease in AR was suppressed as 14.1%. Furthermore, in Experiment 3, the average value of AR in the second experiment decreased by 33.4%, whereas in Experiment 4, the decrease in AR was suppressed as 2.5%. From these results, the arousal effect by magnetic stimulation was also confirmed in this verification experiment.

Furthermore, in the result of Experiment 3, despite the fact that the magnetic stimulation was applied in the first half as compared with Experiment 1, the AR of the second half experiment was greatly reduced. In this result, it was suggested that the arousal effect remaining time by applying the magnetic stimulation may be less than 1 h.

From the above results, the arousal effect by the magnetic stimulation was confirmed, suggesting the possibility that the remaining time is less than 1 h. However, when conducting two experiments on the same day, the influence of fatigue by experimental task was also confirmed. Therefore, it is considered that verification experiments on driver arousal effect in the presence or absence of magnetic stimulation should not be done on the same day but should be done separately.

## 6 Verification of Driver Arousal Effect Using Magnetic Stimulation

Based on the results of the verification in the previous chapter, it became clear that the verification experiment of arousal effect on the presence or absence of the magnetic stimulation need to be conducted separately and the rationality of the verification experiment so far was obtained. In this chapter, we further conducted experiment by increasing the number of subjects, and tried to improve the reliability of driver arousal method using physiological magnetic stimulation.

### 6.1 *Experimental Method*

#### **Experimental Conditions**

The experimental conditions were the same as those shown in Sect. 5.1. In this verification, the subjects were 10 men, and the experimental procedure is as follows. Experiments that apply magnetic stimulation and experiments that do not apply magnetic stimulation were conducted separately each day.

#### **Experimental Procedure**

Experiment was conducted in the following procedure.

1. Apply magnetic stimulation to the driver for 30 min before driving. In the case of not applying magnetic stimulation, setting the magnetic field intensity to 0.
2. Measure EEG for 3 min before driving ( $AI_1$ ).
3. Subjects drive a course simulating a night expressway for 20 min with magnetic stimulation. In the case of not applying magnetic stimulation, setting the magnetic field intensity to 0.
4. Measure EEG for 3 min after driving ( $AI_2$ ).

### 6.2 *Experimental Result*

Figure 13 shows the result for 10 subjects we have examined so far [32]. In this result, the AR of 9 out of 10 subjects was higher in the experiment that applies the magnetic stimulation than the experiment which does not apply magnetic stimulation. As a result of significant difference test by Wilcoxon signed-rank test, a significant difference was confirmed with a significance level of less than 1% ( $P = 0.000934$ ).

Figure 14 shows the experimental results of 10 subjects newly obtained in this additional verification. In this result, the AR of all 10 subjects was higher in the experiment that applies the magnetic stimulation than the experiment which does not apply magnetic stimulation. As a result of significant difference test by Wilcoxon

signed-rank test, a significant difference was confirmed with a significance level of less than 1% ( $P = 0.00506$ ).

Figure 15 shows the average value of AR of 20 subjects when magnetic stimulation is not applied and when magnetic stimulation of 1 to 21 Hz is applied. In this result, compared with the case without magnetic stimulation, the average value of AR when applying magnetic stimulation was 29.5% higher. In addition, as a result of significant difference test by Wilcoxon signed-rank test, a significant difference was confirmed with a significance level of less than 1% ( $P = 0.00014$ ).

### 6.3 Consideration

In the previous verifications, there were 9 out of 10 subjects who got higher AR in the case of applying magnetic stimulation than in the case without applying magnetic stimulation. As a result of additional verification this time, there were all 10 subjects

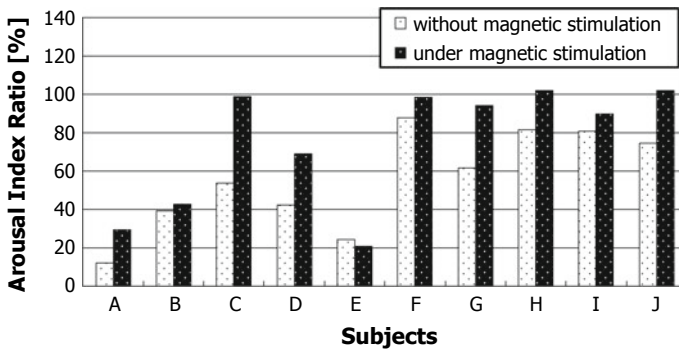


Fig. 13 AR of the 10 subjects obtained in the previous study

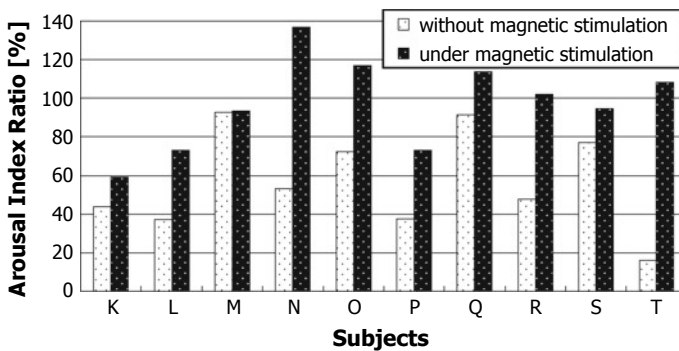
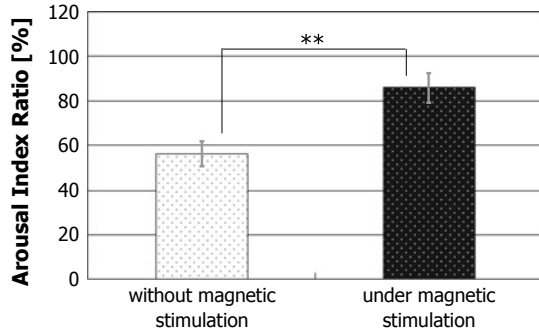


Fig. 14 AR of the 10 subjects obtained in this verification

**Fig. 15** Average AR of 20 subjects



who got higher AR in the case of applying magnetic stimulation than in the case without applying magnetic stimulation. Even when these results were integrated, and the number of subjects was increased to 20, a tendency that the AR increased when the magnetic stimulation was applied was similarly obtained, and a significant difference was also confirmed. Based on these results, we believe that the reliability of the driver arousal method by magnetic stimulation has further increased.

## 7 Conclusion

In this study, we conducted experiments on the presence or absence of magnetic stimulation on the same day and newly verified the order effect, residual effect and the effect of fatigue by experimental tasks. In addition, by further increasing the number of subjects, additional verification experiments were conducted to improve the reliability of driver arousal effect by physiological magnetic stimulation.

Experimental results on the presence or absence of magnetic stimulation during the same day confirmed the arousal effect by magnetic stimulation and suggested that the remaining time of the arousal effect may be less than 1 h. However, when conducting two experiments on the same day, the influence of fatigue caused by the experimental task was also confirmed, so we decided to increase the number of subjects and verify them in the same way as in previous verification experiments. As a result, even in the case of increasing the number of subjects, the effectiveness of the driver arousal effect by magnetic stimulation was confirmed.

We will continue to prove that the driver's arousal effect by magnetic stimulation is obtained based on the Magneto-protonics principle. In addition, in order to confirm whether there is a frequency band particularly effective for driver arousal, we will examine the driver arousal effect when narrowing the range of the theoretical frequency band.

## References

1. Usui, S., Nomura, N., Kumagai, H., Sekine, H.: Development of improvements to driver assistance system “EyeSight” for reduction of traffic accidents. *J. Soc. Appl. Electromagn. Mech.* **25**(4), 383–389 (2017)
2. Kuwahara, T., Iguchi, Y., Hamaue, I., Yamamoto, S.: Development of driver control function. *Fujitsu Ten Tech. Rep.* **33**(1), 9–15 (2015)
3. Matsuzaki, T., Miyazaki, T., Mori, O., Iwanuma, T., Yajima, M.: Practical application of hot stamping patchwork technology for crash safety and weight reduction. *Subaru Tech. Rev.* **41**, 109–113 (2014)
4. Hirai, K., Koyama, K., Goto, T., Kume, T.: Evolution of Mazda advanced safety technology “i-ACTIVSENSE”. *Maz. Tech. Rev.* **34**, 157–162 (2017)
5. National Police Agency Traffic Bureau: The occurrence situation of traffic accident in Heisei 29 (2018)
6. Tokushima way 16 people casualty accident. [http://www.topics.or.jp/localNews/news/2017/08/2017\\_15037889124309.html](http://www.topics.or.jp/localNews/news/2017/08/2017_15037889124309.html)
7. Naito, K., Sugimoto, D., Takano, H., Kojima, H., Kawamura, H., Nakamura, K.: Development of Real-time Doze Detection Method Using Blink Bursts and Isolated Blinks. *IEICE Tech. Rep. (MBE)* **113**(61), 1–5 (2013)
8. Wakui, H., Hirata, Y.: Eye movements and pupil fluctuation reflecting alertness and their neuronal mechanisms. *Jpn. Neural Netw. Soc.* **21**(1), 20–31 (2014)
9. Sano, S., Tomimori, H., Masuda, Y., Odagiri, J., Kato, H., Nakano, Y.: Development of drowsiness detection system using ear clip-type sensor. In: *DICOMO 2014, Japan*, pp. 24–29 (2014)
10. Nakamura, T., Nakamura, S., Terada, M., Hashimoto, H.: Signal Processing Method for Car-mounted Vital Signs Monitor System. *Trans. Soc. Instrum. Control. Eng.* **52**(4), 228–233 (2016)
11. Oyama, H., Arakawa, T.: Development of warning system that estimates driver’s arousal level based on unsteady driving phenomenon and evaluation of driver’s condition based on EEG. *J. Soc. Automot. Eng. Jpn.* **52**(12), 89–94 (2004)
12. Kume, T., Naito, T., Ishida, K., Kawai, S., Matsunaga, S., Nishii, K., Kitajima, H.: Development of absentminded state detection and resolution method using vehicle equipments. *Soc. Automot. Eng. Jpn.* **45**(3), 567–572 (2014)
13. Saigo, S., Raksinchareonsak, P., Nagai, M.: Investigation on individual adaptive driver state diagnosis method based on driver model in car-following situation. *Trans. JSME* **80**(815), 1–17 (2014)
14. Ebe, K., Kimura, K., Inagaki, H., Doi, S.: Characteristics of alarms and perceived urgency: a proposal of urgency-map. *Soc. Automot. Eng. Jpn.* **56**(3), 27–32 (2002)
15. Okuwa, M., Kurahashi, T., Fujieda, N., Tsuda, T., Hattori, A.: A study of tactile driver interface using seat vibrations. *Soc. Automot. Eng. Jpn.* **39**(6), 59–64 (2008)
16. Kakamu, Y., Yoshikawa, M., Shimizu, T., Yanagida, Y., Nakano, T., Yamamoto, S., Yamada, M.: Study on awakening effect by fragrance presentation against drowsy driving and construction of fragrance presentation system. *IEEJ Trans. EIS* **131**(2), 349–354 (2011)
17. FUJITSU JOURNAL: Wearable sensor supports drivers by detecting drowsiness in advance. <http://journal.jp.fujitsu.com/en/2015/02/03/01/>
18. BOSCH: Bosch Driver Drowsiness Detection, Press release 29 Mar 2012. <https://www.bosch-press.de/pressportal/de/en/bosch-driver-drowsiness-detection-41616.html>
19. Masuda, K., Yamazaki, H., Kawasumi, M., Nakano, T., Yamamoto, S., Yamada, M.: Verification of sleep rebound effect based on the electroencephalogram. In: *ITS Symposium 2012, 1-D-07, Japan*, pp. 241–245 (2012)
20. Mohri, K., Fukushima, M., Matsumoto, M.: Gradual decrease of electric resistivity in water triggered by Milli-Gauss low frequency pulsed magnetic field. *Trans. Mag. Soc. Jpn.* **1**(1), 22–26 (2001)
21. Mohri, K., Fukushima, M.: Milligauss magnetic field triggering reliable self-organization of water with long-range ordered proton transport through cyclotron resonance. *IEEE Trans. Magn.* **39**(5), 3328–3330 (2003)

22. Mohri, K., Uchiyama, T., Yamada, M., Watanabe, T., Inden, Y., Kato, T., Iwata, S.: Arousal effect of physiological magnetic stimulation on elder person's spine for prevention of drowsiness during car driving. *IEEE Trans. Magn.* **47**(10), 3066–3069 (2011)
23. Mohri, K., Uchiyama, T., Yamada, M., Mohri, Y., Endo, K., Suzuki, T., Inden, Y.: Physiological magnetic stimulation for arousal of elderly car driving evaluated with electro-encephalogram and spine magnetic field. *IEEE Trans. Magn.* **48**(11), 3505–3508 (2012)
24. Sakai, K., Kawasumi, M., Nakano, T., Yamada, M., Mohri, Y., Mohri, K., Uchiyama, T.: Experimental Verification of Arousal Effect by Spinal Magnetic Stimulation on Driver, DIA2012, I-15, Japan, pp. 172–175 (2012)
25. Kato, W., Mohri, Y., Nakano, T., Yamada, M., Mohri, K., Uchiyama, T.: An Experimental Verification of Arousal Effect for Car Drivers by the Magneto-Protonics Principle, National Convention Record I.E.E., Japan, pp. 121–122 (2013)
26. Kato, W., Ogawa, Y., Mohri, Y., Nakano, T., Yamada, M., Mohri, K.: A new arousal method for vehicle drivers using physiological magnetic stimulation and EEG measurements, Tokai-Section Joint Conference 2013, Po1-30, Japan (2013)
27. M. Kawaguchi, S. Kojima, Y. Mohri, T. Nakano, M. Yamada, K. Mohri: An examination on the practical application of driver arousal technique by Physiological Magnetic Stimulation, ITS Symposium 2014, 2-2B-04, Japan (2014)
28. Y. Hisada, M. Kawaguchi, S. Kojima, Y. Mohri, T. Nakano, M. Yamada, K. Mohri: Magnetic Field Frequency Dependence on the Driver Arousal Method by Physiological Magnetic Stimulation, ITS Symposium 2015, 2-2A-02, Japan (2015)
29. Mohri, Y., Yamada, M., Uchiyama, T., Mohri, K.: Arousal effect of alternating distributed static magnetic field stimulation on car driver's spine evaluated with electro-encephalogram and back magneto-cardiogram. *IEEJ Trans. EIS* **135**(1), 52–57 (2015)
30. Mohri, Y., Kawaguchi, M., Kojima, S., Yamada, M., Nakano, T., Mohri, K.: Arousal retention effect of magnetic stimulation to car drivers preventing drowsy driving without sleep rebound. *IEEJ Trans. EIS* **136**(3), 383–389 (2016)
31. Takegawa, S., Hisada, Y., Mohri, Y., Nakano, T., Yamada, M., Mohri, K.: Examination on Effective Frequency for Driver Arousal Technique with Physiological Magnetic Stimulation, ITS Symposium 2016, 1-A-04, Japan (2016)
32. Takegawa, S., Hisada, Y., Mohri, Y., Nakano, T., Mohri, K., Yamada, M.: Examination of arousal effect by driving simulator system equipped with arousal technique by magnetic stimulation. The IEICE General Conference, Proceedings of the Student Poster Session, Japan, p. 151 (2017)
33. Tsukada, M., Takegawa, S., Hisada, Y., Mohri, Y., Nakano, T., Mohri, K., Yamada, M.: Examination on Magnetic Field Frequency Dependence for the Driver Arousal Technique with Physiological Magnetic Stimulation, The IEICE General Conference, Proceedings of the Student Poster Session, Japan, p. 155 (2017)
34. Urade, Y.: Adenosine as a sleeping substance. *J. Health Phys. Educ. Recreat* **60**(12), 805–811 (2010). Kyorin Shoin
35. ICNIRP Publication: ICNIRP Guidelines for limiting exposure to time-varying electric, magnetic, and electromagnetic fields (upto 300 GHz). *Health Phys.* **77**(4), 494–522 (1998)
36. Noda, A., Koike, Y.: Polysomnography. *Med. Biol. Eng.* **46**(2), 134–143 (2008)
37. Fujisawa, K., Mizuno, T., Omori, Y., Miyaji, K., Mizukami, K.: Information processing of EEG data on spatial field distributions. *Res. J. Jin-Ai Univ.* **1**, 71–83 (2002)
38. Institute for Traffic Accident Research and Data Analysis: Investigation of Accidents Caused by Degradation of Concentration of Drivers, Traffic Accident Investigation and Analysis Report (2008)

# Study on Simultaneous-Action Discrimination System Using the Neural Network



Takahiko Murayama, Masato Ito, Hatsuo Yamasaki, Tomoaki Nakano and Muneo Yamada

**Abstract** Along with the rapid spread of a smartphones, accidents caused by “simultaneous-walking” which is walking while operating a smartphone and “simultaneous-cycling” which is cycling while operating a smartphone has become a social problem. Our research group has been studying algorithms to detect simultaneous-walking and simultaneous-cycling using the smartphone itself, and proposed a method to switch each detection algorithm based on GPS speed. However, in an environment that could not obtain the GPS information, there were problems that cannot be used this conventional method and the detection accuracy changes greatly depending on the surrounding environment. In this study, our research group suggests a discrimination method of simultaneous-walking and simultaneous-cycling which is robust against the above problem by learning tri-axial acceleration sensor information of a smartphone with a neural network.

**Keywords** Simultaneous-action · Smartphone · Neural network

---

T. Murayama (✉) · M. Ito

Division of Information Engineering, Graduate School of Science and Technology, Meijo University, 1-501, Shiogamaguchi, Tempaku-ku, Nagoya, Aichi 468-8502, Japan  
e-mail: [183426021@ccmailg.meijo-u.ac.jp](mailto:183426021@ccmailg.meijo-u.ac.jp)

M. Ito

e-mail: [173426004@ccalumni.meijo-u.ac.jp](mailto:173426004@ccalumni.meijo-u.ac.jp)

H. Yamasaki

Faculty of Science and Technology, Department of Electrical and Electronic Engineering, Meijo University, Nagoya, Japan  
e-mail: [yamasaki@meijo-u.ac.jp](mailto:yamasaki@meijo-u.ac.jp)

T. Nakano · M. Yamada

Faculty of Science and Technology, Department of Information Engineering, Meijo University, Nagoya, Japan  
e-mail: [tnakano@meijo-u.ac.jp](mailto:tnakano@meijo-u.ac.jp)

M. Yamada

e-mail: [myamada@meijo-u.ac.jp](mailto:myamada@meijo-u.ac.jp)

© Springer Nature Singapore Pte Ltd. 2019

T. Mine et al. (eds.), *Intelligent Transport Systems for Everyone's Mobility*, [https://doi.org/10.1007/978-981-13-7434-0\\_7](https://doi.org/10.1007/978-981-13-7434-0_7)



## 1 Introduction

Simultaneous-walking which is walking while operating a smartphone (hereinafter referred to as SP) and Simultaneous-cycling which is cycling while operating a SP is a cause of serious accidents. Actually, many accidents caused by simultaneous-action are occurring all over the world [1–9]. In 2016 Shinagawa Tokyo, the woman felled station home while simultaneous-walking. Thereafter she was hit by a train and was dead [1]. In addition, in 2017 Kawasaki Tokyo, an accident that a woman at the simultaneous-cycling collides with an elderly pedestrian and caused her to die has also occurred [2]. As described above, simultaneous-action has the danger of causing serious fatal accidents and it is necessary to take countermeasures immediately. Our research group has studied the detection method of simultaneous-action using a SP itself [10–12] and the warning method to a SP user [13]. However, in the conventional method of detecting simultaneous-action, since a GPS sensor was used for discriminate between walking and cycling, there were problems such as a method cannot be used in an environment where a GPS sensor does not work and the detection accuracy greatly changes depending on the environment. In this study, in order to solve the above problem, a method of improving simultaneous-action discrimination accuracy without using GPS information was studied by a neural network (hereinafter referred to as NN) that learned information of tri-axial acceleration sensor information of a SP.

## 2 Conventional Study on Simultaneous-Action

Many studies for identifying the status of a SP users by using various sensor devices mounted on the SP have been reported so far [13–17]. In the research by Kodama et al. [13], in view of the fact that SP users cannot stop simultaneous-walking despite recognizing the risk of it, a system that supports simultaneous-walking as safe as possible was suggested. Specifically, the degree of danger is calculated based on the distance to the object close to the SP user, the relative speed, etc., and the degree of danger and the direction are displayed on the upper part of the SP screen (risk display area). Then, the color of the risk display area is changed from blue (safety) to red (danger) according to the calculated degree of danger, and furthermore, the discoloration point is changed according to the direction in which the object exists. In addition, to avoid impairing the functions of existing a SP, overlay method was employed for risk display. The distance from the user to the adjacent object is acquired not by using the SP sensor but by using the range image sensor CamBoard pico flexx. Attach this sensor to the waist so as to be perpendicular to the ground, and photograph the entire surface in the horizontal direction with the ground. The range image sensor is connected to the laptop on which the degree of danger calculation program is activated by a USB connection. During the verification experiment, the laptop is stored in the backpack. As a result of the evaluation experiment by two

subjects, the collision rate with pedestrians was 13.3 [%] when not assisting by the proposed system during simultaneous-walking. On the other hand, by supporting with the proposed system, the collision rate decreased to 2.2 [%]. However, since the proposed system requires sensors other than the SP terminal, the user's satisfaction level was low. As future studies, installing a range image sensor on a SP case and studying another danger notification method was planned.

In the research by Yoshida et al. [14], a system that detects the collision possibility by GPS sensor mounted on a SP and gives warning to a SP user was proposed for the purpose of preventing collision accident between bicycle and pedestrian. In this system, the position of the bicycle and the pedestrian are respectively measured by the GPS, and the position information is shared with each other through the Bluetooth communication. Furthermore, the distance from the position of the other party that received the position information to its own position is calculated, and if the distance is equal to or smaller than the prescribed threshold value, a warning is issued. However, since positional information obtained from a GPS generally causes errors due to various factors, when measurement errors are large, it is necessary to acquire GPS information a plurality of times. As a result of verification experiment with the GPS error tolerance set to 16.9 m and warning distance set to 30 m, the result that collision between pedestrian and bicycle can be avoided with accuracy of 100 [%] has been obtained. As the warning distance becomes longer, the warning will be issued at an early stage. Therefore, considering usability in a real environment, there is concern about the troublesome warning and the reliability of warning. Since "detection error" and "warning delay" are in a trade-off relationship, examination of the optimum ratio of both is cited as a future study.

In the above-mentioned method of Kodama et al., installation of a range image sensor in addition to the SP terminal is required, so practical problems such as system cost and troublesome mounting are considered to be significant. On the other hand, in the method of Yoshida et al., It is important to be able to share location information by communication, so further examination and verification of the communication method with multiple SPs and the influence of radio wave interference by obstacles is considered to be essential. More than anything, with this method, collision with a general pedestrian who does not own the SP cannot be avoided. In this study, we aim to realize a system that can prevent accidents by discriminating simultaneous-action using only the sensors installed in a SP and giving warnings to the SP user.

### **3 Conventional Simultaneous-Action Detection**

#### ***3.1 Definition of Simultaneous-Action***

In this study, the state where the SP operation and the movement operation are simultaneously performed was defined as "simultaneous-action". The state in which SP operation and walking are performed at the same time was defined as "simultaneous-

walking”. The state in which SP operation and cycling are performed at the same time was defined as “simultaneous-cycling”. On the other hand, the walking state without SP operation was defined as “non-simultaneous-walking”. Likewise, the cycling state without SP operation was defined as “non-simultaneous-cycling”. During non-simultaneous-walking or non-simultaneous-cycling, the SP was assumed to be stored in the user’s pants pocket. A state in which the SP is operated without moving operation was defined as “stationary-state”. In our previous studies, we focused on this feature and proposed a method to detect it as simultaneous-action when moving operation and SP operation are simultaneously detected.

### ***3.2 Detection of the Movement While Simultaneous-Action***

The movement behavior of the SP user is detected by using a tri-axial acceleration sensor that is standard installed in the SP. Since the characteristics of acceleration in simultaneous-walking and simultaneous-cycling are different, the movement state is discriminated on the basis of the moving speed of the SP measured by the GPS and each operation is detected by applying each detection algorithm. The detection method of simultaneous-walking and simultaneous-cycling are explained below.

### ***3.3 Detection of Simultaneous-Walking***

During simultaneous-walking, the SP was stabilized more than non-simultaneous-walking because the shaking of the SP accompanying walking is absorbed by the operator’s arm. Figure 1 show the time series data of tri-axial acceleration scalar values of simultaneous-walking. And Fig. 2 show the time series data of tri-axial acceleration scalar values of non-simultaneous-walking. In Figs. 1 and 2, significant differences in acceleration amplitude and frequency can be confirmed between simultaneous-walking and non-simultaneous-walking. Therefore, simultaneous-walking can be detected by setting thresholds for the amplitude and frequency of acceleration.

#### **3.3.1 Detection of Simultaneous-Cycling**

As with simultaneous-walking, even during simultaneous-cycling, the swing of the SP accompanying cycling is absorbed by the operator’s arm. However, when cycling, the left and right wobbling due to steering wheel operation was reflected in the swing of the SP, so the stable periodicity of the acceleration was lost. Therefore, we focused on the variance value as the feature quantity instead of the amplitude and frequency of the acceleration scalar value. Figure 3 show the variance value of the tri-axial acceleration scalar value for simultaneous-cycling. And Fig. 4 show the variance value of

**Fig. 1** Time series behaviors of acceleration scalar value of simultaneous-walking

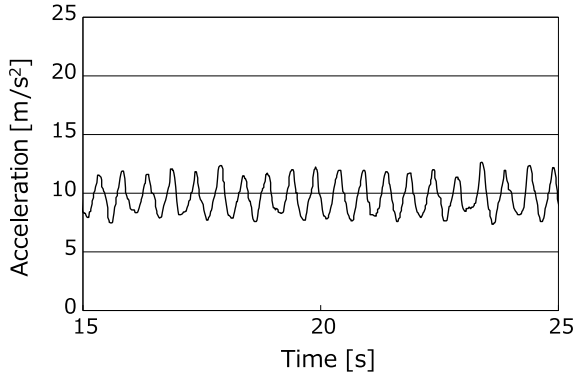


**Fig. 2** Time series behaviors of acceleration scalar value of non-simultaneous-walking

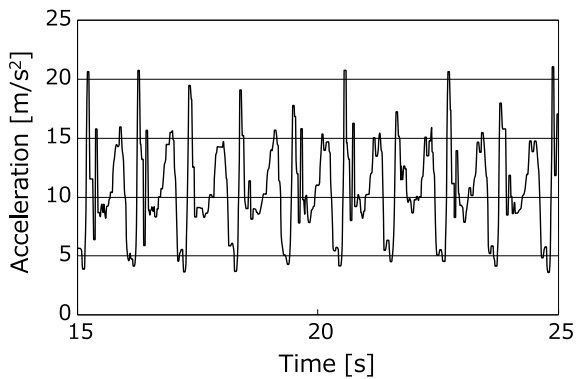
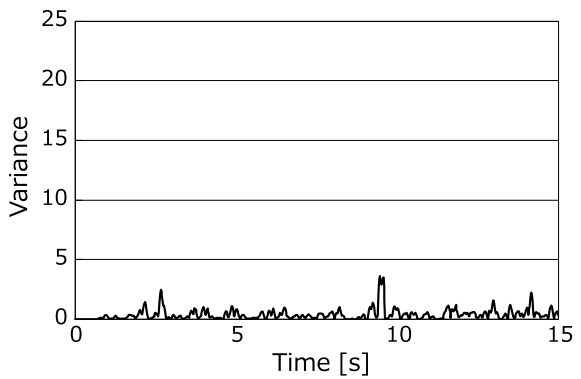
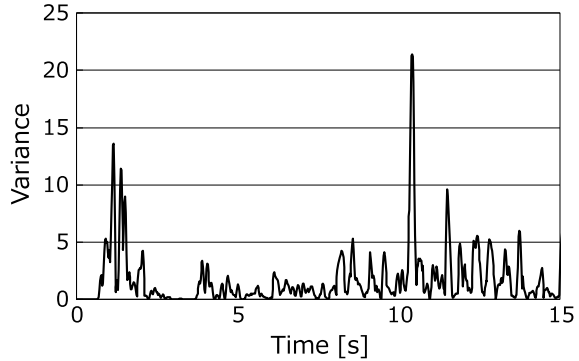


**Fig. 3** Time series behaviors of variance of acceleration scalar value of simultaneous-cycling



the tri-axial acceleration scalar value for non-simultaneous-cycling. In Figs. 3 and 4, between simultaneous-cycling and non-simultaneous-cycling, remarkable difference can be seen in the variance value of the acceleration scalar value. Therefore, simultaneous-cycling can be detected by setting thresholds for variance value.

**Fig. 4** Time series behaviors of variance of acceleration scalar value of non-simultaneous-cycling



### 3.4 Detection of SP Operation

The SP operation detection is based on the following three elements, and when two or more elements were detected, it was determined as SP operation.

- Detection of touch event of the SP screen by touch sensor
- Screen gaze detection by camera image analysis
- Detection of tilting angle of the SP by angle sensor.

## 4 Discrimination of Simultaneous-Action Using the Neural Network

In the conventional method that was explained Sect. 3, since the moving state was discriminated using GPS speed, there was a problem such as the method cannot be used in an environment where a GPS sensor does not work. In this study, we proposed the discrimination method of each simultaneous-action by the NN that was learned acceleration data without using a GPS sensor. In simultaneous-action, since a SP screen was fixed in order to gaze on a SP screen, the high frequency component of the acceleration data tends to be small. Also, a tri-axial acceleration components shows the attitude of a SP, which can discriminate whether simultaneous-action or not. For these reasons, we studied a method to discriminate simultaneous-action by the NN learning tri-axial acceleration data. The definition of input/output data and the structure of the network are explained below.

#### 4.1 Input/Output Data

The input data is the acceleration frequency spectrum (Fig. 5) calculated from the tri-axial acceleration components by FFT and the acceleration average value (Fig. 6) of the tri-axial acceleration components. The sampling frequency was 50 Hz, and the number of sampling points was 256 points. The number of input data of the acceleration frequency spectrum was total of 378 points which 126 points excluding near zero frequency calculated from x axis component, y axis component and z axis component respectively. The number of input data of the acceleration average value is three components of x axis, y axis and z axis. Therefore, the total number of input data to NN was 381 points. The output is the likelihood of five states of stationary-state, simultaneous-walking, non-simultaneous-walking, simultaneous-cycling and non-simultaneous-cycling.

#### 4.2 The Network Structure

The NN structure was the three-layer hierarchical (Fig. 7), with 381 units for the input layer and 5 units for the output layer. Since the determination of the number of hidden layer units and the learning times leads to improvement in expressive ability and generalization ability of a NN [18], these values have studied by preliminary verification. As a result, the hidden layer was 100 units and the number of learning was 50 times. RPROP [19] was employed for the learning algorithm. The sigmoid function was employed as the activation function of RPROP, and the learning was terminated when the specified number of times was satisfied.

**Fig. 5** The acceleration frequency spectrum

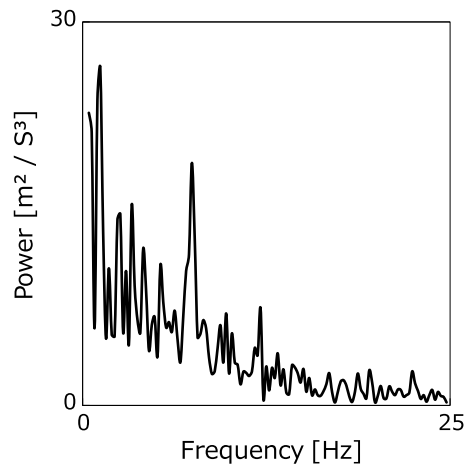


**Fig. 6** The average of the acceleration value

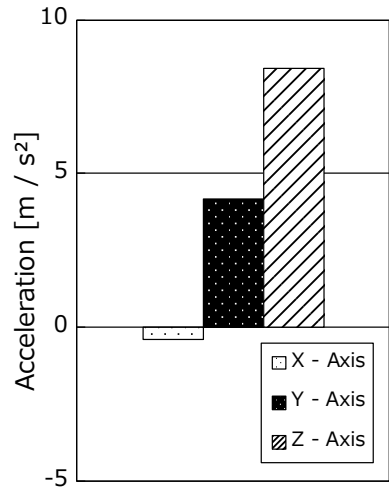
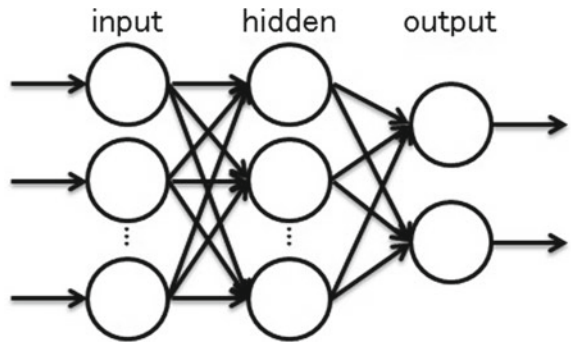


**Fig. 7** The three-layer hierarchical neural network



## 5 Verification Experiment

By measuring the tri-axial acceleration data of a SP in various real environments, various kinds of simultaneous-action discrimination accuracy by the conventional method described in Sect. 3 and the method by the NN of this proposal were compared and verified. Measurement experiments of the tri-axial acceleration data of a SP is explained below. Subjects were seven men in their twenties.

**Fig. 8** Flat road

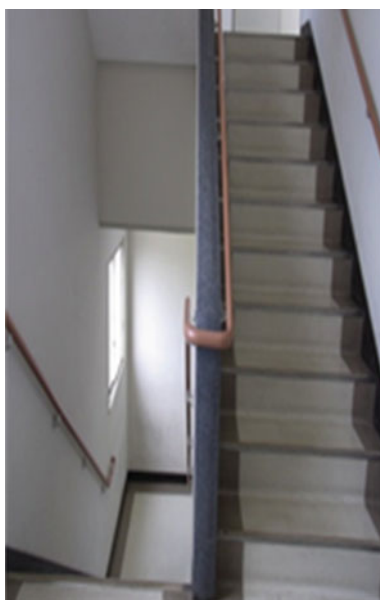
### ***5.1 Measurement Experiment of Acceleration Data in Simultaneous-Walking***

In simultaneous-walking and non-simultaneous-walking, experiments were conducted in three environments; flat road, slope and stairs. Experimental environments on flat road, slope and stairs are shown in Figs. 8, 9 and 10, respectively. Subjects were walked 70 steps in each of three environments. Subjects performed this sequence for ten times in each walking environment and acquired acceleration data in both simultaneous-walking and non-simultaneous-walking.

### ***5.2 Measurement Experiment of Acceleration Data in Simultaneous-Cycling***

In simultaneous-cycling and non-simultaneous-cycling, experiments were conducted in three environments that flat road, slope and uneven road. Since the probability of simultaneous-cycling occurring on the uphill slope is low, this study only focuses downhill slope. Experimental environments on flat road, slope and uneven road are shown in Figs. 11, 12 and 13, respectively. Subjects were cycling 70 m in each of three environments. Subjects performed this sequence for ten times in each cycling environment and measured acceleration in both simultaneous-cycling and normal-cycling.



**Fig. 9** Slope**Fig. 10** Stairs

**Fig. 11** Flat road



**Fig. 12** Slope



**Fig. 13** Uneven road

### ***5.3 Measurement Experiment of Acceleration Data in Stationary-State***

In the stationary-state, subjects were asked to perform SP operation for 60 s while sitting on a chair. Similarly, subjects performed this sequence ten times and measured acceleration of stationary-state.

### ***5.4 Experimental Verification of Discrimination Accuracy by the NN***

As a verification method of discrimination accuracy by NN, K-fold cross-validation [20] was employed. Let  $K = 7$ , learning the data of 6 subjects, and the discrimination rate were calculated using the remaining 1 subject's data. This sequence was done seven times so that the data of all subjects would be test data.

## **6 Experimental Result**

Figure 14 show the comparison results on discrimination rate between the conventional method and the proposed method. From the result in Fig. 14, the average dis-

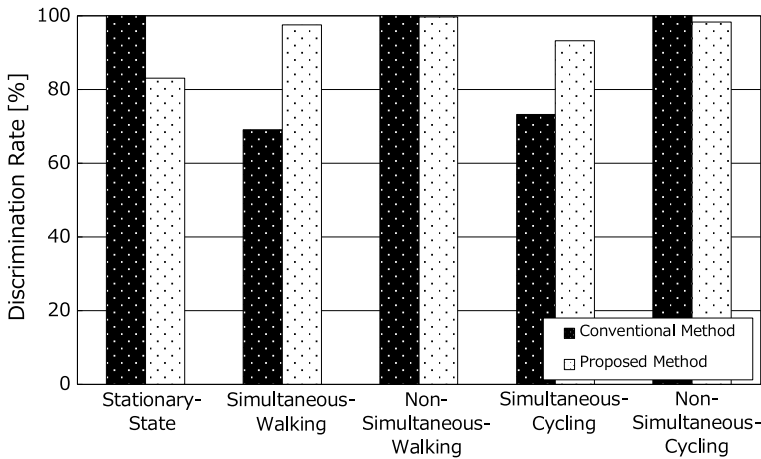


**Fig. 14** Discrimination rate of the conventional method and proposed method

crimination rate for five states was 86.09 [%] in the conventional method and 95.49 [%] in the proposed method, it was confirmed that the proposed method improves the discrimination rate of 9.4 [%] as compared with the conventional method. In the proposed method, accuracy of the stationary-state was 83.12 [%], which was much lower than other state. In addition, when comparing the discrimination results between the conventional method and the proposed method, the discrimination rate of the proposed method was improved by 20 [%] or more in simultaneous-walking and simultaneous-cycling. On the other hand, for the stationary-state, the discrimination rate of the proposed method was reduced by about 17 [%]. For non-simultaneous-walking and non-simultaneous-cycling, there was no significant difference in the discrimination rate between the conventional method and the proposed method.

### 6.1 Discussion

Table 1 shows the breakdown of the discrimination results by the proposed method. In the results of Table 1, among the misjudgment of the proposed method, the highest rate of misjudgment was 16.49 [%] which erroneously discriminates stationary-state as simultaneous-cycling. The next highest rate of misjudgment was 5.11 [%] which erroneously discriminates simultaneous-cycling as stationary-state. From these results, it was confirmed that the misjudgment has occurred between stationary-state and simultaneous-cycling. Factors in which misjudgment tend to occur between two states, stationary-state and simultaneous-cycling, were discussed from the viewpoint of input data. Figure 15 shows the acceleration average value of various state of simultaneous-action. The acceleration average value of each axis was information indicating the attitude of the SP. From the results in Fig. 15, it can be confirmed that

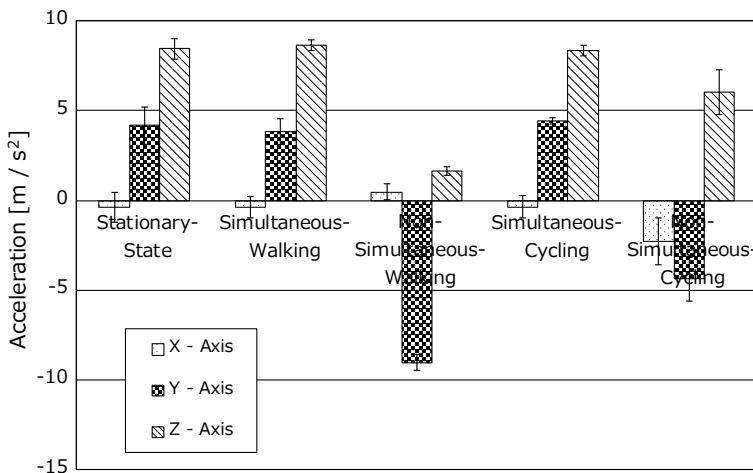


**Fig. 15** Acceleration average value of various simultaneous-action

there was no significant difference in the acceleration average value in stationary-state, simultaneous-walking and simultaneous-cycling. Next, Fig. 16 shows the acceleration frequency spectrum of the z axis of various state of simultaneous-action. Here, the acceleration frequency spectrum of the z axis was used as a comparison target because a waveform characteristic to the acceleration frequency spectrum of the z axis of the SP was confirmed. In simultaneous-walking and non-simultaneous-walking, the spectrum peak as the walking cycle was confirmed around 1.7 Hz. On the other hand, in simultaneous-cycling and non-simultaneous-cycling, no characteristic spectrum corresponding to cycling was confirmed. Based on the above discussion, we thought that misjudgment had occurred because it could not be confirmed the significant difference in the two states of stationary-state and simultaneous-cycling in the acceleration average value and the acceleration frequency spectrum used as the input data.

## 6.2 Study on Improvement of Discrimination Accuracy

In order to improve the discrimination accuracy of the NN, it is necessary to use a feature quantity in which a difference between the stationary-state and the simultaneous-cycling appears conspicuously as input data. Therefore, data obtained from various sensors mounted on the SP were compared and examined. As a result, it was confirmed that there was a remarkable difference in the value of the tilting angle sensor capable of detecting the holding angle of the SP (Fig. 17). In the stationary-state, users tend to bring the SP closer to the position of the line of sight where the SP can be easily operated. As a result, the user tends to possess a SP perpendicular to

**Table 1** Breakdown of discrimination rate of the proposed method

Average discrimination rate [%]	True class					
	Stationary-state	Stationary-state walking	Non-simultaneous-walking	Simultaneous-cycling	Non-Simultaneous-cycling	
Detection class	Stationary-state	83.12	0.18	0.00	5.11	0.47
	Simultaneous-walking	0.00	97.52	0.00	1.32	0.12
	Non-simultaneous-walking	0.00	0.00	99.73	0.08	0.82
	Simultaneous-cycling	16.49	2.30	0.00	93.32	0.22
	Non-simultaneous-cycling	0.39	0.00	0.27	0.17	98.37

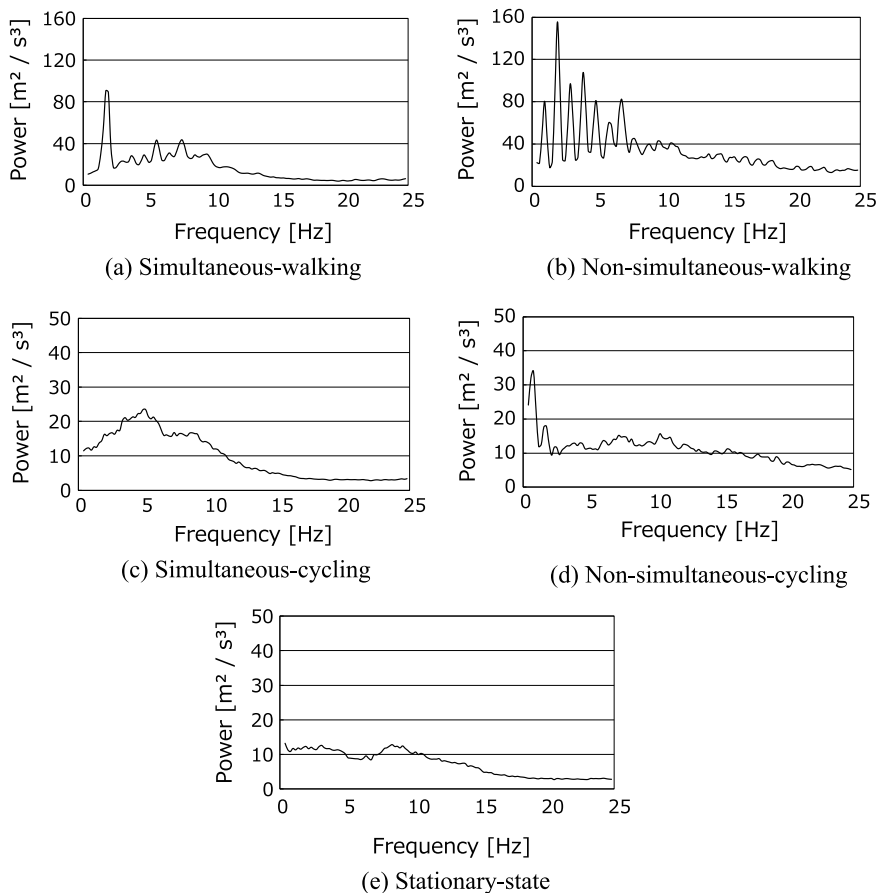
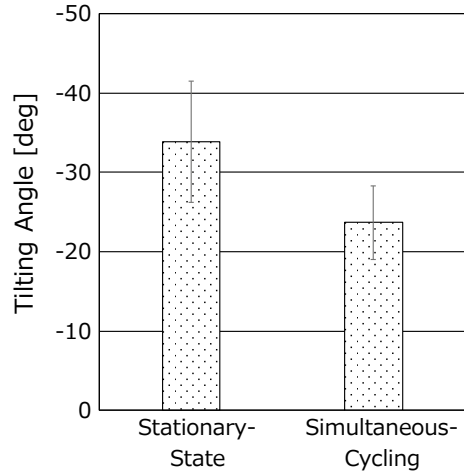


**Fig. 16** Acceleration frequency spectrum of various simultaneous-action

the ground. On the other hand, in simultaneous-cycling, the user tends to possess a SP horizontally with respect to the ground in order to avoid falling of the SP. For these reasons, it is considered that the difference in the tilting angle of the SP appears between the stationary-state and the simultaneous-cycling. From the above discussion, it is considered that if the tilting angle of a SP is added as a new feature quantity, the accuracy of discriminating simultaneous-action by the NN can be improved.

**Fig. 17** The tilting angle of the smartphone of stationary-state and simultaneous-cycling



## 7 Future Problems to be Studied

### 7.1 Problems Related to Real Time Property

In this study, the acceleration data used as the input data of the NN was data of 256 points sampled at 50 Hz. In this method, since 256 points of acceleration data were acquired at 0.2 s intervals, input data was created every 5.12 s. Therefore, the discrimination by the NN is performed only about every 5 s, and the problem of real time property is pointed out. This problem is thought to be solved by creating input data while shifting by one point instead of creating input data every 256 points. By this method, it is possible to discriminate by the NN every 0.2 s, and to secure real time property without re-learning of the NN.

### 7.2 Problems Related to Learning Data of the NN

In this study, the number of data used for learning the NN was 5127 and the data for testing was 854. In general, it is preferable to use more data sets in order to realize the NN with high generalization ability. There is concern about the shortage of learning data for the scale of the network proposed in this study. In the future, we plan to solve this problem by increasing the number of subjects and collecting more acceleration data.



## 8 Conclusion

In this study, as a detection method of simultaneous-action moving while operating a smartphone, a discrimination method by a neural network was newly examined and compared with the conventional method. As a result, the average discrimination rate of simultaneous-action by the conventional method was 86.09 [%], whereas in the proposed method it was 95.49 [%], and the discrimination accuracy improvement of 9.4 [%] was achieved. On the other hand, in the result of the proposed method, only the stationary-state discrimination rate was reduced by 17 [%] compared to the conventional method. We will investigate new features reflecting the features of various simultaneous-actions and improve the accuracy of further discrimination by creating more learning data sets by increasing the number of subjects.

## References

1. Yahoo! Japan News. <https://news.yahoo.co.jp/byline/satohitoshi/20160601-00058313/>
2. Kanagawa Shimbun. <http://www.kanaloco.jp/article/297652>
3. Yahoo! Japan News. <https://news.yahoo.co.jp/byline/satohitoshi/20180824-00094364/>
4. Chunichi Web. <http://www.chunichi.co.jp/article/shizuoka/tokai-news/CK2018072102000099.html>
5. Info Com Newsletter. [http://www.icr.co.jp/newsletter/global\\_perspective/2014/Gpre2014079.html](http://www.icr.co.jp/newsletter/global_perspective/2014/Gpre2014079.html)
6. Info Com Newsletter. [http://www.icr.co.jp/newsletter/global\\_perspective/2014/Gpre2014057.html](http://www.icr.co.jp/newsletter/global_perspective/2014/Gpre2014057.html)
7. Yahoo! Japan News. <https://news.yahoo.co.jp/byline/satohitoshi/20170623-00071983/>
8. Yahoo! Japan News. <https://news.yahoo.co.jp/byline/satohitoshi/20180516-00085280/>
9. Yahoo! Japan News. <https://news.yahoo.co.jp/byline/satohitoshi/20171210-00079134/>
10. Yamamoto, T., Takagi, K., Okumura, A., Yamasaki, H., Nakano, T., Yamada, M.: A proposal of detection technique for simultaneous state detection using smartphone considering actual environment. In: 2016 ITS-Symposium, Proceedings (CD-ROM), 3-C-07 (2016)
11. Ishizuka, A., Okumura, A., Takagi, K., Nakano, T., Yamasaki, H., Yamada, M.: Study on a detection technique for simultaneous-walking in actual environments by neural network. In: Symposium on ITS 2016, 3-C-03 (2016)
12. Ito, M., Ishiduka, A., Yamamoto, T., Yamasaki, H., Nakano, T., Yamada, M.: Study on detection of simultaneous-walking using smartphone considering holding direction of an owner of a smartphone. In: Tokai-Section Joint Conference on Electrical, Electronics, Information, and Related Engineering, Po2-24 (2017)
13. Ito, M., Ishiduka, A., Yamamoto, T., Yamasaki, H., Nakano, T., Yamada, M.: Study on warning method for deterring simultaneous-state. In: The 2017 IEICE General Conference Proceedings of the Student Poster Session, ISS-SP-154 (2017)
14. Kodama, S., Enokibori, Y., Mase, K.: Examination of safe-walking support system for texting while walking using a time-of-flight range image sensor. 2016 IPSJ SIG Technical Report (2016)
15. Yoshida, H., Nakano, M., Sugiyama, M.: A study of accident prevention both of bicycle and pedestrian by approaching detection based on mobile GPS. 2015 IPSJ SIG Technical Report (2015)
16. Sawano, T., Akiho, T., Niitsu, Y.: Detection method of smartphone use while walking using smartphone sensors. 2012 IEICE Student Research Presentation, B-7 (2013)

17. Nasaka, K., Kato, T., Nishigaki, M.: A system to avoid accidents while careless use of smart-phone. IPSJ SIG Technical Report (2012)
18. Hagiwara, Katsuyuki: Basics and some recent advances in neural networks. *J. Plasma Fusion Res.* **82**(5), 282–286 (2006)
19. Riedmiller, M., Braun, H.: A direct adaptive method for faster backpropagation learning: the RPROP algorithm. In: *IEEE International Conference on Neural Networks* (1993)
20. Ishi, K., Ueda, N., Maeda, E., Murase, H.: *Easy Pattern Recognition*, pp. 69–70. Ohmsha, Japan (1998)

**Part II**  
**ITS-Based Smart Mobility**

# Prediction of Travel Time over Unstable Intervals Between Adjacent Bus Stops Using Historical Travel Time in Both the Previous and Current Time Periods



Mansur As and Tsunenori Mine

**Abstract** Travel time prediction is an important issue for many people who want to know their departure time from an origin and arrival time at a destination in order to make decisions (e.g., postpone departure time at certain hours) and to reduce their waiting time at bus stops. Accurate predictions of bus travel time are necessary to know whether the travel time over target intervals between pairs of adjacent bus stops is stable or not. For this purpose, at first, we classified intervals between adjacent bus stops into two classes: stable and unstable. Next, we identified two statistically significant factors: variations of travel time in the same time periods over days and correlation of travel time between eight time-periods, which influence the bus travel time in the current time-period over unstable intervals. Then, we developed nonlinear dynamical models for predicting bus travel time over each unstable interval between adjacent bus stops for 7 time periods in a day. The proposed method basically utilizes time series methods based on Artificial Neural Network (ANN), Support Vector Machine Regression (SVR) and Random Forest (RF). We conducted experiments using bus probe data collected from November 21st to December 20th, 2013 and provided by Nishitetsu Bus Company, Fukuoka, Japan. In addition, to evaluate our proposed approach, we conducted a comparison experiment between our proposed model and the model in our previous study. Experimental results show that our proposed models can effectively improve the previous study model on the prediction accuracy of travel times over unstable intervals.

---

M. As

Graduate School of Information Science and Electrical Engineering, Kyushu University,  
744 Motoooka, Nishi-ku, Fukuoka 819-0395, Japan  
e-mail: [manjoer82@gmail.com](mailto:manjoer82@gmail.com)

T. Mine (✉)

Faculty of Information Science and Electrical Engineering, Kyushu University,  
744 Motoooka, Nishi-ku, Fukuoka 819-0395, Japan  
e-mail: [mine@ait.kyushu-u.ac.jp](mailto:mine@ait.kyushu-u.ac.jp)

© Springer Nature Singapore Pte Ltd. 2019

T. Mine et al. (eds.), *Intelligent Transport Systems for Everyone's Mobility*, [https://doi.org/10.1007/978-981-13-7434-0\\_8](https://doi.org/10.1007/978-981-13-7434-0_8)

# 1 Introduction

## 1.1 Background

Prediction of bus travel time is a crucial tool that lets passengers know their departure time from and arrival time at origin and destination locations, and reduces their waiting time at the bus stops. Furthermore, it can also play an important role in evaluating the effectiveness of public bus transportation. On the other hand, realizing accurate prediction of bus travel times has been a challenging research problem over the last several years in the study of intelligent transport systems. Thus, previous studies have investigated a lot of cases, such as travel time over routes, distributions of travel times, delay of arrival/departure time, using weather and/or traffic conditions [1, 2, 6, 21].

Our recent research activities [2–5], have also attempted to predict travel time over shorter intervals such as the interval between pairs of adjacent bus stops using an Artificial Neural Network (ANN) model built from real bus probe data. This research succeeded in classifying the intervals into stable and unstable ones [2], and in obtaining accurate prediction results on average [1, 3, 5], but has not focused only on unstable intervals for travel time prediction. This paper focuses on unstable intervals to predict travel time and clarifies the characteristics of the prediction of travel time over unstable intervals.

On the other hand, a lot of studies [1, 6, 8, 11, 20], have employed other machine learning techniques such as Support Vector Machine (SVM), Artificial Neural Network (ANN) and Random Forest (RF) to build prediction models for bus travel time and showed that these models were practical, useful and reliable, although they assumed cases where the traffic flow was relatively small and stable. In this study, we propose a prediction model for travel time over unstable intervals using Support Vector Regression (SVR), Artificial Neural Network (ANN) and Random Forest (RF) with the time series approach method and try to clarify the characteristics of the prediction of travel time over the unstable intervals.

We first conducted statistical analyses on the observed travel time over the unstable intervals between pairs of adjacent bus stops so that we could clarify the correlation of the travel time between adjacent time periods and the variability of travel time in the same time periods over the past several days. Based on the results of these analyses, we employed two types of input data: dynamic average travel time (DATT) in the time period right before the current one and historical average travel time (HATT) in the same time-period over the past several days to build our prediction model of travel time over unstable intervals. We will explain the two types of data, DATT and HATT in Sect. 3.3.

## 1.2 Objective and Scope

The main objective of this study is to develop prediction models of bus travel time over unstable intervals between pairs of adjacent bus stops. We use Support Vector Regression (SVR), Artificial Neural Network (ANN) and Random Forest (RF) to build the models. We divide the day into 8 time periods according to the bus time tables in the probe data, and perform precise prediction of travel time over the intervals for each time period. These eight time periods are defined in Table 1. Since we use two types of input data: DATT and HATT, where DATT requires a time period just before the current one and there is no time period just before EM, we focus on the prediction of travel time for 7 time-periods omitting EM and we conduct experiments comparing our proposed model in this study and a model in our previous study. This is done in order to grasp the rough characteristics of average travel time over the intervals in each time period over several instances of the same day of the week, which is a weekday. We will discuss the details in Sect. 4.4.

On the other hand, in this study, we perform precise prediction for average travel time over unstable intervals for each time-period only for weekdays. This means that the prediction of the travel time for each time period in this study is influenced by the travel time in the previous time periods of a day and is more sensitive than the previous work [5]. To this end, this study broadly divided all intervals into stable and unstable ones based on their travel time in each time period using 20-weekday data; we examine the correlations of travel time over intervals, especially unstable intervals between adjacent time periods, and the variability of travel time over the intervals during the past several days. Based on these results, we identified the characteristics of unstable intervals and noted, in particular, if there are any recurrent properties in their time series data. Considering the characteristics identified, we chose two types of input data: DATT and HATT to build a prediction model. We summarize our objectives in this study as follows:

**Table 1** Time periods

Periods	Ranges of time
Early morning (EM)	5:00:00–7:29:59
Morning peak (MP)	7:30:00–9:29:59
Late morning (LM)	9:30:00–11:59:59
Midday (MD)	12:00:00–12:59:59
Early afternoon (EA)	13:00:00–15:29:59
Afternoon peak (AP)	15:30:00–17:29:59
Evening (E)	17:30:00–19:29:59
Late night (LN)	19:30:00–25:59:59

1. Compute historical average travel time in each of eight time periods in a day and distinguish stable and unstable intervals using 20 days of weekday probe data.
2. Carry out an exploratory data analysis to clarify correlations of travel time over unstable intervals between adjacent time periods and variability of travel time over the intervals in the same time period during the past several days.
3. Evaluate prediction results by comparing the results with the model in our previous study.

The rest of this paper is organized as follows: Sect. 2 describes our data and methodologies; Sect. 3 describes the preliminaries for model development in our study and shows some results of analysis; Sect. 4 discusses the experimental setup and presents the results our study using three machine learning techniques. Next, we compare the results of our proposed model with those of our previous study. Finally, we conclude the paper.

## 2 Data and Methodologies

### 2.1 Data

Probe data generated by vehicles include data obtainable from navigation systems, such as the time and position (longitude and latitude), i.e. data on the vehicle's running history, and front-rear acceleration or right-left acceleration, i.e. data on the vehicle's performance history. Since these probe data can be obtained continuously over time from the vehicles, they allow one to monitor the state of road traffic at any chosen location or point in time and provide intelligence regarding traffic information. Thus probe data offers the potential to develop a prediction model and can improve the accuracy of prediction results [15, 17].

The probe data we used in this research were provided by NISHITETSU Bus Company. The data were collected from the 21st of November to the 20th of December in 2013. The probe data include (1) Bus route number, (2) Number of buses, (3) Identity of Vehicle, (4) GPS position of buses, (5) Time of the day, (6) Bus stop code, (7) Actual arrival and departure times at the beginning of the route, end of the route and at every bus stop along the route, (8) Direction: inbound or outbound.

The typical travel time unit of a bus on its route is the time it takes to move from one bus stop to the next bus stop, as shown in Fig. 1, which is determined by the time position when a bus departs from one and arrives at the other of two adjacent bus stops along route. The bus will not travel on the same segment twice in a single trip, although it could travel on the same segment more than once in a single trip, but in the opposite direction i.e. inbound and outbound directions.

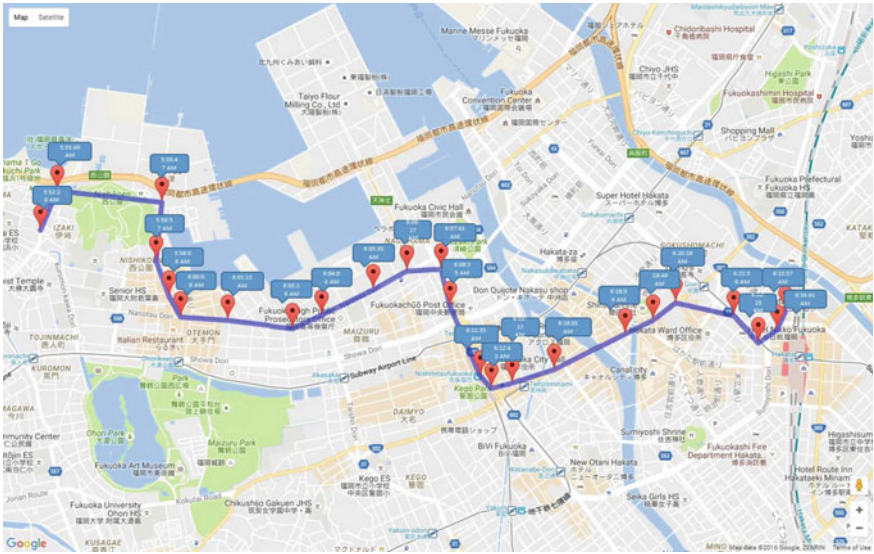


Fig. 1 Samples of pairs of the position and time of the bus on the route are obtained by GPS

Bus routes are operated for around 18 hours a day. Buses run in different patterns on weekdays, Saturdays and Sundays/holidays according to their timetable. Here, in this paper, we just deal with travel time on 20 weekdays, excluding Saturdays and Sundays/holidays because of the paucity of data for those days. We analyzed 77 routes that contain 824 intervals for inbound and 1196 intervals for outbound directions, and calculated travel time over each interval between pairs of adjacent bus stops.

## 2.2 Methodologies

### 2.2.1 Travel Time over Intervals

In order to calculate the average bus travel time in each time period, first we classified the travel time data into eight time periods in a day. This is because bus travel times are influenced by the traffic conditions, ridership and weather conditions in each time period, which often change even when buses run over intervals between pairs of adjacent bus stops [2, 3, 5, 13].

The following explains how to calculate bus travel time over an interval between adjacent bus stops.

We first define travel time  $T_{AB}(i, tp, d)$  in Eq. (4), which is the length of time when bus # $i$  runs between adjacent bus stops:  $A$  and  $B$ , in time-period  $tp$  ( $\in$  (EM, MP, LM, MD, EA, AP, E, LN)) on day  $d$ , which is always a weekday in this paper.



**Fig. 2** Bus travel time over an interval between adjacent bus stops: A and B

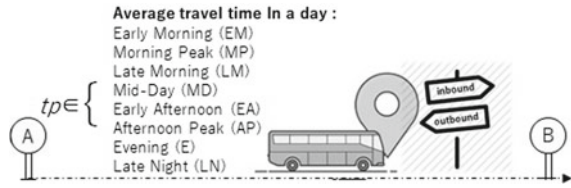


Figure 2 illustrates the calculation of travel time over the interval between adjacent bus stops for each time period, and Table 1 shows the ranges in each time periods.

$$Tt_{AB}(i, tp, d) = t_B(i, tp, d) - t_A(i, tp, d), \quad (1)$$

where  $t_B(i, tp, d)$  and  $t_A(i, tp, d)$  are the time when the bus # $i$  arrives at bus stop  $B$  and departs from bus stop  $A$  in time-period ( $tp$ ) on a day ( $d$ ), respectively.

Using Eq. (1), we calculate the average travel time  $Tt_{AB}(tp, d)$  as follows:

$$Tt_{AB}(tp, d) = \frac{1}{N} \sum_{i=1}^N Tt_{AB}(i, tp, d), \quad (2)$$

where  $N$  is the number of buses running on the interval between adjacent bus stops:  $A$  and  $B$ , and may vary according to each interval.

### 2.2.2 Distinguishing Stable and Unstable Intervals

First, we transform the data of average of travel time over each interval in each time period using *natural logarithm*. Then, we calculate the average travel time  $Tt_i(tp)$  over interval  $i$  in time period  $tp$  over  $n$  weekdays, where  $n = 20$  in this research.

$$Tt_i(tp) = \frac{1}{n} \sum_{d=1}^n Tt_i(tp, d) \quad (3)$$

Then, we put a number onto each interval from 1 to  $N$ , where  $N$  is the total number of intervals; we calculate  $Tt_i$ , which is the average travel time over interval  $i$  ( $1 \leq i \leq N$ ) among  $TP = \{EM, MP, LM, MD, EA, AP, E, LN\}$ , a set of eight time periods of a day.

$$Tt_i = \frac{1}{|TP|} \sum_{tp \in TP} Tt_i(tp) \quad (4)$$

Then, we calculate  $StDev_i$ , which is the standard deviation of the average travel time over interval  $i$  to find out whether travel time over each interval is stable or not. To make a fair comparison for all routes considering the differences of distance of all

the intervals, we divide the standard deviation of the average travel time over each interval by the average travel time over the interval.

$$StDev_i = \frac{\sqrt{\frac{1}{|TP|} \sum_{tp \in TP} (Tt_i(tp) - Tt_i)^2}}{Tt_i} \tag{5}$$

Then, we calculate  $\sigma$ , the standard deviation of the standard deviation of the average travel time over all the intervals.

$$\sigma = \sqrt{\frac{\sum_{i=1}^N (StDev_i - \mu)^2}{N - 1}} \tag{6}$$

Here  $\mu$  is the average of the standard deviation over the intervals.

$$\mu = \frac{1}{N} \sum_{i=1}^N (StDev_i) \tag{7}$$

According to  $StDev_i$ , interval  $i$  is classified into logarithm ranges of interval criteria as shown in Table 2. We roughly classified all intervals into two classes: stable and unstable; if the standard deviation of travel time over an interval is less than  $\mu$ , then the interval is classified as stable, or otherwise, unstable [2, 3, 5]. Then, we further classified each of the two into three sub-classes: weak, medium and strong (we present the results in Sect. 3.2).

Next, we briefly present references and the outline of nonlinear time series prediction using machine learning techniques for prediction of bus travel time over unstable intervals in seven time periods of a day; we used Support Vector Regression (SVR), Artificial Neural Network with NARX and Random Forest (RF) Regression.

### 2.2.3 Support Vector Regression (SVR) Method

Support Vector Machine (SVM) has been developed to work on a non-linear problem by incorporating the concept of the kernel in high-dimensional space; SVR is an

**Table 2** Logarithmic ranges of interval criteria

Interval category	Ranges
Strong stable	if $StDev_i \leq \mu - 2\sigma$
Medium stable	if $\mu - 2\sigma < StDev_i \leq \mu - \sigma$
Weak stable	if $\mu - \sigma < StDev_i \leq \mu$
Weak unstable	if $\mu < StDev_i < \mu + \sigma$
Medium unstable	if $\mu + \sigma \leq StDev_i < \mu + 2\sigma$
Strong unstable	if $StDev_i \geq \mu + 2\sigma$

application of SVM to the case of regression [19], which was designed to overcome the over-fitting and to yield a good performance [18, 20].

We assume there are  $n$  numbers of training data  $(x_i, y_i)$  ( $i = 1, \dots, n$ ), where  $x_i$  is an input vector, and  $y_i$  is a scalar output. With SVR, we want to assign a function  $f(x)$ , which has the significant deviation  $\varepsilon$  from the actual target  $y_i$  for all training data. If the value of  $\varepsilon$  becomes equal or near to 0, a good regression model is obtained [20].

The main purpose of the SVR model is to construct a linear model in  $m$ -dimensional feature space which input  $x$  is mapped onto. Using mathematical notation, the linear model  $f(x, w)$  is given below [12]:

$$f(x, w) = \sum_{j=1}^n w_j g_j(x) + b, \quad (8)$$

where  $w_j$  and  $g_j(x)$  denote the  $j$ th weight and nonlinear transformation, respectively, and  $b$  is a bias. Next, prediction performance is measured by the loss function  $L(y, f(x, w))$ . SVR uses a new type of loss function called  $\varepsilon$ -insensitive loss function proposed by Vapnik [19]:

$$L_\varepsilon(y, f(x, w)) = \begin{cases} 0 & \text{if } |y - f(x, w)| \leq \varepsilon \\ |y - f(x, w)| - \varepsilon & \text{otherwise} \end{cases} \quad (9)$$

SVR performs linear regression in the high-dimensional feature space using  $\varepsilon$ -insensitive loss, and at the same time, tries to reduce model complexity by minimizing  $\|w\|^2$ . This can be described by introducing (non-negative) slack variables  $\zeta_i, \zeta_i^*$  ( $i = 1, \dots, n$ ), to measure the deviation of training data outside the  $\varepsilon$ -insensitive zone. Thus SVR is formulated as a minimization of the following function:

$$R_{(w, \zeta)} = \frac{1}{2} \|w\|^2 + C \sum_{i=1}^n (\zeta_i + \zeta_i^*) \quad (10)$$

subject to :

$$\begin{cases} y_i - f(x_i, w) \leq \varepsilon + \zeta_i^* \\ f(x_i, w) - y_i \leq \varepsilon + \zeta_i \\ \zeta_i, \zeta_i^* \geq 0, (i = 1, \dots, n) \end{cases}, \quad (11)$$

where  $(1/2)\|w\|^2$  is a weight vector norm, and  $C$  is a regularized constant determining the trade-off between the empirical error and the regularized term.  $\varepsilon$  is called the tube size of SVR and it is equivalent to the approximation accuracy placed on the training data points. By introducing optimal constraints, this optimization problem can be transformed into a dual problem whose solution is given by:

$$f(x) = \sum_{i=1}^{n_{sv}} (a_i - a_i^*) K(x_i, x) \quad (12)$$

subject to:  $0 \leq a_i^* \leq C, 0 \leq a_i \leq C$ , where  $n_{sv}$  is the number of Support Vector (SVs) and  $K$  is a kernel function. The kernel parameters should be carefully chosen as they implicitly define the structure of high dimensional features and thus controls the complexity of the final solution. However, generalization performance, here prediction accuracy, depends on a good setting for parameters  $C, \varepsilon$ , kernel parameters, and input values ( $x$ ) of the training data [12, 20].

We selected Radial Basis Function (RBF) as the kernel function in this study. For measurement of performance ( $C$ ) in the training process, we selected RBF network ( $\lambda, \varepsilon$ ) at the minimum error as an SVR model [12].

#### 2.2.4 Artificial Neural Network (ANN) with NARX

Next, we use an ANN-based time series prediction method to perform the prediction of travel time over intervals between adjacent bus stops on all of the routes. The method is based on a Nonlinear Auto Regressive model with the eXogenous input (NARX) model. The NARX model is well suited for modeling dynamic nonlinear systems, especially, with time series characteristics. The NARX model is a subset of the Nonlinear Auto-Regressive Moving Average with Exogenous Inputs (NARMAX), which are nonlinear non-parametric identification models [10, 22]. The mathematical function which models a real world system is very complex and usually unknown. However, the NARX model can be constructed using a simpler function structure such as neural networks [9]. The NARX model formulation [9] [10] is described as follows:

$$y(t) = f(y(t-1), \dots, y(t-n_y), u(t-1), \dots, u(t-n_u)) + e(t), \quad (13)$$

where  $y(t)$ ,  $u(t)$  and  $e(t)$  are the model output, model input, and noise at time  $t$ , respectively.  $n_y$  and  $n_u$  are the maximum lags in the output and the input, respectively;  $f(\cdot)$  is some vector-valued non-linear function, but can be approximated using some known simpler function such as neural networks [9].

In our model, we used a multilayer perceptron (MLP) with a single hidden layer to approximate any bounded continuous function. The MLP contains one or more layers of hidden units. The hidden units enable the MLP to learn complex tasks and meaningful features from the input/output relationships. Moreover, high degree of connectivity between the MLP layers is determined by the weights of the network [22]. We conducted MLP training with the Levenberg-Marquardt algorithm and evaluated the model using the measure of Mean Squared Error (MSE) in training and testing. The MSE is a default indicator in training the ANN model. The ANN model with the smallest MSE value is considered to be the best model [22].

### 2.2.5 Random Forest (RF) Regression

The present Section is not intended to provide a detailed description of Random Forest (RF); the parameters are described in Sect. 4.1.

Random Forest (RF) Regression is a regression technique that combines the performance of numerous Decision Tree (DT) algorithms to predict the value of a variable [7]. Therefore, regression using RF can be implemented for time series prediction purposes. That is, when RF receives a  $\mathbf{u}$  input vector, made up of the values of the different evidential feature analyses for a given training area, RF builds  $k$  numbers of regression trees and averages the results.

Assumed that the  $\underline{\mathbf{u}}$  is a random vector with  $k$  elements, the aim is to predict  $\underline{v}$  by estimating the regression function [16]:

$$m(\mathbf{u}) = E[\underline{v} | \underline{\mathbf{u}} = \mathbf{u}] \quad (14)$$

given fitting sample:

$$S_s = ((\mathbf{u}_1, v_1), \dots, (\mathbf{u}_s, v_s)) \quad (15)$$

which are independent realizations of the random variable  $(\underline{\mathbf{u}}, \underline{v})$ . Therefore, the aim is to construct an estimate  $m_s$  of the function  $m$ .

A random forest is a predictor constructed by growing  $M$  randomized regression trees. For the  $j$ -th tree in the family, the predicted value at  $\mathbf{u}$  is denoted by  $m_s(\mathbf{u}; \underline{\theta}_j, S_s)$ , where  $\underline{\theta}_1, \dots, \underline{\theta}_M$  are independent random variables, distributed as  $\underline{\theta}$  and independent of  $S_s$ . The random variable  $\underline{\theta}$  is used to resample the fitting set prior to the growing of individual trees and to select the successive directions for splitting [16]. The prediction is then given by the average of the predicted values of all trees. Before constructing each tree, the observations are randomly chosen from the elements of  $\mathbf{u}$ . These observations are used for growing the tree. To avoid the correlation of the different trees, RF increases the diversity of the trees by making them grow from different training data subsets created through a procedure called bagging.

Hence, some data may be used more than once in the training, while other data might never be used. Thus, greater stability is achieved, as it makes it more robust when facing slight variations in input data and, at the same time, it increases prediction accuracy [7]. On the other hand, when the RF makes a tree grow, it uses the best feature of split point within a subset of evidential features which has been selected randomly from the overall set of input evidential features. Therefore, this can decrease the strength of every single tree, but it reduces the correlation between the trees, which reduces the generalization error [7]. Another characteristic of interest is that the trees of a RF classifier grow with no pruning, which makes them light, from a computational perspective [14]. However, The performance of the RF algorithm depends on the tuning of its parameters and the variable selection (also known as feature selection) [7, 16].

### 2.2.6 Measures of Model Performance and Prediction Results

The model parameters are evaluated by Root Mean Squared Error (RMSE). The model with the smallest RMSE error value is chosen as it shows the best performance. Next, we select Mean Absolute Percentage Error (MAPE) as the measure of prediction accuracy and calculate it for all prediction results. RMSE and MAPE are defined below:

$$RMSE = \sqrt{\frac{1}{N} \sum_{i=1}^N (t_{Actual}(i) - t_{Predicted}(i))^2} \quad (16)$$

$$MAPE = \sum_{i=1}^N \left| \frac{t_{Actual}(i) - t_{Predicted}(i)}{t_{Actual}(i)} \right|, \quad (17)$$

where  $t_{Actual}$  is the observed bus travel time over an interval in each time-period;  $t_{Predicted}$  is the predicted bus travel time over the interval in the same time-period.  $N$  is the number of observations.

## 3 Preliminaries to Model Development

In general, travel time variability has been classified into recurrent and non-recurrent, where recurrent variability is a result of insufficient capacity, such as traffic congestion in rush hour. While the non-recurrent variability is caused by transient events, sources of unexpected congestion include accidents, inclement weather, construction and special events [20, 21].

The variability of bus travel time has been one of crucial issues in many studies because understanding the variance of travel time on a route helps to understand the situation of traffic flows on the urban networks. Results from this analysis motivate the modeling assumptions described in Sect. 1. Although calculation of the variability of route travel time is based on a simple accumulation of travel times, the difference in travel time between time periods in a day may show changes in road conditions caused frequently or unexpectedly. In this study we investigated two things: first, variability of bus travel time between time periods and discrimination between stable and unstable intervals.

### 3.1 Variability of Bus Travel Time Between Time Periods

Many measures of travel time variability have been proposed in previous studies [3, 5, 21]. The goal of the data analysis is to explore characteristics of the data that can be

**Table 3** Periodical variance of travel time over unstable intervals on weekdays

Day	Inbound			Outbound		
	Pooled StDev (ln)	F-value	P-value	Pooled StDev (ln)	F-value	P-value
Mon	0.339	21.35	0.00	0.329	43.397	0.00
Tue	0.346	20.512	0.00	0.33	37.093	0.00
Wed	0.344	19.642	0.00	0.333	43.699	0.00
Thu	0.347	21.733	0.00	0.338	43.004	0.00
Fri	0.351	26.551	0.00	0.342	46.791	0.00

used for building prediction models [20]. Using the method mentioned in Sect. 2.2, we calculated average travel time during eight time-periods in a day over 20 days. Next, we investigated the relationship of travel time between days over intervals between pairs of adjacent bus stops on all routes in each time period and ascertained the daily characteristics of bus travel time. We also intended to prove an assumption that travel time in certain time periods has a strong correlation with travel time in other time periods in a day; during off-peak hours such as early morning (EM), midday (MD), or late night (LN), both traffic volume and travel time decrease. Meanwhile, during peak hours such as morning peak (MP), late morning (LM), and evening (E), the traffic volume increases dramatically and causes the travel time to increase as well. Thus, the travel time should be different between different time periods in a day [2, 3, 20].

Using statistical analysis, we compared the average travel time among eight time periods for five weekdays. Table 3<sup>1</sup> shows the resulting f-values and p-values for five weekdays for the inbound and outbound directions.

The results show, for five weekdays, p-values  $\leq 0.05$ ; this indicates that there are statistically significant differences in the average travel time among the eight time periods for the five weekdays. Further, on Thursday and Friday, the pooled standard deviation values are higher than other days for the inbound and the outbound directions. It is true that the characteristics of travel time over intervals between pairs of adjacent bus stops may vary between time periods day to day. During the morning peak, late morning, and evening on weekdays, bus travel time may significantly increase due to the heavy traffic volume. This result also explains why we chose eight time periods in a day as input variables in our proposed model.

---

<sup>1</sup>All the data has been transformed using a natural logarithm to make the data conform to normality distribution.

### 3.2 Stable and Unstable Interval

Next, using the method described in Sect. 2.2.2, we roughly divided all intervals into two classes: stable and unstable, which could be further classified into weak, medium or strong. The width of the category ranges of weak, medium and strong of stable and unstable intervals is one standard deviation from mean; their ranges are between mean plus-minus one standard deviation, from mean plus-minus one standard deviation to mean plus-minus two standard deviations, and more or less than two standard deviations from mean, respectively (see our method in Sect. 2.2).

Figure 3 shows the percentage of stable and unstable travel times over all the intervals on weekdays. There is a significant amount of variability in the travel time over each interval on all routes on weekdays. The percentages of the three unstable interval classes: weak, medium and strong, are 28.52%, 13.35% and 3.16% for the inbound direction, and 31.10%, 12.79% and 3.51% for the outbound direction, respectively. The results clearly indicate the existence of unstable intervals whose percentage is not negligible (see Fig. 3, Ratio of stable and unstable intervals). Therefore, in this study we focus on these unstable intervals in the above data to develop a prediction model for travel time over each interval.

#### 3.2.1 Variability of Travel Time over Unstable Intervals for Several Days of Data in Each Time Period

In the second part of the data analysis, we verified the daily variance of travel time over unstable intervals. In this analysis, data from the same time period on different

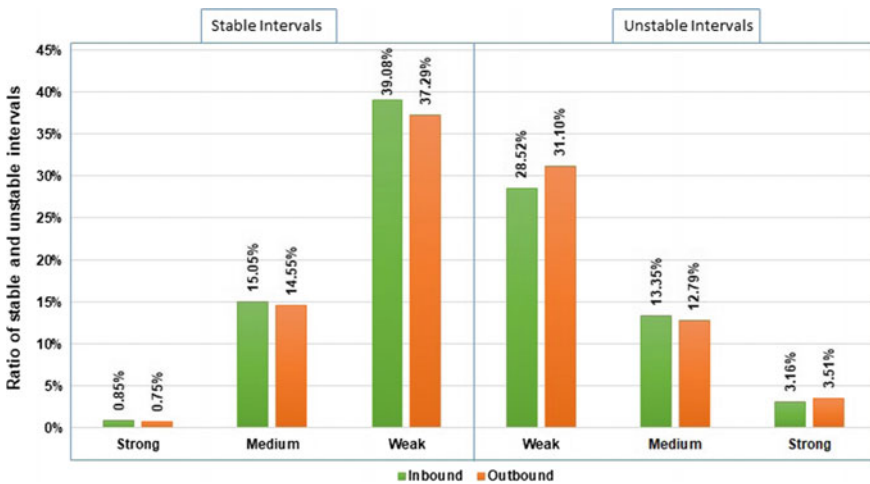


Fig. 3 Ratio of stable and unstable intervals



weekdays were compared. This analysis aims to find the variability of travel time over unstable intervals, and to confirm whether the variability tends to be recurrent or non-recurrent day to day as we described in Sect. 3.

The results of the variability analysis of travel time obtained by using one-way ANOVA in SPSS are shown in Table 4, where **0.000** denotes less than 0.0005. Table 4 shows that some specific time periods, especially rush hours: MP, AP and E for both the inbound and the outbound directions, have smaller p-values than 0.05 although travel time in LM for the outbound direction has also a smaller p-value than 0.05. Interestingly, the other time periods have greater p-values than 0.05, even when the target intervals are unstable ones. The results indicate that historical average travel times in time periods other than rush hours seem to have recurrent properties and to help in the prediction of travel times even over the unstable intervals. The results also support the same assumption as our previous study [5] that travel times over intervals in the same time period have recurrent and non-recurrent properties between several days. However the time periods with recurrent and non-recurrent properties shown in Table 4 are different from those of our previous study [5]. This is because this study only focuses on unstable intervals, unlike our previous study.

### 3.2.2 Correlation of Travel Time Between Adjacent Time Periods

In Sect. 3.2.1, we mentioned that travel times over unstable intervals showed recurrent and non-recurrent properties for several time periods day to day. In addition, in our previous study [5], we found there are correlations between adjacent time periods, for example, travel time in late morning (LM) is affected by that in morning peak (MP) and travel time in evening (E) is affected by that in afternoon peak (AP). However, unlike our previous study, this study only focuses on unstable intervals. Thus, we conducted experiments to confirm if there are any correlations in travel time between the eight time periods in a day. The experimental results denote that there are strong or moderate correlations between time periods in a day over unstable intervals, in

**Table 4** Daily variance of travel time over unstable intervals

Time period	Inbound		Outbound	
	F-value	P-value	F-value	P-value
EM	0.325	0.997	1.005	0.451
MP	1.380	<b>0.015</b>	6.615	<b>0.000</b>
LM	0.462	0.977	1.953	<b>0.008</b>
MD	0.810	0.697	1.034	0.416
EA	0.611	0.901	1.395	0.117
AP	1.483	<b>0.003</b>	3.010	<b>0.000</b>
E	2.577	<b>0.000</b>	4.435	<b>0.000</b>
LN	0.686	0.836	0.539	0.947

particular when two time periods are near to each other. The results were similar to our previous study [5]. So we can say that travel times in the previous time periods is a useful factor in predicting travel times in the later time periods and in building a prediction model for travel times.

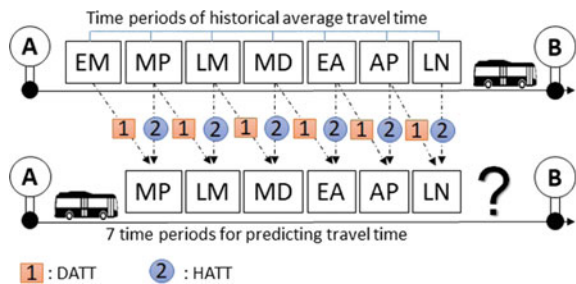
In summary, there are three results we obtained from the statistical analysis of travel time over unstable intervals. First, the characteristics of travel time between pairs of adjacent bus stops may vary between time periods in a day. Second, the daily variance of travel time tends to be recurrent or non-recurrent. Third, There are strong correlations of travel time between time periods in a day. These results show that there is great potential to predict the travel times over unstable intervals.

### 3.3 Selection of Input Variables

The results of the analyses described in Sects. 3.2.1 and 3.2.2 explain why we consider travel time in each time period as input variables of the prediction model. We chose two input variables: DATT and HATT. Figure 4 illustrates how the model uses the two input variables for travel time prediction.

1. **DATT** is expected to adjust the prediction of travel time in the current time-period using the travel time observed in the period just before the current one. For instance, we predict travel time in morning peak (MP) using the travel time observed in early morning (EM) and so on. It is more effective for detecting unexpected dynamic events than only using HATT.
2. **HATT** denotes the average travel time in the same time period during the past several days. It is an important input variable of the prediction model because travel time over intervals in some time periods tends to have recurrent properties between days.

**Fig. 4** Two input variables: DATT and HATT for prediction model



## 4 Experimental Setup

### 4.1 Prediction Model Building

We carried out experiments to predict travel time over each unstable interval between pairs of adjacent bus stops on the route using the SVR, ANN and RF methods with two input variables: DATT and HATT. In the experiments, because DATT relies solely on the travel time observed in the time period just before the current one and there is no time period before EM, prediction of travel time was performed for each of 7 time-periods in a day: MP, LM, MD, EA, AP, E and LN. Therefore we just used HATT for the EM period. We used SVR and RF of **WEKA version 3.8**. For SVR, RBF was selected as the kernel function in this study. Other parameters are  $C : 1.0$ ,  $\varepsilon : 1.0E-12$ , and  $\varepsilon$  parameter tolerance: 0.001. In addition, the number of features used for training at each node split is *mtry*.

For RF, observations per a tree default = 1.0; features per node scalar default =  $nvars/3$ ; maximum tree depth = unlimited and the method of calculating variable importance = 0,1. In addition, we used  $M = 500$  trees, which is equal to their default values in the Weka RF package, and a node size = 5. The parameter *mtry* is controlled during the validation phase to avoid over-fitting.

Next, in ANN, we used a multilayer perceptron (MLP) with a single hidden layer to approximate any bounded continuous function. Also, we selected a narxnet network architecture, where the number of hidden neurons is 10, and the number of delays is 2. Furthermore, in the training network, we used the Levenberg-Marquardt algorithm in MATLAB `trainlm`. After every  $n$  epoch we applied Series-parallel (SP) mode to actual values of the target series data in order to form the regression of the target series data, and to minimize over-fitting in the training process; we performed validation using the validation data.

The optimal performance parameters of SVR, ANN and RF were found by calculating the average performance of each training model, while the search for the optimal value of the parameter was performed in a grid. The RMSE was used to measure the performances. The optimal parameters minimizing the RMSE were selected.

### 4.2 Training Data and Prediction Iteration

In the training phase, we used two sets of input data: DATT and HATT, for each model: SVR, ANN and RF. In the first prediction step, we used 14-days data as training data, 1-day data as validation data, and 1-day data as testing data. We prepared five days of data as testing data and selected one day among them in each iteration without duplication. In the training process, predicted results were evaluated by RMSE, conducting out-of-sample prediction with validation data; when the RMSE value fell below the threshold, the training was stopped to avoid over-training. We

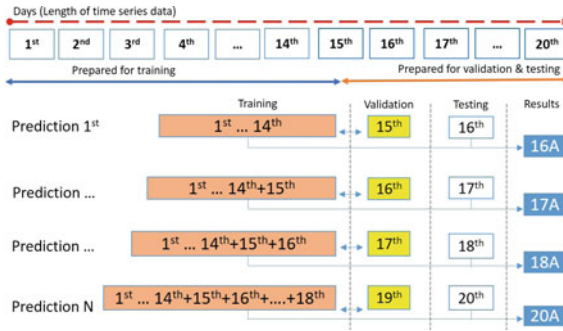


**Fig. 5** Training data and prediction iteration

repeated all the above steps five times selecting another 1-day data in the 5-day test data. In the next iteration step, we added the validation data in the previous iteration step into the training data and used the test data in the previous iteration step as the validation data. Then, the quantity of training data was increased by one day data in each iteration step. The iteration of the prediction model is shown in Fig. 5. Unlike our previous study [5], this procedure does not add the prediction result in the current step, but adds the validation data in the current step into the training data in the next step. Further, in this study, we used not only ANN, but also other machine learning models: SVR and RF.

Further, we investigated if just adding the validation data used in the previous step into training data in the current step has any effect. To this end, instead of just adding the validation data, we implemented a moving window model such that the length of training data is the same 14 days in each iteration. This model changes the training data by moving one day forward so that each data set has the same 14 day training data size. Accordingly, the validation data in the previous step was added into training data in the current step, but the earliest day data in the training data in the previous step was removed. In summary, the difference between the proposed models in this study and the model proposed in our previous study [5] is that the previous study model just adds both the predicted result and the validation data in the previous step into the training data in the current step, but the proposed model in this study replaces the earliest day data in the training data with the validation data in the current step for the next step by taking the moving window model. Figure 6 illustrates the experimental procedure of the proposed model in the training process.

### 4.3 Prediction Performance Evaluation

When building prediction models, the primary goal is to make a model that most accurately predicts the desired target value for actual data. To measure the model error, we used mean absolute percentage error (MAPE) as described in Sect. 2.2.6.

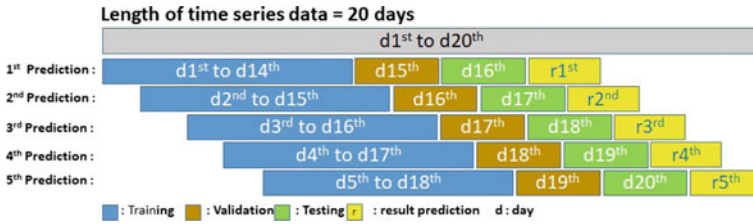


Fig. 6 The training process in the proposed model

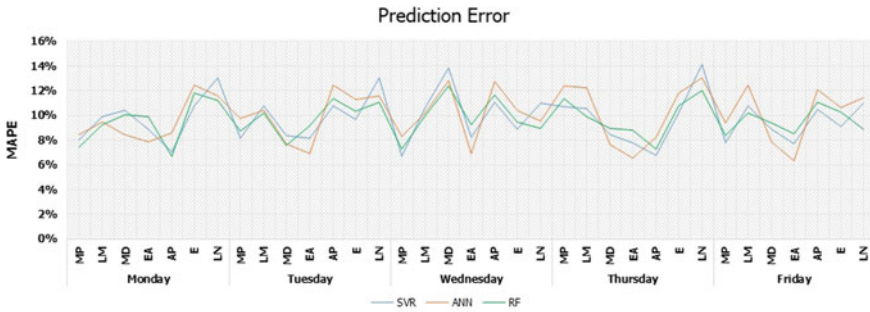


Fig. 7 Prediction error for the inbound direction

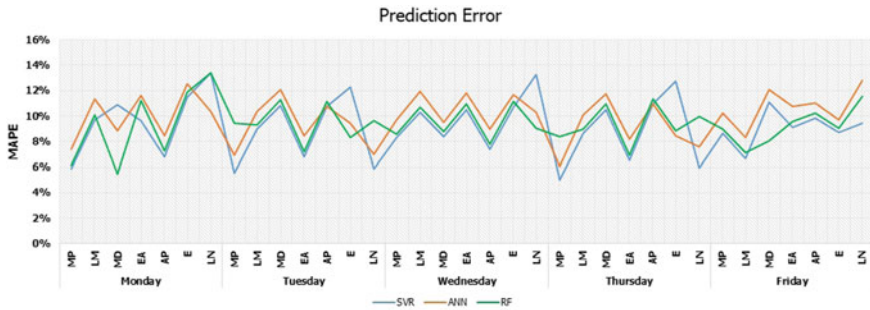


Fig. 8 Prediction error for the outbound direction

Figures 7 and 8 present the MAPE values of the prediction models in each time period for five days by performing one step ahead prediction on weekdays.

First, we observed the prediction results for five days. For the inbound direction on Monday in morning peak (MP), the RF model obtained the lowest prediction error of approximately 6.72% and on Wednesday in morning peak (MP), the SVR model obtained the lowest prediction error of approximately 6.70%. Next on Tuesday, Thursday and Friday always in early afternoon (EA), the ANN model obtained the lowest prediction error of approximately 6.94%, 6.57% and 6.31% respectively. While, for the outbound direction, the RF model obtained the lowest prediction error on Monday for midday (MD) of approximately 5.46%, the SVR model was next,

**Table 5** Average MAPE of prediction error

Models	Direction	MP (%)	LM (%)	MD (%)	EA (%)	AP (%)	E (%)	LN (%)
SVR	Inbound	8.27	10.53	9.99	8.16	9.22	9.74	12.45
	Outbound	6.68	8.85	10.33	8.52	9.13	11.19	9.58
ANN	Inbound	9.65	10.95	8.90	6.93	10.82	11.33	11.43
	Outbound	8.07	10.40	10.84	10.16	10.01	10.35	9.61
RF	Inbound	8.63	9.90	9.67	9.14	9.63	10.52	10.42
	Outbound	8.30	9.24	8.89	9.17	9.55	9.84	10.71

obtaining the lowest prediction error for several days i.e., on Tuesday in morning peak (MP), Wednesday in afternoon peak (AP), Thursday in morning peak (MP) and on Friday in late morning (LM), with values of approximately 5.55%, 7.37%, 5.02% and 6.69% respectively.

In general, the observations indicate that there is no significant difference in the distribution of MAPE between the three models. However, it can be clearly seen for the inbound direction that the ANN model outperformed the SVR and RF models for the prediction travel time on several days, especially in time periods with recurrent variability i.e., early afternoon (EA). On the other hand, for the inbound and outbound directions the SVR and RF models give better prediction results compared to the ANN model in predicting travel time in time periods with non-recurrent variability i.e., in morning peak (MP), afternoon peak (AP) and evening (E). Recurrent and non-recurrent variability of travel time were observed as described in Sect. 3.2.1.

Second, in order to clarify the above discussion, we carried out further analysis on overall average MAPE for each time period for the three models. The analysis results can be seen in Table 5.

As can be seen in Table 5, the SVM and the RF models have the lowest MAPE value in morning peak (MP), afternoon peak (AP) and evening (E). However, the SVR model obtained worse prediction results for the inbound direction in late night (LN) and midday (MD), with values of approximately 9.99% and 12.45% respectively. At the same time, the RF model also obtained worse prediction results in late night (LN) for the outbound direction, compared with the ANN model. In summary, the SVR and RF models outperform the ANN model in most cases, but there were no significant differences between the three models. Also, the results of three models showed acceptable performance and are in the reasonable error range in predicting the travel time over unstable intervals.

#### 4.4 Model Comparison

In order to discover the characteristics of the training data in our previous study [5], we conducted other experiments predicting travel time in each time period for the

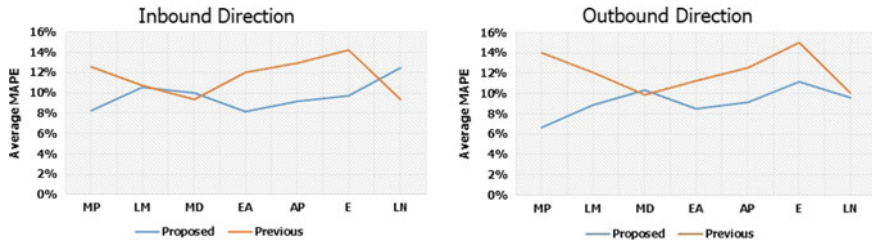


Fig. 9 Comparison of the prediction error

inbound and the outbound directions according to the training model in our previous study. Since the SVR model had the best performance in this study, we repeated the experiments five times as we conducted experiments in Sect. 4.2.

On the other hand, to make a fair comparison with this study, we conducted experiments on our previous model using time series data for 20 days; each day is divided into eight time periods and we predicted for 7 time periods in a day. Next, we conducted experiments using **WEKA version 3.8** as described in Sect. 4.1. RBF was selected as the kernel function, parameters were  $C : 1.0$ ,  $\varepsilon : 1.0E-12$ , and  $\varepsilon$  parameter tolerance: 0.001.

We compared the results between our proposed model and the previous model using average MAPE values. The experimental results shown in Fig. 9 illustrate that our proposed model obtained lower MAPE results than our previous model, except for two time periods of travel time i.e., midday (MD) and late night (LN) for the inbound direction and midday (MD) for the outbound direction. In addition, we focused on the time periods with non-recurrent properties: morning peak (MP), late morning (LM), afternoon peak (AP), and evening (E), for the inbound and the outbound directions. The results above indicate that our proposed model outperformed the previous model, especially in prediction for the time periods with non-recurrent variability of travel time.

Next, we conducted a t-test in SPSS software to see if there are any significant differences between the prediction results. In this procedure, we compared our proposed model and previous model in each time period for all days. Table 6 shows that there are significant differences between the proposed and previous models; for the inbound direction there are five such time periods i.e., morning peak (MP), early afternoon (EA), afternoon peak (AP), evening (E) and late night (LN). While, for the outbound direction there are four such time periods i.e., morning peak (MP), early afternoon (EA), afternoon peak (AP) and evening (E). Considering the above results, we can say that the proposed model in this study outperformed our previous model and there are significant differences between them.

**Table 6** Paired sample test

Proposed versus Previous	Inbound		Outbound	
	T-value	P-value	T-value	P-value
Pair 1 MP	-8.427	<b>0.001</b>	-7.829	<b>0.001</b>
Pair 2 LM	-0.647	0.553	-2.367	0.077
Pair 3 MD	1.113	0.328	1.633	0.178
Pair 4 EA	-13.083	<b>0.000</b>	-3.270	<b>0.031</b>
Pair 5 AP	-3.847	<b>0.018</b>	-3.924	<b>0.017</b>
Pair 6 E	-7.039	<b>0.002</b>	-3.567	<b>0.023</b>
Pair 7 LN	6.057	<b>0.004</b>	-0.270	0.801

## 5 Conclusion and Future Work

It is a challenging problem to accurately predict bus travel time over each unstable interval between pairs of adjacent bus stops because the characteristics of the travel time over unstable intervals include non-recurrent properties as well as recurrent ones. In this study, we built our prediction model using three machine learning techniques: SVR, ANN and RF, with a time series model approach. We applied the models to more than 2000 intervals on 77 routes to predict travel time over unstable intervals. Before building the prediction model, we conducted exploratory data analyses to clarify its characteristics, especially the variability of the unstable intervals. Based on the analysis results, we determined two input variables: HATT and DATT, for the prediction model.

To validate the proposed model, we conducted experiments using 20-weekday data, where we used 14-days data as training data, 1-day data as validation data, and 1-day data as test data in the prediction step at the beginning. From the second prediction step, we added validation data from the previous step to the training data, used the test data in the previous step as validation data, and chose another 1-day data from the 5-day test data as test data in the current prediction step. We repeated the prediction step five times and each prediction step produced prediction results for one step ahead.

Experimental results showed that our proposed model provided promising performance in predicting travel time over unstable intervals compared to our previous model. The results also indicated that our proposed model accurately and dynamically predicted travel time over unstable intervals for each time-period in a day, especially for the time periods with non-recurrent variability of travel time. This means that bus travel time can be reasonably estimated using both DATT and HATT data over unstable intervals.

In our future work, we will strive to continuously improve our prediction models focusing on rush/peak hours and off-peak periods of travel time.



**Acknowledgements** The probe data used in this study were provided by **NISHITETSU Bus Company in Fukuoka, Japan**. This work is partially supported by **JSPS KAKENHI Grant Number JP15H05708**.

## References

1. Amita, J., Jain, S., Garg, P.: Prediction of bus travel time using ANN: A case study in Delhi. *Transp. Res. Procedia* **17**, 263–272 (2016)
2. As, M., Mine, T.: Empirical study of travel time variability using bus probe data. In: *IEEE International Conference on Agents (ICA)*, pp. 146–149. IEEE (2016)
3. As, M., Mine, T.: Estimation of travel time variability using bus probe data. In: *6th IEEE International Conference on Advanced Logistics and Transport (ICALT)*, pp. 68–74. IEEE (2017)
4. As, M., Mine, T.: An adaptive approach for predicting bus travel time over unstable intervals. In: *The 16th ITS Asia-Pacific Forum FUKUOKA, (ITS AP)*, pp. 146–160. ITS Asia Pacific and ITS Japan (2018)
5. As, M., Mine, T.: Dynamic bus travel time prediction using an ANN-based model. In: *The 12th International Conference on Ubiquitous Information Management and Communication (IMCOM)*, p. 8. ACM (2018)
6. Bai, C., Peng, Z.R., Lu, Q.C., Sun, J.: Dynamic bus travel time prediction models on road with multiple bus routes. *Comput. Intell. Neurosci.* **2015**, 63 (2015)
7. Breiman, L.: Random forests. *Mach. Learn.* **45**(1), 5–32 (2001). <https://doi.org/10.1023/A:1010933404324>
8. Chen, M., Liu, X., Xia, J., Chien, S.I.: A dynamic bus-arrival time prediction model based on APC data. *Comput. Aided Civ. Infrastruct. Eng.* **19**(5), 364–376 (2004)
9. Chen, S., Billings, S., Grant, P.: Non-linear system identification using neural networks. *Int. J. Control* **51**(6), 1191–1214 (1990)
10. Diaconescu, E.: The use of NARX neural networks to predict chaotic time series. *Wseas Trans. Comput. Res.* **3**(3), 182–191 (2008)
11. Gal, A., Mandelbaum, A., Schnitzler, F., Senderovich, A., Weidlich, M.: Traveling time prediction in scheduled transportation with journey segments. *Inf. Syst.* **64**, 266–280 (2017)
12. Müller, K.R., Smola, A., Rätsch, G., Schölkopf, B., Kohlmorgen, J., Vapnik, V.: Using support vector machines for time series prediction. In: *Advances in Kernel Methods-support Vector Learning*, pp. 243–254 (1999)
13. Patnaik, J., Chien, S., Bladikas, A.: Estimation of bus arrival times using APC data. *J. Public Transp.* **7**(1), 1 (2004)
14. Rodriguez-Galiano, V., Sanchez-Castillo, M., Chica-Olmo, M., Chica-Rivas, M.: Machine learning predictive models for mineral prospectivity: an evaluation of neural networks, random forest, regression trees and support vector machines. *Ore Geol. Rev.* **71**, 804–818 (2015)
15. Satoshi, F.: On the subject of probe data. Director of the Research Center for Advanced Information Technology (2011)
16. Tyralis, H., Papacharalampous, G.: Variable selection in time series forecasting using random forests. *Algorithms* **10**(4), 114 (2017)
17. Uno, N., Kurauchi, F., Tamura, H., Iida, Y.: Using bus probe data for analysis of travel time variability. *J. Intell. Transp. Syst.* **13**(1), 2–15 (2009)
18. Vanajakshi, L., Rilett, L.R.: Support vector machine technique for the short term prediction of travel time. In: *2007 IEEE Intelligent Vehicles Symposium*, pp. 600–605. IEEE (2007)
19. Vapnik, V.: *The Nature of Statistical Learning Theory*. Springer Science & Business Media (2013)
20. Wu, C.H., Ho, J.M., Lee, D.T.: Travel-time prediction with support vector regression. *IEEE Trans. Intell. Transp. Syst.* **5**(4), 276–281 (2004)

21. Wu, X., Zhang, H.: Analysis of time-dependent travel time reliability for urban corridors: a case study in Houston. In: 2016 IEEE 19th International Conference on Intelligent Transportation Systems (ITSC), pp. 1939–1944. IEEE (2016)
22. Yassin, I.M., Taib, M.N., Adnan, R.: Recent advancements & methodologies in system identification: a review. *Sci. Res. J.* **1**(1), 14–33 (2013)

# Dynamic Arrival Time Estimation Model and Visualization Method for Bus Traffic



Kei Hiroi, Hitomi Imai and Nobuo Kawaguchi

**Abstract** Bus transportation service is more strongly influenced than other public transport modalities by various factors such as traffic congestion, weather conditions, number of passengers, and traffic signals. These factors often cause delays, and users may feel inconvenienced when waiting at a bus stop. Few studies have analyzed the relationship between operational situations and multiple different factors by visualization. Thus, we propose an arrival time estimation method and a visualization model. The arrival time estimation model dynamically updates the accuracy via an estimation method using a combination of a multiple-regression model and a Kalman filter. The visualization model analyzes relationships between delays and various factors. The goal of this study is to realize a society where people can use buses more comfortably.

## 1 Introduction

Many people use public transport in the form of bus service. According to a survey by the Ministry of Land, Infrastructure, Transport and Tourism [1], in Japan, approximately 12 million people use this service every day. Recently, traffic data have begun to be collected by various systems [2], for example, bus arrival information systems.

---

K. Hiroi (✉) · H. Imai  
Graduate School of Engineering, Nagoya University, Furo-cho, Chikusa-ku,  
Nagoya, Aichi 464-8603, Japan  
e-mail: [k.hiroi@ucl.nuee.nagoya-u.ac.jp](mailto:k.hiroi@ucl.nuee.nagoya-u.ac.jp)

H. Imai  
e-mail: [imai@ucl.nuee.nagoya-u.ac.jp](mailto:imai@ucl.nuee.nagoya-u.ac.jp)

N. Kawaguchi  
Graduate School of Engineering/Institutes of Innovation for Future Society,  
Nagoya University, Furo-cho, Chikusa-ku, Nagoya, Aichi 464-8603, Japan  
e-mail: [kawaguti@nagoya-u.jp](mailto:kawaguti@nagoya-u.jp)

Such systems obtain bus information using GPS: arrival or departure time, traveling locations (latitude and longitude), etc. In addition, the number of passengers and the behavior of the driver are also recorded. On the other hand, bus operation situations are more strongly influenced than other public transport modalities by traffic congestion [3], weather condition [4], number of passengers [5, 6], traffic signals [7], etc. These factors [8] are related to delays, and the motion of buses changes in a complicated manner [9, 10]. Many services inform the users of departures from a bus stop [11, 12], but few services provide specific estimated arrival or delay times. Few studies have analyzed the relationships between operational situations and multiple factors by visualization. When a bus is delayed, passengers may feel inconvenienced when waiting at the bus stop. Thus, we propose an arrival time estimation method and a visualization model: “EMRF (Extended Multiple Regression Filter) model”. The arrival time estimation model dynamically updates the accuracy via an estimation method using a combination of a multiple-regression model and a Kalman filter. The multiple-regression model estimates the trend in advance, and the Kalman filter updates the estimation to the optimal state based on the trend in Fig. 1. As a feature of this method, the closer the bus is to the terminal station, the better the accuracy. “Bus Tapestry” is the visualization model, which analyzes relationships between delays and factors. This model creates a heat map of operational situations (delays or premature arrival) and adds bus stop positions, signal positions, and bus traffic data. We can thereby visually find factors related to delays. The goal of this study is to realize a society whereby people can use buses more comfortably.

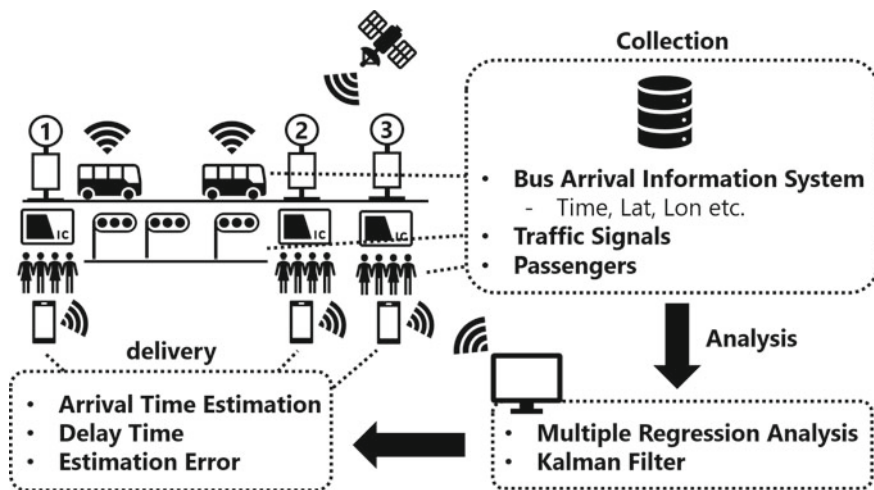


Fig. 1 Outline of the proposed system

## 2 Literature Review

### 2.1 Multiple-Regression Analysis

Multiple-regression analysis is a linear model and derives the dependent variable  $Y$  using multiple independent variables  $X_i (i = 0, 1, \dots)$  by Eq. 1 as follows:

$$Y = a_0 + a_1X_1 + \dots + a_iX_i \quad (1)$$

where  $a_i$  is a coefficient calculated for each independent variable. In the study by Jayakrishna and Chien [13], the dependent variable was the estimated time taken between bus stops. Independent variables, such as the time required for the timetable, the distance between bus stops, the number of passengers, and the time to open and close the door, were factors that influenced delays. The estimation under this model was highly accurate. However, multiple-regression analysis is a static estimation based on the past data and does not consider increased passengers due to rainy weather or events being held near the bus stop. Therefore, it is difficult to respond to such a real-time changing environment and present the estimated arrival time to users.

### 2.2 Kalman Filter

The Kalman filter is a powerful mathematical tool for estimating the future states of variables even without knowing of the precise nature of the system modeled. In the study by Chen et al. [14], the time required in the next interval was dynamically estimated based on the time required for the timetable and information accumulated from the starting station. Although the Kalman filter can process information including errors and perform estimation dynamically, accurate estimation is difficult when a bus stop interval is characteristic.

## 3 Model Development

### 3.1 Arrival Time Estimation

The EMRF model consists of a multiple-regression model and Kalman filter. Before departure, the multiple-regression model estimates changes in inputs, and after departure, the Kalman filter performs estimation dynamically from the difference between the measured value and the estimated value based on the preliminary estimation.

First, we explain the multiple-regression analysis in this study. The dependent variable is the estimated time taken between bus stops [13]. The independent variables are factors that influence delays [15] such as bus stop sections, delays ahead of  $n$  stations, the time zone, the day of the week, the time required for the timetable, and the number of passengers. The delay is defined as the difference between the required time for the timetable and the actual required time. For the time zone, Early Morning is defined as until 7:00, Late Morning is defined from 8:00 to 10:00, Early Noon is defined from 10:00 to 13:00, Late Noon is defined as from 13:00 to 17:00, Evening is defined from 17:00 to 19:00, and Night is defined after 19:00. For the number of passengers, the number of people getting onto the bus is compared with the number getting off, and the higher number is recorded.

Second, we describe our Kalman filter in Fig. 2. Based on the estimation of the multiple-regression model, the Kalman filter estimates the required time for each bus stop interval. The end point is defined as the bus stop  $N$ . At a given bus stop  $k$ , the EMRF model estimates the times required for bus stop intervals  $k - (k + 1)$ ,  $k - (k + 2)$ ,  $\dots$ ,  $k - N$ . We input values estimated by a multiple regression model as the initial state of the system. Specifically, for  $k = 1$ , an estimated value is calculated using past data. For  $k > 1$ , the model calculates the real time differences (delay or premature arrival) using the estimated value for the bus stop interval  $(k - 1) - N$ , together with the timetable used in the calculation, and it inputs the results that are re-estimated using the multiple-regression model. After the bus leaves the starting station, the model updates the system status and estimated value each time it arrives at the bus stop and repeats this motion until it reaches the end point. By repeating the update, it is possible to correct the value even if the estimated and actual measured values are different from each other. Additionally, as the bus approaches the end point, the accuracy of the estimation can be improved.

In general, the Kalman filter estimates the state of the system at time  $(k + 1)$  using the state equation based on the previous state by Eq. 2 as follows:

$$x_{k+1,j} = \Phi_{k+1}x_{k,j} + u_k + Wk,j \tag{2}$$

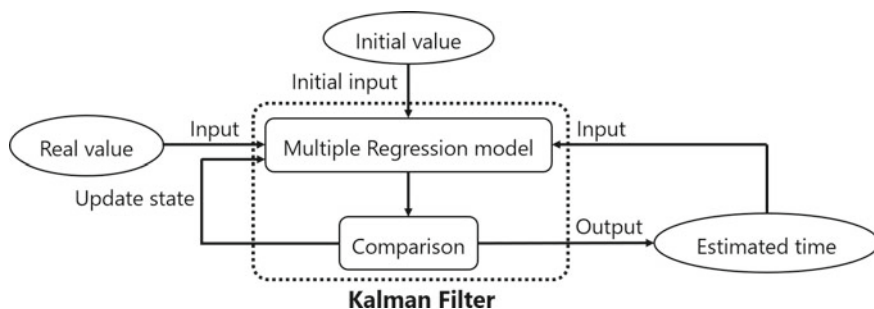


Fig. 2 Outline of the proposed method

where  $x_{k+1,j}$  is the state of the system at time  $(k + 1)$ ,  $\Phi_{k+1}$  is the state-transition model,  $u_k$  is the state vector, and  $W_{k,j}$  is noise. We use a multiple-regression model (Eq. 1) instead of the state vector  $u_k$  in Eq. 2. The relationship between an observation value  $z_k$  and a state variable  $x_{k,j}$  is expressed by the observation equation of Eq. 3.

$$z_k = H_k x_{k,j} + v_{k,j} \quad (3)$$

where  $H_k$  is the observation model and  $v_{k,j}$  is noise. We define the state variable  $x_{k,j}$  as the estimated time  $E_{k,j}$  and the real time required  $R_k$  in Eq. 4 as follows:

$$x_{k,j} = (E_{k,j}, R_k) \quad (4)$$

where  $E_{k,j}$  is the total value from an arbitrary bus stop  $k$  to the bus stop  $j$  and  $R_k$  is the total value from the starting station to the bus stop  $k$ .

### 3.2 Visualization

Bus Tapestry creates a heat map of operational situations (delays or premature arrival) and adds bus stop positions, signal positions, and bus traffic data. This visualization method attempts to determine and find a tendency of bus delays and their reasons to use large-scale bus traffic data as a scatter plot. The vertical axis is the time zone, the horizontal axis is the distance from the starting to the ending bus stop, and each position is the accumulated distance.

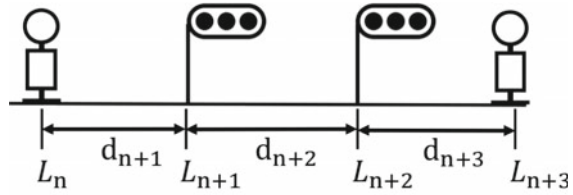
First, we explain how to process the data. Our visualization expresses operational situations by the difference between the actual time required and the required time. The value is positive when the bus is later than the timeline suggests, and it is negative when the bus is earlier than the timeline suggests. The route distance is the total value based on the bus stop and the location information of the signal (latitude and longitude) in Fig. 3a. Our method calculates the interval distances  $d_{n+1}$  from  $L_n$  to  $L_{n+1}$  using the information at each position. The total distance  $L_{n+1}$  is the sum of their values in Eq. 5 as follows:

$$L_{n+1} = L_n + d_{n+1} \quad (5)$$

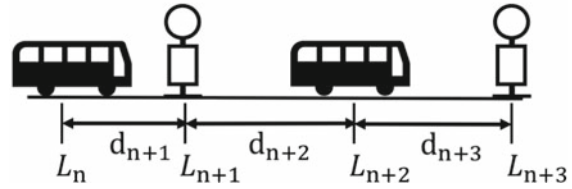
In this study, our method does not consider the curvature of the road, for example. We did not process data from the bus arrival information system because these data might include errors. Similarly, the travel distance of the bus is also the sum of the distances between the locations traveled in Fig. 3b. For the travel distance, the location of the bus stop is the point at which the departure information was recorded.

Second, we describe how to visualize the data. Our method visualizes operational situations and the signal position using our created data. The heat map represents operational situations (delays or premature arrivals), where the vertical axis is the time zone (hour) and the horizontal axis is the distance (km). The horizontal axis

**Fig. 3** Definition of interval and total distance



(a) Case of Bus Stops and a Signal.



(b) In Case of Bus.

expresses the distance between bus stops by putting the same data every 0.01 km within each bus stop interval. We add the signal position data (mileage) and make the number of traffic signals between routes visible. Consequently, we can analyze the influence of the signals between bus stops and operational situations of each time zone. Furthermore, we can evaluate the operational situations in greater detail by adding the location information of each bus to the visualized data.

## 4 Data Collection

In this study, data were collected from the bus arrival information system. The recorded area is located in the Aichi Prefecture and includes information on position, time, route, bus stop, etc. These data were provided by the Transportation Bureau City of Nagoya [11] and the Meitetsu Bus Company Limited [12] through the Location Information Service Research Agency (Lisra) [16]. The above data were recorded when arriving and departing a bus stop and during communications at 30 s intervals. The range for the data collection was from December 13–22, 2014. This dataset includes 1030 buses, 3784 bus stops and 664 routes. These data were recorded only when departing the bus stop. The range for data collection was for July 1–15, 2016 and from January through October 2017. This dataset includes 710 buses, 1539 bus stops and 523 routes. The number of passengers was provided by the Meitetsu Bus Company Limited. In addition, we indicate each position of traffic signals on the target bus routes.



## 5 Analysis of Results

### 5.1 Independent Variables and Coefficients of Multiple-Regression Model

We analyze whether the independent variables assumed in Sect. 3.1 are necessary and sufficient manner. First, we add “The amount of precipitation”, “Temperature”, “The number of signals in the bus stop sections” and “Interval distance” as the independent variables of our model. Table 1 shows a result of the multiple-regression analysis on the data for 1 month in March 2017 and 10 months from January to October 2017. In the multiple-regression analysis with the independent variables in Sect. 3.1, the coefficient of determination was 0.77 for the one month of data and 0.79 for the 10 months of data. In the multiple-regression analysis using Sect. 3.1’s variables, the amount of precipitation was 0.77 and 0.79. Although the coefficients slightly improved due to the increase in the data volume, we cannot confirm large changes due to the addition of independent variables.

### 5.2 Influence of Data Volume on p Value

Figure 4 shows the comparison results for the p value calculated by the multiple-regression analysis using the independent values of Sects. 3.1 and 5.1. The independent variables in Fig. 4 are arranged in descending order of p value for the data for 10 months. The coefficients of “bus stops interval 1–2”, “Early Morning” and “Monday” are 0, and the significance level (p value < 0.05) is represented by a red dotted line. According to Fig. 4, there are variables with significantly different p values for the data for 1 month and 10 months. Specifically, with regard to “The amount of precipitation”, “Temperature”, some “bus stop interval”, “Time zone”, “Day of week”, and “Delay in front of 2 stations”, the p value using the data for 1 month did not satisfy the baseline value. These independent variables resulted in less influence on the required time than the other factors; however, the p values changed significantly for the 10 months of data, and the p values that met the significance

**Table 1** Independent variables and coefficients

Independent variables	Coefficients (1 month)	Coefficients (10 months)
–	0.7715	0.7934
The amount of precipitation	0.7716	0.7935
Temperature	0.7715	0.7934
The number of signals	0.7715	0.7934
Interval distance	0.7715	0.7934

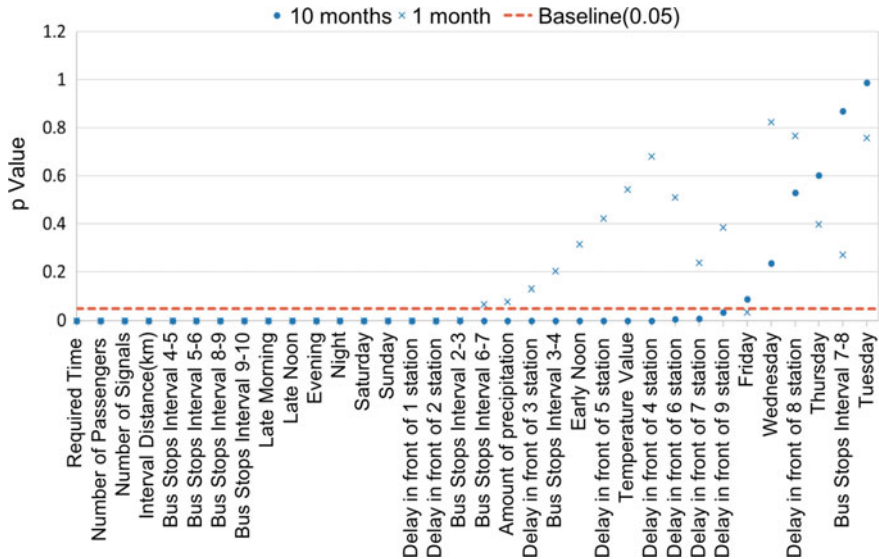


Fig. 4 p value of each independent variable

level increased. We think that this is because although these independent variables have minimal influence on the required time in the case using the data for one month, the data for 10 months include the day on which these independent variables work well. However, some independent variables using data for 10 months exceeded the level of significance, with the result that “Tuesday”, “Wednesday”, “Thursday”, and “Friday” had minimal impact. It seems that this was because of the similar operating conditions on weekdays and weekends. In addition, it was found that this situation considered more data, and the effectiveness of the independent variable increases. On the other hand, when using 10 months of data for “The amount of precipitation”, “temperature”, “number of signals” and “interval distance”, no p value remarkably increased compared to other p values. Therefore, these independent variables are thought to affect the required time.

### 5.3 Correlation between the Independent Variables

The added variables of “The amount of precipitation”, “temperature”, “number of signals” and “interval distance” were found to affect the required time; thus, we investigate the correlation between the independent variables. We calculate the correlation coefficient  $R$  for all independent variables assumed in this study, and we show the variables with  $|R| > 0.4$  in Fig. 5. “The delay in front of  $n$  stations” showed a strong correlation overall. This seems to be because the delay at the previous bus stop influences the delay of the next bus stop directly. There was also a strong correlation

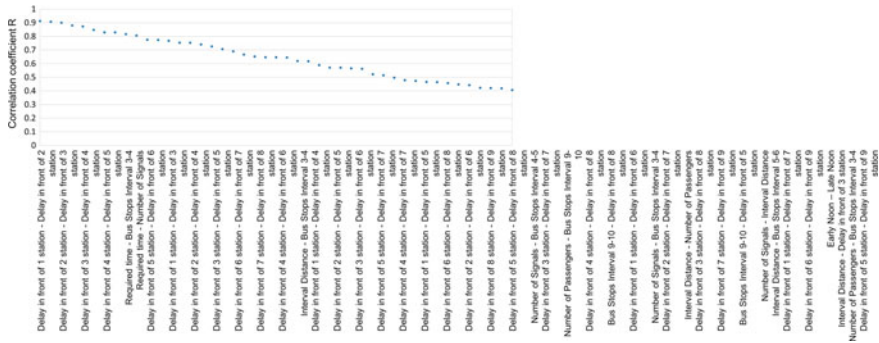
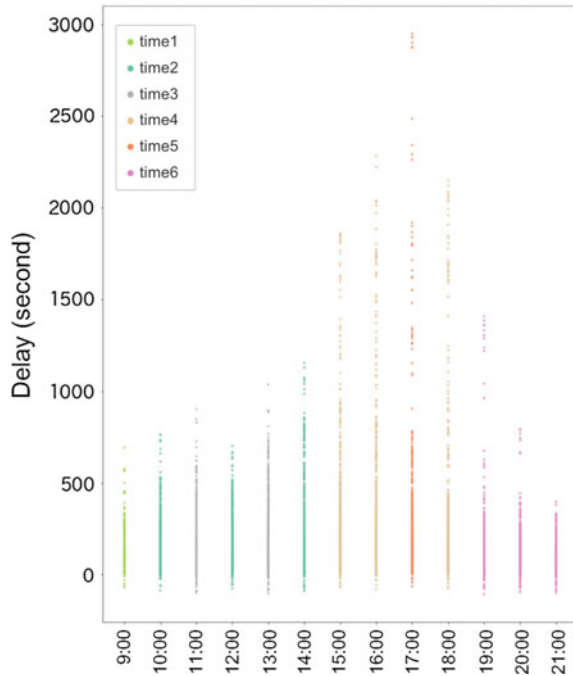


Fig. 5 Independent variables whereby  $|R| > 0.4$

between “The required time” and “Number of signals”. This is why no significant change was observed in the decision coefficient even when “number of signals” was added as an independent variable; thus, “the number of signals” could be one of the factors in setting the required time. In addition, the “number of signals” also shows a strong correlation with “interval distance”, and this tends to increase the number of signals as the distance increases. “Bus stop interval” sometimes showed strong correlation with other independent variables; however, “Bus stops interval” was a dummy variable and occurred because the values indicated by the factors were biased. However, “Early Noon” and “Late Noon” are dummy variables set under the same condition, and they must be independent variables. Since this time zones were arbitrarily categorized, we thought that the correlation could be weakened by rearranging it according to the bus location data of each area. Therefore, we classified the time zones into 6 classes based on the median, maximum and minimum of the time zone lag using k-means clustering. K-means is a typical non-hierarchical classification method that divides a set of data into  $l$  clusters. First, an arbitrary centroid  $\mu_i (i = 1, \Delta\Delta\Delta, l)$  is defined in the cluster as an initial value. Then, each point of the data is assigned to the cluster  $c_i$  having the closest centroid, and the centroid is updated to the average point of the data included in the cluster. The cluster assignment and the update of the centroid are repeated until the dispersion within the cluster is minimized to calculate the optimum classification result. Figure 6 shows the result of the classification of time zones in a route. Using this classification result, the correlations between time zones all achieve  $|R| > 0.4$ . Then, we removed “Number of signals” from the independent variables and improved the multiple-regression model for “time zone” tailored to each route.

**Fig. 6** Clustering result for time zone



#### 5.4 R-squared by Multiple-Regression Analysis

The results of a multiple-regression analysis are shown in Fig. 7. The data are from the Meitetsu Bus Company Limited, having a range of March 1–31, 2017. For comparative purposes, the R-squared for the Nagoya City Bus data is collected in Fig. 7. The range of the utilized data is for December 13–19, 2014. The R-squared value indicates how well an independent variable accounts for the variability of another, dependent variable. The value of R-squared ranges from zero to one, with values closer to one indicating a lower degree of relative error. The highest R-squared value was 0.90. However, since the coefficients had abnormally large values, such as  $5.86 \times 10^{11}$ , multiple-regression analysis could not be performed properly. This is because the route contains 25 bus stops, and as such, there are too many independent variables. On the other hand, the smallest R-squared value is 0.46. This seems to be caused by irregular congestion in a bus stop interval. The average value for Meitetsu Bus was 0.69, which was close to the average value of the Nagoya City Bus (0.76). However, the value of Meitetsu Bus was slightly lower than that of the Nagoya City Bus because there was less data on Meitetsu Bus than on Nagoya City Bus. Data of Nagoya City Bus were recorded when arriving and departing the bus stop and when communicating every 30 s, but data of Meitetsu Bus were only recorded when departing the bus stop. The relationship between the R-squared and the number of bus stops is shown in Fig. 8. The R-squared is 0.0053, and there was no correla-

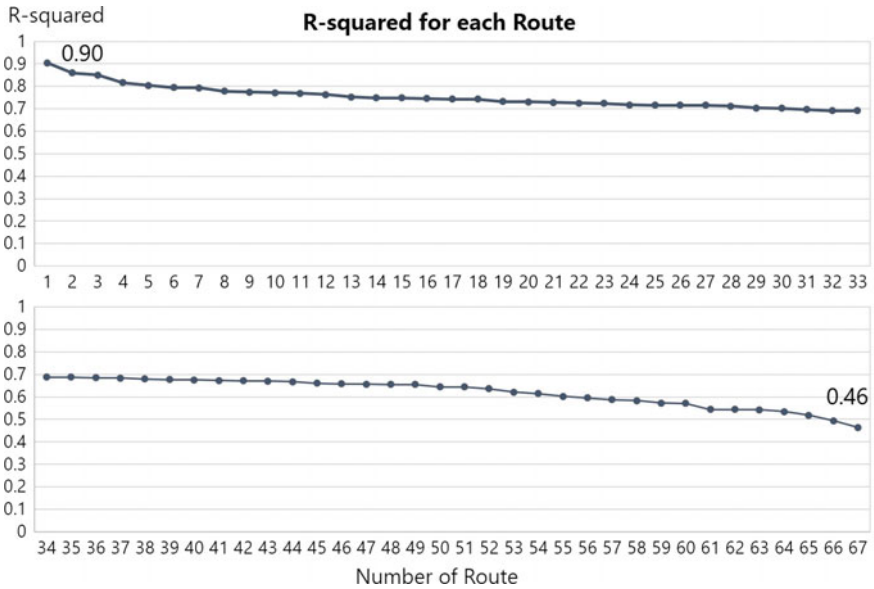


**Fig. 7** R-squared for Meitetsu Bus

**Table 2** R-squared for Nagoya City Bus

Route ID	R-squared
8415	0.79
8471	0.76
8784	0.69
8921	0.58
8939	0.80
8990	0.80
9014	0.80
9015	0.88
Average	0.76

tion between the multiple-regression analysis and the number of bus stops in Fig. 8 (Table 2).

### 5.5 Accuracy Verification by Changing the Amount of Data

We verified how a change in the amount of data affects the estimation accuracy using the multiple-regression model using the data from Meitetsu Bus Company Limited. The compared data were data for 14 days (July 1–14, 2016), 101 days (July

**Fig. 8** The relationship between the R-squared and the number of Bus Stops

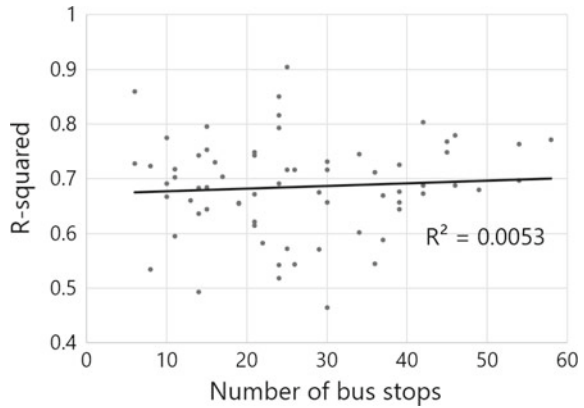


**Table 3** Variation of R-squared for Route 9

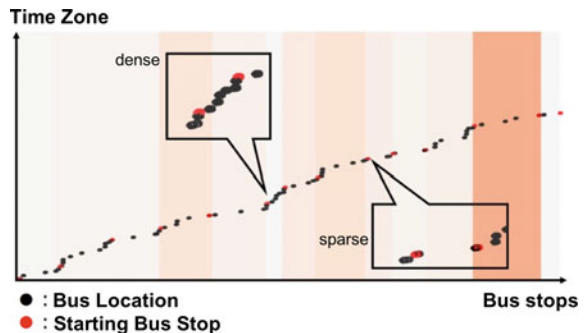
The type of data	R-squared
14 days	0.34
101 days	0.44
Excluding	0.55

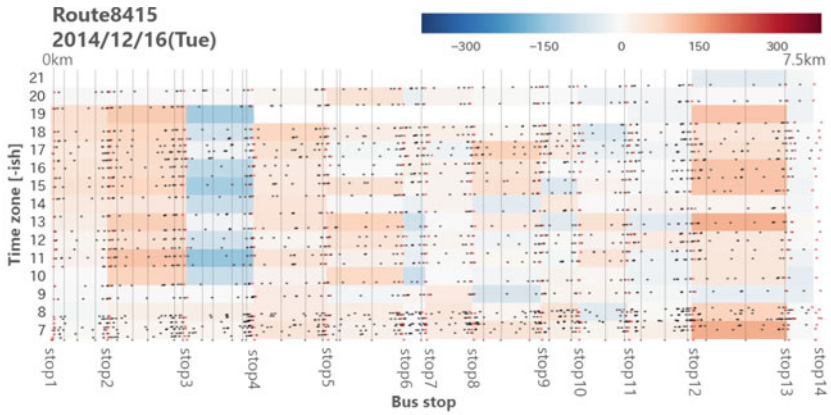
1–14, 2016 and from January to March 2017), and 101 days excluding the abnormal values. The estimated date is July 15, 2016. We removed the abnormal values using the interquartile range. We calculated the R-squared by comparing the estimated and actual values for route 9 (Fig. 7) in Table 3. Table 3 shows that the R-squared increased as the amount of data increased. Additionally, excluding the abnormal values further improved the estimation accuracy.

### 5.6 Visualization

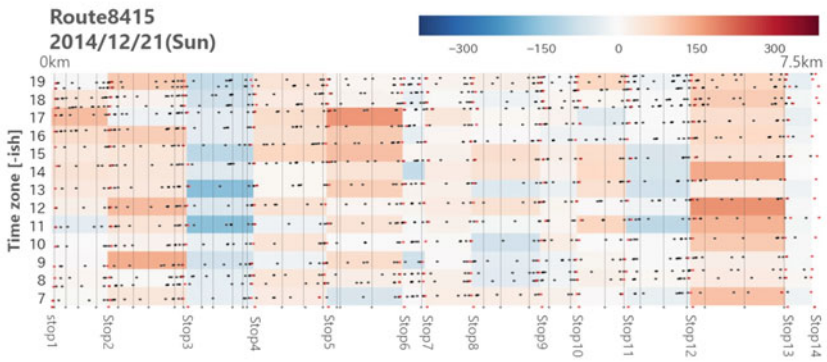
We used the data from the Transportation Bureau City of Nagoya on December 16 and 21, 2014. The result of our visualization is presented in Fig. 10. The black dots

**Fig. 9** Bus Tapestry sample

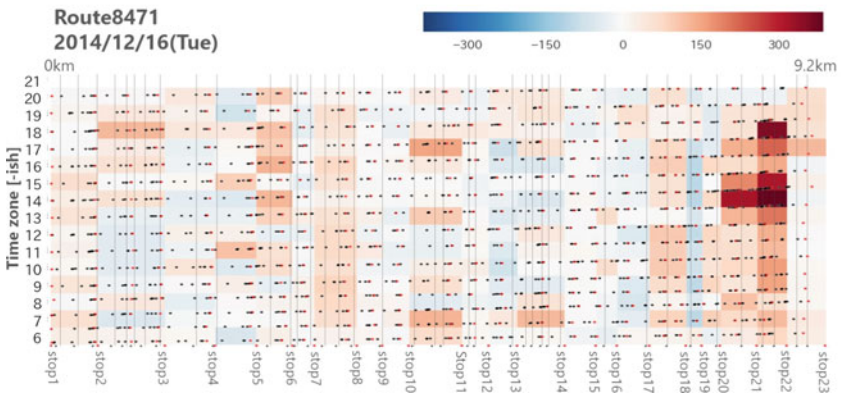




(a) Visualization for Route 8415 (Tue).



(b) Visualization for Route 8415 (Sun).



(c) Visualization for Route 8471 (Tue).

Fig. 10 Result obtained by Bus Tapestry

are the running positions of the bus, the red dots are the bus stop positions, and the dotted lines are the signal positions. The white areas in the heat map are the time zones during which the bus was not running. For example, Fig. 9 is an enlarged view of the initial time in Fig. 10a, where the bus travels along the y axis as time elapses. The points representing the positions of the bus are divided into sparse and dense points, where the bus does not move much when the points are dense but does move when the points are not dense.

Figure 10a, b are other days of the same route and show a similar delay condition overall. However, in the range of bus stop 5 to bus stop 6, we find that the delay on Sunday is greater than those on Tuesdays from 16:00 to 17:00. Figure 10a, c are the other route on the same day. They show that route 8471 has a large delay near three stations before the end point compared to route 8415. Moreover, in Fig. 10a, the signal between bus stop 2 and bus stop 3 does not significantly affect the delay because there are few points before it. On the other hand, the signal between stop 11 and stop 12 is likely to affect the delay because there are many points before it. Thus, we can visually identify the relationship between delay and factors using our visualization method.

## 6 Evaluation of the Model

We used the data from Meitetsu Bus Company Limited for March 1–31, 2017 for Route 9. The estimated date is Tuesday, January 31, 2017. The model was created for 30 days, excluding the estimated date. For the estimated date, the number of passengers and delay in front of  $n$  stations were the average of 30 days.

### 6.1 Comparison by Estimation Errors

For Schedule 10430, the estimation errors by the multiple-regression model and our model are presented in Fig. 11. Schedule 10430 is a bus running from 20 to 21 h. The estimation errors are the difference between the estimated value and the actual value. The error is positive when the EMRF model estimates are longer than the actual value and negative when the model estimates are shorter than the actual value. Figure 11 shows that the estimation errors are smaller than those of the multiple-regression model, and the EMRF model corrects the estimation.

### 6.2 Comparison by RMSE

We evaluate the models using the RMSE (Root Mean Squared Error) in Eq. 6 as follows:



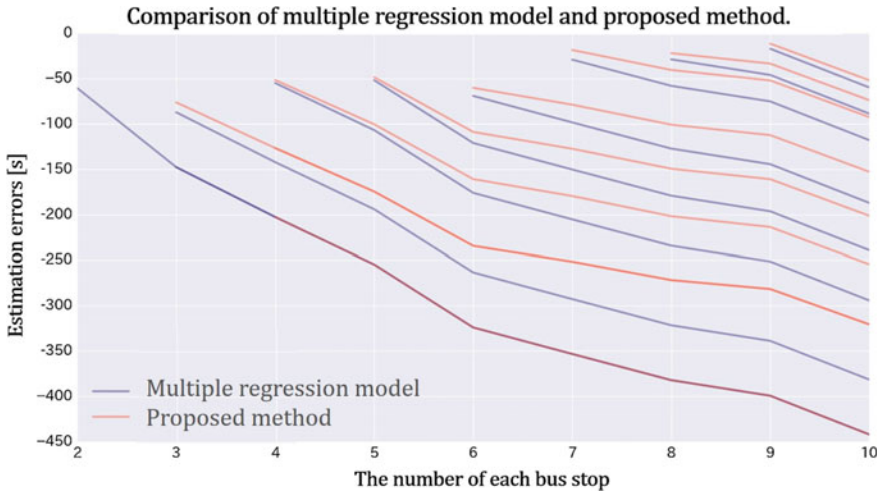
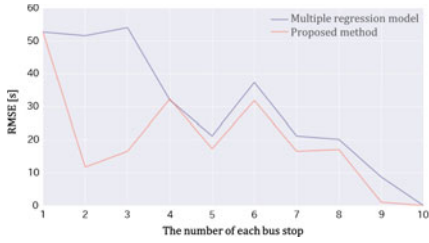


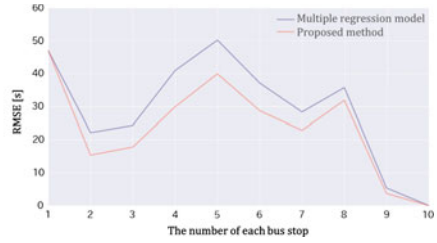
Fig. 11 Estimation error in route 9, schedule: 10430

$$RMSE = \sqrt{\frac{1}{N} \sum_{i=1}^N (y_i - \hat{y}_i)^2} \quad [s] \tag{6}$$

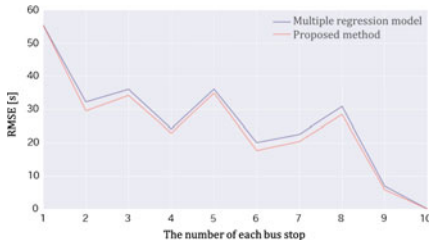
where  $N$  is the number of bus stop intervals,  $y_i$  is the actual value of the  $i$ -th bus stop interval, and  $\hat{y}_i$  is the estimated value of the  $i$ -th bus stop interval. The RMSE is an evaluation method that quantifies the difference between the estimated value and the actual value. An RMSE closer to 0 indicates a more accurate estimation. Figure 12 presents the the RMSE obtained by the multiple-regression model and our model. Schedule 10430 is a bus running from 10 to 11 h. The estimated date varied from March 1 to 31. The horizontal axis is the estimated bus stop, and the vertical axis is the RMSE. Figure 12a, b, presenting March 31 using data of other dates, show that the RMSE by our model is smaller than that obtained solely by using the multiple regression model. Especially in Fig. 12a, the estimation was well corrected at bus stop 2. In Fig. 12c, showing March 13, the results are approximately equal to those under the multiple-regression model. Then, we estimated the other route in Fig. 12d. Most of the RMSE values under our model showed a higher accuracy than the multiple-regression model except for bus stops 5 and 10. Similarly, for all schedules, the average RMSE is presented in Fig. 13. This figure shows that the RMSE was smaller in our model even in the case of using the average value for the data of one month. Therefore, it is assumed that our model can improve the estimation accuracy.



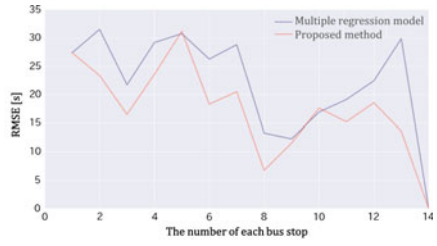
(a) Route 9, Schedule: 10400 (3/31).



(b) Route 9, Schedule: 10425 (3/31).



(c) Route 9, Schedule: 10400 (3/13).



(d) Route 10, Schedule: 11209 (3/31).

**Fig. 12** The RMSE for route 9 and route 10



**Fig. 13** The average RMSE

## 7 Examination of Presentation Method

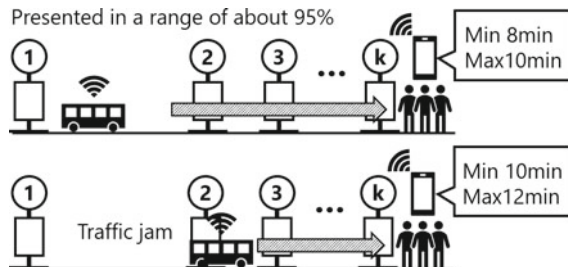
We propose a method for presenting the arrival time including estimation errors. Using the standard deviation, the estimated required time is calculated with some leeway and presented to users with an accuracy of approximately 95% using Eq. 7 as follows:

$$E' = E \pm 2SD(E - R) \tag{7}$$

where  $E'$  is the required time including estimation errors,  $E$  is the estimated required time, and  $R$  is actual required time. Showing users the earliest arrival time allows them to broaden their choice of actions, as in Fig. 14. For example, users might think “If this time is the earliest possible, let’s go to a convenience store” or “Since there is no need to hurry, let’s walk slowly”. Presenting the latest arrival time has the effect of alleviating the anxiety of “How long will I have to wait at the bus stop?” Our method can also show the estimated arrival time at the destination stop and inform the users of it because our model can be applied to all bus stop intervals. Presenting the specific estimated arrival times in this way gives users a more accurate idea of operational situations, making it easier to act upon such data.

Moreover, to investigate the viewpoints of the users on the presentation method of the estimated arrival time, we performed an investigation using questionnaires. This period was for January 29–30, 2018. We obtained responses from 184 people using SNS, where valid responses from 169 people were obtained. Respondents were asked to evaluate how they viewed estimation errors with 5 responses: “Never”, “Hardly ever”, “Neutral”, “Some of the time”, or “All of the time”. When the estimation errors are less than 1 min, “All of the time” accounted for approximately 90% of all responses. When the estimation errors are within 1–5 min, “All of the time”, “Some of the time” and “Neutral” accounted for approximately 90% of all responses. Therefore, it is assumed that the standard for estimation errors is less than 5 min. Figure 15 shows the results of the questionnaire on the presentation method. There were 4 types of sample types: “Estimated delay time”, “Estimated arrival time”, “Estimated time remaining”, and “Graphical presentation”. “Estimated arrival time” and “Estimated time remaining” each accounted for approximately 40% of all responses. Thus, we found that the users prefer to display the arrival time over the delay time. It is assumed

**Fig. 14** How to present the results to users



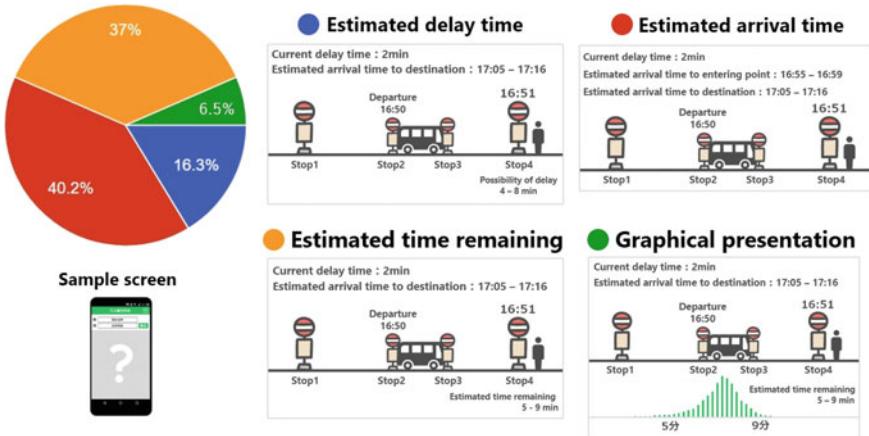


Fig. 15 The result of the questionnaire about the presentation method

that the users could comfortably use an application in which they could select the presentation method because the answers were divided.

## 8 Conclusion

In this study, we proposed the EMRF model and Bus Tapestry. The EMRF model is a dynamic model for arrival time estimation combining the multiple-regression model and the Kalman filter. We verified the accuracy of the estimation using the R-squared and evaluated the EMRF model by the RMSE. The results showed that the average estimation error improved from 186 s to 17 s. We also presented the estimated arrival time including estimation errors. We performed an investigation using the questionnaires and obtained 184 answers concerning the presentation method. The results showed that the standard estimation error was less than 5 min, and the users preferred to display the arrival time rather than the delay time.

Bus Tapestry is a visualization method for analysis of operational situations. We can visually compare the operational situations of other days or routes and potentially find different features. Additionally, we can see the relationship between delays and number of signals in greater detail. In the future, it may be possible to estimate abnormal values and use machine learning. Furthermore, to start an estimation service, it is necessary to conduct a demonstration experiment and collect the opinions of users.

**Acknowledgements** We wish to thank Meitetsucom Co. Ltd and Meitetsu Bus Co., Ltd for insightful suggestions and provision of bus traffic data. This research and development work was supported by the JST OPERA and the MIC/SCOPE #172106102.

## References

1. Ministry of Land, Infrastructure, Transport and Tourism. <http://www.mlit.go.jp/en/index.html> (Cited January 2018)
2. Yu, B., Lu, J., Yu, B., Yang, Z.: An adaptive bus arrival time prediction model. *Easten Asia Soc. Transp. Stud.* **8**, 1126–1136 (2010)
3. Michael, L.: Anderson: subways, strikes, and slowdowns: the impacts of public transit on traffic congestion. *Am. Econ. Rev.* **104**(9), 2763–2796 (2014)
4. Stover, V.W., McCormack, E.D.: The impact of weather on bus Ridership in Pierce County. *Washington J. Public Transp.* **15**(1), 95–110 (2012)
5. Zhang, C., Teng, J.: Bus dwell tme estimation and prediction : a study case in Shanghai-China. *Proced. Soc. Behav. Sci.* **96**, 1329–1340 (2013)
6. Shalaby, A., Farhan, A.: Prediction model of bus arrival and departure times using AVL and APC data. *Public Transp.* **7**(1), 41–61 (2004)
7. Tan, C.-W., Park, S., Liu, H., Qing, X., Lau, P.: Prediction of transit vehicle arrival time for signal priority control: algorithm and performance. *IEEE Trans. Intell. Transp. Syst.* **9**(4), 688–696 (2008)
8. Iu, A.: Adrian Friday: statistical modelling and analysis of spare bus probe data in Urban areas. In: *International IEEE Annual Conference on Intelligent Transportation Systems Madeira Island*, pp. 1256–1263 (2010)
9. Nagatani, T.: Dynamical transitions to chaotic and periodic motions of two shuttle buses. *Phys. A Statist. Mech. Appl.* **319**(1), 568–578 (2003)
10. Nagatani, T.: Chaos control and schedule of shuttle buses. *Phys. A Statist. Mech. Appl.* **371**(2), 683–691 (2006)
11. Toransportation Bureau City of Nagoya. <http://www.kotsu.city.nagoya.jp/en/pc/OTHER/TRP0001448.htm> (Cited January 2018)
12. Meitetsu Bus Company Limited. <http://www.meitetsu-bus.co.jp/english/index.html> (Cited January 2018)
13. Jayakrishna, P.S., Chien, A.B.: Estimation of bus arrival times using APC data. *J. Public Transp.* **7**(1), 1–20 (2004)
14. Chen, M., Liu, X., Xia, J.: Dynamic prediction method with schedule recovery impact for bus arrival time. *Transp. Res. Record J. Transp. Res. Board*, 208–217 (2005)
15. Tirachini, A.: Estimation of travel time and the benefits of upgrading the fare payment technology in Urban bus services. *Transp. Res. Part C: Emerg. Technol.* **30**, 239–256 (2013)
16. Location Information Service Research Agency. <http://lisra.jp/en> (Cited January 2018)

# Simulation for Passengers Convenience Using Actual Bus Traffic Data



Kei Hiroi, Takehiro Arai and Nobuo Kawaguchi

**Abstract** Public transport bus service is an important means of transportation for commuting, schooling and daily life. However, many unpredictable problems arise, resulting in delays caused by traffic congestion or an increased number of passengers. Changing the operation schedule may alleviate these problems; however, determining the optimal schedule change requires an iterative process of trial and error. As the number and diversity of changes increase, it becomes necessary to notify users many times, which places a heavy burden on both users and bus operators. In addition, it is difficult to evaluate what kind of schedule is best for passengers and bus operators. Therefore, in this study, we propose a framework for simulating and analyzing various driving situations. We define a “dissatisfaction degree” based on factors related to the convenience of passengers, such as the waiting time or the congestion rate, from simulations based on actual bus traffic data. Then, we measure and evaluate the dissatisfaction degree when the driving situation changes quantitatively. Additionally, we develop a tool to confirm how operations change based on the conditions of the simulation, such as the number of buses or passengers.

## 1 Introduction

Public transport bus service is an important means of transportation for commuting, schooling and daily life. For the convenience of the passengers, it is desirable for bus service to operate on time. Public transport bus service, however, is subject to many

---

K. Hiroi (✉) · T. Arai  
Graduate School of Engineering, Nagoya University, Furo-cho, Chikusa-ku,  
Nagoya, Aichi 464-8603, Japan  
e-mail: [k.hiroi@ucl.nuee.nagoya-u.ac.jp](mailto:k.hiroi@ucl.nuee.nagoya-u.ac.jp)

T. Arai  
e-mail: [arai@ucl.nuee.nagoya-u.ac.jp](mailto:arai@ucl.nuee.nagoya-u.ac.jp)

N. Kawaguchi  
Graduate School of Engineering/Institutes of Innovation for Future Society,  
Nagoya University, Furo-cho, Chikusa-ku, Nagoya, Aichi 464-8603, Japan  
e-mail: [kawaguti@nagoya-u.jp](mailto:kawaguti@nagoya-u.jp)

factors that interfere with scheduled operations. The bus operation situation is easily influenced by various factors, such as traffic congestion or weather conditions. The number of passengers is also a factor that affects the delay: the more passengers need to get on and off, the more time the bus will spend at the bus stop, and the more the arrival time at the next stop will be delayed as the number of passengers increases. These factors lead to bus delays and make bus service inconvenient.

On the other hand, bus location systems have recently emerged that can easily obtain various data, such as arrival and departure times and travel locations. Using such bus location data, we have analyzed the bus delays in Aichi Prefecture, Japan, and confirmed that there are delays at specific times and places, such as during commuting time in the morning and near the main station on holidays. Naturally, bus operators have been working to resolve these delay factors and planning to operate according to a given time schedule. However, bus operators must periodically revise their schedules since the road situation and the number of passengers are constantly changing as the population increases and as changes are made to nearby facilities and the operation plans for other transportation systems. Bus operation simulations are used for this purpose.

Wang et al. considered the optimization of bus operations by using time-dependent passenger demands and traffic patterns [1]. Duzha et al. simulated public transportation to mitigate congestion in the morning and evening through cooperation between municipalities and public transport operators [2]. Reference [3] simulated travel optimization by adjusting the departure times at specific stops to adjust bus departure times. These studies sought efficient and low-cost operation. However, it seems that these approaches show little consideration for the convenience of passengers.

In this study, we develop a simulation system to achieve both better bus operations and greater convenience for passengers using actual bus traffic data. We adopt the concept of a “dissatisfaction degree” as an index for measuring the convenience of passengers with respect to bus operations. We simulate bus operations in Okazaki City, Aichi Prefecture, where buses are delayed by 20 to 30 min on a daily basis due to congestion. The simulation calculates passenger appearance rates at each bus stop every hour based on passenger number data. Bus operations are simulated based on actual operation information and the numbers of passengers getting on and off. Various operation conditions are reproduced by adjusting the appearance probability of passengers and the bus arrival timing at bus stops. Then, in the area where traffic congestion occurs frequently, we evaluate how the dissatisfaction degree varies with the situation using our simulation. Furthermore, we develop a system for visualizing the simulation results and visually confirming the influence of changes in operation conditions. This research contributes (a) to the construction of a system for pursuing greater convenience for both bus operators and bus users and (b) to the efficient use of actual bus operation information and passenger number information.

## 2 Related Research

Many researchers have attempted to improve bus operations by using alternative methods to replace the optimization problem. Reference [4] addressed the optimization problem by representing the bus network with nodes and edges, [5] studied optimal bus operation with a genetic algorithm, [6] considered optimal bus operation using a random variable to represent the bus arrival time, and [7] used an ant colony algorithm to calculate the bus delay as a stochastic value. In [8], because of the difficulty of completely optimizing bus operations, inequalities were derived to obtain suboptimal solutions as a basis for optimization. Reference [9] studied the application of evolutionary algorithms to the operations of each bus individually.

Researchers have also attempted to reproduce bus operations using computer simulations. Reference [3] simulated bus optimization by adjusting bus arrival intervals by adjusting the departure times of buses at specific stops. References [10, 11] simulated the construction of a bus network considering road congestion and delays due to passengers getting on and off. In [2], in cooperation with local governments and public transportation facilities, the authors studied how to eliminate congestion in the morning and evening by simulating the operation of bus routes based on the population composition of the target city and road conditions.

Moreover, research on a new form of bus operation called on-demand bus operation, in which the passenger demand is observed in real time and used to determine travel plans, was conducted in [12]. The authors of [13, 14] are developing a system to determine the travel routes of buses in real time according to passenger demand.

In the research discussed above, optimization or simulation has been performed with the aim of mitigating congestion and delays in bus operations; however, appropriate optimization with respect to user preferences has not been done. For example, it is expected that during commuting and school hours, many people would prefer to arrive at their destinations as soon as possible even at the cost of some congestion. By contrast, those who are coming home from the shopping mall might prefer to take their time and be able to find a seat when boarding the bus. Therefore, in this study, in addition to improving the efficiency of operations from the bus operator's perspective, we also consider optimization from the user's perspective. Taking into account the changing seasons, different times of day, and the locations between which users require bus operations, we consider a system that will enable optimal bus operations at all times.

## 3 Proposal of the Dissatisfaction Degree for Bus Service

### 3.1 Definition of the Dissatisfaction Degree

We first present the “dissatisfaction degree”, which is used to quantify passenger convenience in bus use. The “dissatisfaction degree” is defined as an index that quantifies the difference between the operations desired by passengers and the actual



operations. This quantification of passenger convenience makes it possible to verify the effectiveness of various simulated bus operation schedules. In situations in which passengers' desired operations and the actual operations differ, passengers will typically use the bus under the assumption that the bus will be operated in accordance with the given timetable; thus, it is expected that any difference from passengers' desires will be caused by the actual operations being different from the timetable. The difference between the timetable and actual operations can be represented as a delay, and this delay has two components: a passenger's waiting time at the bus stop until the passenger boards the bus and the delay of the arrival time of the bus at its destination. Furthermore, if the passengers' buses are crowded, they will not be able to expect comfortable transportation to their destinations. The operation delay and level of congestion are thought to vary with various factors, such as the season, time of day, location, and weather.

This study therefore considers the "dissatisfaction degree", denoted by  $S$ , derived from the above three factors: the waiting time at the bus stop before boarding the bus,  $T_{wait}$ ; the delay of the arrival time at the destination,  $T_{delay}$ ; and the level of congestion,  $C$ , during boarding. We express the dissatisfaction degree by converting these factors into functions:  $f(T_{wait})$ ,  $g(T_{delay})$ , and  $h(C)$ . Although these factors are closely related (for example, a bus that is delayed in arriving at a bus stop where passengers are waiting will also be delayed in arriving at its destination), this paper assumes that each factor is independent, and the "dissatisfaction degree"  $S$  is expressed as a combination of the values associated with each factor as expressed in the following equation. Since each factor can vary due to seasonality or time of day, each function is given a weight,  $\omega_i$ :

$$S = \omega_1 f(T_{wait}) + \omega_2 g(T_{delay}) + \omega_3 h(C) \quad (1)$$

### 3.2 Derivation of the Functions Contributing to the Dissatisfaction Degree

Figure 1 shows the derivation of each function contributing to the dissatisfaction degree. The function  $f(T_{wait})$  is derived from the passenger's waiting time at the bus stop. In other words, it depends on the extent to which the actual arrival time is delayed with respect to the timetable. When the passenger must wait for 5 min or more because of bus delays, the value of the dissatisfaction degree increases. Since we expect that the longer the waiting time is, the greater the passenger's dissatisfaction will be,  $f(T_{wait})$  is assumed to increase linearly with the waiting time. However, it is not realistic to suppose that a passenger will remain waiting for a long time during daily bus use in a region with many operating buses. The delay of the target bus is likely to be related to a delay of the previous bus, meaning that waiting passengers will be able to board the previous bus instead. Therefore, the maximum bus waiting time is set to 20 min, and the upper limit of the function value is accordingly fixed to 30.

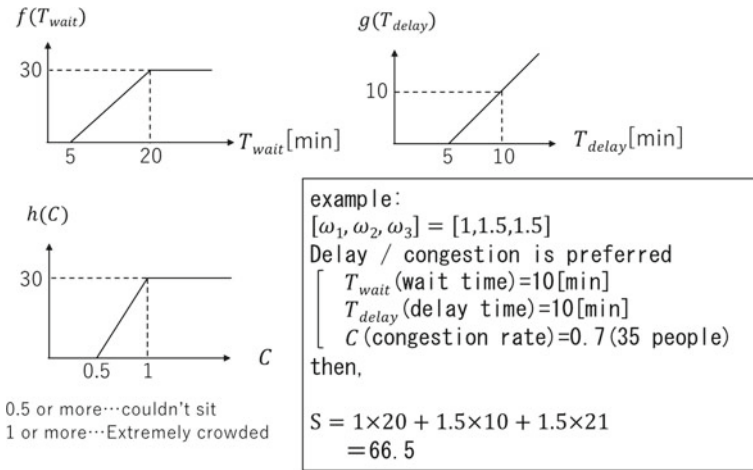


Fig. 1 Dissatisfaction degree function

The function  $g(T_{delay})$  is derived from the delay of the arrival time at the destination. When  $T_{delay}$  is 5 min,  $g(T_{delay})$  is defined as 0, and  $g(T_{delay})$  is defined to linearly increase as  $T_{delay}$  increases. Finally, we derive  $h(C)$  from the level of congestion on the bus. We set the level of congestion  $C$  to 1 when 50 people are on board. The seating capacity of our target buses is approximately 25 people; thus, a  $C$  value of 0.5 represents the threshold determining whether a passenger can find a seat when boarding. We expect that dissatisfaction will increase when passengers are not able to sit. The more passengers are on the bus and the more crowded the bus becomes, the more dissatisfied the passengers will be. However, because there is an upper limit on the number of passengers that can ride on one bus, the upper limit on  $h(C)$  is fixed to 30.

In this paper, these functions are designed using linear functions. However, various possibilities can be considered for function determination. To design a dissatisfaction degree that faithfully expresses the convenience of passengers, it is necessary to consider which functions are suitable. In this paper, we demonstrate the derivation of our dissatisfaction degree on the basis of simulations using actual data and the linear functions shown here, and we discuss the validity of the resulting values.

## 4 Simulation of the Dissatisfaction Degree

### 4.1 Outline

The dissatisfaction degree is derived from simulations based on actual bus traffic data. Our aim is to propose a method of optimizing operations by analyzing how the dissatisfaction degree varies with changes in the bus operation schedule. We

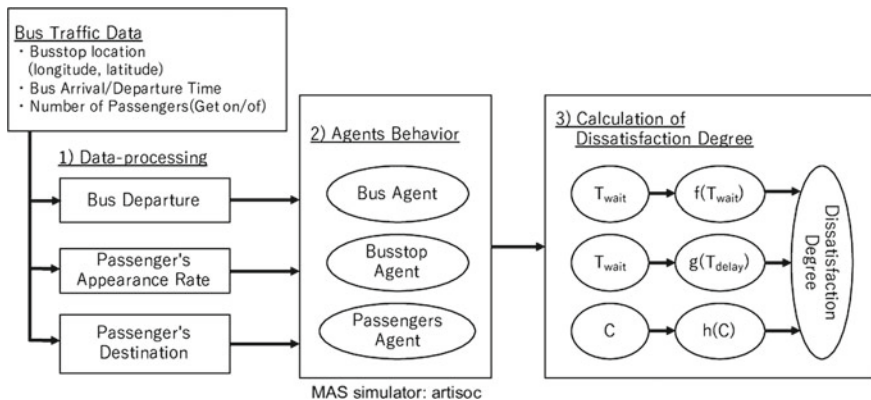


Fig. 2 Diagram of the simulation procedure

repeatedly simulate changes to the bus operation schedule and derive the resulting dissatisfaction degree to observe the changes in its numerical value. The methodology applied in this research is shown in Fig. 2. To reproduce bus operations, we generate three kinds of agents (bus agents, bus stop agents, and passenger agents), which imitate the actual movements and characteristics of the corresponding real agents based on actual data. (1) We use three types of data, namely, bus departure data, passenger appearance rate data, and passenger destination data, to calculate the dissatisfaction degree from simulations using actual data. (2) We simulate the behaviors of each agent based on these data. (3) We substitute the  $T_{wait}$ ,  $T_{delay}$ , and  $C$  values obtained from these data into the equations presented in the previous section to calculate the value of each function.

## 4.2 Bus Traffic Data

The actual data used are bus operation data collected by Meitetsu Bus Co., Ltd., through a bus arrival information system. Their bus arrival information system records data for each bus, including the unique bus ID, the actual/scheduled arrival/departure times at each bus stop, and the numbers of passengers who get on/off at each bus stop. This study uses data from Okazaki City, Aichi Prefecture, Japan, which is a major city with a large number of buses and passengers. Meitetsu Bus Co. has 710 buses, 1539 bus stops and 523 routes in Okazaki City. The data ranges correspond to July 1–16, 2016, and from January through October 2017. In particular, we use the data collected on July 8, 2016, the day when the number of passengers was the largest between July 1 and 16, 2016.

### **4.3 Multi-agent Simulator**

We develop our simulation using a multi-agent simulator (MAS): artisoc [15]. An MAS performs agent-based simulations in which an agent representing each object is placed in a defined space and each agent takes actions in accordance with behaviors determined for each step. In this study, three kinds of agents are defined: “bus stop agents”, “bus agents”, and “passenger agents”. We design the behaviors of these agents based on actual bus traffic data. The simulation outputs the data necessary for calculating the dissatisfaction degree. Then, we modify the bus operation schedule and analyze the resulting changes in the dissatisfaction degree for various operation schedules. The agents perform predetermined operations in each step. In this study, 1 step = 1 s.

#### **4.4 (1) Data Processing**

Based on the actual data, we generate three kinds of agents: bus agents, bus stop agents, and passenger agents. The data processing described here is the procedure used to determine the behavior of each agent based on the actual bus traffic data.

##### **4.4.1 Bus Departure**

The bus departure data comprise the bus stop route of each bus agent and the arrival and departure times at the bus stops. The bus departure data are generated using actual bus traffic data provided by Meitetsu Bus Co., Ltd. The bus traffic data consist of the unique bus IDs, the scheduled arrival/departure times, and the actual arrival/departure times. Based on these data, we created a database consisting of the target bus IDs and the corresponding routes (the lists of bus stops visited and their order) within the target area, Okazaki City. Furthermore, we generated a reference database for the bus departure steps in the simulation from the actual arrival and departure times of each bus at each bus stop. During our simulation, each bus agent refers to these databases to determine its behavior.

##### **4.4.2 Passenger Appearance Rate**

The passenger appearance rate data describe the proportion of passengers appearing at each bus stop as a function of time. This rate is a value calculated from the data on the boarding/alighting of passenger agents based on the actual bus traffic data. Although we have data on the number of passengers present at each bus stop, we cannot know when each passenger arrives at the bus stop and how long the waiting time at the bus stop is. Thus, we generate the passenger appearance rates—representing when passengers visit each bus stop—through simulation.

We calculate the number of passengers at each bus stop from the actual data. To determine the timing of when each passenger appears at the bus stop before the bus arrives, passengers are stochastically generated in accordance with the upper limit on the number of passengers at the target bus stop. Each bus stop agent judges whether a passenger should appear in every step based on the passenger appearance rate data. This judgment is based on a function that returns a random number in accordance with the Poisson distribution. Since  $1 \text{ step} = 1 \text{ s}$  in this study, the passenger appearance rate calculated in units of person/minute is divided by 60 to obtain the rate per second as the argument for this function.

We assume that only a return value of 0 or 1 can be obtained because the value of the argument is very small. This calculation uses the passenger number data for each bus stop and aggregates the data for every 15 min. Then, we divide the number of passengers for every 15 min period by 15 to calculate the passenger appearance rate per minute. We calculate the passenger appearance rate every 15 min.

#### 4.4.3 Passenger Destination

From the actual bus traffic data on the passengers' destinations, we determine the destination of each passenger agent. The destinations of the passengers are determined in accordance with the probabilities that passengers will get off at the various possible bus stops. Based on the data on the number of passengers getting off at each bus stop, we calculate the proportion of passengers getting off at each bus stop. The passengers' destinations are then calculated based on these proportions. For example, we consider a case in which two, three, and four passengers depart from bus stop  $s_1$  and have destination bus stops of  $s_2$ ,  $s_3$ , and  $s_4$ , respectively. The probabilities of alighting at each bus stop are then  $\frac{2}{2+3+4} \approx 0.22$  for  $s_2$ ,  $\frac{3}{2+3+4} \approx 0.33$  for  $s_3$ , and  $\frac{4}{2+3+4} \approx 0.44$  for  $s_4$ .

### 4.5 (2) Agent Behaviors for Bus Operations

Based on the actual data, we generate three kinds of agents: bus agents, bus stop agents, and passenger agents.

#### 4.5.1 Bus Agents

Figure 3 shows the simulation flow for the behavior of the bus agents. Each bus agent moves to the next bus stop and is loaded with waiting passengers. The bus agent has the route information determining the bus stops at which it stops. Each bus also has data on the number of passengers to board and the number of passengers getting off at each bus stop. After the boarding and alighting of passengers, the bus leaves at

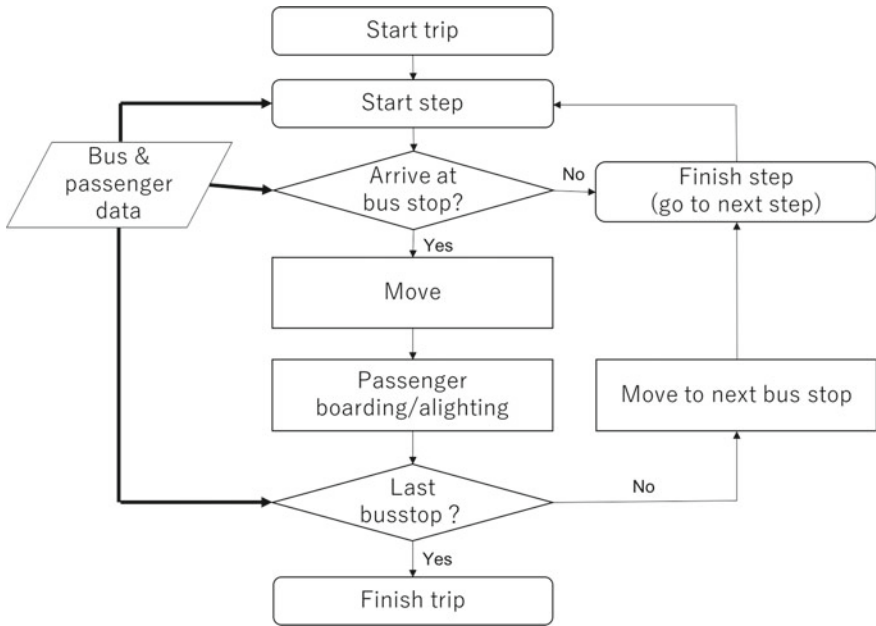


Fig. 3 Behavior flow of bus agents

the departure time recorded in the actual data. Then, the bus repeatedly heads for the next bus stop on its route, arrives, allows passengers to get on and off, and departs until it reaches the terminal station. The simulated arrival time at each bus stop is generated from the arrival times recorded in the actual bus departure data. We use the output of the passenger agent behavior as the data for the passengers’ destinations.

### 4.5.2 Bus Stop Agents

The role of each bus stop agent is to create the passenger agents who will board at the corresponding bus stop. The locations of the bus stop agents and the stopping buses are generated from the latitudes and longitudes of the actual bus stops and the bus route data. Each bus stop agent creates passengers in accordance with the passenger appearance rate at that bus stop. The bus stop agents are assigned individual numbers that identify the corresponding stops. These numbers are used to specify the next bus stop to which each bus should head. In addition, each bus stop agent maintains the passenger appearance rate at the corresponding bus stop for each hour as calculated from the data as a series of constant values.

### 4.5.3 Passenger Agents

Passenger agents are generated by bus stop agents. Each passenger agent has information on the destination bus stop name based on the passenger destination data. When a bus arrives at the bus stop, each passenger agent determines whether its desired destination exists on the route served by that bus. The passenger agent gets on the bus if the destination bus stop exists in the route data of the bus. The passenger agent moves along with the boarded bus. When the bus arrives at the destination bus stop, the passenger agent gets off the bus and deletes itself from the simulation field.

The simulation flow of the passenger agents is shown in Fig. 4. Passengers appear in accordance with the probability of appearance at each bus stop. For each step of the simulation, a random number that corresponds to the number of appearances every second (that is, the x axis of the Poisson distribution) is generated in accordance with the Poisson distribution corresponding to the appearance probability per second. Since the appearance rate per second is low, almost all of the random numbers generated from the Poisson distribution will be 0 or 1. When the value is 1, a passenger appears at the corresponding bus stop.

When a bus arrives at the bus stop, the simulation judges whether each passenger's destination exists on the route served by that bus. If the route of the bus agent includes the bus stop corresponding to the passengers agent's destination, that passenger agent gets on the bus. When the bus agent arrives at the destination bus stop, the passenger agent gets off the bus. The simulation records the times at which each passenger gets on and off the bus.

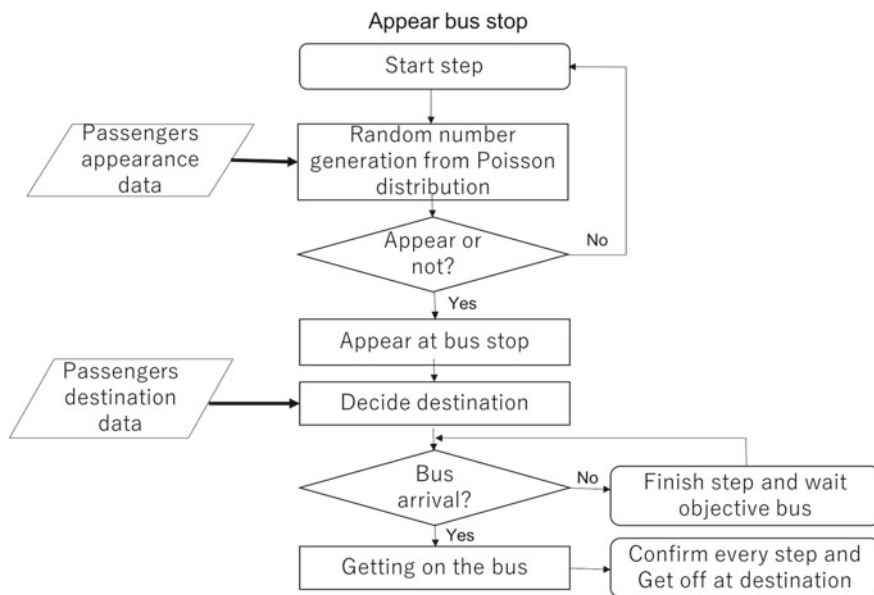


Fig. 4 Behavior flow of passenger agents

### 4.6 (3) Calculation of the Dissatisfaction Degree

We describe the procedure for calculating the dissatisfaction degree from the behavior of each agent. The simulation outputs the appearance times of passengers waiting for a bus at each bus stop from the behaviors of the passenger agents. The difference between the appearance time and the arrival time of the bus is  $T_{wait}$ . To calculate  $f(T_{wait})$ , we substitute  $T_{wait}$  into:

$$f(T_{wait}) = \begin{cases} 2T_{wait} - 10 & (T_{wait} \leq 20) \\ 30 & (T_{wait} > 20) \end{cases} \quad (2)$$

Furthermore, the simulation records the time at which each passenger agent gets off at the destination bus stop. The difference between the scheduled arrival time and the agent's alighting time is  $T_{delay}$ . To calculate  $g(T_{delay})$ , we similarly substitute  $T_{delay}$  into:

$$g(T_{delay}) = 2T_{delay} - 10 \quad (3)$$

Each bus agent holds data on the number of passengers on the bus. Let  $C$  be the number of passengers when the target passenger agent boards; to calculate  $h(C)$ , we substitute this value into:

$$h(C) = \begin{cases} 60C - 30 & (C \leq 1) \\ 30 & (C > 1) \end{cases} \quad (4)$$

Finally, we calculate the dissatisfaction degree  $S$  of each passenger by substituting  $f(T_{delay})$ ,  $g(T_{wait})$ , and  $h(C)$  into Eq. (1).

### 4.7 Visualization Tool

Although this study aims to quantify the convenience of passengers and use the resulting dissatisfaction degree to optimize the bus operation schedule, it is also critical to consider the analysis of bus operations from the viewpoint of the bus operator. Hence, we have developed a visualization tool, called Harmoware-VIS,<sup>1</sup> to present the result of the proposed simulations. Harmoware-VIS is based on deck.gl,<sup>2</sup> a WebGL-based big data visualization framework developed and published by Uber. The deck.gl framework can perform the analysis and drawing tasks based on a GPU implementation and can combine multiple layers. Using this multi-layer capability, we can visualize various data, such as the behavior of passengers at each bus stop or

<sup>1</sup>Harmoware-VIS: <https://github.com/Harmoware/Harmoware-VIS>.

<sup>2</sup>deck.gl: <https://deck.gl/>.





Fig. 5 Bus operation visualization using Harmoware-VIS

the weather conditions, in addition to the bus operation output from the simulation for the purpose of observing the interactions between bus operations and other factors.

Figure 5 shows the Harmoware-VIS interface displaying bus traffic data and the number of passengers at each bus stop. In this figure, light purple circles represent bus stops, and green, yellow and red circles represent buses. The different colors represent different degrees of delay for the buses. When a bus is delayed, the color of the circle representing it changes. The circle is red when the bus is delayed and is green when it is operating on time. The data are described in a json file, and the display is updated according to the passage of time. The vertical bar at each bus and bus stop shows the corresponding number of passengers. The bar at each bus stop indicates the number of people waiting to get on at that time.

## 5 Simulation Result

In this section, we will explain the results of our simulations. The simulation results obtained using artisoc are shown. We carried out simulations with fixed passenger appearance rates and varying bus operation schedules. The passenger appearance rates were fixed to those observed on July 8, 2016, and the simulations were conducted by varying the bus operation schedules to correspond to those observed from July 4 to 8, 2016. The simulation results can be presented in two forms: the change in the number of passengers over time and the change in the number of passengers waiting to board at a bus stop over time.

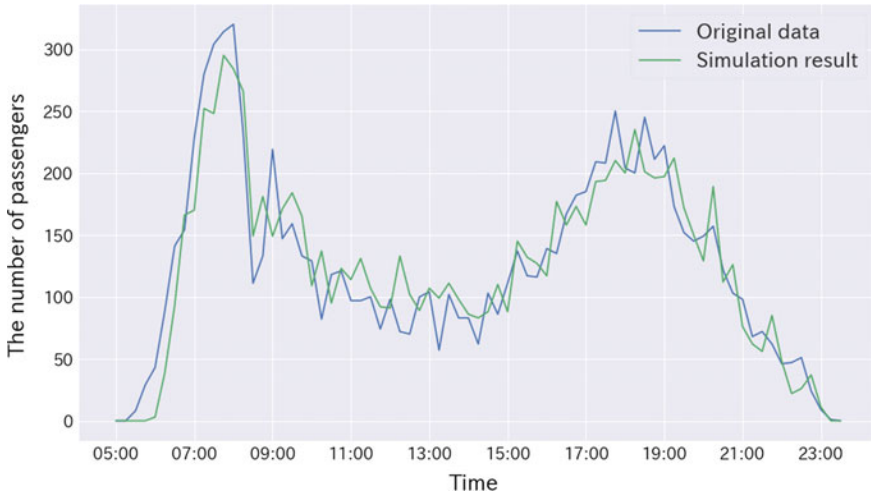


**Fig. 6** Simulation result of number of passengers at all busstops

### ***5.1 Time Transition of the Number of Passengers***

The transition of the number of passengers over time is shown in Fig. 6. The horizontal axis represents time, and the vertical axis represents the number of passengers by showing the number of people who boarded every arriving bus at all stops. Notably, the granularity of a representation of all rides at every time point is too fine for good visibility; therefore, the aggregated number of passengers for every 15 min period is shown instead. In this way, it can be seen that the simulated numbers of passengers are close to the actual data. The correlation coefficient between the actual data and the simulation result is 0.94. Next, a graph showing the change in the number of passengers over time at a given bus stop is shown in Fig. 7. It can be seen that even for a single bus stop, the change in the number of passengers can be reproduced with a quality similar to that achieved for the bus system as a whole.

### ***5.2 Time Transition of the Number of Passengers Waiting for Boarding***

The transition of the number of passengers waiting to board at all bus stops over time is shown in Fig. 8. It can be seen that the passenger volume is concentrated during commuting hours, whereas the curve is more gentle in the afternoon when various people are riding. It seems that some degree of reproducibility is obtained. A more detailed examination of the degree of reproducibility will be addressed in future work. In addition, these data were obtained by excluding the changes at the

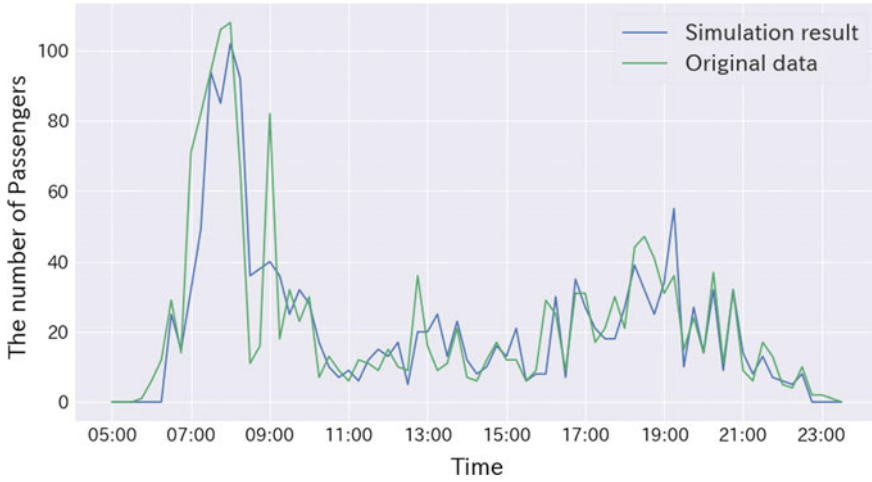


Fig. 7 Simulation result of number of passengers at busstop: “Okazaki station”

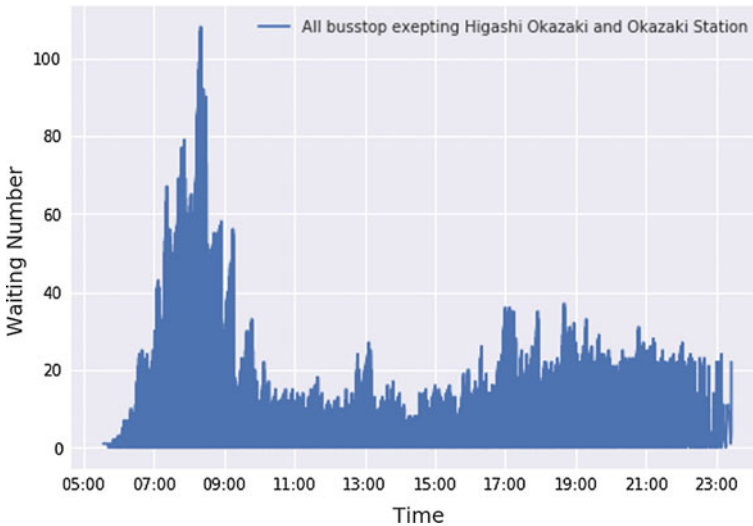


Fig. 8 Time transition of the number of passengers waiting for boarding excepting “Higashi Okazaki” and “Okazaki Station”

Higashi Okazaki and Okazaki Station stops. The results were not accurate when these stops were included. These stops are the main stops in Okazaki City, where people with a wide variety of destinations gather. Since the destination probabilities of the passengers run throughout the day, there is a possibility that a passenger may appear even though there is no bus scheduled that is heading towards that passenger’s destination at that time.

**Table 1** Simulation result (Passenger Appearance Rate: July 8, 2016, Bus Operation: from July 4 to 8, 2016)

	July 4 (Mon)	July 5 (Tue)	July 6 (Wed)	July 7 (Thu)	July 8 (Fri)	July 9 (Sat)	July 10 (Sun)
Level of Congestion	0.40	0.39	0.40	0.39	0.40	0.48	0.48
Wait time (s)	502	485	500	500	489	528	539
Delay time (s)	265	268	216	254	443	327	185
Dissatisfaction Degree	59.1	58.7	57.7	58.7	63.3	61.0	58.1
Number of Buses	415	415	415	415	415	372	372

### 5.3 Simulation Results for Different Operation Dates

Table 1 shows the results of simulations with the same passenger appearance rates and varying operation schedules. In the current method of calculating the dissatisfaction degree, when the level of congestion is 0.5 or less, the dissatisfaction degree due to congestion becomes 0. The average level of congestion is 0.39–0.48; therefore, the influence of this index on the overall dissatisfaction is considered to be low. Consequently, the main factors affecting dissatisfaction are delay and waiting time. On Saturdays and Sundays, the number of buses is decreased compared to that on weekdays, and the waiting time is correspondingly increased; however, the bus delays are simultaneously reduced. As a result, the dissatisfaction degree remains approximately the same. Delay is the main reason why the dissatisfaction degree on the 8th is found to be especially large; indeed, the bus delay on this day was approximately 1.7 times the delay on other days (including weekdays), so it seems that the influence of this factor is clear.

### 5.4 Simulation Result of Various Passengers Rate

Then, we show the results of the simulation, changing the number of passengers. The simulation result using the bus operation condition on July 6, and the passengers appearance rate from from July 4 to 8, 2016 is shown in Table 2 (A). The bus operated on the same schedule on weekdays and on weekends. The number of passengers of the targeted area were 483, 950, 878, 947, 908, 367, 476 passengers, from July 4 to 8, respectively, passengers on July 4, 9, 10 were small. Therefore, the dissatisfaction degree on July 4, 9, 10 was calculated especially low. The maximum congestion rate was 0.7.

This paper defines three functions:  $f(T_{delay})$ ,  $g(T_{wait})$ ,  $h(C)$  for calculating the dissatisfaction degree. We evaluate these kinds of functions by manipulating the

**Table 2** Simulation result of various passengers rate at all busstops

	July 4 (Mon)	July 5 (Tue)	July 6 (Wed)	July 7 (Thu)	July 8 (Fri)	July 9 (Sat)	July 10 (Sun)
(A) $f(T_{delay}), g(T_{wait}), h(C)$	58.4	61.4	61.3	60.7	61.1	59.6	59.6
(B) $f(T_{delay}), g(T_{wait})$	19.2	21.0	20.9	19.7	20.4	19.5	20.5
(C) $f(T_{delay}), h(C)$	45.0	45.0	45.0	45.0	45.0	45.0	45.0
(D) $g(T_{wait}), h(C)$	58.4	61.5	61.3	60.7	61.1	59.6	59.6

**Table 3** Simulation result of various passengers rate at terminal busstops

	July 4 (Mon)	July 5 (Tue)	July 6 (Wed)	July 7 (Thu)	July 8 (Fri)	July 9 (Sat)	July 10 (Sun)
(A) $f(T_{delay}), g(T_{wait}), h(C)$	56.7	61.4	61.1	60.4	60.2	59.6	60.5
(B) $f(T_{delay}), g(T_{wait})$	17.1	21.1	21.5	19.3	20.0	18.8	20.3
(C) $f(T_{delay}), h(C)$	45.0	45.0	45.0	45.0	45.0	45.0	45.0
(D) $g(T_{wait}), h(C)$	56.7	61.4	61.1	60.4	60.2	59.6	60.5

combination of functions, as to whether these functions are necessary or not. The Table 2 (B) is a simulation result performed using only  $f(T_{delay})$  and  $g(T_{wait})$  in Eq. (1). The dissatisfaction degree on this condition shows dissatisfaction only by the bus arrival time delay and the delay to the destination. The dissatisfaction degree on July 4 and July 6 were 19.2, 20.9, which were not so much difference. However, each maximum value of the congestion rate is 0.5, 0.7. The number of passengers on July 4 was crowded to the extent that passengers could sit, on the other hand, the passengers on July 6 were in a situation where some passengers could not sit. It seems that there is a difference in the situation of passengers on the bus on the 2 days, although the differences could not be properly expressed by not using  $h(C)$ .

Furthermore, Table 2 (C) is a simulation result performed using only  $f(T_{delay})$  and  $h(C)$  in Eq. (1). Though we can observed delay, all dissatisfaction degree was equal. It was impossible to adequately represent a decline in convenience to passengers due to delay. Dissatisfaction degree could not adequately represent a decline in convenience of passengers due to delay.

Table 2 (D) is a simulation result performed using only  $g(T_{wait})$  and  $h(C)$  in Eq. (1). The simulation using these two functions is almost the same as A), however, there was a difference from A) only on July 5. The arrival time to the destination is related to the waiting time for bus. Thus the longer the waiting time, the higher the possibility that the arrival time will be delayed. However, due to traffic congestion on the way to the destination, the arrival time may be delayed, and dissatisfaction degree simulation including  $f(T_{delay})$  can correspond to various situations.

Table 3 shows the result of calculating the dissatisfaction degree by extracting only the bus heading near the terminal station, which has a particularly large number of passengers in the target area. We fixed the bus operation to July 6, and simulated the passenger appearance rate from July 4 to 8, 2016. Thus the results are similar to

Table 2, result on July 4 is 56.7, which is lower than 58.4 of Table 2 (A). Passengers heading to terminal stations are considered to be commuters on weekdays or train passengers on weekends. It seems that the dissatisfaction degree on July 4 is low, because the passengers are fewer and delay is less than other busstops.

### 5.5 Simulation Result for Various $\omega_i$

We show the simulation results by changing  $\omega_i$  to various values. In previous section, the simulations were performed using weights of  $\omega_i = [1, 1.5, 1.5]$ . However, we believe that the value of  $\omega_i$  will take various depending on the characteristics or conditions of passengers. That is, the possible values of  $\omega_i$  can be changed according to the situation in which it is in a hurry condition such as commuting to school or office. In shopping situation, passengers will tolerate some delay but would like to get on the empty bus as possible. It is also thought that the elderly people will give priority to sitting when taking a bus from delay. Thus, we assume the several combination of  $\omega_i$  for various situations.

The simulation results with the passengers appearance rate and operation condition of July 6 are shown in Tables 4 and 5. Here, (i) is a set of  $\omega_i$  for commuters,  $\omega_i = [1.5, 1.5, 0.5]$ . This  $\omega_i$  includes the factors:  $T_{delay}$ ,  $T_{wait}$  of functions  $f(T_{delay})$ ,  $g(T_{wait})$  and  $h(C)$ , that is, the definition that the delay greatly affects passengers' dissatisfactions. (ii) is a set of  $\omega_i$  for the elderly people,  $\omega_i = [1.0, 0.5, 1.5]$ . We thought that the waiting time for bus and bus congestion rate— $T_{wait}$  and  $C$ —have a great influence on dissatisfaction. (iii) is a set of  $\omega_i$  assuming a time-constrained situation such as shopping,  $\omega_i = [1.0, 1.0, 1.0]$ .

Table 4 shows the simulation results using various  $\omega_i$ . We simulate the dissatisfaction degree, extracting the data of passengers heading for busstop near two terminal stations in the target area. We compare the dissatisfaction degrees with the timezone of Weekday (7: 00–10: 00), Weekday (10: 00–12: 00), Weekday (13: 00–16: 00), Weekends (13: 00–16: 00) for (i), (ii), (iii). In all the time zones of Weekday and Weekends, (ii) Elders' dissatisfaction degree got higher than (i) Commuters'. For the passengers heading to the terminal stations, the extracted timezone has particularly commuters, the dissatisfaction degree was calculated large for (ii) Elders. For Weekday (13: 00–16: 00) not commuting time, (i), (ii), (iii) all got a lower dissatisfaction degree.

**Table 4** Simulation result for various  $\omega_i$  (To Terminal Station)

	Weekday (7:00–10:00)	Weekday (10:00–12:00)	Weekday (13:00–16:00)	Weekday (13:00–16:00)
(i) Commuters	40.0	44.3	37.4	46.9
(ii) Elders	62.2	64.5	60.0	66.3
(iii) Others	47.2	49.5	45.0	51.2

**Table 5** Simulation result for various  $\omega_i$  (To Hospital)

	July 4 (Mon)	July 5 (Tue)	July 6 (Wed)	July 7 (Thu)	July 8 (Fri)
(i) Commuters	38.1	31.7	35.5	49.2	40.3
(ii) Elders	60.4	56.1	58.7	67.8	61.8
(iii) Others	45.4	41.1	43.7	52.8	46.8

Table 5 is the result of extracting passengers heading to five hospitals in the target area. We extracted the data of 8:00–12:00, as to hospital business hours. Especially (ii) Elders' dissatisfaction degree is high on July 4, which is crowded with passengers heading to hospital on the first day after the holidays, thus possibly the dissatisfaction degree has increased. On July 7, the dissatisfaction degree is higher in (i), (ii), (iii). The simulation results that the number of passengers increases on a specific day of the week and the dissatisfaction degree increases. (ii) Elders' dissatisfaction degree was also particularly high, whereas, the dissatisfaction degree of (i) Commuters and (iii) Others was calculated relatively low.

## 6 Conclusion

In this study, for the optimization of bus operations through simulation, we have proposed the concept of the “dissatisfaction degree”, which is an index that varies with the operation evaluation criteria for each user. By doing so, we aim not only to improve the efficiency of operations from the bus operator's point of view but also to ensure comfortable bus operations from the perspective of each passenger. Using actual transportation data provided by Meitetsu Bus Co., Ltd., we constructed a simulation to reproduce bus operations using the MAS artisoc. We confirmed that the simulation performed correctly by approximating the number of passengers per hour, achieving a correlation coefficient of 0.94 between the simulation results and actual operation data. In addition, visualization software that displays on a map the number of people waiting to board at each bus stop and the number of passengers on each bus has been made available by means of the visualization library BusDataVisualizer using deck.gl.

In future work, a clear definition of the dissatisfaction degree should first be developed. It will be necessary to examine the correlations of factors such as location and time with operation times and congestion levels and to further investigate the influence of operation time and congestion level on the overall dissatisfaction degree. Next, it will be necessary to calculate the passenger destination probabilities with respect to time to achieve more accurate probabilities and then to examine the extent to which the numbers of people waiting to board over time are accurately reproduced. Moreover, in the current simulation, the bus behavior is completely determined over time, and there is no model for modifying the delays during the simulation. Therefore,

it will be necessary to address this shortcoming. Then, we will examine the resulting influence on the dissatisfaction degree when the operation schedule is changed.

In addition, we intend to further develop the visualization tool in the future. With the current specifications, it is not possible to compare multiple operation schedules simultaneously on one screen, so it will be necessary to implement the ability to review various simulation results at the same time. The tool should also provide the ability to simultaneously review various types of information, such as delay logs, which is a subject to be studied in the future.

The purpose of visualizing the simulation results is to visually confirm how the passenger flow changes when the simulation conditions change. The simulation conditions considered are the bus operation times, the number of operating buses, and the passenger appearance rates. We will make various modifications to ensure the faithful reproduction of various driving scenarios (such as different days of the week and seasons) and to improve the definition of the dissatisfaction degree.

**Acknowledgements** We wish to thank Meitetsucom Co. Ltd and Meitetsu Bus Co., Ltd for insightful suggestions and provision of bus traffic data. This research and development work was supported by the JST OPERA and the MIC/SCOPE #172106102.

## References

1. Wang, Y., Dongxiang Zhang, L.H., Yang, Y.: Loo Hay Lee: data-driven and optimal bus scheduling model with time-dependent traffic and demand. *IEEE Trans. Intell. Transp. Syst.* **18**(9), 2443–2452 (2017)
2. Duzha, E., Hakrama, I.: *Public Transportation Simulation by Using Agent Based Simulation: Case of Tirana* (2015)
3. Cats, O., Larijani, A.N., Koutsopoulos, H.N.: Impacts of holding control strategies on transit performance: a bus simulation model analysis, CTS Working Paper, Vol. 2216 (2013)
4. Pattnaik, S.B., Mohan, S., Tom, V.M.: Urban bus transit route network design using genetic algorithm. *J. Transp. Eng. Am. Soc. Civil Eng.* **124**(4), 368–375 (1998)
5. Bielli, M., Caramia, M., Carotenuto, P.: Genetic Algorithms in Bus Network Optimization. *Transp. Res. Part C: Emerg. Technol.* **10**(1), 19–34 (2002). Elsevier
6. Wei, M., Chen, X., Sun, B., Zhu, Y.-Y.: Model and algorithm for resolving regional bus scheduling problems with fuzzy travel times. *J. Intell. Fuzzy Syst.* **26**, 2689–2696 (2015). IOS Press
7. Wei, M., Li, Y.: Collaborative ant colony algorithm for online regional bus scheduling. *J. Intell. Fuzzy Syst.* **31**(6), 3029–3037 (2016). IOS Press
8. Foulhoux, P., Ibarra-Rojas, O.J., Kedad-Sidhoum, S., Rios-Solis, Y.A.: Valid Inequalities for the synchronization bus timetabling problem. *Eur. J. Oper. Res.* **251**(2), 442–450 (2016) Elsevier
9. Zuo, X., Chen, C., Tan, W., Zhou, M.: Vehicle scheduling of an urban bus line via an improved multiobjective genetic algorithm. *IEEE Trans. Intell. Transp. Syst.* **16**(2), 1030–1041 (2015)
10. Meignan, D., Simonin, O., Koukan, A.: Simulation and evaluation of urban bus-networks using a multiagent approach. *Simul. Model. Pract. Theory* **15**(6), 659–671 (2007)
11. Meignan, D., Simonin, O., Koukan, A.: Multiagent approach for simulation and evaluation of urban bus networks. In: *5rd AAMAS Conference* (2006)
12. Tactical Design of High-demand Bus Transfers: C Angelo Guevara, Gonzalo A Donoso. *Transport policy*, Elsevier **32**, 16–24 (2014)



13. Nakashima, H., Matsubara, H., Shiraishi, K.H.Y., Sano, S., Kanamori, R., Noda, I., Tomohisa, Y., Koshiba, H.: Design of the smart access vehicle system with large scale MA simulation. In: Proceedings of the 1st International Workshop on Multiagent-Based Societal Systems (MASS 2013), Saint Paul (2013)
14. Nakashima, H., Sano, S., Hirata, K., Shiraishi, Y., Matsubara, H., Kanamori, R., Koshiba, H., Noda, I.: One Cycle of Smart Access Vehicle Service Development Serviceology for Designing the Future, pp. 247–262. Springer (2016)
15. Kozo KEIKAKU Engineering Inc, artisoc. <http://mas.kke.co.jp/> (Cited January 2018)
16. Hitachi, Bus service plan simulation. [http://www.hitachi.co.jp/products/bus/selection/8031738\\_38322.html](http://www.hitachi.co.jp/products/bus/selection/8031738_38322.html) (Cited January 2018)

# Adaptive Traffic Signal Control Methods Based on Deep Reinforcement Learning



Chia-Hao Wan and Ming-Chorng Hwang

**Abstract** Smart cities are characterized by their use of intelligent transportation systems (ITS), which utilize advanced traffic signal control methods to achieve effective and efficient traffic operations. Recently, due to significant progress in artificial intelligence, research has focused on machine learning-based frameworks of adaptive traffic signal control (ATSC). In particular, deep reinforcement learning (DRL) can be formulated as a model-free technique and applied to optimal action selection problems. We propose a DRL-based ATSC method for two kinds of neural network models: deep neural networks (DNN) and convolutional neural networks (CNN). In the training processes, the microscopic simulator Vissim builds a virtual intersection that the agent uses to scan all possible observations and makes interactive decisions. For each testing scenario, five random experiments are generated. The average system total delay (ASTD) over the five experiments is compared for the two proposed neural network models and a fixed timing plan by way of the Webster delay formulas. Based on these preliminary tests, the DNN-model (CNN-model) signal control agent performed a lowest value of ASTD for the unsaturated (oversaturated) cases. Moreover, the CNN-model has better feature extraction capabilities than the DNN-model particularly for the oversaturated cases. We found that situations with specific traffic maneuvers, such as a spillback of a protected left-turn bay, are well learned by the proposed CNN-model, even the training scenario remains only unsaturated.

**Keywords** Adaptive traffic signal control · Convolutional neural network · Deep neural network · Reinforcement learning

---

C.-H. Wan (✉) · M.-C. Hwang  
ITS Research Center, China Engineering Consultants, Inc., 28F., No.185, Sec.2, Sinhai Rd.,  
Taipei, Taiwan  
e-mail: [b97501066@gmail.com](mailto:b97501066@gmail.com)

M.-C. Hwang  
e-mail: [mchwang@ceci.org.tw](mailto:mchwang@ceci.org.tw)

## 1 Introduction

The adaptive traffic signal control (ATSC) method is a powerful approach to mitigate urban congestion, as it can deal with intersection traffic fluctuations. While receiving and processing real-time data from traffic sensors, the ATSC method instantly determines green splits to optimize intersection performance [1]. Theoretically and practically, the ATSC method is a better alternative for signalized intersections than pre-timed and actuated control approaches. Several well-known ATSC methods have been investigated and developed in the literature (e.g., SCOOT [2], SCATS [3], and OPAC [4]). However, these methods demand a pre-defined traffic system to describe the operational characteristics of intersection and then to be the inputs of computing optimal signal timing. These model-based methods are usually disputed to achieve a reasonable and affordable representation of the environment encountered. Moreover, these methods require human interventions both in design and operation phases. That makes the robustness of these methods deteriorated from mapping complex nature of traffic situations into optimal control actions.

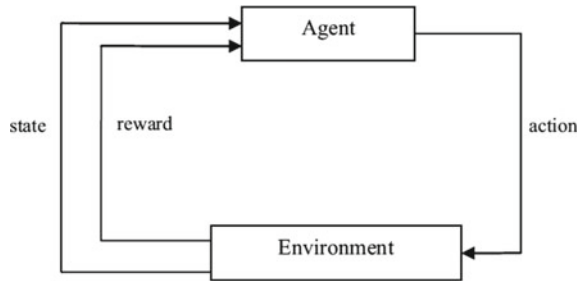
In contrast, reinforcement learning (RL) can be formulated as a self-training and model-free procedure without any supervision or the use of human data [1]. This key property is exploited to allow the proposed ATSC methods to self-train by autonomously interacting with a traffic simulator. A simulated intersection is set up as the environment for the RL agent to interact with. The states, actions, and rewards within the RL framework are vehicle-presence, signal phase selection, and total system delay, respectively. The RL agent is trained to find a phase selection policy that optimizes the total system delay on the simulated intersection. We consider deep neural network (DNN) and convolutional neural network (CNN) models to address the non-linear relationship among states, rewards, and actions.

The rest of this paper is structured as follows. Section 2 reviews the literature. Section 3 describes the modeling of the proposed deep-RL based ATSC methods. Section 4 discusses the results of training and testing for the different methods. Section 5 provides a brief conclusion and proposes future works.

## 2 Literature Review

Reinforcement learning (RL) is a machine learning paradigm focused on stochastic sequential decision-making problems [5]. Figure 1 depicts a typical RL model [6], which formulates the interactions between learners and corresponding environments to achieve a goal. In this model, the learner/decision-maker is called the agent. The agent interacts with the environment by selecting actions. Actions cause a state-change of the environment, and may incur rewards, which the agent continuously seeks to optimize. The entire RL algorithm helps the agent learn how to achieve a goal via sequential decision-making.

**Fig. 1** A typical RL framework



There are three major categories of RL methods: dynamic programming, Monte-Carlo, and temporal difference (TD) learning methods. Dynamic programming algorithms are model-based and require a model of the Markov decision process [7, 8]. Monte-Carlo methods are model-free and learn directly from experience. Unlike dynamic programming methods, Monte-Carlo methods do not need the complete probability distribution of all possible transitions [5, 8]. TD learning is a combination of Monte Carlo and dynamic programming concepts [5, 9]. Temporal difference learning does not require the entire trajectory sample because it updates the state value from part of the trajectory [5].

Q-learning is a TD method [10, 11] that aims to learn an action-value function,  $Q(s, a)$ , which ultimately gives the expected utility of taking a given action  $a$  in a given state  $s$  and following an optimal policy thereafter. Deep Q-networks (DQN) are a variant of Q-learning [12], and have been successfully used in Atari games. Recent advances in deep neural networks [13–15] allow DQN using DNN to play the role of the action-value function  $Q(s, a)$ .

On the other hand, there have also been attempts to introduce artificial intelligence to traffic signal control to create innovative solutions. Beginning in the early 2000s, several studies have adopted the RL technique for adaptive signal control [16–18]. After Google’s DeepMind first proposed the term Deep Reinforcement Learning (DRL) in 2013 [19], another wave of DRL in signal control was triggered [20–24]. Previous efforts have established a clear DRL signal control framework for an isolated intersection. In this paper, we continue these experiences but focus on whether different traffic scenarios affect the agent’s learning process and performance.

### 3 DQN Signal Control Model

In this section, we first discuss how to fit the signal control problem into an RL model by defining the state element, action space, and reward. Then, we introduce an algorithm for the traditional DQN method. Finally, we improve the inefficient parts of DQN to make it suitable for the signal control problem.

### 3.1 Environment, State, Action, and Reward

**The environment** is a Markov process, and a reinforcement learning agent learns by interacting with its environment. In this case, our environment is an isolated signalized intersection with four identical approaches as shown in Fig. 2.

Because we cannot let the agent directly learn from the real world, we establish the environment in the microscopic simulator Vissim, which is a world-renowned traffic simulation software. Two lanes and a left turn bay (about 20 m) approach the intersection from each direction. The arrival rates at the four arms are random in each episode, but their sum is constant to ensure a baseline demand is maintained. All movement ratios are also constant. Random number seeds are changed for each episode to guarantee randomness in every simulation. The approaches are 1000 m from the stop line to ensure all queuing vehicles are included in the total delay (we explain this further when discussing rewards).

**The state** is described by the input data. In general, using more information to describe a state helps the network more precisely determine the value of the state. For example, Fig. 3 describes the state using cell occupancy [22, 24].

**Fig. 2** The isolated signalized intersection layout

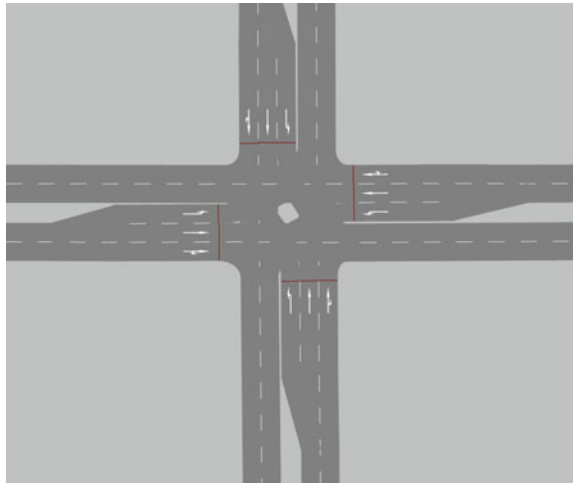


**Fig. 3** Using cell occupancy to describe traffic states

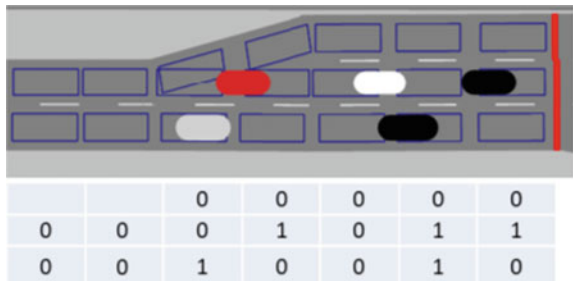
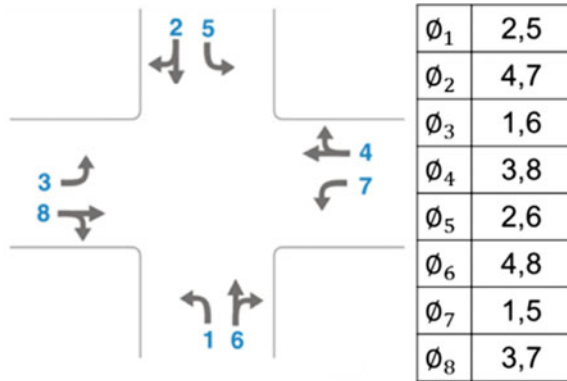


Fig. 4 Phase configurations



Each lane approaching the intersection is divided into many cells. If a cell is occupied by a vehicle, the cell is set to 1; otherwise, it is set to 0. This state description method provides a great deal of information to the agent and almost resembles an image data input. Therefore, this method is expected to work well with the image recognition vehicle detector. In this research, each cell is 5 m long, which is about the length of a car in the simulation. In total, there are 260 cells across the four approaches. The farthest cell from the stop line is about 200 meters away.

**The action** refers to the choice of a signal phase. Figure 4 shows possible signal phase configurations. The agent picks one of these eight phases once a second. The inter-green limitation and minimum green time are taken into consideration. Thus, if the agent decides to change the current phase, it cannot make any new actions in the next time period. However, if the agent decides to maintain the current phase, it can select the same signal phase. This implies the agent needs to learn the consequences of different actions in different states.

**The reward** is a guide that allows the agent to know whether it is moving in the right direction. In this case, we choose system delay as our reward. Since the agent is performing a sequential decision-making process, each state-action generates an instant reward called  $r_t$ . Here, we use a time-step accumulated system delay as  $r_t$ , meaning that  $r_t$  is the accumulated system delay between two actions. At the terminal time  $T$ , the total reward  $R$  will equal the accumulated system delay:

$$R = \sum_{t=1}^T r_t \tag{1}$$

### 3.2 DQN Framework Application

The basic concept of DQN is to find an equation  $Q$  that inputs the current state and outputs each action’s expected total reward. The optimal action-value function with environment  $\epsilon$  can be expressed using Bellman’s equation as

$$Q^*(s, a) = \mathbb{E}_{s' \sim \epsilon} \left[ r + \gamma \max_{a'} Q^*(s', a') | s, a \right] \tag{2}$$

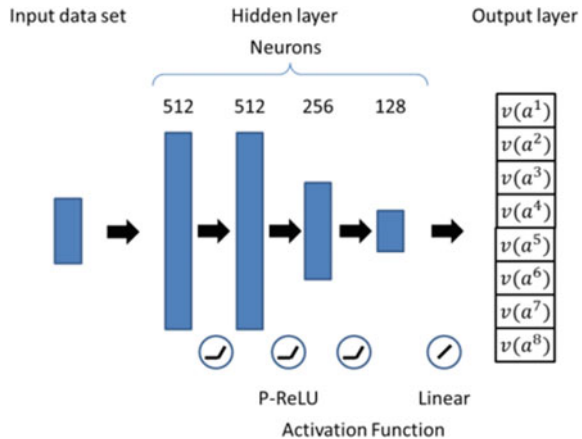
Here, a neural network is used as a non-linear approximation to estimate the action-value function. To train the neural network, TD error is considered the loss. The loss function is expressed as

$$L_i(\theta_i) = \mathbb{E}_{s, a \sim \rho(\cdot)} [(y_i - Q(s, a; \theta_i))^2] \tag{3}$$

where  $\theta_i$  are parameters,  $y_i = \mathbb{E}_{s' \sim \epsilon} [r + \gamma \max_{a'} Q(s', a'; \theta_{i-1}) | s, a]$  is the target for iteration  $i$ , and  $\rho(s, a)$  is a probability distribution over sequences. Finally, we perform a gradient descent with respect to  $\theta$  and we update parameters. Algorithm 1 describes this process.

The algorithm’s two key features are memory replay [25] and target network [12]. Memory replay allows the agent to learn from earlier experience and speed up learning. Target network helps the agent learn the  $Q$  function more stably. We use a Deep Neural Network (DNN) as the estimator  $Q$  in Eq. (2). The DNN model architecture is shown in Fig. 5. There are 300,000 trainable parameters in this DNN model.

**Fig. 5** DNN model architecture



**Algorithm 1**

**Deep Q-learning Network**  
**off-line learning with memory replay and  $\epsilon$ -greedy**

---

```

Initialize replay memory D to capacity N
Initialize action-value function Q with random parameters  $\theta$ 
Initialize target action-value function  $\hat{Q}$  with parameters  $\hat{\theta} = \theta$ 
for episode = 1..M do
  Initialize environment and  $s_t$ 
  for t=1..T do
    With probability  $\epsilon$ , select a random action  $a_t$ 
    Otherwise select  $a_t = \max_a \hat{Q}^*(s_t, a; \hat{\theta})$ 
    Execute action  $a_t$  in environment and observe reward  $r_t$  and next state  $s_{t+1}$ 
    Store transition  $(s_t, a_t, r_t, s_{t+1})$  in D
    If the size of D is larger than N then
      Remove the oldest data in D
  end for
  for k=1..C do
    Sample random minibatch of transitions  $(s_j, a_j, r_j, s_{j+1})$  from D
     $y_i = r_i + \gamma \max_{a'} \hat{Q}(s_{j+1}, a'; \hat{\theta})$ 
    Perform a gradient descent step on  $(y_j - Q(s_j, a_j; \theta))^2$ .
    -with respect to network parameters  $\theta$ 
  end for
  Reset  $\hat{Q} = Q$ 
end for

```

The discount factor  $\gamma$  must be considered carefully. As mentioned in 3.1, the action is phase selection. Figure 6, which shows a simple action-based example, reveals an execution time difference between actions. In this example, taking the upper action requires 1 time-step and taking the lower action requires 2 time-steps. If we use the function in Algorithm 1,  $y_i = r_i + \gamma \max_{a'} \hat{Q}(s_{j+1}, a'; \hat{\theta})$ , to do the iteration, we find that the bottom state for  $t = 5$  has been discounted twice, but the top state for  $t = 5$  has been discounted five times. This simple case demonstrates that regardless of the relationship between reward and action, an action based-structure will lead to a biased estimation of the Q value.

Therefore, we incorporate the action execution time  $E$ , which is the time interval between two sequential decisions, into the discount factor. In the equations below,  $\delta$  is the dynamic discount factor depending on  $E$  and the original fixed discount factor  $\gamma$ .

$$\delta = 1 - E(1 - \gamma) \quad (4)$$

$$y_i = r_i + \delta \max_{a'} \hat{Q}(s_{j+1}, a''; \hat{\theta}) \quad (5)$$

The dynamic discount factor in Eq. (4) is derived from the summation of an infinite geometric series. By using Eq. (5), we can ensure that at each time-step, the Q value will have the same level of discount. We expect this modification to make the agent



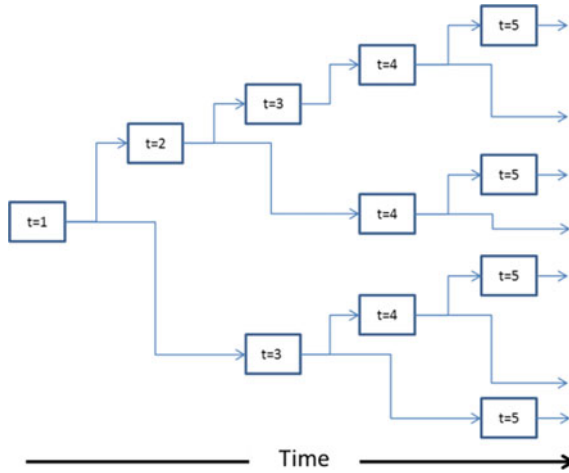


**Fig. 6** Time difference between actions' execution

more inclined to maintain the same phase compared with fixed  $\gamma$ , which repeatedly reduces the Q value for each action. Maintaining the same phase means more actions during a certain period of time and more discounts than changing a phase.

### 3.3 Convolutional Neural Networks Model

Convolutional Neural Networks (CNN) are a class of DNN inspired by biological processes [26]. The basic concept of CNN is to learn filters via the machine itself. The filter detects features of the input data to increase the efficiency of the training process and to improve performance. In this paper, the filter works as Fig. 7.

Here, we want the CNN model to distinguish queuing features, such as spillback from the left turn bay, and to then apply these to each approach. Unlike the common 2D convolution used in image recognition, we build up the model with 1D convolution layers because we use cell occupancy to describe traffic states, which is more similar to 1D data. We hope the CNN model, whose architecture is shown in Fig. 8, helps the agent converge faster and more accurately. There are 256,040 trainable parameters in this CNN model.

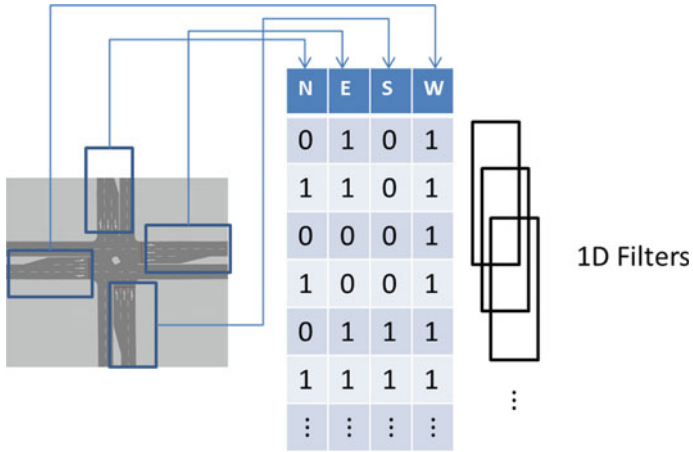


Fig. 7 The filters detect the queuing features in a single approach

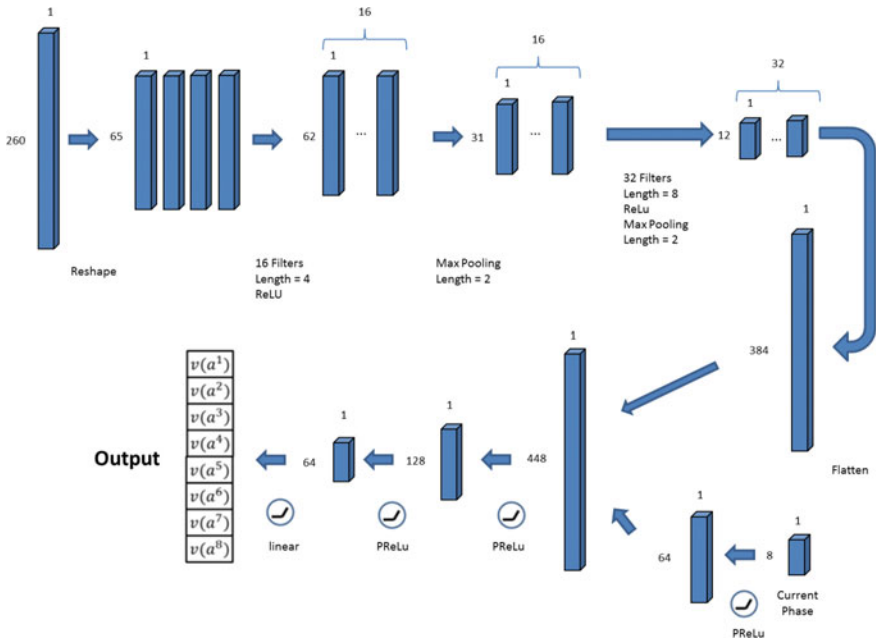


Fig. 8 CNN model architecture

## 4 Training and Scenario Testing

### 4.1 Training

The performance of DQN is evaluated with the traffic metric known as the system total delay. We also observe the loss value over episodes to determine whether the agent has achieved a converged Q value function. Each episode is set to simulate 1,200 simulation seconds from the initial state. After each episode, the target network is updated with the same parameter as the model. The rest of the settings are shown in Table 1.

Note that before training, data was collected under a random action policy. This was to ensure that the agent was learning from a stochastic experience instead of from the initial network parameters. The data was collected and stored in the memory replay space. The agents have the opportunity to re-use these experiences before they are removed. The training was processed in a python script and used TensorFlow as the backend. The training results are shown in Figs. 9 and 10. In each episode, the model performed 500 gradient descents and the model's parameters were updated.

Figure 9 shows that both the DNN and CNN models reached convergence. However, the DNN model was much easier to train and had lower loss compared with the CNN model. Both models reduced the total system delay to around  $-50,000$  s, but the CNN model had more variation in its results, as seen in Fig. 10.

**Table 1** Training Settings

Parameter	Value
Simulation times	1200 s
Arrival rates	1000 passenger car units(pcu)/h at each approach
Network parameter update rate	1/episode
Memory replay capacity: N	100,000
Episode	2000
Epochs in one episode: C	500
$\epsilon$	0.2
$\epsilon$ decrease rate	0.002/episode
Optimizer	Adam [27]
Loss function	Mean square error of TD
Amber period	3 s
All red	3 s

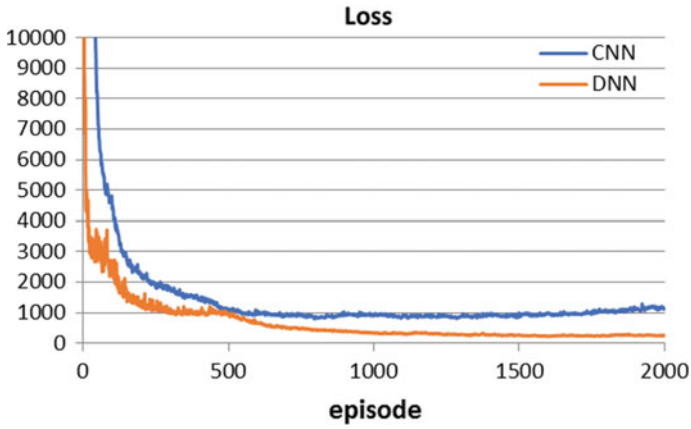


Fig. 9 The training process of the DNN and CNN models

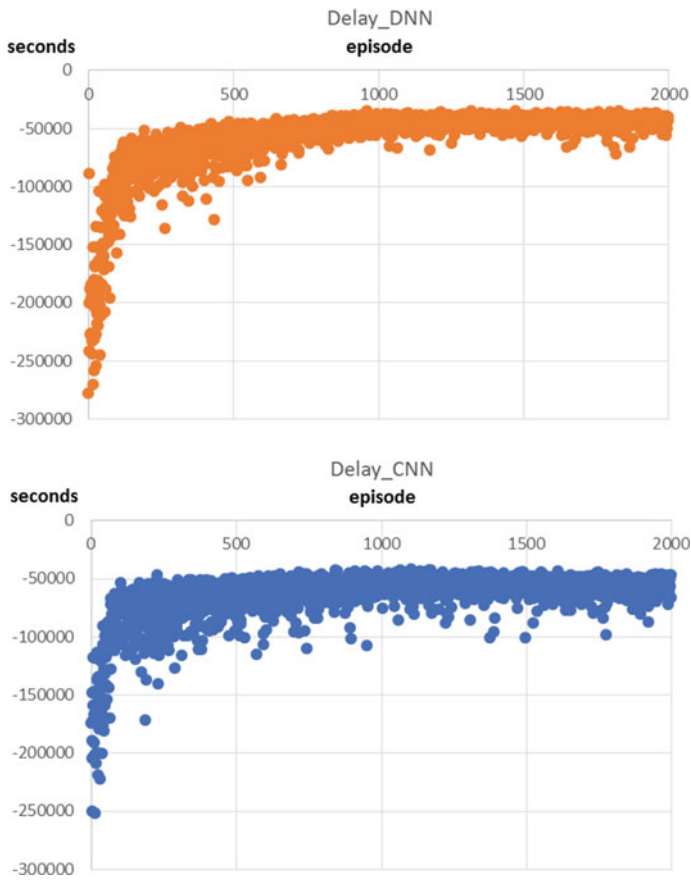


Fig. 10 The total system delay over episodes for the DNN and CNN models

### 4.2 Scenario Testing

Here, we set up two arrival rate scenarios, unsaturated and oversaturated, to test the models' performance. The arrival rates are set to 1000 pcu/h for each approach in the unsaturated scenario, which is the same total demand as in the training setting. In the oversaturated scenario, we set the arrival rates to 1800 pcu/h input on the North and West boundaries, and 200 pcu/h on the East and South. We maintain the same turning movement ratios for training.

We compare the performance of the DNN model, the CNN model, and the Fixed Timing plan, which is calculated via the delay formulas from Webster [28] for unsaturated situations.

We also set up an unsaturated scenario with noise in arrival rates. That is, the arrival rates are slightly different in each simulation ( $N(1000,100)$ ), although they are equal for the comparison between the DNN model, the CNN model, and the fixed timing plan. For the oversaturated scenario, the fixed timing plans were derived empirically. We set a 180-s cycle and split it into green periods weighted by the ratio of arrivals to the saturation flow.

The evaluation index is the system total delay because it was the reward during the training and it is a common traffic performance indicator. For each scenario, we ran simulations three times with different random seeds to ensure variability in the scenarios. Figure 11 shows the results of the comparison.

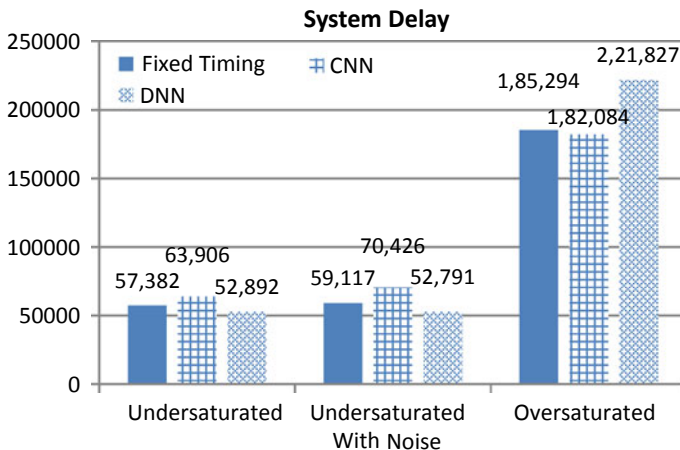


Fig. 11 Average system total delay

## 5 Discussion

The comparison in Fig. 11 shows some interesting results. The DNN model had the best score in the under-saturated scenario, reducing system delay by about 8% compared with the fixed timing plan. Similarly, the DNN reduced delay by about 10% in the under-saturated with noise scenario. In contrast, the results of CNN were worse than the fixed timing plan for both under-saturated scenario.

Surprisingly, the DNN model had the worst score in the oversaturated scenario, and the CNN model performed slightly better than the fixed timing plan. This might be because the training sample does not have similar experiences to learn from. Furthermore, if the state can improve the description of arrival rates, this might support the application of the DRL model in oversaturated scenarios.

We expected the CNN model to have better performance. The unexpectedly poor results could be because the vehicle queue pattern is not suitable for fetching feature values with 1D filters. In contrast, the DNN model has a fully connected structure, which is more appropriate for the queue patterns herein. If the simulator could produce an infinite sample to train the model, this might eliminate the advantage of the CNN model for oversaturated scenarios.

Our results are markedly different from reference [29]. However, it is worth noting that the state and reward settings are different in this study and in [29], which could be an explanation for the disparity. Regardless, there is no doubt as to the potential of DRL signal control.

## 6 Conclusions and Further Work

In this paper, we applied a DRL method called DQN to the traffic signal control problem. Some modifications were made in the DQN algorithm to suit this task. Training and scenario testing were conducted. The results showed that the DNN model performed better in under-saturated scenarios than both the fixed timing plan and the CNN model, but performed poorly in oversaturated scenarios where the state did not have any descriptions of the arrival rates.

In future research, we plan to focus on applying DRL to multi-intersections. The DQN framework can only be used while the action set is discrete. The inclusion of a multi-intersection signal phase is a type of continuous action problem. There are several DRL algorithms designed to solve continuous action tasks such as Actor-Critic, DDPG (Deep Deterministic Policy Gradient), and PPO (Proximal Policy Optimization). The question of how to apply these state-of-the-art approaches to traffic signal control will be one of the hottest topics in the next generation of ITS.

## References

1. Roess, R.P., Prassas, E.S., McShane, W.R.: Traffic Engineering, 3rd edn. Prentice Hall (2004)
2. Hunt, P.B., Robertson, D.I., Bretherton, R.D., Winton, R.L.: SCOOT—a traffic responsive method of coordinating signals. Transportation Research Lab., Crowthorne, U. K., Tech. Report (1981)
3. Sims, A.G., Dobinson, K.W.: The Sydney coordinated adaptive traffic (SCAT) system philosophy and benefits. *IEEE Trans. Veh. Technol.* **29**(2), 130–137 (1980)
4. Gartner, N.H.: OPAC: a demand-responsive strategy for traffic signal control. *Transp. Res. Rec.* **906**, 75–81 (1983)
5. Sutton, R.S., Barto, A.G.: Reinforcement Learning: An Introduction. MIT Press, Cambridge, Massachusetts, USA/London, England (2011)
6. Kaelbling, L.P., Littman, M.L., Moore, A.W.: Reinforcement learning: a survey. *J. Artif. Intell. Res.* **4**, 237–285 (1996)
7. Bertsekas, D.P.: Dynamic Programming and Optimal Control, vol. 2, 3rd edn. Athena Scientific (2007)
8. Abdulhai, B., Kattan, L.: Reinforcement learning: Introduction to theory and potential for transport applications. *Can. J. Civ. Eng.* **30**, 981–991 (2003)
9. Abdulhai, B., Kattan, L.: Reinforcement learning: introduction to theory and potential for transport applications. *Can. J. Civ. Eng.* **30**, 981–991 (2003)
10. Watkins, C.J.C.H.: Learning from Delayed Rewards. Doctoral dissertation, Cambridge University (1989)
11. Watkins, C.J.C.H., Dayan, P.: Q-learning. *Mach. Learn.* **8**(3), 279–292 (1992)
12. Mnih, V., Kavukcuoglu, K., Silver, D., Rusu, A.A., Veness, J., Bellemare, M.G., Graves, A., Riedmiller, M., Fidjeland, A.K., Ostrovski, G., Petersen, S.: Human-level control through deep reinforcement learning. *Nature* **518**(7540), 529–533 (2015)
13. Bengio, Y.: Learning deep architectures for AI. *Found. Trends Mach. Learn.* **2**, 1–127 (2009)
14. Krizhevsky, A., Sutskever, I., Hinton, G.: ImageNet classification with deep convolutional neural networks. *Adv. Neural. Inf. Process. Syst.* **25**, 1106–1114 (2012)
15. Hinton, G.E., Salakhutdinov, R.R.: Reducing the dimensionality of data with neural networks. *Science* **313**, 504–507 (2006)
16. Abdulhai, B., Pringle, R., Karakoulas, G.J.: Reinforcement learning for true adaptive traffic signal control. *J. Transp. Eng.* **129**(3), 278–285 (2003)
17. Wiering, M.: Multi-agent reinforcement learning for traffic light control. In: ICML, pp. 1151–1158 (2000)
18. Bingham, E.: Reinforcement learning in neurofuzzy traffic signal control. *Eur. J. Oper. Res.* **131**(2), 232–241 (2001)
19. Mnih, V., Kavukcuoglu, K., Silver, D., Graves, A., Antonoglou, I., Wierstra, D., Riedmiller, M.: Playing Atari with deep reinforcement learning (2013). arXiv preprint [arXiv:1312.5602](https://arxiv.org/abs/1312.5602)
20. Rijken, T.: DeepLight: Deep reinforcement learning for signalised traffic control. Master's thesis. University College London (2015)
21. Ozan, C., Baskan, O., Haldenbilen, S., Ceylan, H.: A modified reinforcement learning algorithm for solving coordinated signalized networks. *Transp. Res., Part C Emerg. Technol.* **54**, 40–55 (2015)
22. Genders, W. and Razavi, S., 2016. Using a deep reinforcement learning agent for traffic signal control. <https://arxiv.org/abs/1611.01142>. Accessed November 2016
23. Li, L., Lv, Y., Wang, F.Y.: Traffic signal timing via deep reinforcement learning. *IEEE/CAA J. Autom. Sin.* **3**(3), 247–254 (2016)
24. van der Pol, E., 2016. Deep reinforcement learning for coordination in traffic light control. Master's thesis, University of Amsterdam
25. Lin, L.J.: Self-improving reactive agents based on reinforcement learning, planning and teaching. *Mach. Learn.* **8**(3–4), 293–321 (1992)

26. Matusugu, M., Mori, K., Mitari, Y., Kaneda, Y.: Subject independent facial expression recognition with robust face detection using a convolutional neural network. *Neural Netw.* **16**(5), 555–559 (2003)
27. Kingma, D.P., Ba, J.: Adam: A Method for Stochastic Optimization (2014). [arXiv:1412.6980](https://arxiv.org/abs/1412.6980) [cs.LG]
28. Webster, F.V.: Traffic Signal Settings. Road Research Technical Paper No. 39. London: Great Britain Road Research Laboratory (1958)
29. Wan, C.H., Hwang, M.C.: A Study on Applying Deep Q-learning Network to Isolated Intersection Adaptive Signal Control. ITS Asia-Pacific Forum FUKUOKA 2018 (2018)



# Analysis of Quality/Quantity Trade-Off of Images Collected by On-Vehicle Fisheye Cameras for Super Resolution



Shintaro Ono, Teruhisa Takano, Hiroshi Kawasaki and Katsushi Ikeuchi

**Abstract** Fisheye cameras or wide-angle cameras used on automobiles have various applications as distributed sensors and their image resolution can be enhanced using super resolution (SR) technology. However, when an object is observed while the vehicle moves or by multiple vehicles, the object regions are often captured with very low quality (low resolution and large blur) resulting from the character of the lens. Therefore, applying SR requires a decision as to which images to use as inputs: a greater number of lower-quality images or fewer higher-quality images. We evaluated and discussed the input image quality necessary to obtain effective SR results, especially focusing on degree of image blur. Then, we considered its potential use as a requisite in observing road environments.

**Keywords** Reconstruction-based super resolution · On-vehicle fisheye/super wide-angle camera · Number of input images · Trade-off between image quality and quantity

---

S. Ono (✉)

Institute of Industrial Science, The University of Tokyo, 4-6-1 Komaba, Meguro-ku Tokyo 1538505, Japan  
e-mail: [onoshin@its.iis.u-tokyo.ac.jp](mailto:onoshin@its.iis.u-tokyo.ac.jp)

T. Takano

Graduate School of Interdisciplinary Information Studies, The University of Tokyo, 4-6-1 Komaba, Meguro-ku, Tokyo 1538505, Japan  
e-mail: [teruhisa-takano@cvi.iis.u-tokyo.ac.jp](mailto:teruhisa-takano@cvi.iis.u-tokyo.ac.jp)

H. Kawasaki

Faculty of Information Science and Electrical Engineering, Kyushu University, 744 Motoooka, Nishi-ku, Fukuoka 81900395, Japan

K. Ikeuchi

Interfaculty Initiative in Information Studies, The University of Tokyo, Tokyo, Japan  
e-mail: [katsushi.ikeuchi@outlook.jp](mailto:katsushi.ikeuchi@outlook.jp)

Microsoft Research Asia, 11801 97th Ln NE, Kirkland, WA 98034, USA

© Springer Nature Singapore Pte Ltd. 2019

T. Mine et al. (eds.), *Intelligent Transport Systems for Everyone's Mobility*, [https://doi.org/10.1007/978-981-13-7434-0\\_12](https://doi.org/10.1007/978-981-13-7434-0_12)

# 1 Introduction

Road sensing using general-purpose automobiles for business and personal use is becoming more feasible as well as using dedicated-purpose vehicles such as MMS (mobile mapping system). Particularly, web-connected on-vehicle cameras, driving video recorders, and parking assistance cameras have gained popularity. Although image and position data collected by such sensing devices have relatively low quality or poor accuracy, the quantity of data is very large and the quality and accuracy can potentially be improved through post-processing.

Regarding on-vehicle cameras in general-use vehicles, super wide-angle lenses, including fisheye lenses, are often used to view wider areas using fewer cameras, leading to lower image quality around the peripheral area. It is even possible to generate images with higher resolution through post-processing, using super resolution (SR) technology.

However, because of its lens character, on-vehicle image sensing with such a super wide-angle camera faces a trade-off problem on the quality and quantity of the collected images and it is hard to meet both of them at the same time, as described in 3.2 with Fig. 2 in detail. Therefore, the inclusion or exclusion of the collected images from input of post-processing becomes an important issue.

Here, focusing on SR of the fisheye images collected by on-vehicle camera, we examine and consider the inclusion or exclusion of images that will enable better SR result. Then, we discuss the possibility of the blur level of the image region being a criterion for the inclusion/exclusion of input images.

Specifying the inclusion/exclusion criteria for input images of SR can be a contribution to ITS-. It can assist in inferring requisites for on-vehicle sensing, including the number of observations, speed, and camera specifications (frame rate and lens character), depending on the distance of the observed objects. Moreover, it can also provide basic information for assessing the necessity for cloud-based sharing of data captured by other vehicles and on the requisites for the shared data quantity and frequency.

## 2 Related Works

### 2.1 Sensing by Vehicle for Dedicated Use or General Use

Regarding road sensing by a vehicle, a system composed of special sensing devices such as LiDARs and cameras has been commonly used on a dedicated-use vehicle. Such a system is generally called MMS (mobile mapping system) and widely developed by survey companies. In this case, the specification of the sensor can be intentionally designed to obtain enough data quality; however, its cost makes it unrealistic to frequently survey wide area. The features are summarized in Table 1.

**Table 1** Sensing using dedicated-use vehicles and general-use vehicles

	Dedicated-use vehicles (MMS)	General-use vehicles
Sensing system specifications	Can be designed intentionally	An inexpensive and multi-purpose system is generally assumed
Accuracy of acquired data	Relatively high	Relatively low, but might be improved through post-processing
Quantity of acquired data	Depends on the operational opportunities of the vehicle itself	Potentially capable of collecting a large quantity of data through sharing, if the system becomes widely used
Sensing for wide areas and/or with frequent opportunities	Typically, costly and not very realistic	Relatively realistic, if the system becomes widely used

Conversely, exploiting general-use vehicles for probe survey became more feasible today. For example, it is quite practical to analyze motion data of general-use vehicles to sense traffic congestion, road-surface condition, dangerous driving, etc.

Moreover, web-connected on-vehicle cameras, including driving video recorders, and parking assistance cameras, have gained popularity. Exploiting such online/offline data enables to visually share situations of congested spots [1], estimate per-lane as well as per-road traffic congestion [2], construct near-miss incident or traffic accident database [3, 4], etc.

Although image and position data collected by such a sensing scheme lacks high quality or accuracy than dedicated sensing scheme, it is realistic to sense wider area with higher frequency. Since the quantity of data is large, the issue of quality and accuracy can potentially be improved in post-processing. These characters are confronted in Table 1. Image sensing by this scheme will lead to more expansive applications, such as map construction and criminal investigation, if issues regarding personal data protection are resolved.

## 2.2 Improving Resolution of Fisheye Images

Improving image resolution is a basic signal processing technique to generate a high-resolution image as output from inputted low-resolution images, called super resolution (SR). A method named reconstruction-based SR is known well. In this method, multiple images are provided as inputs and the image positions are registered in sub-pixel order.

Several related studies have been conducted on SR for fisheye/super wide-angle cameras [5–8]. Although their problem settings are in part similar to ours, they consider only limited cases in which the shape and blur level of the image region of

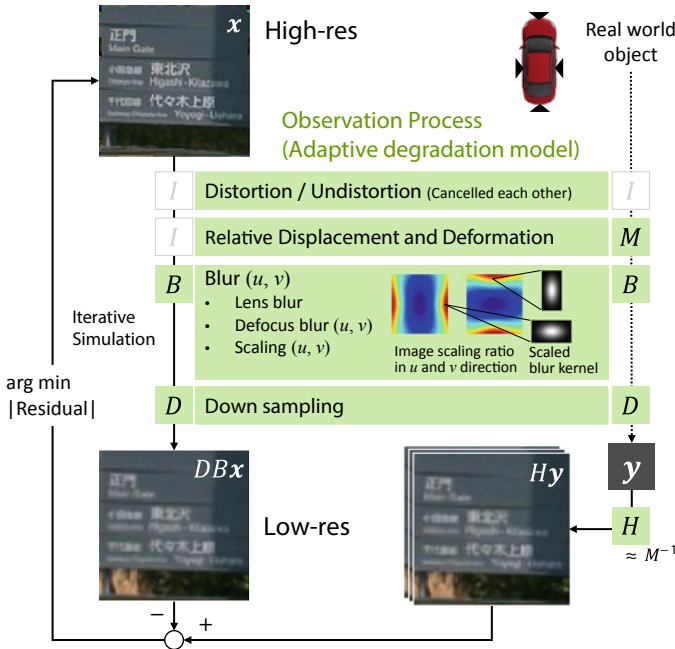


Fig. 1 Process of SR for fisheye images based on the adaptive degradation model

interest (ROI), the region in which the object is observed, are constant throughout all of the input images. This differs from the conditions in our study. To our knowledge, no other study has been reported discussing the relation between SR results and constraints on the input images.

### 3 SR Using a Fisheye Camera on a General-Use Vehicle

#### 3.1 SR Method Based on Adaptive Deformation and Blur Model

SR for fisheye image is fundamentally based on the conventional reconstruction-based SR method. Figure 1 illustrates the problem of reconstruction-based SR for fisheye images. After successively shooting a real-world object and before it is stored as observed image data, a process with degradation model is assumed that includes displacement, blur, down sampling, and noise. The SR can be realized by finding an ideal high-resolution image that minimizes the difference between the actual observed images and the “degraded ideal image” using the same model and parameters.

Particularly, in the case of dealing with fisheye images, unlike the case of ordinary images, the image degradation model includes some special processes: lens distortion/undistortion, deformation, and scaling of the blur caused by the undistortion. Please note that these effects are not uniform but dependent on position in the image. Therefore, we call the model as “adaptive degradation model”. We have developed an improved SR method based on this model in [9].

The problem can be formulated as shown in Eq. (1), where  $\mathbf{x}$  is an ideal image (in column-vector form),  $\mathbf{y}_k$  is rectangular regions in the observed images after correcting lens distortion.  $k$  is the image index, and  $H_k$ ,  $B_k$ , and  $D$  are degradation matrix operations representing registration (deformation and displacement), blur, and downsampling (a constant matrix given as problem setting).

$$\min_{\mathbf{x}} \sum_k |DB_k\mathbf{x} - H_k\mathbf{y}_k| \quad (1)$$

The approximate solution can be found through the following iterative calculation [10] as shown in Eq. (2), where  $\beta$  is a convergence step,  $\lambda$  is a smoothness constraint,  $\alpha$  is an attenuation by distance, and  $S_x^l$ ,  $S_y^m$  are image translations.

$$\begin{aligned} {}^{n+1}\mathbf{x} = {}^n\mathbf{x} - \beta & \left\{ \sum_k B_k^T D_k^T \text{sign}(D_k B_k {}^n\mathbf{x} - H_k \mathbf{y}_k) \right. \\ & + \lambda \sum_l \sum_m \{ \alpha^{|l|+|m|} (I - S_y^{-m} S_x^{-l}) \text{sign}({}^n\mathbf{x} - S_x^l S_y^m {}^n\mathbf{x}) \} \\ & \left. - p \leq l \leq p, 0 \leq m \leq p, l + m \geq 0 \right. \end{aligned} \quad (2)$$

The deformable image registration  $H_k$  is assumed to be represented by a homographic conversion and can be found using image-to-image block matching and point-to-point correspondences inside the images by using Speeded-up Robust Features (SURF). Through this process, images are theoretically registered in sub-pixel order including rotation and deformation.

The blur  $B_k$  consists of three components: (1) a blur generated by the lens itself by the optical interference (point spread function), (2) the defocus depending on the depth of field, and (3) image scaling resulting from correcting lens distortion. These components are assumed to be integrated and represented approximately by convoluting a two-dimensional Gaussian function. The standard deviation of the Gaussian function corresponds to the degree of blur. We refer to this value as the “blur size” in this paper.

The blur size is assumed to be the product of the lens blur size (1) and the image scaling ratio (3). The defocus (2) is not assumed, i.e., the camera focus is fixed to the object depth. The lens blur (1) can be estimated by fitting a Gaussian function to intensity values across a black/white edge in the captured raw image, which is focused and theoretically and ideally observed as a step function. The image scaling ratio caused by undistortion (3) can be calculated from lens distortion parameters.

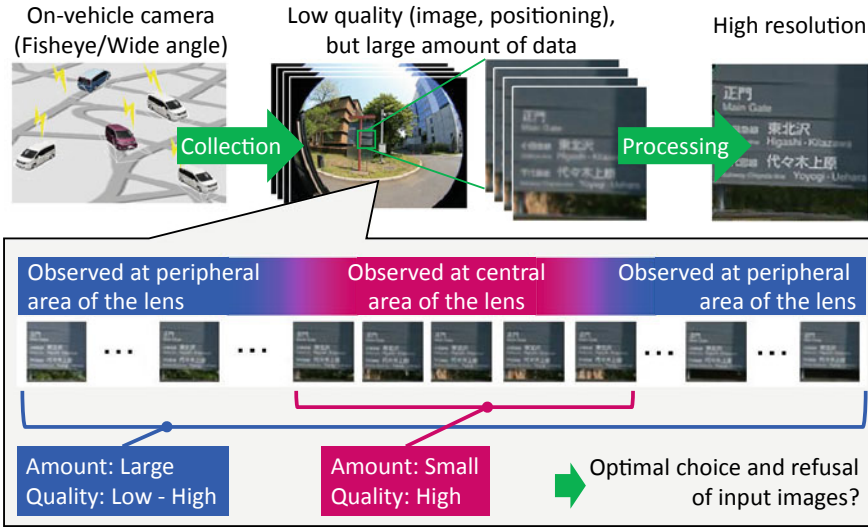


**Fig. 2** Trade-off of quality and quantity in collecting images using an on-vehicle fisheye/wide-angle camera and SR

Finding the ideal image  $x$  requires the initial value  $^0x$ , which is determined by scaling one of the  $y_k$  values using linear interpolation and iterative calculation.

### 3.2 Trade-Off of Input Images: Quality Versus Quantity

A super wide-angle lens, especially a fisheye lens, generally captures an image with greater distortion and lower resolution, especially in the peripheral area of the lens. Let us assume a situation in which such a camera is on a vehicle moving directly forward, observing a static object.

As Fig. 2 illustrates, if an object is observed around peripheral area of the lens, its image quality becomes lower, and if observed in central area, its image quality becomes higher. Meanwhile, the peripheral-area observation has more chance to occur rather than the central-area observation. Therefore, the quality and the quantity cannot be compatible. This is inevitable for fisheye lens, unless some extra sensing scheme is assumed such as collecting sensing data by multiple vehicles.

Reconstruction-based SR technology theoretically requires sufficient information as input, i.e., sufficiently many input images. However, at the same time, low-quality input images cause errors in estimating image observation parameters (such as displacement or blur) required in the SR process and lower the quality of the result. In other words, there is a trade-off problem between the quality and quantity of the input image for SR. Whether to include or exclude the images from post-processing

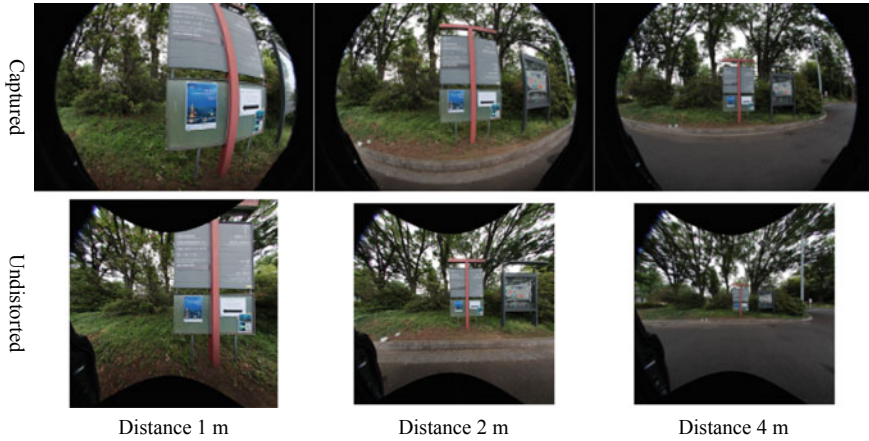


**Fig. 3** Examples of the captured fisheye images and the undistorted images

affects the final quality of the output image, however, it is unknown which images have to be included/excluded to obtain better results.

In this study, we focus on the size of the blur parameter of the image region as the criterion, and we discuss the problem by comparing several choice/refusal patterns based on this criterion.

## 4 Quantitative Analysis of the Trade-Off Problem

For quantitative analysis of the trade-off problem, we assumed an experimental situation including outdoor objects observed by an on-vehicle camera.

### 4.1 Acquisition of the Experimental Data

We successively observe a signboard by an on-vehicle fisheye camera. The vehicle proceeds in a straight line parallel to a planar signboard. The signboard is on the left side of the path and the camera is directed to the left. The distance between the board and the line (depth to the object) are one, two, and four meters.

We used *Canon EOS Kiss Digital X/Sigma 8 mm F3.5 EX DG Circular Fisheye* for the camera and the lens, with its focal length fixed. Figure 3 shows some examples of the captured images in the upper row.

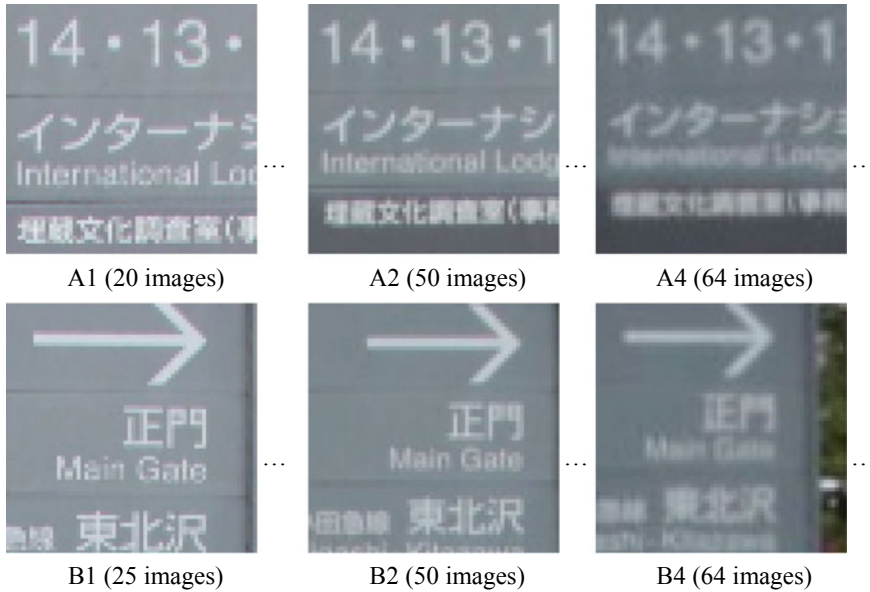


**Fig. 4** Examples of registered image sets

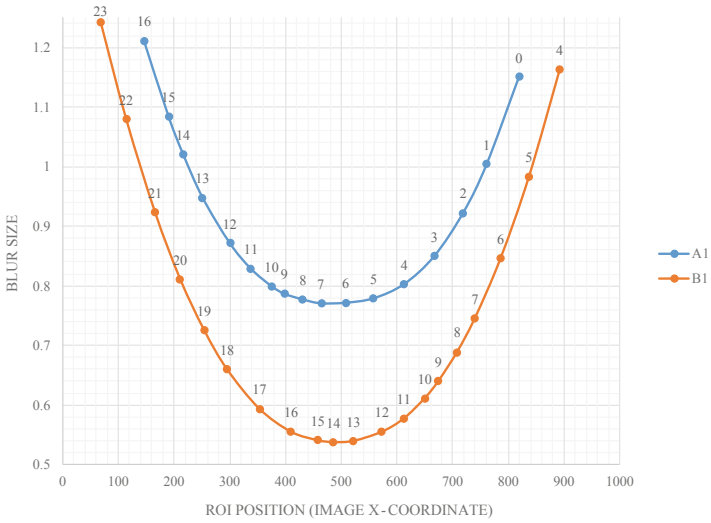
## 4.2 Deformable Image Registration and Blur Estimation

As pre-processing, the captured images are first undistorted, i.e., converted into perspective images by removing lens distortion. We use the calibration method/tool of [11] for undistortion. Figure 3 shows the images after undistortion in the lower row. In addition, to normalize roughly the apparent dimensions of the signboard for later comparison, the undistorted images captured at one meter and two-meter distances are resized into 1/4 and 1/2 scale, respectively.

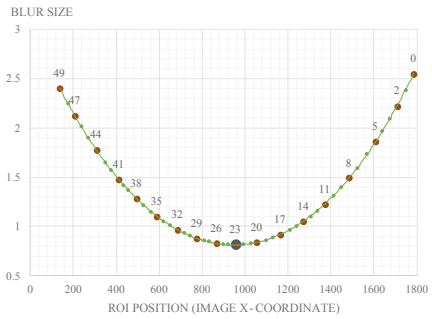
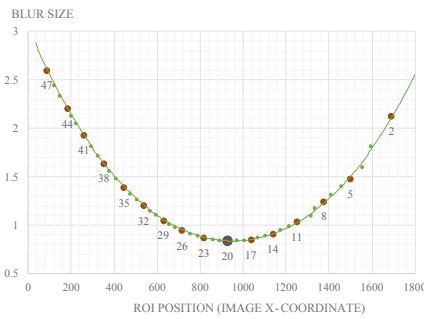
Then, two rectangular ROIs, A and B, ( $64 \times 64$  pixels) for SR are extracted from the observed images. For each sequential frame, the regions corresponding to A and B are tracked using block matching and registered with image deformation. In addition, the blur sizes of A and B, i.e., how much the pixels in the regions are blurred compared to a sharp edge, are estimated.

Hereafter, the registered sequential image sets of the ROIs A and B, with the shooting depth  $d = 1, 2, 4$  m, are described as  $A_d$  and  $B_d$ . Figure 4 shows some of the deformable registration results, and Fig. 5 plots their estimated blur sizes. Since the lens distortion effect is internally approximated by a polynomial function in [6], the blur size values also follow a continuous curve. Although the pixel scaling ratio varies strictly for each pixel, they are averaged within the ROI for approximation on the graphs.

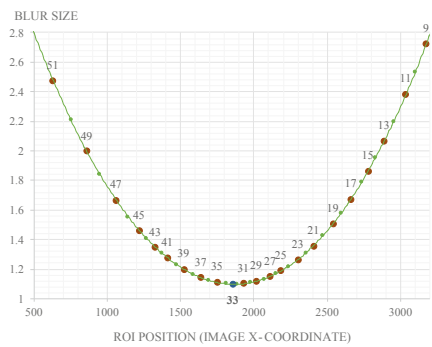
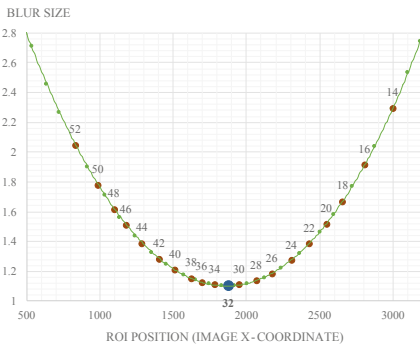




(a) A1 and B1



(b) A2 and B2



(c) A4 and B4

**Fig. 5** Blur size of the ROI. The images chosen for SR are indicated by dots and image indices. Images with smaller blur size are chosen by priority

### 4.3 Choosing Input Images

Then, we selected several input images for SR from  $A_d$  and  $B_d$  and examined how the SR result varies depending on the input images, and especially their blur sizes.

To select the input images for SR from  $A_d$  and  $B_d$ , the images are first sorted by ascending order of the blur size. As shown in Fig. 5, for example, in A1 and B1 the orders are  $(A_1^7, A_1^6, A_1^8, \dots, A_1^{16})$  and  $(B_1^{14}, B_1^{13}, B_1^{15}, \dots, B_1^{23})$ , respectively. In A2, B2, A4, and B4, only some key images indicated with large dots with image indices in Fig. 5 are subject to selection.

Then, with these orders, the first four images are selected as the first sets, and the first six, eight, ten, and further images are selected as the second, third, fourth, and further sets.

Throughout all of the inclusion/exclusion patterns, the minimum number of input image is four, and the maximum size of the blur is 2.72. The more input images are chosen, the larger the amount of information there is, but at the same time, low-quality images with larger blur size and lower registration accuracy are included.

### 4.4 SR Result

SR is performed to increase the resolution twice, generating a  $128 \times 128$ -pixel image as output from the  $64 \times 64$ -pixel input images. The parameters in (2) in the appendix are set as  $\beta = 1.0$ ,  $\lambda = 0.2$ ,  $\alpha = 0.5$ ,  $p = 3$ . The initial value of the SR image is provided by resizing one of the input images using linear interpolation.

Figure 6 shows examples of SR images. Although some images partially include false color effects caused by the image border, the SR effect can be recognized. Additionally, the effect of SR can also be seen in Fig. 7 (described later), in which the gradients of the pixel intensity around edges, usually caused by factors such as the border of a character, became steeper compared to the linearly-scaled image, and yet, the difference in the intensity values was not enlarged more than the input, in contrast to unsharp masking.

### 4.5 Evaluation

Peak signal-to-noise ratio (PSNR) is a well-known score for evaluating image degradation and restoration. It requires a ground-truth image for comparison; however, the ground truth is unknown in SR of real images. Setting a camera to low- and high- resolution modes and regarding the former as input for SR and the latter as the ground truth does not work, because even the latter image contains a blur caused by the lens itself and, hence, differs from the ground truth.

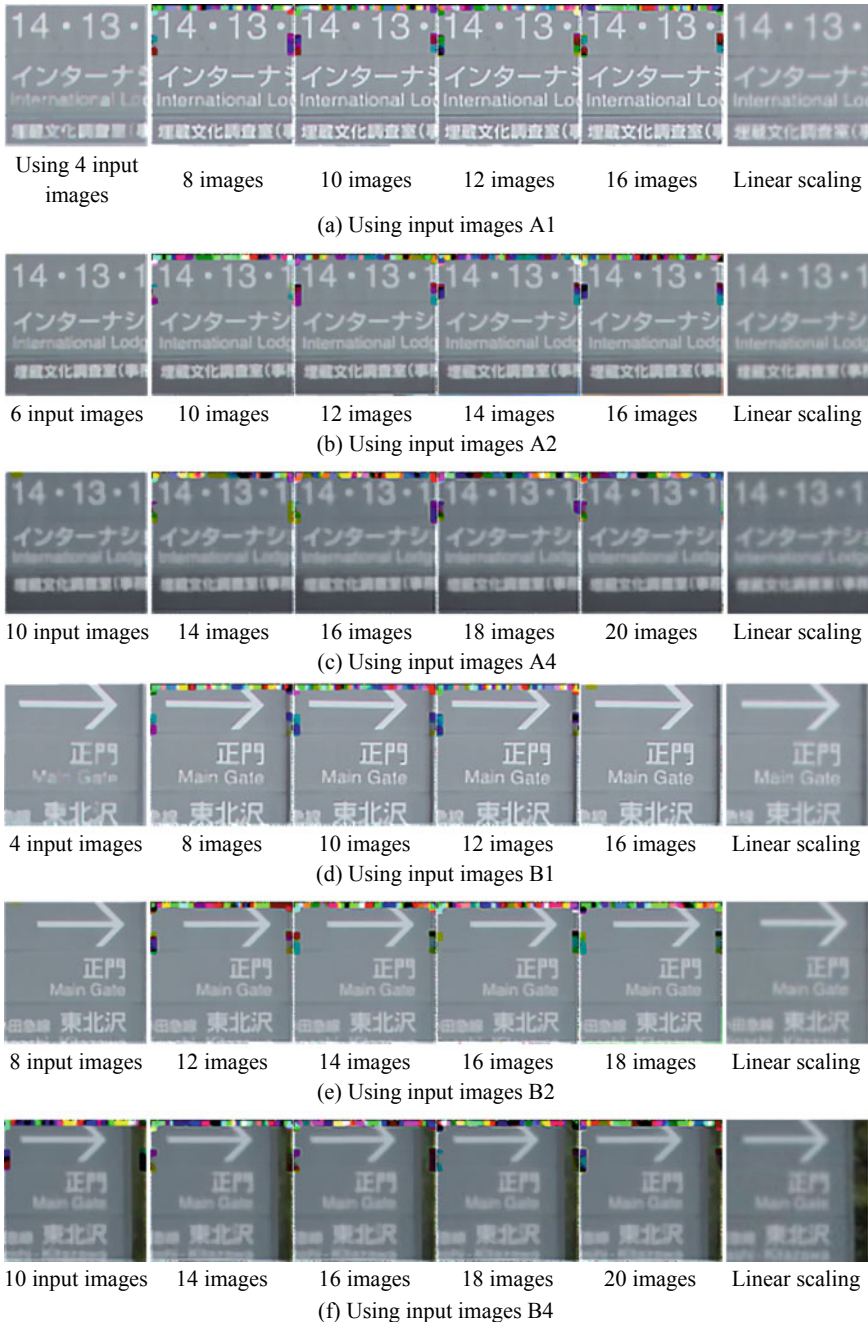


**Fig. 6** Result images of SR with varying numbers of input images (calculation iterations = 1,000). The linear scaling is not a result of SR. It is included just for comparison

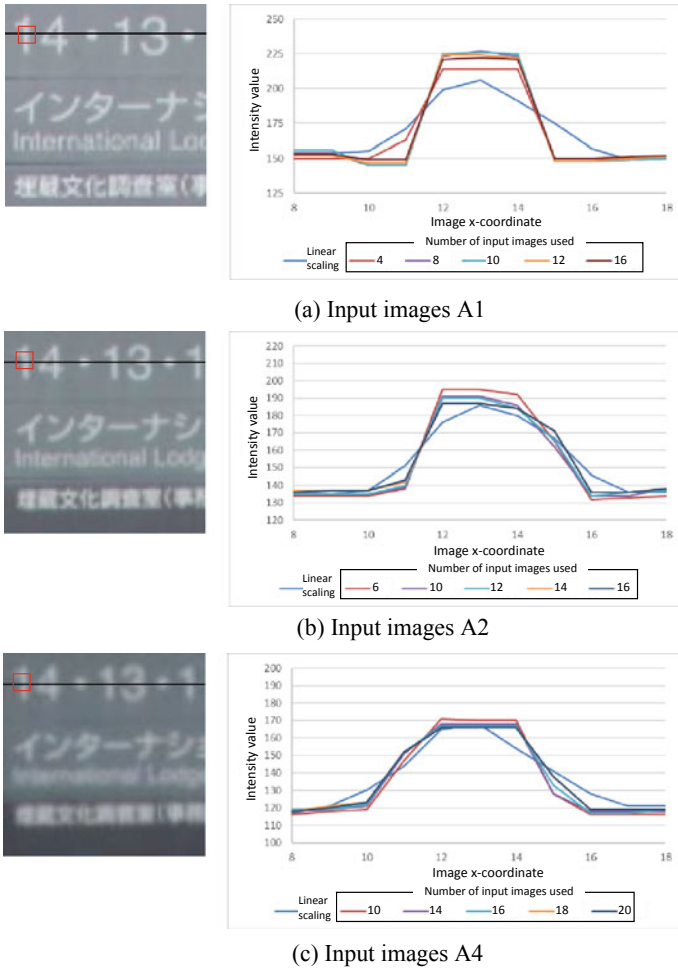
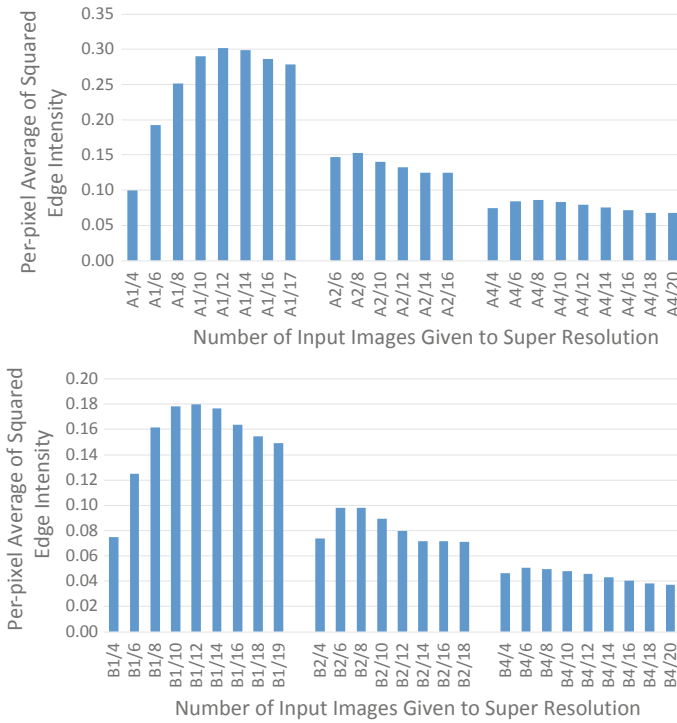


Fig. 7 Pixel intensity values around an edge (across the character “1” on the left) along the horizontal line in a result image of SR

In this study, we focus on edges in the image and their gradients to evaluate the results of SR, because SR generally restores the high-frequency component.

Evaluation using the Edge Intensity Gradient. Figure 7 shows some examples of the intensity value of the SR results around the edge. For A1, as more input images were provided for SR, the gradient became steeper in the result. On the other hand, for A2 and A4, when more than ten input images were provided, the gradient became lower, meaning that the edge became less sharp.

To evaluate these edge attributes comprehensively and quantitatively, as Fig. 8 shows, the mean square value of the edge intensity  $(dI/dx)^2 + (dI/dy)^2$  within the image (except the image border with a false color effect) was calculated. The score



**Fig. 8** Mean value of squared edge intensity in a result image of SR

achieved a maximum, indicating the best SR result, when 12 images were provided as input for A1, and eight images for A2 and A4. The same tendency can be seen for B1, B2, and B4.

Let us check the maximum blur size of the input image when the edge intensity achieves its maximum value as above. As Fig. 5 shows, for A1, the maximum blur size is 1.25 with 12 input images. This indicates that the observed images that have larger blur than this value are to be excluded from the input of SR, and that the blur size can be a criterion.

In the same manner, the maximum blur sizes that provide choice/refusal criteria in the other cases (A2, A4, B1, B2, and B4) were found to range from 1.08 to 1.45.

### 4.6 Discussion

Theoretically, the number of input images used cannot itself be a causative factor for low-quality result images in reconstruction-based SR.

In contrast, errors in pre-processing, deformable image registration, and blur estimation are considerable factors. Among these, blur estimation is unlikely to be a causative factor since it is a process common throughout all of the cases (A1 ~ B4) and its scaling ratio can be found analytically. Deformable image registration is most likely the causative factor in worsening the quality of the result images, because including larger blur in the input images and searching corresponding points for deformable image registration results in lower accuracy.

## 5 Conclusion

The work reported in this paper regarding the SR of on-vehicle fisheye camera images made the following contributions.

- It pointed out the problem of trade-off between quality and quantity of input images and evaluated the effects of choice/refusal of input images on the SR results.
- It found that the results worsen when more input images are included with a maximum blur greater than 1.08 ~ 1.45, as a result of image registration errors.
- It estimated that the blur size can potentially be a criterion for inclusion/exclusion of input images.

Future work includes improving the blur estimation process, experiments using more commonly-used inexpensive cameras, consideration of motion blur, and discussion of the requisites for better SR results.

## References

1. Pioneer Corporation, Pioneer Introduces New CYBER NAVI Car Navigation Systems for Japan Market. <https://global.pioneer/en/news/press/index/1617> (2018)
2. Toyota Motor Corporation, Toyota Plans Trial Provision of Lane-specific Traffic-congestion Information Based on Driving Video Data from 500 Tokyo Taxis. <https://newroom.toyota.co.jp/en/detail/19231576/> (2018)
3. Kataoka, H., Suzuki, T., Oikawa, S., Matsui, Y., Satoh, Y.: Drive video analysis for the detection of traffic near-miss incidents. In: IEEE International Conference on Robotics and Automation (ICRA) (2018)
4. Chan, F.-H., Chen, Y.-T., Xiang, Y., Sun, M.: Anticipating accidents in dashcam videos. In: The 13th Asian Conference on Computer Vision (ACCV) (2016)
5. Kawasaki, H., Ikeuchi, K., Sakauchi, M.: Super-resolution omnidirectional camera images using spatio-temporal analysis. *Electron. Commun. Jpn.* **89**(6), 47–59 (2006)
6. Nagahara, H., Yagi, Y., Yachida, M.: Super-resolution from an omnidirectional image sequence. In: Proceedings of 26th Annual Conference of the IEEE Industrial Electronics Society (IECON), vol. 4, pp. 2559–2564 (2000)
7. Zhang, F., Zhu, Q.-D.: Super-resolution image reconstruction for omni-vision based on POCs. In: Proceedings of 21st Annual International Conference on Chinese Control and Decision (CCDC), pp. 5045–5049 (2009)

8. Arican, Z., Frossard, P.: Joint registration and super-resolution with omnidirectional images. *IEEE Trans. Image Process.* **20**(11) (2011)
9. Takano, T., Ono, S., Matsushita, Y., Kawasaki, H., Ikeuchi, K.: Super resolution with fisheye camera images for visibility support of vehicle. In: *IEEE International Conference on Vehicular Electronics and Safety (ICVES)* (2015)
10. Farsiu, S., Robinson, D., Elad, M., Milanfar, P.: Fast and robust multiframe super resolution. *IEEE Trans. Image Process.* **13**, 1327–1344 (2004)
11. Scaramuzza, D., Martinelli, A., Siegwart, R.: A toolbox for easy calibrating omnidirectional cameras. In: *Proceedings to IEEE International Conference on Intelligent Robots and Systems (IROS)* (2006)

# Architecture and Development of Agent-Based Unified Simulation Environment for ITS Services



Ryo Fujii, Takahiro Ando, Kenji Hisazumi, Tsunenori Mine, Tsuneo Nakanishi and Akira Fukuda

**Abstract** Agent-based traffic simulation has become increasingly interesting and important for developing new intelligent transport systems (ITS) services. Till date, a variety of studies and developments that combine simulators and evaluate ITS services on the combined simulators have been conducted. In this paper, we propose a simulation environment called as Agent-based unified simulation environment (USE) for ITS services. To confirm the effect of ITS services on the society via simulation, it is generally necessary to implement a model of the service on a simulator. The Agent-based USE provides an easy-to-build simulation environment for ITS-related services. Particularly, by connecting simulators with ITS services, the Agent-based USE determines behaviors to be changed on the simulators using the data of the services such as recommendation results generated by the services and communicates the decisions to the simulators; the Agent-based USE then obtains the data representing the current situation on the simulators and sends it to the services as feedback so

---

R. Fujii (✉)

Graduate School of Information Science and Electrical Engineering, Kyushu University, 744 Motoooka, Nishi-ku, Fukuoka 819-0395, Japan  
e-mail: [r\\_fujii@f.ait.kyushu-u.ac.jp](mailto:r_fujii@f.ait.kyushu-u.ac.jp)

T. Ando

Faculty of Information Science and Electrical Engineering, Kyushu University, 744 Motoooka, Nishi-ku, Fukuoka 819-0395, Japan  
e-mail: [ando.takahiro@f.ait.kyushu-u.ac.jp](mailto:ando.takahiro@f.ait.kyushu-u.ac.jp)

K. Hisazumi

System LSI Research Center, Kyushu University, 744 Motoooka, Nishi-ku, Fukuoka 819-0395, Japan  
e-mail: [nel@slrc.kyushu-u.ac.jp](mailto:nel@slrc.kyushu-u.ac.jp)

T. Mine · A. Fukuda

Faculty of Information Science and Electrical Engineering, Kyushu University, Fukuoka, Japan  
e-mail: [mine@ait.kyushu-u.ac.jp](mailto:mine@ait.kyushu-u.ac.jp)

A. Fukuda

e-mail: [fukuda@ait.kyushu-u.ac.jp](mailto:fukuda@ait.kyushu-u.ac.jp)

T. Nakanishi

Department of Electronics Engineering and Computer Science, Faculty of Engineering, Fukuoka University, 8-19-1 Nanakuma, Jonan-ku, Fukuoka 814-0133, Japan  
e-mail: [tun@fukuoka-u.ac.jp](mailto:tun@fukuoka-u.ac.jp)

© Springer Nature Singapore Pte Ltd. 2019

T. Mine et al. (eds.), *Intelligent Transport Systems for Everyone's Mobility*, [https://doi.org/10.1007/978-981-13-7434-0\\_13](https://doi.org/10.1007/978-981-13-7434-0_13)



as to enable the services to generate the next recommendation. Additionally, using the Agent-based USE, it is possible to construct a co-simulation environment where simulation is performed by synchronizing some types of simulators and services and by sharing simulation information. In this paper, we introduce the overview and architecture of the Agent-based USE for traffic simulation and discuss its usefulness.

## 1 Introduction

With the development of the internet of things (IoT) technology, there have been increasing expectations to become a smart mobility society equipped with new social information infrastructure systems. Information infrastructure systems that support the smart mobility society are called smart mobility systems, and research on system life cycle that includes the development of such a system has become increasingly important. The realization of a sustainable smart mobility society is currently being discussed as a challenging task [2]. Particularly, many issues concerning the development of smart mobility systems such as services and applications related to intelligent transport systems (ITS) that are responsible for the social infrastructure still remain to be addressed.

While developing ITS services, it is important to confirm their effect on the society affected by them, and field trials are often conducted before their full-scale introduction. However, the field trials are time-intensive and expensive, and the cost of their preparation is also considerable; therefore, it is not realistic to conduct the field trials several times on a single system. Therefore, it is common to check the effect of these systems via simulation before their field trials or release.

Generally, while checking the effect of ITS services via simulation, we need to create models on the behavior of ITS services in addition to modeling the vehicles, pedestrians, and road networks. Apart from the ITS services, we have to create the behavior model with the same function that the services have.

In addition to the method of performing simulation, there exists a method of preparing a simulation system for each service individually. In that case, it is necessary to modify the whole or a part of the simulation system at each service update. At least it is necessary to implement the behavior models of the services on the simulation system repeatedly. If the implementation of the behavior model is omitted, the simulation cost can be reduced.

For a purpose similar to the abovementioned, combining different simulators or combining simulators and services has been attempted. However, simulators and services are combined directly during the attempts, and the main objective of the attempts is to exchange data with each other. There are considerable researches on Agent-based simulation incorporating the decision-making model of the entity (agent) to be simulated. Such a decision-making model is implemented in the simulator; however no consideration is given to connecting it with other simulators or services. Even for simulators including such decision-making models, the services can be connected by introducing a mechanism to connect simulators and services as

described above. However, in order to introduce decision-making models on other simulators, it is necessary to newly implement the decision-making model. Additionally, while implementing a decision-making model for each simulator, because the simulator information used in each decision-making model is different and sharing of simulator information is generally difficult, it is not easy to ensure consistency between different implementations of the decision-making models.

We propose a simulation environment, called the Agent-based unified simulation environment (USE) for ITS services. It is possible to apply a common decision-making model to multiple simulators and to services associated with the object by introducing one decision-making model for each object. Therefore, there is no inconsistency between the above decision models. Even if it is necessary to use different decision-making models in different simulators, it can be dealt with by handling them as different objects (entities). In this paper, we describe the overview of this Agent-based USE and discuss case studies to verify its effectiveness.

The rest of this paper is organized as follows. In Sect. 2, we introduce traffic simulators used for observing the effects of ITS services. In Sect. 3, we describe motivational examples of development of our Agent-based USE. In Sects. 4 and 5, we present an overview of the Agent-based USE and its architecture. In Sect. 6, we discuss case studies to confirm the effect of the Agent-based USE using its prototype implementation. Section 7 describes related work, and we conclude the paper in Sect. 8.

## 2 Traffic Simulator

Traffic simulators simulate the behavior of a moving object such as a vehicle or a pedestrian on a road network and the behavior of a signal system in a virtual space. These simulators observe the behavior of the moving objects and the condition of traffic in the virtual spaces. The traffic simulators are classified into macro traffic simulators, micro traffic simulators, and human flow simulators according to the size of the virtual space to be focused on and the observation granularity of the moving objects. An appropriate simulator is selected according to the simulation purpose. The characteristics of the different simulators are given below.

**Macro traffic simulator** This covers a relatively wide area and targets a large-scale road network. Additionally, it does not treat moving objects individually object-wise, but as fluids that flow over a network, and observes their flow rates.

Visum [9] is an example of a macro traffic simulator.

**Micro traffic simulator** This covers a relatively smaller area. Additionally, it treats moving objects individually and simulates their detailed motion. SUMO [4], Vis-sim [8], Aimsun [13] etc. are few examples of micro traffic simulators.

**Human flow simulator** This primarily covers areas such as stations or commercial facilities and simulates the movement of people in such spaces. In the simulation of the evacuation of people during a disaster, artisoc [3] is used as a human flow simulator.

### 3 Motivational Example

In this section, we describe motivational examples of development of our Agent-based USE.

#### 3.1 Connection of Simulator and Multiple Services

First, we describe the motivational example illustrated in Fig. 1. Figure 1 shows a situation in which vehicles and pedestrians move within an area having few buildings and parking lots.

A vehicle traveling in this area uses a service of the system for recommending the available parking lots and determines a destination parking lot. Additionally, it uses a service of the car navigation system and determines the travel route to its destination.

On the other hand, a pedestrian in this area uses a service of the pedestrian navigation system, determines a route based on the information provided by the service, and moves between some buildings and parking lots along the route.

In the above situation, there may be demands for observing the interference between services for an object receiving multiple services, and between objects

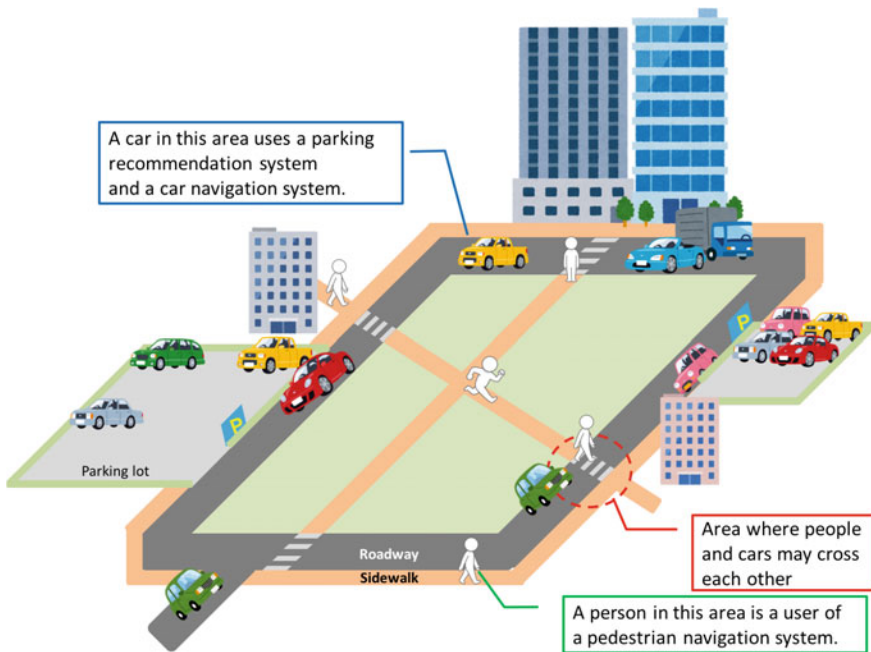


Fig. 1 Motivational example for connection of simulator and multiple services

receiving different services. In order to observe this interference via simulation, it is necessary to implement all the factors of the services into one simulation system. This is a considerably tough job.

Therefore, in our Agent-based USE, we decided to provide a mechanism to connect the simulator and implementations of services. Using this mechanism, we can easily connect a simulator and multiple services without modeling them and reduce construction costs of a simulation system.

### 3.2 Connection of Different Kinds of Simulators

Next, we describe the motivational example illustrated in Fig. 2. The figure shows how the flow of people on each floor and the behavior of each elevator interact with each other in a building with multiple elevators.

A person is a user of a service that recommends which elevator to ride; the person determines a target elevator based on the information from the service, and moves up to the target elevator on the floor. The varying degree of congestion in front of the elevators affects the behavior of the elevators. Consequently, the behavior of the elevators or users riding the elevators also affects the behavior of the elevator recommendation service, which cyclically affects the flow of people again.

In order to observe the situation mentioned above, the following simulation is desired.

- Human flow and elevator behavior are simulated using different simulators: a human flow simulator and an elevator simulator that are appropriate to the human flow and elevator behavior, respectively.

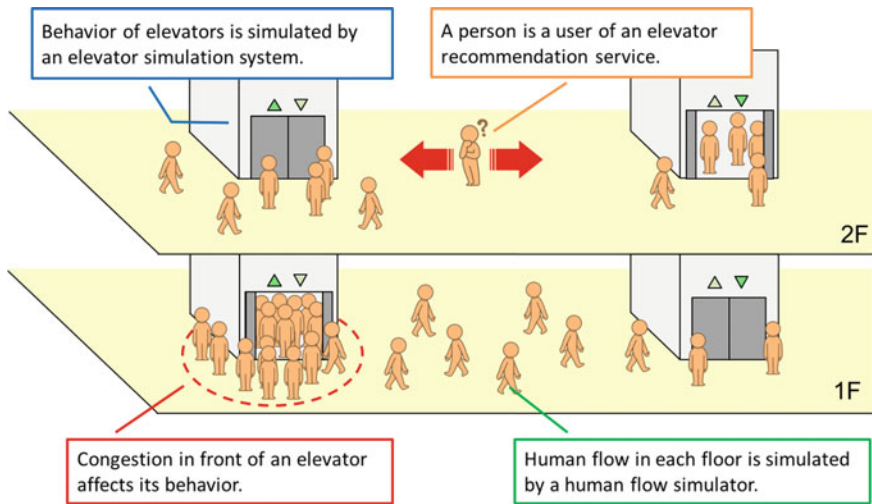


Fig. 2 Motivational example for connection of different kinds of simulators

- The simulation is performed by synchronizing the different simulators, sharing each simulation result at each timing of synchronization.
- In the simulation, the shared results at a step are used as each simulator’s input for the next step of the simulation.

Such a simulation is called co-simulation, and it is difficult to construct it.

Therefore, our Agent-based USE provides a mechanism that enables connecting different simulators with each other. Using this mechanism, the construction costs of the co-simulation environment can be reduced.

### 4 Overview of the Agent-Based USE

In this section, we describe the Agent-based USE that is currently under development, and which uses ITS services.

Figure 3 illustrates a simulation system using the Agent-based USE that consists of three main parts: simulators, ITS services, and our Agent-based USE. The roles of the components in the simulation system are as follows.

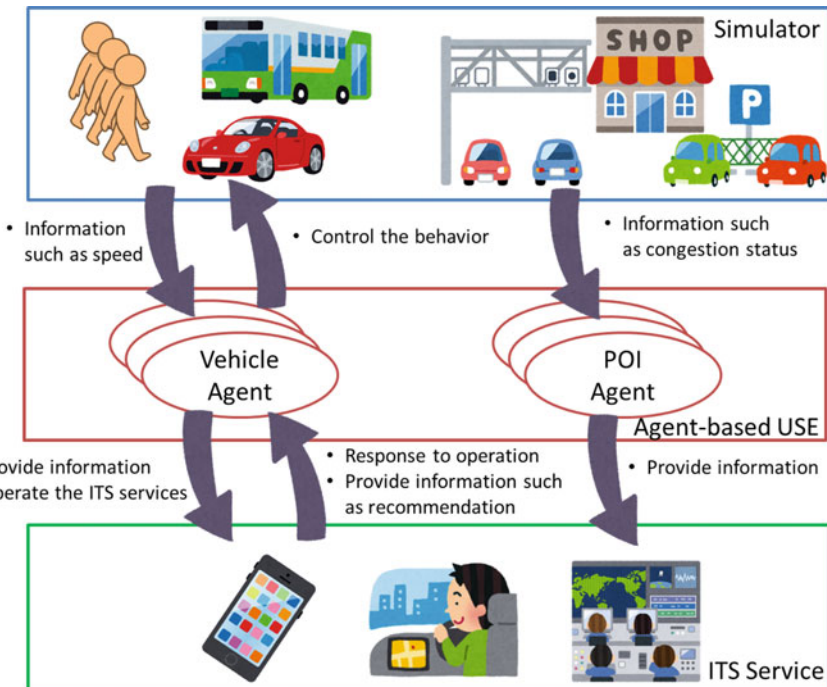


Fig. 3 Conceptual diagram of the Agent-based USE

**Simulator** A simulator simulates the movements of objects in the simulator. In terms of a traffic simulator, it simulates only “driving a car” to the destination and does not voluntarily “change” the destination of the car.

**ITS Service** An ITS service provides useful information to determine the destination of a moving object and a route to the destination. Some services acquire information such as the current location of the object and point of interest (POI) information such as the congestion status of the destination and provide information based on the acquired information.

**Agent-based USE** The Agent-based USE connects simulators and ITS services with each other. It changes the parameters of moving objects from outside the simulator such as for determining and changing the destination of a moving object on the simulator and changing the route. It also gathers the information necessary for the service from the simulator and sends it to the service. It determines changes in the parameter values of moving objects on the simulators, based on the information provided by the connected ITS services.

By connecting the implementation of the ITS service with the traffic simulator, simulation can be performed without creating a model representing the behavior of the ITS service on the simulator.

Moreover, because the traffic simulator and the implementation of ITS services can exchange information in real time through the Agent-based USE during the simulation, the behavior of the ITS services affects the environment being simulated in real time. Additionally, it is also possible to observe that the environmental change on the simulator affects the behavior of ITS services in real time.

The Agent-based USE can connect to multiple ITS services with the traffic simulator. This enables us to observe the interference between influences of each service. More specifically, it enables us to observe whether the effect of multiple cooperating services is as expected.

Furthermore, the Agent-based USE enables mutual connection between the ITS services and the different kinds of simulators; it enables the simulation of the following scenarios:

1. Under the guidance of a car navigation system, a car moves to a parking lot closest to the destination, which is a target building such as a commercial facility. The driver walks to the commercial facility after getting off the car.
2. The driver walks from the entrance to the target store within the commercial facility, using the in-facility guidance system.

In this scenario, simulation is performed using a micro traffic simulator outside the commercial facility and a human flow simulator inside. The two types of simulators are executed at the same time. In the simulation, the moving object performing the scenario behaves as a moving object on the micro traffic simulator when present outside the facility and as a moving object on the human flow simulator when present inside the facility.

## 5 Architecture of the Agent-Based Unified Simulation Environment

### 5.1 Modules of Agent-Based USE

In this section, the architecture of the Agent-based USE, which is currently under development, is outlined based on the architecture diagram shown in Fig.4. This Agent-based USE comprises several types of core modules and objects as follows:

**Unified Simulation Field** This module forms the base of the Agent-based USE and is responsible for managing instances of each module appearing in the Agent-based USE.

**Sim** This module is responsible for connecting an individual simulator and the Agent-based USE.

**Vehicle** This object is responsible for connecting with a moving object on a simulator. When a moving object moves into the space of another simulator, it is moved to another Sim module by the unified simulation field module.

**POI** This object is responsible for connecting with a POI object within a simulator.

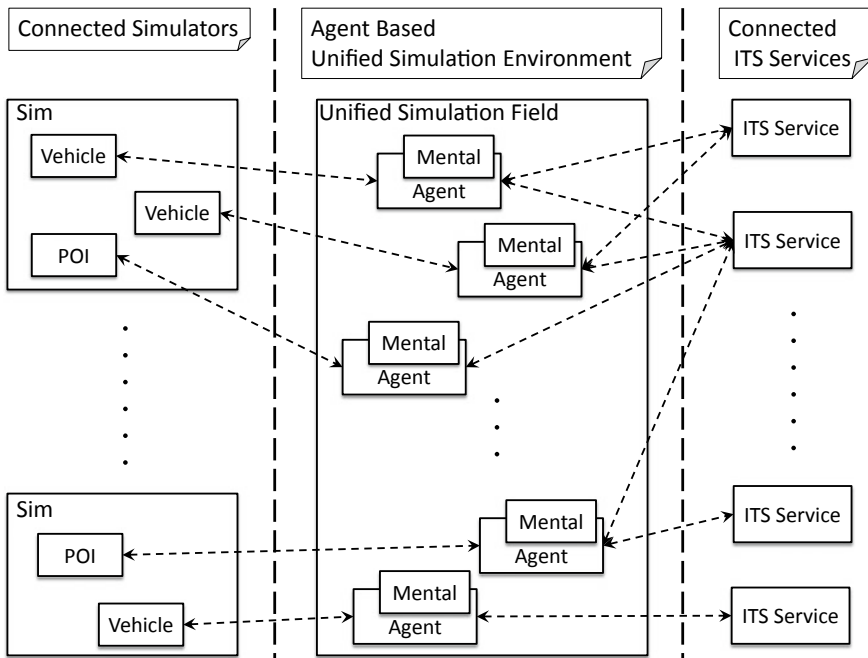


Fig. 4 Architecture of the Agent-based USE for traffic simulation

**Agent** This object plays the role of an intermediary for exchanging information between a vehicle object and the ITS services or between a POI object and the ITS services. This object is also responsible for changing the movement of a moving object that it is connected with.

**Mental** This object is a component of an Agent object, and plays the role of a decision-maker for the Agent object. It is responsible for determining of the parameter of the moving object after the behavior change based on the information is received by the Agent object.

## ***5.2 Information Transmitted and Received in the Agent-Based USE***

In each connection between the modules and objects, information is transmitted and received as follows.

**Information from the vehicle on the simulator to the Agent** The present location and speed of the moving object are acquired from the simulator through the vehicle object and sent to the Agent object in charge.

**Information from the POI on the simulator to the Agent** The POI information such as the degree of congestion is acquired from the simulator through the POI object and sent to the Agent object in charge.

**Information from the Agent to the ITS services** The Agent object that obtains the information from the simulator transmits it to the ITS services. Additionally, the Agent acting as an intermediary with the moving object transmits what operation is to be performed and the information necessary for the operation to the ITS services, on behalf of the moving object that performs the operation.

**Information from the ITS service to the Agent** The ITS service returns appropriate response information for the operation to Agent. For example, a route recommendation service recommends a proper route to the user. This information is used by Mental that is a component of Agent to create a decision to change the object behavior.

**Information from the Agent to the vehicle on the simulator** The Agent responsible for the moving object sends a decision to change the behavior of the moving object created by Mental.

## ***5.3 Connections of Each Component in the Simulation System Using the Agent-Based USE***

We describe connection of each component in the simulation system using the Agent-based USE. Presently, an interface called traffic control interface (TraCI) [14] to connect the Agent-based USE with the simulators. The Agent-based USE acquires object



status and handles object behaviors through the interface. Additionally, the TCP/IP and REST APIs are supported for the communication between the Agent-based USE and ITS services. The Agent-based USE communicates with the services, sends necessary information through a request to the services, and receives a response. Using this mechanism, it is possible to construct a simulation environment reflecting the results in real time.

We are currently developing a prototype of this Agent-based USE based on the architectural design using Python. Functions to connect different types of simulators have not been implemented yet; however, connection between the same kind of simulator and multiple kinds of ITS services is already supported.

### 5.4 Connecting Multiple Simulators

In this section, we describe connecting multiple simulators in our simulation environment. Our proposed simulation environment enables connection of multiple traffic simulators. Presently, its prototype is able to connect only those simulators with the same simulation time granularity; however, we plan to implement the feature to connect simulators with different time granularity as well.

In Fig. 5, we explain the management of multiple simulation times and the time of our simulation environment.

The time of each connected simulator never overtakes the time of the simulation environment. The time of each connected simulator and the simulation environment satisfies the following conditions, where  $Tick_{env}$  is a tick of the simulation environment and  $Tick_i$  is the tick of simulator  $S_i$  respectively.

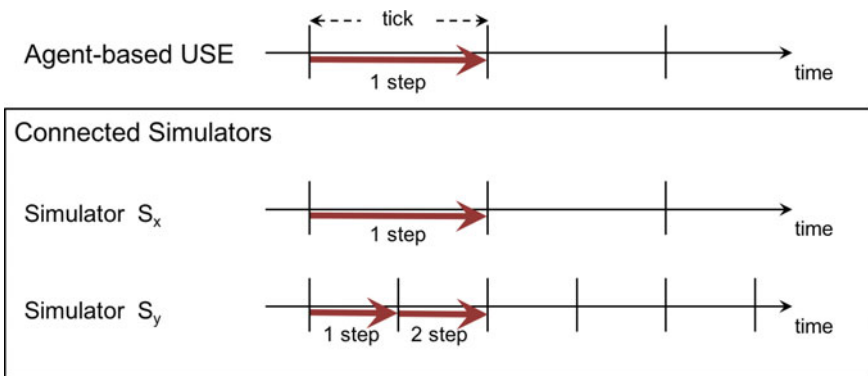


Fig. 5 Management of simulation tick

1.  $Tick_i \leq Tick_{env}$
2. The least common multiple of each connected simulator tick is a tick of the simulation environment. Therefore, the following formula gets established.

$$Tick_{env} = m_i \times Tick_i \quad (m_i \in \mathbb{N})$$

In generally, since the tick of the simulator takes values such as 1, 5 and 1000 ms, we believe that it is acceptable.

Also, connecting multiple traffic simulators requires consideration of objects moving between different traffic simulators. In Fig. 6, we explain how to handle the objects moving between traffic simulators.

For objects moving to another simulator space, the corresponding Agent is added to the list of transferred objects and to the destination simulation space in the next simulation step. Since the Agent has the information of the corresponding object, it can hold the information in the simulation space of the destination. In this manner, the moved object is recognized as the same one on the simulation environment, and the object information can also be handed over and handled.

## 5.5 Connecting Multiple Services

In this section, we describe connecting multiple services and our simulation environment.

Our proposed simulation environment is connectable to multiple services. This is realized by having the client of the service in the Agent. If you have multiple clients in an Agent, you can connect to multiple services.

When the Agent uses the service, it receives the recommendation information as a result. It accepts the recommendation information and judges whether to replace the information owned by the Agent by Mental model. Further, the same Agent may use multiple services and receive a plurality of recommendation information. Even in this case, we decide which information to accept depending on the Mental model. To judge the recommendation information by the Mental model, the evaluation value of the recommendation information is calculated and decided based on the value. The following equation is an expression for calculating the evaluation value.

$$V = \sum_i f_i(e_i)$$

$V$  represents an evaluation value, and  $e_i$  represents an element relating to the evaluation, e.g., a distance, congestion rate etc.  $f_i$  is the weight of the element. For example, when  $e_i$  is a distance and its evaluation function  $f_i$  is a linear function, the evaluation value  $f_i(e_i)$  is proportional to the distance. Based on this evaluation formula, the evaluation value of the recommendation information and the information competing with the recommendation information is calculated and evaluated.

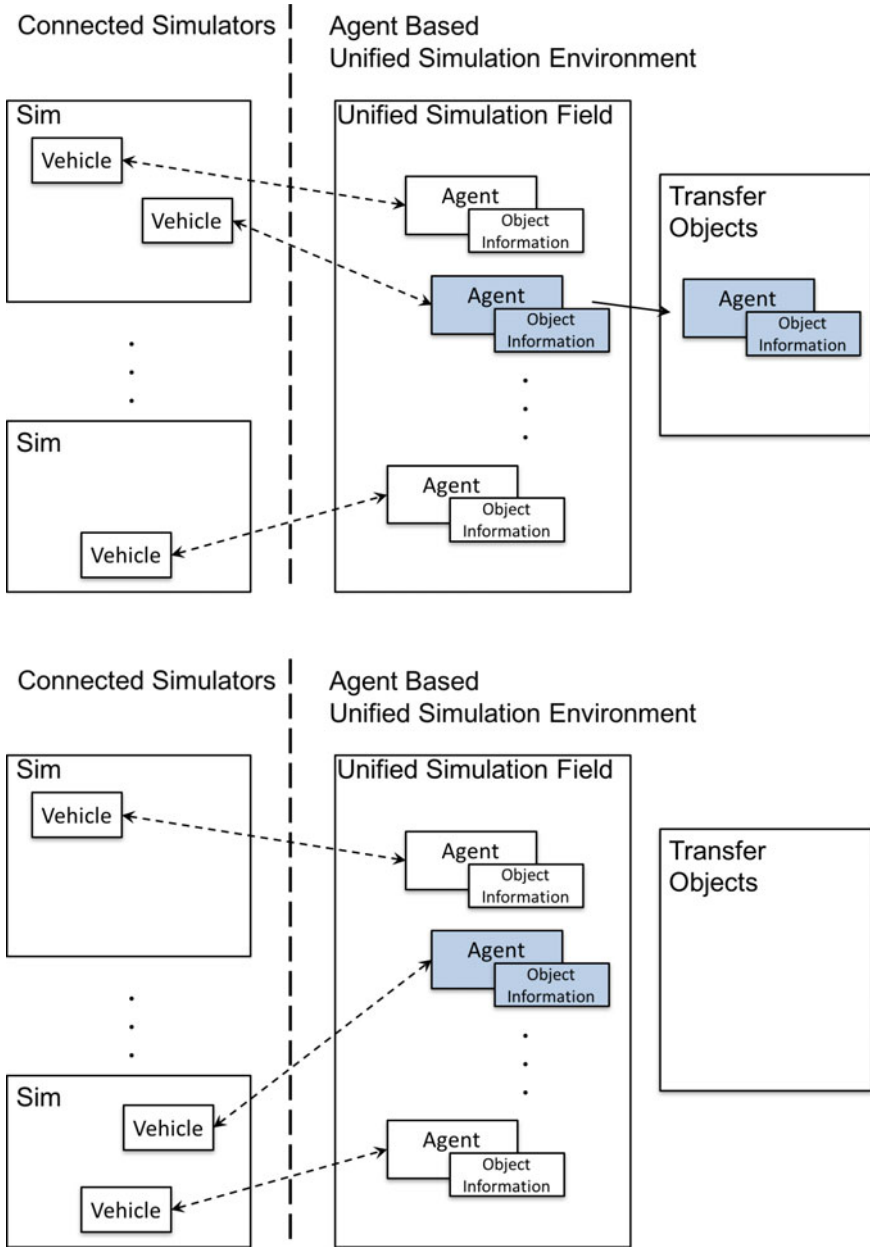


Fig. 6 Management of a transfer object

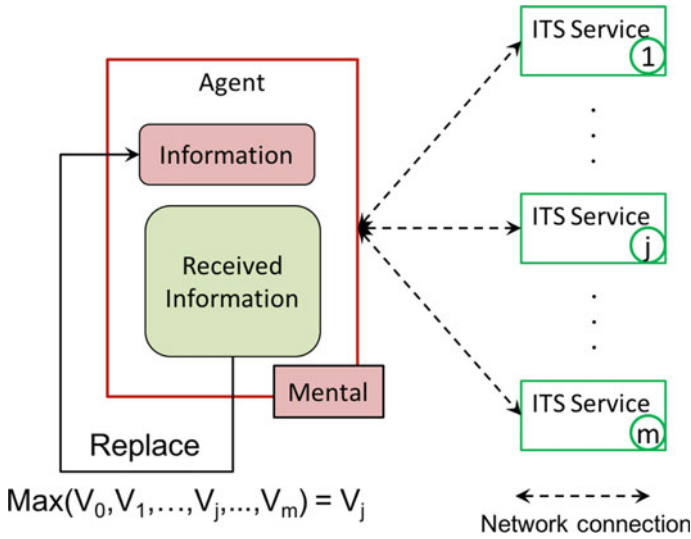


Fig. 7 Connection of multiple services

Figure 7 shows the overview of replacing information owned by the Agent based on the result of the obtained evaluation value. As an example, we will explain the flow of receiving recommendation information from  $m$  connected services and replacing that information.

1. The Agent requests the recommendation information to  $m$  competing recommendation services.
2. The Agent receives recommendation information from the  $m$  services.
3. For each unit of recommendation information, each evaluation value ( $V_1 \dots V_m$ ) is calculated using the evaluation formula.
4. Calculate the evaluation value of the recommendation information, and also calculate the evaluation value ( $V_0$ ) of the information currently owned by the Agent.
5. From all the calculated evaluation values, find the one with the maximum evaluation.
6. If the one with the highest evaluation value is obtained from the recommendation information, it replaces the information that the Agent originally owned.

## 6 Case Study

In this section, we describe a case study of simulation using the prototype of the Agent-based USE under implementation in Python language based on the architecture design shown in Sect. 5. In this case study, we implemented several simple ITS services and connected them with SUMO as a traffic simulator.

### 6.1 Connected with Multiple ITS Services

We introduce a case study connecting two ITS services that we prepared for the simulator to observe the interference between the services.

#### Data Used for the Simulation Execution

Road Network:

road network shown in Fig. 8 was prepared as the application space of the case study. Three places marked in gray represent parking lots that are POIs. Additionally, the POI information of each parking lot is assumed to be the degree of congestion at that time, and the maximum number of cars which each parking lot can accommodate is 40, 40, and 25 in order from parking lot 1.

Vehicle Data:

The data of the vehicles moving on the road network were created using the tool attached to SUMO. Each vehicle emerges from any one of the left, right, or lower end, and moves to one of the three parking lots.

In this case study, the number of execution steps in the simulation is 3,600 and the vehicles on the simulator are generated in one of the steps and discarded on reaching one of the parking lots. Additionally, some vehicles use one of the ITS services described below and conform to the recommendation information from the ITS services. Depending on the recommendation information from the ITS services, the vehicles may change the destination from one parking lot to another. The number of vehicle units using each ITS service is shown in Table 1.

ITS Service:

We implemented a simple ITS service that connects to the simulator and recommends vacant parking lots according to the degree of congestion of the parking lot.

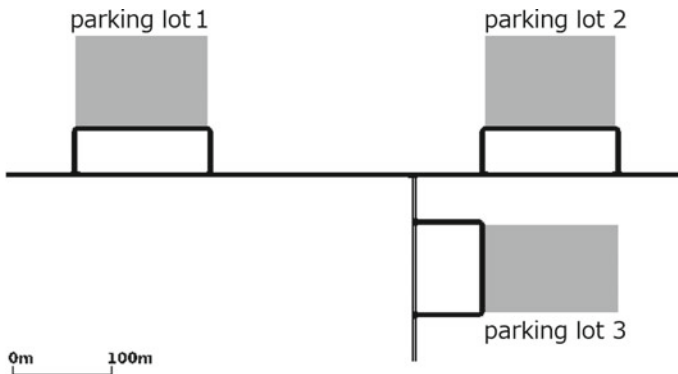


Fig. 8 Road network for simulation

**Table 1** Number of vehicles according to the recommendation of an ITS service

ITS service 1	83 units
ITS service 2	98 units
NOT use service	119 units
Total	300 units

We prepared two simple parking lot recommendation services, where two services monitor two different parking lots. They recommend one of the two parking lots monitored.

The first service monitors parking lots 1 and 3 and recommends either of the two, and the second service monitors parking lots 2 and 3 and recommends either of the two.

In this case study, simulations were carried out by simultaneously connecting the above two simple parking lot recommendation services to the Agent-based USE.

**Result of the Simulation Execution**

Simulation was performed using various data described in the previous section and the prototype of the Agent-based USE currently under development. Consequently, the simulation was executed without abnormal termination up to the set step, and it was confirmed that simulation using the implementation of ITS services is possible by using this Agent-based USE.

Furthermore, we observed the change in the degree of congestion of the parking lot during simulation, as shown in the graph of Fig. 9. In this graph, the horizontal

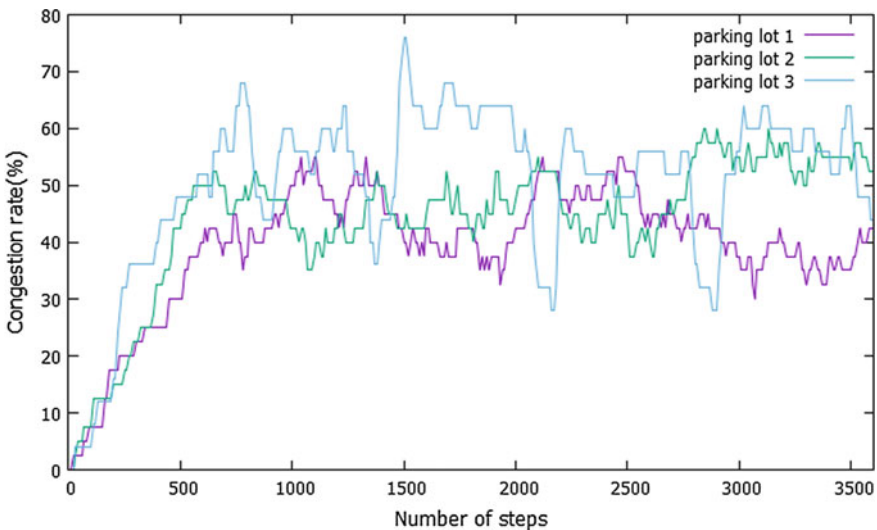


**Fig. 9** Result of parking congestion ratios

line represents the number of steps, and the vertical represents the congestion rate of the parking lot. The congestion rate of the parking lot is calculated by the following equation.

$$(\text{Congestion rate}) = \frac{(\text{Number of vehicles parked})}{(\text{Maximum number of storable cars})} \times 100$$

In this graph, when the simulation step reaches around 1,500, the congestion rate of parking lot 3 suddenly rises and exceeds 70%. This can be easily confirmed. This is because parking lot 3 was less congested than parking lots 1 and 2 in the immediately preceding step, and parking lot 3 was recommended at the same time by both the services.

From the aforementioned, it can be seen that this Agent-based USE is useful for manifesting the mutual interference situation influenced by multiple ITS services.

## 6.2 *Connecting with Mixed Reality Environment*

Secondly, we introduce a case study in which a mixed reality device and a simulator are connected and the simulation result is projected onto the mixed reality in real time. We used Microsoft HoloLens [5] as a mixed reality device, and a simulation monitor application on the device was connected to our Agent-based USE as an ITS service.

Prepared Simulation Monitor Application:

We prepared a 3D map [16] corresponding to the simulation area and the 3D model of a vehicle to project the simulation result in the mixed reality. Further, we prepared scripts that acquire information such as the location and orientation of each vehicle from the vehicle Agent and control the behavior of a 3D vehicle model. From the view point of the Agent-based USE, the monitor application is connected as an ITS service.

### Screen Shots of the Example Application

Figure 10 is a screen shot of the simulation result on the simulator at a certain moment and Fig. 11 of the mixed reality device at the same instant.

Using our Agent-based USE, we can easily connect with a mixed reality application similar to connecting with the ITS services, and we can easily build an environment that allows to observe a more stereoscopic result of the simulation.

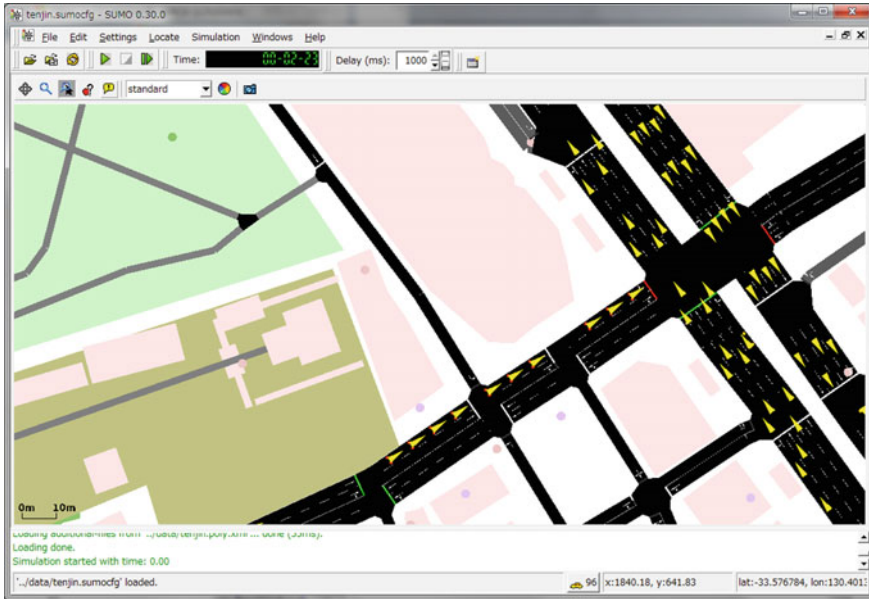


Fig. 10 Screen shot of the simulation result on the simulator



Fig. 11 Screen shot on the HoloLens at the same instant of Fig. 10



## 7 Related Work

Among the research on environmental development of traffic simulation, research [1, 7] on the construction of an integrated simulation environment connecting a traffic simulator and various simulators, research [14] on an interface-enabling connection with a traffic simulator, and similar other researches have been conducted.

In the literature [1], an integrated simulation environment that combines various simulators such as Vissim, MATLAB [11], and ns-3 [15] to create a simulation environment of vehicle-to-everything (V2X) communication technology has been proposed. In the literature [7], an integrated simulation environment traffic and network simulation environment (TraNS) for vehicle ad hoc networks (VANETs) has been proposed, in which the traffic simulator SUMO and the network simulator ns-2 [12] are interconnected by TraCI that is described below. These simulation environments are focused on the V2X communication technology system or VANETs system. However, our proposed simulation environment is focused on the overall ITS services. In the literature [6], a simulation environment that integrates different domain simulators such as a traffic, and an electronic simulator has been proposed. Additionally, the design of each domain simulator has been also proposed, and the design is constructed toward simulation integration. Our Agent-based USE also has the function to integrate simulators. However, we suppose that each integrated simulator is an existing one which has been used in each domain. The simulator is not necessarily constructed for simulator integration.

In the literature [14], an interface known as TraCI for interconnecting a traffic and a network simulator has been proposed. By using TraCI, it becomes possible to acquire congestion information on the road, via the traffic simulator, or to control the behavior of the moving object in real time during the simulation. The Agent-based USE proposed in this study uses TraCI to realize the connection between the simulator and the implementation of the ITS service.

In the literature [10], a platform that integrates a traffic simulator and multi-driving simulators has been proposed. In this platform, the data is exchanged in real time between the driving simulators and the traffic simulator, and simulation results are mutually reflected. Our simulation environment also exchanges information between the simulators and services in real time. However, our simulation environment is targeted for the services that can communicate using network protocols such as TCP/IP, and therefore it is possible to exchange information in real time between the services and simulators.

## 8 Conclusion

In this paper, we discussed a simulation environment called Agent-based USE that does not require modeling of the ITS services for simulation, and outlined the Agent-based USE and its architectural design. The Agent-based USE has the following features.

- The Agent-based USE does not require modeling of the ITS services; however, it provides a simulation environment connecting the implementation of the ITS services to the simulators.
- In the Agent-based USE, information is exchanged between the simulator and the ITS service when the simulation is executed, and it is possible to simulate the ITS service behavior and environmental changes mutually affecting each other in real time.
- The Agent-based USE provides an environment enabling connection between a simulator and multiple ITS services, and confirms how the effects of each ITS interfere with each other.
- The Agent-based USE provides an environment in which multiple or different types of simulators can be connected, and a simulation can be performed on objects moving to different simulator worlds.

Further, we developed a prototype of the Agent-based USE in Python language based on the proposed architectural design. By using the prototype implementation, it was possible to perform the simulation of an environment where multiple ITS services are affected by each other. Using case studies, the effectiveness of the proposed Agent-based USE was confirmed.

In future work, we plan to develop and implement the feature to connect even simulators with different time granularity. Further, we plan to build a meta simulation environment that can deploy a simulation environment with our Agent-based USE more easily. Continuing development of the Agent-based USE, conducting case studies, and getting feedback of the case studies, we will find a way of solving the uncertainty problems before or during the designing phase of the Agent-based USE and establish a process for strengthening the Agent-based USE.

**Acknowledgements** This work is partially supported by JSPS KAKENHI Grant Number JP15H05708.

## References

1. Choudhury, A., Maszczyk, T., Math, C.B., Li, H., Dauwels, J.: An integrated simulation environment for testing V2X protocols and applications. *Procedia Comput. Sci.* **80**, 2042–2052 (2016)
2. Fukuda, A., Hisazumi, K., Ishida, S., Mine, T., Nakanishi, T., Furusho, H., Tagashira, S., Arakawa, Y., Kaneko, K., Kong, W.: Towards sustainable information infrastructure platform for smart mobility-project overview. In: 2016 5th IIAI International Congress on Advanced Applied Informatics (IIAI-AAI), pp. 211–214 (2016)
3. KOZO KEIKAKU ENGINEERING Inc.: artisoc 4. <http://mas.kke.co.jp/modules/tinyd0/index.php?id=13> (2016)
4. Krajzewicz, D., Erdmann, J., Behrisch, M., Bieker, L.: Recent development and applications of SUMO-Simulation of Urban MObility. *Int. J. Adv. Syst. Meas.* **5**(3&4), 128–138 (2012)
5. Microsoft: Microsoft HoloLens. <https://www.microsoft.com/ja-jp/hololens> (2016)

6. Nakajima, Y., Hattori, H.: A simulator integration platform for city simulations. In: Kinny, D., Hsu, J.Y.J., Governatori, G., Ghose, A.K. (eds.) *Agents in Principle, Agents in Practice: 14th International Conference, PRIMA 2011, Wollongong, Australia, November 16–18, 2011. Proceedings*, pp. 484–495. Springer, Berlin (2011). [https://doi.org/10.1007/978-3-642-25044-6\\_39](https://doi.org/10.1007/978-3-642-25044-6_39)
7. Piórkowski, M., Raya, M., Lugo, A.L., Papadimitratos, P., Grossglauser, M., Hubaux, J.P.: TraNS: realistic joint traffic and network simulator for VANETs. *ACM SIGMOBILE Mob. Comput. Commun. Rev.* **12**(1), 31–33 (2008)
8. PTV Group: PTV Vissim 9. <http://vision-traffic.ptvgroup.com/en-uk/products/ptv-vissim/> (2016)
9. PTV Group: PTV Visum 16. <http://vision-traffic.ptvgroup.com/en-us/products/ptv-visum/> (2016)
10. Sun, J., Ma, Z., Li, T., Niu, D.: Development and application of an integrated traffic simulation and multi-driving simulators. *Simul. Model. Pract. Theory* **59**, 1–17 (2015). <http://www.sciencedirect.com/science/article/pii/S1569190X15001173>
11. The MathWorks: MATLAB. <https://www.mathworks.com/products/matlab.html>
12. The Network Simulator ns-2. <http://www.isi.edu/nsnam/ns/>
13. TSS-Transport Simulation Systems: Aimsun 8.1. <https://www.aimsun.com/aimsun/> (2015)
14. Wegener, A., Piórkowski, M., Raya, M., Hellbrück, H., Fischer, S., Hubaux, J.P.: TraCI: an interface for coupling road traffic and network simulators. In: *Proceedings of the 11th Communications and Networking Simulation Symposium*, pp. 155–163. ACM (2008)
15. Wehrle, K., Güneş, M., Gross, J.: The ns-3 network simulator. In: *Modeling and Tools for Network Simulation*, pp. 15–34 (2010)
16. ZENRIN CO., LTD.: Japanese Matsuri City. <https://assetstore.unity.com/packages/3d/environments/urban/japanese-matsuri-city-35619> (2015)

# Traffic State Estimation Using Traffic Measurement from the Opposing Lane—Error Analysis Based on Fluctuation of Input Data



Katsuya Kawai, Atsushi Takenouchi, Masahiko Ikawa and Masao Kuwahara

**Abstract** In this study, we propose a method of estimating traffic states using the traffic data observed from the opposing lane. As input data, our proposed method requires (1) probe vehicle trajectory on the target section and (2) vehicle data observed by vehicles running in the opposing lane. These input data identify the cumulative vehicle counts along the trajectories of the probe vehicles and observation vehicles in the time-space of interest. We applied the variational theory based on the kinematic wave to estimate vehicle trajectories over the entire time-space using the identified cumulative vehicle counts as the boundary condition. Furthermore, we used the Clark approximation to analytically examine the sensitivity of the estimate to the stochastic fluctuations of the input data and measurements. Validation using a hypothetical network confirms that the proposed method reasonably reproduces the traffic states and that the Clark approximation can accurately estimate the sensitivity.

**Keywords** Kinematic wave · Vehicle trajectory · Variational theory · Traffic flow · Data assimilation

---

K. Kawai · M. Ikawa

Advanced Technology R&D Center, Mitsubishi Electric Corporation, 8-1-1,  
Tsukaguchi-hommachi, Amagasaki 661-8661, Japan  
e-mail: [Kawai.Katsuya@dn.MitsubishiElectric.co.jp](mailto:Kawai.Katsuya@dn.MitsubishiElectric.co.jp)

M. Ikawa

e-mail: [Ikawa.Masahiko@aj.MitsubishiElectric.co.jp](mailto:Ikawa.Masahiko@aj.MitsubishiElectric.co.jp)

A. Takenouchi (✉) · M. Kuwahara

Graduate School of Information Sciences, Tohoku University, 6-6-06, Aoba, Aramaki, Aoba-ku,  
Sendai 980-857, Japan  
e-mail: [takenouchi@plan.civil.tohoku.ac.jp](mailto:takenouchi@plan.civil.tohoku.ac.jp)

M. Kuwahara

e-mail: [kuwahara@plan.civil.tohoku.ac.jp](mailto:kuwahara@plan.civil.tohoku.ac.jp)

© Springer Nature Singapore Pte Ltd. 2019

T. Mine et al. (eds.), *Intelligent Transport Systems for Everyone's Mobility*, [https://doi.org/10.1007/978-981-13-7434-0\\_14](https://doi.org/10.1007/978-981-13-7434-0_14)

# 1 Introduction

## 1.1 Background

Understanding the traffic flow is important for tackling various problems in road traffic, such as congestion, accidents, and environmental load. Owing to the popularization of high-precision positioning made possible by the global positioning system (GPS), deployment of communication infrastructure and road infrastructure, advances in the electronic control of vehicles, and widespread use of in-vehicle sensors, in recent years, the type and amount of information that can be collected as probe vehicle data has become enormous. Traffic monitoring is expected to be based on such information.

In this study, we assume that forward-moving passing vehicles can be counted by the measurement vehicle running on the opposite lane (we call this the *backward probe vehicle*) using advanced technologies such as video recording, millimeter wave radars, and vehicle-to-vehicle communications. We are still developing a measurement device to be equipped on the backward probe vehicle. However, we believe that such sensing technologies can be deployed in the near future, especially under the connected and automated vehicle environment.

We employed the variational theory (VT) to estimate the traffic states utilizing the count measurement from the opposite lane (backward probe) in addition to probe vehicle data in the forward direction (forward probe). The VT was employed because the vehicle counts by the backward probe vehicle are used directly for the boundary condition of the VT. In addition, we propose an analytical method that examines the sensitivity of the estimates in relation to the variabilities of the input data and measurements.

## 1.2 Previous Researches

Here, we review mainly the studies that estimate traffic states based on physical traffic flow dynamics utilizing various sensing data.

Mehran and Kuwahara [10, 9] examined a method that estimates vehicle trajectories in a simple section with signalized intersections based on the VT proposed by Daganzo [3, 4] using a traffic detector, probe vehicles, and signal-timing data. In addition, they extended the method to consider the inflow and outflow at intersections in the middle of the study section. Takayasu and Kuwahara [14] examined the sensitivity of the estimated cumulative counts in relation to the variability of the input data considering the correlation among the data. Kawasaki et al. [8] carried out a similar analysis using VT with traffic detector and probe vehicle data, considering the variability of the fundamental diagram. Several studies reported filtering techniques for data assimilation considering the stochasticity of traffic flow models and sensing data (Herrera and Bayen [5], California. Allströma et al. [1], Yuan et al.

[16], Nantes et al. [11], Jiang et al. [7], Xie et al. [15]). Patire et al. [12] examined the amount of Eulerian and Lagrangian data needed based on an ensemble filter using traffic detector and probe vehicle data. Canepa and Claudel [2] and Sun et al. [13] formulated optimization problems for data assimilation.

The aforementioned studies basically focused on a simple road section without any alternative routes. Hofleitner et al. [6] proposed a model that estimates traffic states in a two-dimensional network. However, the vehicle routing is not related directly to the estimated traffic states.

None of these previous studies employed measurements from a vehicle running in the opposite lane.

### 1.3 Purpose

To solve the above problem, we propose a method to estimate the traffic state using the traffic flow data from the opposite lane as measured by vehicle sensors such as cameras and millimeter wave radars, instead of using data measured by a fixed vehicle detector. By applying this method, we can estimate the traffic state using data measured by vehicles alone with the same accuracy as when using the fixed vehicle detector data. In this paper, we describe the results obtained using the VT model as an estimation model of the proposed method and the evaluation results using simulated data.

## 2 Proposed Method

### 2.1 Overview of the VT

In the VT, we assume a two-dimensional space (a time-space diagram). The time and position of road segments form the axes of the diagram. Then, we consider the traffic volume accumulated from the origin to each point on the diagram as the value at the point. As Fig. 1a shows, the line where the value is known on the space is called the boundary. Daganzo proves that  $NP$ , the value of a non-boundary point  $P$ , can be expressed as Eq. (1) using  $NB$ , the value of an arbitrary boundary point  $B$ , and  $\Delta BP_{max}$ , the maximum number of vehicles that overtake a virtually moving observer from  $B$  to  $P$ . In other words,  $NB$  is the minimum value of  $NP + \Delta BP_{max}$ , when the vehicle moves from point  $B$  on all boundaries accessible to point  $P$ . Note that to evaluate  $NB$ , we must access  $P$  from all the accessible directions and, then, find the minimum value.

$$NP = \inf B\{NB + \Delta BP_{max}\} \text{ for any Boundary point } B \quad (1)$$

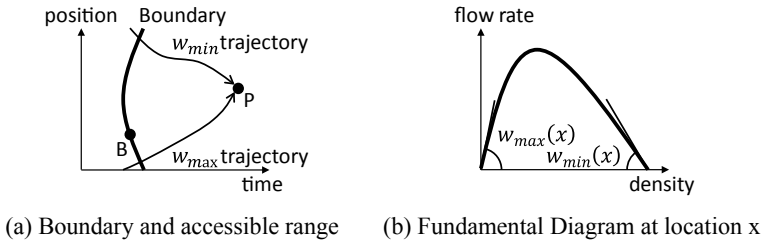
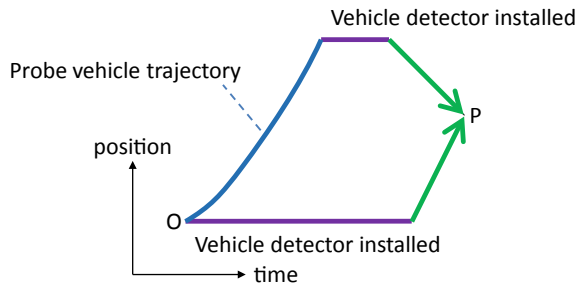


**Fig. 1** Movement range of a mobile observer

**Fig. 2** Boundaries determined by the vehicle detectors and probe vehicle



As Fig. 1 shows, if a fundamental diagram showing the relationship between traffic flow rate and density (FD) is given for all positions  $x$  of the target road section, the accessible range can be found using the maximum value  $w_{max}(x)$  and minimum value  $w_{min}(x)$  of the wave speed of the Fundamental Diagram (FD) at that position. In addition,  $\Delta B P_{max}$  can be calculated from FD using the relative capacity (Daganzo).

### 2.2 Example of Application of the VT in Previous Researches

Mehran, Kuwahara et al. showed an example of applying the VT using trajectories of probe vehicles and fixed vehicle detector data. The cumulative traffic volume can be calculated from the number of passing vehicles at the point where vehicle detectors are installed. In addition, the cumulative traffic volume on the probe vehicle trajectory is constant. The thick line in Fig. 2 shows the boundaries determined by the vehicle detector data and the probe vehicle trajectories. As Fig. 2 shows, if the target section has a homogeneous FD, Eq. (1) should be evaluated from all the boundaries of the thick line between the maximum and minimum values of the wave speed of the FD.

A method for conveniently evaluating Eq. (1) using these boundaries is described in this paragraph. We assume that the forward wave speed is defined as  $v$  and the backward wave speed as  $-w$  about the linear fundamental diagram of the target section area, as Fig. 3 shows (For simplicity, it is assumed that all sections have the same FD). At first, the time axis is divided into uniform minute sections. Next, as

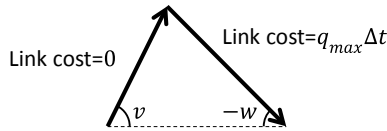


**Fig. 3** Liner fundamental diagram

**Fig. 4** Boundaries and network for path search

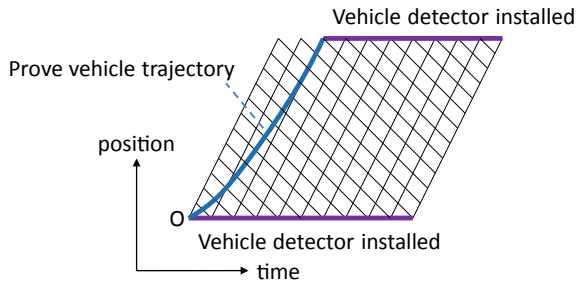


Fig. 4 shows, the lines with a slope of speed  $v$  and  $-w$  for each discretized time are noted, and the network that has these lines as directed links and these intersections as nodes is configured. The forward links (they have the slope of forward wave speed) are set to zero as the link cost, and the backward links (they have the slope of backward wave speed) are set to  $q_{max} \Delta t$ . Then, the cumulative number of arbitrary nodes proved to be the cost of the shortest path from origin O to the node.

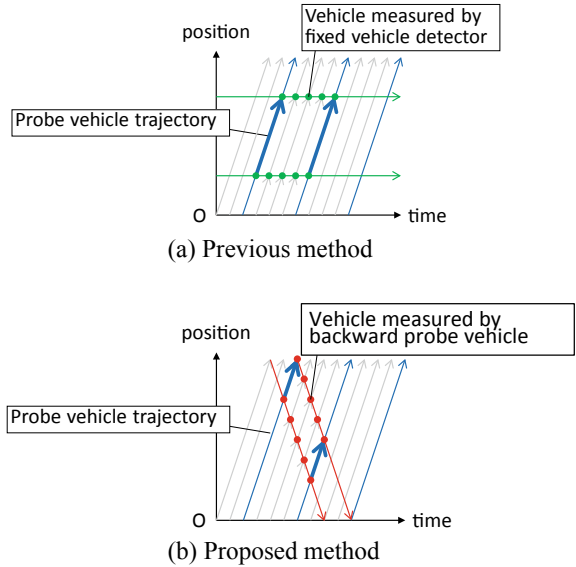
In this paper, the path with the minimum total cost from one point to another is called the shortest path between the points, and the total cost of the shortest path is called the minimum cost between the points.

### 2.3 Application of the Boundary of the Proposed Method

In contrast to previous studies that employed fixed vehicle detector data, the proposed method uses the measurement data measured by backward probe vehicles. Figure 5 shows schematic diagrams of the boundaries. In Fig. 5b, blue solid lines are probe vehicle trajectories, and red dots are the space-time points of the vehicles measured by the backward probe vehicles. If the boundaries can be defined at sufficient intervals, it is possible to estimate the traveling trajectories of general vehicles between the probe vehicles by applying the VT as it is.



**Fig. 5** Schematic diagrams of the boundaries



### 3 Analysis of Estimation Errors in the Proposed Method

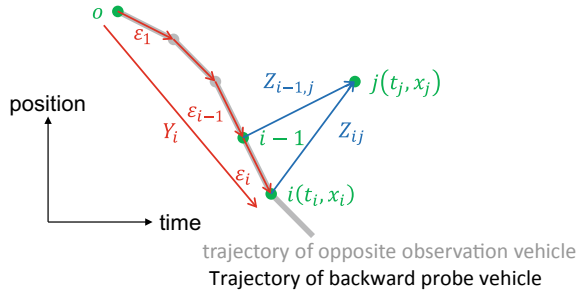
#### 3.1 Overview of the Analysis

To apply the proposed method to the actual traffic flow, it is necessary to consider the influence of the variation of the input condition such as driver’s driving behavior and terminal traffic volume. In this section, we use the boundary condition obtained from one trip of the backward probe vehicle to analyze the effect of probability variation of the input condition on the result of estimation.

Figure 6 shows the analysis target on the search network. We assume the starting point of the boundary as origin node  $o$  and analyze the cumulative traffic volume from  $o$  to any node (target node  $j$ ). Since the cumulative traffic volume of target node  $j$  is calculated as the minimum cost from origin node  $o$  to  $j$ , we develop the probability for the minimum path from  $o$  to  $j$  and calculate the expectation value.

Among the candidate paths that can reach target node  $j$ , the shortest path through a node on a certain boundary (boundary node  $i$ ) can be determined to one. Thus, we calculate the minimum cost for each passing boundary node. Here, we define a set of boundary nodes that the path to target node  $j$  may pass through as  $\Omega_j : \{1, 2, 3, \dots, n_j\}$ . We classify the path from origin node  $o$  through boundary node  $i$  to target node  $j$  into a boundary partial path (from  $o$  to  $i$ , the red line in Fig. 6) and the internal partial path (from  $i$  to  $j$ , the blue line in Fig. 6), and calculate each minimum cost. Furthermore, we analyze the probability of selecting the whole path together with these partial paths as the shortest path.

Fig. 6 Target of analysis



### 3.2 Minimum Cost of the Boundary Partial Path

Fluctuation of the terminal traffic volume of the target interval by the demand fluctuations and the detection errors of the vehicle sensor on the backward probe vehicle is considered as a fluctuation on the boundary. Therefore, this fluctuation can be treated as a variation of the minimum cost  $Y_i$  in the boundary partial path.

Here, since the boundary that the backward probe vehicle generates monotonically increases on the time axis (monotonically decreases on the spatial axis because it proceeds in the opposite direction), the probability distribution of  $Y_i$  is not independent but correlated with each other. That is,  $t_i > t_k$ ,  $x_i \leq x_k$  and  $Y_i \geq Y_k$ . In addition, demand fluctuations and detection errors are cumulative and affect the next fluctuations. Then, we consider  $\varepsilon_i$  (on  $i \in \Omega_i$ ), which is the traffic volume including the fluctuation components from node  $i-1$  to node  $i$ . The probability distribution of  $\varepsilon_i$  is assumed an independent identical distribution (iid) that has the reproductive property. Then, the expectation and dispersion of this probability distribution are defined as  $\mu_{\varepsilon_i}$  and  $\sigma_{\varepsilon_i}^2$ . The Poisson distribution, normal distribution, etc., are described as the probability distributions with a reproduction property, and the following is a description of the normal distribution, for example.

$$\varepsilon_i \sim iid N(\mu_{\varepsilon_i}, \sigma_{\varepsilon_i}^2) \tag{2}$$

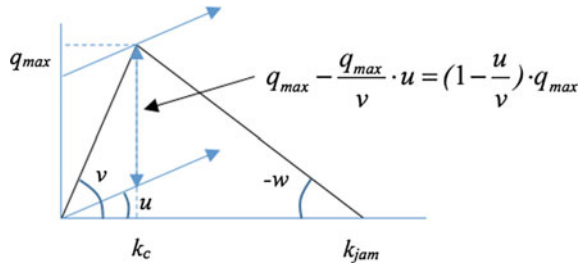
Then,  $Y_i$  can be expressed as a sum of  $\varepsilon_i$ , and it follows the normal distribution that has an expectation  $\mu_{Y_i}$  and a dispersion  $\sigma_{Y_i}^2$ .

$$Y_i = \sum_{k=1}^i \varepsilon_k \sim iid \cdot N(\mu_{Y_i}, \sigma_{Y_i}^2) \tag{3}$$

$$\mu_{Y_i} = \sum \mu_{\varepsilon_i} \tag{4}$$

$$\sigma_{Y_i}^2 = \sum \sigma_{\varepsilon_i}^2 \tag{5}$$

**Fig. 7** Linear fundamental diagram



### 3.3 Minimum Cost of the Internal Partial Path

Fluctuation of the vehicle trajectory due to the variation of the driving behavior is considered as a fluctuation within the network. Therefore, this fluctuation can be treated as a variation of the minimum cost  $Z_{ij}$  in the internal partial path. In general, the changes in cumulative traffic volume from boundary node  $i$  to target node  $j$  can be written as follows.

$$Z_{ij} = \int_{t_i}^{t_j} \sup_{k(x,t)} (q(k(x,t), x) - k(x,t)u(x,t))dt \tag{6}$$

Here, as shown below, we assume the Fundamental Diagram (FD) in which the forward and backward waves are linear. Then, the maximum traffic flow rate and the critical traffic density in the path via boundary node  $i$  are defined as  $q_{max}^{ij}$  and  $k_c^{ij}$ , respectively. Furthermore,  $q_{max}^{ij}$  and  $k_c^{ij}$  are assumed to follow normal distributions and to be iid with the maximum traffic flow rate and the critical traffic density in the path via other boundary nodes. Then, the expectation and dispersion of  $q_{max}^{ij}$  are defined as  $\mu_q$  and  $\sigma_q^2$ , respectively, and those of  $k_c^{ij}$  are defined as  $\mu_k$  and  $\sigma_k^2$ , respectively (Fig. 7).

$$q_{max}^{ij} \sim iid N(\mu_q, \sigma_q^2) \tag{7}$$

$$k_c^{ij} \sim iid N(\mu_k, \sigma_k^2) \tag{8}$$

Then,  $Z_{ij}$  follows the normal distribution that has an expectation  $\mu_{Z_{ij}}$  and a dispersion  $\sigma_{Z_{ij}}^2$ .

$$\begin{aligned} Z_{ij} &= \int_{t_i}^{t_j} q_{max}^{ij} \left(1 - \frac{u}{v}\right) dt = q_{max}^{ij} \left(1 - \frac{u}{v}\right) (t_j - t_i) \\ &= q_{max}^{ij} (t_j - t_i) - k_c^{ij} (x_j - x_i) \sim iid N(\mu_{Z_{ij}}, \sigma_{Z_{ij}}^2) \end{aligned} \tag{9}$$

### 3.4 Minimum Distribution of Path Costs

The cumulative traffic volume  $U_{ij}$  of the path from origin node  $o$  through boundary node  $i$  to target node  $j$  can be expressed as shown in the following equation.

$$U_{ij} = Y_i + Z_{ij} \quad (10)$$

Therefore, the distribution of the minimum values of all path costs can be written as follows.

$$\begin{aligned} P(\min \text{ Path Cost} > n) &= P(U_0 > n, U_1 > n, \dots, U_i > n) \\ &= P(Y_0 + Z_{0j} > n, Y_1 + Z_{1j} > n, \dots, Y_i + Z_{ij} > n) \end{aligned} \quad (11)$$

## 4 Approximate Calculation of Estimation Errors in the Proposed Method

### 4.1 Overview of the Approximate

Since the minimum distribution has a probability fluctuation  $Y_0, Y_1, \dots, Y_i$ , which are correlated with each other, it is difficult to calculate analytically. Therefore, we use the Clark approximation method to calculate the expectation and standard deviation of cumulative traffic volume.

The Clark approximation method allows approximating the maximum value of the probability variable according to two multivariate normal distributions as a probability variable according to a new multivariate normal distribution. In this method, we calculate the covariance and the correlation coefficient of two probability variables from the expectation and variance of each probability variable and, then, recursively calculate the correlation coefficient and maximum value of multiple probability variables. Here, we write the expectation and variance of the probability variable  $X$  as  $E(X)$  and  $V(X)$ , respectively, and the covariance and correlation coefficient of the two probability variables  $X$  and  $Y$  as  $Cov(X, Y)$  and  $\rho(X, Y)$ , respectively. In addition, we omit  $j$  of the affixed character to make the expression concise.

### 4.2 Confirmation to Multivariate Normal Distribution Check

We show that the cumulative traffic volume  $U_i$  is a multivariate normal distribution.

Since  $\varepsilon_i$  and  $Z_i$  are normally distributed according to formulas (2) and (9), the iid standard normal distribution  $x_i$  and standard multivariate normal distribution  $X$  can be defined as shown below.

$$x_i = \frac{\varepsilon_i - \mu_{\varepsilon_i}}{\sigma_{\varepsilon_i}} = \frac{Z_i - \mu_{Z_i}}{\sigma_{Z_i}} \sim iid N(0, 1) \tag{12}$$

$$X = (x_{1j}, x_{2j}, \dots, x_{ij})^t \tag{13}$$

Therefore,  $U_i$  can be represented by the linear transformation of the standard multivariate normal distribution  $X$ . It is a multivariate normal distribution, and the Clark approximation can be applied.

$$U_i = AX + C \tag{14}$$

where

$$A = \begin{pmatrix} \sigma_{\varepsilon_1} + \sigma_{Z_1} & 0 & \dots & 0 \\ \sigma_{\varepsilon_1} & \sigma_{\varepsilon_2} + \sigma_{Z_2} & \dots & 0 \\ \vdots & \vdots & \ddots & \vdots \\ \sigma_{\varepsilon_1} & \sigma_{\varepsilon_2} & \dots & \sigma_{\varepsilon_i} + \sigma_{Z_i} \end{pmatrix} \tag{15}$$

$$X = \begin{pmatrix} x_{1j} \\ x_{2j} \\ \vdots \\ x_{ij} \end{pmatrix} \tag{16}$$

$$C = \begin{pmatrix} \mu_{\varepsilon_1} + \mu_{Z_{1j}} \\ \mu_{\varepsilon_1} + \mu_{\varepsilon_2} + \mu_{Z_{2j}} \\ \vdots \\ \sum_{k=1}^i \mu_{\varepsilon_{1k}} + \mu_{Z_{ij}} \end{pmatrix} \tag{17}$$

### 4.3 Calculation of Correlation Coefficients

This subsection describes how to determine the correlation coefficient of the two probability variables that are known to be expected and distributed.

If  $0 < \varepsilon_{ik}$ , the covariance  $Cov(U_i, U_{i-k})$  of the probability variables  $U_i$  and  $U_{i-k}$  can be described as follows.

$$\begin{aligned} E(U_i, U_{i-k}) &= E(Y_i + Z_i)(Y_{i-k} + Z_{i-k}) \\ &= E(Y_{i-k} + \varepsilon_{ik} + Z_i)(Y_{i-k} + Z_{i-k}) \\ &= E(Y_{i-k}Y_{i-k}) + E(Y_{i-k})E(Z_{i-k}) + E(\varepsilon_{ik})E(U_{i-k}) + E(Z_i)E(U_{i-k}) \\ &= V(Y_{i-k}) + E(Y_{i-k})E(Y_{i-k}) + E(Y_{i-k})E(Z_{i-k}) + E(\varepsilon_{ik})E(U_{i-k}) + E(Z_i)E(U_{i-k}) \end{aligned}$$

$$\begin{aligned}
&= V(Y_{i-k}) + E(Y_{i-k})E(U_{i-k}) + E(\varepsilon_{ik})E(U_{i-k}) + E(Z_i)E(U_{i-k}) \\
&= V(Y_{i-k}) + E(U_i)E(U_{i-k})
\end{aligned} \tag{18}$$

$$Cov(U_i, U_{i-k}) = E(U_i, U_{i-k}) - E(U_i)E(U_{i-k}) = V(Y_{i-k}) \tag{19}$$

Therefore, if  $Y_{i-k} < Y_i$ , the correlation coefficient  $\rho(U_i, U_{i-k})$  of the probability variable  $U_i$  and  $U_{i-k}$  can be calculated as follows.

$$\begin{aligned}
\rho(U_i, U_{i-k}) &= \frac{Cov(U_i, U_{i-k})}{\sqrt{V(U_i)}\sqrt{V(U_{i-k})}} \\
&= \frac{V(Y_{i-k})}{\sqrt{V(Y_i + Z_i)}\sqrt{V(Y_{i-k} + Z_{i-k})}} \\
&= \frac{V(Y_{i-k})}{\sqrt{V(Y_i + Z_i)}\sqrt{V(Y_{i-k} + Z_{i-k})}}
\end{aligned} \tag{20}$$

#### 4.4 Maximum Value Recursion

Clark showed that when considering multivariate normal distributions  $U_1$  and  $U_2$ , the first moment  $\alpha_{12}$  and the second moment  $\beta_{12}$  of the probability variable  $Max(U_2, U_1)$  are as shown in formulas (21) and (22).

$$\alpha_{12} = E(U_1)\Phi(\gamma) + E(U_2)\Phi(-\gamma) + c\phi(\gamma) \tag{21}$$

$$\begin{aligned}
\beta_{12} &= (E(U_1)^2 + V(U_1))\Phi(\gamma) + (E(U_2)^2 + V(U_2))\Phi(-\gamma) \\
&+ (E(U_1) + E(U_2))c\phi(\gamma)
\end{aligned} \tag{22}$$

where

$$\phi(\omega) = (2\pi)^{-1/2} \exp\left(\frac{-\omega^2}{2}\right) \tag{23}$$

$$\Phi(\omega) = \int_{-\infty}^{\omega} \phi(t)dt \tag{24}$$

$$c^2 = V(U_1) + V(U_2) - 2\sqrt{V(U_1)V(U_2)}\rho(U_1, U_2) \tag{25}$$

$$\gamma = \frac{E(U_1) - E(U_2)}{c} \tag{26}$$

Then,  $Max(U_1, U_2)$  can be approximated by the following normal distribution.

$$Max(U_2, U_1) \sim N(\alpha_{12}, \beta_{12} - \alpha_{12}^2) \tag{27}$$

In addition, the correlation coefficient  $\rho(U_3, \text{Max}(U_2, U_1))$  is obtained as follows.

$$\rho(U_3, \text{Max}(U_2, U_1)) = \frac{\sqrt{V(U_1)}\rho(U_1, U_3)\Phi(\gamma) + \sqrt{V(U_2)}\rho(U_2, U_3)\Phi(-\gamma)}{(\beta_{12} - \alpha_{12}^2)^{1/2}} \tag{28}$$

Using the above definition and by applying formulas (23)–(26) to  $U_3$  and  $\text{Max}(U_2, U_1)$ , the first moment  $\alpha_{123}$  and second-order moment  $\beta_{123}$  of  $\text{Max}(U_3, \text{Max}(U_2, U_1)) = \text{Max}(U_3, U_2, U_1)$  are obtained in the same way as shown in formula (21) and (22).

The expectation and variance of  $\text{Max}(U_3, U_2, U_1)$  are obtained as follows.

$$\text{Max}(U_3, U_2, U_1) = \text{Max}(U_3, \max(U_2, U_1)) \sim N(\alpha_{123}, \beta_{123} - \alpha_{123}^2) \tag{29}$$

By repeating this treatment for  $U_i$ , the expectation of  $\text{Max}(U_1, U_2, \dots, U_i)$  can be calculated.

## 5 Validation on a Hypothetical Network

### 5.1 Validation of Traffic State Estimates

#### 5.1.1 Generating True Traffic States

To validate the proposed method, the true traffic states are first constructed on a simple network shown in Fig. 8. The total length of the straight pipe section is 5.0 km; however, as presented in Table 1, the first 3.5 km and the last 1.5 km sections have different fundamental diagrams. Although both sections have the same forward and backward speeds of 60 km/h and  $-15$  km/h, respectively, they have different capacities of 1,500 veh/h and 750 veh/h, respectively. As Table 2 indicates, the demand from origin O to destination D is generated time-dependent. The first and last 20-min periods have a demand of 1,200 veh/h, which exceeds the capacity of 750 veh/h on the 1.5-km section (ND). Therefore, a queue is generated from node N during the periods.



Fig. 8 Simple network

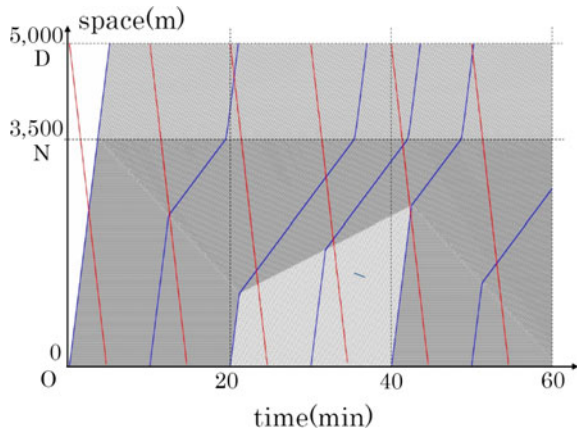
**Table 1** Simulation conditions

Item			Value
Simulation time span			60 min
FD	q <sub>max</sub> : Saturation flow rate	O → N	1,500 veh/h
		N → D	750 veh/h
	Forward wave speed		60 km/h
	Backward wave speed		15 km/h

**Table 2** Traffic demand

Origin → Destination	Time (min)		
	0–20	20–40	40–60
O → D	1,200 veh/h	500 veh/h	1,200 veh/h

**Fig. 9** True traffic state



To construct the true traffic state, we employ a simple simulation with a 1 s scanning interval in which each vehicle moves forward based on the speed-spacing relationships defined by the assumed fundamental diagrams. Figure 9 shows the constructed true traffic state, where a queue grows during the first and last 20-min periods from node N because of the demand exceeds the capacity of the 1.5-km section; however, the queue decreases for the next 20 min because the demand decreases. The forward and backward probe vehicles are generated every 10 min, as shown by the blue and red lines, respectively, in Fig. 9. The backward probe vehicles are assumed to move at a free flow speed of 60 km/h.



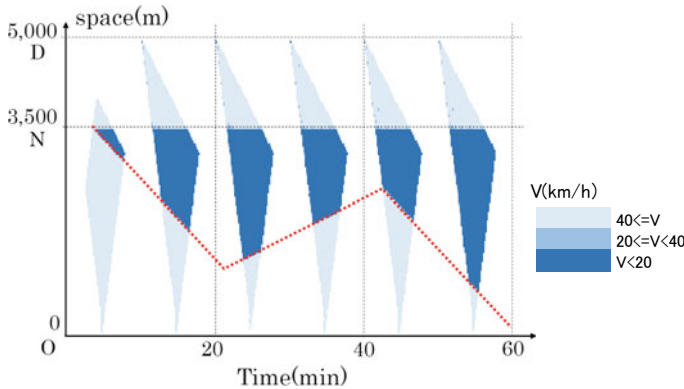


Fig. 10 Estimated traffic states

### 5.1.2 Estimating Traffic States

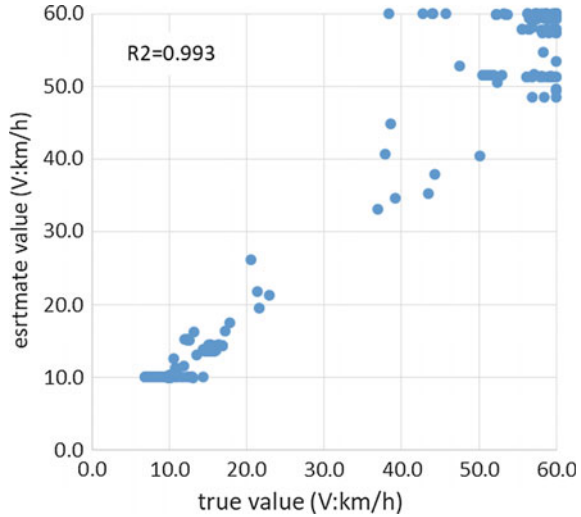
Using the proposed method, the traffic state is estimated from the forward and backward probe data. For the VT, a triangular network is constructed. In this network, a time step  $dt$  is equal to 1 s. Figure 10 shows the estimated traffic states, and Fig. 11 shows the relationship between the true and estimated velocities. The result estimated using only backward probe vehicle data is almost equivalent that estimated using forward and backward probe vehicle data. Both of the results show good agreement with the true states, especially the locations of the queue tail described by the red dots are well reproduced. However, the regions in which traffic state can be estimated are limited. Since the simple simulation and the proposed method employ the same fundamental diagram and no measurement errors are included in the estimation, the errors in the estimates arise from the time and space discretization in the VT. An important conclusion is the traffic state can be reasonably estimated only from the backward probe data. In previous studies, both forward probe data and traffic detector data are needed, and the traffic state could not be reproduced in the absence of any one type of data.

## 5.2 Validation of Sensitivity of the Estimates

In this section, we examine the sensitivity of the estimates attributed to the variabilities in the input data. In particular, we examine the sensitivity resulting from the measurement noises of the backward probe vehicle measurements since the traffic count measurements may contain errors due to sensing technology and occlusions caused by obstacles on the median and adjacent moving vehicles.

The true sensitivity is created that the boundary cumulative counts measured by the backward probe vehicles are stochastically fluctuated. Specifically, in Eq. (3),  $\mu_{Y_i}$

**Fig. 11** Relationship between true and estimated velocities



is assumed as the cumulative counts set in the previous section, and  $\sigma_{Y_i}^2$  is assumed the same as  $\mu_{Y_i}$ . By focusing on the backward probe vehicle measurements,  $\mu_{Z_{ij}}$  and  $\sigma_{Z_{ij}}^2$  are assumed zero, implying that the variability due to driving behaviors is neglected in this examination. By following the stochastic distribution, the simple simulation based on the velocity-spacing relationship mentioned earlier is repeated 30 times to evaluate the true standard deviations of the cumulative counts.

Figure 12 compares the estimated standard deviations for the Clark approximation with the true standard deviation. Since the measurement noises on the cumulative boundary are accumulated, the standard deviation increases with the cumulative counts, and this natural tendency is observed both in the true and estimated standard deviations. Furthermore, the standard deviations estimated by the Clark approximation at the same location and time agree well with the simulated values with the correlation coefficient of 0.963.

## 6 Conclusion

This study proposes a method that estimates traffic states using measurements from a vehicle running on the opposite lane (*backward probe measurements*) in addition to conventional probe vehicle data (*forward probe measurements*) and examines the sensitivity of the estimates in relation to the variabilities of the input data and measurements. Assuming that the backward probe vehicle can measure the counts of passing vehicles running forward, we employ the VT to estimate the traffic states by utilizing count measurements. This method seems advantageous in that it allows quick responses to unexpected incidences such as accidents and vehicle malfunctions.

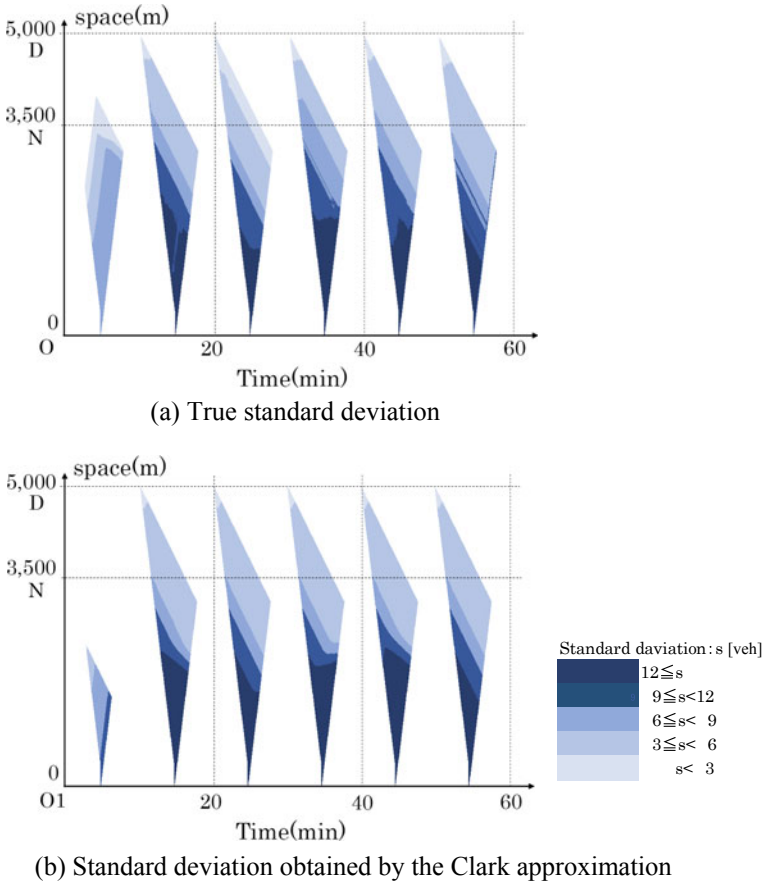


**Fig. 12** Standard deviation due to backward probe measurement noises

This is because the backward probe vehicle is expected to observe such incidents without much delay. In addition, we use the Clark approximation to analytically examine the sensitivity of the estimates in relation to variabilities of the input data and measurements.

The validation confirms that the proposed method can estimate traffic states reasonably without using traffic detector data. Furthermore, the Clark approximation provides the accurate standard deviations of the estimates when the input and measurement data have stochastic noises.

**Acknowledgements** This research was supported by “Study on probe data utilization method in traffic control system,” research commissioned by Mitsubishi Electric Co., Ltd.

## References

- Allströma, A., Bayen, A.M., Fransson, M., Gundlegårda, D., Patirec, A.D., Rydergrena, C., Sandina, M.: Calibration framework based on bluetooth sensors for traffic state estimation using a velocity based cell transmission model. *Transp. Res. Procedia* **3**, 972–981
- Canepa, E.S., Claudel, C.G.: Networked traffic state estimation involving mixed fixed-mobile sensor data using Hamilton-Jacobi equations. *Transp. Res. Part B* **104**, 686–709 (2017)
- Daganzo, C.F.: A variational formulation of kinematic waves: basic theory and complex boundary conditions. *Transp. Res. Part B* **39**, 187–196 (2005)
- Daganzo, C.F.: A variational formulation of kinematic waves: solution methods. *Transp. Res. Part B* **39**, 934–950 (2005)
- Herrera, J.C., Bayen, A.M.: Incorporation of Lagrangian measurements in freeway traffic state estimation. *Transp. Res. Part B* **44**, 460–481 (2010)
- Hofleitner, A., Herring, R., Bayen, A.: Arterial travel time forecast with streaming data: a hybrid approach of flow modeling and machine learning. *Transp. Res. Part B* **46**, 1097–1122 (2012)
- Jiang, Z., Chen, M., Ouyang, Y.: Traffic state and emission estimation for urban expressways based on heterogeneous data. *Transp. Res. Part D* **53**, 440–453 (2017)
- Kawasaki, Y., Hara, Y., Kuwahara, M.: Real-time monitoring of dynamic traffic states by state space model. *Transp. Res. Procedia* **21**, 42–55 (2017)
- Mehran, B., Kuwahara, M.: Fusion of probe and fixed sensor data for short-term traffic prediction in urban signalized arterials. *Int. J. Urban Sci.* **17**(2), 163–183 (2013)
- Mehran, B., Kuwahara, M., Naznin, F.: Implementing kinematic wave theory to reconstruct vehicle trajectories from fixed and probe sensor data. *Transp. Res. Part C* **20**, 144–163 (2012)
- Nantes, A., Ngoduy, D., Bhaskar, A., Miska, M., Chung, E.: Real-time traffic state estimation in urban corridors from heterogeneous data. *Transp. Res. Part C* **66**, 99–118 (2016)
- Patire, A.D., Wright, M., Prodhomme, B., Bayen, A.M.: How much GPS data do we need? *Transp. Res. Part C* **58**, 325–342 (2015)
- Sun, Z., Jin, W., Ritchie, S.G.: Simultaneous estimation of states and parameters in Newell's simplified kinematic wave model with Eulerian and Lagrangian traffic data. *Transp. Res. Part B* **104**, 106–122 (2017)
- Takayasu, A., Kuwahara, M.: Traffic State Estimation considering stochasticity of input data based on variational theory. In: *The 21st International Conference of Hong Kong Society for Transportation Studies* (2016)
- Xie, X., van Lint, H., Verbraeck, A.: A generic data assimilation framework for vehicle trajectory reconstruction on signalized urban arterials using particle filters. *Transp. Res. Part C* **92**, 364–391 (2018)
- Yuan, Y., Duret, A., van Lint, H.: Mesoscopic traffic state estimation based on a variational formulation of the LWR model in Lagrangian-space coordinates and Kalman filter. In: *18th Euro Working Group on Transportation, EWGT 2015*, 14–16 July 2015, Delft, The Netherlands, *Transportation Research Procedia*, vol. 10, pp. 82–92 (2015)

# Development of a Statistical Model to Predict Traffic Congestion in Winter Seasons in Nagaoka, Japan Using Publicly Available Data



Hiroaki Ikeuchi, Kiichiro Hatoyama, Ryota Kusakabe and Ikumi Kariya

**Abstract** Since the weather condition can be a cause of serious traffic congestion, it is necessary to establish a methodology to forecast future traffic congestions caused by rainfall and snowfall. However, there are few studies with simple methods that are applicable for practitioners such as road administrators. Therefore, in this paper we challenged to construct a statistical model to predict locations and levels of traffic congestion in a city, using only existing data that is open to the public. We collected hourly precipitation amount, hourly snowfall amount and cumulative snowfall amount from the Japan Meteorological Agency as weather observation data and images of Google Maps as traffic congestion data. As a result of the correlation analysis, we found that the hourly precipitation amount and the hourly snowfall amount did not correlate much with the relative congestion level whereas the correlation between the cumulative snowfall amount and 18-hour snowfall amount was found to be high. Consequently, a logistic regression analysis was conducted to explain the relative congestion level at various points on the roads using the 18-h snowfall amount and the cumulative snowfall amount. As a result, the model demonstrated good performance to reproduce the occurrence of increase in traffic congestion levels with >80% hit rates. In future, we would like to improve the present model to forecast potential road congestion based on weather forecast by using highly accurate weather information and longer term data.

---

H. Ikeuchi

Institute of Industrial Science, The University of Tokyo, Tokyo 153-8505, Japan

e-mail: [ikeuchi@rainbow.iis.u-tokyo.ac.jp](mailto:ikeuchi@rainbow.iis.u-tokyo.ac.jp)

R. Kusakabe · I. Kariya

Department of Civil Engineering, The University of Tokyo, Tokyo 113-0032, Japan

e-mail: [ryota-k@eri.u-tokyo.ac.jp](mailto:ryota-k@eri.u-tokyo.ac.jp)

I. Kariya

e-mail: [kariya@concrete.t.u-tokyo.ac.jp](mailto:kariya@concrete.t.u-tokyo.ac.jp)

K. Hatoyama (✉)

Department of Civil and Environmental Engineering, Nagaoka University of Technology,

Niigata 940-2188, Japan

e-mail: [kii@vos.nagaokaut.ac.jp](mailto:kii@vos.nagaokaut.ac.jp)

© Springer Nature Singapore Pte Ltd. 2019

T. Mine et al. (eds.), *Intelligent Transport Systems for Everyone's Mobility*, [https://doi.org/10.1007/978-981-13-7434-0\\_15](https://doi.org/10.1007/978-981-13-7434-0_15)

## 1 Introduction

### 1.1 Needs for Traffic Congestion Prediction

In Japan, the areas along the Sea of Japan often suffer from heavy snowfall every year due to the mountain range and the moist air brought by the northwest seasonal wind. In these areas, the weather conditions can be a cause of serious traffic congestion particularly in large cities, even those with well-developed road networks. The major causes include frozen road surfaces, road width reductions due to snow removal works, poor visibility due to bad weather, etc. In February 2018, in Fukui and Ishikawa prefectures, more than thousand drivers were stuck overnight in their vehicles on a national highway due to a rare and heavy snowfall [1]. To avoid such incidents, it is necessary for these cities to develop a strategy to predict traffic congestion caused by rain and snow. Thus, we attempted to establish a method that analyzes traffic congestion directly, and consider the applicability for practitioners such as road and traffic administrators.

### 1.2 Objective of this Study

Based on the above context, the objective of this study is to develop a simple method to predict locations and levels of traffic congestion in a city, using only publicly available data. Specifically, in this research, we attempted to build a statistical model to explain the relationship between weather performance data and traffic congestion data as a preparation process for future traffic congestion predictions.

## 2 Literature Review

### 2.1 Transportation Engineering Studies

In the field of traffic engineering, there are some related studies that analyzed the impact of weather conditions on saturation flow rates, vehicular speeds, traffic volumes, and traffic capacities.

Several papers have investigated vehicular speed under various weather conditions. Zhao et al. observed freeway speed in New York in snowy and icy conditions and developed a regression model [2]. Kyte et al. revealed that free-flow speed of traffic on American rural interstate freeways is likely to be affected by pavement conditions, visibility, and wind speeds under poor weather conditions [3]. In Japan, Terauchi et al. conducted a survey in Fukui prefecture to calculate reduced traffic speed during snowfall [4]. However, these studies did not deal with traffic congestion directly.

Asamer and Van Zuylen measured saturation flow rates through a video survey at several signalized intersections in Vienna, and found that snow may reduce the saturation flow [5]. Ivanović and Jović showed the impact of rainfall intensity on saturation flow rates in Belgrade [6]. Sun et al. focused on saturation flow rates of left-turn lanes in Shanghai following the same survey method as Ivanović and Jović and found less significant differences under the condition of light rain [7]. However, to conduct these studies, it is necessary to perform time-consuming video analyses.

Akin et al. measured vehicular speed and traffic capacity in Istanbul using detectors and showed that rainfall reduced the average vehicular speed and traffic capacity [8]. Jia et al. also studied the effect of rainfall on traffic flow in Beijing to carry out microscopic simulation [9]. Agarwal et al. conducted a survey following the same method as Jia et al. in the northern metropolitan areas of America and found that speed reduction due to heavy snow was significantly lower than capacity reduction [10]. These studies indicate that heavy snow, unlike rain, may not reduce vehicular speed, but may reduce traffic volume itself. However, the observed situations in these studies are different from the situation of areas receiving heavy snowfall areas in Japan, where snow might not affect traffic volume. Ibrahim et al. confirmed that under similar traffic volume conditions, speed and traffic capacity reduce during heavy snowfall in Ontario [11] and the same phenomenon was observed by Weng et al. through a case study in Beijing [12]. Most of these studies used data from detectors; however, it is difficult to install a number of detectors outside metropolitan areas.

Some studies suggested that traffic congestion may occur because of precipitation and accumulated snowfall. Chung collected traffic flow data from a vehicle detection system in Korean freeways and found that rainfall and snowfall increased traffic congestion, whereas extremely heavy snowfall sometimes reduced traffic demand itself [13]. Lee et al. also attempted to predict traffic congestion using a linear regression model with weather forecasting factors [14]. Thus, it is safe to say that the number of studies targeting traffic congestion from a meteorological point of view is limited.

## ***2.2 Recent Technologies***

Recently, several studies demonstrated the use of advanced technology to predict traffic conditions using meteorological data. Qiu et al. used a neural network, principal component analysis, and the precipitation-correction fusion model to predict traffic volume under rainy conditions [15]. Tselentis et al. attempted to compare statistical and Bayesian combination models with classical ones to predict short-term traffic [16]. Furthermore, there are some studies which introduced deep learning methodology for short-term traffic flow prediction [17] or modeling with social media data [18]. However, these studies used complicated models to analyze the relationship between precipitation, snowfall amount, and traffic congestion levels.

## **3 Data**

### ***3.1 Target Area***

For the target area in this study, we selected the roads situated on the west side of Station Nagaoka of Japan Railways. A major reason for this choice is that it frequently suffers from severe traffic congestion and heavy snowfall.

### ***3.2 Target Period***

The target period was 21 December 2016 to 25 January 2017. In this period, a heavy snowfall event with 80 cm of cumulative snowfall occurred. This snowfall event was the largest within the target period.

### ***3.3 Weather Observation***

Hourly weather observation data can be downloaded as csv files from the website of the Japan Meteorological Agency [19]. Hourly precipitation, hourly snowfall, and cumulative snowfall data observed at Nagaoka were obtained. For analyses, we used the cumulative snowfall over an antecedent of 18 hour because the Niigata Prefecture provides predictions of snowfall during the coming 18 h twice per day [20].

### ***3.4 Traffic Congestion***

Traffic congestion data of public roads were obtained from Google Maps using a function to display traffic conditions on roads, called ‘Google Traffic’ [21]. This function enables to display traffic congestion by four different levels. Green and red indicate fast and slow traffic conditions, respectively. We automatically obtained images of the traffic congestion maps once per hour by taking screen shots with the domain and the scale fixed using a shell script.

### ***3.5 Image Analysis of Traffic Congestion***

Four traffic congestion levels were digitized from the Google Traffic images. First the RGB values corresponding to each congestion level were investigated as summarized in Table 1. Next, the traffic congestion levels on the Google Traffic images were determined by referring to the RGB values (Fig. 1). All analyses were conducted



**Table 1** RGB values of 4 traffic congestion levels

	Red	Green	Blue
Level 4	0.620	0.075	0.075
Level 3	0.902	0.000	0.000
Level 2	0.941	0.490	0.008
Level 1	0.518	0.792	0.314

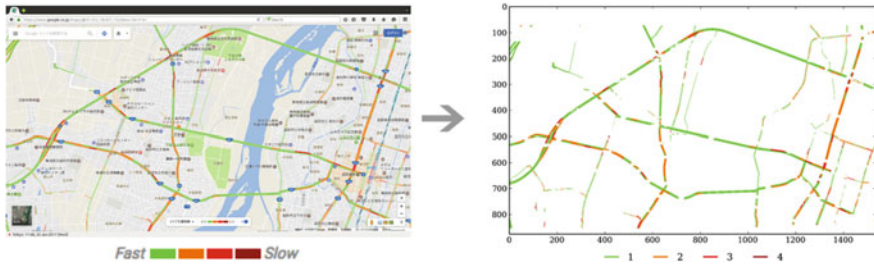


**Fig. 1** An example of the digitization of traffic congestion levels from Google Traffic

using Python. Note that we cannot use raw data with regard to traffic volume or traffic velocity because they are not available.

It is expected that traffic conditions strongly depend on time, i.e., the day of the week or time in a day. Therefore, to eliminate such temporal effects on traffic conditions, we calculated the difference in traffic congestion levels between the actual traffic conditions and the ‘typical’ conditions at the same time and day of the week. The ‘typical traffic conditions’ can be displayed on Google Traffic at a given time and day of a week, and we assumed that the typical traffic data reflected the effects of temporal information on traffic condition. Figure 2 shows an example of this method at 6 PM on 25 January 2017. Hereinafter we call this difference as the ‘relative traffic congestion levels’.

## 4 Correlation Analysis Between Traffic and Weather Data

### 4.1 Method

We conducted a correlation analysis between the relative traffic congestion levels and weather data to investigate the impact of weather conditions on traffic congestion. For each time (hour-long periods from 6 AM to 10 PM) over the target period (from 21 December 2016 to 25 January 2017), we calculated the correlation coefficients between (a) the number of pixels within the map images of traffic congestion that have positive values of relative traffic congestion levels, and (b) four types of weather observations, i.e., hourly precipitation, hourly snowfall, and cumulative snowfall, over the preceding 18 h, and cumulative snowfall at the time period. Figure 3 shows

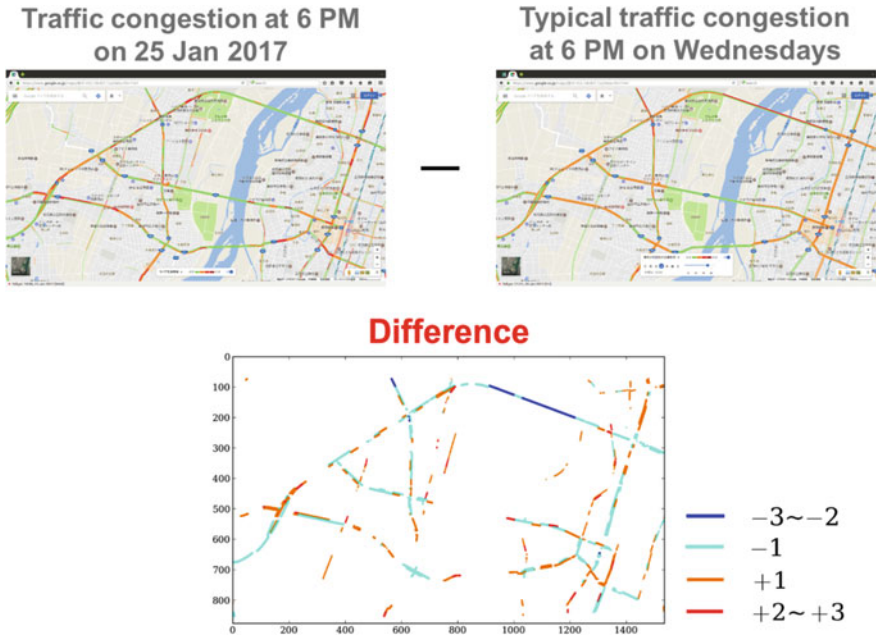


Fig. 2 Illustration of the calculation of the difference in traffic congestion levels between the actual and typical traffic conditions

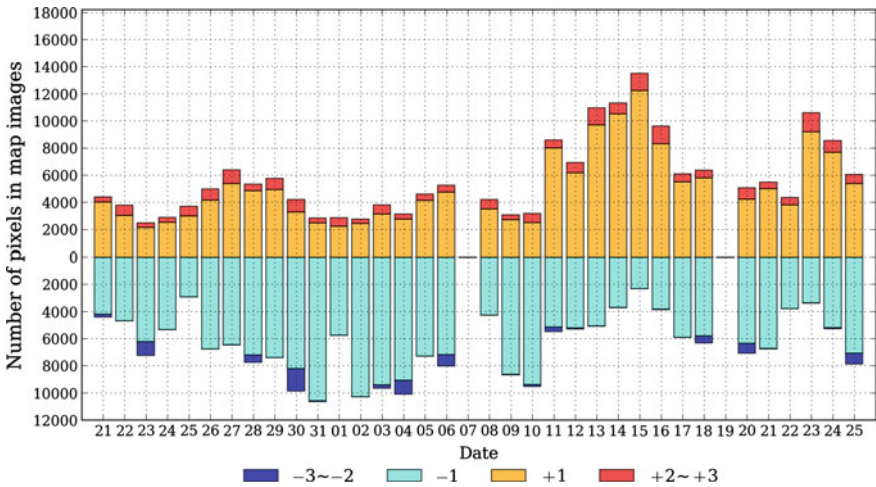


Fig. 3 An example of the time series of the number of pixels (y axis) with relative traffic congestion levels at 6 PM during the target period (x axis). Warm and cool colors indicate positive and negative values of relative traffic congestion levels. Bar graphs with zero data such as 7 or 19 January indicate missing data

an example of the time series of relative traffic congestion levels at 6 PM. Note that the bar graphs with zero data (i.e., 7 or 19 January) indicate missing data due to technical errors in retrieving Google Traffic images.

## 4.2 Result

Figure 4 shows an example of the correlation analysis between the relative traffic congestion levels and weather observations at 6 PM. In this case, the correlation coefficients were 0.143 for hourly precipitation, 0.460 for hourly snowfall, 0.604 for cumulative snowfall over the preceding 18 h, and 0.701 for cumulative snowfall; thus, the latter two show a relatively good positive correlation with relative traffic congestion levels.

Figure 5 shows the correlation coefficients between the positive relative traffic congestion levels and weather observations for each time from 6 AM to 10 PM calculated over the entire target period. The overall averages of correlation coefficients for each weather factor were 0.277 for hourly precipitation, 0.170 for hourly snowfall, 0.488 for 18-h cumulative snowfall, and 0.530 for cumulative snowfall, respectively.

Two points can be pointed out from this analysis. First, hourly precipitation and hourly snowfall have a weak correlation with the increase in traffic congestion, whereas 18-h cumulative snowfall and cumulative snowfall have a moderate correlation. Therefore, we assumed that these two parameters were the factors which may determine traffic congestion. Second, even though we subtracted typical traffic condition to eliminate temporal effects on traffic congestion, there still remains a certain temporal dependence between the time of a day and correlation between the weather and traffic congestion. This implies that we should consider the time of day as a factor to determine traffic congestion as well.

## 5 Logistic Regression Analysis

### 5.1 Method

Logistic regression analysis was employed to estimate whether a pixel  $i$  shows an increase in traffic congestion using cumulative and 18-h cumulative snowfall ( $x_{1i}$  and  $x_{2i}$ , respectively) and time ( $x_{3i}$ ) information. Logistic regression analysis is a method to develop a statistical model to estimate the probability of occurrence ( $p_i$ ) of a certain phenomenon using linear regression by maximum likelihood estimation with regard to factors that can determine the occurrence of the phenomenon. Thus, logistic regression analysis can be considered as a proper way to represent the statistical relationship between snowfall and traffic congestion. In this case, the regression equation can be described as follows:

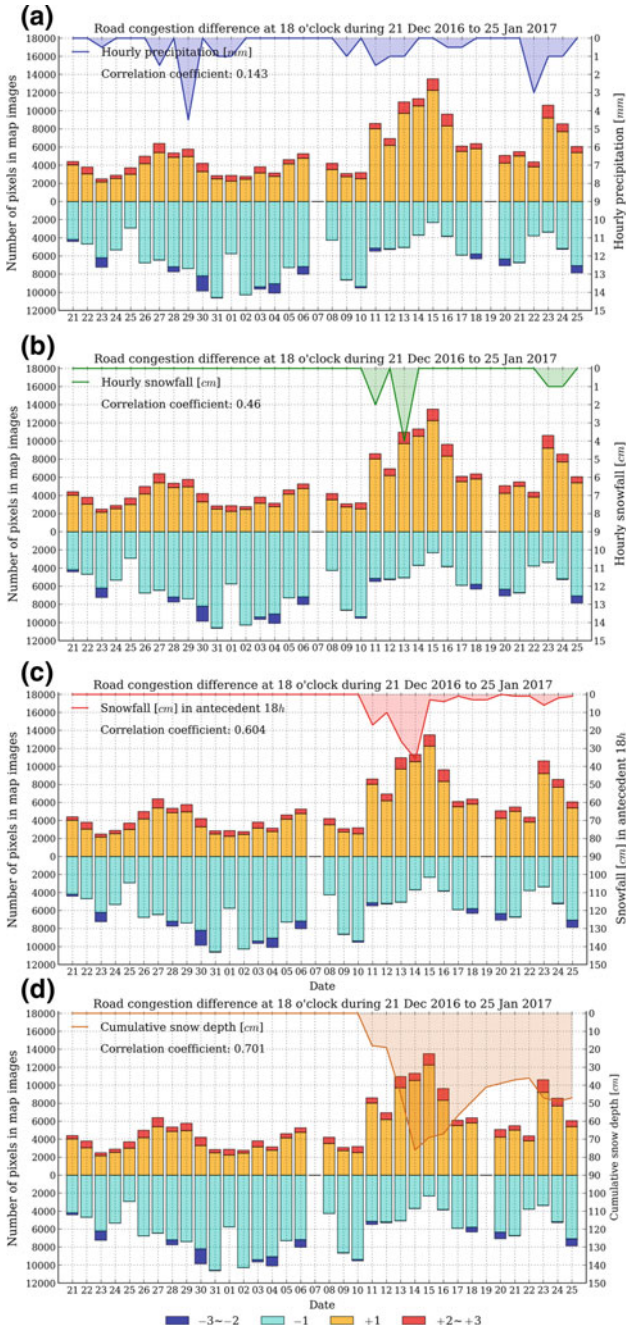


**Fig. 4** An example of correlation analysis between relative traffic congestion levels and weather observation at 6 PM, that is, **a** hourly precipitation, **b** hourly snowfall, **c** cumulative snowfall over the antecedent 18 h, and **d** cumulative snowfall

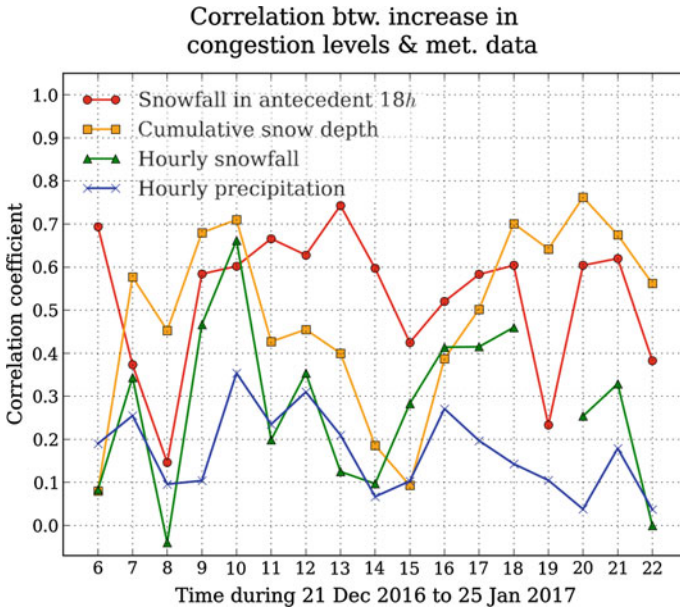


**Fig. 5** Correlation coefficients between the total number of pixels within each map image that have positive relative traffic congestion levels and the weather observations for each time during the target period

$$p_i = \frac{\exp(\beta_0 + \beta_1 x_{1i} + \beta_2 x_{2i} + \beta_3 x_{3i})}{1 + \exp(\beta_0 + \beta_1 x_{1i} + \beta_2 x_{2i} + \beta_3 x_{3i})} \tag{1}$$

where  $\beta_j$  means the parameters to be optimized.

We used a generalized linear model (GLM) in the programming language R. Two models were developed for two different thresholds (1 or 2) with regard to the increase in relative congestion levels to predict moderate (1) and severe (2) traffic congestion. First, the relative traffic congestion levels were converted into binary data, where 1 means that the relative traffic congestion level is greater than or equal to the threshold, whereas 0 means it is not. Next, logistic regression analysis was applied for each pixel by using the converted binary data and weather observations (Fig. 6). Finally, by using the coefficients obtained from logistic regression analysis and past weather observations, the past occurrence of traffic congestion was estimated to validate the applicability of the statistical model developed here. The probabilities calculated by the optimized parameters and input variables (i.e., weather observations and time) were converted to binary data by rounding, and then hit rates were calculated as percentages of the true prediction for each pixel. Note that the pixels that always contains values of 0 were excluded from analysis because they do not represent the traffic conditions.

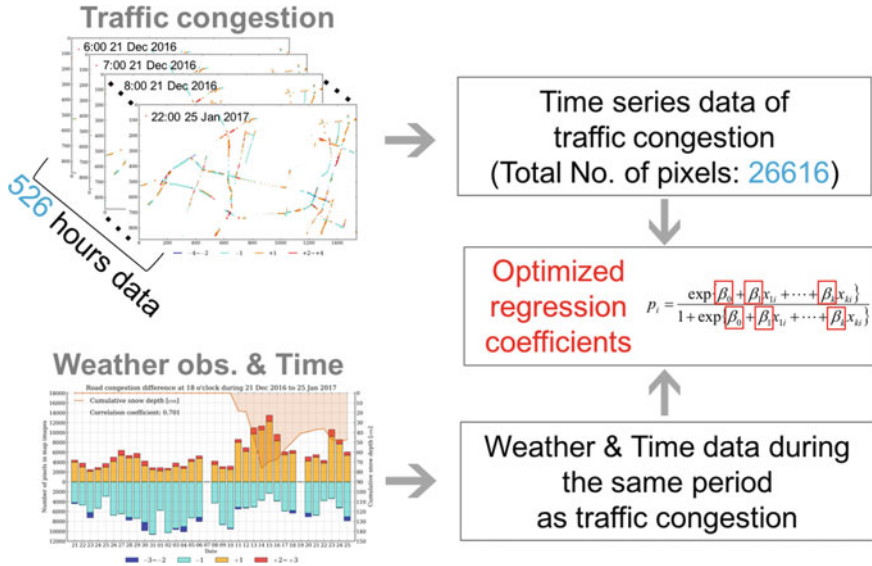


Fig. 6 Flowchart of logistic regression analysis

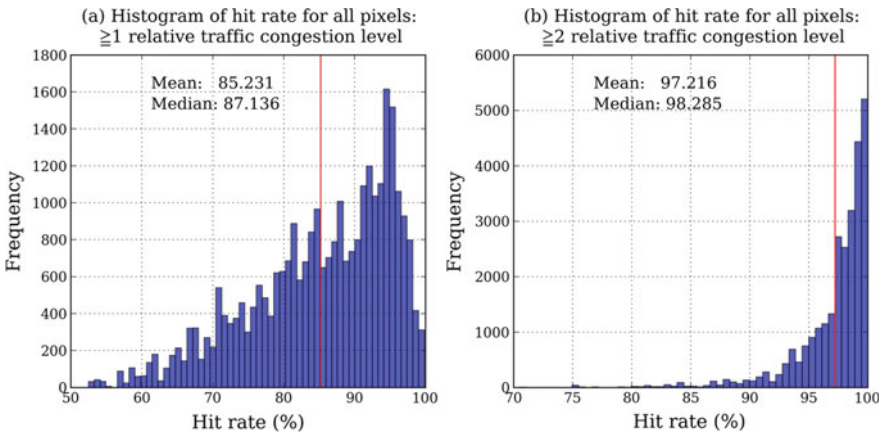


Fig. 7 Histogram of hit rates (%) of predictions for a positive relative traffic congestion level and b relative traffic congestion level  $\geq 2$ . The red lines indicate the mean values

### 5.2 Result

Figure 7 shows the histogram of hit rates (%) for all pixels. The mean and median values of hit rates were 85.231% and 87.136% in the case of a threshold of 1, and 97.216% and 98.285% in the case of a threshold of 2, respectively. These high values indicate that the statistical model proposed here is valid to predict the occurrence of traffic congestion due to weather conditions.

## 6 Discussion

This study has some limitations. First, this study ignores several factors that can determine traffic congestion. For example, although snowfall has a significant impact on the occurrence of traffic congestion as demonstrated in this study, the reason for traffic congestion is not necessarily the weather conditions. It can be caused by other factors, such as traffic accidents and road construction or repairs. In addition, we did not take into account human activities to mitigate the adverse impacts of snowfall, such as snow shoveling, snow removal, and the operation of snowplows and snow-melting pipes. Therefore, if such effects become significant to determine traffic congestion, the statistical model developed in this study may not accurately predict traffic congestion.

Second, the reliability of the Google Traffic data is an important issue that should be discussed. Google Traffic displays four levels of traffic congestion, but it does not provide concrete information about traffic parameters such as traffic speed, volume, or how to calculate traffic congestion levels. Hence, it is necessary to validate the accuracy of the Google Traffic data by comparing it with observed traffic congestion situations. To evaluate the reliability of the Google Traffic data, a potential solution may be to use ETC2.0 data [22]. It provides probe information obtained via mutual communication between ETC2.0 devices on cars and roadside devices. Therefore, if we can collect abundant data from ETC2.0, it may be possible to check whether the Google Traffic data appropriately captures actual traffic conditions.

In this study, although we obtained ETC2.0 data along the National Route 8 within the central part of Nagaoka City (Fig. 8), it was difficult to use the data to validate the Google Traffic data in this study because of a technical issue. According to the ETC portal, the number of cars which have ETC2.0 is around 3 million throughout Japan, but only 1,158 in Niigata Prefecture [22]. Owing to this, the data obtained from ETC2.0 shows an inconsistency in the number of the cars available for observation. Figure 9 shows that only 5 to 10 cars per hour are detected via ETC2.0 even in

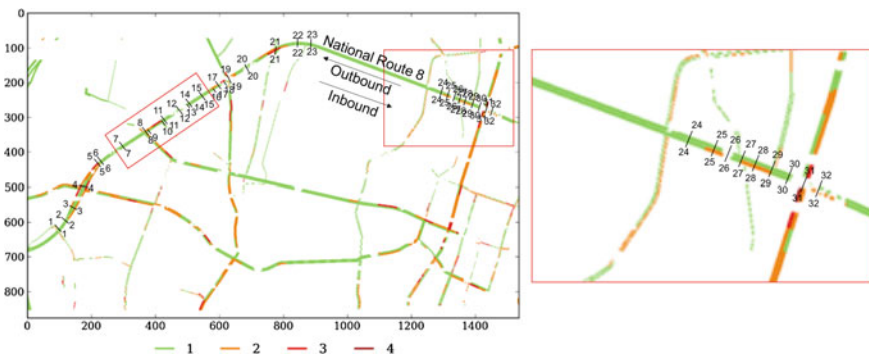
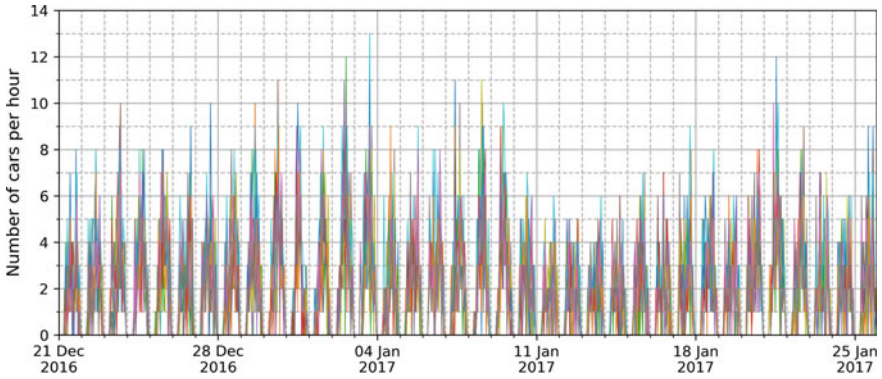
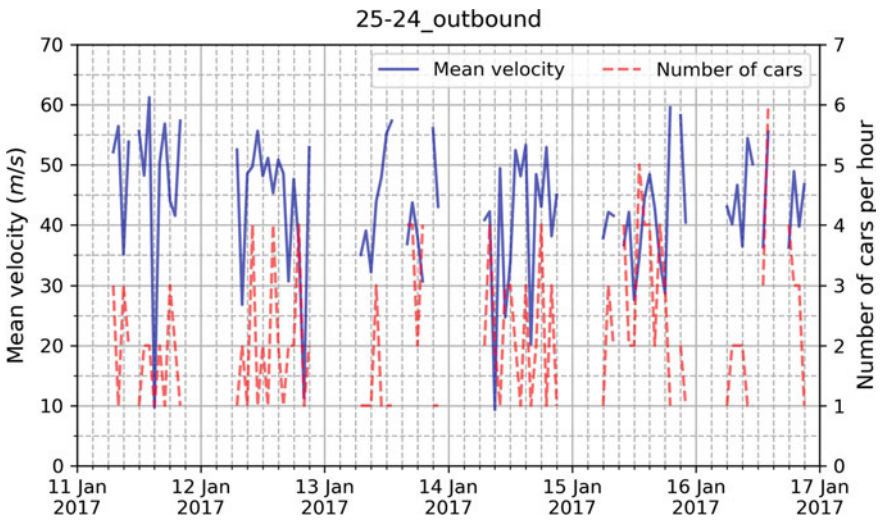


Fig. 8 Road sections where ETC2.0 data were available along the National Route 8



**Fig. 9** Time series of the number of cars detected per hour. Each line indicates one road section



**Fig. 10** An example of mean velocity per hour at the outbound road section from 25 to 24 in the Fig. 8

daytime, while more than 1,000 vehicles per hour pass through this road even in off-peak hours. When focusing on the hourly average speed of detected vehicles, it is observed that the calculated average speed shows large variation (Fig. 10). If the ETC2.0 system becomes more popular than now, this information can provide a reliable basis to validate the Google Traffic data. Despite these limitations, our statistical model developed to predict traffic congestion during snowfall is highly reliable.



## 7 Conclusion

In this study, we proposed a simple method to predict traffic congestion caused by weather conditions using free, publicly-available data. Nagaoka City in Niigata Prefecture, Japan, was selected as a target region because of the recurrent traffic congestion induced by heavy snowfall in the winter. Weather observations were obtained as a csv file, and traffic congestion data were digitized from Google Traffic, a web page that can demonstrate live and typical traffic congestion levels. We found a positive correlation between the increase in traffic congestion levels and cumulative snowfall, and therefore proceeded to use logistic regression analysis to formulate the relationship between them. Validation of the performance of the developed statistical model demonstrated that it can predict the occurrence of traffic congestion compared to typical traffic conditions with a hit rate of greater than 80% on average. This high hit rate indicates the validity of the model.

Future work that stems from the present study will include the incorporation of anthropogenic impacts on the relationship between traffic congestion and snowfall with data of a longer period that includes more snowfall events.

**Acknowledgements** We thank Nagaoka National Highway Office, Hokuriku Regional Development Bureau, Ministry of Land, Infrastructure, Transport and Tourism, Japan for providing us with the ETC2.0 data. We also thank Jun Ito, an assistant professor and Noriyuki Sakai, a master's student at Nagaoka University of Technology, Japan for extracting and organizing the necessary information from the raw ETC2.0 data.

## References

1. The Asahi Shinbun: 1,400 drivers in Hokuriku stuck overnight by heavy snow. <http://www.asahi.com/ajw/articles/AJ201802070039.html> (2018). Last accessed 29 Aug 2018
2. Zhao, Y., Sadek, A.W., Fuglewicz, D.: Modeling the impact of inclement weather on freeway traffic speed at macroscopic and microscopic levels. *Transp. Res. Rec. J. Transp. Res. Board* **2272**, 173–180 (2012). Transportation Research Board of the National Academies
3. Kyte, M., Khatib, Z., Shannon, P., Kitchener, F.: Effect of weather on free-flow speed. *Transp. Res. Rec. J. Transp. Res. Board* **1776**, 60–68 (2001)
4. Terauchi, Y., Usami, S., Honda, Y.: An investigation on road traffic characteristics for road traffic management in snowfall season. *J. Snow Eng. Jpn.* **15**, 203–210 (1999). (in Japanese with English abstract)
5. Asamer, J., Van Zuylen, H.J.: Saturation flow under adverse weather conditions. *Transp. Res. Rec. J. Transp. Res. Board* **2258**, 103–109 (2011)
6. Ivanović, I., Jović, J.: Sensitivity of street network capacity under the rain impact: case study of Belgrade. *Transport* **33**, 470–477 (2018)
7. Sun, H., Yang, J., Wang, L., Li, L., Wu, B.: Saturation flow rate and start-up lost time of dual-left lanes at signalized intersection in rainy weather condition. *Procedia Soc. Behav. Sci.* **96**, 270–279 (2013)
8. Akin, D., Sisiopiku, V.P., Skabardonis, A.: Impacts of weather on traffic flow characteristics of urban freeways in Istanbul. *Procedia Soc. Behav. Sci.* **16**, 89–99 (2011)

9. Jia, Y., Wu, J., Du, Y.: Modeling and simulation of rainfall impacts on urban traffic flow: a case study in Beijing. *Theory Methodol. Tools Appl. Model. Simul. Complex Syst.* **643**, 475–484 (2016)
10. Agarwal, M., Maze, T.H., Souleyrette, R.: Impacts of weather on urban freeway traffic flow characteristics and facility capacity. In: *Proceedings of the Mid-Continent Transportation Research Symposium*, Ames, Iowa, August (2005)
11. Ibrahim, A.T., Hall, F.L.: Effect of adverse weather conditions on speed-flow-occupancy relationships. *Transp. Res. Rec.* **1457**, 184–191 (1994)
12. Weng, J., Liu, L., Rong, J.: Impacts of snowy weather conditions on expressway traffic flow characteristics. *Discret. Dyn. Nat. Soc.* **2013**, 791743 (2013)
13. Chung, Y.: Assessment of non-recurrent congestion caused by precipitation using archived weather and traffic flow data. *Transp. Policy* **19**, 167–173 (2012)
14. Lee, J., Hong, B., Lee K., Jang Y.: A prediction model of traffic congestion using weather data. In: *2015 IEEE International Conference on Data Science and Data Intensive Systems*, Sydney, New South Wales, pp. 81–88 (2015)
15. Qiu, H., Li, R., Liu, H.: Integrated model for traffic flow forecasting under rainy conditions. *J. Adv. Transp.* **50**, 1754–1769 (2016)
16. Tselentis, D.I., Vlahogianni, E.I., Karlaftis, M.G.: Improving short-term traffic forecasts: to combine models or not to combine? *IET Intell. Transp. Syst.* **9**(2), 193–201 (2015)
17. Polson, N.G., Sokolov, V.O.: Deep learning for short-term traffic flow prediction. *Transp. Res. Part C* **79**, 1–17 (2017)
18. Lin, L., Ni, M., He, Q., Gao, J., Sadek, A.W.: Modeling the impacts of inclement weather on freeway traffic speed-exploratory study with social media data. *Transp. Res. Rec.* **2482**(1), 82–89 (2015)
19. Japan Meteorological Agency. <http://www.data.jma.go.jp/gmd/risk/obsdl/>. Last accessed 28 Aug 2018
20. Niigata Prefecture. <http://www.chiiki.pref.niigata.jp/yuki/index-e.html>. Last accessed 28 Aug 2018
21. Google Traffic. <https://www.google.co.jp/maps/@37.453,138.827,15z/data=!5m1!1e1>. Last accessed 28 Aug 2018
22. ETC2.0 <http://www.go-etc.jp/english/etc2/index.html>. Last accessed 28 Aug 2018

# Warning Notification of Potential Collisions for Comfort Intelligence on Autonomous Vehicles



**Taishi Sawabe, Shohei Ota, Masayuki Kanbara, Norimichi Ukita, Tetsushi Ikeda, Luis Yoichi Morales Saiki, Atsushi Watanabe and Norihiro Hagita**

**Abstract** Previous studies about autonomous vehicles only focus on safety and efficiency, however, it is also necessary to consider passenger comforts inside autonomous vehicles including autonomous wheelchairs in order to use by a widespread in the society. Therefore, in this research, we emphasize an importance of considering passenger comforts in designing a real autonomous navigation for a concept of comfort intelligence (CI) in future autonomous society. There are many different factors that reduce passenger anxiety relates to comforts in autonomous scenarios. For example, passengers on autonomous vehicles often feel stress by potential collisions around blind intersections due to lack of information. In contrast to the

---

T. Sawabe (✉) · S. Ota · M. Kanbara  
Nara Institute of Science and Technology, 8916-5 Takayama Town,  
Ikoma City, Nara, Japan  
e-mail: [sawabe.taishi.so0@is.naist.jp](mailto:sawabe.taishi.so0@is.naist.jp)

M. Kanbara  
e-mail: [kanbara@is.naist.jp](mailto:kanbara@is.naist.jp)

N. Ukita  
Toyota Technological Institute, 2-12-1 Hisakata,  
Tenpaku Ku, Nagoya, Aichi, Japan  
e-mail: [ukita@toyota-ti.ac.jp](mailto:ukita@toyota-ti.ac.jp)

T. Ikeda  
Hiroshima City University, 3-4-1 Ozuka Higashi,  
Asaminami Ku, Hiroshima, Japan  
e-mail: [ikeda@hiroshima-cu.ac.jp](mailto:ikeda@hiroshima-cu.ac.jp)

L. Y. M. Saiki  
Nagoya University, Furo-cho, Chikusa Ku, Nagoya, Aichi, Japan  
e-mail: [morales\\_yoichi@coi.nagoya-u.ac.jp](mailto:morales_yoichi@coi.nagoya-u.ac.jp)

A. Watanabe  
SEQSENSE Inc, 303 Meiji university, research center, 2-3227 Mita,  
Tama Ku, Kawasaki City, Kanagawa, Japan  
e-mail: [tsushi.w@ieee.org](mailto:tsushi.w@ieee.org)

N. Hagita  
Advanced Telecommunications Research Institute International,  
2-2 Hikoridai 2 choume, Seika Town, Souraku, Gun, Kyoto, Japan  
e-mail: [hagita@atr.jp](mailto:hagita@atr.jp)

previous method that controls the velocity of vehicles based on the passenger's visibility, this paper proposes another reduction method by showing information. In this research, we examine three types of methods to find the best method for showing information includes a previous method without showing any information, the method uses a convex mirror sets up at the edge of a blind corner, and other method uses a tablet device mounted on the vehicle to display texts and play sounds to inform oncoming moving objects. Experiments are performed with physiological indexes to 16 participants to verify results. These results showed the convex mirror method and the tablet device with texts and sounds method reduce passengers stress.

## 1 Introduction

Growing technologies in autonomous navigation in the state of the art have made it possible to realize autonomous vehicles in human life [1, 2]. Recently, there are many different types of autonomous vehicles that are developed depending on scenarios, such as high-speed desert driving without manual intervention in DARPA Grand Challenge [3], autonomous mobilities used in urban area [4], and autonomous wheelchairs for assisting elderly people [5]. Main purposes of developing these autonomous vehicles are to reduce traffic accidents and traffic jams caused by human errors, to walking assist for people, and to improve human comforts [6–8].

Most of the research mainly focuses on safety issue and efficiency problems of vehicles, however, it is also necessary to consider passenger comforts in autonomous vehicles for a widespread in society. Therefore, in this work, we emphasize the importance of considering passenger comforts in an autonomous navigation for a concept of comfort intelligence (CI) for future autonomous society. The comfort intelligence for autonomous vehicles defines as the intelligent system that considers human comforts both inside and outside people of any kinds of autonomous vehicles.

There are already related works about human comfort during navigational tasks by using autonomous vehicle [9–11]. In contrast to these previous approaches in stress measurement methods, we use physiological indexes to detect and analyze the stress level of passengers during navigational tasks to reduce passenger's anxiety in autonomous navigation with objective measurements.

In this research, the stress of reducing human comfort that occurred when a passenger predicts potential collisions with oncoming objects in blind spots are targeted (see Fig. 1). Showing notification with a convex mirror and a tablet device for displaying texts and playing sounds of information about blind spots are proposed. Compared with the previous scenario of no warning notification, especially inside a building environment. Verification experiment is held with physiological indexes (the heart rate sensor and the galvanic skin response) to analyze the effectiveness of methods.

The rest of the paper is organized as follows: Sect. 2 presents related works of autonomous vehicles considering human comfort, and stress measurement by using physiological sensors. Section 3 describes two proposed methods to show

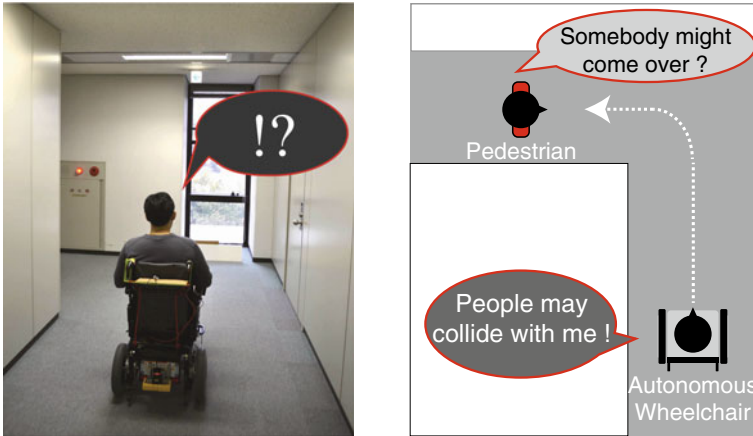


Fig. 1 Scenario for riding vehicles when passengers feel stress from collision prediction

information of the blind spots while riding the autonomous wheelchair, Sect.4 describes an experimental procedure and results including hypothesis and implementation of the autonomous wheelchair and, finally Sects.5 and 6 present discussions and conclusions respectively.

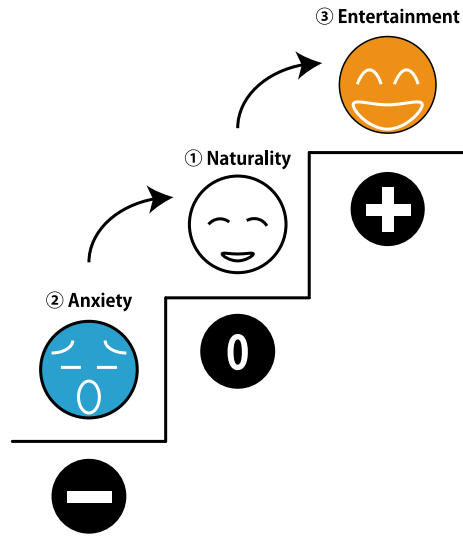
## 2 Related Works

### 2.1 Comfort Intelligence for Autonomous Vehicles

For the widespread in the human society, it is important to consider human comfort in autonomous vehicles of the concept of comfort intelligence for future autonomous society. In this paper, comfort intelligence (CI) is defined as the system that considers passenger comfort inside autonomous vehicles. In the idea of CI contains both a negative state to a positive state of passengers' feeling inside vehicles.

Doi says that there are 3 levels of human feeling state when they meet with new tools or devices in the field of human interface [12]. This concept idea is also the same as riding autonomous vehicles for the first time (see Fig.2). State 1 is the naturality that passenger want to use its vehicles as the assisted walking tools as the ordinary use case. This is the first goal for autonomous vehicles to achieve for widespread use in the human society. State 2 is a feeling of anxiety (or fears) of riding autonomous vehicles. This is the important and most difficult parts in psychological and physiological for passengers to meet with new vehicles for the first time. Doi also explained that when people meet with new devices, they tend to get anxiety about using it. This anxiety increases if people do not understand its devices. State 3 is the

**Fig. 2** The concept idea of human interface with a different state from anxiety to entertainment



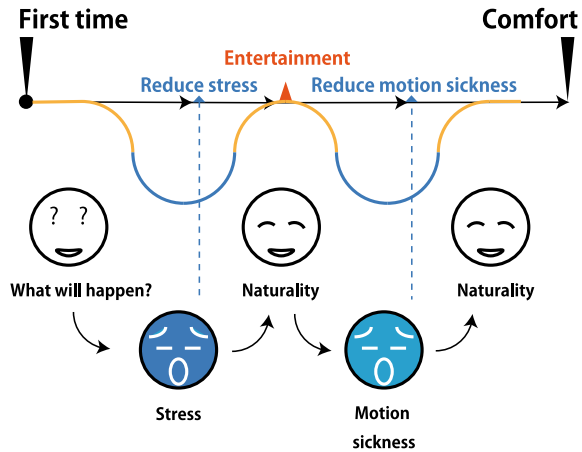
entertainment (or having fun) when passengers get used to riding with autonomous vehicles. Many passengers want to spend their time doing work or having fun with entertainment inside vehicles.

Main anxiety factor is motion sickness in autonomous vehicles. Michael et al. [13] suggest that it is necessary to focus more on motion sickness in autonomous vehicles since there will be more high possibility for passengers to get motion sickness because of passengers have more time for entertainments after they are released from driving.

Therefore, some research mentions the importance of reducing motion sickness when the vehicle becomes autonomous. In the autonomous environment, it is more high possibility to become car sickness since passenger has hardly recognized the direction of acceleration effects [14]. Moreover, many car accessory companies try to make new HUD for navigation with AR and VR in the future autonomous vehicles [15–17]. Isobe [18] mentions the existence of new kinds of motion sickness when people tend to ride autonomous vehicles from these technological trends. That is mixed with car sickness and VR sickness called Autonomous Vehicles Motion Sickness (AVMS). In that research, the existence of AVMS is explained through experiments by comparing different types of environments, car sickness, autonomous vehicle motion sickness, and VR sickness environment.

There is also research about motion sickness reduction in future autonomous vehicles. Wada [19] propose an algorithm to measure motion sickness based on vehicles' behavior parameters. In that research state that motion sickness reduction method is also important for passengers' comfort in future autonomous vehicles. Sawabe et al. [20] propose the solution to reduce motion sickness in autonomous vehicles by usingvection illusions to induce passengers' body movements to let sensory organs to know the behavior of vehicles and its acceleration.

**Fig. 3** Concept idea of comfort intelligence (CI) with changing passengers feeling in autonomous vehicles



Another main anxiety factor is stress in autonomous vehicles. Mohamed et al. [21] summarize recent researches related to autonomous vehicles. It states the importance of stress reduction for passenger comforts in autonomous situations.

Ota et al. [22] classify stressors of passengers by measuring physiological indexes while they are in a semiautonomous driving situation, and defined these kinds of stress on autonomous vehicles as “Autonomous Vehicle Stress (AVS)”. From experimental result, the classification table of stressors and solutions to reduce these stress are summarized. In the table, control vehicles’ behavior and show information are the effective solutions to be adequate to reduce stress in autonomous vehicles.

In this research, the stress factor is focused more since more possibility to feel anxiety when they ride autonomous vehicles at first time (see Fig. 3).

## 2.2 Stress Reduction Method by Controlling Vehicle Behavior

There are previous studies related to control vehicles. Gulati et al. [23] propose and demonstrate the concept of high-performance control for a graceful motion of an intelligent wheelchair. González et al. [24] introduces the continuous curvature path planning algorithm that can avoid obstacles. The previous study related to the human comfort of reducing stress by controlling vehicle, Morales et al. [25] evaluated the passenger’s stress of riding an autonomous wheelchair from the static environment. In this work, the relationship between the visibility of the environment and the stress is evaluated by using laser range-finder to collect 3D information of the static environment and use this information to estimate the visibility of passenger. Moreover, Nomura et al. [26] proposed the path planning algorithms for reducing the stress of passengers on autonomous wheelchairs in static environments. These two

types of research mainly focus on the stress caused by static environments. Furthermore, Sawabe et al. [27] proposed a method for velocity control of the autonomous wheelchair based on the concept of “Behaviour Dependent Observability (*BDO*)” to reduce stress from collision prediction in blind regions. By using *BDO*, the velocity of the autonomous wheelchair is computed so that passengers feel comfortable. The approach is to use the method of controlling vehicle-based on passengers’ visibility to reduce predicted stress.

### ***2.3 Stress Reduction Method by Showing Information***

There are already previous works related to stress reduction by showing information. Hashimoto et al. address stress reduction by showing information about the behavior of the autonomous wheelchair to the passenger [28]. This work evaluates the relationship between stimulus intensity (strong or weak) or duration of stress factor (long or short) and physiological indexes by analyzing reactions to each physiological indexes of different kinds of stress events such as sudden accelerations, jerking movements and passing too close to walls. Moreover, it demonstrates that stress is reduced by showing the behavior of the autonomous wheelchair to the passenger.

Sasai et al. [29] propose a system to reduce stress by using augmented reality to show the blind spot of its vehicle with using physiological indexes for stress measurements. In this work, the see-through image with AR to show the relationship between the tires and the position of the road directly for stress reduction from colliding prediction with static environments. This research targets the reduction of stress from collision prediction with other dynamic objects in blind spots, and not many studies have not targeted yet.

Generally, autonomous wheelchairs enter corners with suitable velocity, only considering the efficiency of movement, but without visual information. In this case, the stress by predicting the crossing collision with other dynamic objects because the passenger will not be able to see what will happen after entering the blind corner due to the lack of information. Therefore, in this research, we propose methods to show information with the convex mirror and the tablet device to display texts and play sounds.

We use the tablet device displaying texts and playing sounds about coming objects. The approach is compared towards a static convex mirror that is normally used in blind environments in normal road situations. Moreover, verification experiments are held to validate the efficiency of showing information methods by using physiological indexes.



## 2.4 Physiological Indexes for Stress Monitoring

This section explains objective measurements for related researches by using physiological indexes for stress measurements. There are many ways to measure human stress, however, in this research, the heart rate sensor of LF/HF value and the galvanic skin response for sweat value is focused more for riding autonomous vehicles.

### 2.4.1 Heart Rate (HR)

The analysis of heart rate (HR) data for stress measurement is a well known in physiological indexes [30, 31]. In this research, HR information is measured with a thoracic HR band and an electrocardiograph circuit (Fig. 4 left). Then, to evaluate the stress level, the ratio LF/HF is used.

The LF/HF value is the value that is computed from the ratio of LF: Low Frequency, 0.05–0.15 Hz to HF: High Frequency, 0.15–0.40 Hz by analyzing the frequency of the heart rate data. To compute a value on whether a person is stressed or not, a comparison between a few seconds before and after the LF/HF rate is done.

### 2.4.2 Galvanic Skin Response (GSR)

The analysis of the galvanic skin response (GSR) for stress measurement is well known and have been used in main previous works. Many cognitive psychology studies show that changes in skin response are linked to psychological processes such as emotion, stress and pain [32, 33].

Passengers use terminals in two of his fingers to measure the electric value of personal skin conductance (Fig. 4 right). In this research, we use the eSense Skin Response GSR sensor by Mindfield Biosystems Inc. For passenger stress evaluation, we analyze the variation of GSR rate in time series. To compute a value on whether a person is stressed or not, an analyzing the change of GSR rate, if it is rapidly changing the person get stress from that event.

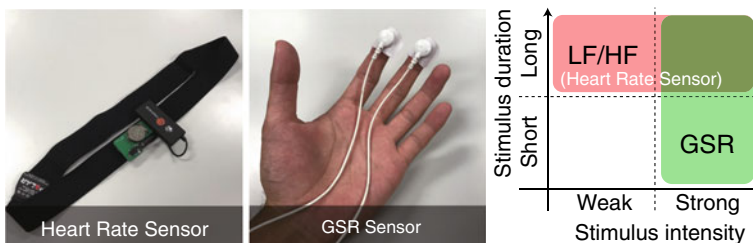


**Fig. 4** Physiological indexes for measuring stress. The HR band and an electrocardiograph circuit (left), the GSR sensor (middle), and the classification result (right) [28]

### 2.4.3 Stress Measurements for Autonomous Vehicles with Physiological Indexes

There is previous research to measure the mental stress of the passenger who drives the autonomous wheelchair by using HR and GSR [28]. In this previous work, different behavior of autonomous wheelchair and the influence of the stress can be classified based on physiological indexes. As the result, the stress can be classified as the stimulus intensity (strong or weak) and the duration (long or short) of events while moving. Evidence regarding stimulus intensity and duration are shown on experimental results of Sect. 4. If the event has long stimulus, LF/HF ratio can detect the stimulus, and if the event has strong short stimulus, GSR is more appropriate to detect it.

In this research, stress comes from collision prediction that is weak stimulus intensity and long duration is targeted, and it can detect by using the heart rate sensors (see Fig. 4 in the right).

## 3 Reducing Stress by Showing Information

There are already studies for stress reduction by showing information of vehicles' behavior or surrounded static environments in related works (Sect. 2). In contrast, we propose a method with visual and sound effects in order to reduce stress caused by collision predictions from dynamic objects in blind spots. In the experiment, we test 3 methods to verify effects. First, autonomous vehicles without showing any information to the passenger. Second, a static convex mirror that normally sets at the edge of blind corners in outside situations is used. Third, a visual and a sound notification from a tablet device is used. Following paragraphs explain the convex mirror method and tablet device method.

### 3.1 *Showing Blind Spots Information with the Static Convex Mirror Set in the Environment*

The use of static convex mirrors is common in street traffic outside environment. Generally, in-car driving roads with blind spots, there are convex mirrors near corners to show information about blind spots for the safety and human comfort [34]. The driver can see blind information before turning corners by using convex mirrors. By being aware of such information, stress from collision prediction also decrease. In this research, the convex mirror called "Square Indoor Mirror: View-mirror" by the NAC group Co., Ltd. is used to show information. The specification of the convex mirror is shown in Table 1 and the image is shown in Fig. 5.

**Table 1** Specifications of the convex mirror

Size [mm]	H420 * W620 * D320
Radius [mm]	R1500
Material	Methacrylic resin

**Fig. 5** The convex mirror used to show information in a blind corner

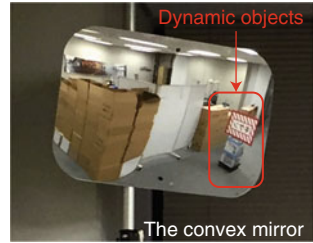


**Fig. 6** The procedure of displaying texts and playing sounds

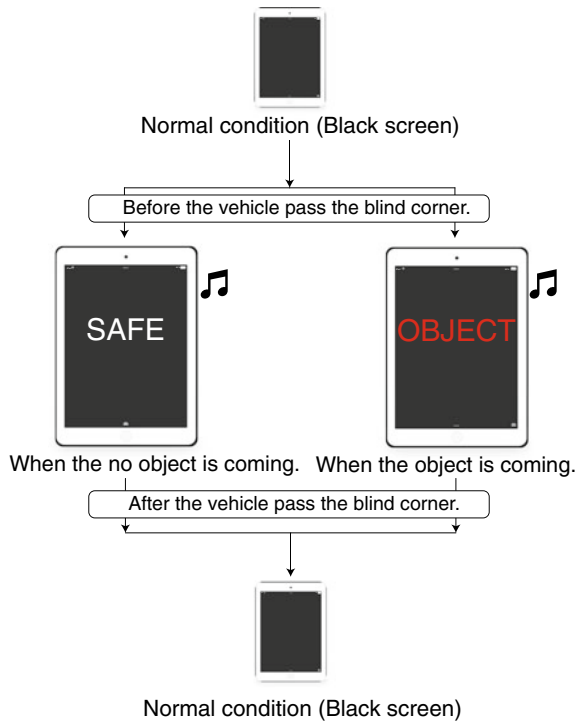


**Table 2** Display texts and play sounds from the tablet device

Object	Text	Sound
Yes	Object	Object is coming
No	Safe	It is safe

In order to reduce stress from collision prediction, showing information about blind spots by using a tablet device for displaying texts and playing sounds is proposed. In this research, the iPad is used to for notifications. Figure 6 shows the procedure of displaying text and playing sounds in the iPad screen. The sound is created by using the speech synthesis system called the rospeex, and implement in the application for iOS by using the Swift programming language. The rospeex is a cloud-based multilingual communication package for ROS, and it can easily support speech recognition and speech synthesizes in different languages [35].

The content of displaying texts and playing sounds notification is shown in Table 2 depends on situations. The normal condition when the autonomous wheelchair is moving, there is no contents and no sound from the tablet device, however, if the vehicle close to the blind spot, the device displays texts and play sounds depending on two situations. One is when the dynamic object is not coming, the text shows “SAFE” in the screen and make sound saying “It is safe”, and another is when the dynamic object is coming from the corner, the tablet device display the text “OBJECT”, and make sound saying “Object is coming”.

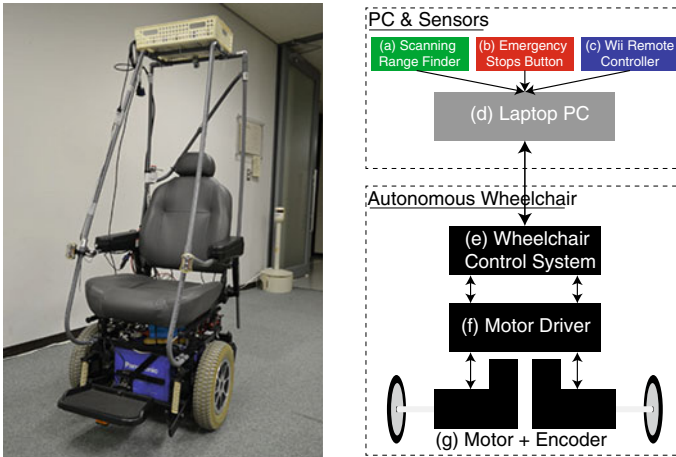
## 4 Experimental Procedure and Results

### 4.1 Hypothesis

The purpose of this research is to find the best method for showing information to reduce stress on autonomous vehicles, compared with previous ways of showing no information, use of the convex mirrors, and use of the tablet devices with text and sound notification. The hypothesis of the experiment is that uses the convex mirror, and uses the tablet device by displaying texts and playing sounds notification will reduce passengers potential collision stress compared with showing no information no\_Info. This is, by checking at LF/HF values of the same passenger between two intervals to analyze stress level. The convex mirror and the tablet device methods will have the LF/HF values decreases or stays constants compared to the conventional method of showing no information. In the experiment, the autonomous wheelchair travels the routine stated path which includes the blind spots, while measuring the weak and long stress caused by collision prediction with other objects. Table 3 shows the hypothesis of the experiment with different methods of showing information.

**Table 3** Condition and hypothesis of the experiment

	No_Info	Info A	Info B
Showing information	–	Mirror	Text and Sound
LF/HF value	Increase	Decrease or constant	Decrease or constant
GSR Value	No change	No change	No change

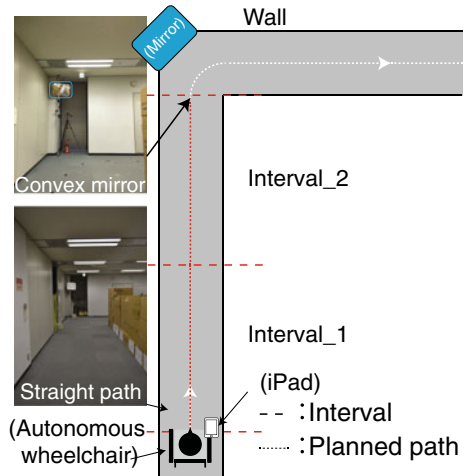
**Fig. 7** The autonomous wheelchair used in the experiment (left) and constructed system (right)

## 4.2 Implementation

In the implementation, the maximum linear velocity  $v_{max}$  is fed to the motion planner implemented as a ROS node [11]. The motion planner operates as a trajectory tracker which computes vehicle's angular ( $w$ ) velocity of the vehicle to follow a given global path at maximum linear velocity ( $v_{max}$ ). The source code of the trajectory tracker is implemented in ROS framework available at <http://openspur.org/atsushi.w/packages/>.

The system of the autonomous wheelchair is composed of two parts (see in Fig. 7). First parts, PC & sensors which include the laptop PC, a scanning rangefinder, an emergency stops button for the passenger, a wireless Bluetooth controller used as the emergency button for the experiment observer. Second parts, the whole hardware wheelchair which includes a wheelchair control system, a motor driver, and motors with encoders.

**Fig. 8** Experimental environments with intervals and the planning path



### 4.3 Experimental Procedure

In the verification experiment, we called 16 Japanese people at the age of about 20 years old to ride the autonomous wheelchair in an indoor path includes the blind spot. In this experiment, the maximum velocity of the autonomous wheelchair is 1.2 m/sec as the default velocity, and the velocity of other dynamic objects is considered as 1.2 m/sec which is typical fast velocity enough for human walking [36]. Left side of Fig. 8 shows the top view of the experimental environment. For objective evaluation, physiological indexes, such as HR and GSR are used to evaluate stress. In this research, the stress from the collision prediction is classified as the weak-long stress. The stress can be verified by the changing of LF/HF value in two different intervals.

To evaluate stress, we subtract the average value of LF/HF at the interval of straight path (which is in the interval\_1) and before entering the corner (which is in the interval\_2) as shown in Fig. 8. There are two different intervals: the interval\_1 is the basic straight path where the passenger visibility is guaranteed, and the interval\_2 contains “L” intersection with the blind spot. The interval line between the interval\_1 and the interval\_2 is decided with the timing of showing information.

Three different methods were compared: *no\_Info* of the conventional method, *Info A* of with using the convex mirror method, and *Info B* of using the tablet device with display texts and play sounds notification.

For the experiment, we prepared three different types of runs.

- Test runs: we allow the participant to get accustomed to the autonomous wheelchair and its driving. Basically, this run is held in the same environment (same path and same velocity) as the experimental run.

- Dummy runs: these runs are to make the participant aware that there might be people walking in the blind spots in the environment. We asked people who helped us to walk near the autonomous wheelchair when it turns the blind corner.
- Experimental runs: these runs are used for the evaluation of stress level. No\_Info of not showing information, Info A using the convex mirror, and Info B of using the tablet device to display texts and play sounds is conducted. No moving obstacles were present in these experimental runs.

The procedure of this experiment is as follows:

1. Each participant has 15 runs in total.
2. First, 3 test runs are performed. No\_Info, Info A (mirror), and Info B (text and sound) with the dummy runs.
3. Then 12 experimental runs are done.
  - a. 3 dummy runs carried out.
  - b. 9 experimental runs are evaluated.
  - c. Conditions were randomized to avoid ordering effects
4. Finally, an interview is held at the end of each experiment.

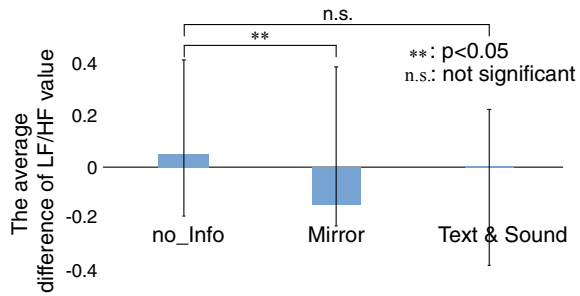
From preliminary experimental results between no\_Info and Info A, Info B, we know that there are few passengers who do not predict collisions with possible moving objects in blind spots. This causes that LF/HF ratio value of the Info method is bigger in the interval 2 with the blind spots corner compared with the interval 1 in the straight corridor. This suggests the fact that stress from the collision prediction is smaller than the other factors (e.g. wheelchair velocity). For these reasons the data of passengers who do not predict collisions are excluded from the evaluation data to evaluate the stress (in this case 8 participants' data are excluded in the result).

#### 4.4 Evaluation Results

In the experiment, evaluation of the stress is conducted to 8 participants looking at the change of the average value of LF/HF (No predicting data are excluded). Figure 9 is the result of the subtracted value of the average LF/HF between interval 1 (in the straight line area) and interval 2 (before entering the blind corner area) for all 8 passengers. The figure shows the result of the showing no information no\_Info, the convex mirror Info A, and the tablet device Info B. The horizontal axis shows the method of showing information, in order of no\_Info, Info A, and Info B. The vertical axis shows the subtraction of the average LF/HF in two intervals with 0.2 scale intervals. The average LF/HF value for all passengers for no\_Info is 0.041, Info A is  $-0.152$ , and Info B is 0.003.

Moreover, the  $t$ -test is used to validate the significance of the result of each LF/HF. In the graph, the significance is shown as the black line on the top of the bar.

**Fig. 9** The average LF/HF values for all passengers with each method



*T – test* mainly use *p – value* to validate significance. If the *p – value* is smaller than 0.05 the result is significant, smaller than 0.1 and bigger than 0.05 the result is marginally significant and bigger than 0.1 the result is not significant.

## 5 Discussion

From experimental results from Fig. 9, the stress from collision prediction with moving obstacles was reduced with the convex mirror and the tablet device with display texts and play sounds as the LF/HF value decreased between intervals 1 and 2, compared with a no\_Info run. Moreover, data suggests that the convex mirror is effectively working to reduce targeted stress for passengers on the autonomous wheelchair. In addition, the *t – test* shows the result of using the mirror to be of significance (from *p – value* in the Table 4). However, the using the tablet device with texts and sounds show that there is no significant difference.

The main reason for this is because of the lack of trust in the tablet device by displaying texts and playing sounds, given that it does not show the moving objects. The mirror shows moving obstacles at blind spots. It seems that the mirror is more insightful. Another reason might be the lack of the number of participants that influence the verification results (Fig. 9).

Furthermore, from the interview result, in the mirror method experiment, participants have still anxiety from the crossing collision that comes from the area outside of the mirror since the mirror has the limitation of displaying the whole environmen-

**Table 4** *t – test* statistical significance values for each condition

<i>t – test</i>	No:mirror	No:text and sound
<i>p – value</i>	0.011	0.378
Significance	Significant	Not significant



tal view. In the tablet device with texts and sounds method experiment, participants tend to trust the device after they have enough experience of using the tablet device to predict the objects from the blind corner.

## 6 Conclusions

This paper proposes an importance of considering human comforts in the autonomous vehicle in the concept of comfort intelligence (CI), and to presents a new approach for human passenger anxiety reduction while riding autonomous wheelchairs due to collision prediction stress in blind corners by showing information. Experimental results suggest that the use of the convex mirror and displaying texts and playing sounds reduce the collision prediction stress from occurred regions. Physiological indexes with  $t$  - test are used to evaluate the result of LF/HF. From the result, the convex mirror method shows the significant and effective for most of the passengers. Moreover, data from participant interviews suggest that suitable method of showing information is depends on the passenger characteristics.

As future work, a verification with the larger number of subjects is needed in different types of blind spots to verify the effectiveness of these approaches. In addition, more variety of approaches to show information such as using a static camera to display blind spots or to use argument reality to see through the blind corner have to be tested for stress reduction.

## References

1. Morales, Y., Takeuchi, E., Carballo, A., Aburadani, A., Tsubouchi, T.: Autonomous robot navigation in outdoor cluttered pedestrian walkways. *J. Field Robot.* **26**, 609–635 (2009)
2. Nummerle, R.K., Ruhnke, M., Steder, B., Stachniss, C., Burgard, W.: Autonomous robot navigation in highly populated pedestrian zone. *J. Field Robot.* **4**, 565–589 (2015)
3. Thrun, S., Montemerlo, M., Dahlkamp, H., Stavens, D., Aron, A., Diebel, J., Fong, P., Gale, J., Halpenny, M., Hoffmann, G., Lau, K., Oakley, C., Palatucci, M., Pratt, V., Stang, P., Strohband, S., Dupont, C., Jendrossek, L., Koelen, C., Markey, C., Rummel, C., Niekerc, J., Jensen, E., Alessandrini, P., Bradski, G., Davies, B., Ettinger, S., Kaehler, A., Nefian, A., Mahoney, P.: Stanley: the robot that won the DARPA grand challenge. *J. Field Robot.* **23**, 661–692 (2006)
4. Institute, Todd Litman Victoria Transport Policy: Autonomous Vehicle Implementation Predictions Implications for Transport Planning, pp. 1–35 (2018)
5. Scudellari, M.: Self-Driving Wheelchairs debut in Hospitals and Airports, the autonomous vehicles sense positions, select routes, and stop for obstacles. *IEEE Spectr.* (2017). <https://spectrum.ieee.org/the-human-os/biomedical/devices/selfdriving-wheelchairs-debut-in-hospitals-and-airports> (Cited 30 Aug 2018)
6. National Strategy Office of ICT and Government of Japan: Declaration to be the World's Most Advanced IT Nation, pp. 1–48 (2013)
7. Cabinet Office Government of Japan: Traffic safety in Japan 2010, Abridged edn. White Paper (2010)
8. Ormu, O., Ormuz, K., Mufti, O.: Main ambient factors influencing passenger vehicle comfort. In: Proceedings of 2nd International Ergonomics Conference, vol. 2, pp. 77–84 (2004)

9. Gulati, S., Jhurani, C., Kuipers, B., Longoria, R.: A framework for planning comfortable and customizable motion of an assistive mobile robot. In: *IEEE/RSJ International Conference on Intelligent Robots and Systems (IROS2009)*, pp. 4253–4260 (2009)
10. Morales, Y., Kallakuri, N., Shinozawa, K., Miyashita, T., Hagita, N.: Human-comfortable navigation for an autonomous robotic wheelchair. In: *IEEE/RSJ International Conference on Intelligent Robots and Systems (IROS2013)*, pp. 2737–2743 (2013)
11. Morales, Y., Watanabe, A., Ferreri, F., Even, J., Ikeda, T., Shinozawa, K., Miyashita, T., Hagita, N.: Including human factors for planning comfortable paths. In: *IEEE International Conference on Robotics and Automation (ICRA2015)*, pp. 6153–6159 (2015)
12. Doi, M.: Human interface. *Nikkei X TECH* (2004). <https://tech.nikkeibp.co.jp/dm/article/NEWS/20050407/103547/> (Cited 30 Aug 2018)
13. Sivak, M., Schoettle, B.: Motion Sickness in Self-Driving Vehicles. The University of Michigan Transportation Research Institute, Technical Report (2015)
14. Diels, C., Bos, J.E.: Self-driving carsickness. *Appl. Ergon.* (2015)
15. Continental Inc.: Head-up Displays-Safety. <http://continental-head-up-display.com/>. (Cited 30 Aug 2018)
16. Etherington, D.: Wayrays ar in-car hud convinced me huds can be better. *Techcrunch* (2018). <https://techcrunch.com/2018/01/09/wayrays-ar-in-car-hud-convinced-me-huds-can-be-better/>. (Cited 30 Aug 2018)
17. Ng-Thow-Hing, V., Bark, K., Beckwith, L., Tran, C., Bhandari, R., Sridhar, S.: User-centered perspectives for automotive augmented reality. In: *IEEE International Symposium on Mixed and Augmented Reality* (2013)
18. Isobe, R.: Evaluation of motion sickness in mixed environment of car sickness and vr sickness in autonomous vehicle. Master 学位论文. Nara Institute of Science and Technology (2018)
19. Wada, T.: Motion sickness in automated vehicles. In: *International Symposium on Advanced Vehicle Control* (2016)
20. Sawabe, T., Kanbara, M., Hagita, N.: Diminished reality for acceleration-motion sickness reduction withvection for autonomous driving. In: *International Symposium on Mixed and Augmented Reality (ISMAR) Adjunct Proceedings*, pp. 297–299 (2016)
21. Elbanhawi, M., Simic, M., Jazar, R.: In the passenger seat: investigating ride comfort measures in autonomous cars. *Intell. Trans. Syst. Mag.* 7(3), 4–17 (2015)
22. Ota, S., Kanbara, M., Ukita, N., Kitahara, I., Kameda, Y., Ohta, Y., Ikeda, T., Morales Saiki, L.Y., Shinozawa, K., Hagita, N.: Stress of Autonomous Vehicles Stress measurement of Autonomous Vehicles driver by physiological indices. In: *The Institute of Electronics, Information and Communication Engineers IEICE*, vol. 114, no. 369, pp. 87–92 (2014)
23. Gulati, S., Kuipers, B.: High performance control for graceful motion of an intelligent wheelchair. *IEEE International Conference on Robotics and Automation (ICRA2008)*, pp. 3932–3938 (2008)
24. González, D., Pérez, J., Lattarulo, R., Milanés, V., Nashashibi, F.: Continuous curvature planning with obstacle avoidance capabilities in urban scenarios. In: *IEEE 17th International Conference on Intelligent Transportation Systems (ITSC2014)*, pp. 1430–1435 (2014)
25. Morales, Y., Even, J., Kallakuri, N., Ikeda, T., Shinozawa, K., Kondo, T., Hagita, N.: Visibility analysis for autonomous vehicle comfortable navigation. In: *IEEE International Conference on Robotics and Automation (ICRA2014)*, pp. 2197–2202 (2014)
26. Nomura, N., Hashimoto, R., Ukita, N., Kanbara, M., Ikeada, T., Morales, Y., Watanabe, A., Shinozawa, K., Hagita, N.: Human-comfortable path planning for an autonomous robotic wheelchair based on physiological indices. In: *IEICE Technical Committee on Pattern Recognition and Media Understanding (PRMU2014-86)*, vol. 114, pp. 123–128 (2014)
27. Taishi, S., Kanbara, M., Ukita, N., Ikeada, T., Morales Saiki, Y., Watanabe, A., Hagita, N.: Comfortable autonomous navigation based on collision prediction in blind occluded regions. In: *2015 IEEE International Conference on Vehicular Electronics and Safety (ICVES)*, pp. 75–80 (2015)

28. Hashimoto, R., Nomura, N., Kanbara, M., Ukita, N., Ikeada, T., Morales, Y., Shinozawa, K., Hagita, N.: Evaluation of comfortable navigation with behavior information sharing for an autonomous wheel chair. In: IEICE Technical Committee on Cloud Network Robotics (CNR2014-14), vol. 114, pp. 27–32 (2014)
29. Sasai, S., Kitahara, I., Kameda, Y., Ohta, Y., Kanbara, M., Ukita, N., Ikeda, T., Morales, Y., Hagita, N., Shinozawa, K.: Stress-free driving for autonomous vehicle: stress reduction using augmented reality. In: IEICE Technical Committee on Intelligent Transport Systems Technology (ITS2014-36), vol. 114, pp. 93–98 (2014)
30. Hayano, J.: Assessment of autonomic nervous activity by heart rate variability. **29**, 342–350 (1997)
31. Japan Society for Neurovegetative Research: Autonomic. Nervous Function Test, 4th edn. Bunkodo (2007)
32. Dehais, F., Sisbot, E.A., Alami, R., Causse, M.: Physiological and subjective evaluation of a human robot object hand-over task. *Appl. Ergon.* **42**, 785–791 (2011)
33. Khalifa, S., Isabelle, P., Jean-Pierre, B., Manon, R.: Event-related skin conductance responses to musical emotions in humans. *Neurosci. Lett.* **328**, 145–149 (2002)
34. Department of Planning and Transport and Infrastructure and Government of South Australia: Convex Traffic Mirror Operational Instruction. Transport Services Division and Transport Services Division. Version No. 3, 1–7, (2012)
35. Komei, S., Chiori, H., Koji, Z.: Rospeex: a cloud-based spoken language communication toolkit for ROS. In: The Institute of Electronics, Information and Communication Engineers (IEICE) and Cloud Network Robot (CNR), vol. 113, no. 248, pp. 7–10 (2013)
36. Bršćić, D., Zanlungo, F., Kanda, T.: Density and velocity patterns during one year of pedestrian tracking. *Trans. Res. Proc.* **2**, 77–86 (2014)

**Part III**  
**Next-Generation Mobility**

# Exploring System Characteristics of Autonomous Mobility On-Demand Systems Under Varying Travel Demand Patterns



Farid Javanshour, Hussein Dia and Gordon Duncan

**Abstract** Shared Autonomous Mobility on-Demand (AMoD) systems are prescribed by many as a solution to tackle congestion. In these systems, customers are serviced on demand by a fleet of shared Autonomous Vehicles (AV). The main aim of this novel mobility system is meeting travel aspirations of people while reducing the number of passenger cars on roads. Our study explores the relationship between fleet size and induced Vehicle-Kilometres Travelled (VKT) in AMoD systems in the context of a case study in Melbourne, Australia. To achieve this, an agent based simulation model was developed to investigate this relationship through scenario analysis. Our results show that fleets of on-demand shared AVs have the potential to reduce the number of vehicles by 79% on our roads. These systems, however, lead to 61% more VKT within the transport network. This finding indicates that the vast majority of literature is overoptimistic about the potential of AMoD systems for mitigating congestion. This paper also reports on an investigation into the effects of travel demand pattern on the performance of these systems, and shows that the impact of this phenomenon on their efficiency is not trivial. Further, our simulation results reveal a quadratic relationship between AMoD fleet size and induced VKT in the system, which holds for all travel demand patterns.

**Keywords** Autonomous vehicles · Shared autonomous Mobility-on-Demand systems, Agent-based modelling · Disruptive mobility

---

F. Javanshour (✉) · H. Dia  
Swinburne University of Technology, Melbourne, VIC, Australia  
e-mail: [faridjavanshour@gmail.com](mailto:faridjavanshour@gmail.com)

H. Dia  
e-mail: [hdia@swin.edu.au](mailto:hdia@swin.edu.au)

G. Duncan  
Autodesk, Inc, London, UK  
e-mail: [gordon.duncan@autodesk.com](mailto:gordon.duncan@autodesk.com)

# 1 Introduction

Urban mobility suffers from various problems such as congestion, road trauma, and emissions. This issue becomes even more serious for large and capital cities, which are considered the best place to thrive by members of the public. Undoubtedly, our cities would fail to deliver the prosperity people expect as long as urban arterials are clogged by private vehicles, seeking the best route to their desired destinations. Hence, providing urban environments with an efficient and sustainable transport system remains critical [22].

Public transport is one of the most sustainable transport solutions to the current mobility challenges. These systems, however, are not always successful in encouraging people to relinquish their personally owned vehicles mainly because they often lack the comfort and privacy one could find in private cars. Their high construction costs, especially for underground metro lines is another matter that discourages authorities from a vast deployment of mass transit systems.

All these issues have prompted experts and city councils to find an alternative to mass transit, which is not only a more cost-effective system to operate but also appealing to private vehicle users.

Autonomous Mobility on-Demand (AMoD) systems have recently been at the centre of attention as the key solution to the current urban transport problems [7, 23, 24, 31]. AMoD systems are made up of a fleet of shared Autonomous Vehicles (AVs) that could provide their customers with almost the same degree of comfort and privacy. Given in these shared systems travelers only purchase the mobility as a service whenever needed, the overall number of vehicles within the city declines dramatically.

Shared AMoD systems, however, could induce more Vehicle-Kilometres Travelled (VKT) in the network due to additional empty travels that would be undertaken by AVs to pick-up customers. The major part of the current literature suggest very little amounts of empty VKT (eVKT), which is contradictory to our findings.

In this paper, we will discuss the possible reasons for these discrepancies, and explore the relationship between AMoD fleet size and induced VKT more rigorously using a Melbourne case study. Further, we have proposed a new measure for assessing the performance of AMoD systems, called “travel demand pattern”. Our investigations show that this measure could have a significant impact on the efficiency of AMoD systems.

The remainder of this paper is organized as follows. Section 2 provides a review of the current literature on AMoD systems and identifies their drawbacks. We have described our methodology, in Sect. 3, and explained the study area and travel demand in Sect. 4. Sections 5 and 6 deals with the simulation framework, and results respectively. Section 7 looks into how travel demand pattern could affect the efficacy of AMoD systems and whereby VKT. Section 8 outlines some policy insights based on the findings of this paper. Finally, Sect. 9 presents the conclusions of the study and puts forward a few research directions for the future studies.

## 2 Related Work

The current literature on AMoD systems envisage a wide range of implications as a result of deploying these new mobility means. Different articles have investigated the potential impacts of AMoD systems from various perspectives such as their effect on road capacity, travel behaviour, travel cost or environmental issues [9, 27].

Our study would investigate transport network-impacts of AMoD systems using four performance measures: 1. fleet size, 2. VKT, 3. customer waiting times, 4. trip success-rate. The available studies that have explored the AMoD systems with almost the same measures of this research could be categorised into two groups namely, analytical models, and simulation models.

Analytical models, most of which are based upon the method proposed by James R. Jackson in 1957 [21], utilise mathematical techniques to model transport networks. The main drawback of analytical models is their reliance on quite unrealistic assumptions such as disregarding the effects of congestion in the network. Although using such models could have been justifiable back in time when powerful computers did not exist, deploying them for answering today's transport questions does not make sense.

One of the analytical models was developed for Singapore [30] in which researchers showed a fleet of AMoD system could meet the same travel demand as today using only a third of the current number of passenger vehicles. Another analytical model [32] also suggests that an AMoD system could meet the current taxi demand in Manhattan using only 70% of the current New York taxi fleet.

A recent study published in Nature [31] deploys an analytical approach to explore its AMoD scenarios. The model uses a travel demand consisting of 150 million trips undertaken in New York City over the calendar year of 2011. It has also utilised historical data to estimate travel times between the origins and destinations. The results of this research suggest a 30% reduction in fleet size compared to the current taxi fleet in New York City.

All of these models, however, have overlooked the effects of AMoD systems on VKT. Further, two of them [30, 32] have assumed Euclidean distances between their origins and destinations rather than utilising the real road network, which ultimately lead to less realism.

There are also many simulation models in the literature, which have suggested AMoD systems could meet the current demand using much fewer numbers of vehicles than that of today at the expense of an increase in VKT.

Many studies suggest very little amounts for the potential increase in VKT that ranges from 6 to 14% [4, 6, 10, 16, 17, 26]. The Stockholm study [8] also predicts a 24% increase in VKT when AMoD systems are operational. However, studies such as [20, 25] suggest AMoD studies could translate into high induced VKT in the system.

Some other simulation models also exist [1, 29] that although have showed the potential impact of AMoD services on reducing the current private vehicle fleet size, they have not reported on the amount of increase in VKT due to use of shared systems.

MATSim is the main package that has been used in many of the reviewed studies. MATSim is an agent-based traffic simulation tool tailored for large-scale scenarios [19]. In MATSim, traffic flow is represented at a mesoscopic level that disregards the interactions between vehicles. Further, simulating movement of empty AVs travelling to pick-up their customers is not possible. Thus, the studies, which has deployed MATSim as their modelling platform, have only estimated the eVKT based on the Euclidean distances between origins and destinations rather than simulating them on the real network.

Apart from the limitations, the open access nature of the MATSim has provided a good opportunity for the researchers and experts across the world to enhance the functionalities of this software through developing new modules and sharing them with other MATSim users [3, 4, 5, 14, 18].

Our research, which is an extension of the work reported in [11] aims at exploring the relationship between AMoD fleet size and induced VKT through a more meticulous model compared to other studies in order to find the possible causes for the aforementioned discrepancies among reported VKTs in the literature.

### 3 Methodology

An agent-based traffic simulation package, called Commuter [2], has been utilised as the modelling tool for this research. Commuter uses a microscopic traffic flow model, meaning the interactions between vehicles are taken into account. It uses three well-known car-following and lane-changing models namely, Gipps, Wiedemann, and Fritzsche (used in this study). Users can also define their own car-following algorithms using the tool's Application Programming Interface (API) [2, 12, 13].

In Commuter, each traveller and vehicle is considered an agent, and any information related to it is recorded over the course of the simulation. In this program, simulating the movement of empty AVs on the real network is also possible as opposed to the other models appraised in Sect. 2. Travel demand in Commuter is defined to the model through a matrix similar to other simulation tools such as Vissim and Aimsun.

Due to spatiotemporal characteristics of travel demand, AMoD systems are liable to become imbalanced in terms of vehicle availability within the network. In this study, a real time optimum rebalancing model developed by [28] has been implemented. This algorithm is responsible for sending idle AVs to service customers in areas where no AV exists so that the total induced eVKT remains minimum in the system. In other words, whenever rebalancing algorithm is invoked, it distributes idle vehicles within the network such that system reaches again to a stable condition without the need to scaling up the fleet size. To date, this algorithm has only been tested in Matlab, which is a low fidelity simulation tool.

In order to embed this rebalancing model into Commuter, a code was written in Java, and installed in the model as a new plugin. Once the simulation is run, at the end of each specific time-step (e.g. each 5 min), an optimal Linear Program (LP) is



solved by the simplex method based on the current information the model receives from the network, and sends idle AVs from where they are accumulated to where they are needed. This time-step will be referred to as Optimisation Time-Step (OTS) throughout the paper. In other words, OTS is the amount of time the fleet operator has to wait before rebalances the AVs. In fact, the optimisation process minimises the total induced eVKT within the network.

Note, although the travel demand has already been imported to the model, the rebalancing algorithm takes no account of that and distributes the idle AVs without any a priori information. That is to say, the travel demand is assumed unknown to the fleet operator in this study.

Let  $v_i(t)$  be the total number of vehicles available at station  $i$ . Now, if station  $i$  has  $c_i(t)$  customers, then the excess vehicles at station  $i$  is  $v_i^{excess}(t) = v_i(t) - c_i(t)$ . These are the vehicles that station  $i$  has currently available to send to other stations in need. Thus, the total number of excess vehicles in the system is  $\sum_i v_i^{excess}(t) = V - \sum_i c_i(t)$ . Note that by definition,  $\sum_i v_i(t) = V$ . At the end of a time-step, the excess vehicles will be sent by solving for the objective function (1). The objective function represents minimisation of the total travel time experienced by unoccupied AVs, which will ultimately result in minimum eVKT in the system.

$$\min (\text{eVKT}) = \min \sum_{i,j} T_{ij} \text{num}_{ij} \tag{1}$$

Subject to,

$$v_i^{excess}(t) + \sum_{j \neq i} (\text{num}_{ji} - \text{num}_{ij}) \geq v_i^d(t) \quad \text{num}_{ij} \in N \forall i, j \in N, i \neq j \tag{2}$$

where,

$\text{num}_{ij}$ : number of rebalancing vehicles from station  $i$  to station  $j$  ( $\text{num}_{ij}$  is reverse for  $\text{num}_{ji}$ )

$T_{ij}$ : travel time from station  $i$  to station  $j$

$v_i^d(t)$ : desired number of vehicles at station  $i$  at time  $t$  following rebalancing

$v_i^{excess}(t)$ : excess vehicles at station  $i$  at time  $t$ .

For this study,  $v_i^d(t)$  is assumed zero, which means that at the time of optimisation, AMoD stands with an excess number of vehicles would send all their idle vehicles upon request, and stands with a deficit number of vehicles would receive as many vehicles as pick-up requests are logged at those AMoD stands. In other words, if  $v_i^d(t)$  were assumed one for a sender stand, it would send all its idle vehicles except one vehicle, which will remain at the AMoD stand. Similarly, if  $v_i^d(t)$  is assumed one for a receiver stand, it would receive as many vehicles as it needs plus one more vehicle.

It is obvious that the proper determination of  $v_i^d(t)$  could only happen when demand is certain, which is difficult to predict. For example, if it is known that there is an upcoming demand at a station (say one person will come in 2 minute-time), the system will keep one idle vehicle to service this forthcoming request. Similarly, this

pre-emptive action could apply to receiver AMoD stands. Note that investigating the optimum approaches of determining  $v_i^d(t)$  is out of the scope of this paper.

If constraint (2) is rewritten considering that  $v_i^d(t)$  is zero, and  $v_i^{excess}(t) = v_i(t) - c_i(t)$ , constraint (3) becomes:

$$\sum_{j \neq i} (num_{ji} - num_{ij}) \geq c_i(t) - v_i(t) \quad num_{ij} \in N \forall i, j \in N, i \neq j \quad (3)$$

## 4 Study Area and Travel Demand

Part of Melbourne with an area around 88.75 km<sup>2</sup> (Fig. 1), which features 95 signalised intersections was chosen as the case study for this research. Travel demand is imported into the model through centroids located at the centre of blocks shown in Fig. 1, whose sides range from 200 to 700 M across the whole study area. These centroids will be referred to as Origins and Destinations (ODs) in the current paper. In fact, ODs are the places where trips originate or end during the simulation period. In total, the study area consists of 53 ODs.

A hypothetical travel demand, constituted of 2000 trip requests have been employed in this study. All trips happen within the study area, meaning both trip origins and destinations are located inside the boundaries shown in Fig. 1. Further, it is assumed that the central parts of the study area attract more trips than the other regions. In other words, central parts of the city are more attractive than other areas, and as a result receive more travel.

No through traffic has been considered in the modelling environment, and the simulation is conducted only for the morning peak (07:00–09:00 am).

## 5 Simulation Framework

In the present model, first, a Base Case (BC) scenario that represents the current condition in which all travellers use their own private vehicles to arrive in the desired destinations would be considered. The BC scenario would be followed by several AMoD scenarios in order to explore the potential impacts of these systems on the current situation. It is worth noting that, calibration and validation of these scenarios is not feasible given AMoD systems are not operational yet.

For this study, a station-based AMoD system has been configured so that there is an AMoD stand at each centroid (Fig. 1), where customers can be picked-up or dropped-off by the AVs. In other words, in this system, travellers would have to walk from their residences to these stations to be able to use the AMoD service provided.

In this paper, we have assumed that demand is uncertain to the fleet operator and vehicle rebalancing is performed without any priori information. As a result, the initial number of AVs would be distributed equally between different stations within

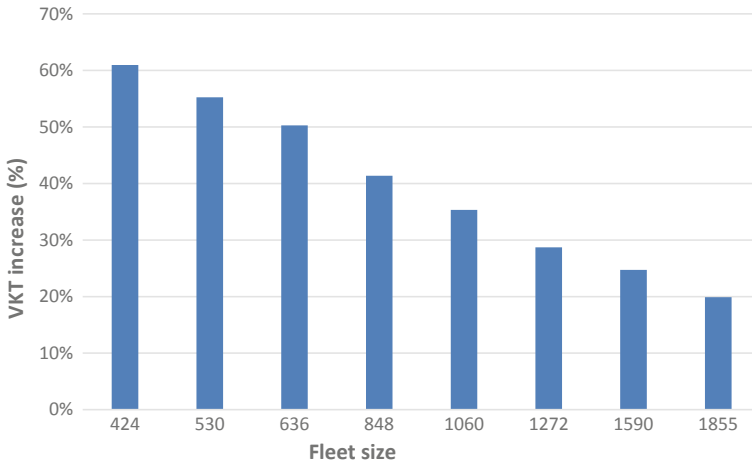


Fig. 1 The study area and spatial distribution of ODs within that

the study area. Further, it is assumed that trips are one-way travels among origins and destinations. Note that for the all AMoD scenarios, OTS would always be set to 5 min.

When customers enter any station if no AV is available, they would wait up to 15 min. Travellers would leave the station if no AV were found within 15 min. In the current modelling framework in two conditions, a customer could receive an AV:

1. There is an occupied AV on the way to the station where the customer is waiting. In this case, the AV can pick-up the waiting customer after having its on-board passenger dropped-off.



**Fig. 2** Amount of increase in VKT for different AMoD fleet sizes

2. Otherwise, the customer should wait until the next rebalancing process is performed. It means, in the meantime, no AV will be assigned from the neighbouring stations to service the waiting customer.

In this paper, no ride-sharing has been modelled including car-pooling or dynamic ride sharing such as the one discussed in [15]. In other words, in this study, the AMoD scenarios represent car-sharing systems in which each AV serves only one traveller at a time. These travellers are the ones who used to drive their own vehicles in the BC scenario.

For the AMoD scenarios, we deployed eight different fleet sizes ranging from 424 to 1855 AVs. All fleet sizes are shown in Fig. 2. The minimum fleet size was selected so that all the travel requests were met for the OTS of 5 min. That is to say, through simulation, different fleet sizes were examined and finally it became clear that 424 AVs is the smallest fleet size that could meet the whole demand. Afterwards, the fleet size was gradually scaled up such that we could track the general change in the performance of the system.

Note, the fleet sizes must be chosen such that the equal distribution of AVs between 53 AMoD stations is possible. For instance, when fleet size is 848, each station would have 16 vehicles (i.e.  $848/53 = 16$ ) at the start of the simulation.

## 6 Simulation Results

This section reports on the simulation outputs of nine scenarios conducted in this study. The obtained results suggest that all the AMoD fleet sizes successfully met the whole travel demand with passenger waiting times always less than 5 min.

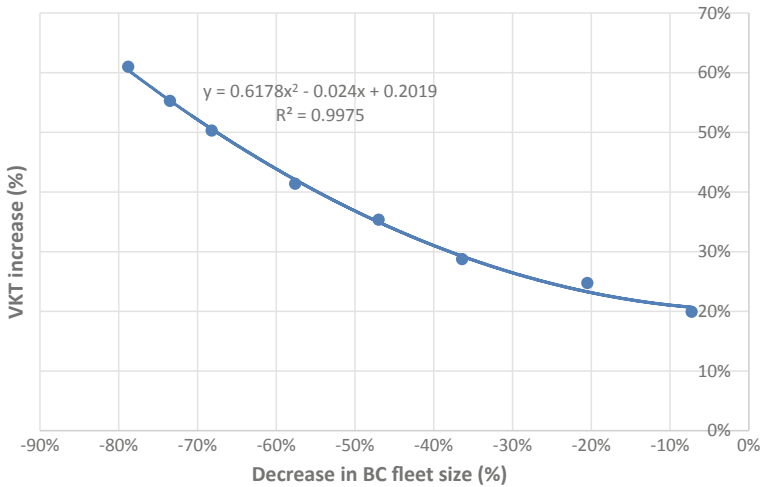


**Fig. 3** The relationship between the amount of decrease in the BC fleet size and VKT

The model, however, shows that AMoD scenarios lead to significant increase in VKT compared to the BC scenario. As shown in Fig. 2, the AMoD system featuring 424 AVs would translate into 61% more VKT in the network. As the fleet size grows, the increase in VKT drops gradually. The least increase in VKT (20%) has been recorded for the AMoD system comprised of 1855 AVs.

Note that the estimated VKTs in this study are much higher than the ones suggested in many studies in the literature. Most of the available AMoD models e.g. [4, 16, 17] suggest a VKT increase around 10% for the fleet size, almost 90% smaller than the BC one. Whereas our model suggests 61% increase in VKT with the AMoD fleet size (424 AVs), 79% smaller than the current fleet size.

Figure 3 shows how VKT increases as the fleet size is cut down. Each point on this graph represents an AMoD fleet size described in comparison to the BC fleet size. For instance, we can represent the AMoD system made up of 424 AVs as a system 79% smaller than the BC fleet size and so on. As clear from Fig. 3, there is a quadratic relationship between fleet size and VKT.

The key reason for these discrepancies might be rooted in some simplifying assumptions that have been made in these studies. For instance, these studies moved rebalancing AVs on Euclidean distances between different areas rather than simulating them on the real network. This could certainly translate into less VKT in the network.

Further, unlike our model, these studies assumed a perfect knowledge of demand and provided as many AVs as required at the start of simulation, which is quite unrealistic. Rebalancing of AVs at the start of simulation could generate considerable amounts of eVKT.

These disparities might also be due to the fact in these models, a high percentage of travellers have shared ride with other customers. These studies, however, have never

mentioned the inclusion of ride-sharing scenarios in their modelling environment. Obviously, employing ride-sharing services especially with high car-occupancy rates would result in unrealistic impression regarding the contributions of AMoD systems.

Difference between the Travel Demand Pattern (TDP) of these studies and ours might be another factor that has led to these discrepancies. The effects of this phenomenon is discussed in the next section.

## 7 Effects of Travel Demand Pattern on VKT

In this section, we aim at investigating the effects of TDP on the potential increase in VKT as a result of deploying AMoD systems. To achieve this, in addition to the TDP used in the previous section (D1), three other hypothetical TDP constituted of 2000 trip requests would be introduced into the model namely, D2, D3, D4. In other words, all demands (D1, D2, D3, D4) feature the same amount of travel requests (2000 trips) with different TDPs.

In this paper, TDP will be represented by the distribution of a parameter, called Net Trip Rate Ratio (NTRR) within the study area along with their associated Standard Deviation (SDV) values. By definition, for each TDP ( $D_j$ ), the value of NTRR for each area ( $i$ ) will be computed as follows,

$$NTRR_{ij} = \frac{\text{Total number of incoming trips to area } i}{\text{Total number of outgoing trips from area } i} \quad (4)$$

where,

$NTRR_{ij}$  : net trip-rate ratio of area  $i$  when TDP is  $D_j$

The value of SDV for the whole study area when TDP is  $D_j$  will be calculated as follows,

$$SDV_j = SDV(NTRR_{1j}, NTRR_{2j}, \dots, NTRR_{ij}) \quad (5)$$

where,

$SDV_j$  : Standard deviation of NTRR values for the whole study area when TDP is  $D_j$ . For this study,  $i \in (1, 2, 3, \dots, 53)$  and  $j \in (1, 2, 3, 4)$

By definition, if the NTRR for an area is equal to 1, then it attracts as many trips as it generates. On the other hand, if the NTRR is zero, this indicates this area does not attract any trips. Similarly, an area will attract more trips than it generates if its NTRR is more than 1.

The distribution of NTRR within the study area for each TDP and their related SDV is shown in Fig. 4. As clear from the graph, in the first and second TDPs (D1, and D2), the central parts of the study area (i.e. area 9–34) have the highest NTRR values (5.50 for D1, 3.33 for D2) meaning these regions are popular in comparison to

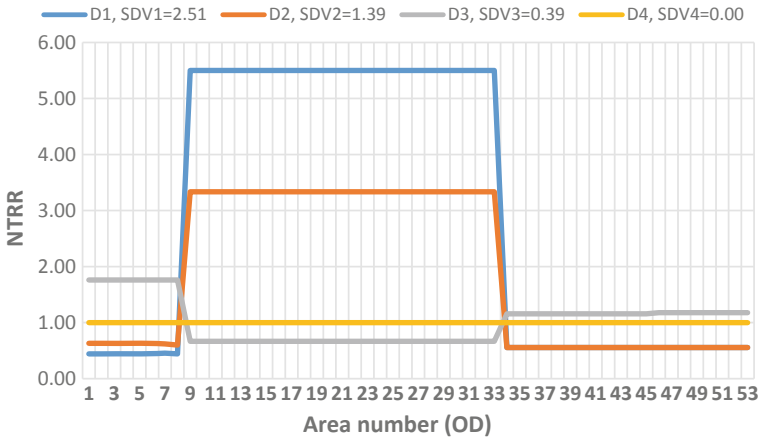


**Fig. 4** The distribution of NTRR within the study area for various travel demand patterns

the other areas.<sup>1</sup> While, for the third TDP (D3), the central parts of the study area are less attractive than other regions with a NTRR value of 0.67. Finally, for the fourth TDP (D4), the NTRR of the all areas within the study area is equal to 1, meaning the attractiveness of all regions is on a par.

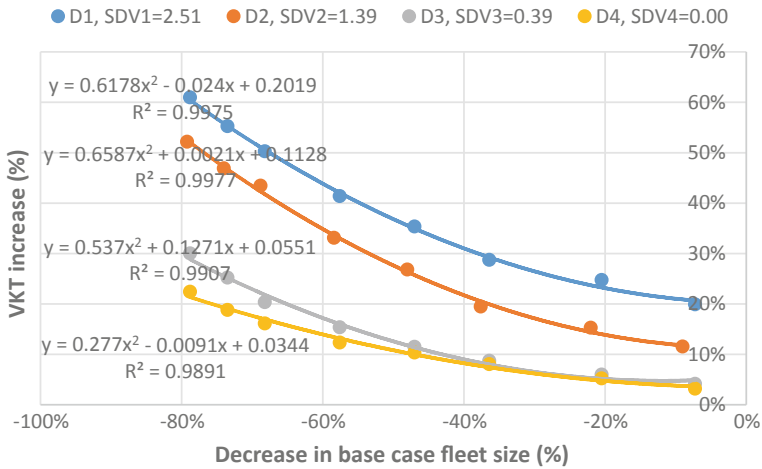
As shown in Fig. 4, as TDP moves from D1 to D4, the value of SDV gradually declines from 2.51 to 0. In fact, D1 represents the case in which the study area is constituted of regions with very different attractiveness levels, and as TDP approaches D4; all areas display an equal attractiveness.

It is most likely to observe a TDP, similar to D1 or D2 between suburbs and city centres over peak hours when most people travel from their residences to CBD for work. During off-peak hours, travel demand distribution within the city could approach D3 or D4. However, observing a TDP similar to D4 in reality is quite difficult.

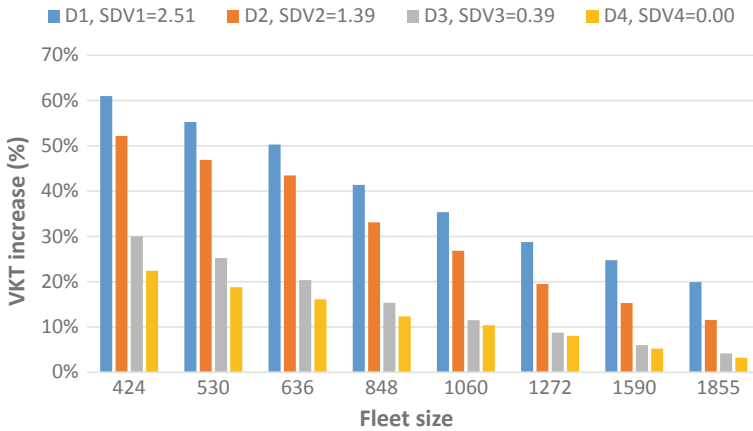
Figure 5 illustrates the simulation results for all 32 AMoD scenarios conducted in this section. Obviously, it shows there is still a quadratic relationship between fleet size and induced VKT irrespective of demand pattern. In other words, given the simulation results obtained through out this study, it can be deduced that there is always a quadratic relationship between fleet size and induced VKT irrespective of TDP. In this section, the all scenarios were successful in meeting the whole demand with customer waiting times always less than 5 min.

Figure 6, however, shows that demand pattern has a substantial effect on the induced VKT. As seen in this graph, for a specific fleet size there is a considerable difference between the VKT generated in each TDP. For instance, when fleet size is 424, the induced VKT for D1 is 39% more than that of D4. Note that the number of trips (demand) are the same (2000 trips) for all of the scenarios investigated in this section.

<sup>1</sup>Note that the NTRR values in D1 and D2 are the same (0.56) for the area 34–53 (Fig. 4).



**Fig. 5** The relationship between fleet size and VKT for a constant demand with various patterns



**Fig. 6** Induced VKT for different fleet sizes with a constant demand but various patterns

This happens due to the fact that in D1, customers in the non-attractive areas whose NTRR is so low could only be serviced through sending idle vehicles from the attractive areas (central parts in this study) whose NTRR is so high. Whereas, in D4, customers are not only reliant on rebalancing AVs to be serviced. Travellers in these areas could also be picked-up by AVs, carrying passengers from other parts of the city to this area.

The occupied AVs could pick-up waiting customers at these areas after having their on-board passengers dropped-off. In fact, the incoming travels from other parts of the urban area is the key reason, which have led to less VKTs in D4. While in D1, non-attractive areas could barely receive any trips from other parts. As a result, in



D1, the AMoD system is heavily dependent on the rebalancing process to meet the travel demand, which ultimately leads to high VKTs.

## 8 Policy Insights

The findings of this research are of direct relevance to policy makers and will help them arrive at informed and realistic decisions. Some of the policy insights gained from this research are outlined below.

1. Deploying AMoD systems for servicing customers within the whole urban area would lead to sizable increase in VKT if they are not shared. Therefore, implementing ride-sharing schemes in these systems is imperative in order to avoid the potential growth in congestion.  
Governments should also invest more in researching the possible factors influencing travellers to share rides with their fellow citizens. Having a realistic insight into people's travel behaviour and expectations would assist governments in introducing new schemes that encourage more ride-sharing.
2. Given that AMoD systems may lead to significant potential for increasing VKT in urban areas, they would be more suited for improving accessibility to current mass public transit systems particularly as related to first and last kilometre travel. Implementing shared AVs between residential areas and public transport stations and hubs would promote more mass transit use. In other words, introducing AMoD systems as first/last kilometre solutions could prompt more people to use them and reduce the number of vehicles on roads.  
Further, the increased interest in mass transit would attract more funds to enhance the current public transport systems, and thereby the number of travellers using these systems would grow. This strategy would not only cut VKT, but also establish a more sustainable mobility system.
3. This study, for the first time in the literature, proposed a method to explore the impacts of Travel Demand Patterns on the efficiency of AMoD systems. The results showed that this phenomena can substantially affect the efficacy of these systems and render them unsustainable.  
The study showed that deploying AMoD system during peak hours between suburbs and city centres might not be a viable solution to fix congestion problem in urban areas. Governments should also take this issue into account along with other decision factors while establishing new urban transport agendas in the age of emerging technologies.
4. Public transport investments, particularly high capacity rail, will remain critical even in future mobility scenarios. Together with walking and cycling, these should continue to be promoted as prominent modes of transport particularly in urban areas.
5. Transport policies and deployment strategies should consider the shape, type and size of AMoD fleets and ensure that the right mix between public transport

and shared vehicles is reached to minimise empty running and avoid increased congestion and emissions in cities.

6. Environmental benefits will depend on vehicle technology, car occupancy, and total VKT in the system. An AMoD fleet comprised of efficient and advanced AVs that deploys ride-sharing schemes will most likely succeed in delivering an environmentally friendly transport system.
7. To ensure the public transport industry remains viable and relevant, it needs to be more entrepreneurial and step forward to be an actor in shaping the regulatory frameworks and future use of AVs. Otherwise it will be mainly shaped by the automobile and technology companies. The industry can achieve this by supporting public transport AV trials to raise profile and increase public awareness. The regulatory frameworks will need to be adapted to allow public transport operators to innovate and launch such pilot studies.
8. Authorities should promote and adapt policies to prepare citizens for the shared use of vehicles. This can be achieved through demonstrating support, removing barriers and providing tax incentives to shared mobility schemes to support the trends in declining car ownership and favour shared ownership of vehicles. More shared mobility and more digital services today will lay the foundation for AV fleets and AMoD services tomorrow.
9. The commercial sector and provider of AMoD should design fare systems and pricing structures of mobility services that ensure the sustainability of the service. To the traveller, it will not matter in the future who will provide the service but more importantly the type and cost of the service. These services will need to be run in line with public policy goals to provide safe, clean, equitable, accessible and affordable mobility solutions.

## 9 Conclusions and Future Directions

This paper explored the performance of shared AMoD systems when travel demand is uncertain to the fleet operator. We explicitly investigated the relationship between AMoD fleet size and VKT and showed that there is a quadratic relationship among them.

The simulation results also showed that a large portion of the literature is overoptimistic about the potential of AMoD systems for mitigating congestion in urban areas. We proposed and discussed four possible causes, which might have led to this unrealistic optimism about AMoD systems.

Further, this study, for the first time, introduced a new measure called “travel demand pattern” for assessing the performance of AMoD systems. Our model suggests that this phenomenon has a significant impact on the efficiency of AMoD systems and the potential increase in VKT due to deployment of these systems. However, for different travel demand patterns, the general quadratic relationship between fleet size and VKT always holds.

The current study also showed that the worst performance of AMoD systems occur during peak hours between suburbs and city centres. That is to say, over peak hours when the majority of trips happen between suburbs and central parts of urban areas, implementing AMoD systems might even worsen the congestion level in the city.

In this paper, however, we did not consider the effects of ride-sharing scenarios on the performance of AMoD systems. In the future, we will quantify the implications of these systems in the presence of ride-sharing schemes as well.

Future studies could also make an effort to formulate the relationship between AMoD fleet size, VKT and the amount of increase in capacity due to need to fewer parking lots. Discovering this relationship will be a valuable contribution to the knowledge and assist us in gaining a more comprehensive insight into the potential of AMoD systems.

## References

1. Alonso-Mora, J., et al.: On-demand high-capacity ride-sharing via dynamic trip-vehicle assignment. In Goodchild, M. (ed.) *Proceeding of the National Academy of Science of the United States (PNAS)*, pp. 462–467. <http://www.pnas.org/content/114/3/462.full.pdf> (2017). Accessed 10 Apr 2017
2. Azalient: Commuter. <http://www.azalient.com/1.php> (2013)
3. Bischoff, J., Maciejewski, M.: Agent-based simulation of electric taxicab fleets. *Trans. Res. Proc.* [https://ac.els-cdn.com/S2352146514002981/1-s2.0-S2352146514002981-main.pdf?\\_tid=5ce5880c-b2d3-11e7-a2bf-0000aab0f6c&acdnat=1508200832\\_92c562321ddaf059e952239e87c6428b](https://ac.els-cdn.com/S2352146514002981/1-s2.0-S2352146514002981-main.pdf?_tid=5ce5880c-b2d3-11e7-a2bf-0000aab0f6c&acdnat=1508200832_92c562321ddaf059e952239e87c6428b) (2014). Accessed 17 Oct 2017. (Munich, Elsevier)
4. Bischoff, J., Maciejewski, M.: Simulation of city-wide replacement of private cars with autonomous taxis in Berlin. *Proc. Comput. Sci.* (2016) (Elsevier)
5. Bischoff, J., Nagel, K.: Integrating explicit parking search into a transport simulation. *Proc. Comput. Sci.* [https://ac.els-cdn.com/S1877050917310906/1-s2.0-S1877050917310906-main.pdf?\\_tid=6fb9929e-b877-11e7-ae35-0000aab0f6b&acdnat=1508821058\\_5bcb0a2dbd58fc51a31f0b11a38fea67](https://ac.els-cdn.com/S1877050917310906/1-s2.0-S1877050917310906-main.pdf?_tid=6fb9929e-b877-11e7-ae35-0000aab0f6b&acdnat=1508821058_5bcb0a2dbd58fc51a31f0b11a38fea67) (2017). Accessed 24 Oct 2017 (Elsevier)
6. Boesch, P.M., Ciari, F., Axhausen, K.W.: Autonomous vehicle fleet sizes required to serve different levels of demand. *Trans. Res. Rec. J. Trans. Res. Board* **2542**, 111–119. <http://trrjournalonline.trb.org/doi/10.3141/2542-13> (2016). Accessed 16 Mar 2017
7. Brownell, C., Kornhauser, A.: A driverless alternative. *Trans. Res. Rec. J. Trans. Res. Board* **2416**, 73–81. <http://trrjournalonline.trb.org/doi/10.3141/2416-09> (2014). Accessed 16 Oct 2017
8. Burghout, W., Rigole, P.J., Andreasson, I.: Impacts of shared autonomous taxis in a Metropolitan area. In: *Transportation Research Board 94th Annual Meeting* (2015)
9. Burns, L.D., Jordan, W.C., Scarborough, B.A.: Transforming personal mobility. <http://wordpress.ei.columbia.edu/mobility/files/2012/12/Transforming-Personal-Mobility-Aug-10-2012.pdf> (2012)
10. Chen, T.D., Kockelman, K.M., Hanna, J.P.: Operations of a shared, autonomous, electric vehicle fleet: Implications of vehicle and charging infrastructure decisions. *Trans. Res. Part A Policy Pract.* **94**, 243–254. <http://www.sciencedirect.com/science/article/pii/S096585641630756X> (2016). Accessed 19 Apr 2017
11. Dia, H. & Javanshour, F.: Autonomous shared mobility-on-demand: Melbourne pilot simulation study. *Trans. Res. Proc.* 285–296. <http://www.sciencedirect.com/science/article/pii/S2352146517301709> (2017). Accessed 27 June 2017 (Istanbul, Elsevier)

12. Duncan, G.: Commuter user's manual (2013)
13. Duncan, G.: From microsimulation to nanosimulation: visualizing person trips over multiple modes of transport. *Trans. Res. Board (TRB)* **2175**(15), 130–137 (2010)
14. Fagnant, D.J., Kockelman, K.M.: Dynamic ride-sharing and fleet sizing for a system of shared autonomous vehicles in Austin, Texas. *Transportation* 1–16. <http://link.springer.com/10.1007/s11116-016-9729-z> (2016). Accessed 16 Mar 2017
15. Fagnant, D.J., Kockelman, K.M.: Dynamic ride-sharing and optimal fleet sizing for a system of shared autonomous vehicles. In: *Proceedings of the 94th Annual Meeting of the 19 Transportation Research Board in Washington DC*. Washington DC. <https://pdfs.semanticscholar.org/e960/62a0e83885f41d2d83090989c71aec44f2a5.pdf> (2015). Accessed 16 Oct 2017
16. Fagnant, D.J., Kockelman, K.M.: The travel and environmental implications of shared autonomous vehicles, using agent-based model scenarios. *Trans. Res. Part C Emerg. Technol.* **40**, 1–13 (2014)
17. Fagnant, D.J., Kockelman, K.M., Bansal, P.: Operations of a shared autonomous vehicle fleet for the Austin. *Trans. Res. Board (TRB)*, **2536** (2015)
18. Horl, S.: Agent-based simulation of autonomous taxi services with dynamic demand responses. *Proc. Comput. Sci.* 899–904. <http://www.sciencedirect.com/science/article/pii/S1877050917310943> (2017). Accessed 17 Oct 2017 (Elsevier)
19. Horni, A., Nagel, K., Axhausen, K.: The multi-agent transport simulation MATSim. In: 2016th ed. Horni, A., Nagel, K. (eds.) Ubiquity Press. <http://www.ubiquitypress.com/site/books/10.5334/baw/> (2016). Accessed 16 Mar 2017
20. ITF: Urban mobility system upgrade: How shared self-driving cars could change city traffic (2015)
21. Jackson, J.R.: Networks of waiting lines. *Oper. Res.* **5**(4), 518–521. <http://pubsonline.informs.org/doi/abs/10.1287/opre.5.4.518> (1957). Accessed 26 May 2017
22. Kane, M., Whitehead, J.: How to ride transport disruption—a sustainable framework for future urban mobility. *Aust. Plan.* 1–9. <https://www.tandfonline.com/doi/full/10.1080/07293682.2018.1424002> (2018). Accessed 9 June 2018
23. Kornhauser, A., et al.: Uncongested mobility for all: New Jersey's area-wide aTaxi system (2013)
24. Lazarus, J., et al.: Shared automated mobility and public transport. In: Springer, Cham, pp. 141–161. [http://link.springer.com/10.1007/978-3-319-60934-8\\_13](http://link.springer.com/10.1007/978-3-319-60934-8_13) (2018). Accessed 9 June 2018
25. Levin, M.W., et al.: A general framework for modeling shared autonomous vehicles with dynamic network-loading and dynamic ride-sharing application. *Comput. Environ. Urban Syst.* **64**, 373–383. [http://ac.els-cdn.com/S019897151630237X/1-s2.0-S019897151630237X-main.pdf?\\_tid=88a6ddd2c-8ee5-11e7-a347-00000aacb361&acdnat=1504250395\\_dc74d0b6c822eac4bacd9dee7ac24634](http://ac.els-cdn.com/S019897151630237X/1-s2.0-S019897151630237X-main.pdf?_tid=88a6ddd2c-8ee5-11e7-a347-00000aacb361&acdnat=1504250395_dc74d0b6c822eac4bacd9dee7ac24634) (2017). Accessed 1 Sept 2017
26. Liu, J., et al.: Tracking a system of shared autonomous vehicles across the Austin, Texas network using agent-based simulation. *Transportation*, 1–18. <http://link.springer.com/10.1007/s11116-017-9811-1> (2017). Accessed 16 Oct 2017
27. Milakis, D., van Arem, B., van Wee, B.: Policy and society related implications of automated driving: a review of literature and directions for future research. *J. Intell. Trans. Syst.* **21**(4), 324–348. <https://www.tandfonline.com/doi/full/10.1080/15472450.2017.1291351> (2017). Accessed 16 Oct 2017
28. Pavone, M., et al.: Robotic load balancing for mobility-on-demand systems. *Int. J. Robot. Res.* **31**(7), 839–854 (2012)
29. Shen, W., Lopes, C.: Managing autonomous mobility on demand systems for better passenger experience. In: *Principles and Practice of Multi-Agent Systems*. Springer international publishing, pp. 20–35 (2015)
30. Spieser, K., et al.: Toward a systematic approach to the design and evaluation of automated mobility-on-demand systems: a case study in Singapore. In: Springer International Publishing, pp. 229–245. [http://link.springer.com/10.1007/978-3-319-05990-7\\_20](http://link.springer.com/10.1007/978-3-319-05990-7_20) (2014). Accessed 16 Mar 2017

31. Vazifeh, M.M., et al.: Addressing the minimum fleet problem in on-demand urban mobility. *Nature* **557**(7706), 534–538. <http://www.nature.com/articles/s41586-018-0095-1> (2018). Accessed 9 June 2018
32. Zhang, R., Pavone, M.: Control of robotic mobility-on-demand systems: A queueing-theoretical perspective. *Int. J. Robot. Res.* **35**(1–3), 186–203. <http://ijr.sagepub.com/cgi/doi/10.1177/0278364915581863> (2016). Accessed 30 Sept 2016

# Strategies to Increase the Response Rate of Smartphone-Based Travel Surveys in Afghanistan: Exploring the Effects of Incentives and Female Survey Conductors



Qudratullah and Takuya Maruyama

**Abstract** Smartphone-based travel surveys have been used widely in developed countries as promising alternatives to traditional travel data collection methods. In addition, researchers in developed countries have employed several strategies to increase response rate of the surveys. However, few studies have investigated these issues in developing countries. Therefore, to consider the case of a developing country, we conducted three smartphone-based travel surveys in two Afghanistan cities. The first survey was conducted in 2015 in Kabul. In 2017, we have conducted two additional surveys in Kabul and Khost cities. Two improvements were made to the survey method: offering rewards to increase response rate and appointing female survey conductors to target female participants. The main objectives of this study are: (1) to investigate the effect of rewards on the response rate. (2) to demonstrate female survey conductor's effects on female response rate. (3) to compare response rates of Khost and Kabul surveys. The results reveal that the overall survey response rate in Kabul increases significantly after the improvements are made to the survey method. Rewards have shown to increase male response rate, and female response rate is improved by female survey conductors.

**Keywords** Smartphone-based travel survey · Developing countries · Reward · Female survey conductors · Response rate

---

Qudratullah

Department of Civil and Architectural Engineering, Kumamoto University, 2-39-1 Kurokami, Kumamoto 860-8555, Japan

e-mail: [en\\_qudrat00@yahoo.com](mailto:en_qudrat00@yahoo.com)

Shaikh Zayed University, Khost, Afghanistan

T. Maruyama (✉)

Center for Water Resource, Marine Environment, and Disaster Management, Kumamoto University, 2-39-1 Kurokami, Kumamoto 860-8555, Japan

e-mail: [takumaru@kumamoto-u.ac.jp](mailto:takumaru@kumamoto-u.ac.jp)

© Springer Nature Singapore Pte Ltd. 2019

T. Mine et al. (eds.), *Intelligent Transport Systems for Everyone's Mobility*, [https://doi.org/10.1007/978-981-13-7434-0\\_18](https://doi.org/10.1007/978-981-13-7434-0_18)

# 1 Introduction

## 1.1 Background

Transportation researchers continuously attempt to collect comprehensive, accurate and temporal travel behavior data to develop transport planning policies. In traditional paper-based survey method, obtaining accurate travel behavior data such as the exact locations of origin and destination, travel time, trajectory of the recorded trip, and multi-day data is not an easy task [1, 5, 44]. Thus, the use of smartphones as a means of technological data collection, which have been found to improve data accuracy and efficiency, is a promising alternative to traditional survey methods [15, 43]. In contrast to other tools such as global positioning system (GPS), smartphones as personally-owned devices are ubiquitous and versatile that are rarely forgotten by users; the embedded GPS and accelerometer in smartphones reduces the burden of carrying an extra devices as well as instrument cost [3, 33].

In spite of these advantages of smartphone-based surveys method, some concerns such as battery drain and the different penetration rate of smartphones are main causes of recruiting small and nonhomogeneous samples [6, 13, 14, 48, 49]. In addition, the privacy concerns of the respondents may also negatively affect the response rate.

Another issue of smartphone-based travel surveys is that the experiences mainly been limited to developed countries, and the implementation of these types of survey in developing countries has not been fully investigated. Several studies have revealed that people in developed countries are more willing to participate in smartphone-based travel surveys than paper-based surveys [22, 46]. In particular, younger, wealthier, and more educated individuals have high smartphone-ownership rate, and those fall in this demographic are more willing to participate in smartphone-based travel surveys [35, 37, 51]. However, very little research has been conducted investigating the socioeconomic and demographic factors that influence the response rates of smartphone-based surveys in developing countries.

Researchers have been striving to implement strategies to increase the response rates and collect representative samples in smartphone-based travel surveys [36, 45]. One of these strategies is offering incentives to respondents in order to increase the response rate and collect a homogeneously distributed sample [31, 32, 34]. However, few literatures have examined the effects of incentives for smartphone-based surveys in developing countries.

Smartphones, internet, and other technological tools are expanding globally; however, the technology ownership gap between developed countries and developing communities still remains [38]. In addition, the level of education, literacy of using technology, and freedom of making decision to participate in smartphone-based survey may vary among large and rural cities which may result in different response rate.

Based on these motivations, this paper investigates strategies to increase response rate and studies the socioeconomic and demographic factors affecting response rate

in developing countries. As a case study, we examine the smartphone-based travel surveys conducted in a rural city and a large city of Afghanistan.

We conducted three smartphone-based travel surveys in Afghanistan. Our first survey was conducted in 2015 in Kabul without a participation incentive, and had a limited response rate. We found that a strategy is needed to increase the overall response rate. We also found that females are hard-to-reach population in traditional and patriarchal community of Afghanistan, and particular considerations are required to capture female respondents. For instance, our previous study revealed that cultural restrictions and privacy concerns may negatively affect response rate of female respondents in developing countries [41]. Considering these concerns, we conducted two additional smartphone-based travel surveys in 2017 with the following improvements.

- (1) Conducted surveys in rural city (Khost) as well as large city (Kabul)
- (2) Offered incentive to increase response rate
- (3) Assigned female survey conductors to target female participants

With the implementation of these improvements, this study aims to investigate the following issues using our smartphone-based travel survey data collected in 2015 and 2017 in Kabul and Khost cities.

- (1) Compare response rates of smartphone-based travel surveys in large and rural cities in Afghanistan
- (2) Compare response rates of surveys with and without reward
- (3) Demonstrate the effects of using female survey conductors on the female response rate

The current experiences of smartphone-based travel survey are limited to developed countries [4, 5, 12, 17, 18, 22, 23, 31, 33, 42, 47]. In the case of developing countries, the experience of this survey method is limited. Hence, the originality of this study is the investigation of smartphone-based travel surveys in Afghanistan as a developing country. In addition, investigating the effects of different strategies (e.g., incentive and female survey conductors), and residential area type (e.g., rural and large cities) on response rate is another contribution of this study.

The structure of this paper is organized as follows: Sect. 2 focuses on the literature review of passive and active data. Section 3 explains the methodology of our smartphone-based travel survey. Section 4 is allocated for the results analysis and discussions, and Sect. 5 includes a summary of our findings and conclusions.

## 2 Literature Review

The recent advancements in technology (e.g., GPS, smartphones, and so on) provide opportunities for automatic collection of a larger amount of data with a higher accuracy compared to the traditional survey methods. In the field of transportation, several technological tools (e.g., GPS, mobile phones, and so on) have been used



for data collection. Data can be automatically collected from several sources such as: fixed-location sensors (e.g., roadside sensors for vehicle counting data collection), installed sensors on moving objects (e.g., GPS installed on the vehicles), and mobile phones and smartphones [19]. Technological devices allow researchers to obtain passive data (e.g., from mobile phone) and active data (e.g., from smartphone applications) for transportation. The merits and demerits of passively-generated and actively-collected datasets are described in the following subsections.

## ***2.1 Passive Data Collection***

Capturing massive amounts of spatial and temporal data from individuals is one of the significant advantages of recent technological advancements. Passive data can be collected from various sources. For instance, smart card datasets [2, 8, 24, 30, 53], mobile phone datasets [11, 21, 50, 54], and GPS installed in taxis [29, 55]. Smart cards and taxis with installed GPS sources can be used for particular groups of people. For example, smart card datasets can provide insight into the travel patterns of users of public transport, and the travel behaviors of taxi drivers and passengers can be captured from the GPS installed in the taxis. The mobile phone, as a ubiquitous versatile product, has become an integral part of everyday life. Therefore, data collection through mobile phones is a reliable and widely used method for capturing the mobility patterns of individuals [11]. Hence, researchers and transportation planners have attempted to use this device for collection of data from individuals for transportation [20]. There are two ways (call detail records and sighting records) that can offer the opportunity to obtain an individual's movement data using a mobile phone [11]. In the call details record (CDR) dataset, each phone call represents an observation. In order to channel the call to the cell tower, the cellular network operator system needs to know the location of the individuals who initiate/receive calls. Hence, information such as the location of caller/callee, the start time of the call, and the duration of the call can be recorded in the cellular network operation system [10, 11, 26]. Another type of mobile phone dataset is sightings data [9, 10, 11]. In the sightings dataset, each record represents the change in the position of the mobile phone. There are various factors that distinguish CDR data from the sightings data. The sightings data have higher temporal (a single call in CDR can generate a single record while the same call may generate multiple sightings if the caller/callee change their positions during the call) and spatial (the recording location is the location of the cellphone tower in CDR, while the recording location in sightings is the device location) resolutions when compared to the CDR data. In addition, the information from both the caller and callee can be simultaneously observed for each call in the CDR, while it cannot be observed in the case of sightings data collection [3, 9, 11]. The collection of massive amounts of data and real positioning are the dominant merits of passive data. However, there are several shortcomings in passively-generated data such as:

1. *Lack of individual attribute information*: Due to privacy concerns of individuals, the passive dataset usually comprises anonymized records. In other words, the demographic and socioeconomic information of individuals cannot be obtained from passive data sources [7, 9, 19, 28, 30].
2. *Sample unrepresentativeness*: There are several concerns regarding the representativeness of the sample. Passive data sources can provide insight into travel patterns of particular groups. For instance, the smart card can only capture the travel pattern of individuals who use public transport. In the case of GPS data from taxis, the data can only collect the behaviors of drivers and passengers. The concern of sample unrepresentativeness also exists for mobile phone data. While some mobile phone users may own several devices, others may have only one or no mobile phone. In addition, the frequency of using mobile phones varies among people. Therefore, most of the sample consists of those who own mobile phones and frequently use the device; the sample lacks data for those who rarely use mobile phones or have no mobile devices. Furthermore, the penetration rate of the mobile phone may vary among cellphone carriers. Hence, using single cellphone carrier data may lead to an unrepresentative sample collection [9, 11, 16].
3. *Inaccurate measurements*: In the passive data obtained from mobile phones, the term “displacement” has been used instead of travel distance. Displacements are straight-line distances between two consecutive records. Therefore, the accuracy of these measurements can be low [11].

The route and mode choice cannot be easily obtained from passive data collected through mobile phones. Some researchers have attempted to infer the route choice by using the intermediate point between the origin and the destination. Overlaying the intermediate points with the transport networks may help to determine the possible route choices [11]. In addition, the trip purpose cannot be directly derived from the passive data obtained from mobile phones. However, for obtaining the trip purpose, researchers have used several methods such as frequency-based measurements (e.g., return home if the location was frequently visited during night time, work-based trip if the location was frequently visited during day time) [39], and statistical approaches (e.g., using regression models for predicting the location type) [10].

In the case of actively-collected dataset, smartphone-based travel survey is one of the promising methods for collection of individuals’ travel behaviors. The merits and drawbacks of this survey method are described in the subsection below.

## 2.2 Active Data Collection

Several studies have investigated the implementation of the active travel data collection using smartphones [31, 42, 52]. The embedded technology in the smartphones and the available survey apps have enabled researchers to obtain temporal, accurate, and effective travel information. In smartphone-based travel surveys, the survey app

allows respondents to validate their travel information (e.g., validating trip purpose, trip mode, and so on); this is not applicable in the case of passive data collection methods. In addition, the survey app can automatically record the travel distance, departure/arrival time, travel mode (e.g., by vehicle, on foot, or on a cycle), and so on. Unlike the passive data collection method, the recruitment of individuals to participate is the integrated part in the smartphone-based travel survey methods. Consenting individuals are then trained and guided to participate in the survey. If the respondents consented to participate, they have agreed to part with their data confidentiality and privacy. In addition, by using supplementary (e.g., web-based, paper-based) questionnaires, the collection of information on attributes (e.g., demographic, socioeconomic, and so on) of consenting individuals is possible in smartphone-based travel survey methods. Considering these unique features of smartphone-based travel survey methods, data accuracy, and ability to capture detailed information of respondents are the advantages of this data collection method when compared to the passively-generated data collection method.

Despite the abovementioned advantages of smartphone-based travel surveys, there are several shortcomings of this survey method such as:

1. *Small sample size and small amount of data:* The small size of the sample is one of the main concerns in smartphone-based travel survey methods. Therefore, several strategies have been used by researchers to increase the sample size of smartphone-based travel surveys. For instance, using incentives is an effective strategy for increasing the sample size [31, 48]. In addition, some technology-related (e.g., fast battery drain, slower device operation speed while app is running, and app malfunctioning) and respondent-related (e.g., concerns about being tracked) challenges are the main barriers for collecting long-term (several days) data from smartphone surveys [6, 13, 14, 17, 27, 33, 34, 40, 42, 48, 51].
2. *Cost issues:* Active data collection through smartphone-based travel surveys necessitates several financial costs. For example, the internet consumption by the survey app and provision of incentive to attract individuals can incur financial burden for the researchers [31, 40]. This does not occur in the case of passive data collection.
3. *Sample unrepresentativeness:* The penetration rate of smartphones is different from country to country, and from population to population. Some studies have stated that the ease of accessibility to the internet and the smartphones devices is different for developed and developing countries [25, 38]. The inaccessibility to the internet and the low penetration rate of smartphones could adversely affect the sample representativeness. In addition, the choice to participate in smartphone-based surveys may not be random. Therefore, the unrepresentativeness of the sample is one of the dominant concerns in the smartphone-based travel surveys as well as in methods involving passive data collection from mobile phones. This is one of the motivations of this research.

### 3 Methodology and Survey Overview

This survey was designed and implemented to investigate the feasibility of smartphone-based travel surveys in Afghanistan and to obtain daily trip information regarding each user's travel behaviors. The respondents were invited to participate in the survey through the personal network of the survey conductors. The respondents that consented were instructed to download and install the MOVES application. MOVES was an existing application, which was available for Android and iOS in Google Play and App Store, respectively, without cost. This application records temporal (travel time, departure and arrival time), spatial (location, travel distance) and mode (e.g., vehicle, walk, cycling) information.

Prior to starting the survey, face-to-face instructions regarding the use of the application were given to each participant. Moreover, a printed user guide and privacy policy documents were distributed to those who accepted our invitation. The user guide helps the respondents to download and install the application, generate an account using a provided ID, run the app, and stop running the app when the smartphone battery drains. Additional information, such as the survey objectives, security of the respondent's privacy, types of data, and usage of the data are described and provided in the privacy policy documents. Incentives were promised to the respondents, and those who successfully complete the two-week survey were entitled to the reward of 100 AFN to be provided as a phone credit.

#### 3.1 Survey Overview

Tables 1 and 2 summarize the survey recruitment methods and survey sample data, respectively. In 2015, 200 participants were recruited, and the response rates of male and female respondents were 36.2% and 40.0%, respectively. Furthermore, in 2017, the total recruited sample sizes of the Kabul and Khost surveys were 137 and 218, respectively. For Kabul survey, the male response rate was 70.5%, and the female response rate was 49.0%, while in Khost survey, the response rates were 52.2% and 23.2% for the male and female respondents respectively.

#### 3.2 Data Collection in 2015

In our survey of 2015 in the city of Kabul, the respondents were recruited through the personal networks of the research team. The overall response rate was low for both males and females [41]. The survey conductor team consisted of males, and due to some traditional restrictions, a small sample size of females were collected. The personal information (gender, age, occupation, and smartphone ownership history) of the consenting participants was collected through a web-based question-

**Table 1** Survey recruitment methods

Survey items	Kabul survey (Aug 2015)	Kabul survey (Sep 2017)	Khost survey (Sep 2017)
Survey period	1 month	2 months	2 months
Application	MOVES	MOVES	MOVES
Incentive	Not offered	100 AFG	100AFG
Gender of survey conductors	Male	Male and female	Male and female
Requested participation period	2 weeks	2 weeks	2 weeks

**Table 2** Overview of survey samples

Demographic information	Kabul survey (Aug 2015)		Kabul survey (Sep 2017)		Khost survey (Sep 2017)	
	n	%	n	%	n	%
<b>Total (Recruited)</b>	200	100	137	100	218	100
<b>Gender</b>						
Male	135	67.5	88	64.2	123	56.4
Female	65	32.5	49	35.8	95	43.6
<b>Response</b>						
Male	49	65.3	62	72.1	65	75.0
Female	26	34.7	24	27.9	22	25.0
<b>Response rate<sup>a</sup></b>						
Male		36.2		70.5		52.8
Female		40.0		49.0		23.2

<sup>a</sup>Response rate = (Agreed participants/Total)

naire. However, we were not able to collect the personal information of those who rejected the invitation, with the exception of gender and apparent age. Therefore, this knowledge was used to improve the recruitment methods and conduct two additional smartphone-based travel surveys in 2017.

### 3.3 Data Collection in 2017

In 2017, we conducted two smartphone-based travel surveys reinforced by paper-based questionnaires in the cities Kabul and Khost. In these surveys, the following strategies were implemented to increase the sample sizes and obtain more detailed information.

- Providing an incentive as mobile credit of 100 AFG (equivalent to approximately 1.2 USD) to increase sample sizes and investigate its effect on the response rate
- Appointing female survey conductors to target female and increase their response rates
- Obtaining information from non-respondents through a paper-based questionnaire

Prior to starting the main survey, a pilot survey was conducted to ensure that the survey worked as intended. Furthermore, feedback was received from the respondents of the pilot survey, which allowed us to enrich the survey documentation. For instance, the feedback from the respondents of the pilot survey allowed us to add answers and more detailed information to the Frequently Asked Questions documentation. In the pilot survey, we recruited 38 and 59 respondents in Kabul and Khost, respectively. From these recruits, 22 respondents in Kabul and 19 respondents in Khost agreed to participate in our survey, and the data collected during this stage was added and analyzed in combination with the data obtained from the main surveys.

The main surveys were conducted following the pilot survey. We recruited 137 individuals in Kabul, and from these recruits, 62 males and 24 females accepted the invitation and participated in the survey. The non-consenting respondents consisted of 26 males and 25 females. In the city of Khost, we recruited 218 people, and 65 males and 22 females agreed to participate in the survey. The number of those who declined their participations were 58 males and 73 females, as outlined in Tables 3 and 4.

**Table 3** Response and non-response rate of Kabul survey (2017)

		Response rate		Non-response rate		Total	
		n	%	n	%	n	P-value
Gender	Male	62	70.5	26	29.5	88	0.013*
	Female	24	49.0	25	51.0	49	
Age	Age < 30	45	70.3	19	29.7	64	0.087
	Age > 31	41	56.2	32	43.8	73	
Marital status	Married	52	65.0	28	35.0	80	0.52
	Single	34	59.6	23	40.4	57	
Education	Educated	80	70.1	34	29.9	114	$6.6 \times 10^{-5}$ **
	Uneducated	6	26.0	17	74.0	23	
Occupation	Employed	54	68.3	25	31.7	79	0.11
	Unemployed	32	55.0	26	45.0	58	

\* $p < 0.05$ ; \*\* $p < 0.01$

**Table 4** Response and non-response rate of Khost survey (2017)

		Response rate		Non-Response rate		Total	
		n	%	n	%	n	P-value
Gender	Male	65	52.8	58	47.2	123	$9.0 \times 10^{-6**}$
	Female	22	23.1	73	76.9	95	
Age	Age < 30	55	44.7	68	55.3	123	0.09
	Age > 31	32	33.6	63	66.4	195	
Marital status	Married	52	38.5	83	61.5	135	0.44
	Single	35	43.8	45	56.2	80	
Education	Educated	86	47.5	95	52.5	181	$1.0 \times 10^{-5**}$
	Uneducated	1 <sup>a</sup>	2.9	33	97.1	34	
Occupation	Employed	45	43.3	61	56.7	106	0.55
	Unemployed	42	39.3	67	60.7	109	

\*\* $p < 0.01$ , <sup>a</sup>Due to small number of uneducated respondents, the fisher exact test has been applied

## 4 Results and Discussion

### 4.1 Response Rate of Kabul Survey (2017)

After the improvements made to the survey, the overall response rate of Kabul survey is 62.8%, while male and female have response rate of 70.5% and 49.0% respectively. A significant difference between male and female response rates is confirmed after conducting statistical test ( $p = 0.013 < 0.05$ ), as shown in Table 3. This significant difference may be due to females rejecting their participations on the basis of traditional restrictions and privacy concerns.

Figure 1 reveals the response rate in term of age and gender. The lowest response rate (22.2%) of female aged under 20 could be due to their dependency on male member of family in patriarchal society of Afghanistan. Male over 51 years of age show the lowest response rate (25.0%), which may be due to their less familiarity of using smartphones. However, the difference of response rate between respondents aged under 30 and over 31 years of age is not statistically significant ( $p = 0.087 > 0.05$ ), as shown in Table 3.

The response rates are also shown for each gender and marital status in Table 3. Those who are married have a response rate of 65.0%, while those who are single have a response rate of 59.6%, though this difference is not statistically significant ( $p = 0.52 > 0.05$ ). As shown in Fig. 2, single females have the lowest response rate (30.0%), whereas single males have the highest response rate (75.7%). The lowest response rate being single females may be due to their dependency regarding decision-making rights.

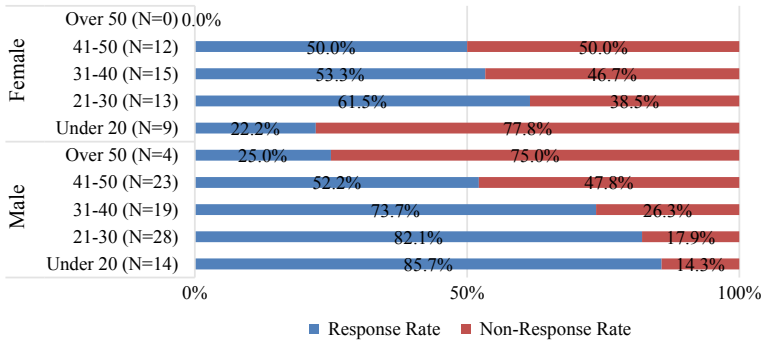


Fig. 1 Response and non-response distribution by gender and age (Kabul)

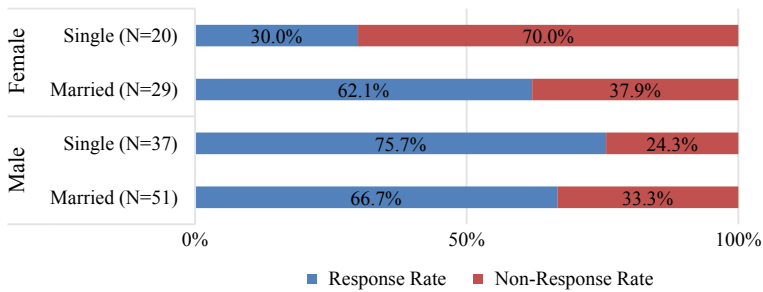


Fig. 2 Response and non-response distribution by gender and marital status (Kabul)

The difference in response rates between single and married males is not statistically significant ( $p = 0.36 > 0.05$ ), whereas the difference between single and married females is statistically significant ( $p = 0.02 < 0.05$ ). The difference between the response rates of married males and married females is not statistically significant ( $p = 0.68 > 0.05$ ), whereas the difference is significant between single males and single females ( $p = 8 \times 10^{-4} < 0.01$ ).

Figure 3 compares the response rates in terms of education level for both genders. Those classified as illiterate have the highest non-response rates of 73.3 and 75.0% for males and females, respectively. The results confirm a statistically significant difference in the response rates between those who are literate (school-educated and university-level individuals) and those who are illiterate ( $p = 6.6 \times 10^{-5} < 0.01$ ), as shown in Table 3. More specifically, when statistically comparing the response rates of the literate and illiterate groups for both genders, it is confirmed that the difference in male response rates for those two groups is statistically significant ( $p = 4 \times 10^{-5} < 0.01$ ), while a statistically significant difference is not apparent for females of those two groups ( $p = 0.14 > 0.05$ ).

The effect of employment conditions on the response rate has also been considered. Male students have the highest response rate (86%), while the highest response rate for females is the private organization workers category (78%). A statistical test



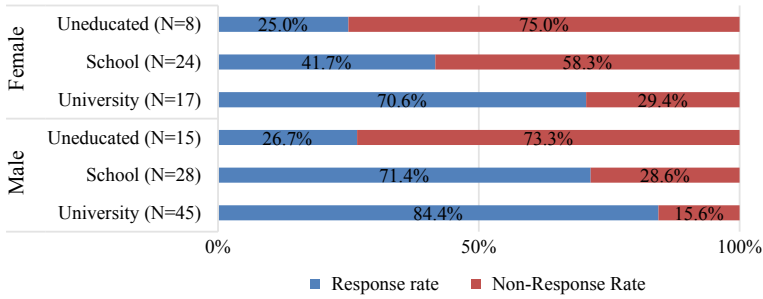


**Fig. 3** Response and non-response distribution by gender and education level (Kabul)

reveals that the response rate difference between those that are employed (government employees, private organization workers, and self-employed) and those that do not hold a job (students and unemployed) is not statistically significant ( $p = 0.11 > 0.05$ ), as shown in Table 3.

### 4.2 Response Rate of Khost Survey (2017)

The overall response rate of Khost survey is 40%, while that rate of male and female is 52.8 and 23.2% respectively. A significant difference between male and female response rates is confirmed after conducting statistical test ( $p = 9.0 \times 10^{-6} < 0.01$ ) as shown in Table 4. This significant difference could be due to traditional and privacy concerns of females. Please note that 3 females strongly declined their participations and we could not able to record their demographic (except their gender and apparent age) and socioeconomic information.

Figure 4a reveals the response rates in term of age and gender. Males over 41 years of age have the lowest response rate (23.8%), while females under 20 and over 41 years of age share lowest response rates of 15.2 and 15%, respectively. It is confirmed that the difference in the response rates of those under 30 and over 31 years of age is not statistically significant ( $p = 0.09 > 0.05$ ), as shown in Table 4.

Figure 4b explains the response rates in term of marital status for each gender. Single females have the lowest response rate (21.9%), while their male counterparts have the highest response rate (58.3%). A statistically significant difference between married and single respondents is not observed ( $p = 0.44 > 0.05$ ), as shown in Table 4. More specifically, the response rate difference between single and married males is not statistically significant ( $p = 0.33 > 0.05$ ), and such is the case for females ( $p = 0.6 > 0.05$ ), as shown in Fig. 4b. We also compared the response rates of married males and married females, as well as between single males and single females; statistically significant differences are confirmed in both cases ( $p = 9.0 \times 10^{-3} < 0.01$  and  $p = 1.2 \times 10^{-3} < 0.01$ , respectively).

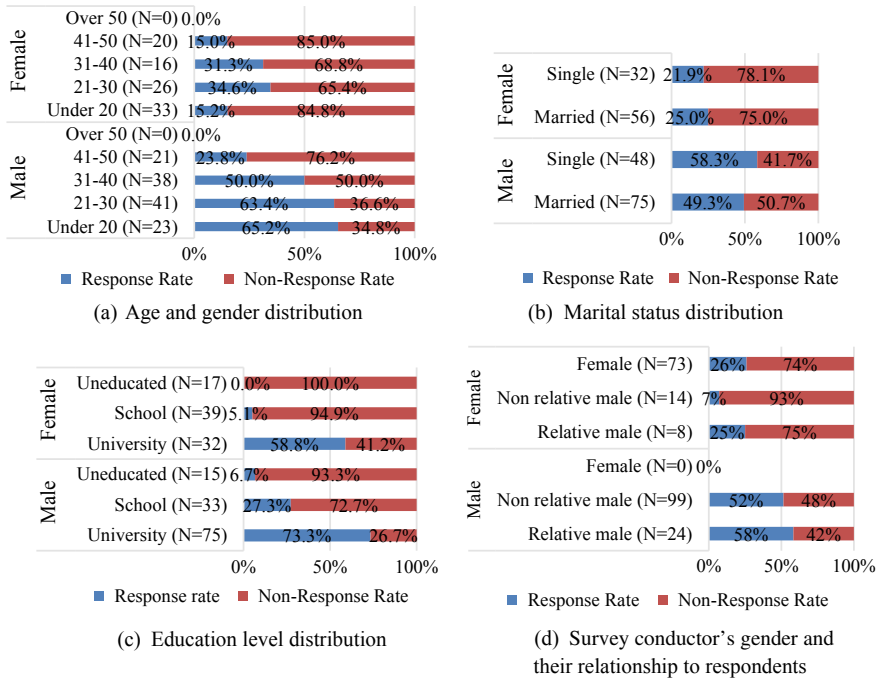


Fig. 4 Response and non-response rate distribution of Khost survey (2017)

Figure 4c compares the response rates in terms of education level for both genders. Those who are illiterate have the highest non-response rates of 93.3% and 100% for males and females, respectively. The response rate differences between those who are literate and those who are illiterate is statistically significant ( $p = 1.0 \times 10^{-5} < 0.01$ ). These differences may be due to the increased familiarity of smartphone usage for the educated respondents compared with those who are less educated.

We have also considered the effects of employment conditions on the response rates. Male students and female government employees have the highest response rates of 71% and 57%, respectively. In addition, the response rates of the unemployed, self-employed, and private organizational female workers are zero. This may be due to their unfamiliarity with smartphone usage and privacy concerns. A statistical test between those who are employed (government employees, private organization workers, and self-employed) and those who do not hold a job (students and unemployed) does not show a statistically significant difference ( $p = 0.55 > 0.05$ ), as shown in Table 4.

Figure 4d describes the response rates of males and females in terms of genders of the survey conductors and their relationships with the respondents. We conducted a statistical test between the response rates and non-response rates of females recruited by males, and females recruited by females, and the difference is not statistically significant ( $p = 0.22 > 0.05$ ), as shown in Fig. 4d. Please note that the female

**Table 5** Comparison of response and non-response rates of Khost and Kabul (2017)

		Response rate		Non-Response rate		Total	
		n	%	n	%	n	<i>P-value</i>
Male	Kabul	62	70.5	26	29.5	88	$9.9 \times 10^{-3**}$
	Khost	65	52.8	58	47.2	123	
Female	Kabul	24	49.0	25	51.0	49	$1.6 \times 10^{-3**}$
	Khost	22	23.2	73	76.8	95	
Both gender	Kabul	86	62.8	51	37.2	137	$2.7 \times 10^{-5**}$
	Khost	87	40.0	131	60.0	218	

\*\* $p < 0.01$

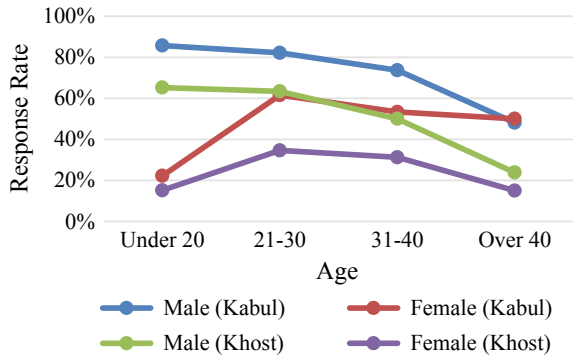
survey conductors did not attempt to recruit male respondents; however, all survey conductors were requested to target the respondents without considering gender.

### 4.3 Comparison of Response Rate in Kabul and Khost Surveys (2017)

The overall response rate of Kabul survey is 62.8%, whereas the overall response rate for the Khost survey is 40.0%. We compared the response rates from these two surveys, and the difference is statistically significant ( $p = 2.7 \times 10^{-5} < 0.01$ ), as shown in Table 5. More specifically, the difference between the response rates of the two surveys in terms of males and females is also statistically significant ( $p = 9.9 \times 10^{-3} < 0.01$  and  $p = 1.6 \times 10^{-3} < 0.01$ , respectively). The main reason behind these differences can potentially be attributed to the concern of smartphone battery drainage in rural locations because there is no accessibility to public electricity. The high non-response rate of rural females may be due to traditional restrictions that force them to reject survey participation.

Figure 5 compares the response rates of the Kabul and Khost surveys in terms of age and gender. The response rate declines greatly with increasing age of the male participants in both surveys. Moreover, the middle-age female participants have the highest response rate, while response rates of younger and elderly females are lower. The lower response rate of younger females may be due to their dependency on male family members. In addition, the lower response rate from elderly respondents may be due to their relatively lower education level and unfamiliarity with smartphone usage.

**Fig. 5** Response rate distribution in term of age and gender of (Kabul and Khost)



### 4.4 Investigation of Incentive and Female Survey Conductors Effects

To investigate the effects of incentives, we compared the response rates from the 2015 survey without an incentive and the 2017 survey with an incentive. It is confirmed that the difference between the response rates of the two surveys is statistically significant ( $p = 5.0 \times 10^{-6} < 0.01$ ), as shown in Table 6. Thus, we can conclude that this difference is likely due to the improvements made to the 2017 survey methods.

To determine the improvement in the results for each gender, the response rates of each gender are statistically compared. The difference in the male response rates is statistically significant ( $p = 6.1 \times 10^{-7} < 0.01$ ), while the difference in the female response rates is not statistically significant ( $p = 0.33 > 0.05$ ), as shown in Table 6. From these results, we can conclude that the strategies implemented to increase the

**Table 6** Comparison of response and non-response rates of Kabul (2015 and 2017)

		Response rate		Non-Response rate		Total	P-value
		n	%	n	%		
Male	Kabul (2017)	62	70.5	26	29.5	88	$6.1 \times 10^{-7**}$
	Kabul (2015)	49	36.2	86	63.8	135	
Female	Kabul (2017)	24	49.0	25	51.0	49	0.33
	Kabul (2015)	26	40.0	39	60.0	65	
Under 30	Kabul (2017)	45	70.3	19	29.7	64	$1.2 \times 10^{-3**}$
	Kabul (2015)	48	44.9	59	55.1	107	
Over 31	Kabul (2017)	41	56.2	32	43.8	73	$4.2 \times 10^{-4**}$
	Kabul (2015)	27	29.0	66	71.0	93	
Total	Kabul (2017)	86	62.8	51	37.2	137	$5.0 \times 10^{-6**}$
	Kabul (2015)	75	37.5	125	62.5	200	

\*\* $p < 0.01$

response rate may vary between genders. An incentive will significantly increase the male response rate, whereas the female response rate will not be greatly affected by an incentive.

We also considered the effects of incentives on younger and elderly respondents. The response rates of the younger respondents (under 30 years of age) from the 2015 survey and 2017 survey were statistically compared, and the test shows that the difference is statistically significant ( $p = 1.2 \times 10^{-3} < 0.01$ ). We also compared the response rates of those over 31 years of age from both surveys, and a statistically significant difference ( $p = 4.2 \times 10^{-4} < 0.01$ ) is confirmed, as shown in Table 6. We can conclude that the use of incentives for increasing the response rate is effective for both younger and elderly respondents; however, the younger respondents are more affected than the elderly. In the case of developed countries, offering incentive is an effective strategy in order to improve response rate of smartphone-based travel survey. For instance, [31] reported that the effects of incentive was significant on the improvement of response rate of smartphone-based travel survey conducted in the city of Kumamoto, Japan.

In the 2015 survey, females were less likely to participate in the survey due to the male survey conductors. Considering this fact, we assigned female survey conductors to target and recruit females in the 2017 survey. Figure 6a reveals that females are more willing to join the survey if the survey conductors are female. A statistical test confirms that the difference between the response rates of females recruited by males and those recruited by females is significant ( $p = 3.18 \times 10^{-5} < 0.01$ ), as shown in Fig. 6a. The reason behind this significant difference may be due to cultural restrictions, as females may feel more comfortable communicating with other females. In addition, we instructed that the conductors recruit respondents without considering gender, but the female survey conductors did not attempt to recruit male respondents. Furthermore, we have also compared the female response rates of the 2015 survey without female survey conductors with the response rates of female recruited by females in survey of 2017, and a statistical significant difference ( $p = 0.001 < 0.01$ ) is confirmed, as shown in Fig. 6b. Considering these significant differences, we can conclude that it is important to consider gender in smartphone-based surveys in traditional communities, such as Afghanistan. These findings may be not applicable in the case of developed countries, since there could be no traditional restrictions against females' participation.

## 5 Conclusion

This study aimed to investigate the effects of survey method improvements on increasing the response rates of smartphone-based travel surveys in Afghanistan. We conducted three smartphone-based travel surveys in the cities of Kabul and Khost. The first survey was conducted in Kabul in 2015, and the other two surveys were simultaneously conducted in Kabul and Khost in 2017. The high non-response rate of the 2015 survey led us to improve the recruitment methods to generate an increased

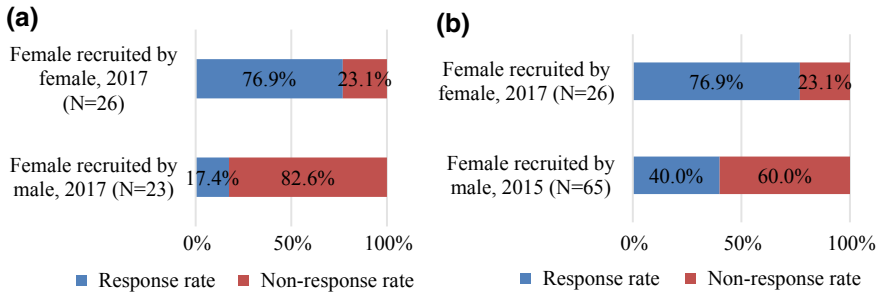


**Fig. 6** Female survey conductor’s effects on respondent’s recruitment

response rate in the 2017 surveys. The improvements employed in the 2017 survey were as follows:

- (1) Conducted smartphone-based travel surveys in the rural city Khost, and the capital city, Kabul
- (2) Offered an incentive of 100 AFN (approximately equivalent to 1.2 USD) to respondents who participate in the survey for two weeks
- (3) Included female survey conductors to target female respondents

The overall response rate of the survey in Kabul increased significantly after the survey improvements were implemented. Various studies in developed countries have demonstrated that an incentive can be a useful strategy in increasing the response rates of young people, regardless of gender. However, in the case of a developing country, we found that the effects of incentives differ between males and females, and the impacts of an incentive differ depending on a rural or urban environment.

The following conclusions were obtained from this study:

- (1) The response rate of the survey varies between capital residents and rural communities.
- (2) Incentives have a significant impact on increasing the overall response rate of the smartphone-based survey. However, the effect of an incentive differs between the younger and elderly.
- (3) Recruiting female participants by male survey conductors is a sensitive issue in traditional countries, and thus, female survey conductors significantly increase the response rate of females.

Therefore, unlike developed countries, it is necessary to take certain countermeasures for increasing the response rates of smartphone-based surveys in developing countries, taking the cultural and traditional backgrounds into consideration.

Based on the data collected from our surveys in 2017, we propose further investigation of the factors associated with the non-responses in the Kabul and Khost surveys. In addition, analyzing the GPS data from our surveys to generate trip and time related measurements is a future research consideration.

## References

1. Alio, X.D., Marquet, O., Guasch, C.M.: Keeping track of time: A smartphone-based analysis of travel time perception in suburban environment. *Travel Behav. Soc.* **9**, 1–9 (2017)
2. Alsger, A., Tavassoli, A., Mesbah, M., Ferreira, L., Hickman, M.: Public transport trip purpose inference using smart card fare data. *Trans. Res. Part C* **87**, 123–137 (2018)
3. Asakura, Y., Hato, E., Maruyama, T.: Behavioral data collection using mobile phones. In: Rasouli, S., Timmermans, H., (ed.) *Mobile technologies for activity-travel data collection and analysis*. Heshey PA, USA, 17–35 (2014)
4. Assemi, B., Jafarzadeh, H., Mesbah, M., Hickman, M.: Participants' perceptions of smartphone travel surveys. *Trans. Res. Part F* **54**, 338–348 (2018)
5. Berger, M., Platzler, M.: Field evaluation of the smartphone-based travel behavior data collection app "SmartMo". *Trans. Res. Proc.* **11**, 263–279 (2015)
6. Bhat, C.R.: Conducting travel survey using portable devices-challenges and research needs. *Trans. Res. Proc.* **11**, 199–205 (2015)
7. Boyd, D., Crawford, K.: Critical questions for big data. *Inf. Commun. Soc.* **15**(5), 662–679 (2012)
8. Briand, A.S., Côme, E., Trépanier, M., Oukhellou, L.: Analyzing year-to-year changes in public transport passenger behavior using smart card data. *Trans. Res. Part C* **79**, 274–289 (2017)
9. Calabrese, F., Diao, M., Lorenzo, G.D., Jr, J.F., Ratti, C.: Understanding individual mobility patterns from urban sensing data: a mobile phone trace example. *Trans. Res. Part C* **26**, 301–313 (2013)
10. Chen, C., Bian, L., Ma, J.: From traces to trajectories: How well can we guess activity locations from mobile phone traces? *Transp. Res. Part C* **46**, 326–337 (2014)
11. Chen, C., Ma, J., Susilo, Y., Liu, Y., Wang, M.: The promises of big data and small data for travel behavior (aka human mobility) analysis. *Transp. Res. Part C* **68**, 285–299 (2016)
12. Comendador, J., López-Lambas, M.E.: Pain and joy of a panel survey on transport studies. *Trans. Res. Proc.* **18**, 248–255 (2016)
13. Cottrill, C., Pereira, F., Zhao, F., Dias, I., Lim, H., Ben-Akiva, M., Zegras, P.: Future Mobility Survey: Experience in developing a smartphone-based travel survey in Singapore. *Transp. Res. Rec.* **2354**, 59–67 (2013)
14. Danalet, A., Mathys, N.A.: The potential of smartphone data for national travel surveys. Paper presented at the 17th Swiss transport research conference, Monte Verità/Ascona, 17–19 May 2017 (2017)
15. Demissie, M., Phithakkitnukoon, S., Sukhvibul, T., Lisboa Bento, B.C.: Inferring passenger travel demand to improve urban mobility in developing countries using cell phone data: a case study of Senegal. *IEEE Trans. Intell. Transp. Syst.* **17**, 2466–2478 (2016)
16. Experian Simmons: The 2011 mobile consumer report. <http://www.experian.com/assets/simmons-research/white-papers/experian-simmons-2011-mobile-consumer-report.pdf> (2011). Accessed 19 Aug 2018
17. Gadzinski, J.: Perspective of the use of smartphones in travel behavior studies: findings from a literature review and a pilot study. *Transp. Res. Part C* **88**, 74–86 (2018)
18. Geurs, K.T., Thomas, T., Bijlsma, M., Douhou, S.: Automatic trip and mode detection with MoveSmarter: First results from the Dutch mobile mobility panel. *Trans. Res. Proc.* **11**, 247–262 (2015)
19. Gohar, M., Muzammal, M., Rahman, A.: SMART TSS: Defining transportation system behavior using big data analytics in smart cities. *Sustain. Cities Soc.* **41**, 114–119 (2018)
20. Gonzalez, M.C., Hidalgo, C.A., Barabasi, A.L.: Understanding individual human mobility patterns. *Nature* **453**(5), 779–782 (2008)
21. Gould, J.: Cell phone enabled travel survey: the medium moves the message In: Zmud, J., Lee-Gosselin, M., Munizaga, M., Carrasco, J.A. (eds.) *Transportation survey methods*, 1st edn. Bingley, UK, pp. 51–70 (2013)
22. Greaves, S., Ellison, R., Rance, D., Standen, C., Rissel, C., Crane, M.: A web-based diary and companion smartphone app for travel/activity surveys. *Trans. Res. Proc.* **11**, 279–310 (2015)

23. Hoogendoorn-Lanser, S., Schaap, N.T.W., OldeKalte, M.: The Netherlands mobility panel: an innovative design approach for web-based longitudinal travel data collection. *Trans. Res. Proc.* **11**, 311–329 (2015)
24. Ingwardson, J.B., Nielsen, O.A., Raveau, S., Nielsen, B.F.: Passenger arrival and waiting time distributions dependent on train service frequency and station characteristics: A smart card data analysis. *Trans. Res. Part C* **90**, 292–306 (2018)
25. Internet live stats. <http://www.internetlivestats.com/internet-users/afghanistan/> (2016). Accessed 19 Aug 2018
26. Iqbal, S., Choudhury, C.F., Wang, P., González, M.C.: Development of origin–destination matrices using mobile phone call data. *Transp. Res. Part C* **40**, 63–74 (2014)
27. Ketelaar, P.E., Van, B.M.: The Smartphone as your follower: The role of smartphone literacy in the relation between privacy concerns, attitude and behavior toward phone-embedded tracking. *Comput. Hum. Behav.* **78**, 174–182 (2018)
28. Kitchin, R.: The real-time city? Big data and smart urbanism. *Geo J.* **79**, 1–14 (2014)
29. Liu, Y., Kang, C., Gao, S., Xiao, Y., Tian, Y.: Understanding intra-urban trip patterns from taxi trajectory data. *Geo. Syst.* **14**, 463–483 (2012)
30. Long, Y., Thill, J.C.: Combining smart card data and household travel survey to analyze job–housing relationships in Beijing. *Comput. Environ. Urban Syst.* **53**, 19–35 (2015)
31. Maruyama, T., Sato, Y., Nohara, K., Imura, S.: Increasing smartphone-based travel survey participants. *Trans. Res. Proc.* **11**, 280–288 (2015)
32. Mohammadian, K., Bricka, S.: Conducting travel surveys using portable devices-role of technology in travel surveys. *Trans. Res. Proc.* **11**, 242–246 (2015)
33. Montini, L., Prost, S., Schrammel, J., Schussler, N.R., Axhausen, K.W.: Comparison of travel diaries generated from smartphones data and dedicated GPS devices. *Trans. Res. Proc.* **11**, 227–241 (2015)
34. Nitsche, P., Peter, W., Simon, B., Brandle, N., Maurer, P.: A strategy on how to utilize smartphones for automatically reconstructing trips in travel surveys. *Proc. Soc. Behav. Sci.* **48**, 1033–1046 (2012)
35. Nitsche, P., Peter, W., Simon, B., Brandle, N., Maurer, P.: Supporting large-scale travel surveys with smartphones—a practical approach. *Transp. Res. Part C* **43**, 212–221 (2014)
36. Pedersen, M.J., Nielsen, C.V.: Improving survey response rates in online panels: effects of low-cost incentives and cost-free text appeal interventions. *Soc. Sci. Comput. Rev.* **34**(2), 229–243 (2016)
37. Pew Research Center: App vs. web for surveys of smartphone users (2015)
38. Pew Research Center: Smartphone ownership and internet usage continues to climb in emerging economies (2016)
39. Phithakitnukoon, S., Horanont, T., Lorenzo, G.D., Shibasaki, R., Ratti, C.: Activity-aware map: identifying human daily activity pattern using mobile phone data. *Human Behav. Underst.* **6219**, 14–25 (2010)
40. Qudratullah, Maruyama, T.: Reasons for non-response to smartphone-based travel survey in two Afghanistan cities. *Asian Trans. Stud.* **5**(3), 523–542 (2019)
41. Qudratullah, Khalid, A., Maruyama, T., Sato, Y.: Investigating response, data sending, and completion rates of a smartphone-based travel survey conducted in Kabul, Afghanistan, presented at 15th World Conference on Transport Research - WCTR 2019 Mumbai 26–31 May (2019)
42. Safi, H., Assemi, B., Mesbah, M., Ferreira, L.: An empirical comparison of four technology-mediated travel survey methods. *J. Traffic Trans. Eng.* **4**(1), 80–87 (2017)
43. Sato, Y., Maruyama, T.: Examining difference between paper-based and web-Based self-Reported departure/arrival time using smartphone-based survey, to be presented at 15th World Conference on Transport Research-WCTR 2019 Mumbai 26–31 May (2019)
44. Shin, D., Aliaga, D., Tuncer, B., Arisona, S.M., Kim, S., Zund, D., Schmitt, G.: Using smartphones for transportation mode classification. *Comput. Environ. Urban Syst.* **53**, 76–86 (2015)
45. Stopher, P.: *Collecting, Managing, and Assessing Data Using Sample Survey*, 1st edn. Cambridge University Press, New York, USA (2012)



46. Susilo, Y., Woodcock, A., Liotopoulos, F.: Deploying traditional and smartphone app survey methods in measuring door-to-door travel satisfaction in eight European cities. *Trans. Res. Proc.* **25**, 257–2275 (2017)
47. Thomas, T., Puello, L.L.P., Geurs, K.: Intrapersonal mode choice variation: evidence from a four-week smartphone-based travel survey in the Netherlands. *J. Trans. Geogr.* (2018) (in press)
48. TRB Travel survey methods committee (ABJ40): The online travel survey manual: a dynamic documents for transportation professionals, chapter 26.0 using smartphones for travel behavior studies (2014). Accessed 20 Aug 2018
49. Vich, G., Marquet, O., Guasch, C.M.: Suburban commuting and activity spaces: using smartphones tracking data to understand the spatial extent of travel behavior. *Geogr. J.* **183**, 426–439 (2017)
50. Wang, Z., He, S.Y., Leung, Y.: Applying mobile phone data to travel behavior research: a literature. *Travel Behav. Soc.* **11**, 141–155 (2018)
51. Zegras, P.C., Li, M., Kilic, T., Lozano-Gracia, N., Ghorpade, A., Tiberti, M., Aguilera, A.I., Zhao, F.: Assessing the representativeness of a smartphone-based household travel survey in Dar es Salaam. *Tanzan. Trans.* **45**(2), 335–363 (2018)
52. Zhao, F., Pereira, F.C., Ball, R., Kim, Y., Han, Y., Zegras, C., Ben-Akiva, M.: Exploratory analysis of a smartphone-based travel survey in Singapore. *Transp. Res. Rec.* **2494**, 45–56 (2015)
53. Zhao, Z., Koutsopoulos, H.N., Zhao, J.: Individual mobility prediction using transit smart card data. *Trans. Res. Part C* **89**, 19–34 (2018)
54. Zhong, G., Yin, T., Zhang, J., He, S., Ran, B.: Characteristics analysis for travel behavior of transportation hub passengers using mobile phone data. *Transportation* (2018) (in press)
55. Zhu, J., Ye, X.: Development of destination choice model with pairwise district-level constants using taxi GPS data. *Transp. Res. Part C* **93**, 410–424 (2018)

# Sensing Information Dissemination Strategy for Collective Perception in VANET Based on the Relative Position of Vehicles and the Road Structure



Kaito Furukawa, Mineo Takai and Susumu Ishihara

**Abstract** Sharing local sensing data about objects in vicinity among the surrounding vehicles by using Vehicle-to-Vehicle (V2V) communication expands the perceptual range of vehicles as compared with a case of using only onboard sensors. In order to recognize the presence of non-V2V-equipped vehicles with high accuracy, vehicles need to receive messages containing information about vehicle locations in a non-line-of-sight region frequently. However, packet collisions caused by high vehicle density and the hidden terminal problem make it difficult to deliver messages containing sensing data about nearby vehicles. To ensure delivering sensing data of vehicles in non-line-of-sight regions, it is important to give high priority for sending packets to vehicles that are in better positions to observe obstacles and other vehicles. In this paper, we propose a strategy to control the sensing information transmission frequency based on the positional relationship of vehicles and road structure in order to improve the surrounding awareness of vehicles. Furthermore, we investigate the effectiveness of the proposed strategy through simulations.

**Keywords** Collective perception · VANET · V2V

## 1 Introduction

In recent years, vehicles equipped with Advanced Driver Assistance System (ADAS) applications have been becoming popular [1–3]. For example, they have functions for detecting obstacles by using onboard sensor equipment, e.g. RADAR and camera

---

K. Furukawa (✉) · S. Ishihara (✉)  
Shizuoka University, Hamamatsu 432-8561, Japan  
e-mail: [furukawa.kaito.17@shizuoka.ac.jp](mailto:furukawa.kaito.17@shizuoka.ac.jp)

S. Ishihara  
e-mail: [ishihara.susumu@shizuoka.ac.jp](mailto:ishihara.susumu@shizuoka.ac.jp)

M. Takai (✉)  
University of California, Los Angeles, CA, USA  
e-mail: [mineo@ieee.org](mailto:mineo@ieee.org)

Osaka University, Suita, Japan

© Springer Nature Singapore Pte Ltd. 2019  
T. Mine et al. (eds.), *Intelligent Transport Systems for Everyone's Mobility*, [https://doi.org/10.1007/978-981-13-7434-0\\_19](https://doi.org/10.1007/978-981-13-7434-0_19)

and supporting collision avoidance. Most of today's ADASs provide the driver with support for collision avoidance or avoidance of traffic congestion by detecting the presence of road participants within the Field-of-View (FoV) of their onboard sensors or Road Side Units (RSUs).

Today, vehicles with the Vehicle-to-Vehicle (V2V) communication function are sold in some regions. Vehicles equipped with the V2V communication function (hereinafter referred to as V2V-equipped vehicles) periodically broadcast messages (hereinafter referred to as beacons) containing its status information (e.g., position, speed, direction, etc.) to notify its presence to the surrounding vehicles in Vehicular Ad Hoc Network (VANET) [4]. The beacons improve the range of surrounding awareness of vehicles compared with a case that vehicles use only onboard sensors and do not have the V2V communication function. Nevertheless, it remains difficult to recognize the presence of vehicles that are out of the FoV of onboard sensors of vehicles and do not have a V2V communication function (hereinafter referred to as non-V2V-equipped vehicles). If RSUs detect the presence of out-of-sight vehicles by sensors and/or collect the location information from a vehicle that detects the presence by onboard sensors, vehicles can recognize the presence of vehicles by receiving the location information from the RSUs. However, RSUs are not fully installed on roads and It will be difficult to become such environments. We, therefore, assume that the RSUs are not installed in the rest of the paper.

In order to expand the range of surrounding awareness of vehicles, the collective perception technology recently collects much attention [5]. The concept of collective perception envisions sharing of sensing data obtained by onboard perception sensors, e.g., RADAR, camera, LIDAR, etc. between road participants. Location information of road participants detected by such sensors is attached to sensing data. Vehicles that receive the sensing data recognize the presences of other road participants. Figure 1 shows that a situation that the car A which does not detect the non-V2V-equipped car D being the out-of-sight perceives the presence of D using by collective perception. The authors of [5] evaluate the performance of a collective perception through real-world tests using a small number of vehicles [6]. The test results showed that a vehicle can recognize the presence of an obstacle installed on a road about three times faster than the case of without the collective perception.

On the other hand, they also mention that the collective perception suffers from scalability issues as the network grows. For V2V communication in US, Europe, and Japan based on IEEE 802.11 wireless LAN technology is used [7–9]. It uses Carrier

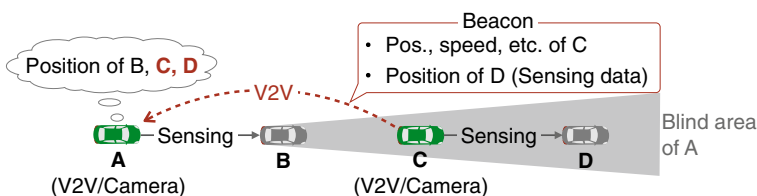


**Fig. 1** Detection of the presence of a car being out-of-sight using by collective perception

Sense Multiple Access/Collision Avoidance (CSMA/CA) as the access mechanism [10]. The higher the density of V2V-equipped vehicle periodically transmitting beacons, the more the vehicles on the network send a beacon simultaneously. Therefore, in such a situation, it is pointed out that the reception rate of beacons deteriorates due to collisions of beacons caused by high vehicle density, the hidden terminal problem and congestion of communication channels [11]. Accordingly, it becomes difficult to recognize the presence of the surrounding road participants with an accuracy for operating ADAS applications satisfactorily.

In order to satisfy the requirements of packet delivery in ADAS applications, we introduce a strategy for transmitting beacons from vehicles at important positions with relatively high transmission frequency in this paper. This strategy controls the frequency of beacon transmission and/or transmission power so that a vehicle with a sensor covering areas not covered by sensors of other vehicles can obtain more transmission opportunities based on a positional relationship of vehicles and road structure.

The remainder of this paper is organized as follows. In Sect. 2, we present work related to the transmission control of beacons in a vehicular network. Section 3 proposes the data transmission control strategy based on the positional relationship of vehicles and road structure. In Sect. 4, we investigate the range of surrounding awareness of vehicles in collective perception by simulation of a simple highway scenario when giving a high priority to vehicles at important positions. Finally, Sect. 5 concludes the paper and presents future direction of this study.

## 2 Related Work

When vehicle density is high, the packet collisions frequently occur and transmission delay increases due to the congestion of the communication channel and the hidden terminal problem. To reduce packet collisions and to improve the beacon reception rate, in such an environment, methods for controlling the beaconing have been proposed.

The authors of [12] propose Distributed Fair Power Adjustment for Vehicular Network (D-FPAV) that controls the transmission power of beacons based on channel utilization. Vehicles increase the transmission power until the beaconing load exceeds the maximum network load. As a result, D-FPAV can keep network load below a given constant, and vehicles can use channels fairly.

European Telecommunications Standards Institute (ETSI) standardizes Decentralized Congestion Control (DCC) algorithm as a part of medium access control (MAC) protocol of Vehicle-to-X (V2X) in Europe [13]. DCC controls transmission parameters (e.g., power, frequency, datarate, etc.) of beacons based on a Channel Busy Ratio (CBR). Vehicles estimate the current level of channel utilization and control the transmission parameters according to the level. Whenever an average received signal level in a vehicle exceeds a predefined threshold, the vehicle regards the current level of channel utilization as busy. In this case, the vehicle controls the

transmission parameters so that vehicles in the vicinity can receive beacons stably. On the other hand, if the vehicle does not regard the current level of channel utilization as busy, vehicles control the transmission parameters to deliver beacons to farther vehicles at a higher frequency.

Sommer et al. propose a method to control the transmission frequency of beacon based on an available channel capacity and a message utility, Adaptive Traffic Beacon (ATB) [14]. Vehicle detects the number of collisions and the Signal-to-Noise Ratio (SNR) of the beacon in the current communication channel. If the channel is overloaded, the beaconing period of the vehicles is extended, resulting in fewer beacons per time. In constant, if the channel is still underutilized, the beaconing frequency of the vehicles is increased up to a certain upper limit. The message utility is used to describe the importance of traffic information to be sent. This importance is estimated given information such as the distance to an event and the age of a message. ATB allows messages that have been sent by vehicles closer to an event and newer information to spread faster.

These methods essentially control beaconing based on the density of V2V-equipped vehicle and do not take into account the positional relationship of vehicles in terms of increasing the reliability of packet transmission and decreasing the transmission delay. Therefore, packets from vehicles in an important location, e.g. at the head of a cluster, where a vehicle can perceive obstacles in front of the cluster, could fail to deliver beacons to a vehicle that needs the information contained in the beacon packets. It is considered that vehicles capable of transmitting beacons useful for collision avoidance are different for individual vehicles depending on the positional relationship of the vehicles and road structure. In order to increase the transmission opportunities of such useful beacons and delivery the beacon with short transmission delay, we propose a strategy to control the transmission frequency based on the positional relationship of vehicles.

### 3 Data Transmission Control Strategy

In this section, we firstly present the problem of controlling the transmission power/frequency of the beacon according to vehicle density with some examples. Then, we propose a strategy for controlling beacon transmission according to the positional relationship of vehicles and road structure.

We classify the range of surrounding awareness of a vehicle into the following two areas: a *simple perception area* and an *extended perception area*. As shown in Fig. 2, we define a simple perception area as the area a vehicle can directly sense with its own sensors, and an extended perception area as the combined area of a vehicle's simple perception area and simple perception areas of other vehicles that have sent a beacon received by the vehicle.

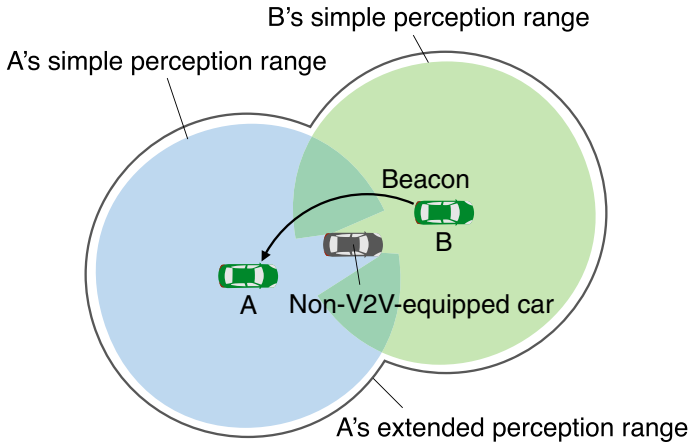


Fig. 2 Simple perception area and extended perception area

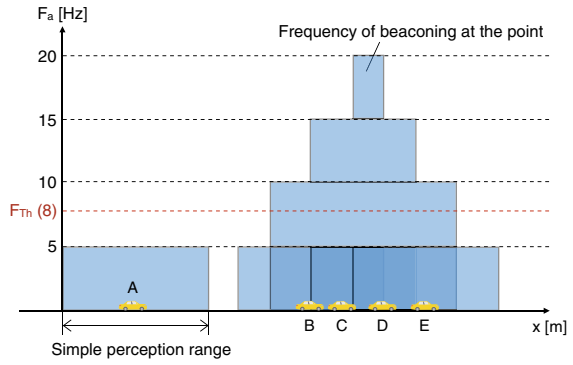
### 3.1 Why Is Vehicle Density-Based Traffic Control Not Always Effective?

#### 3.1.1 No Occlusion Case

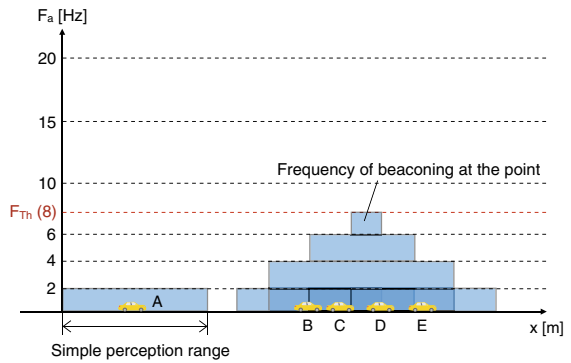
Figure 3 shows beacon transmission frequency of each vehicle on a road, and the aggregated beacon transmission frequency on the road. In this figure, we model a road in one-dimension for the sake of simplicity. We assume that the communication range of each vehicle is significantly long and the vehicles calculate the same vehicle density. We do not consider the effect of occlusion here. Each vehicle can always detect other vehicles and obstacles within its sensing range. In other words, the simple perception area of a vehicle and the sensing range of the vehicle are the same. The aggregated beacon transmission frequency of a location is calculated by summing the beacon frequency of onboard sensors of vehicles that are covering the location. Let  $F_T$  be the threshold of the transmission frequency of a beacon necessary for a vehicle to grasp the road conditions (including the existence of vehicles and obstacles) with sufficient accuracy to prevent accidents, and  $F_{Th} = 8\text{Hz}$  in Fig. 3. Let  $F_a$  be the aggregated frequency of beacon transmission of each location on the road. If two vehicles are in the same position and they have the same simple perception areas, the  $F_a$  in the areas is  $2F$ . If there is only one vehicle that has a simple perception area not overlapped with other vehicle's simple perception area,  $F_a$  in the simple perception area of the vehicle is  $F$ .

Figure 3a shows a case when the beacon transmission frequency of all vehicles is set to a constant value. If the transmission frequency of all the vehicles,  $F$  is 5, the transmission frequency of sensing information in a simple perception area of car A is 5Hz. Thus,  $F_a$  in the area is less than  $F_T$ . On the other hand,  $F_a$  in an area where the simple perception area of car B, C, D and E overlap is the sum of the

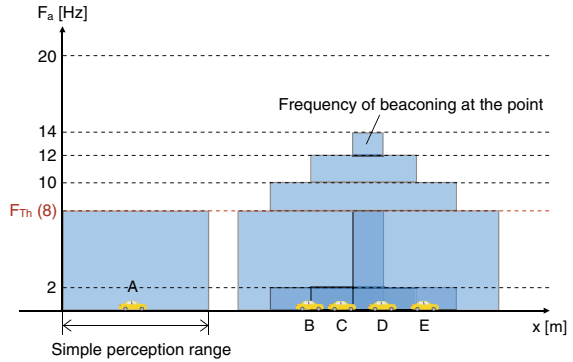
**Fig. 3** Aggregated transmission frequency of information



(a) All vehicles use a constant frequency.



(b) Vehicles reduce their beacon frequency according to vehicle density, "high".



(c) Simple perception area-based beacon transmission frequency control

$F$  of the vehicles. Therefore,  $F_a$  in the overlapping area is greater than  $F_T$ .  $F_a$  in the non-overlapping area, however, is less than  $F_T$ . In the most overlapping area,  $F_a$  ( $=20$ ) is more than twice of  $F_T$ . This means that beacons are being transmitted excessively.

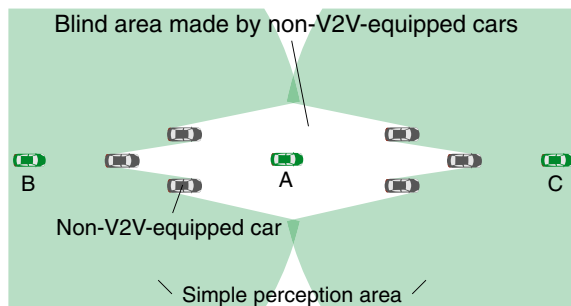
Figure 3b shows  $F_a$  of a case where beacon transmission frequencies of vehicles are controlled according to the vehicle density. If the vehicles regard the vehicle density is high, they will reduce their beacon transmission frequency. Let us assume  $F = 2$ . In such a case,  $F_a$  in the area where the simple perception areas mostly overlapped can be reduced. However, only the area satisfies the required condition  $F_a > F_{Th}$ .

Figure 3c shows a case of controlling the beacon transmission frequency by considering the overlap of the simple perception area of vehicles. In this case,  $F$  of a vehicle in the area with a small degree of overlap of simple perception areas is increased to 8. On the other hand, vehicles in the most overlapped area decrease their  $F$  to 2. As a result,  $F_a$  in the simple perception area of all vehicles satisfies  $F_T$ . In addition,  $F_a$  in the area where the simple perception area is the most overlapped is lower than when using a constant value of  $F$ .

### 3.1.2 Occlusion Case

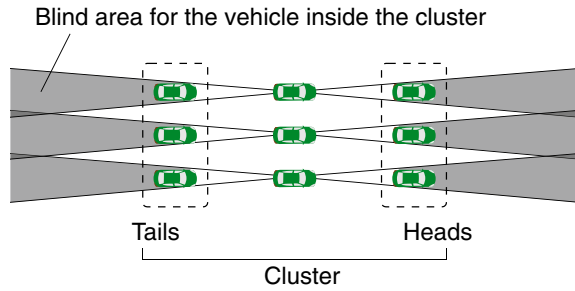
Figure 4 shows a situation where simple perception areas of V2V-equipped vehicles are blocked by bodies of non-V2V-equipped vehicles. In this case, the area surrounded by the non-V2V-equipped is out-of-sight of the V2V-equipped vehicles' sensors. Hereinafter, we refer to such an area as a blind area. If a V2V-equipped vehicle  $A$  is in a blind area, increasing the chance of sending beacons from  $A$  will assist other vehicles out of the blind area know the condition in the area. In a case when controlling beacon transmission frequency according to only vehicle density, each vehicle uniformly controls the beacon transmission frequency. Thus, the beacon transmission opportunity of vehicle  $A$  becomes the same as one of other vehicles and beacons transmitted by vehicle  $A$  become will be hard to be received by other vehicles. In order to increase the beacon transmission opportunity of  $A$ , the transmission

**Fig. 4** Blind area for V2V-equipped vehicles made by non-V2V-equipped vehicles





**Fig. 5** Blind area for vehicles inside a cluster



frequency of the vehicle  $B$  and  $C$  should be reduced. By this control, the blind area for vehicles  $B$  and  $C$  can be covered with high aggregated beacon frequency.

Figure 5 shows a cluster that is traveling by keeping a constant inter-vehicle distance and the blind area for vehicles inside the cluster. Sensors of vehicles in the head and the tail group of the cluster can observe an area that is not covered by sensors of other vehicles in the cluster. In a case when controlling beacon transmission frequency according to only vehicle density, as discussed above, the beacon transmission opportunity of each vehicle is the same. For this reason, beacons transmitted by the vehicles in the head and the tail of a cluster become hard to be received by other vehicles in the cluster. Therefore, in order to increase the opportunity of transmitting beacons from vehicles at the head and tail of the cluster, the transmission frequency of other vehicles in the cluster should be reduced. In this way, it will be possible to cover the blind area at the front and rear of the cluster for the vehicles in the cluster, so that the vehicles can notice the existence of vehicles approaching the cluster from the front or the back.

### 3.2 Basic Concept for Giving a Higher Priority of Sending Sensor Information

In order to disseminate useful sensing data for ADAS, in our strategy, vehicles having such sensing data transmit beacons including sensor data with a higher priority than others (i.e., a chance of beacon transmission of the vehicles is more than others). In this section, we discuss the positional relationship between vehicles with such useful sensing data and other vehicles. In addition, we discuss the relationship between such vehicles and road structures.

#### 3.2.1 Blind Area in a Cluster

As described in the previous subsection discussing the effect the occlusion, the line-of-sight of onboard sensors of vehicles inside a cluster are blocked by bodies of outer

side vehicles. We define a cluster as a group consisting of V2V-equipped and non-V2V-equipped vehicles that are moving in the same direction and keeping a constant inter-vehicle distance. Head/tail vehicles of a cluster can observe a wider area, while vehicles in the inside of the cluster are hard to observe outside of the cluster. If an obstacle is in front of the cluster or a motorcycle approaches to the cluster rapidly, vehicles inside the cluster are hard to detect the existence of the obstacle or the motorcycle directly. From these reasons, vehicles at the head or the tail of a cluster have useful sensing data for ADAS.

### 3.2.2 Overlapping of Simple Perception Areas

Sensing data obtained by vehicles observing an area that is not covered by sensors of other vehicles should be transmitted more frequently than sensing data of vehicles observing an area overlapping with a simple perception area of other vehicles in order to disseminate useful sensing data for ADAS. If the size and the shape of simple perception area of onboard sensors of all vehicles are the same, as shown in Fig. 6a, most of the simple perception area of a vehicle that is in a group of vehicles at the head/tail of a cluster and is on the center lane overlap with simple perception areas of other vehicles of the group on the left and the right lanes. Furthermore, vehicles at the side edge of the group of vehicles at the head/tail of the cluster have more useful sensing data for ADAS than others in the group because they can observe right/left side of the cluster in addition to the front/back of the cluster.

So far, we have discussed cases where vehicles at the head of cluster or the tail of the cluster are moving side by side. Drivers, however, tend to avoid driving vehicles side by side because it is hard to see a vehicle moving together side by side in the neighboring lane. Thus, the shape of the head group of a cluster is not flat as shown in Fig. 6b. In such a case, the overlapped area of the simple perception area of the head vehicle of a cluster and one of vehicles at the head of other lanes can be small, and the head vehicle of the cluster has wider view of the outside of the cluster. That is, a vehicle at the head or the tail of a cluster has more useful sensing data for ADAS.

### 3.2.3 Long Cluster

When a size of a cluster is long in the traveling direction of the vehicles in the cluster, a vehicle not detected by sensors of vehicles in the head group or the tail group may approach to the cluster from the side of the cluster. Figure 6c shows a car not detected by sensors of vehicles in the head and tail group approaches to a long cluster from the side of the cluster. The approaching car *A* is detected by sensors of car *B*. Car *B* can notify cars in the cluster the existence of car *A*, and notify car *A* of the existence of cars in the cluster. In this case, *B* obtains useful sensing data for the surrounding cars in the cluster. That is, vehicles at the edge of a cluster have useful sensing data for ADAS. The outer side of the cluster can be efficiently covered by sensors on vehicles the sensor coverage distance away from the vehicles in the head or the tail

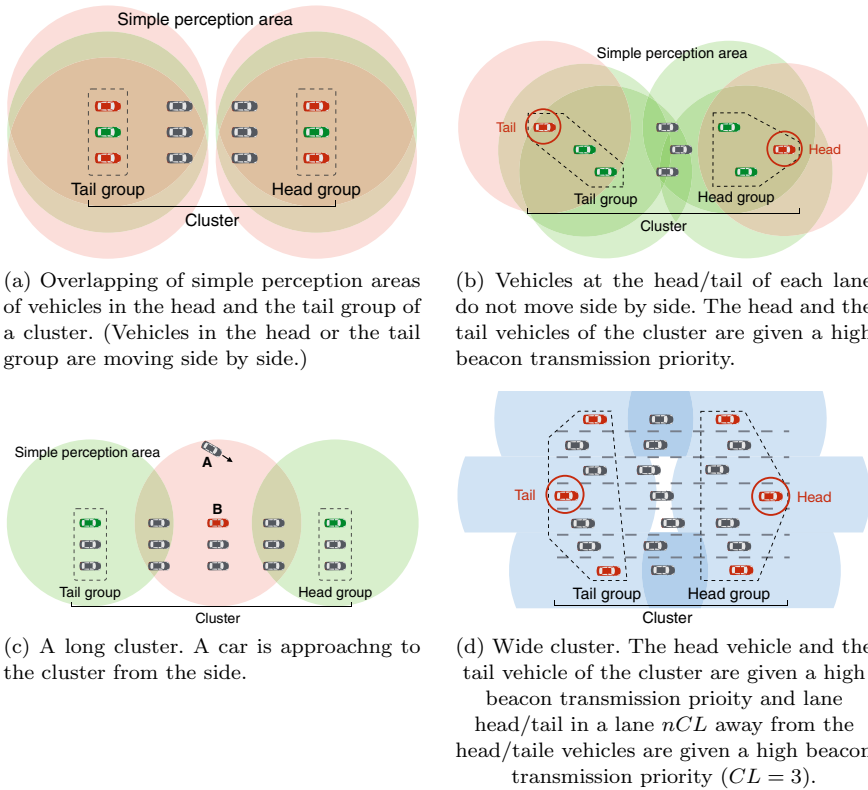


**Fig. 6** Cars having useful sensing data for ADAS in cluster

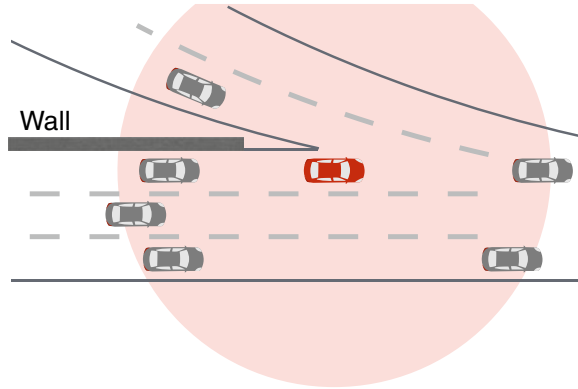
group of the cluster. Thus, it is reasonable to give such vehicles a higher priority of sending sensor data.

### 3.2.4 Wide Cluster

Let us assume that a size of a cluster is wide laterally with respect to the traveling direction in the cluster (e.g. highway with many lanes). Here, we focus on the accuracy of detecting an object by sensors. The accuracy of detecting an object of a perception sensor such as LIDAR drops when the distance between the sensor and a detection target is long. Thus, for obtaining higher accuracy of object detection, we should avoid using longer range of sensors.

Let  $CL$  be the number of lanes that can be covered by sensors of vehicles with high accuracy. Vehicles at the head and the tail groups of a cluster can efficiently cover an area outside the cluster with high accuracy if a vehicle at the head of vehicles group

**Fig. 7** A car having useful sensing data for ADAS on a merging lane



on each lane selected at an interval of  $CL$  lanes is given a higher beacon transmission priority.

Figure 6d shows a case when  $CL = 3$ . Red cars are given a higher beacon transmission priority. We can see that the sensor coverage with high accuracy of the red cars cover an area outside the cluster with small overlapping areas.

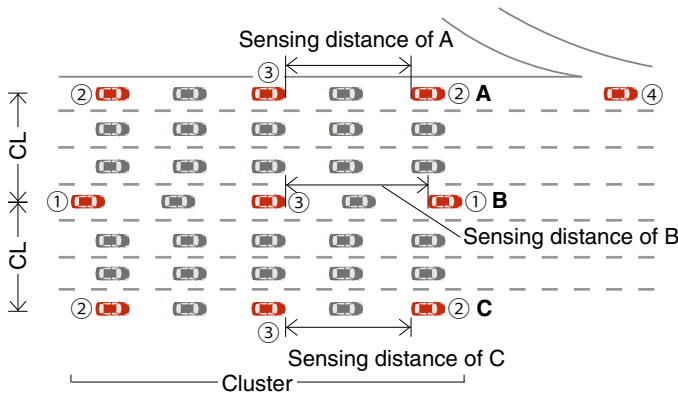
### 3.2.5 Merging Lanes

Figure 7 shows a case where lane merges with a road with multiple lanes. One red car that is close to the merging point is given a higher beacon transmission priority because it has a view covering both two merging lanes and has useful sending data for ADAS.

## 3.3 Proposed Strategy

Based on discussions in the Sect. 3.2, in our strategy, a vehicle transmits beacons with a high priority if the vehicle satisfies one of the following conditions:

- Condition 1 It is at the head or the tail of a cluster.
- Condition 2 It is at the head of a vehicles on a lane in the cluster and the lane is  $CL$  lanes away from the lane where the head of the cluster exists.
- Condition 3h It is at the tail of a vehicles on a lane in the cluster and the lane is  $CL$  lanes away from the lane where the tail of the cluster exists.
- Condition 3t If the distance between the vehicle and a vehicle satisfies the first or the second condition in the same lane is almost the same as the sensing range with high accuracy.
- Condition 4 It is the closest to the lane merging point.



**Fig. 8** Vehicles disseminating beacons with high priority in our strategy

Figure 8 shows that cars satisfying one of the above conditions in red. The encircled numbers in the figure correspond to the condition index numbers.

## 4 Simulation Study

To demonstrate the effectiveness of the proposed strategy for controlling beacon transmission frequency and/or transmission power according to the positional relationship of vehicles and road structure, we evaluate the effect of the strategy through simulation using Scenargie wireless network simulator [15]. We focus on the second pattern presented in Sect. 3.3 and controlling the beacon transmission frequency.

### 4.1 Simulation Scenario

We arranged three clusters of cars on a 770 m straight highway with 7 lanes in the simulator as shown in Fig. 9. In each cluster, the distance between cars on the same lane is 20 m, and the length of the cluster is about 100 m. The distance between neighboring clusters is 80 m. All cars keep their positional relationship during the simulation. In other words, all cars move parallel at the same speed. The size of each car is 4.7 m × 1.7 m. We assume that all cars are equipped with a LIDAR sensor. They can detect objects on the road in 150 m range unless their line-of-sight is not blocked by bodies of other cars. Table 1 summarizes other simulation parameters. All cars have the V2V communication function and they transmit beacons including LIDAR sensing data at a given frequency according to their positional relationship.

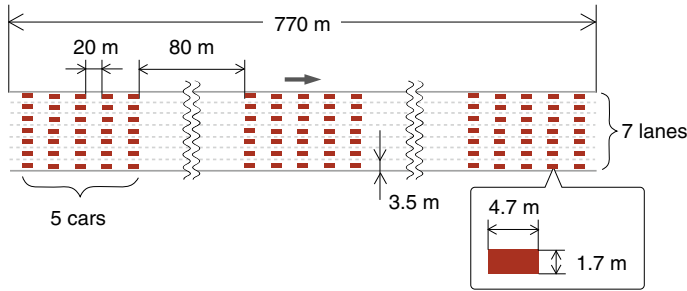


**Fig. 9** Cars and road layout in the simulation

**Table 1** Simulation parameters

Radio	IEEE 802.11p at 5.9 GHz
Bandwidth	10 MHz
Data bitrate	6 Mbps
Propagation model	Free space
Transmission power	20 dBm
Receiver sensitivity threshold	-85 dBm
Carrier sense level	-65 dBm
Packet size	1500 Bytes
LIDAR sensor range	150 m
LIDAR sensor horizontal FoV	360°
Sensing interval	0.1 s
Simulation time	30 s
Number of runs	10

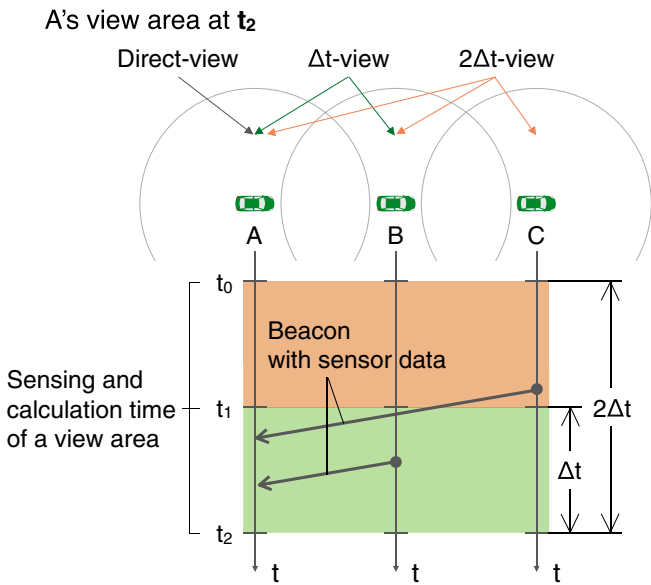
We simulated various patterns of beacon transmission frequency. The patterns are summarized in Table 2. In the table, “Head & tail (all lanes) 10-1” means that a head and tail of a cluster in all lanes transmit beacons with 10Hz and the others transmit beacons with 1 Hz, and this transmission pattern is referred to as HTA101. Furthermore, “Center lane 10-1” means that cars in a center lane transmit beacons with 10Hz, and the others transmit beacons with 1 Hz and “const. 1” means that all cars transmit beacons with constant frequency 1 Hz.

### 4.2 Performance Metrics

We introduce performance metrics,  $\Delta t$ -view and  $2\Delta t$ -view, for evaluating the effectiveness of the proposed strategy.  $\Delta t$ -view is an extended perception area obtained

**Table 2** Beacon transmission pattern

Group	Allocation of beaconing frequency	Name
Proposed (context aware beaconing frequency)	Head & tail (all lanes) 10-1	HTA101
	Head & tail (all lanes) 10-5	HTA105
	Head & tail (center lane) 10-1	HTC101
	Head & tail (center lane) 10-5	HTC105
	Head & tail (edge lanes) 10-1	HTE101
	Head & tail (edge lanes) 10-5	HTE105
	Center lane 10-1	CL101
	Center lane 10-5	CL105
Constant frequency	Const. 1	CT1
	Const. 5	CT5
	Const. 10	CT10



A's  $\Delta t$ -view and  $2\Delta t$ -view at  $t_0$  and  $t_1$  is same as A's Direct-view

**Fig. 10**  $\Delta t$ -view,  $2\Delta t$ -view and direct-view

from beacons sent within the past  $\Delta t$  time duration. Figure 10 illustrates the definition of  $\Delta t$ -view.  $2\Delta t$ -view is also defined in the similar manner. Direct-view is defined as a simple perception area obtained from only line-of-sight of onboard sensors of the car. We assume that each beacon includes information of the simple perception area of the beacon sender car. Even if a car's onboard sensor's view is blocked by other car's body, if the blocked area is covered by the view of other cars that have sent a beacon to the car, the car can obtain the view area blocked from its sensor. We assume that sensing data would reach all cars one hop away. As time passes, information in a beacon becomes old. If the ADAS allows  $\Delta t$  delay of sensing information,  $\Delta t$ -view tells the effective extended perception area for the ADAS system. We assume cars evaluate direct-view,  $\Delta t$ -view, and  $2\Delta t$ -view every 100 ms and  $\Delta t = 100$  ms.

### 4.3 How to Calculate the View Area

For calculating the view area of a car, we virtually placed points at a constant interval on each lane and counted the number of the points perceived by the cars.

#### 4.3.1 Points Detected by a Car's LIDAR

Points for calculating the view area are virtually placed on the center of all lanes at a 0.5 m interval. Figure 11 shows points detected by the LIDAR of car A and points not detected by the LIDAR. A's LIDAR can detect a point if there are no obstacles between A and the point. On the one hand, A's LIDAR cannot detect a point if there is a body of another car between A and the point. More specifically, the LIDAR of A can detect a point  $P$  satisfying the following two conditions:

1. a line drawn from the center point of A to point  $P$  does not intersect the line forming the body of another car.
2.  $P$  is within the sensor range of the LIDAR of A.

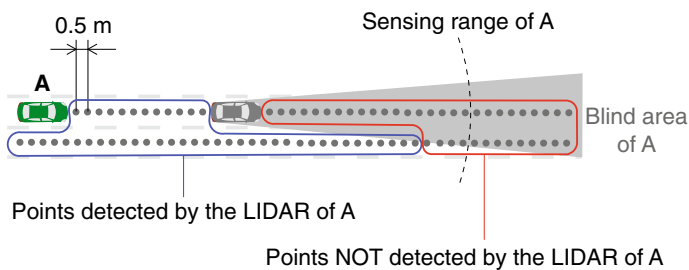


**Fig. 11** Points detected by the LIDAR of car A and points not detected by the LIDAR



### 4.3.2 Calculation of the View Area

Direct-view  $V_{direct}$  of a car is calculated as follows:

$$V_{direct} = \frac{N_{p\_detected}}{N_{p\_road}} \quad (1)$$

$N_{p\_detected}$  is number of points detected by the LIDAR of the car,  $N_{p\_road}$  is number of points on the road.

$\Delta t$ -view  $V_{\Delta t}$  of a car is calculated as follows:

$$V_{\Delta t} = \frac{N_{p\_detected} + N_{p\_beacon}}{N_{p\_road}} \quad (2)$$

$N_{p\_beacon}$  is the number of points obtained from beacons sent within the past  $\Delta t$  time duration.  $2\Delta t$ -view is also calculated in the similar manner.

## 4.4 Simulation Results

Figure 12 plots the relationship of view area ( $\Delta t$ -view,  $2\Delta t$ -view and direct-view) of a car at the center of the right hand cluster in Fig. 9 and the amount of communication traffic of each beacon transmission pattern when  $\Delta t$  is 100 ms. We calculate the amount of communication traffic as the sum of beacon frequency of all cars. For example, in case of HTE101, the communication traffic is 483 beacons/s. Each black dotted frame in the figure indicates a beacon traffic pattern, and green, blue and red plots in a frame correspond to  $\Delta t$ -view,  $2\Delta t$ -view and direct-view of the traffic pattern, respectively. The values of a view area are normalized. Ideally, the communication traffic should be smaller and the perception area should be larger. If points of a beacon transmission pattern are plotted closer to the bottom right of the graph, the result indicates the beacon traffic pattern is more effective.

In all cases, the value of direct-view is the same (0.09) because all cars move parallel at the same speed. In case of CT1, CT5 and CT10,  $\Delta t$ -view and  $2\Delta t$ -view are less than 0.2. In contrast, in the case of the beacon transmission patterns derived from the proposed strategy,  $\Delta t$ -view and  $2\Delta t$ -view are about 0.8 or larger than 0.8. For example,  $2\Delta t$ -view of HTA105 is about 10 times wider than one of CT10. There are two possible reasons why the view values based on constant transmission patterns is lower than the ones based on proposed transmission patterns. First, packet collisions occur frequently and packets suffer a long waiting time before transmission due to the high communication traffic and the same transmission chance of packets of all cars. Second, the number of transmissions of valuable information for expanding an extended perception range, i.e. information about out of the cluster, is smaller than the proposed transmission patterns due to the same beacon transmission chance

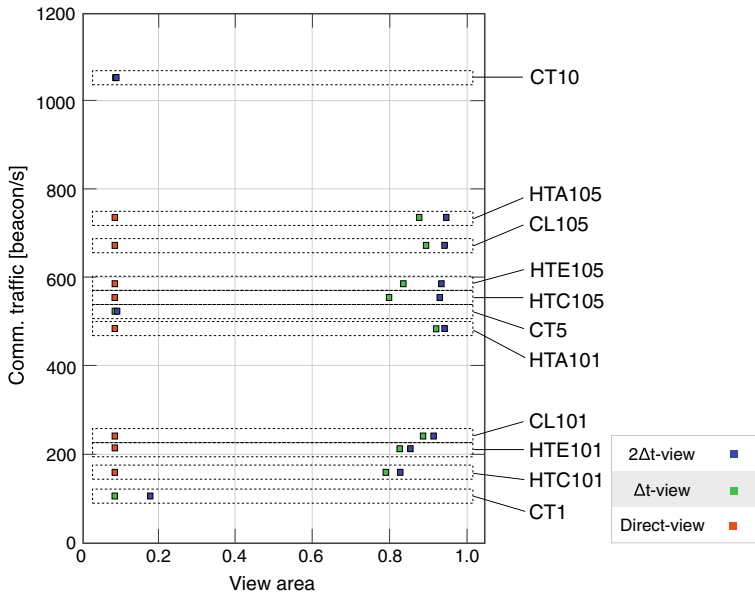


**Fig. 12** Relationship between the communication traffic and the view area of a car at the center of the right hand cluster when  $\Delta t$  is 100 ms

of all cars. The beacon transmission pattern that achieves the largest  $\Delta t$ -view and  $2\Delta t$ -view is HTA101.

These results show that when cars transmit beacons according to the proposed beacon transmission strategy,  $\Delta t$ -view and  $2\Delta t$ -view can be wider than using constant beacon transmission patterns. That is, controlling transmission frequency of beacon according to the positional relationship of cars can expand an extended perception

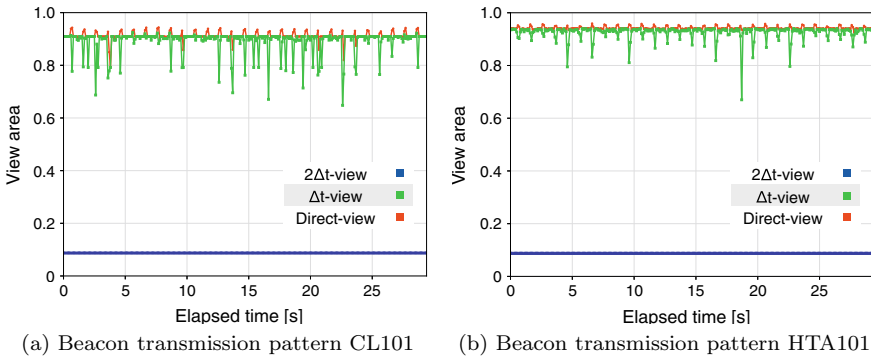


**Fig. 13** Time transition of view area of the car at the center of the right hand cluster over time when  $\Delta t$  is 100 ms

area of a car wider than controlling transmission frequency uniformly.  $\Delta t$ -view and  $2\Delta t$ -view of CL101 are larger than ones of HTE101, although communication traffic of CL101 is almost the same as one of HTE101. Additionally, as described in Sect. 3.3, the cars are more likely to cover a wider area in a left and right of a center lane by sensors of the cars compared to sensors of other cars when the number of lanes is large. Thus,  $\Delta t$ -view and  $2\Delta t$ -view of CL101 are larger than ones of HTE101 due to cars covering wider area inside a cluster than the others transmit beacons with higher transmission frequency than other cars.

Figure 13 shows the time transition of view area ( $\Delta t$ -view,  $2\Delta t$ -view and direct-view) of the car at the center of the right hand cluster over time when  $\Delta t$  is 100 ms. Figure 13a and b shows the result when beacons transmission pattern are CL101 and HTA101 respectively. In both figures, we can see that  $\Delta t$ -view sometimes drops, while  $2\Delta t$ -view is stable. This indicates that loss of sensing data from other cars is compensated by following beacon packets from other cars.

## 5 Conclusions

In this paper, we proposed a data transmission control strategy that controls the transmission power and/or frequency of messages according to the positional relationship of vehicles and road structure in order to exchange the data of onboard perception sensors that cover a region that is not covered by onboard perception sensors of other vehicles. Our proposed strategy assume vehicles recognize traffic conditions by collective perception. In order to avoid collision accidents using onboard perception sensors and V2V communication, it is necessary for vehicles to recognize surrounding traffic conditions with sufficient accuracy. We presented that vehicles can recognize surrounding traffic conditions efficiently by controlling beacon transmission considering areas of surrounding awareness of vehicles compared to controlling beacon transmission simply based on vehicle density and road structure. The strength of using this strategy is summarized as follows. (i) Vehicles can recognize the positions of objects in a blind area of its sensors with high accuracy, (ii) The load of the V2V communication channel is reduced.

We presented preliminary simulation results to demonstrate the effectiveness of the proposed strategy. We showed that the surrounding awareness of vehicles can be improved by controlling opportunities for beaconing transmission of vehicles based on the positional relationship of vehicles and road structure compared to a case of controlling the opportunities uniformly.

For our future work, we plan to design a concrete algorithm for calculating a suitable priority for sending beacons and evaluate the performance through simulations of realistic traffic scenarios.

**Acknowledgements** This work was supported by JSPS KAKENHI Grant Number 15H02689.

## References

1. Toyota Motor Sales: Toyota safety sense. <https://www.toyota.com/safety-sense/animation/pcs>. Accessed 21 January 2018
2. AUDI AG.: Driver assistance systems. <https://www.audi-mediacycenter.com/en/technology-lexicon-7180/driver-assistance-systems-7184>. Accessed 21 January 2018
3. Volvo Car Corporation: IntelliSafe—driver support and safety. <http://support.volvocars.com/uk/Pages/article.aspx?article=7a660a63632ab9b7c0a80151706a5baa>. Accessed 21 January 2018
4. Hartenstein, H., Laberteaux, K.: VANET: Vehicular Applications and Inter-Networking Technologies. Wiley Online Library (2010)
5. Günther, H.-J., Trauer, O., Mennenga, B., Wolf, L.: Realizing collective perception in a vehicle. In: Proceedings of the 2016 IEEE Vehicular Networking Conference (VNC). Columbus, Ohio, USA (2016)
6. Günther, H.-J., Riebl, R., Wolf, L., Facchi, C.: Collective perception and decentralized congestion control in vehicular ad-hoc networks. In: Proceedings of the 2016 IEEE Vehicular Networking Conference (VNC). Columbus, Ohio, USA (2016)
7. National Highway Traffic Safety Administration: Federal motor vehicle safety standards, V2V communications. Fed. Regist. **82**(8), 3854–4019 (2017)
8. European Telecommunications Standards Institute: Intelligent Transport Systems (ITS), Access layer specification for intelligent transport systems operating in the 5 GHz frequency band, ETSI EN 302 663 V1.2.0 (2012)
9. Association of Radio Industries and Businesses: 700 MHz band intelligent transport systems, ARIB STD-T109 v1.3 (2017)
10. IEEE: Wireless LAN medium access control (MAC) and physical layer (PHY) specifications, IEEE Computer Society, Std 802.11-2012 (2012)
11. Torrent-Moreno, M., Jiang, D., Hartenstein, H.: Broadcast reception rates and effects of priority access in 802.11-based vehicular ad-hoc networks. In: Proceedings of the 1st ACM International Workshop on Vehicular Ad Hoc Networks (VANET), ACM, pp. 10–18 (2004)
12. Torrent-Moreno, M., Santi, P., Hartenstein, H.: Distributed fair transmit power adjustment for vehicular ad hoc networks, IEEE SECON2006, pp. 39–48 (2006)
13. European Telecommunications Standards Institute: Intelligent transport systems (ITS), Decentralized congestion control mechanisms for intelligent transport systems operating in the 5 GHz range. Access layer part, ETSI, TS 102 687 V1.1.1 (2011)
14. Sommer, C., Tonguz, O.K., Dressler, F.: Traffic information systems: efficient message dissemination via adaptive beaconing. IEEE Commun. Mag. **49**(5), 173–179 (2011)
15. Space-Time Engineering. <https://www.spacetime-eng.com>. Accessed 21 January 2018

# Increase of Traffic Efficiency by Mutual Concessions of Autonomous Driving Cars Using Deep Q-Network



Tomohisha Yamashita, Ichitaro Ogawa, Soichiro Yokoyama, Hidenori Kawamura, Akira Sakatoku, Tadashi Yanagihara, Tomohiko Ogishi and Hideaki Tanaka

**Abstract** In recent years, autonomous operation technology has been actively developed in various research institutions and companies. Many experiments have been conducted on public roads to confirm whether an autonomous driving car can drive safely. However, there is a lack of research on autonomous driving operation for improving traffic efficiency with inter-vehicle communication. In our research, we implement mutual concessions of autonomous driving cars with Deep Q-Network (DQN), which is a deep neural network structure used for estimating the Q-value of the Q-learning method. Mutual concessions are a collective behavior in which a vehicle sometimes gives way to other vehicles and sometimes is given way by other vehicles. To verify the influence of mutual concessions, an experiment environment has been developed with radio control (RC) cars. Our experiment environment consists of up to 16 RC cars equipped with infrared LED markers and RaspberryPi3, an infrared camera for location estimation of the RC cars, a laptop controlling the RC cars through Wi-Fi, and a course of 6 m in length and 6 m in width. In this

---

T. Yamashita (✉) · I. Ogawa · S. Yokoyama · H. Kawamura  
Graduate School of Information Science and Technology, Hokkaido University, Kita 14, Nishi 9,  
Kita-ku, Sapporo, Hokkaido 060-0814, Japan  
e-mail: [tomohisa@complex.ist.hokudai.ac.jp](mailto:tomohisa@complex.ist.hokudai.ac.jp)

I. Ogawa  
e-mail: [ogawa\\_ogawa@complex.ist.hokudai.ac.jp](mailto:ogawa_ogawa@complex.ist.hokudai.ac.jp)

S. Yokoyama  
e-mail: [yokoyama@complex.ist.hokudai.ac.jp](mailto:yokoyama@complex.ist.hokudai.ac.jp)

H. Kawamura  
e-mail: [kawamura@complex.ist.hokudai.ac.jp](mailto:kawamura@complex.ist.hokudai.ac.jp)

A. Sakatoku · T. Yanagihara · T. Ogishi · H. Tanaka  
KDDI Research Inc., 2-1-15, Ohara, Fujimino, Saitama 356-8502, Japan  
e-mail: [ak-sakatoku@kddi.com](mailto:ak-sakatoku@kddi.com)

T. Yanagihara  
e-mail: [td-yanagihara@kddi.com](mailto:td-yanagihara@kddi.com)

T. Ogishi  
e-mail: [ogishi@kddi-research.jp](mailto:ogishi@kddi-research.jp)

H. Tanaka  
e-mail: [hide@kddi-research.jp](mailto:hide@kddi-research.jp)

paper, mutual concessions of autonomous cars are implemented at the confluence at a roundabout. DQN is applied for the decision-making mechanism to decide speed at the roundabout based on the status of other cars. As a result of the experiment in our experiment environment, it is confirmed that mutual concessions at the roundabout were acquired with DQN, and that mutual concessions can increase traffic efficiency.

## 1 Introduction

The recent development of automatic operation technology has been remarkable, the Japanese government has come up with a policy of practical use of unmanned automatic operation mobile services in limited areas in 2020 [16]. Definition of the current automatic operation has followed the definition of the International Society of Automotive Engineers (SAE), which is a standardized mechanism established in the United States in 1905.

The guidelines for automatic operation of the Japanese government are given in “Public-Private ITS Initiative Roadmap 2017”, where the four levels of classification of the automatic operation was changed to a five-level classification. According to the current level classification of the automatic operation, the implementation of all operating task system in certain conditions, which aims to commercialization by 2020, corresponds to level 4.

Various sensors such as stereo camera, a lidar, a millimeter-wave radar, a GPS, and an odometer are mounted on the autonomous driving car. With these sensors, the autonomous driving car detects other vehicles, obstacles, and pedestrians and estimates self-position and surrounding situation. Particularly in analysis of the camera image, the tertiary artificial intelligence boom has been significant, and since convolutional neural network (CNN: Convolutional Neural Network) [7] results have been applied, a significant improvement in the object sensitivity has been observed. Stable operation control for driving along a driving line and maintaining appropriate distance from other vehicles is realized by learning the method of adjusting the steering and the acceleration/deceleration by using the acquired sensor data. Learning of driving behavior is one of the most important among automatic operation technologies.

ICT is also important in order to perform the learning of the driving action in automatic driving. NVIDIA’s Grzywaczewski [3] reported a trial calculation of the data capacity and the amount of computation required for the learning of the driving behavior for automatic operation vehicles. As a modest estimate, even if only five cameras are focused on, every hour, 1 TB or more of the data is generated in one autonomous driving car. In consideration of the compression and sampling of data, 204.8 PB of data is generated in 100 cars during 260 business days (8 h per day).

Because it is necessary to aggregate the large amount of driving data from the vehicles, the fifth-generation mobile communication system (5G), with large capacity, low latency, and high reliability, is required for learning driving behavior. Further, because 5G can support real-time sharing of location information, 5G is expected to

contribute not only aggregation of the learning data, but also to accident prevention and improvement of traffic efficiency.

In previous research, many researchers have worked on avoidance of accidents and collisions by learning driving behavior, and the alleviation of congestion by central information system. However, approaches addressing interaction among vehicles have received relatively little attention. Because there is intensive interaction among the vehicles in transportation systems, operation control of a single vehicle and information sharing among vehicles are not sufficient to enhance the safety and efficiency.

For example, assume a situation where multiple cars are simultaneously approaching an intersection without a traffic signal. When each vehicle is controlled independently, there is a possibility that all vehicles simultaneously advance to an intersection or stop. The adjustment process of vehicle behavior through a central system consists of the transmission of information from the vehicles to a central system, the adjustment of the central system, and the notification of adjustment results to the vehicles. Therefore, there is a possibility of a delay in the response and inappropriate adjustment due to lack of information.

Based on this research background, we have been working on collaborative learning with radio control cars (RC cars) using DQN (Deep Q-Network) [9]. DQN is a combination technique of Q learning and Deep Neural Network (DNN) to infer the action-value function of the table form of the Q table in the approximate function using the DNN. In this study, we implement mutual concessions of autonomous driving cars with DQN. To verify the effectiveness of the proposed mutual concessions, we developed an experiment environment for verification of autonomous operation with RC cars. Our experiment environment consists of 16 RC cars equipped with



Fig. 1 Appearance of the course on which the RC cars run

infrared LED markers and RaspberryPi3, and a course of 6 m in length and 6 m in width., shown in Fig. 1.

We found that “mutual concessions” are valid for the improvement of the traffic efficiency of the vehicles. It is one outcome of the collaborative research [10] of Hokkaido University and KDDI Research, Inc. since 2016 that the autonomous-driving cars learn mutual concessions of driving path, and the overall traffic efficiency can be thereby increased. The demonstration video of mutual concessions with the RC cars has been opened to the public on YouTube [8].

In Sect. 2, mutual concessions among vehicles is explained. In Sect. 3, previous studies where machine learning is used for acquiring the driving behavior of the autonomous driving car are reviewed. In Sect. 4, the experiment environment with RC cars and the learning of mutual concessions with DQN are described. In Sect. 5, the influence of mutual concessions in the experiment environment is confirmed. Finally, our paper is summarized in Sect. 6.

## 2 Implementation of Mutual Concessions

This section is focused on mutual concessions of the autonomous driving car in a roundabout, and explaining how mutual concessions work. First of all, in this study, “mutual concessions” between the autonomous driving cars are considered as per the situation shown in Fig. 2. The roundabout is an intersection format in which inflow vehicles to intersection are handled in a one-way manner on an annulus around the central island, and follows a control scheme with priority over vehicles driving on the ring road. In the roundabout, there is priority to the vehicles driving on the

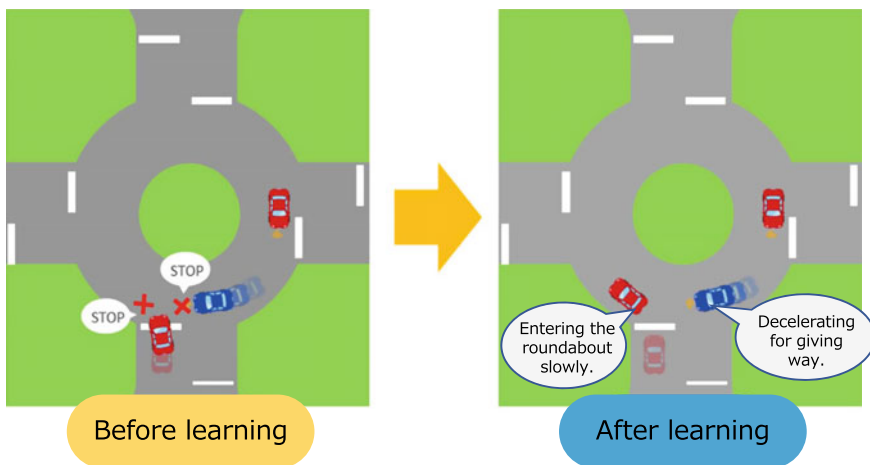


Fig. 2 Outline of mutual concessions acquired by using machine learning



central circle than the vehicles attempting to enter the central circle from the outside. Therefore, the vehicle driving on the central circle can move without stoppage.

However, it is possible to increase traffic efficiency if the vehicles driving on the circular path give way to the vehicles attempting to enter from the outside. From the point of view of the individual vehicle driving on the circular path, not to give way is always the dominant strategy. On the other hand, from the point of view of all vehicles, to give way is sometimes assumed to result in increasing the traffic efficiency of all vehicles collectively.

Improvement of traffic efficiency by giving way can be observed in various real contexts.

For example, suppose that at an intersection with no right turn lanes on one side of a two-lane road, a leading vehicle to turn right is waiting for passage of one oncoming vehicle. Some vehicles are also waiting after the leading vehicle in the same lane, but they have intention to go straight on the intersection. In this case, if a vehicle approaching the intersection in the opposite lane gives way to the leading vehicle to turn right, it is possible to improve the collective traffic efficiency.

It is easy to understand that giving way under such a simple circumstance can increase collective traffic efficiency. However, it is not revealed that the collective traffic efficiency can be increased by mutual concessions, which is a collective behavior in which a vehicle sometimes gives way to other vehicles and sometimes is given way by other vehicles. Therefore, in this paper, we verify the following two hypotheses; (1) mutual concessions can be acquired by machine learning, and (2) mutual concessions can increase the traffic efficiency of all vehicles.

In practice, mutual concessions, such as the veteran driver giving priority road to beginner learner driver, are usually observed. This kind of mutual concession is different from driving according to traffic signals and road signs, because it is not based on clear rules. For that reason, it has been asserted that it is difficult to realize mutual concession in an automatic operation in which the machine judges the situation on behalf of a person and performs a driving operation. If autonomous driving cars learn mutual concessions, the realization of the automatic driving in the general road will be one step closer.

### 3 Related Research

The present section offers a review of research on acquisition of driving behavior with machine learning and research related to mutual concessions.

Bojarski et al. at NVIDIA [2] reported an automatic operation system that performs learning of the driving behavior in the End-to-End. In this operation system with CNN, direct learning of driving behavior of wheel operation and acceleration/deceleration is performed based on the image acquired from a camera mounted on the driver's seat.

In the research of Kendall et al. at Wayve Co. [6], in the learning environment where an automated driving vehicle moves back into the lane when the automated

driving vehicle is out of the lane, applying the Actor-Critic method led to the automatic driving car successfully learning to drive inside the lane with a 20-minute training.

Ishikawa et al. [5] tried to apply Q-learning to acquire driving behavior of an autonomous driving car based on traffic simulation. This research adopted a cooperative learning framework in which a plurality of agents (vehicles) refer to and update the same behavior value function  $Q$  by applying a compensation setting that gives a negative compensation to a stop or a distance equal to or greater than a certain distance. As a result, agents learned the timing of acceleration and deceleration of automated driving vehicles and lane change in single-track bottleneck, and it was confirmed that the traffic flow rate increased as a result.

David et al. [4] sought to combine automatic operation and DQN. It has been reported that in the passage throughput of an intersection without traffic signal, the control of autonomous driving car by using a DQN is better than rule-based control.

The demonstration of the “collision-free car” proposed by Nippon Telegraph and Telephone Corporation, Toyota Motor Corporation, Preferred Networks can be cited as an example of the research applying this approach with RC cars. In this demonstration, under the environment in which a camera is set over a driving area to detect the position data of the vehicles, acceleration/deceleration and steering control of the vehicle to prevent collision was acquired by using the DQN [12].

Researching the control method of the autonomous driving cars in a junction, Jackeline et al. [14] reported that there are distributed type and centralized type, and that many schemes have been proposed for each. In another paper, Jackeline et al. [13] evaluated fuel economy of autonomous driving cars by centralized control in a junction.

Turning to research trends in information sharing of autonomous driving cars, Tanari et al. [11] have proposed a spatial information platform to share autonomous driving cars status and path through servers. Moreover, Sato et al. [15] substantiated that the actual vehicle can share information by using the Local Dynamic Map (LDM) for integrally managing information of vehicles and pedestrians.

## 4 Development of Experiment Environment

The present section elaborates on the experiment environment with the RC car. At first, we explain the whole of the experiment environment. Then, we explain two main sub-systems of the experiment environment. One is the location estimation system for acquiring the position of the RC cars. The other is the driving operation system, consisting of an accel PWM module, steering PWM module, and learning module of mutual concessions with DQN.

### 4.1 System Outline

The experiment environment shown in Fig. 3 consists of RC cars (up to 16 units) equipped with IRLEDs and Raspberry Pi 3, a camera for location estimation of the RC car, a laptop PC for driving control, and a log viewer. Figure 4 shows the appearance of the RC car, and Fig. 5 shows the RC car without the body. The present subsection explains the function and processing procedure of the experiment environment.

The experiment environment using the RC car constructed in this research is located between the experiment by the actual autonomous driving car and the traffic simulation of the software.

An advantage of the experiment environment using RC cars is that it is possible to conduct experiments safely and inexpensively compared with experiments using real automatic driving vehicles. The experiment environment using RC cars is a useful approach because it can naturally capture realistic elements such as location estimation, communication delay, and environmental disturbance compared to software simulation.

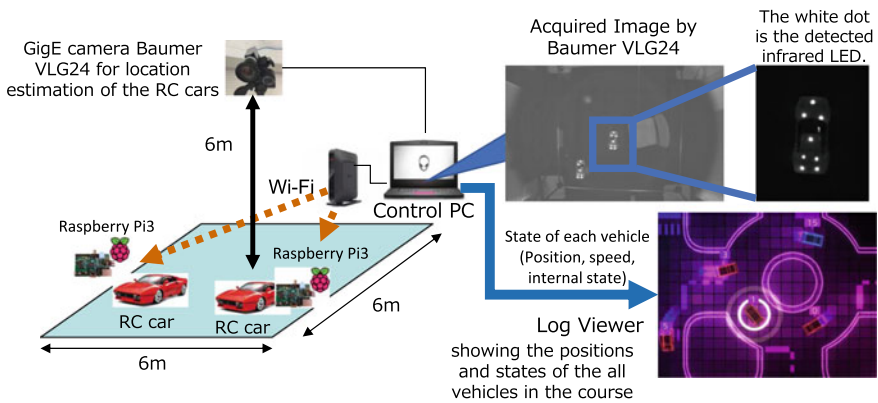
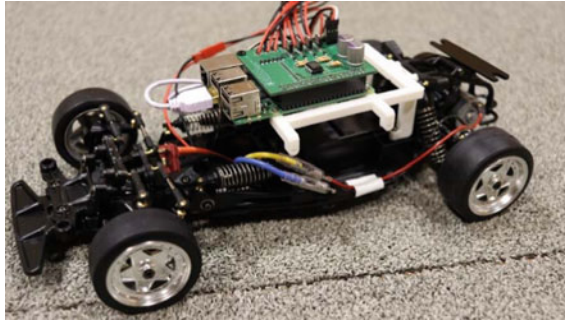


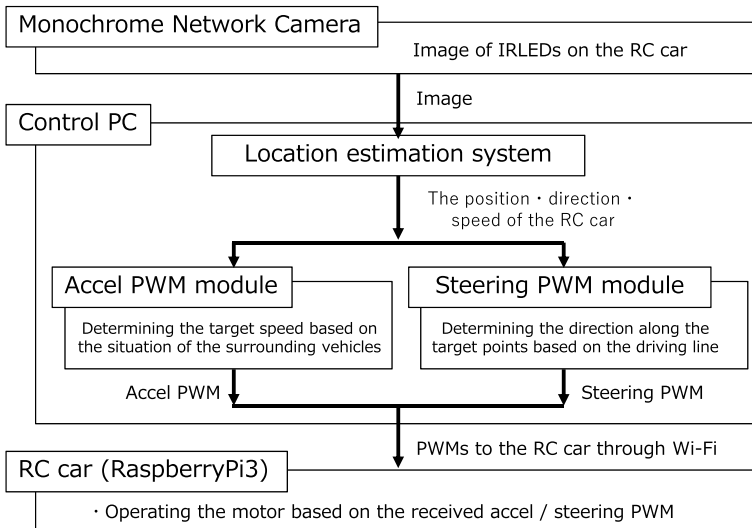
Fig. 3 System outline of the experiment environment

Fig. 4 Appearance of the RC car





**Fig. 5** Inside of the RC car



**Fig. 6** Procedure of location estimation and determination of accel and steering PWM in the experiment environment

The control PC determines the traveling direction and the traveling speed of each RC car based on the positions of all the vehicles, and it transmits them to the Raspberry Pi 3 mounted on each RC car. Wi-Fi is applied for communication between the control PC and RC cars. The Raspberry Pi 3 installed in the RC cars operate the motors based on the accelerator/steering PWM received from the control PC. The log viewer receives the position, speed, and internal information of the RC cars from the control PC and visualizes it, shown in Fig. 3.

In the experiment environment, the RC car is controlled based on its position and the surrounding car situation, as shown in Fig. 6. The monochrome network camera shoots the images of IRLEDs on the RC car and sends them to the control PC. The location estimation system in the control PC calculates the position, direction, and

the car ID of the RC car from the positional relationship of IRLEDs attached to the ceiling of the RC car. The accel PWM module determines the target speed based on the situation of the surrounding vehicles and outputs the PWM for accel control. The steering PWM module determines the direction along the target points based on the driving line and outputs the PWM for steering control. The RC car receives the PWMs and operates the motors based on accel/steering PWM modules.

### 4.2 Location Estimation

In location estimation, the position, direction, and ID of the RC car are determined from the positional relationship of IRLEDs attached to the ceiling of the RC car. Up to eight IRLEDs are attached to the RC car. Three IRLEDs are used for the position recognition, and up to five IRLEDs are used for the car ID recognition. Location estimation consists of camera image transformation, camera distortion correction, perspective transformation, and position and ID recognition of the RC cars (Fig. 7).

At first, in camera image transformation, the infrared network camera of VLG24M with VS-0618H1 lens set at 6 m above the ground shoots the IRLEDs of all RC cars on the course. Frame rate of the camera is at the highest 38.5 *fps* and resolution is 1920 × 1200. The camera images acquired by the camera are sent to the control PC via a LAN cable at 27.8 *fps*.

The control PC calculates the center of gravity of the white areas (IRLEDs) in the image and performs distortion correction of the camera to determine the position in the Cartesian coordinate system based on the algorithm proposed by Suzuki

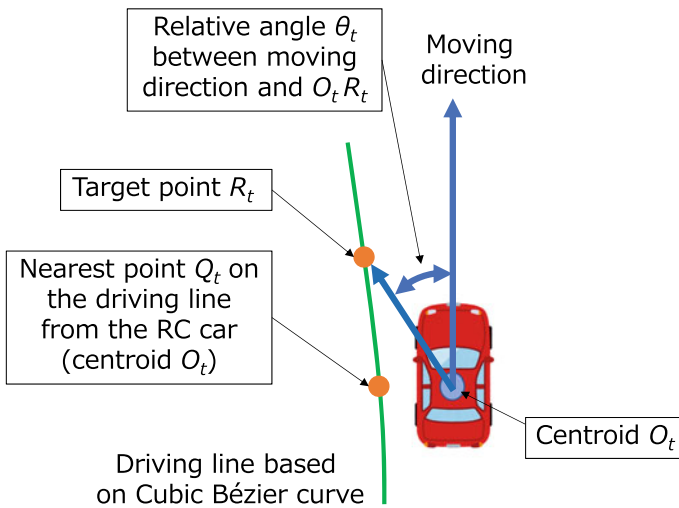


Fig. 7 Position of target point for steering PWM

et al. [17]. Correction of the relative camera distorted coordinates of the detected IRLED corrects the height by the detected position of the IRLED real coordinates. The position, direction, and car IDs of the RC cars are determined from the positional relationship of IRLEDs and are converted into real coordinates by perspective transformation [18]. Please refer to the reference [10] for detailed explanation of camera distortion correction, perspective transformation, and position and ID recognition.

### 4.3 Driving Operation

In driving operation of the RC car, there are two operation types. One is steering operation, to move to the target point. The other is accel operation, to move at the target speed. The present subsection explains the steering and accel operations of the RC car.

#### 4.3.1 Steering Control

In steering operation of the RC car, the RC car is supposed to move to a target point. To implement this operation, the steering PID control is applied. The output of the steering PID control is the steering PWM.

To move to a target point, it is necessary to calculate relative angle  $\theta_t$  from the current moving direction to target point  $R_t$  in step  $t$ . Target point  $R_t$  in step  $t$  is calculated as described in the next paragraph.

Here, the direction and centroid of the RC car in step  $t$  are described as  $dir_t$  and centroid  $O_t$ . The driving line is defined based on Cubic Bézier curve and the figure of a road. Point  $Q_t$  in step  $t$  is defined as the nearest point to the RC car on the driving line (centroid  $O_t$ ). Target point  $R_t$  is determined based on the length of  $O_t Q_t$ .

At first, based on the length of  $O_t Q_t$ , the length from target point  $R_t$  to point  $Q_t$  is determined using the following formula 1.

$$Q_t R_t [m] = \begin{cases} 1.2 & (O_t Q_t \leq 0.3) \\ 3.2 & (0.8 \leq O_t Q_t) \\ 4.0 O_t Q_t & (\textit{otherwise}) \end{cases} \quad (1)$$

The parameters in formula (1) are adjusted heuristically in order to make the RC car follow the driving line as closely as possible.

Subsequently, point  $R_t$  is selected as the point satisfying that the length is  $Q_t R_t$  and that it is above the driving line. When the position of target point  $R_t$  is determined, relative angle  $\theta_t$  from the current moving direction to target point  $R_t$  in step  $t$  is determined. Finally, steering PWM is calculated using the following formula (2), and is sent to the steering motor.

$$PWM_t^{steering} = \theta_t \times K_P + \sum_t \theta_t \times K_I + (\theta_t - \theta_{t-1}) \times K_D, \tag{2}$$

where PID parameter  $K_P$  is 80.0,  $K_I$  is  $5.0 \times 10^{-5}$ , and  $K_D$  is 70.0.

### 4.3.2 Accel Control

The accel PWM module determines the target speed and outputs the PWM for operating the accelerator motor shown in Fig. 8.

In the accel PWM module, the target speed candidates calculating module calculates the following five target speed candidates.

Emergency stop for collision avoidance

The emergency stop is a safety device for when there is another RC car in front of the RC car. The target speed for emergency stop is given by formula (3).

$$TS_t^{EmergencyStop}(v_t, d_t^{front}) = \begin{cases} 0 & (d_t^{front} < d_{thr\_EmergencyStop}) \\ v_t & (otherwise), \end{cases} \tag{3}$$

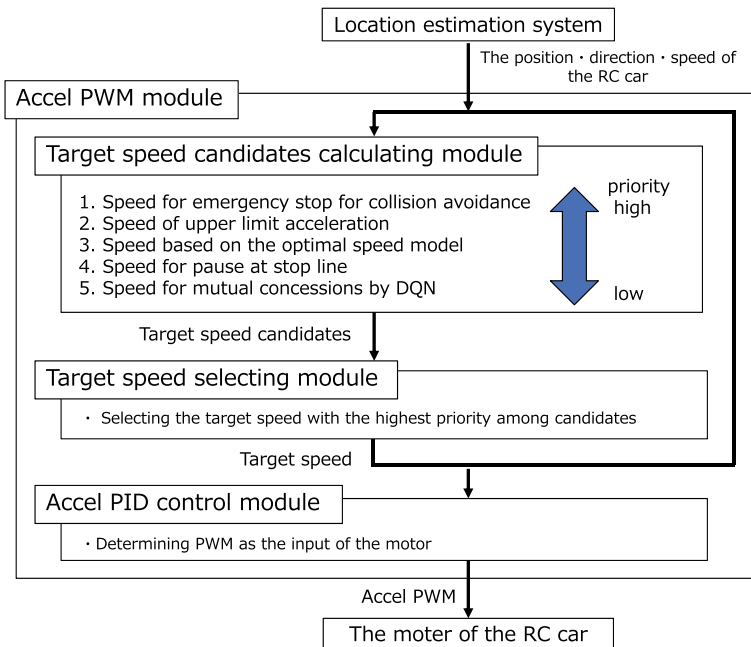


Fig. 8 Procedure of determination of the accel PWM

where  $v_t$  is the other candidate speed in step  $t$ ,  $d_t^{front}$  is the distance to the RC car in front, and  $d_{thr\_EmergencyStop}$  is the activation threshold of emergency stop. Here,  $d_{thr\_EmergencyStop}$  is set as  $1.0 \times 10^{-1}$ .

Upper limit of speed change

The upper limit of speed change is set to suppress sudden braking at deceleration. The target speed based on the upper limit of speed change is given by formula (4).

$$TS_i^{AccelLimit}(v_t, v_{t-1}) = \begin{cases} v_{t-1} + a_{thr\_upper} \Delta t & (a_{thr\_upper} < v_t - v_{t-1}) \\ v_{t-1} - a_{thr\_lower} \Delta t & (v_t - v_{t-1} < -a_{thr\_lower}) \\ v_t & (otherwise), \end{cases} \quad (4)$$

where  $a_{thr\_upper}$  is the upper limit of acceleration,  $a_{thr\_lower}$  is the lower limit of acceleration, and  $\Delta t$  is the time for 1 step. Here,  $a_{thr\_upper}$  and  $a_{thr\_lower}$  are set as 2.0 and 2.0, respectively.  $\Delta t$  is set as  $8.3 \times 10^{-2} sec (=12 fps)$ .

Optimal speed model

The Optimum Speed Model (OVM) [1] is a method of deciding the speed based on the distance from the RC car driving ahead. This model is used for speed determination during normal driving. The target speed based on the OVM is given by formula (5).

$$TS_i^{OVM}(d_t^{front}) = a * (\tanh(d_t^{front} - c) + \tanh(c)), \quad (5)$$

where  $d_t^{front}$  is the distance to the car in front, and  $a$  and  $c$  are the parameters of OVM. When there is no preceding car within  $d_{max}$  ahead,  $d_t^{front}$  is set as the maximum distance  $d_{max}$ . Here,  $a$ ,  $c$ , and  $d_{max}$  are set as 1.0,  $7.0 \times 10^{-1}$ , and 3.0, respectively.

Speed for stopping at stop lines

There are places where it is necessary to accurately stop at a stop line, such as the confluence and T-junction in the course. This speed is used to decelerate and stop when the distance to the stop line becomes less than or equal to a certain value. The target speed for stopping at a stop line is given by formula (6).

$$TS_i^{StopLine}(v_t, d_t^{StopLine}) = \begin{cases} 0 & (d_t^{StopLine} < d_{thr\_Stop}) \\ v_{min} + 1.6(d_t^{StopLine} - 0.4) & (d_{thr\_Stop} \leq d_t^{StopLine} < d_{thr\_Deceleration}) \\ v_t & (otherwise), \end{cases} \quad (6)$$

where  $d_t^{StopLine}$  is the distance to the stop line,  $v_{min}$  is the minimum speed of the RC car, and  $d_{thr\_Stop}$  and  $d_{thr\_Deceleration}$  are the activation threshold of stop and deceleration for stopping on stop line, respectively. Here, thresholds  $d_{thr\_Stop}$  and  $d_{thr\_Deceleration}$  are set as 0.4 and 1.2, respectively.



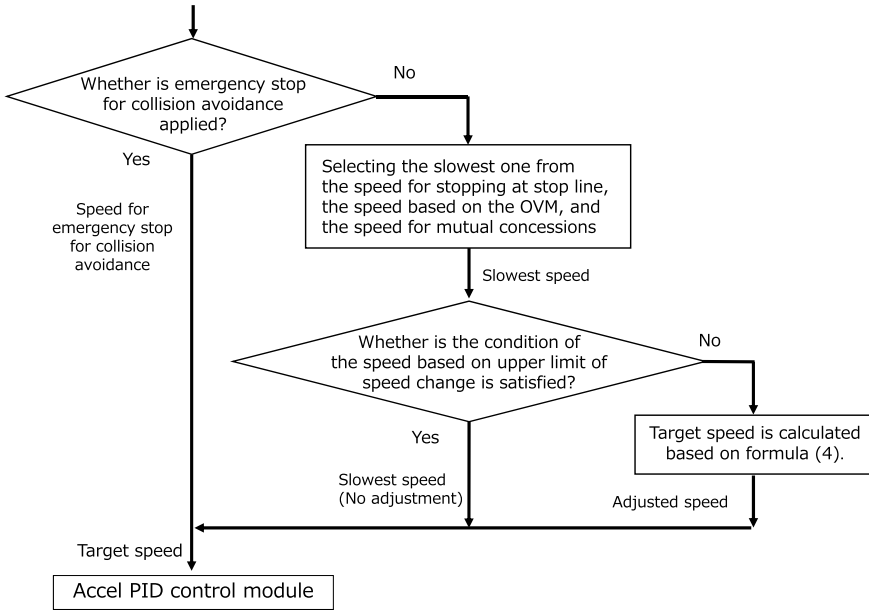


**Fig. 9** Procedure of selection of the target speed

### Mutual concessions

The speed setting for mutual concessions with DQN is explained in the next subsection.

Target speed selecting module selects target speed  $v_t^*$  from the five candidates based on the procedure in Fig. 9. If the condition of emergency stop is satisfied, the target speed is determined as the speed for emergency stop for collision avoidance. Otherwise, target speed selecting module selects the slowest one from the speed for stopping at stop line, the speed based on the OVM, and the speed for mutual concessions. And then, the condition of the speed based on upper limit of speed change is applied to the slowest one, and the target speed is determined.

For example, if there are other vehicles within 0.1 m in front of the RC car, the target speed selecting module selects the speed for emergency stop as the target speed  $v_t^*$ . In this case, even if the target speed for stopping at the stop line has been calculated, the target speed selecting module selects the speed for an emergency stop because the priority of emergency stop is higher than that of stopping at the stop line.

As another example, if there is no preceding car within 10m ahead of the RC car and it is close to the stop line, the target speed selecting module selects the speed for stopping at the stop line because it is the minimum speed.

Finally, the accel PWM is calculated using the following formula (7).

$$PWM_t^{accel} = PWM_t^{accel\_Main} + PWM_t^{accel\_Corr}, \tag{7}$$

The accel PWM consists of a main component term  $PWM_t^{accel\_Main}$  and a correction term  $PWM_t^{accel\_Corr}$ . The main component term  $PWM_t^{accel\_Main}$  is calculated based on the relation of the accel PWM input to the motor and the actual speed of the RC car. In preliminary experiments, it was recorded the speed of the RC car observed when a certain PWM was input. This record is used as a measure to determine the PWM for driving the target speed. Please refer to reference [10] for the preliminary experiment for investigating the relationship between the input PWM and the speed of the RC car.

However, even if a certain PWM is input to the motor, the same speed cannot always be obtained depending on the current speed and acceleration. Therefore,  $PWM_t^{accel\_Corr}$  for correcting  $PWM_t^{accel\_Main}$  is required according to the situation of the RC car. The correction term  $PWM_t^{accel\_Corr}$  is given by formula (8).

$$\begin{aligned}
 PWM_t^{accel\_Corr} = & \\
 & (v_t^* - v_t) \times K_P + \\
 & + \{(v_t^* - v_t) + (v_{t-1}^* - v_{t-1}) + (v_{t-2}^* - v_{t-2})\} \times K_I \\
 & + (v_t^* - v_t) \times K_D,
 \end{aligned} \tag{8}$$

where PID parameter  $K_P$  is 40.0,  $K_I$  is  $1.0 \times 10^{-4}$ , and  $K_D$  is 1.0.

#### 4.4 Learning Module of Mutual Concessions with DQN

The present subsection explains the setting of applying the method of learning module with DQN for acquiring mutual concessions.

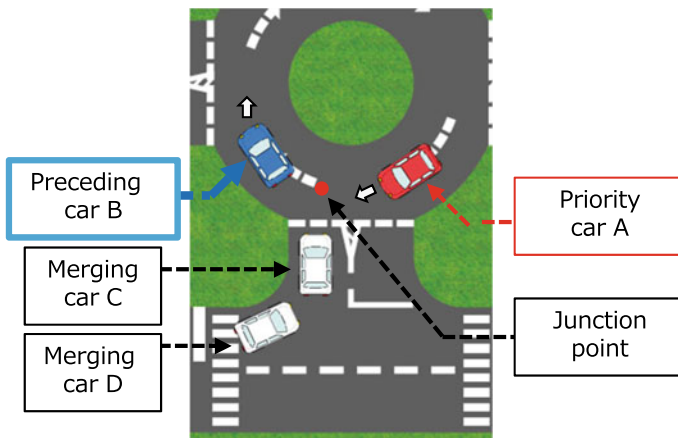
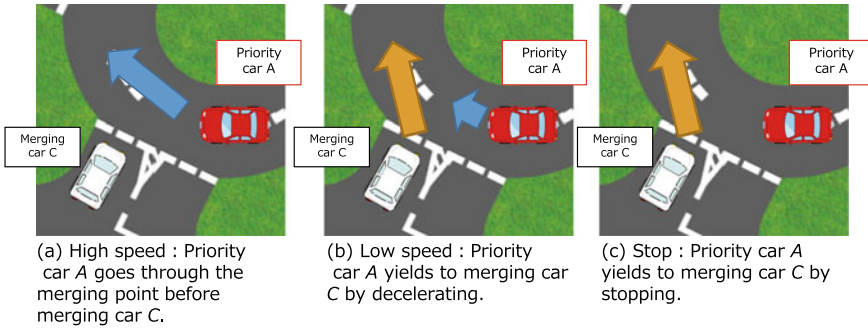


Fig. 10 Setting of car names at roundabout



**Fig. 11** Influence of action choice by priority car

**Table 1** Setting of state, action, and reward used in DQN

State	Current speed of car A
	Current speed of car B
	Current speed of car D
	Distance between car A and junction point $O(AO)$
	Distance between car B and junction point $O(BO)$
	Distance between car A and car D ( $AD$ )
	Number of merging cars
	Number of cars on roundabout
	Number of all cars
	Average speed of all cars
Action	Speed of car A : stop (0 m/s)
	Speed of car A : low speed (0.50 m/s)
	Speed of car A : high speed (0.65 m/s)
Rewards	Addition: average speed of all RC cars
	Deduction: emergency stop (-100.0)
	Deduction: stop time of car A exceeds 10 s (-100.0)

In this paper, DQN is applied to determine the target speed for mutual concessions shown in Fig. 8. DQN is a deep neural network structure used for estimating the Q-value of the Q-learning method. As shown in Fig. 10, when there is a preceding car B or merging car C at the roundabout, we implement mutual concessions by learning the speed of priority car A.

DQN learning mutual concessions use the states, actions, and reward described in Table 1. As shown in Fig. 11, we assume a scenario of mutual concessions in which priority car A selects “stop” or “low speed” and gives way to merging car C. On the other hand, priority car A selects “high speed” and goes through the merging point before merging car C.

In order to increase the overall speed, the average speed of all cars is rewarded. In order to avoid continuing emergency stop and stop, each reward is set to  $-100$ .

In the configuration of the DQN model, the number of input units is 10 units, equal to the number of states, the number of intermediate layers is three, and the number of units is 10 in each layer. The number of output units is three units, corresponding to the three actions listed in Table 1. *ReLu* and *RMSProp* are used as the activation function and the optimization function. Epsilon  $\epsilon$  in *RMSProp* is 0.01.

DQN learns 227,358 data offline for 100,000 epochs (1 epoch is 100 steps). Because the data collected in the experiment environment consists of the position, speed, and direction of all RC car, the status in Table 1 can be calculated based on the data. Data of 100 steps selected randomly is used for experience play. The target network is updated every 100 steps.

## 5 Verification of Effect of Mutual Concessions

This section reports application of the the experiment environment to verify the influence of mutual concessions. We analyze the difference in the driving situation with and without DQN and verify whether DQN has learned mutual concessions, and mutual concessions can increase traffic efficiency.

The course used for the experiment consists of the roundabout shown in Fig. 1 and the road around it. This course has a one-way lane on one side and there is no passing.

To evaluate the influence of the concession on the traffic flow, we conduct an experiment when using DQN and when not using it and compare the results. As the experiment settings, three trials are conducted with 12 RC car for 5 min. With respect to the 5-minute data, the data of the first minute is not used because the initial position at the start of driving of the RC car is affected and the variation is large. Only the data of the last 4 min is used for learning of DQN.

As a first experimental result, mutual concessions at the roundabout were confirmed in each trial with DQN. Table 2 shows in each trial the number of times that mutual concessions occur, the number of times that mutual concessions did not occur, and the ratio in which mutual concessions occur in the situation where there is a priority car at the roundabout and there is also a merging car. Here, the occurrence of mutual concessions means that, when the priority car drives in the roundabout

**Table 2** Number of times that mutual concessions occur in three trials

	Trial 1	Trial 2	Trial 3	Average
Number of times that mutual concessions occur	28	22	14	21.3
Number of times that mutual concessions did not occur	86	80	96	87.3
Ratio that mutual concessions occur	0.24	0.22	0.13	0.20

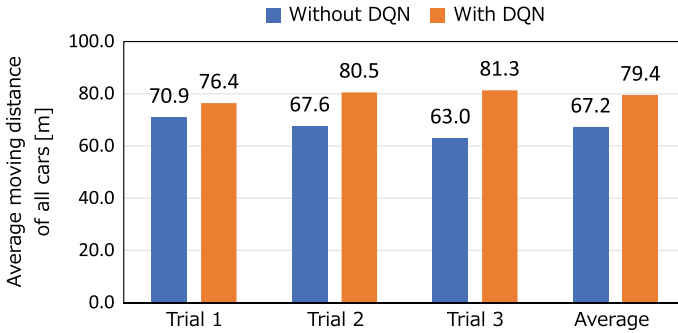


**Fig. 12** Average moving distance of all 12 RC cars

and the merging car approaches the roundabout, the priority yields to the merging car by decelerating or stopping. At the roundabout, it was confirmed that mutual concessions occurred in about 20 percent of all opportunities that it occurs.

As a second experimental result, mutual concessions can be confirmed to improve traffic efficiency. Figure 12 shows the average moving distances of all RC cars for 4 min with and without DQN. From the graph, the average moving distance increases with the introduction of DQN. Therefore, in the case with DQN, it is confirmed that since mutual concessions to the invasion to the roundabout has been acquired, it is possible to increase the average moving distance of all the RC cars by mutual concessions.

## 6 Conclusion

In this paper, we address machine learning of driving behavior in autonomous driving and explain an outline of mutual concessions among vehicles. Then, related researches on acquisition of driving behavior with machine learning and researches related to mutual concessions are overviewed.

Next, the experiment environment using the RC car is explained. The experiment environment consists of RC cars (up to 16 units) with Raspberry Pi 3, a camera for location estimation of the RC car, a laptop PC for vehicle control, log viewer showing the status of the RC cars, and a course of 6 m in length and 6 m in width.

In location estimation, the position, direction, and ID of the RC car are determined from the positional relationship of IRLEDs attached to the ceiling of the RC car. In steering operation of the RC car, steering PWM module determines the direction along the target points based on the driving line and sends Steering PWM to the RC car. In accel operation of the RC car, accel PWM module selects the target speed with the highest priority among candidates and sends accel PWM to the RC car. DQN is applied for learning of mutual concessions among the RC cars at the roundabout.

To evaluate the influence of the concession on the traffic flow, an experiment when using DQN and when not using it are conducted under the settings with 12 RC car for 5 min. Finally, the experiment in our experiment environment results that mutual concessions at the roundabout was acquired with DQN, and that mutual concessions can increase traffic efficiency.

## References

1. Bando, M., Hasebe, K., Nakayama, A., Shibata, A., Sugiyama, Y.: Dynamical model of traffic congestion and numerical simulation. *Phys. Rev. E* **51**(2), 1035 (1995)
2. Bojarski, M., Testa, D.D., Dworakowski, D., Firner, B., Flepp, B., Goyal, P., Jackel, L.D., Monfort, M., Muller, U., Zhang, J., Zhang, X., Zhao, J., Zieba, K.: End to end learning for self-driving cars. In: arXiv preprint. [arXiv:1604.07316](https://arxiv.org/abs/1604.07316) (2016)
3. Grzywaczewski, A.: Training AI for self-driving vehicles: the challenge of scale. In: NVIDIA Developer Blog. <https://devblogs.nvidia.com/training-self-driving-vehicles-challenge-scale/> (2018)
4. Isele, D., Cosgun, A.: To go or not to go: a case for q-learning at unsignalized intersections. In: Proceedings of the 34th International Conference on Machine Learning, p. PMLR 70 (2017)
5. Ishikawa, S., Arai, S.: Cooperative learning to achieve driving strategy for suppression of traffic jam. In: Proceedings of the Annual Conference of JSAI JSAI2016, 1H4OS05a4–1H4OS05a4 (2016)
6. Kendall, A., Hawke, J., Janz, D., Mazur, P., Reda, D., Allen, J.M., Lam, V.D., Bewley, A., Shah, A.: Learning to drive in a day. In: arXiv preprint. [arXiv:1807.00412](https://arxiv.org/abs/1807.00412) (2018)
7. Krizhevsky, A., Sutskever, I., Hinton, G.E.: Imagenet classification with deep convolutional neural networks. *Adv. Neural Inf. Process. Syst.* **25**, 1097–1105 (2017)
8. Laboratory of Harmonious Systems Engineering, Research Group of Synergetic Information Engineering, Division of Computer Science and Information Technology, Graduate School of Information Science and Technology, Hokkaido University: CEATEC2017 demonstration. YouTube. <http://bit.ly/2g8cPXE> (2017)
9. Mnih, V., Kavukcuoglu, K., Silver, D., Rusu, A.A., Veness, J., Bellemare, M.G., Graves, A., Riedmiller, M., Fidjeland, A.K., Ostrovski, G., Petersen, S., Beattie, C., Sadik, A., Antonoglou, I., King, H., Kumaran, D., Wierstra, D., Legg, S., Hassabis, D.: Human-level control through deep reinforcement learning. *Nature* **518**(7154), 529–533 (2015)
10. Ogawa, I., Yokoyama, S., Yamashita, T., Kawamura, H., Sakatoku, A., Yanagihara, T., Ogishi, T., Tanaka, H.: Implementation of mutual concessions of autonomous cars using deep q-network. In: Proceedings of The 16th ITS Asia-Pacific Forum FUKUOKA 2018, p. 110 (2018)
11. Okada, S., Omae, M.: Study on cooperative driving of automated driving vehicles through shared spatial information infrastructure. *J. Automot. Eng*
12. Preferred Networks, Inc.: Autonomous robot car control demonstration in CES2016. YouTube. <https://youtu.be/7A9UwxvgeV0> (2016)
13. Rios-Torres, J., Malikopoulos, A.A.: Automated and cooperative vehicle merging at highway on-ramps. *IEEE Trans. Intell. Transp. Syst.* **18**(4), 780–789 (2017)
14. Rios-Torres, J., Malikopoulos, A.A.: A survey on the coordination of connected and automated vehicles at intersections and merging at highway on-ramps. *IEEE Trans. Intell. Transp. Syst.* **18**(5), 1066–1077 (2017)
15. Sato, K., Hashimoto, M., Suganuma, N., Kato, S., Shiba, N., Hanai, M., Takada, H., Amanuma, M., Ktsuna, M., Oishi, J.: Field experiment of ldm global concept for cooperative automated driving. In: The Proceedings of 13th ITS Symposium (2015)
16. Strategic Conference for the Advancement of Utilizing Public and Private Sector Data, Strategic Headquarters for the Advanced Information and Telecommunications Network Society:

- Public-private its initiative/roadmaps 2017. [https://japan.kantei.go.jp/policy/it/itsinitiative\\_roadmap2017.pdf](https://japan.kantei.go.jp/policy/it/itsinitiative_roadmap2017.pdf) (2017)
17. Suzuki, S., Abe, K.: Topological structural analysis of digitized binary images by border following. *Comput. Vis. Graph. Image Proc.* **30**(1), 32–46 (1985)
  18. Zhang, Z.: A flexible new technique for camera calibration. *IEEE Trans. Pattern Anal. Mach. Intell.* **22**(11), 1330–1334 (2000)

# Floating Car Data-Based Real-Time Road Traffic Prediction System and Its Application in Macau Grand Prix Event



Ngoc-vai Chiang, Lap-mou Tam, Kin-hou Lai, Ka-in Wong  
and Wai-meng Si Tou

**Abstract** Traffic congestion is a major concern in Macau. To alleviate the situation, this study aims to develop an effective and reliable real-time road traffic prediction system for Macau. In most existing studies, traffic prediction systems are developed based on moving-average models and using only historical traffic data. Considering that new arriving data usually contain the most updated and useful traffic information, this study proposes to construct the prediction model using a novel machine learning algorithm, namely extreme learning machine, which is capable of learning the data behavior in an extremely fast and online manner. To collect real-time traffic data, floating car data from public transportation are employed as the data source in this study. By performing online learning and real-time traffic prediction simultaneously, the proposed system is able to provide reliable real-time forecasting traffic information, even in the presence of undesired traffic changes. To evaluate the performance of the proposed system, a case study on the Macau Grand Prix event is conducted. During this event, many road sections are closed and more than half of the bus routes need to be diverted. The evaluation results show that the proposed system is effective for predicting future traffic conditions under the complicated traffic situation and different time frames. Based on the forecasting information, the traffic authorities will be able to make corresponding traffic management measures and provide optimal route guidance for the citizens.

---

N. Chiang · K. Lai · K. Wong (✉) · W. Si Tou  
Transport Bureau, Macau, China  
e-mail: [rwong@dsat.gov.mo](mailto:rwong@dsat.gov.mo)

N. Chiang  
e-mail: [NVChiang@dsat.gov.mo](mailto:NVChiang@dsat.gov.mo)

K. Lai  
e-mail: [KHLAI@dsat.gov.mo](mailto:KHLAI@dsat.gov.mo)

W. Si Tou  
e-mail: [WMSITOU@dsat.gov.mo](mailto:WMSITOU@dsat.gov.mo)

L. Tam  
Department of Electromechanical Engineering, University of Macau, Zhuhai, China  
e-mail: [fstlmt@umac.mo](mailto:fstlmt@umac.mo)



**Keywords** Traffic prediction · Intelligent transport system · Floating car data · Macau grand prix · Extreme learning machine

## 1 Introduction

Being a previous colony of Portugal and now a Special Administrative Region of China, Macau is a beautiful city well-known for its mixed culture of Chinese and Western. Every year, more than thirty millions tourists visit Macau for sightseeing, gambling and attending annual mass events such as Macau Arts Festival and Macau Grand Prix. This brings not only huge benefits to Macau's economy, but at the same time huge impact to Macau's traffic environment. According to Macau Statistics and Census Service, the vehicle density of Macau has already reached 557 vehicles per kilometer in mid-2018. With the ever-increasing number of tourists, more and more travelling buses and taxies need to be put into service, unavoidably increasing the traffic pressure. Moreover, during some of the mass events, temporary traffic arrangement would be implemented, which further worsens the already complicated traffic situation. Taking Macau Grand Prix as an example, many roads need to be temporarily closed during this event, and thus many bus routes have to be diverted or suspended, affecting the traffic conditions of other surrounding roads. The result is that traffic congestion always happens—even at non-rush hour, and the travelling time is almost unpredictable, which can be very inconvenient for road users. Therefore, in order to alleviate the problems, this study aims to develop a road traffic prediction system for Macau, such that, based on the predictions of the proposed system, the traffic authorities are able to make optimal traffic management plans and improve the traffic situation.

Developing an accurate and reliable prediction model for Macau traffic, however, can be extremely challenging due to its complex road characteristics. As limited by the available area, most roads in Macau are only two-lane roads (one lane for each direction), and the road width is usually very narrow (generally around 5.5 m for two-lane). Some statistical studies already indicated that narrow lane width strongly affects the drivers' behavior and the corresponding driving speed [1–3]. Thus, the average flow speed in Macau usually varies a lot, and traffic congestion can happen very easily. Furthermore, the road network of Macau contains too many intersections and loops. When a congestion occurs at the intersections, it is very difficult to sort out because the vehicles can easily get stuck in the surrounding loops, and hence the congestion can spread out quickly. What makes the problem even worse is that there are numerous traffic lights and bus stops around the city, and their distribution is very dense, which further reduces the overall flow speed in Macau. Obviously, all these factors together make the prediction of Macau traffic a highly complex and uncertain problem to deal with.

In the literature, various methods have been proposed to handle complicated traffic prediction problems [4]. A famous one is with the use of historical average models, such as the autoregressive integrated moving average models in [5, 6] and the

vector autoregressive models in [7]. However, these approaches only use time-series data as the model inputs, without considering the spatial information. As the traffic flow of any road in Macau can change rapidly and is correlated to the surrounding traffic, neglecting the spatial data would only lead to poor prediction accuracy. Artificial intelligence (AI) methods, such as neural network [8–10], fuzzy logic [11, 12] and support vector machine (SVM) [13, 14], which have been recently employed for traffic prediction, should be more favorable for the current study. In these AI approaches, the inputs are not restricted to time-series data but anything. That is, any traffic-related factors can be included as the inputs of the prediction model, which can greatly enhance the prediction accuracy as compared to time-series approaches [15]. A previous study by Shi et al. [16] already demonstrated that neural network can be applied to the prediction of Macau traffic. Still, limitations of these conventional AI methods are that: (i) they are usually computationally-intensive; (ii) the model parameters are sub-optimal; and (iii) some of the training algorithms may suffer from overfitting risk, leading to poor generalization performance. Moreover, since these methods can only build the prediction model based on historical data, the new arriving real-time data, which may contain the most updated traffic information, are totally wasted and cannot be used to update the model, unless the model is re-trained from scratch.

Considering the above issues of conventional methods, an emerging AI algorithm called extreme learning machine (ELM) [17–19] is employed in this study. It is a machine learning algorithm that overcomes most of the aforementioned drawbacks, requires extremely low computational complexity, and has the capability of learning new data online [20]. These features are beneficial for addressing the difficulties in Macau traffic prediction. Since the algorithm is a data-driven method, lots of traffic data are required for training the model. Owing to the fact that very limited sensors are currently available in the road network of Macau, this study further proposes to use another emerging and effective way for data collection—floating car data (FCD) [21, 22]. Comparing with other in situ data collection methods such as magnetic loops and microwave radar, FCD have the advantage that the installation location is not limited to the road environment. Any vehicle equipped with global positioning system (GPS) can be used as the source of FCD. They can cover almost everywhere of Macau with very low cost and reflect the real-time traffic very effectively. It is believed that with FCD, the proposed system can provide more accurate traffic predictions for Macau.

In short, this study proposes a traffic prediction system that utilizes FCD as the data source and ELM model as the prediction method. The system is suitable for real-time traffic prediction with online learning ability. To show the effectiveness of the proposed system, a case study on the Macau Grand Prix event in 2017 is conducted for evaluation of the system. Based on the result, possible traffic management plan for the Macau Grand Prix event is discussed and analyzed.

## 2 Design of Proposed System

A schematic diagram of the proposed traffic prediction system is shown in Fig. 1. The purpose of the proposed system is to predict the future traffic flow based on the current traffic flow. It basically consists of three parts: (i) FCD collection system, (ii) data processing system, and (iii) traffic flow prediction system. In the following sub-sections, details of each part of the system are presented.

### 2.1 FCD Collection System

The FCD collection system aims to collect real-time traffic data via internet. Currently, most of the public transportation in Macau (taxies, buses, etc.) are already equipped with Global Positioning System (GPS). Each of them can act as an in situ traffic probe to monitor the real-time traffic. Along with the GPS location of the vehicle (latitude, longitude, head direction), other useful information are also needed for data processing purposes, including the time, vehicle ID, vehicle speed, vehicle state (e.g., whether the taxies are empty, whether the buses are picking passengers) and engine state (e.g., whether the engine is running). All these information are stored together in the form of data packets. At every short interval (around 10–30 s, depending on the number of available vehicles), each vehicle sends one data packet of that instant via 3G wireless transmission back to the central server owned by the Macau government. After the data are received at the central server, they are then transferred to the data processing system.

### 2.2 Data Processing System

Based on the data collected from the FCD collection system, the data processing system utilizes certain algorithms to convert them into useful information for traffic prediction.

Firstly, a quick map-matching algorithm is employed to determine which roads the vehicles are located. This algorithm directly compares the GPS data (latitude and longitude) with an electronic map provided by the Macau government, and validates the result by checking if the head direction of the vehicle is same as the road direction. If no road can be located for the corresponding GPS data, or the head direction is different from that of the located road, the data will be omitted.

After the road of the data are specified, the next step is to filter out the useless data. A filtering algorithm is therefore employed. The algorithm checks the vehicle state and the engine state of the data. For buses and taxies, if the engine is not running, it is assumed that the vehicle is not operating on that street. For taxies, if the engine is running, but the taxi is empty and is not moving for 60 s or the moving distance is

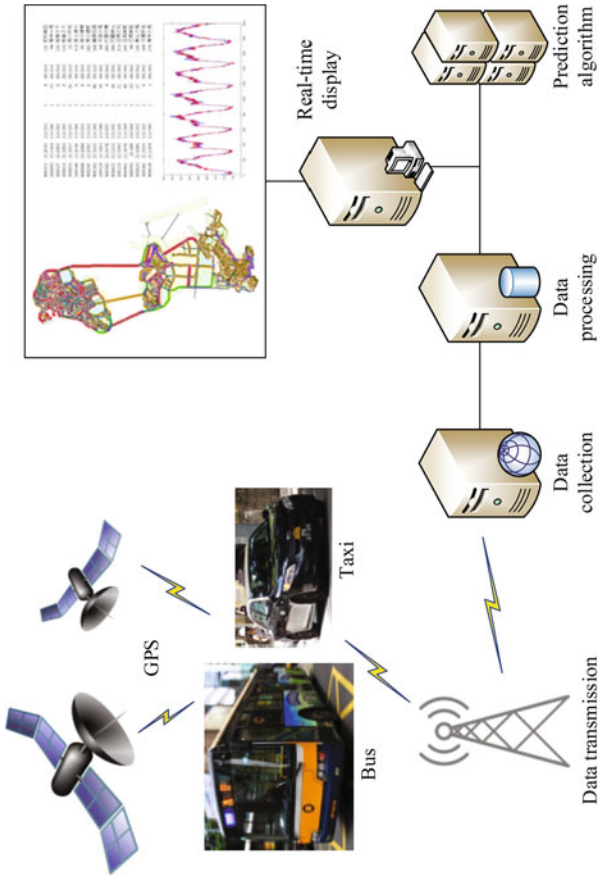


Fig. 1 Overview of the proposed system

less than 8 m, it is assumed that the taxi is waiting for passengers. For buses, if the engine is running, but the bus is near a bus stop and is picking up passengers, it is assumed that the bus is not on the main lane but the bus lane. For all these mentioned cases, the data are filtered.

The last step of this system is to compute the traffic flow of each road. Based on the remaining data, the average vehicle speed of each road is calculated. A time frame of 5-minutes is adopted in this system, and the average speed is updated every minute. That is, at every one-minute interval, the average flow speed of the past 5 min is determined. Finally, the processed data (time, road name, flow speed) are passed to the traffic flow prediction system for training the model and making predictions.

### 2.3 Traffic Flow Prediction System

The traffic flow prediction system is the core of the proposed system. The reliability and accuracy of the prediction depends greatly on the prediction model. As mentioned, an emerging machine learning algorithm, namely ELM, is employed in this study for training the prediction model.

#### 2.3.1 ELM Algorithm

The ELM algorithm [17, 18] was originally designed to overcome the shortcomings of slow learning speed in conventional learning algorithms. The key concept of ELM is that the input weights to hidden nodes of the feature mapping layer need not be tuned, and that the feature mapping layer can be implemented by either random hidden nodes or kernels [19]. In the following, the derivation of the ELM learning algorithm is provided.

The model formulation of ELM is:

$$f(\mathbf{x}) = \mathbf{h}(\mathbf{x})\boldsymbol{\beta} = \sum_{i=1}^L \beta_i h_i(\mathbf{a}_i, b_i, \mathbf{x}) \quad (1)$$

where  $\mathbf{x} = [x_1, \dots, x_n]$  is the input vector,  $\mathbf{h}(\cdot) = [h_1(\cdot), \dots, h_L(\cdot)]$  is the feature mapping vector,  $\boldsymbol{\beta} = [\beta_1, \dots, \beta_L]^T$  is the output weight vector,  $\mathbf{a}_i = [a_{i1}, \dots, a_{in}]^T$  is the input weight vector,  $b_i$  is a bias term added to the hidden nodes,  $L$  is the number of hidden nodes and  $n$  is the number of inputs.

According to theory of ELM [17], as long as the number of the hidden nodes is large enough, the parameters of the hidden nodes can be generated randomly and remain fixed, and the resulting model still retains very high generalization. Therefore, it is only necessary to learn the output weights  $\boldsymbol{\beta}$  of the model. Given a training data set  $\mathcal{D}$ , output weights  $\boldsymbol{\beta}$  can be obtained by solving the following linear system:

$$\mathbf{H}\boldsymbol{\beta} = \mathbf{Y} \quad (2)$$

where  $\mathbf{H} = [\mathbf{h}(\mathbf{x}_1), \mathbf{h}(\mathbf{x}_2), \dots, \mathbf{h}(\mathbf{x}_N)]^T$  is a matrix of the feature mapping output.

The solution of  $\beta$  to Eq. (2) can be obtained with least-squares method:

$$\beta = \mathbf{H}^\dagger \mathbf{Y} \tag{3}$$

where  $\mathbf{H}^\dagger$  is the Moore-Penrose pseudoinverse of matrix  $\mathbf{H}$  that can be calculated using the orthogonal projection method (see [17]).

To improve the generalization performance and robustness of the solution, the regularization factor  $C$  can be added to the diagonal of  $\mathbf{H}^T \mathbf{H}$  or  $\mathbf{H} \mathbf{H}^T$ . According to Barlett's theory, this resulting solution tends to have better and more stable prediction performance, as verified in [18].

### 2.3.2 Online Learning of ELM

Since the training algorithm in ELM is a least-squares method, it can be easily extended to recursive least-squares (RLS) for online learning. The following algorithm shows the RLS form of ELM:

For the  $(k + 1)$ th arriving training data,

- (a) Calculate the hidden layer output matrix  $\mathbf{H}_{k+1}$ ;
- (b) Update the output weights using the following equations:

$$\mathbf{P}_{k+1} = \mathbf{P}_k - \mathbf{P}_k \mathbf{H}_{k+1}^T (\mathbf{I} + \mathbf{H}_{k+1} \mathbf{P}_k \mathbf{H}_{k+1}^T)^{-1} \mathbf{H}_{k+1} \mathbf{P}_k \tag{4}$$

$$\beta^{(k+1)} = \beta^{(k)} + \mathbf{P}_{k+1} \mathbf{H}_{k+1}^T (\mathbf{T}_{k+1} - \mathbf{H}_{k+1} \beta^{(k)}) \tag{5}$$

It should be noted that this algorithm is used when a base ELM model is initialized, so it is only used for updating a trained model with new arriving data.

### 2.3.3 Structure of Prediction Model

Based on the ELM algorithm and FCD, a model can be trained. The purpose of the model is to predict the future traffic flow based on the current traffic condition. As mentioned, the model considers not only the past traffic flow of the road, but also the flow in the surrounding. That is, the average traffic flow into the road and the average traffic flow out of the road. A schematic diagram of the model structure is shown in Fig. 2.

It can be seen from Fig. 2 that the structure of the proposed prediction model only concerns the traffic flow in and out, without considering how many roads are actually linked to the target road. This is a more general structure since even if the driving direction of the target road is changed, it is not necessary to revise the model structure to keep up with the revised road network structure. In this study, the traffic flow in and out are respectively calculated by averaging the flow speed of the surrounding

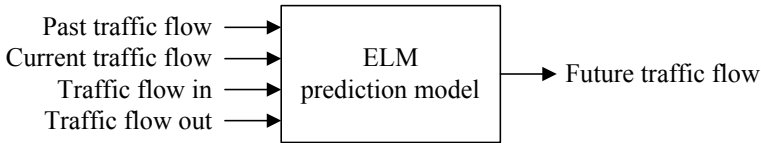


**Fig. 2** Model structure

roads. Further investigation on how they should be obtained would be left for future study. With the prediction model, the traffic authorities can provide any flow speed profile to it for other useful analysis.

### 3 Evaluation of Proposed System

To evaluate the prediction performance of the proposed system, a case study on the Macau Grand Prix event is conducted. In the following sub-sections, background of the event is firstly introduced to show its impact to the traffic situation in Macau and the major difficulties in traffic prediction of this case. Then, traffic prediction models for different prediction time frames are trained based on the data collected before the Macau Grand Prix 2017 event. After that, the trained model is used to predict the traffic conditions during the Macau Grand Prix 2017 event. Finally, the prediction results of the models are compared with the actual traffic conditions to demonstrate its prediction performance.

#### 3.1 Macau Grand Prix and Its Impact

Macau Grand Prix is an annually held motor-racing event in Macau, where top drivers from all around world are attracted to compete on the only street racing circuit in Asia, known as the ‘Guia Circuit’ (see Fig. 3).

Famous by its unique and challenging nature, the Guia Circuit has been one of the most demanding circuits in the world. As shown in Fig. 3, the circuit contains an ultra-long straight that allows vehicles to speed up to its limit, sharply twisting corners that require drivers to have superior driving and handling skills, and a high variation in altitude (over 30 m differences) that challenges the engineers to tune up the vehicles to keep their hill-climbing performance.

Since this circuit is mainly composed of streets, many streets and roads have to be closed as part of the racing track during the Macau Grand Prix event. Access to some of the surrounding roads and areas is also restricted. Carefully planned traffic management measures have to be implemented to minimize the impact of the events and to ensure the transportation of the visitors, event attendants and local citizens







Fig. 4 Examples of traffic management measures taken during Macau Grand Prix (retrieved from news provided by Macau Traffic Bureau)

### 3.2 Prediction Performance

The Macau Grand Prix 2017 event is held in November, so the traffic data collected in November 2017 are employed. The data before the period of Macau Grand Prix event (November 1–15), representing the traffic information under usual situation, are used to train the prediction model of the system, whereas the data during the period of Macau Grand Prix event (November 16–19), representing the traffic information under traffic changed situation, are used to test the prediction model. In order to demonstrate the superiority of the proposed ELM prediction model, SVM is also employed in this study to generate prediction models, so that their performance can be compared.

#### 3.2.1 SVM Model

As SVM model is employed for comparison, its formulation is briefly introduced here. The general form of the SVM model can be represented by:

$$f(x) = h(x)\beta + b \tag{6}$$

where  $\mathbf{h}(\mathbf{x})$  and  $\boldsymbol{\beta}$  are same as those in ELM, that is, the feature mapping vector and the model weight respectively, and  $b$  is a bias term contributes to the shifting of the model origin.

Although it has similar form to the ELM model, the methods for calculating the model weights are totally different. The key to train the SVM is to solve the following optimization problem:

$$\min \frac{1}{2} \|\boldsymbol{\beta}^2\| + C \sum_{k=1}^N (\xi_k + \xi_k^*) \text{ subject to: } \begin{cases} y_k - f(x) - \xi_k \leq \epsilon \\ f(x) - y_k - \xi_k^* \leq \epsilon \\ \xi_k, \xi_k^* \geq 0 \end{cases} \quad (7)$$

where  $y_k$  is the target output,  $N$  is the number of training data,  $\xi_k \geq 0$  and  $\xi_k^* \geq 0$  are two slack variables to control the model accuracy within the “ $\epsilon$ -tube”,  $\epsilon > 0$  is the user-specified precision, and  $C$  is the regularization factor.

Solving of Eq. (7) is a quadratic programming (QP) problem and the resulting SVM model can be re-written in a more detailed form:

$$f(\mathbf{x}) = \sum_{k=1}^N (\alpha_k - \alpha_k^*) K(\mathbf{x}, \mathbf{x}_k) + b \quad (8)$$

where  $\alpha_k, \alpha_k^*$  are the trained support vectors, and  $K(\mathbf{x}, \mathbf{x}_k)$  is a user-specified kernel function satisfying the Mercer’s condition.

Since the learning process of SVM requires solving a QP problem, a large training data set size may incur high computational cost for the learning process. Moreover, as SVM adopts kernel functions and support vectors for feature mapping, it is relatively difficult to extend the algorithm to online learning.

### 3.2.2 Model Parameter Tuning

In the algorithms of both ELM and SVM, certain parameters need to be specified by the user. For ELM, two parameters are needed, namely the regularization factor and the number of hidden nodes, while for SVM, three parameters are needed, including the regularization factor, the basis width parameter of the kernel function and the precision. To select the optimal values for these model parameters, leave-one-out cross-validation is applied in this study.

### 3.2.3 Model Evaluation

Avenida de Venceslau de Moraes, which may suffer from serious traffic congestion issue during the Macau Grand Prix event, is selected in this study for illustrative purpose. This is a long road located near the racing track of Guia Circuit. It is linked to ten roads, and one of them is closed during the Grand Prix event (see Fig. 5). This

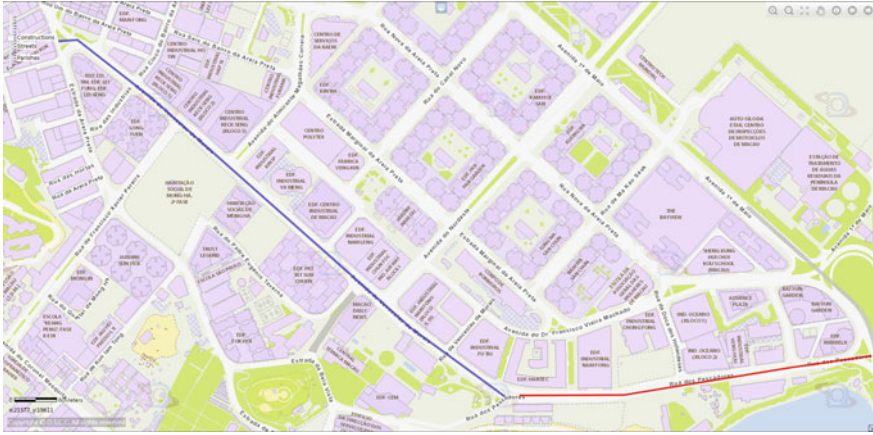


**Fig. 5** Blue: Avenida de Venceslau de Morais; Red: closed during Macau Grand Prix (retrieved from Macau Online Map provided by Macau Cartography and Cadastre Bureau)

illustrative example can evaluate if the model can provide accurate prediction of a road even when some of the surrounding roads are closed or blocked.

As mentioned, the proposed ELM model has the online learning ability that allows adjustment of its prediction performance based on the real-time arriving data. To demonstrate its effectiveness, the prediction model of ELM is updated sequentially when new data are seen. The overall prediction performance of the models is evaluated by using root-mean-squared error (*RMSE*).

For each modeling method, three models are built: one is used to predict the traffic flow for the future 5 min (e.g., at 09:00, the average traffic flow of 09:01–09:05 is predicted); one is for the future 30 min (e.g., at 09:00, the average flow of 09:25–09:30 is predicted); and the remaining one is for the future 1 h (e.g., at 09:00, the average flow of 09:55–10:00 is predicted). These results are included to evaluate whether the models are capability of predicting a longer period of time (i.e., long-term prediction). The results are provided in Fig. 6 and Table 1.

**Table 1** *RMSE* of prediction result for Avenida de Venceslau de Morais

	5 min	30 min	1 h
ELM (without online update)	3.4668	3.6927	3.9215
ELM (with online update)	3.1759	3.5220	3.5470
SVM	4.3081	4.5228	4.9799

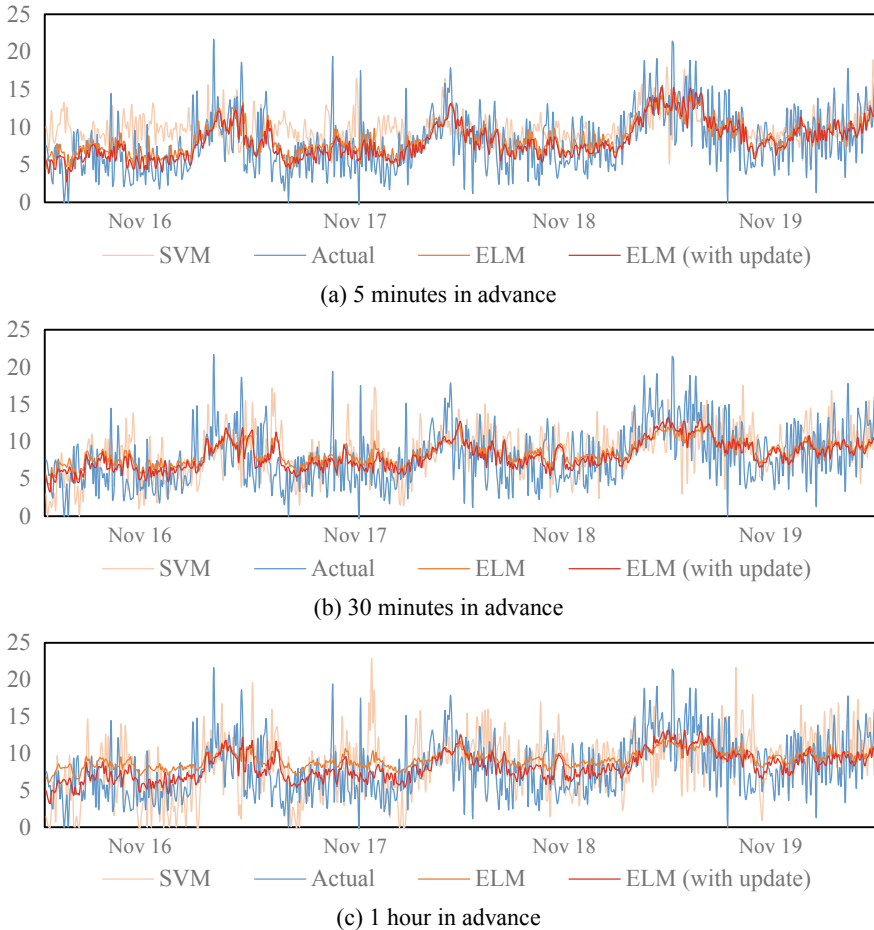


Fig. 6 Prediction result for Avenida de Venceslau de Morais

### 3.3 Discussions of Results

The results from Table 1 and Fig. 6 show that the proposed ELM traffic prediction model can handle the complicated Macau road traffic prediction problem effectively. Although it cannot perfectly match the actual flow speed profile, it can still follow the trend effectively. The reason could be that the model tries to fit all the data and thus all the “spikes” are smoothed out as they might be considered as outliers in the training algorithm. From the results, in terms of both accuracy and tracking ability, the proposed ELM model is superior to another famous AI algorithm, namely SVM. In terms of long-term prediction, worse results are seen for longer prediction period for ELM. This is reasonable because of the high variation in Macau traffic flow.

It is believed that further using some feature extraction methods and adding some representative inputs can help to improve the results, and it would be left for future study. Finally, the results from Table 1 demonstrated that the performance of the proposed ELM model can be improved by updating with the newest data in situ. These results also imply that the model can adapt to any kind of traffic situation, even under a large traffic change event, as long as the data are available for model update.

### 4 Applications of Proposed System

When there is a road being blocked, closed or under traffic jam, it is of great interest to know how the traffic on its surrounding road would be affected. Fortunately, as demonstrated above, such impact can be observed with the prediction model. This can help the government to understand how much impact a road blockage will bring to its surrounding and then decide whether that target road should be closed or not, which is very useful for making optimal traffic management plan.

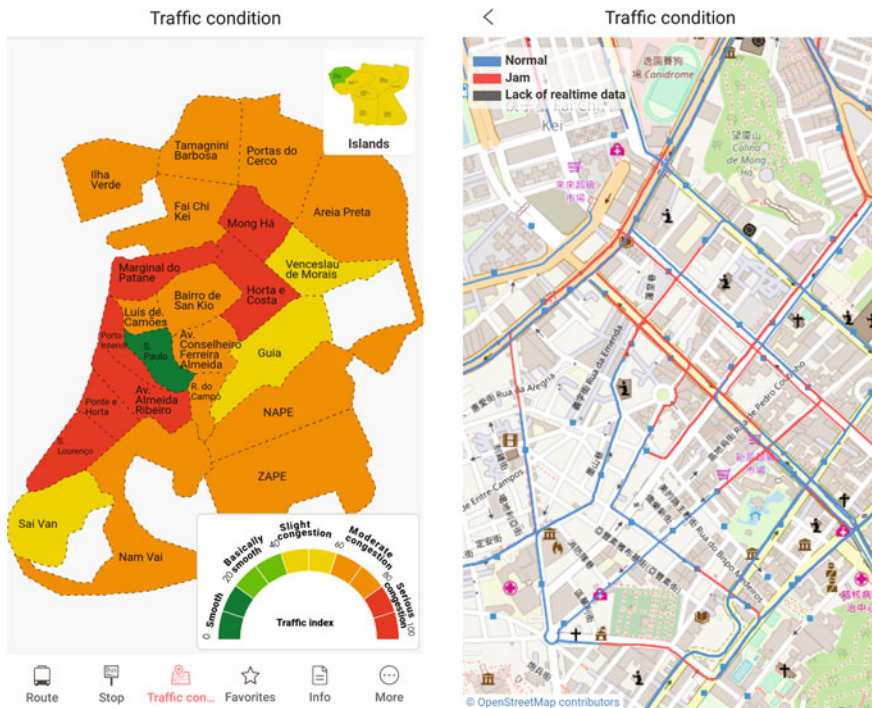


Fig. 7 Mobile app for traffic prediction display

On the other hand, using the prediction system, the traffic authorities can investigate the traffic congestion trend up to 1 h ahead (or even longer if the corresponding models are trained). If the traffic congestion is likely to occur in the near future, the traffic authorities can do some traffic arrangements, such as adjusting traffic lights or assigning police forces to direct the on-site traffic.

Based on the proposed prediction system, the traffic authorities will be able to publish the near term traffic prediction through mobile app and website, so that the general public can have a better understanding about the traffic conditions. An example of the mobile app is shown in Fig. 7, where the traffic conditions at different roads are presented using different color lines.

## 5 Conclusions

In this study, a novel traffic prediction system for Macau is proposed. Two emerging techniques, including a machine learning algorithm called ELM and a data collection strategy called FCD, are employed and combined in the making of this system. The proposed system is able to provide accurate and reliable traffic prediction, even in the presence of undesired traffic changes. A case study on the Macau Grand Prix 2017 event was conducted and the result has demonstrated the effectiveness of the proposed system. With the assistance of the proposed system, the governmental authority can make optimal traffic management plans for improving the traffic situation in Macau.

## References

1. Board TR, National Academies of Sciences E, Medicine Impact of Shoulder Width and Median Width on Safety. The National Academies Press, Washington, DC (2009). <https://doi.org/10.17226/14252>
2. Rosey, F., Auberlet, J.M., Moisan, O., Dupre, G.: Impact of narrower lane width comparison between fixed-base simulator and real data. *Transp. Res. Rec.* **2138**, 112–119 (2009). <https://doi.org/10.3141/2138-15>
3. Liu, S., Wang, J.H., Fu, T.: effects of lane width, lane position and edge shoulder width on driving behavior in underground urban expressways: a driving simulator study. *Int. J. Environ. Res. Public Health* **13**(10) (2016). <https://doi.org/10.3390/ijerph13101010>
4. Vlahogianni, E.I., Karlaftis, M.G., Golias, J.C.: Short-term traffic forecasting: where we are and where we're going. *Transp. Res. Part C Emerg. Technol.* **43**, 3–19 (2014). <https://doi.org/10.1016/j.trc.2014.01.005>
5. Smith, B.L., Williams, B.M., Oswald, R.K.: Comparison of parametric and nonparametric models for traffic flow forecasting. *Transp. Res. Part C Emerg. Technol.* **10**(4), 303–321 (2002). [https://doi.org/10.1016/s0968-090x\(02\)00009-8](https://doi.org/10.1016/s0968-090x(02)00009-8)
6. Williams, B.M., Hoel, L.A.: Modeling and forecasting vehicular traffic flow as a seasonal ARIMA process: theoretical basis and empirical results. *J. Transp. Eng. Asce* **129**(6), 664–672 (2003). [https://doi.org/10.1061/\(asce\)0733-947x\(2003\)129:6\(664\)](https://doi.org/10.1061/(asce)0733-947x(2003)129:6(664))
7. Chandra, S.R., Al-Deek, H.: Predictions of freeway traffic speeds and volumes using vector autoregressive models. *J. Intell. Transp. Syst.* **13**(2), 53–72 (2009). <https://doi.org/10.1080/15472450902858368>

8. Vlahogianni, E.I., Karlaftis, M.G., Golias, J.C.: Optimized and meta-optimized neural networks for short-term traffic flow prediction: a genetic approach. *Transp. Res. Part C Emerg. Technol.* **13**(3), 211–234 (2005). <https://doi.org/10.1016/j.trc.2005.04.007>
9. Chan, K.Y., Dillon, T.S., Singh, J., Chang, E.: Neural-network-based models for short-term traffic flow forecasting using a hybrid exponential smoothing and Levenberg-Marquardt algorithm. *IEEE Trans. Intell. Transp. Syst.* **13**(2), 644–654 (2012). <https://doi.org/10.1109/tits.2011.2174051>
10. Zheng, W.Z., Lee, D.H., Shi, Q.X.: Short-term freeway traffic flow prediction: Bayesian combined neural network approach. *J. Transp. Eng. Asce* **132**(2), 114–121 (2006). [https://doi.org/10.1061/\(asce\)0733-947x\(2006\)132:2\(114\)](https://doi.org/10.1061/(asce)0733-947x(2006)132:2(114))
11. Yin, H.B., Wong, S.C., Xu, J.M., Wong, C.K.: Urban traffic flow prediction using a fuzzy-neural approach. *Transp. Res. Part C Emerg. Technol.* **10**(2), 85–98 (2002). [https://doi.org/10.1016/s0968-090x\(01\)00004-3](https://doi.org/10.1016/s0968-090x(01)00004-3)
12. Stathopoulos, A., Dimitriou, L., Tsekeris, T.: Fuzzy modeling approach for combined forecasting of urban traffic flow. *Comput. Aided Civ. Infrastruct. Eng.* **23**(7), 521–535 (2008). <https://doi.org/10.1111/j.1467-8667.2008.00558.x>
13. Wu, C.H., Ho, J.M., Lee, D.T.: Travel-time prediction with support vector regression. *IEEE Trans. Intell. Transp. Syst.* **5**(4), 276–281 (2004). <https://doi.org/10.1109/tits.2004.837813>
14. Hong, W.C.: Traffic flow forecasting by seasonal SVR with chaotic simulated annealing algorithm. *Neurocomputing* **74**(12–13), 2096–2107 (2011). <https://doi.org/10.1016/j.neucom.2010.12.032>
15. Lippi, M., Bertini, M., Frasconi, P.: Short-term traffic flow forecasting: an experimental comparison of time-series analysis and supervised learning. *IEEE Trans. Intell. Transp. Syst.* **14**(2), 871–882 (2013). <https://doi.org/10.1109/tits.2013.2247040>
16. Shi, Y.D., Pan, Y.Y., Li, J.Q.: Urban short-term traffic forecasting based on grey neural network combined model: Macao experience. In: *Proceeding of 2009 International Workshop on Intelligent Systems and Applications*, 23–24 May 2009, pp. 1–4 (2009). <https://doi.org/10.1109/iwisa.2009.5073229>
17. Huang, G.B., Zhu, Q.Y., Siew, C.K.: Extreme learning machine: theory and applications. *Neurocomputing* **70**(1–3), 489–501 (2006). <https://doi.org/10.1016/j.neucom.2005.121.126>
18. Huang, G.B., Zhou, H.M., Ding, X.J., Zhang, R.: Extreme learning machine for regression and multiclass classification. *IEEE Trans. Syst. Man Cybern. B Cybern.* **42**(2), 513–529 (2012). <https://doi.org/10.1109/tsmcb.2011.2168604>
19. Huang, G.B.: What are extreme learning machines? Filling the gap between Frank Rosenblatt’s dream and John von Neumann’s puzzle. *Cogn. Comput.* **7**(3), 263–278 (2015). <https://doi.org/10.1007/s12559-015-9333-0>
20. Wong, P.K., Gao, X.H., Wong, K.I., Vong, C.M.: Online extreme learning machine based modeling and optimization for point-by-point engine calibration. *Neurocomputing* **277**, 187–197 (2018). <https://doi.org/10.1016/j.neucom.2017.02.104>
21. de Fabritiis, C., Ragona, R., Valenti, G.: Traffic estimation and prediction based on real time floating car data. In: *Proceedings of the 11th International IEEE Conference on Intelligent Transportation Systems*, pp. 197–203 (2008). <https://doi.org/10.1109/itsc.2008.4732534>
22. Simroth, A., Zahle, H.: Travel time prediction using floating car data applied to logistics planning. *IEEE Trans. Intell. Transp. Syst.* **12**(1), 243–253 (2011). <https://doi.org/10.1109/tits.2010.2090521>

**Part IV**  
**Infrastructure Technologies**  
**for Practical ITS**



# Modeling Speed Profile of Two-Way Two-Lane Expressways in Japan



Makoto Kasai, Jian Xing and Shin-ichi Narushima

**Abstract** Recently, several studies have tried to reveal the level of service of traffic flow using data collected with probe cars. In particular, it was reported that the variation of spot speed along the flow direction could be larger than previously believed on two-way two-lane (TWTL) expressways. Although the variation may be due to driver behaviors such as longitudinal alignment and merging at the end of auxiliary lanes, guidelines to effectively improve locally reduced speeds have not been published. Toward this end, in this study a model predicting the speed profile in TWTL sections is proposed. This model is mainly composed of three terms expressing “gradual attenuation” along the flow direction, “merging conflict” causing slow-down after the end of an auxiliary passing lane, and “local speed reduction” at sag sections. The model is calibrated with probe car data collected on representative TWTL expressways in Japan. With respect to the root mean square error, the accuracy of estimation was acceptable. Finally, a future direction for further improvement and way to implement the model are discussed.

**Keywords** Two-way two-lane expressway · Probe data · ETC 2.0 · Speed profile · Prediction model

---

M. Kasai (✉)

Department of Civil Engineering and Architecture, National Institute of Technology, Akita College, 1-1 Iijima-Bunkyo-cho, Akita 011-8511, Japan  
e-mail: [kasai@akita-nct.ac.jp](mailto:kasai@akita-nct.ac.jp)

J. Xing

Traffic and Environment Research Department, Nippon Expressway Research Institute Company Limited, Tokyo, Japan  
e-mail: [xing@ri-nexco.co.jp](mailto:xing@ri-nexco.co.jp)

S. Narushima

Niigata Regional Branch, East Nippon Expressway Company Limited, Tokyo, Japan  
e-mail: [s.narushima.aa@e-nexco.co.jp](mailto:s.narushima.aa@e-nexco.co.jp)

## 1 Introduction

Measurement and improvement of the quality of service (QOS) on highways are major concerns in traffic flow management. Intelligent transportation systems (ITSs), in which traffic flow is monitored on-line and smoothed through dual-communication devices, are expected to play an important role in pro-active traffic management.

ITSs can also contribute to off-line analyses: huge amounts of stored data collected by ITS devices are available for predictions of level of service in the evaluation of alternative plans for road design or re-construction. In Japan, public and private expressway companies as well as the Ministry of Infrastructure, Transport and Tourism (MLIT) have developed and promoted a dual communication device called ETC 2.0 to users (customers). The on-board equipment for ETC 2.0 records and uplinks running data such as time, position, and speed, as measured by a global positioning system [1].

According to the concept of smart utilization of existing road assets advocated by the MLIT in 2015, travel demand management is to be promoted by monitoring traffic flow with probe cars. For this purpose, scientific analyses of huge amounts of stored probe data are essential for determining factors decreasing QOS. In this context, ITSs are expected to store data of traffic flow off-line. In Japan, overtaking using the opposite lane is not allowed and running slower than drivers' expectations may be more common than in countries where such overtaking is permitted. Therefore, drivers in Japan may be highly concerned about speed in their evaluation of level of service.

Off-line analysis with the ETC 2.0 data is a powerful tool to reveal a section of road that is relatively weak in terms of QOS. In rural areas in Japan, expressways are often only two-way two-lane (TWTL) roads rather than multi-lane highways. According to one guideline [2], it is desirable to provide auxiliary lanes to allow overtaking at intervals of approximately 6–10 km. This guideline was written under the assumption that the QOS of traffic flow is not sensitive to longitudinal alignment.

In recent years, several studies (e.g., [3]) using probe car data including ETC 2.0 reported that spot speed tends to vary spatially more than previously believed. This tendency has not previously been observed clearly since detectors that can observe traffic volume and speed are installed only approximately every 10–15 km (strictly speaking, an interchange pair has only one detector). Therefore, it seems that longitudinal alignment possibly affects spot speed in TWTL sections.

This study proposes a model to predict spot speed, accounting for factors such as longitudinal alignment and merging conflict. First, "speed-profile curves" at different flow rates are obtained from ETC 2.0 data. Then, these curves are formulated as functions of flow rate and longitudinal gradient.

## 2 Related Works

### 2.1 *Conventional Measures of Effectiveness*

According to the Highway Capacity Manual (HCM) [4], average travel speed, percentage of time spent following (PTSF), and follower density can all be taken as a measure of effectiveness (MOE) for two-way two-lane expressways. The level of service (LOS) of the overall MOE is expressed in terms of six categories, A to F, in the HCM [4]. These MOEs do not, however, explicitly take longitudinal alignment into account. Other past studies [5, 6] of MOEs for TWTL expressways have also not considered the effect of longitudinal alignment.

Nakamura et al. [5] proposed a performance curve of follower density under the assumption that longitudinal alignment is homogeneous along the flow direction. They pointed out that follower density is the preferable measure to evaluate QOS on TWTL expressways, since average travel time is insensitive to increments of flow rate. Although, of course, PTSF is regarded as a much better approximation of drivers' perception of QOS than average travel time and follower density, it is quite difficult to measure PTSF directly. Consequently, that study related follower density to factors such as length of TWTL, and flow rate.

A criterion for the LOS has also been proposed by the Transportation Development Division of the Oregon Department of Transportation based on field data [7]. However, the criterion does not take longitudinal alignment into account.

### 2.2 *Spatially Varying Speed as an MOE*

To reveal the QOS for representative TWTL expressways in Japan using ETC 2.0 data, "speed profiles" were drawn [3]. The curve shows the speed of the 15th percentile value for every 200-m length of road. Findings of the study can be summarized as follows. (1) There is a tendency for a gradual reduction of speed. In particular, if the length of the TWTL is much larger than the guideline, this tendency is more clearly seen. (2) In some stretches, local reductions of speed are also found (Fig. 1) in sag or ascent sections. For the effective installation of auxiliary passing lanes to improve the LOS, it is important to specify the causes of slow-down and predict locations of slow-down, or predict the LOS of MOEs, such as follower density or PTSF, at every spot.

Since follower density is not directly measured, traffic simulation is often used (e.g., see [5, 8]). The previous study [8] showed that the follower density is not sensitive to traffic conditions, while the speed profile fluctuates strongly. Thus, in the present study, speed profiles that change spot by spot are modeled. The consideration of spot speed is also preferable because it is intuitively comprehensible for users.

In the past, to measure or estimate such MOEs, traffic detector data were often used rather than ETC 2.0 probe data. Traffic detectors are installed at intervals of

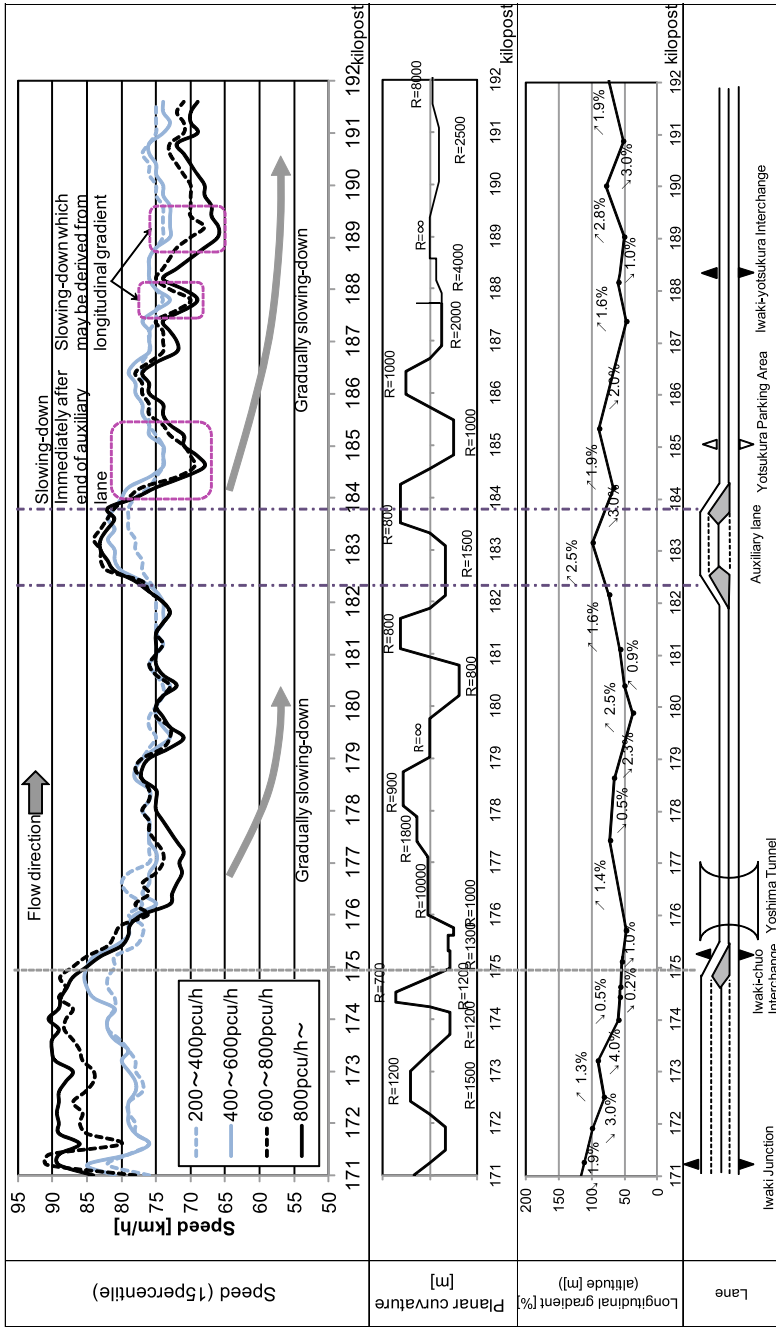


Fig. 1 Speed profile drawn from ETC 2.0 probe data for the Joban Expressway, which is taken as a representative TWTL expressway (revised from [3])

approximately 2 km on interurban expressways in the suburbs of metropolitan areas, while on expressways containing TWTL sections in rural areas of Japan, only one traffic detector is embedded in a basic section (corresponding to an interchange pair). Thus, the fluctuation of spot speed observed by the ETC 2.0 was not revealed until recently. The relation between spot speed and longitudinal gradient was also only discussed to a limited degree due to the sparse installation of traffic detectors.

### 3 Examples of Speed Profile

To aid the modeling of speed profiles for TWTL sections, the speed profiles for the Joban Expressway are shown in Fig. 1. To draw speed profiles, the speed of a probe car is linked with flow rate. The speed distribution of probe cars is specified every 200 m. In Fig. 1, the 15th percentile speed profile is shown for every rank of flow rate. The 15th percentile speed approximately corresponds to the cumulative frequency from  $-\infty$  to  $\mu - \sigma$ , where  $\mu$  is the mean and  $\sigma$  is the standard deviation in a normal distribution.

In Fig. 1, three characteristic behavior can be seen. (1) There is slow-down in the stretch immediately after the disappearance of an auxiliary lane. For instance, from 184 to 185 kp, in cases over 600 pcu/h, the slow-down clearly appears. (2) There is a gradual slow-down along the flow direction in TWTL sections. (3) There is a local reduction of speed in sag sections. Hereinafter, these three characteristics are called “merging conflict”, “gradual attenuation”, and “local speed reduction”, respectively, to avoid cumbersome explanations.

High flow rate tends to amplify the above characteristics. “Merging conflict” seems to appear for high flow rates over 600 pcu/h. “Gradual attenuation” is possibly amplified by increasing flow rate. “Local speed reduction” is similarly amplified by high flow rate in sag sections.

Although detailed considerations of the mechanisms behind these effects are given in the literature [3], we mention them briefly here as follows. (1) The slow-down immediately after merging might be caused by the propagation of a deceleration wave derived from a merging car’s failure to adjust headway distance. (2) The possible cause of the gradual slow-down along flow-direction is attributed to the enlargement of the “platoon”, since a freely running car eventually catches up with the car in front on a long TWTL stretch. (3) The local speed reduction in sag sections could also be explained as the propagation of a deceleration wave, which could trigger a break-down in flow at a bottleneck in multi-lane expressways.

### 4 Model Formulation

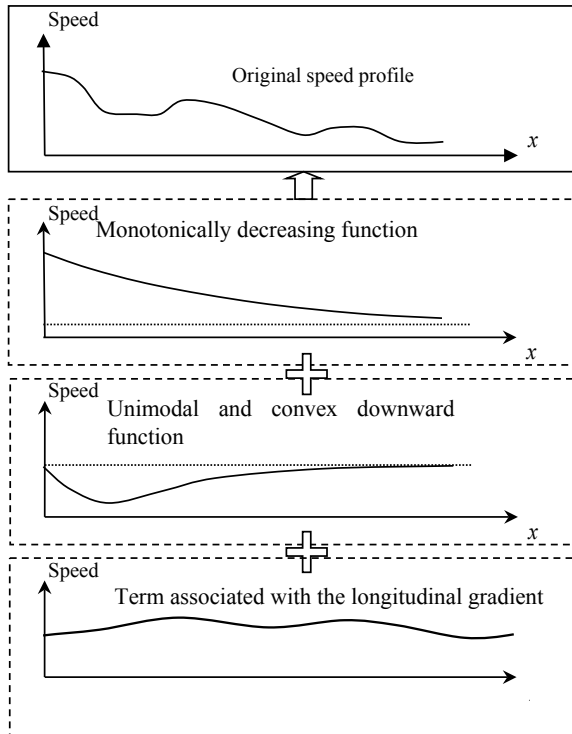
Here, we try to give a basic model of the speed profile. The speed profile is assumed to be decomposed into three components representing the characteristics mentioned above. In this paper, as a pilot study, these characteristics are approximated as follows: (1) the gradual attenuation is assumed to be formulated as a monotonically decreasing function,  $f_1(x)$ ; (2) the merging conflict is assumed to be approximated by a unimodal and convex downward function,  $f_2(x)$ ; and (3) the local speed reduction is formulated as a function depending on longitudinal gradient,  $f_3(x)$ , since the mechanism behind the slow-down may be similar to that in the multi-lane case. The linear summation of these functions in Eq. (1) is regarded as a model of the speed profile. In Fig. 2, the concept is illustrated briefly.

Based on the above assumptions, the speed profile at  $x$ , which is the distance from the end of an auxiliary lane, is formulated as follows:

$$f(x) = f_1(x) + f_2(x) + f_3(x). \tag{1}$$

The gradual attenuation term  $f_1(x)$ , which is a monotonically decreasing function, can be expressed using many alternative functions, such as a linearly decreasing

**Fig. 2** Three components of spot speed



function or a negative exponential function. Here, a negative exponential function is used. The traffic flow rate can also be taken into account in this function since traffic flow rate may affect the rate of decrease.

The second term,  $f_2(x)$ , models merging conflict, which can be seen as the abrupt slow-down immediately after the end of an auxiliary passing lane. Therefore, a unimodal and convex downward function is appropriate for the second term.

The third term,  $f_3(x)$ , reflects local speed reduction and is derived from the longitudinal gradient.

We consider four models whose variations are shown in Table 1. In two models, it is assumed that the gradual attenuation of speed depends on the traffic flow rate, while in the other two models, it is assumed that traffic flow rate has no effect.

Merging conflict is effective in Models II, III, and IV, while in Model I, it is assumed to be negligible. The unimodal and convex downward function is approximated here by a lognormal function. In Models III and IV, it is assumed that the effect of longitudinal gradient on speed is amplified by traffic volume.

The functional forms used in the four models are shown below.

$$f_1(x) = \begin{cases} a_0 + \frac{1}{a_2} \exp\{-(a_1 + a_7q)x\} & \text{for Models I and IV} \\ a_0 + \frac{1}{a_2} \exp(-a_1x) & \text{for Models II and III} \end{cases} \quad (2)$$

$$f_2(x) = \begin{cases} \frac{a_5}{\sqrt{2\pi a_4 q x}} \exp\left[-\frac{\{\log(x-a_3)\}^2}{2(qa_4)^2}\right] & \text{for Models II, III, and IV} \\ 0 & \text{for Model I} \end{cases} \quad (3)$$

$$f_3(x) = \begin{cases} a_6 q i(x) & \text{for Models III and IV} \\ a_6 i(x) & \text{for Models I and II} \end{cases} \quad (4)$$

where,  $a_n$  ( $n = 0, 1, \dots, 7$ ) are parameters,  $q$  is flow rate,  $i(x)$  is longitudinal gradient [%], and  $x$  [km] denotes longitudinal location. If the gradient is descending, the sign of  $i(x)$  is negative.

**Table 1** The different assumptions about the effect of traffic flow rate used in our four models

		Model I	Model II	Model III	Model IV
Monotonically decreasing (Gradual attenuation)	With flow rate $q$	X	–	–	X
	W/O flow rate $q$		X	X	
Unimodal and convex downward (Merging conflict)	Used, with flow rate $q$	–	X	X	X
	Identically zero	X	–	–	–
Longitudinal gradient (Local speed reduction)	With flow rate $q$	–	–	X	X
	W/O flow rate $q$	X	X	–	–

## 5 Model Calibration

### 5.1 Estimated Parameters

The speed profiles of three representative routes (the Joban Expressway, the Tokai-Hokuriku Expressway, and the Okayama Expressway) were used for an implementation test. The numbers of samples and the observed sections are listed in Table 2. For cross-validation, TWTL sections on the three routes are divided into two groups: a group for model calibration and another group for model validation. Successive TWTL sections are placed alternately into the two groups.

For calibration, the simplex method [9], which is an iterative numerical optimization method, was applied. The root mean square error (RMSE) between estimated and actual speeds (i.e., speed profiles) for the sections in the group for model calibration was the objective of the minimization. To confirm the universality of the calibrated model, the RMSE for the sections in the group for validation was also computed. In the model calibration, speed profiles for three different ranks of traffic flow rate (200–400, 400–600, and 600–800 pcu/h) were used simultaneously. In this paper, the highest rank traffic flow rate (over 800 pcu/h) is omitted because it is reported that traffic congestion often occurs in that rank.

In Table 3, estimated parameters and RMSEs are listed. If there is no prior knowledge about the speed, it is natural to assume that speed is constant (invariant) on a TWTL section. We call this Model W in Table 3. The RMSE in this case is 4.20 km/h, and a model that has a smaller RMSE than that is significant. Models II and III satisfy this criterion. However, the estimated value 39.2 km/h of parameter  $a_0$  in Model II is unnaturally low as an initial speed at the start of a TWTL section. So, overall, Model III is better than the other models.

### 5.2 Estimated and Predicted Speed Profiles

The results for Model III are shown in Figs. 3 and 4. In these figures, estimated speed profiles are compared with the actual speed profile. In auxiliary sections, the lines are

**Table 2** Numbers of samples and sections of observation

Expressway	Section	Number of samples
Okayama	Kayo–Ukan	8,800
Tokai-Hokuriku	Shirakawago–Gokayama	5,420
Joban	Iwaki-chuo–Iwaki-Yotsukura	13,453

The number of samples is the average number of cars with ETC 2.0 that successfully recorded and uplinked data for the section shown the central column. The duration of data collection was from October 2014 to September 2015



**Table 3** List of calibrated model parameters, used data, and accuracy of the estimation

	Model I	Model II	Model III	Model IV	Model W
$a_0$	72.9	39.2	70.0	72.8	–
$a_1$	–408	0.00979	0.123	0.202	–
$a_2$	–4532	0.0280	0.188	0.210	–
$a_3$	–	–12.0	–1.03	–4.76	–
$a_4$	–	10.0	1.10	–0.789	–
$a_5$	–	1.08	1.03	3.41	–
$a_6$	–0.71	–0.77	–0.00147	–0.00126	–
$a_7$	71.9	–	–	9.13	–
RMSE for calibrating sections [m]	4.28	3.89	3.98	4.24	4.20
RMSE for cross-validation [m]	3.32	3.05	3.10	3.31	3.32

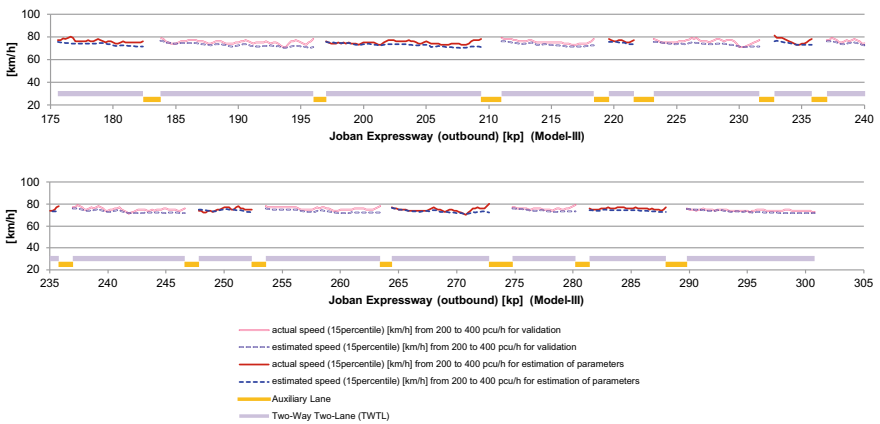


**Fig. 3** Cross-validation of speed profiles based on Model III with estimated parameters for flow rates from 200 to 400 pcu/h on the Joban Expressway

missing. The solid red line and blue dashed line denote actual speed and estimated speed from the calibrated model, respectively. The gray dashed line and the light red line correspond to actual speed and estimated speed used for cross validation, respectively, where speed is estimated with the parameters estimated for sections in the group for the calibration.

As shown in Fig. 3, the estimated speed in the model calibration and predicted speed based on the calibrated model follow the actual speed profile acceptably for 200–400 pcu/h, which is a relatively low flow rate. In case of higher flow rate (as shown in Fig. 4), the discrepancy between the estimated and actual speeds is larger than for the lower flow rate. Large discrepancies are seen around the 208 kp and the 231 kp. A parking area (named “Naraha PA”) is positioned around the 208 kp, and this parking area may affect the actual speed profile. On the other hand, the cause



**Fig. 4** Cross-validation of speed profiles based on Model III with estimated parameters for flow rates from 600 to 800 pcu/h on the Joban Expressway

of the discrepancy around the 231 kp is not clear. Since the longitudinal gradient gradually changes from 3 to 1% uphill, the steep uphill is a factor in slow-down. Further exploration is required and will be included in a future study.

There are two possible ways to improve the accuracy for high flow rates, which will be explored in the future. One way is to calibrate the models for only high flow rate ranks. The other way is to reconsider the model structure. For instance, a non-linear effect of gradient on speed reduction may be included.

A calibrated model using all the data from three routes may have a higher transferability than a model calibrated with data from only one route. On the other hand, the features of a specific route may be not fully captured when using this approach. We examined whether a model calibrated with data from Tokai-Hokuriku Expressway and Okayama Expressway predicts the speed profile of Joban Expressway. As shown in Fig. 5, an acceptable level of reproducibility is achieved.

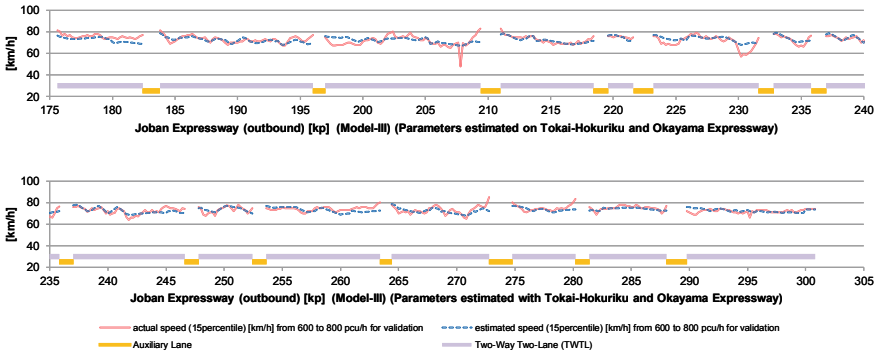


Fig. 5 Predicted speed on the Joban Expressway using a model calibrated with data from the Tokai-Hokuriku and Okayama Expressways

## 6 Conclusions

This study aimed to model speed profiles on TWTL expressways based on ETC 2.0 probe car data. The model could be used to predict spot speeds before the construction of new roads or auxiliary lanes. In particular, the models identified in this paper may be helpful as a guideline for length and location when considering the construction of a new auxiliary lane.

Further exploration is, of course, required to reach the final goal. First, the structure of the model was assumed a priori, considering the three factors of “merging conflict”, “gradual attenuation”, and “local speed reduction”. The correspondence between model output and observations also contributes to an intuitive understanding of the model. Nevertheless, for more accurate prediction, some refinement of model is required. Another challenge is to examine the transferability of the model. In this study, three routes were chosen as representatives of TWTL expressways. In future work, probe data from other TWTL expressways will be used for exploration.

## References

1. Makino, H., Itsubo, S., Toriumi, D., Mizutani, T.: Feasibility study of identifying passable routes after disasters made from ETC 2.0 probe data. In: Proceedings of the 23rd World Congress on ITS, 6 pages (2016)
2. Japan Road Association: Douro Kouzou-rei no Kaisetsu to Unyou (Explanation and operation of road structure ordinance), 206–207 (2015). (in Japanese)
3. Narushima, S., Kasai, M., Xing, J., Goto, H., Tsuji, M.: Analysis of vehicle speeds on two-way two-lane expressways with ETC 2.0 data. JSTE J. Traffic Eng. 3(2), A\_125–A\_134 (2017). (in Japanese)
4. Transportation Research Board: Highway Capacity Manual 2010 (2010)

5. Nakamura, H., Kobayashi, M., Catbagan, J.L.: A study on implementation policy of auxiliary passing lane on two-way two-lane highways considering follower density. *J. Jpn. Soc. Civ. Eng., Ser. D3*, **67**(3), 270–282 (2011). (in Japanese)
6. Catbagan, J.L., Nakamura, H.: Evaluation of performance measures for two-lane expressways in Japan, *Transportation Research Record*, 111–118 (2006)
7. Transportation Development Division Oregon Department of Transportation: *Modeling Follower Density on Two-Lane Rural Highways* (2014)
8. Kasai, M., Xing, J., Narushima, S., Goto, H., Tsuji, M.: A discussion on measure of effectiveness of two-way two-lane expressways. *JSTE J. Traffic Eng.* **3**(2), A\_135–A\_144 (2017). (in Japanese)
9. Jacoby, S.L.S., Kowalik, J.S., Pizzo, J.T.: *Iterative Methods for Nonlinear Optimization Problems*. Prentice-Hall (1972)

# Effect of the Moving-Light-Guide-System on Driving Behavior at Sag



Yuuta Tabira and Yasuhiro Shiomi

**Abstract** There has been an increase in the cases of installation of the Moving-Light-Guide-System (hereafter, MLGS) as a countermeasure against traffic congestion at sag bottlenecks of freeways in Japan. MLGS creates a flow of LED light traveling with constant speed alongside the car. It intends drivers to perceive the speed gap between MLGS and their own vehicles and encourage the spontaneous speed recovery on uphill section at sag. It has been reported that traffic congestion at some bottlenecks were mitigated due to the installation of MLGSs, though its influence on the driving behavior and the mechanism of congestion-mitigation were still unrevealed. In this study, based on a car-following experiment conducted on the Hanshin Expressway Route 3, the influence of the MLGS in the uphill section on driving behavior was analyzed. Based on the rigorous statistical analysis, the following findings were obtained. (1) Regardless of the operating speed, the MLGS tended to exert a change in the inter-vehicle distance on entire section. (2) When the MLGS was operated at a light flow speed of 60 km/h, for drivers who tried to match the vehicle speed with the MLGS light flow speed, the inter-vehicle distance was likely to decrease and traffic capacity improved in the uphill section. (3) The average of the PICUD value in the uphill section was higher in the presence of the MLGS than in their absence, and even in the downhill section of the PICUD value was maintained in the safety level in the uphill section. (4) Although the effect on stability improvement was not found to be statistically significant, the number of drivers who exhibited extreme car-following behavior decreased, which may contribute to an overall improvement of the traffic situation in the entire section.

---

Y. Tabira (✉) · Y. Shiomi  
Ritumeikan University, Kusatsu, Kyotob, Shiga, Japan  
e-mail: [rd0046vi@ed.ritsumei.ac.jp](mailto:rd0046vi@ed.ritsumei.ac.jp)

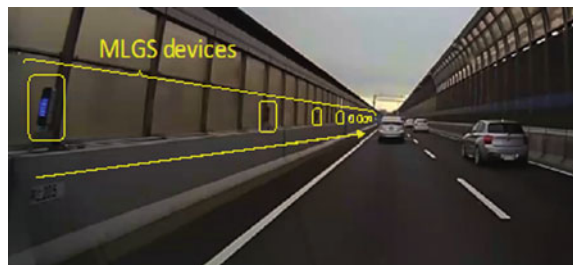
Y. Shiomi  
e-mail: [shiomi@fc.ritsumei.ac.jp](mailto:shiomi@fc.ritsumei.ac.jp)

## 1 Introduction

Freeway congestion has become one of the most serious social problems in many large metropolitan areas. According to Japan's Ministry of Land, Infrastructure, Transport, and Tourism, the amount of time lost due to traffic congestion is estimated to be around 200 million people-hours per year on intercity highways alone, equivalent to about 100,000 workers per year [1]. In particular, sags, which are sections where the road gradient transitions from downhill to uphill, are the primary cause of traffic congestion in Japan. Typically, hard measures to reduce traffic congestion, such as the construction of additional roads, are costly and time consuming. Hence, soft measures for the mitigation of congestion are more attractive in terms of the cost and time.

More specifically, the advanced driver-assistance system and connected and autonomous vehicles have the potential to increase traffic capacity and have attracted considerable research attention in recent years. Ludmann et al. (1997) showed that when the desired time gap is reduced from 1.2 s to below 1.0 s using ACC systems, traffic capacity increases with an increase in the ACC penetration rate in traffic [2]. Goñi Ros et al. [3] proposed a method to prevent the traffic breakdown at sag bottlenecks, in which the acceleration of autonomous vehicles was exogenously controlled [3]. The theory of jam-absorption driving (JAD), which controls the cruising speed of a vehicle to absorb the shockwave was proposed by Nishi et al. [4] and He et al. [5]. Stern et al. [6] experimentally demonstrated that the intelligent control of an autonomous vehicle could dampen waves of stop-and-go traffic [6]. However, the effectiveness of these strategies highly depends on the penetration rate of the vehicles with ACC and CACC and the relative number of connected and autonomous vehicles. Meanwhile, in recent years, the Moving-Light-Guide-System (MLGS, see Fig. 1) has been proposed in Japan as an effective countermeasure against traffic congestion. The MLGS is expected to influence the driver's speed recognition by flashing LED lamps installed along the freeway in a sequential pattern to create a perceived flow of light traveling alongside the car. This mechanism is expected to prompt the driver to suppress excessive speed on downhill sections of the road and to recover speed in the uphill and sag sections of roadways [7]. Thus, MLGSs can potentially alleviate the factors leading to traffic congestion.

**Fig. 1** An example of MLGS devices



The mitigation of congestion from the use of MLGSs has been recently confirmed in real-world conditions. For example, it was reported from a macroscopic viewpoint that in the Tokyo Bay Aqualine, the maximum traffic flow rate during free flowing traffic increased, and the driving speed after a breakdown increased in congested traffic flow [8]. On the Hanshin Expressway, considering the lighting pattern of the MLGS, the congestion time decreased by 60–70%, and congestion amount, which is defined as the integral of the congestion queue length, also decreases by about 70% under MLGS operating conditions [9]. It has also been reported that by analyzing the change in speed and the size of platoons by using a vehicle detector and video recordings, MLGS contributed to preventing platoon formation, and the difference between platoon speeds in the shoulder lane was reduced [10]. These analyses were limited from a macroscopic viewpoint, though the influence of the MLGS on car-following behavior and the mechanism of the contribution of MLGS to increased traffic capacity at bottlenecks have yet to be clarified.

Thus, in this study, car-following experiments were conducted on an expressway with an MLGS installed to examine how the MLGS affects car-following behavior of drivers. In particular, we focused on the variations in inter-vehicle distances and transition of relative speed as a characteristic of car-following behavior. The inter-vehicle distance was related directly with traffic capacity when the speed of the preceding vehicle was constant. The transition of the relative speed becomes an important index in evaluating the stability of the car-following behavior. The inter-vehicle distance for each participant in the experiment was analyzed in relation to the presence or absence of the MLGS, and the results of the questionnaire in which each participant's perception of the MLGS was measured. Regarding the transition of relative speed, we quantified it using Fourier transform and verified whether the driver's car-following behavior was generally stabilized. In addition, to assess the collision risk associated with operation of the MLGS, the potential index for collision with urgent deceleration (PICUD) values in the presence and absence of the MLGS in downhill and uphill sections were analyzed.

The remaining Sections are organized in the following manner. Section 2 outlines the car-following experiments conducted as part of this study and the method of estimating inter-vehicle distance. Section 3 discusses the analytical results of inter-vehicle distance with and without the MLGS, and the cross-tabulation analysis of the questionnaire results and inter-vehicle distance. A verification of the change in traffic capacity with and without the MLGS using a car-following behavior model are described in Sects. 4 and 5 assesses a collision risk for the MLGS. Section 6 assesses the effect of MLGS on the stability of car-following behavior, and finally, the findings of this study and proposed future work are summarized.

## 2 Car-Following Experiment

### 2.1 Outline of the Car-Following Experiment

The section of Hanshin Expressway Route 3, including the Fukae sag (20.5–19.5 kp) bound for Osaka was selected for experimental analysis (see Fig. 2). In this section, the MLGS has been operating since June 2015 to mitigate traffic congestion caused by bottlenecks. The experiments were conducted on weekdays and divided into two periods: the first from July 13–21, 2015, and the second from September 10–17, 2015. The same participants participated in both of the experiments.

The participants included 20 males in their 30–60 s who have been driving for 10 years or more and who routinely use the Hanshin Expressway. Table 1 lists the attributes of the participants. Each participant was asked to drive a car on the route from Uozaki IC past the Fukae Sag to Nishinomiya IC three times when the MLGS was not in operation (hereafter, no MLGS), MLGS operation with a sequential light speed of 60 km/h (hereafter, MLGS 60), and MLGS operation with an 80 km/h light speed (hereafter, MLGS 80). To eliminate any order effects, the order in which these conditions were tested was randomized on each day as shown in Table 2. For each day, in the first and second halves, two subjects participated in the car-following experiment (i.e., four people joined the car-following experiment each day), and over the five-day study periods, the total number of the participants was 20. In Fig. 2, the blue line indicates the driving route, the green arrow indicates the traveling direction for the car-following experiment, and the red line indicates the section of the road in which the MLGS was installed. In this experiment, a conductor of the experiment drove the preceding vehicle maintaining a speed of 60 km/h, while the participant drove the following vehicle and was just instructed to follow the preceding vehicle. All the participants used the same standard vehicle (TOYOTA Succeed) to eliminate variations associated with different vehicle characteristics. After the experiment, a questionnaire regarding the experiment was administered to the participants. In the

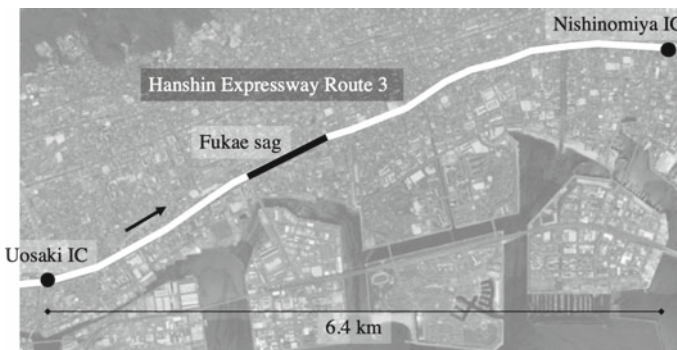


Fig. 2 Travel route overview



**Table 1** List of subject attributes

Subject ID	Age	Driving experience (year)	Usage frequency (Hanshin Expressway)	Usage frequency (Kobe line)
1	30–39	10	1 day a week	1 day a week
2	40–49	29	2 or 3 days a week	2 or 3 days a week
3	40–49	15	1 or 2 days a month	1 or 2 days a month
4	40–49	29	2 or 3 days a week	1 or 2 days a month
5	60–69	44	1 day a week	1 day a week
6	50–59	35	1 day a week	1 or 2 days a month
7	30–39	10	1 or 2 days a month	1 or 2 days a month
8	40–49	24	1 or 2 days a month	1 or 2 days a month
9	50–59	32	1 day a week	1 day a week
10	50–59	38	2 or 3 days a week	1 day a week
11	40–49	20	1 day a week	1 day a week
12	30–39	15	1 day a week	1 or 2 days a month
13	40–49	20	1 or 2 days a month	1 or 2 days a month
14	40–49	28	2 or 3 days a week	2 or 3 days a week
15	40–49	15	2 or 3 days a week	2 or 3 days a week
16	40–49	19	almost every day	almost every day
17	50–59	30	2 or 3 days a week	1 day a week
18	40–49	11	1 day a week	1 or 2 days a month
19	30–39	17	1 or 2 days a month	1 or 2 days a month
20	50–59	32	2 or 3 days a week	1 day a week

questionnaire, we asked whether the participant felt that he tried to fit his driving speed according to the MLGS light flow.

## 2.2 Method for Measuring Inter-vehicle Distance

The GPS data, video image data, and speed data recorded for both the preceding and following drivers were recorded and used to measure inter-vehicle distance. With the GPS, the position of the vehicle was recorded at one-second intervals, and the inter-vehicle distance was estimated by calculating that difference between the positions of the preceding and following vehicles at corresponding points in time. Since the GPS data contained errors, the vehicle position data were corrected by map matching. Consequently, the GPS point sequences were absorbed in the analysis section. Furthermore, the inter-vehicle distance of GPS data at 20.5 kp (the starting point of the analysis section) was compared with the video image data at 20.5 kp to

**Table 2** Lighting conditions for each trial on each day of the experiment

ID	July			September		
	1st round	2nd round	3rd round	1st round	2nd round	3rd round
1	no MLGS	MLGS 60	MLGS 80	MLGS 60	no MLGS	MLGS 80
2	MLGS 80	MLGS 60	no MLGS	MLGS 60	MLGS 80	no MLGS
3	MLGS 60	MLGS 80	no MLGS	MLGS 80	MLGS 60	no MLGS
4	no MLGS	MLGS 80	MLGS 60	no MLGS	MLGS 80	MLGS 60
5	MLGS 60	no MLGS	MLGS 80	no MLGS	MLGS 80	MLGS 60
6	MLGS 60	no MLGS	MLGS 80	MLGS 80	MLGS 60	no MLGS
7	MLGS 80	MLGS 60	no MLGS	MLGS 60	no MLGS	MLGS 80
8	no MLGS	MLGS 60	MLGS 80	MLGS 80	MLGS 60	no MLGS
9	no MLGS	MLGS 80	MLGS 60	MLGS 60	MLGS 80	no MLGS
10	no MLGS	MLGS 80	MLGS 60	MLGS 80	MLGS 60	no MLGS
11	no MLGS	MLGS 60	MLGS 80	MLGS 80	no MLGS	MLGS 60
12	MLGS 80	MLGS 60	no MLGS	no MLGS	MLGS 80	MLGS 60
13	MLGS 60	MLGS 80	no MLGS	no MLGS	MLGS 60	MLGS 80
14	no MLGS	MLGS 80	MLGS 60	MLGS 80	MLGS 60	no MLGS
15	MLGS 80	no MLGS	MLGS 60	no MLGS	MLGS 60	MLGS 80
16	MLGS 80	no MLGS	MLGS 60	no MLGS	MLGS 60	MLGS 80
17	MLGS 80	MLGS 60	no MLGS	MLGS 60	MLGS 80	no MLGS
18	no MLGS	MLGS 60	MLGS 80	MLGS 60	MLGS 80	no MLGS
19	MLGS 60	MLGS 80	no MLGS	no MLGS	MLGS 80	MLGS 60
20	MLGS 60	MLGS 80	no MLGS	MLGS 80	no MLGS	MLGS 60

correct the inter-vehicle distance based on the GPS data. The inter-vehicle distance from the image data was obtained by similarity calculating the width of the bottom portion of the windshield in the following vehicle and the width of the vehicle in the preceding vehicle. The distance between the camera lens and the bottom portion of the windshield was set at 1 m. Although the error was about several meters, it was possible to take the variation characteristic of the inter-vehicle distance because it was possible to confirm that the transition of the inter-vehicle distance from GPS data and that from the drive recorder were virtually identical.

When the subject drivers were involved in congestion during the experiment, the data were excluded as error data. Even when corrected with data from the drive recorder, where the inter-vehicle distance was inappropriate (e.g., negative values) were also excluded. The experimental data from July 16 to September 11, as well as those from the second half of September 14, are missing because of equipment problem. Thus, Table 3 shows the numbers of IDs before and after the removal of erroneous data, and the number of IDs after erroneous data removal is the number of participants for which the inter-vehicle distance can be estimated.

**Table 3** Number of IDs before and after removal of erroneous data

		Number of IDs before error removal	Number of IDs after error removal
No MLGS	July	20	16
	September	20	13
Operated 60 km	July	20	14
	September	20	11
Operated 80 km	July	20	14
	September	20	13

### 3 Fundamental Analysis on Inter-vehicle Distance

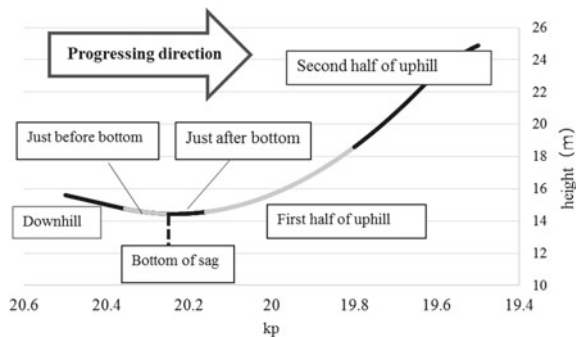
#### 3.1 Outline

In this Section, the analysis of differences in the inter-vehicle distances in the presence and absence of the MLGS is described. To analyze the influence of the MLGS on car-following behavior of the driver as a function of the longitudinal gradient of the road, the section of the road in which the MLGS was installed was divided into 5 sub-sections; (1) downhill, (2) just before the bottom of the sag, (3) just after the bottom of the sag, (4) first half of uphill, and (5) second half of uphill, as shown in Fig. 3. The influence of the MLGS was first analyzed in relation to road geometry, and the attributes of the participants follows.

#### 3.2 Variation of Inter-vehicle Distance in Subsections

As indicated previously, the inter-vehicle distance in the presence of the MLGS was compared with that with no MLGS, MLGS 60 and MLGS 80 for each participant

**Fig. 3** Road geometry of the analysis section and division of the road into sections



in each section shown in Fig. 3. By applying ANOVA and conducting multiple comparisons, the significant variation with 5% level in the inter-vehicle distance in the presence of the MLGS compared to that in their absence was identified for each participant and each subsection. Note that each subsection has a certain distance and approximately more than 10 observational data on inter-vehicle distance was available for analysis. Based on the results, the variation patterns were categorized as (1) “increased”, (2) “stable”, or (3) “decreased”, and the proportions of the measured inter-vehicle distance variations for each of the three categories for MLGS 60 and MLGS 80 are presented.

According to Fig. 4, under MLGS 60 conditions, the inter-vehicle distance “decreased” compared to no MLGS conditions for the largest proportion of drivers. Moreover, this proportion was the largest just after the bottom of the sag, implying that it may be possible to reduce the excessively large inter-vehicle distance that is likely to occur just after the bottom of the sag. While, according to Fig. 5, under MLGS 80 conditions, the ratio of “increase” to “decrease” was relatively larger than that under MLGS 60 conditions. Although there was random variation in inter-vehicle distances, it is interesting to note that the MLGS somewhat influenced the inter-vehicle distance maintained by each driver.

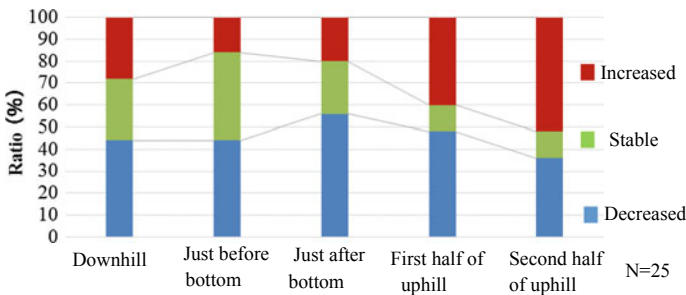


**Fig. 4** Change in inter-vehicle distance with the use of MLGS 60 compared with that without the MLGS

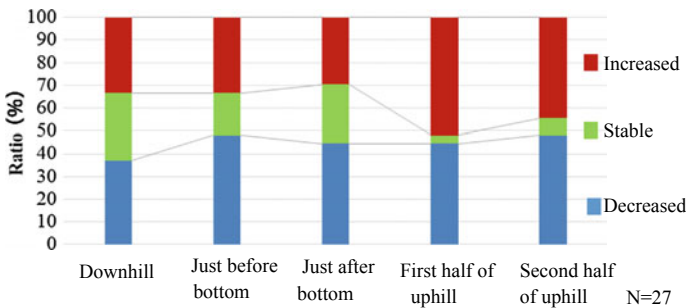


**Fig. 5** Change in inter-vehicle distance with the use of MLGS 80 compared with that without the MLGS

### 3.3 Variations of Inter-vehicle Distance in Driver Perceptions About MLGS

#### 3.3.1 Cross-Tabulation of Inter-vehicle Distance and Questionnaire Results

To examine which driver attributes were significant, cross tabulation analysis was conducted focusing on the relationship between the inter-vehicle distance variation and the responses to the questionnaire conducted during the experiment. In the questionnaire, the participants were asked whether they felt that they tried to adjust their driving speed to that of the MLGS in light traffic. The participants were classified into three categories; “tried to match the speed of the MLGS light flow”, “did not feel anything in particular” or “other”. Note that the participants who answered “other” were excluded from further analysis. The breakdown of inter-vehicle distance variations, “increased”, “stable”, and “decreased”, in the results are shown in Figs. 6 and 7, respectively.

As Fig. 6 shows, in the group of participants who tried to fit the MLGS light flow speed, the proportion of “decrease” in the inter-vehicle distance was relatively large. This decrease was expected to suppress the excessive inter-vehicle distance increase. However, as Fig. 7 shows, under MLGS 80 conditions, the opposite tendency was observed. This was apparently caused by the deviation between the driving speed and the MLGS light flow speed. As Figs. 6 and 7 shows, for the participants who did not try to fit the MLGS light flow speed (noted as “Did not feel anything” in the figures), no clear tendency was observed in the proportions of the variation patterns.

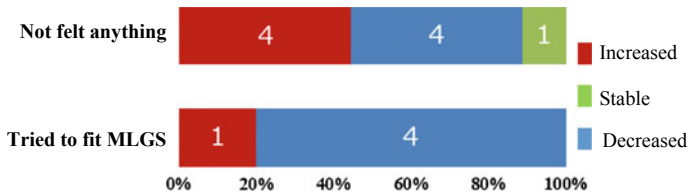


Fig. 6 Inter-vehicle distance changes with MLGS 60

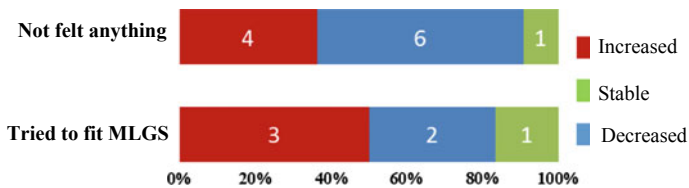


Fig. 7 Inter-vehicle distance changes with MLGS 80

### 3.3.2 Verification by Statistical Significance

Based on the data shown in Fig. 6, it is reasonably clear that the ratio of “decreased” for the participants who tried to fit the MLGS 60 light flow was dominant.

To determine whether there was statistical significance in the relationship between the perception of the MLGS and the decrease in inter-vehicle distance, logistic regression analysis was conducted. The model is expressed as Eq. (1), and the target data were all the participants with available data under MLGS 60 conditions.

$$\ln\left(\frac{p}{1-p}\right) = b_0 + b_1x_1 + b_2x_2 + b_3x_3 + b_4x_4 + b_5x_5, \tag{1}$$

where  $p$  is probability that inter-vehicle distance decreases.  $x_1$  is a dummy variable for which a value of 1 indicates a participant, who answered that he tried to adjust his driving speed to the MLGS light flow and 0 otherwise. Similarly,  $x_2$  is a dummy variable for a participant who answered that he did not have any feelings about following the MLGS.  $x_3$  represents the driving experience of the subject (in years),  $x_4$  represents the age of the subject, and  $x_5$  is a dummy variable for a subject who frequently used the target section of roadway on a daily basis.  $b_0$  to  $b_5$  were the parameters to be estimated, and Table 4 shows the results of the logistic regression analysis.

Based on the data shown in Table 4, the p-values of  $x_1$  and  $x_5$  were less than 0.05, showing that these explanatory variables were significant at a 5% level. Since the parameter  $b_1$  had a positive value, it can be concluded that a driver who tries to fit the speed of the MLGS would be more likely to decrease the inter vehicle distance in the uphill section of the road. Furthermore, it can be interestingly noted that according to the negative value of  $b_5$ , the inter-vehicle distance was less likely to decrease in the up-hill section for drivers who frequently used the target section.

**Table 4** Logistic regression analysis results

Explanatory variable	Regression coefficient	Standard deviation	Z value
Constant term	-2.75	3.70	-0.742
Subjects who wanted to fit MLGS dummy	3.73	1.76	2.12*
Subjects who didn't feel anything dummy	1.79	1.36	1.31
driving experience (year)	-0.0281	0.110	-0.255
Age	0.0968	0.131	0.74
the Kobe line high frequency user dummy	-2.79	1.40	-1.99*

AIC = 36.4, Likelihood ratio = 0.296, N = 25

\* p < 0.05

## 4 Traffic Capacity Estimation Based on Car-Following Model

### 4.1 Outline of the Car-Following Model

According to the results reported thus far, the influence of the MLGS can be considered to influence inter-vehicle distance. However, the impact of the MLGS on traffic capacity is still unclear. Thus, in this Section, the traffic capacity was estimated on an individual basis by applying the car-following model [11] shown in Eq. (2).

$$\ddot{x}_{n+1}(t + T) = \lambda \cdot \frac{\dot{x}_{n+1}(t)^\alpha}{[x_n(t) - x_{n+1}(t)]^\beta} \cdot [\dot{x}_n(t) - \dot{x}_{n+1}(t)], \quad (2)$$

where  $\ddot{x}_{n+1}(t + T)$  represents the acceleration of the following vehicle;  $T$  represents the reaction time;  $\dot{x}_n(t)$  and  $\dot{x}_{n+1}(t)$  represent the speeds of the preceding vehicle and the following vehicle, respectively;  $x_n(t)$  and  $x_{n+1}(t)$  represent the positions of the preceding vehicle and the following vehicle, respectively; and  $\lambda$ ,  $\alpha$ , and  $\beta$  denote parameters. The differential equation (Eq. 2) was mathematically solved by applying variable separation method, where  $T$ ,  $\alpha$ , and  $\beta$  were set as 0, 1, and 3, respectively. The macroscopic relationship between traffic density and average speed are expressed in Eq. (3).

$$\ln v = -\frac{\lambda}{2} \cdot k^2 + \ln v_f, \quad (3)$$

where  $v$  is the speed of the following vehicle,  $\dot{x}_{n+1}(t)$ ,  $k$  is the traffic density,  $v_f$  is the free-flow speed. Herein,  $k = 1/[x_n(t) - x_{n+1}(t)]$  holds. It is assumed that  $v = v_f$  holds when  $k = 0$ . Then, the relationship between  $q$  and  $k$  can be derived as Eq. (4).

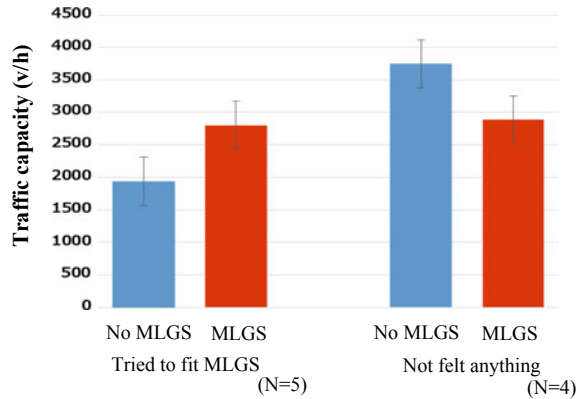
$$q = k \cdot v_f \cdot \exp\left(-\frac{\lambda}{2} \cdot k\right). \quad (4)$$

The traffic capacity is defined as the maximum value of  $q_c$ , which is derived as Eq. (5) at  $k = 1/\lambda$ .

$$q_c = v_f \cdot (\lambda \cdot e)^{-\frac{1}{2}}. \quad (5)$$

Therefore, the traffic capacity,  $q_c$ , can be estimated by supplying the parameters  $\lambda$  and  $v_f$  in Eq. (3). According to the analysis by Takashima et al. [12], the bottleneck of congestion in the Fukae Sag was around 19.8 kp. Thus, in this study, the section from the sag bottom (around 20.25 kp) to 19.8 kp was analyzed.

**Fig. 8** Comparison of traffic capacity with and without the MLGS



## 4.2 Evaluation of Traffic Capacity

The traffic capacity of the participants who tried to fit the speed of the MLGS and those who did not were compared. Considering the number of analytical data, the parameters estimated in Eq. (3) with a coefficient of determination of 0.20 or more was chosen, and data that did not meet this criterion or took on an abnormal value were excluded from the analysis. The average was calculated separately for the participants who tried to fit the speed of the MLGS light flow and those who did not.

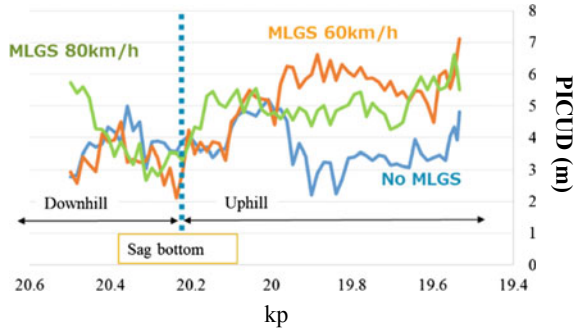
Figure 8 presents the results. For convenience, the data associated with the 60 and 80 km/h MLGS light flow speed and data from July and September were pooled. The results indicated that the participants who felt that they tried to fit the movement of the MLGS light flow speed showed a tendency to increase traffic capacity. It was significant at a significance level of 10% ( $df = 8$ ,  $p\text{-value} = 0.08$ ) based on a  $t$ -test. Meanwhile, the participants who did not feel anything in response to the MLGS light flow speed showed a tendency to decrease traffic capacity, though it was not statistically significant. When comparing traffic capacity with the MLGS operation for both categories of participants, they are interestingly almost equal to each other. This suggests that the MLGS may stabilized the traffic capacity of the entire population of drivers. However, it is necessary to increase the number of samples and continue to enhance the present analysis by improving the model.

## 5 Evaluation of Collision Risks

The change in inter-vehicle distance due to the use of the MLGS was confirmed for a large number of participants. If the inter-vehicle distance decreased due to the MLGS, the risk of a rear-end collision may be higher. Hence, we verified that driving safety was also improved by the MLGS operation. In this study, the safety analysis was performed based on the PICUD (Potential Index for Collision with Urgent



**Fig. 9** Transition of PICUD in MLGS installation section



Deceleration) value proposed by Uno et al. [13] as a collision risk indicator. The PICUD is defined as the distance between vehicles when both cars have stopped after the preceding vehicle suddenly decelerates, and the following vehicle subsequently decelerates with a delayed reaction. In other words, if the PICUD value was less than 0, even if the driver of the following vehicle urgently applied the brake hard, a collision with the preceding vehicle will occur. The PICUD index is expressed by Eq. (6).

$$PICUD = -\frac{V_1^2}{2a} + s_0 - \left( V_2 \cdot \Delta t - \frac{V_2^2}{2a} \right), \tag{6}$$

where  $V_1$  is the speed (m/s) of the preceding vehicle immediately before deceleration,  $V_2$  is the speed (m/s) of the following vehicle at the time of deceleration of the preceding vehicle,  $a$  is the acceleration during the deceleration of both vehicles (assumed to be  $-3.3 \text{ m/s}^2$ ),  $s_0$  is the inter-vehicle distance (m) at the start of the deceleration of the preceding vehicle, and  $\Delta t$  is the reaction delay time for the following vehicle (assumed to be 1.5 s).

The change in the PICUD in the presence of the MLGS was determined according to the MLGS operating speed (60 and 80 km/h). The PICUD was taken as the average value for all participants. About sample number, No MLGS is 30, MLGS 60 is 25, and MLGS 80 is 27 people. Based on the data shown in Figs. 4 and 5, the influence of the MLGS on the inter-vehicle distance was different in the downhill and uphill sections. Hence, the road section to be tested for significant difference in the PICUD was divided into two sections before and after the bottom of the sag. The average PICUDs are shown in relation to the position in the road in Fig. 9. In the downhill section (20.5–20.25 kp), it was confirmed that the PICUD for MLGS 60 conditions was slightly lower than no MLGS conditions just behind the bottom of the sag, but was still larger than 0.

It was shown that there was no significant differences among no MLGS, MLGS 60 and MLGS 80 conditions at a 5% level based on ANOVA in the downhill section, whereas in the uphill section (20.25–19.5 kp), the PICUD values for MLGS 60 and MLGS 80 conditions were significantly larger than those for no MLGS conditions.

The larger the PICUD value in the uphill section of the road, the more likely rear end collisions between the following vehicle when the preceding vehicle decelerates suddenly will be prevented. Therefore, the collision risk does not rise due to the operation of the MLGS and safety is maintained under the use of the MLGS.

## 6 Evaluation on Stability of Car-Following Behaviors

### 6.1 Longitudinal Variation of Relative Speed

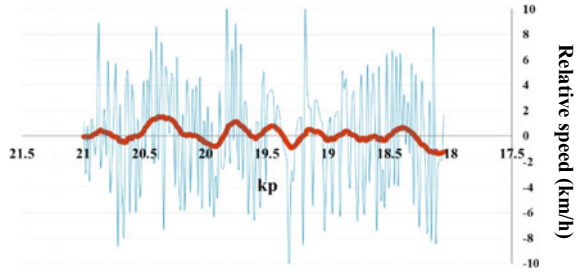
In this section, the traveling speed is estimated using the GPS data installed in the two vehicles in the car-following experiment, and the characteristics of longitudinal variation of relative speed, which can be considered as the stability of the car-following behavior, is examined. The stability of car-following behavior is considered to be a situation in which the speed reduction of the preceding vehicle is not expanded, and the influence of the speed reduction is gradually reduced. Considering the fluctuation of the relative speed, when the fluctuation range is small, the speed difference from the preceding vehicle is small, and it responds quickly to the speed change of the preceding vehicle. If the cycle is large, the variation in the speed difference from the preceding vehicle becomes moderate, which means that the speed adjustment is not excessive.

In this study, we define these states as “stable”. Since the analysis of inter-vehicle distance was based on the average value for each section, it was impossible to evaluate the longitudinal variation in driving behavior. In this study, the relative speed was defined as the “preceding vehicle speed—following vehicle speed”, and the target section was set between 20.5 and 19.5 kp where the MLGS was installed, which was same for inter-vehicle distance analysis. Although it was easy to calculate the speed from GPS data, due to observation errors, the fluctuation range of the transition became excessive. Hence, Kalman smoothing was applied to the relative speed calculated with GPS data. In Kalman smoothing, it was assumed that the transition of the data obtained by GPS included two kinds of observation error and state error. Then, the maximum likelihood estimation method was used to determine the values so that these two kinds of errors were minimized.

Figure 10 shows an example of smoothing. The blue line is GPS data, and the red line is the data after smoothing. It can be seen that random noise can be successfully eliminated. On the basis of data with Kalman smoothing, the average of all the data (i.e., the data for both July and September was calculated for each presence/absence of MLGS and operation speed. Figure 11 presents the results.

From Fig. 11, under MLGS 60 conditions, the fluctuation range of the relative speed was remarkably large in the vicinity of 20.1 kp, and it shifted in smaller increments on the downstream side compared to that at 19.9 kp. Meanwhile, under MLGS 80 conditions, there was a difference in the fluctuation range and the cyclic variation compared to that observed under no MLGS conditions.

**Fig. 10** Smoothing processing example (July ID1 No MLGS)



From these results, the fluctuation range and the cyclic variation apparently varied due to the presence or absence and the difference in the operation speed of the MLGS.

### 6.2 Arrangement of Relative Speed Fluctuation Range and Cycle in Individual Units

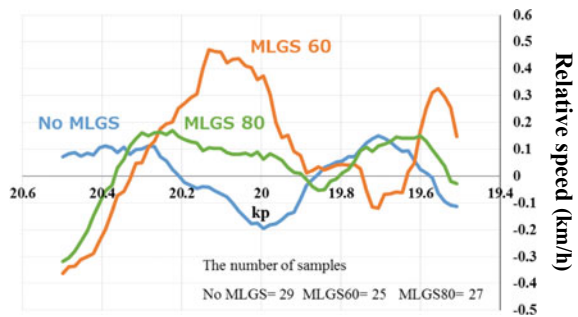
In this section, we analyze and quantitatively evaluate the relative speed fluctuation of an individual driver. We considered the relative speed transition as a waveform and analyzed the waveform amplitude (the variation width of the relative speed) and the frequency (the periodic time of the relative speed) for each participant.

To represent the amplitude, average amplitude was used. Since the relative speed fluctuates between positive and negative values, the method shown by the formula (7) was adopted.  $\Delta v$  is the relative speed, and  $N$  is the number of observations.

$$\bar{x} = \sqrt{\frac{1}{N} \sum \Delta v^2} \tag{7}$$

The frequency was converted to the power spectrum distribution using the Fourier transform (FFT,  $N = 64$ ). In this study, median power frequency ( $f_{med}$ ) was adopted as the representative frequency [14]. Median power frequency is a frequency that divides

**Fig. 11** Relative speed transition result (average of all samples)



the area surrounded by the frequency axis and the power spectrum distribution into two equal areas. When bisecting the area of the power spectrum distribution, it is assumed that the power spectrum is linearly distributed piece-wise.

Based on this result, the distribution of the median power frequency and the average amplitude are shown in the box chart in Fig. 12. Each horizontal line of the box-and-whisker chart indicates the minimum value, the lower quadrant position, the median value, the upper quartile, and the maximum value in ascending order. Regarding the frequency, it was confirmed that although no significant difference was observed between the presence and absence of a MLGS, the observed range of frequency was smaller with an MLGS than without a MLGS.

Regarding the amplitude, although there was no significant difference between observation widths, the medians under MLGS 60 and MLGS 80 conditions were slightly larger than those observed under no MLGS conditions. In other words, the amplitude level tended to be significantly higher with MLGSs than without MLGS, though the observation widths were nearly equal.

Therefore, the amplitude of the relative speed tended to slightly increase, while the frequency (periodic time) was found equalized by operated MLGS.

### 6.3 Evaluation on Stabilization of Car-Following Behavior

In this section, we examine the effect of MLGS on stabilization of car-following behavior of all drivers using median power frequency and average amplitude. To evaluate stability, a coordinate plane is considered in which the horizontal axis is the average periodic time [min] (reciprocal of frequency) and the vertical axis is the average amplitude [km/h]. Both of the values for each participant are plotted as schematically represented in Fig. 13 (this is an example of no MLGS conditions). The stability is then defined as the angle formed by the plotted point and the line connecting the origin and the periodic axis. If the angle is large like  $\theta_1$  in Fig. 13, it is generally considered that the periodic time is small and the amplitude increases, which corresponds to the unstable situation. Conversely, if the angle is small like  $\theta_2$ , the periodic time is large and the amplitude decreases, indicating the stable situation.

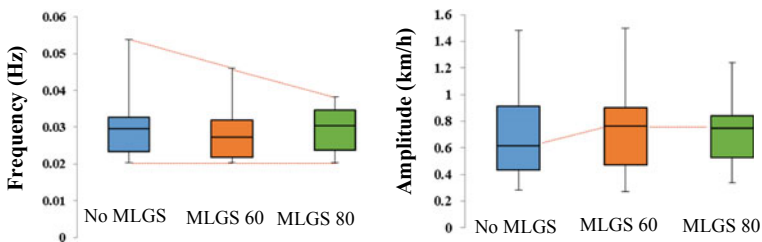
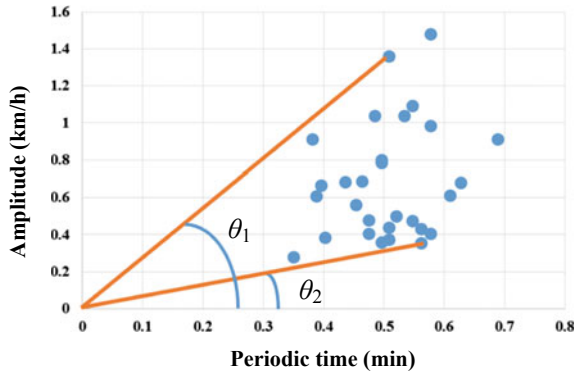


Fig. 12 Median power frequency and average amplitude distribution

In this study, we also examined the dispersion level of the angle under MLGS and no MLGS conditions to evaluate the stabilization of car-following behavior. It is interpreted that the smaller the variance in the angle, the more homogeneous the car driving behavior is, and vice versa.

The histogram of the recorded angle is shown in Fig. 14 for each operation condition of MLGS, and the dispersion value is shown in Fig. 15. From the histogram, it can be seen that the distribution range under no MLGS conditions is wider than that associated with MLGS conditions. When comparing the variance, it was smaller during MLGS operation than without operation of the MLGS. There was a statistically significant tendency in the value of the angle, and there was no significant difference in variance; however, the results suggest that car-following behavior of all drivers could be more homogenous when the MLGS is operational. Therefore, by operating the MLGS, there is a possibility that the number of drivers who exhibit extreme car-following behaviors decreases, which may contribute to an overall improvement in traffic conditions.

**Fig. 13** Stability indicator (No MLGS)



**Fig. 14** Angular distribution (histogram)

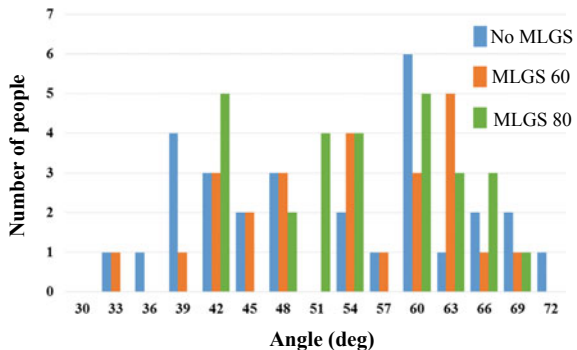
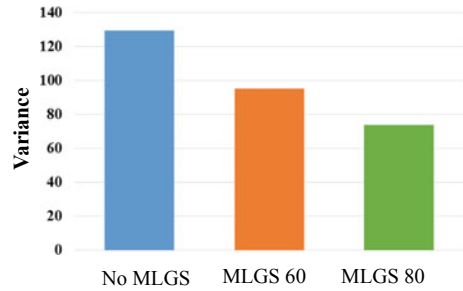


**Fig. 15** Angular variance under each condition



## 7 Conclusions and Future Research

In this study, car-following experiments were conducted on Hanshin Expressway Route 3 at the Fukae Sag. The influence of the MLGS on the driving behavior was analyzed, focusing on the change in inter-vehicle distance, traffic capacity, collision risks and transition of relative speed. Based on the results of our analysis, the influence of the MLGS on the uphill section of the road were as follows: (1) Regardless of the operating speed, the MLGS tended to exert a change in the inter-vehicle distance on entire section. (2) When the MLGS was operated at a light flow speed of 60 km/h, for drivers who tried to match the vehicle speed with the MLGS light flow speed, the inter-vehicle distance was likely to decrease and traffic capacity improved in the uphill section. (3) The average of the PICUD value in the uphill section was higher in the presence of the MLGS than in their absence, and even in the downhill section of the PICUD value was maintained in the safety level in the uphill section. (4) Although the effect on stability improvement was not found to be statistically significant, the number of drivers who exhibited extreme car-following behavior decreased, which may contribute to an overall improvement of the traffic situation in the entire section.

Future research should include an increase in the number of samples for comparison, an analysis using highly accurate inter-vehicle distance and relative speed estimates should also be performed. In this context, collecting vehicle trajectories using video image data might be efficient rather than performing car-following experiments, though it largely depends on the time and cost associated with data collection. It is also important to verify the more detailed mechanisms: how do drivers perceive the optical flow produced by MLGS, how do they change their driving behavior, and how does it influence on the macroscopic traffic flow phenomena. Based on these insights, the operation of the MLGS could be improved to mitigate traffic congestion and traffic accident risks.

## References

1. Ministry of Land, Infrastructure and Transport, Traffic Worst Ranking Summary. <http://www.mlit.go.jp/common/001130029.pdf>
2. Ludmann, J., Neunzig, D., Weilkes, M.: Traffic simulation with consideration of driver models, theory and examples. *Veh. Syst. Dyn.* **27**(5–6), 491–516 (1997). <https://doi.org/10.1080/00423119708969344>
3. Goñi Ros, B., Knoop, V.L., Van Arem, B., Hoogendoorn, S.P.: Optimization of traffic flow at freeway sags by controlling the acceleration of vehicles equipped with in-car systems. *Transp. Res. Part C* **71**, 1–18 (2016). <https://doi.org/10.1016/j.trc.2016.06.022>
4. Nishi, R., Tomoeda, A., Shimura, K., Nishinari, K.: Theory of jam-absorption driving. *Transp. Res. Part B* **50**, 116–129 (2013). <https://doi.org/10.1016/j.trb.2013.02.003>
5. He, Z., Zheng, L., Song, L., Zhu, N.: A jam-absorption driving strategy for mitigating traffic oscillations. *IEEE Trans. Intell. Transp. Syst.* **18**(4), 802–813 (2017). <http://dx.doi.org/10.1109/TITS.2016.2587699>
6. Stern, R., Cui, S., Monache, M., Bhadani, R., Bunting, M., Churchill, M., Hamilton, N., Haulcy, R., Pohlmann, H., Wu, F., Piccoli, B., Seibold, B., Sprinke, J., Work, D.: Dissipation of stop-and-go waves via control of autonomous vehicles: field experiments (2017). arXiv: 1705.01693v1[cs.SY]
7. Transport Facilitation Study Group on Highway Sags: Toward Realization of Effective Transportation Facilitation to Traffic Jam Locations on Highway Sags (2015). [http://www.nilim.go.jp/lab/qcg/japanese/2research/1field/36smoothingsag/201510\\_sag\\_report.pdf](http://www.nilim.go.jp/lab/qcg/japanese/2research/1field/36smoothingsag/201510_sag_report.pdf)
8. Endo, M., Nakagawa, H., Fukase, M., Hashimoto, D.: The measures against traffic congestion in Tokyo Wan Aqua-Line EXPWY. In: Proceedings of the 34th Traffic Engineering Research Paper, pp. 255–261 (2014). [https://doi.org/10.14954/jste.1.4\\_B\\_1](https://doi.org/10.14954/jste.1.4_B_1). (in Japanese)
9. Masumoto, H., Higatani, A., Kodama, T., Kitazawa, T., Suzuki, K.: Evaluating the effect of using the moving light guidance system on Hanshin Expressway against traffic congestion. In: The Proceeding of 55th Infrastructure Planning Conference (2017). (in Japanese)
10. Kameoka, H., Oneyama, H., Watanabe, Y., Sakurai, M.: Verification of effect of alleviating congestion occurrence by dynamic flashing control of roadside light emitters making use of light scattering. In: The Proceeding of 48th Infrastructure Planning Conference (2013). (in Japanese)
11. Edie, L.: Car-following and steady-state theory for non-congested traffic. *Oper. Res.* **9**(1), 66–75 (1961)
12. Takashima, M., Shiomi, Y.: Monitoring traffic flow dynamics at sags: data assimilation approach. *J. JSCE* **73**(5), 1073–1082 (2017). [https://doi.org/10.2208/jscejipm.73.I\\_1073](https://doi.org/10.2208/jscejipm.73.I_1073). (in Japanese)
13. Uno, N., Iida, Y., Itsubo, S., Yasuhara, S.: A microscopic analysis of traffic conflict caused by lane-changing vehicle at weaving section. In: Proceedings of the 13th Mini-Euro Conference “Handling Uncertainty in Transportation Analysis of Traffic and Transportation Systems”, pp. 143–148 (2002)
14. Baba, M., Saga, S., Shiduki, B., Takahashi, S.: A Study on Posture Improvement Support System Using Shoulder Muscle Fatigue Measurement, IPSJ SIG technical reports, (HCI), 2017-HCI-171, pp. 1–8 (2017)

# Proposal of Acoustic Train Detection System for Crowdsensing



Koji Sato, Shigemi Ishida, Jumpei Kajimura, Shigeaki Tagashira  
and Akira Fukuda

**Abstract** Train operation status is an important piece of information for our transportation plans. Without the latest train operation status, commuters might be face transportation inconvenience. Nowadays, train operation status is managed by railway companies. When a railway company delays the status update, commuters do not know the actual train operation status. In rural areas, the status updates are often delayed because railway companies focus more of their efforts on the recovery of train operation. Therefore, we propose a crowdsourced train detection system using a microphone on a smartphone. In our train detection system, a smartphone analyzes the frequency components of sound signals acquired by a microphone. We calculate the probability of a train passing using a logistic regression model on the sound frequency components and apply a hysteresis thresholding with two thresholds to detect passing trains. In addition, simple filtering based on train length is also applied to increase robustness to noise, including the sound of other passing vehicles. We conducted initial experimental evaluations and confirmed that our train detection system can successfully detected trains with an F-measure of 0.99 and a recall of 1.0. Further, we also conducted experiments in a more practical environment where

---

K. Sato (✉) · S. Ishida · J. Kajimura · A. Fukuda  
ISEE, Kyushu University, Fukuoka, Japan  
e-mail: [k\\_sato@f.ait.kyushu-u.ac.jp](mailto:k_sato@f.ait.kyushu-u.ac.jp)

S. Ishida  
e-mail: [ishida@f.ait.kyushu-u.ac.jp](mailto:ishida@f.ait.kyushu-u.ac.jp)

J. Kajimura  
e-mail: [kajimura@f.ait.kyushu-u.ac.jp](mailto:kajimura@f.ait.kyushu-u.ac.jp)

A. Fukuda  
e-mail: [fukuda@f.ait.kyushu-u.ac.jp](mailto:fukuda@f.ait.kyushu-u.ac.jp)

S. Tagashira  
Faculty of Informatics, Kansai University, Suita, Japan  
e-mail: [shige@res.kutc.kansai-u.ac.jp](mailto:shige@res.kutc.kansai-u.ac.jp)



the audio signals were acquired by smartphones in pants's pockets, and confirmed that the acquired audio signals are useful for train detection.

**Keywords** Train detection · Acoustic sensor · Crowdsensing

## 1 Introduction

Trains are fast and high-capacity means of transportation that plays an important role in modern society. In Japan, 2.1 billion people traveled on trains in April 2018 according to a report from the Ministry of Land, Infrastructure, Transport and Tourism [9].

The train operation status is shared on the Internet nowadays because canceled and delayed trains have a substantial influence on numerous train users. A railway company provides the train operation status based on the train location derived from track circuits and tachographs. Train users can rearrange their travel based on the status information when trains are canceled or delayed.

Train operation status, however, is often updated with a considerable delay of more than 20 min after the status changes. The railway company focuses on resuming or recovering the train operation when the operation status changes; the operation status is updated later. A 20-min update delay is often critical for train users, especially in rural areas because the number of trains is limited.

Our goal is to realize a train-operation-status-sharing system that shares latest train operation status based on crowdsensing. Crowdsensing offloads sensors onto users' smart devices to reduce the sensor deployment cost. The train-operation-status-sharing system collects train-location information from the user's devices and checks if the train is running according to schedule.

Several studies have reported train-localization systems using a global positioning system (GPS) module, acceleration sensor, or magnetic sensor [3, 4, 7], which are available on smartphones. These studies assume that the smartphone is on-board, i.e., the user is on a train, and estimate the train location based on the smartphone location, train velocity, or pre-trained sensor signatures. There is little chance of cooperation from train users in rural areas where a limited number of people use trains.

To collect considerably more train-location information, we present a new train-detection system that enables rail-side pedestrians to share the train location. Our key idea is to detect trains using rail-side smartphones and share the detection results along with the smartphone location. We utilize a microphones on a smartphones to detect trains because smartphones are often in a pockets or bags. Our train-localization system analyzes the frequency components of sound signals derived by a smartphones and calculates the probability of a train passing using a logistic regression model on the frequency components. The regression coefficients are trained prior to system usage. Finally, the system applies hysteresis thresholding with two thresholds to detect the passing train.

We conducted an experimental evaluation to demonstrate the basic performance of our train-detection system. We installed a microphone at a house nearby a railway and

recorded the sound of passing trains for approximately 7.5 h. The sound signals were then analyzed using our train detection system to detect passing trains. We confirmed that the train detection system successfully detected trains with an F-measure of 0.99 and a recall of 1.0.

Specifically, our main contributions are twofold:

- We present a train-detection system using a microphone, which enables us to use smartphones in a pockets or bags as sensors. To the best of our knowledge, this is the first attempt to detect trains using a microphone located outside of the trains.
- We demonstrate experimentally that our train detection system shows a high detection performance when we clearly retrieve train sound.

The remainder of this paper is organized as follows. Section 2 shows an overview of our train-operation-status-sharing system utilizing crowdsensing. Section 3 describes existing train localization methods that can be used in the operation-status-sharing system. Section 4 shows our proposed train-detection system for rail-side cooperators in the operation-status-sharing system. Section 5, describes the initial evaluations conducted to demonstrate the basic performance of our system. Section 6 describes the experimental evaluations in a more practical situation. Section 7 discusses possibilities for performance improvement of the train-detection system, and Sect. 8 concludes the paper.

## 2 Train-Operation-Status-Sharing System Utilizing Crowdsensing

Figure 1 shows an overview of our train-operation-status-sharing system utilizing crowdsensing. The status-sharing system relies on three information sources:

1. *Railway company's website:*  
Prior to the system use, the sharing system retrieves the regular train schedule as “ground truth” of the train location. The sharing system also monitors the operation status on the railway company's website.
2. *Smartphones of on-board cooperators:*  
On-board cooperators report their location and time information to the sharing-system server.
3. *Smartphones of rail-side cooperators:*  
Rail-side cooperators report their location and time information when train passing is detected.

The status-sharing system first calculates the train locations based on the “ground truth” train schedule. The status-sharing system then compares the ground truth train location with those collected from cooperators' smartphones to detect irregular train schedules, which are provided to users as a prompt report.

In the case in which insufficient location data is collected by crowdsensing, the sharing system also updates the operation status based on the operation-status

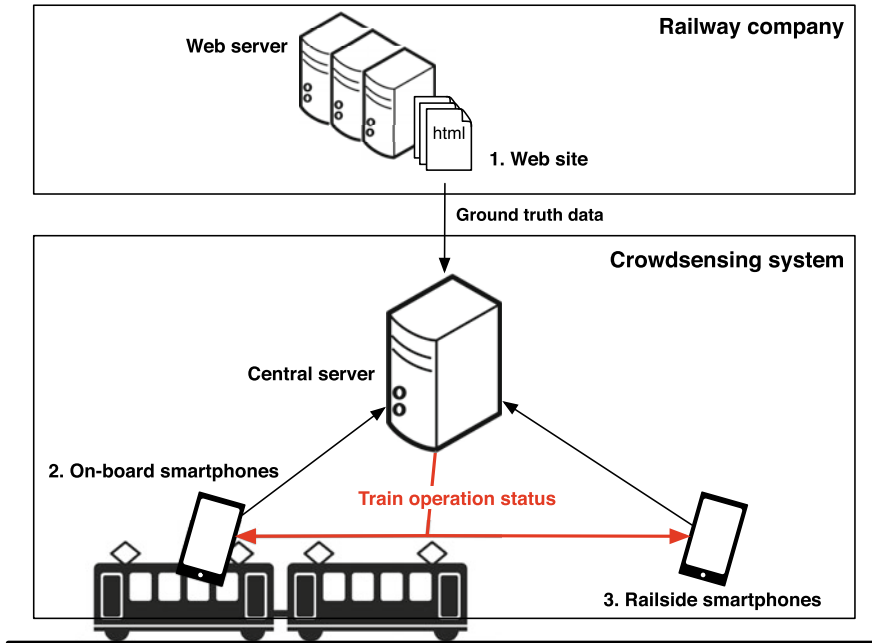


Fig. 1 Overview of train-operation-status-sharing system utilizing crowdsensing

information derived from the railway companies’ website. Information on the railway company’s web site is also used to identify the cause of the irregularity.

As we described in the following section, the first and second aforementioned information sources are already available. We focus on the third information source in this paper.

### 3 Related Work

In this section, we briefly investigate related work on train detection. First, we explain sensor-based train detection methods in use in Japan, which are mainly utilized by railway companies. We then introduce train-detection methods relying on smart-device sensors.

#### 3.1 Existing Train-Localization Methods

This subsection overviews train-localization methods used by railway companies. These methods are used indirectly as *railway company’s website* sources.

There are three main methods used to detect trains: the tachograph, track circuit, and axle counter methods. A tachograph is installed on-board, and the distance from a reference point is calculated using the tachograph output. The reference points are measured using IC tags installed along the railroad track [8]. These systems face a communication problem as reliable communication between the train and ground equipment is required.

A track circuit and axle counter are installed on the railroad track. A track circuit is an electrical circuit using wheels and the axle of a train. Tracks are separated by insulators forming track sections. When a train passes between sections, the circuit is electrically shorted, which indicates the presence of a passing train between the sections. An axle-counter detects a train passing when the train passes over an axle-counter installed on a railroad track. These methods require sensors to be installed on the railroad track, resulting in high deployment and maintenance costs for railroad work, which sometimes restricts on train services. Because these methods require the construction of railroad tracks or customization of train cars, only railway companies can deploy sensing systems using these methods.

Satellite localization systems, including GPS and global navigation satellite system (GNSS), have also been utilized for train localization. The GNSS provides the train location calculated from radio signals from satellites [6, 12]. The GPS and GNSS fail at localization or suffer from high localization errors when radio signals are unavailable or weak, such as in tunnels. Because of these localization error, GPS and GNSS have not been put into practical use in Japan as it has many tunnels.

### 3.2 *Mobile Train-Localization Systems*

Smartphones have a rich set of sensors such as a GPS, magnetic sensor, accelerometer, and microphone. These sensors are used in wide variety of applications and are focused on nowadays as a new area of research field called mobile phone sensing [5]. Several train-localization methods relying on mobile-phone sensing have also been proposed.

Smartphones equipped with GPS modules carried by on-board users are utilized in crowdsensing train-localization systems. Location information and timestamp are sent to a crowdsensing server. As described in the previous section, GPS and GNSS suffer from low localization accuracy with weak radio signals in areas such as in tunnels. To improve the localization accuracy, hybrid approaches that combine inertial measurement units with GNSS have been proposed [1, 10]. In our crowdsensing train-operation-status-sharing system, the GPS and GNSS are promising candidates for on-board cooperators' sensing.

Heirich et al. proposed a train-localization method using an inertial sensor in an on-board smartphone [4]. This method uses location-dependent vibration as a *fingerprnt* that describes the location. Prior to the location estimation, a site survey is conducted; vibration and location data are collected as fingerprints. The train

location is estimated by finding the most similar fingerprint from fingerprints to those collected in the site survey.

A multiple-sensor-based train-localization system using an acceleration sensor and microphone has also been proposed [11]. In this system, an on-board smartphone retrieves acceleration and sound data to estimate the train location. From the vertical acceleration, the system detects trains passing over rail joints. In addition, the vertical acceleration yields the approximate train speed because the acceleration is dependent on the train speed.

Similarly, the sound of the train passing the rail joint is captured by a microphone. The joint-passing sound is emitted when the front and rear wheels of the train pass over the rail joints. From the distance between the front and rear wheels, we can estimate the train speed based on the intervals of the joint-passing sound. Combining these two approaches, the system estimates the actual train speed, which is integrated to calculate the running distance of the train.

All of these methods are utilized in on-board cooperators' crowdsensing in our train-operation-status-sharing system. In rural areas, the number of on-board cooperators may be insufficient to collect train-location data. Our approach, microphone-based rail-side train detection, is proposed to increase the number of cooperators in the status-sharing system.

## 4 Train-Detection System Using a Microphone

Figure 2 illustrates an overview of our train-detection system using a microphone. The train-detection system consists of predict and detect blocks to analyze the sound signals retrieved from a microphone installed near the railroad tracks. A low-pass filter (LPF) is applied prior to the analysis to reduce the influence of high-frequency environmental noise. The predict block calculates the probability of train existence based on the frequency components of the sound signals retrieved from the microphone. The detect block calculates the moving average (MA) over the output of the predict block and applies hysteresis thresholding with two thresholds to detect train passing.

The details of each block are described in the following subsections.

### 4.1 *Predict Block*

A predict block consists of training and prediction phases because the block uses logistic regression, which is a machine-learning method.

In the training phase, regression coefficients of logistic regression are trained using frequency components of the sound signal. In the prediction phase, logistic regression analysis is performed on the frequency components of the sound signal

at each time-point using the regression coefficients trained in the training phase to calculate the existence probability of train passing.

Each phase is described in detail as follows.

### 4.1.1 Training Phase

In the training phase, the system trains the regression coefficients of logistic regression using the training audio data. As shown in Fig. 2, we use frequency components calculated by fast Fourier transform (FFT) as feature values. The sound data is divided into fixed-length time windows. FFT is applied to the each divided data to calculate the amplitude of frequency components. Using the amplitude of the frequency components, the system trains the regression coefficients of the logistic regression.

In a logistic regression analysis for train detection, the system calculates the probability of train existence using the frequency components derived from FFT as feature values. Let  $Y = \{0, 1\}$  be a random variable that describes the existence of a passing train such that  $Y = 1$  when a train exists and  $Y = 0$  when no train exists. The probability of train existence is given by

$$P(Y = 1|\mathbf{X}) = \frac{1}{1 + e^{-\mathbf{A}\mathbf{X}}}, \tag{1}$$

where  $\mathbf{X} = [1, x_1, x_2, \dots, x_n]$  is an input vector, and  $\mathbf{A} = [a_0, a_1, a_2, \dots, a_n]$  is a regression coefficient vector, and  ${}^t\mathbf{Z}$  describes a transpose of vector/matrix  $\mathbf{Z}$ .

In the training process, regression coefficients are calculated by minimizing the cost function  $C(\mathbf{A})$ :

$$C(\mathbf{A}) = \frac{1}{N} \sum_{i=1}^N \log P(Y = Y_i|\mathbf{X}_i), \tag{2}$$

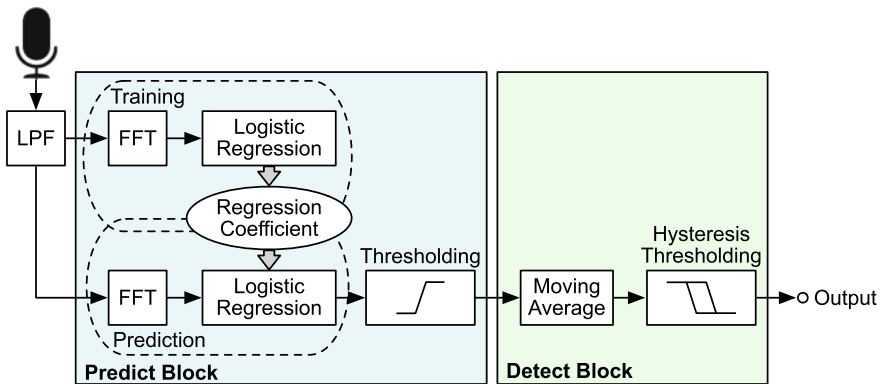


Fig. 2 Overview of train-detection system

where  $\{\mathbf{X}_i, Y_i | i = 1, 2, \dots, N\}$  is a training data set derived from FFT.

### 4.1.2 Prediction Phase

In the prediction phase, the system calculates the existence probability of a passing train using the regression coefficients obtained in the training phase.

Logistic regression analysis is performed using the frequency components calculated by FFT of the sound data. The sound data is divided into a fixed-length time windows. Again, FFT is applied to each divided data to calculate the amplitude of the frequency components  $\mathbf{X}$ . Then, the probability of a train passing at each time is calculated by substituting the regression coefficients  $\mathbf{A}$  obtained in the training phase and the frequency component  $\mathbf{X}$  for the regression model in Eq. (1).

Figure 3 shows an example of the predict block output. A train passed in front of the microphone between 22 and 32 s. As shown in Fig. 3, the predict block outputs high a probability when a train passes in front of the microphone.

## 4.2 Detect Block

A detect block applies moving average and hysteresis thresholding to the output of the predict block to finalize the train detection.

As shown in Fig. 3, the output of the predict block chatters when a train approaches and leaves. The output of the predict block may also increase when a large vehicle passes on a road near the railroad tracks, resulting in a false positive train detection. We apply the moving average to reduce faulty detections caused by the chattering and by passing vehicles. The length of the moving average is set to approximately five seconds based on the time length of the train passing.

Finally, the detect block applies hysteresis thresholding to obtain the final detection results. Figure 4 briefly explains hysteresis thresholding for train detection. The

**Fig. 3** Example of predict block output. The numbers 0 and 1 indicate that a train exists and no train exists, respectively

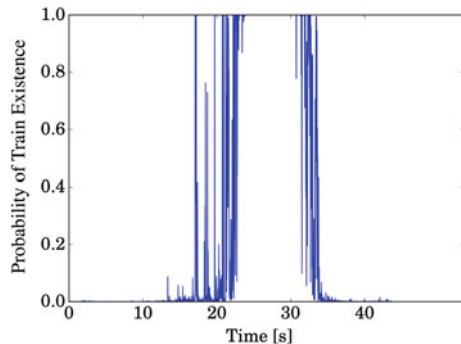
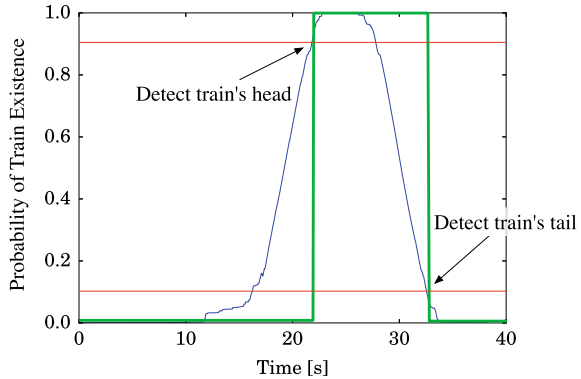


**Fig. 4** Overview of hysteresis thresholding



two red lines represent the thresholds and the blue curve in Fig. 4 represents the output of the moving average, i.e., the averaged probability of train passing. We apply a higher threshold for the rising edge, whereas the falling edge is detected at a lower threshold, deriving the square-shaped wave indicated by the green line in Fig. 4.

## 5 Initial Evaluation

To demonstrate the basic performance of our train-detection system, we conducted an experiment with a microphone installed near a railroad track.

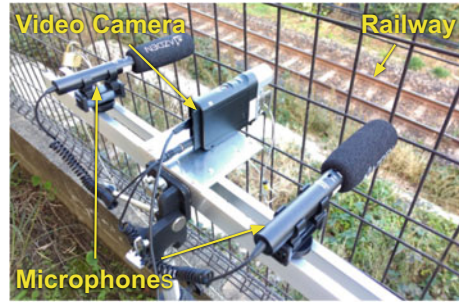
### 5.1 Experiment Setup

Figure 5 shows the experiment setup. A microphone was installed in a backyard of a house near a single-track railroad in Itoshima city, Fukuoka, Japan. We collected audio data for approximately 7.5 h. We also collected audio data at a different location for approximately 3 h; this was used only for training to evaluate the influence of the difference between the locations of training and testing locations. A total of 39 trains passed in the 7.5-h testing data collection, whereas a total of 17 trains passed in the 3-h training data collection. Although two microphones were installed as shown in Fig. 5, we only used one microphone in this study.

The target railroad has a single track, implying that multiple trains never pass simultaneously. The sound was recorded using a SONY HDR-MV1 recorder with an AZDEN SGM-990 microphone at a sampling frequency of 48 kHz and word length of 16 bits. Video monitoring of the target railroad was also recorded using a SONY HDR-MV1 video recorder, which was used as the ground truth.



Fig. 5 Experiment setup



We manually labeled the training data referring to the ground truth, i.e., recorded video: 1 for train passing and 0 for no train passing. The label 1 is used only when a train was passes directly in front of the microphone. The audio data when a train was approaching and was moving away was excluded from the evaluation to improve the training accuracy because these cases might include substantial noise other than the train sound.

We define the train-passing time  $t_p$  as the time at which the train passes directly in front of the microphone. The train passing sound is extracted from  $t_p = 0$  to  $t_p = 5$  s. In the training phase, audio data from  $t_p = -5$  to  $t_p = 0$  s and from  $t_p = 5$  to  $t_p = 20$  s was excluded from the training data because the data includes ambiguous sound signals.

To determine the frequency range of features in logistic regression, we compared the performance between full-range detection and frequency-limited detection. Table 1 shows the frequency range and the numbers of FFT points of the full-range and frequency limited detections.

We evaluated the numbers of true positives (TPs), false negatives (FNs), and false positives (FPs) based on a comparison of the results derived from our train-detection system with video. TP, FN, and FP are defined as the cases in which a train was detected when a train passed, no train was detected when a train passed, and a train was detected when no train passed, respectively.

Using the number of TPs, FN, and FPs, we also evaluated the precision, recall, and F-measure defined, respectively, as:

$$\text{Precision} = \frac{\text{TP}}{\text{TP} + \text{FP}}, \quad (3)$$

$$\text{Recall} = \frac{\text{TP}}{\text{TP} + \text{FN}}, \quad (4)$$

$$F_{\text{measure}} = \frac{2 \cdot \text{Precision} \cdot \text{Recall}}{\text{Precision} + \text{Recall}}. \quad (5)$$

**Table 1** Frequency range and number of FFT points used as feature values in logistic regression

	Frequency range (kHz)	Number of FFT points
Frequency-limited	0 to 1	21
Full-range	0 to 24	512

## 5.2 Detection Performance

We evaluated the detection performance of our train-detection system using two ranges of frequency components, i.e., less than 1 kHz and less than 24 kHz. Logistic regression coefficients were derived using the 3-h training sound data and the 7.5-h sound data was used for the evaluation to include the influence of the recorded location difference between training and testing.

Table 2 shows the detection performance, i.e., the numbers of TPs, FNs, and FPs, as well as the precision, recall, and F-measure. Table 2 indicates the following:

1. Frequency-limited and full-range detections exhibited the same detection performance. This indicates that the frequency components less than 1 kHz were sufficient to practically detect trains.
2. The recall of 1.0 indicates that the train-detection system successfully detected all of the passing trains.
3. The precision of 0.98 indicates that the train-detection system suffered from the small number of FP detections. FP occurred when three motorbikes passed successively near a microphone. Loud sound signals that partially include frequency components of the train sound caused the FP detection. We believe that this type of noise could be excluded if we use a sufficient amount of noise data for training.
4. The F-measure of 0.99 indicates that the train-detection system exhibited extremely high detection performance. One cause of this high performance might be the experiment environment. There was a single railroad track in front of a microphone such that multiple trains never passed simultaneously.

These results reveal that our acoustic-train detection system successfully and effectively detected trains.

**Table 2** Detection performance in (a) frequency-limited and (b) full-range detections

(a)			(b)		
TPs	FNs	FPs	TPs	FNs	FPs
39	0	1	39	0	1
Precision		0.98	Precision		0.98
Recall		1.0	Recall		1.0
F-measure		0.99	F-measure		0.99

**Fig. 6** Regression coefficients of logistic regression in **a** frequency-limited and **b** full-range detections

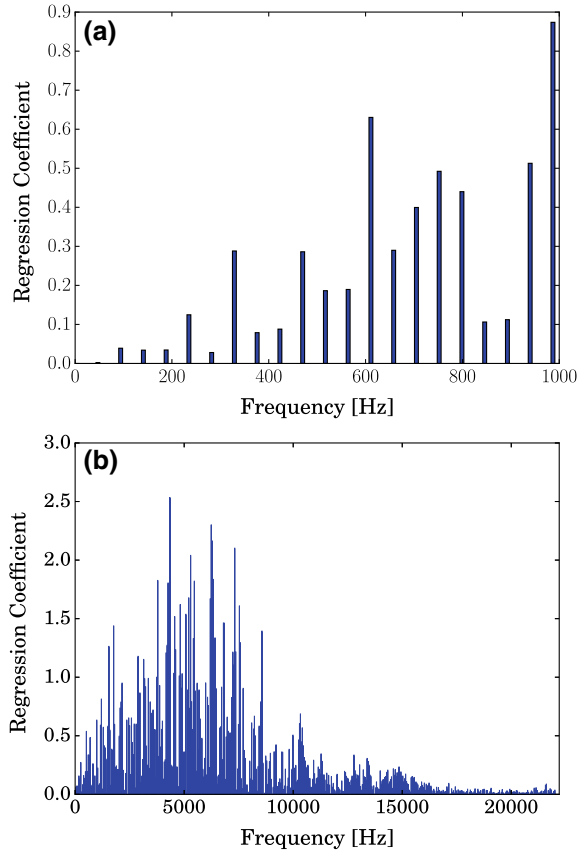


Figure 6 shows the absolute values of the regression coefficients used in the logistic regression, which correspond to the frequency components of the sound signals. The absolute value of the regression coefficient implies a contribution of the corresponding frequency component to the train detection. As shown in Fig. 6b, frequency components of approximately 5–10 kHz contribute substantially to train detection. We still derived a good detection performance in the frequency-limited detection; frequency components of less than 1 kHz were sufficient for the detection of trains.

## 6 Experiment in a Practical Environment

To confirm that our train-detection system can be used in the train-operation-status-sharing system presented in Sect. 2, we conducted an experiment in a more practical environment. Sound data was collected using a mobile phone in a pocket because commuters usually carry their mobile phones in their pockets.

### 6.1 Experiment Setup

We conducted experimental evaluations near Imajuku station in Fukuoka city, Fukuoka, Japan. Figure 7 shows a map of the experiment location. Two railroad tracks run in an east-west direction. An observer equipped with smartphones was on the south side of the tracks. Trains travelling from the east run on the south track, whereas trains travelling from the west run on the north track. Sound data was collected in sitting and walking scenarios:

1. *Sitting scenario:*

The observer sat at the rail-side point indicated in Fig. 7. There is an overpass road above the sitting point. The audio data collected in the sitting scenario therefore includes considerable vehicle sound. The observer sat on a concrete pier of the overpass. For the test data, we collected audio data for approximately 20 min. A total of three trains passed in the 20-min test data collection period.

2. *Walking scenario:*

The observer walked along a sidewalk along the railroad tracks. Figure 8 shows the walking area in the walking scenario. For each train direction, the observer collected audio data of two trains while walking to east or west in the walking area. The audio data of eight passing trains was finally collected. The audio data length was approximately 15 min in total.

The sound was recorded using an ASUS ZenFone 3 Deluxe 5.5 at a sampling frequency of 44.1 kHz and word length of 16bits. Test data was collected from smartphones in the front and rear pockets of jeans, as shown in Fig. 9.

Training data was collected from for approximately 40 min from a smartphone installed at a sidewalk of railroad to evaluate the effect of the difference between the training and test data. A total of six trains passed in the 40-min training data collection period. During our experiment, multiple trains did not pass simultaneously.

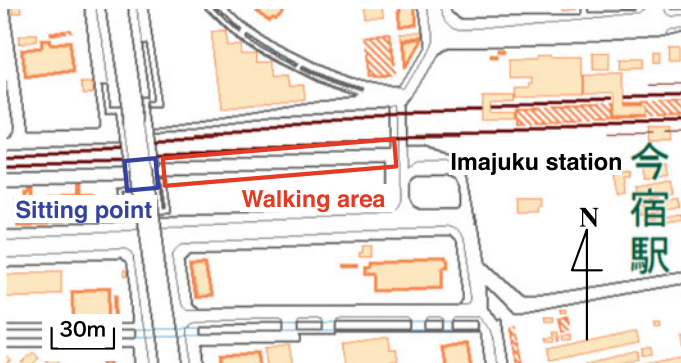


Fig. 7 Map of experiment location (using 1:25,000 scale GSI maps from GSI, Japan [2])

**Fig. 8** Experiment environment: the sidewalk along the railroad



**Fig. 9** Experiment setup: smartphones in front and rear pockets



We manually labeled the train data referring to the ground truth in the same manner as in Sect. 5.1. We used frequency components less than 1 kHz as the feature values, referring to the performance evaluation conducted in Sect. 5. FFT was performed on 1024 samples at a sampling frequency of 44.1 kHz. Therefore, there were 22 FFT points less than 1 kHz.

Comparing the results derived from our train-detection system with ground truth, we evaluated the numbers of TPs, FNs, and FN<sub>s</sub> as well as the precision, recall, and F-measure.

**Table 3** Detection performance in the sitting scenario using a smartphone in (a) front and (b) rear pockets

(a)			(b)		
TPs	FNs	FPs	TPs	FNs	FPs
3	0	0	2	1	0
Precision		1.0	Precision		1.0
Recall		1.0	Recall		0.67
F-measure		1.0	F-measure		0.80

### 6.2 Detection Performance in the Sitting Scenario

Table 3 shows the detection performance in the sitting scenario. Table 3 indicates the following:

1. A precision of 1.0 indicates that the detection system had no FP detection in either pocket. In a crowdsensing system, FP detection is undesirable because they FP confuse the system. Our train-detection system exhibited ideal performance for crowdsensing in terms of FPs.
2. A rear pocket smartphone suffered from an FN detection as indicated by the recall of 0.67. In our experiment, FN detection occurred when a train passed on the north track, i.e., the track far from the observer. FN detections are not as problematic in crowdsensing because crowdsensing relies on many participants; train detections by other participants cover the FN detections.

### 6.3 Detection Performance in the Walking Scenario

Table 4 shows the detection performance in the walking scenario. Table 4 indicates the following:

1. A precision of 1.0 indicates that the detection system again had no FP detection in either pocket.
2. Recalls of 0.38 and 0.25 indicate that the system suffered from too many FN detections.

We found that all of the trains that passed on the north track were undetected. This implies that we need to minimize the influence of distance between the observer and the railroad track for better detection performance.

**Table 4** Detection performance in the walking scenario using a smartphone in (a) front and (b) rear pockets

(a)			(b)		
TPs	FNs	FPs	TPs	FNs	FPs
3	5	0	2	6	0
Precision		1.0	Precision		1.0
Recall		0.38	Recall		0.25
F-measure		0.55	F-measure		0.40

## 7 Discussion

In Sect. 5, we demonstrated that our train-detection system successfully detected trains while a smartphone was in a pocket. Section 6, however, noted that we face an issue for practical use. This section discusses possibilities for performance improvement of the train-detection system.

### 7.1 Frequency Range

In Sect. 5, we conducted an initial evaluation to determine the frequency range for logistic regression based on the frequency components of the train sound signals collected in an open space. Sound signals collected by a smartphone in a pocket in a walking scenario include considerable friction noise caused by the pants’ pocket. The friction noise negatively affected the detection performance, resulting in false negative detections.

**Fig. 10** Amplitude of frequency components of sound signals in sitting and walking scenarios

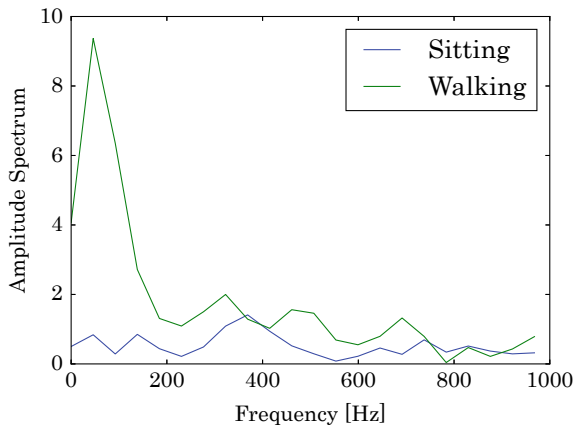


Figure 10 shows the amplitude of each frequency component of the sound signals in the sitting and walking scenarios. In the walking scenario, frequency components under 1 kHz were quite high compared to those in the sitting scenario. We believe that the frequency components were caused predominantly by the friction noise, resulting in the detection of performance degradation.

To reduce the influence of the noise, we need to utilize more wider-bandwidth sound signals in the logistic regression.

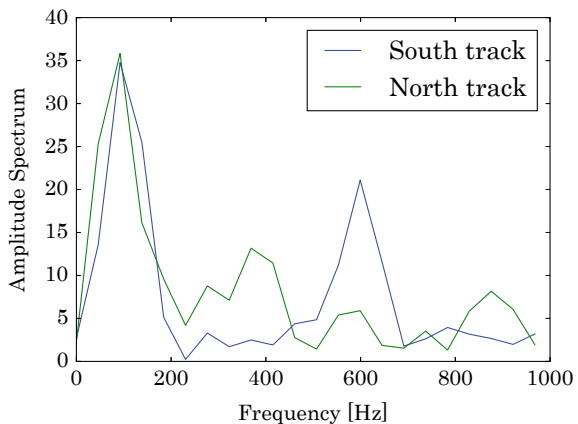
As a reference, we additionally evaluated the detection performance in the walking scenario with frequency components from 0 to 2 kHz in a logistic regression. We confirmed that the F-measures were increased from 0.55 and 0.4 to 0.67 for the front and rear pockets, respectively, with the wider bandwidth. We plan to analyze the influence of frequency components as one of our future works.

### 7.2 Amount of Training Data

In Sect. 6.3, we found that all of the trains that passed on the north track were undetected. The false negative detections were mainly caused by the difference between the frequency components of the sound signals on different tracks.

Figure 11 shows the amplitude of the frequency components of the sound signals for trains on the south and north tracks. Frequency components of approximately 600 Hz of the south-track train are high compared to those of the north-track train. We could not identify the cause of this difference; however we can conclude that we need to collect significantly more training data that in many situations to provide robustness to the environment difference.

**Fig. 11** Amplitude of frequency components of sound signals for trains on the south and north tracks





## 8 Conclusion

In this paper, we proposed a train-operation-status-sharing system using crowdsensing. To realize the status-sharing system, we presented an acoustic train-detection system for rail-side cooperators. In the train detection system, the frequency components of the train sound are analyzed using a logistic regression model to calculate the probability of train passing. We conducted experimental evaluations to demonstrate the detection performance of the train-detection system. Experimental evaluations revealed that the train-detection system successfully detected trains with an F-measure of 0.99 and a recall of 1.0. In addition, we also demonstrated that audio signals collected by smartphones in pants' pockets were capable of train detection. For future works, we plan to improve the detection performance as we discussed in Sect. 7.

**Acknowledgements** The work presented in this paper was supported in part by JSPS KAKENHI Grant Numbers JP15H05708, JP17K19983, and JP17H01741 as well as the Cooperative Research Project of the Research Institute of Electrical Communication, Tohoku University.

## References

1. Cai, B., Wang, X.: Train positioning via integration and fusion of GPS and inertial sensors. *WIT Trans. Built Environ.* **50** (2000)
2. Geospatial Information Authority of Japan (GSI): GSI map. <https://maps.gsi.go.jp/>
3. Heirich, O., Siebler, B., Hedberg, E.: Study of train-side passive magnetic measurements with applications to train localization. *J. Sensors* 2017 8073982 (2017)
4. Heirich, O., Steingass, A., Lehner, A., Strang, T.: Velocity and location information from onboard vibration measurements of rail vehicles. In: *Proceedings of the IEEE International Conference on Information Fusion (FUSION)*, pp. 1835–1840 (2013)
5. Lane, N.D., Miluzzo, E., Lu, H., Peebles, D., Choudhury, T., Campbell, A.T.: A survey of mobile phone sensing. *IEEE Commun. Mag.* **48**(9) (2010)
6. Lu, D., Schnieder, E.: Performance evaluation of GNSS for train localization. *IEEE Trans. Intell. Transp. Syst.* **16**(2), 1054–1059 (2015)
7. Marais, J., Beugin, J., Berbineau, M.: A survey of GNSS-based research and developments for the European railway signaling. *IEEE Trans. Intell. Transp. Syst.* **18**(10), 2602–2618 (2017)
8. Matsumoto, M.: ATACS delivers moving block. *Railw. Gaz. Int.* **167**(3), 43–45 (2011)
9. Ministry of Land, Infrastructure, Transport and Tourism of Japan: Railway transportation statistics month report (in Japanese). <http://www.mlit.go.jp/k-toukei/saisintoukei.html> (2018)
10. Otegui, J., Bahillo, A., Lopetegi, I., Díez, L.E.: A survey of train positioning solutions. *IEEE Sensors J.* **17**(20), 6788–6797 (2017)
11. Su, D., Sano, S., Nagayama, T., Tanaka, H., Mizutani, T.: Train localization by mutual correction of acceleration and interior sound (in Japanese). *J. Struct. Eng.* **62A**, 571–584 (2016)
12. Yordanov, R., Iontchev, E., Miletiev, R., Mladenov, V.: GPS/GPRS/INS system for real-time monitoring of the urban railway. *Int. J. Transp. Syst.* **1**, 48–52 (2016)

# A Study for Social Benefit of VICS WIDE Service by Using Traffic Simulation in Tokyo



Shinya Adachi, Yasuhiko Iwasaki, Kazuhiko Mizushima  
and Hisatomo Hanabusa

**Abstract** VICS (Vehicle Information and Communication System) Center started traffic information service in 1996, now VICS receiver units are mounted on the navigation systems more than 80%, and 4 million units are shipped annually. And in April 2015, VICS Center added a new service “VICS WIDE”. VICS WIDE service provides advanced traffic information that is aimed for more useful DRGS (Dynamic Route Guidance System). We anticipate that this new service will make a convenience of road traffic in the future. Since last year, we have started the study for estimation of the social benefits and economic effects expected by the spread of VICS WIDE service by using the traffic simulator with near-reality road network data and traffic demand data. As a result, the VICS WIDE service got a prospect of reducing the economic cost of traffic congestion by about 10%.

**Keywords** Traffic information · Traffic simulation · Socio-economic benefit

## 1 Introduction

22 years has passed from starting of VICS service. At present VICS receiver units are mounted as an essential function on the navigation system and we estimate that 30% of drivers are using VICS service.

---

S. Adachi (✉) · Y. Iwasaki · K. Mizushima  
Vehicle Information and Communication System Center, Nittochi Kyobashi Bldg, 2-5-7  
Kyobashi, Chuo-Ku, Tokyo, Japan  
e-mail: [s-adachi@vics.or.jp](mailto:s-adachi@vics.or.jp)

Y. Iwasaki  
e-mail: [y-iwasaki@vics.or.jp](mailto:y-iwasaki@vics.or.jp)

K. Mizushima  
e-mail: [mizushima@vics.or.jp](mailto:mizushima@vics.or.jp)

H. Hanabusa  
I-Transport Lab. Co., Ltd, Shin-Surugadai Bldg 9F, 3-10, Kanda-Ogawamachi, Chiyoda-Ku,  
Tokyo, Japan  
e-mail: [hanabusa@i-transportlab.jp](mailto:hanabusa@i-transportlab.jp)

In April 2015, VICS Center doubled the data transmission bandwidth of FM multiplex broadcasting, and started a new service that is named “VICS WIDE”. In the last quarter summary, 80% of the shipped VICS units correspond to VICS WIDE service and we expect to spread rapidly in the near future.

One of the main services added at VICS WIDE is link travel time on ordinary road.

Before the starting of VICS WIDE service, previous VICS services provided only visual traffic jam information on the ordinary road and did not provide link travel time.

For this reason, the route guidance in the previous VICS service has been based on the static link cost that is calculated by the link length and road attributes.

We think that VICS WIDE users can get greater benefits by using DRGS that is calculated with link travel time, and it will contribute to alleviate traffic congestion socially as well.

In this paper, we estimated the economic effect of VICS WIDE by using traffic simulation with near-reality traffic demand data and road network data.

## 2 Objective of This Study

In recent years, several studies have been conducted on the influence and effect on traffic flow by providing traffic information.

In general, by providing traffic information, individual drivers select route which is minimize travel time, so the road network can be effectively utilized and congestion alleviation can be expected.

However, particularly in the crowded road network, along with the increasing of number of vehicles following the traffic information, there is a possibility that the traffic concentration to the unoccupied road may occurs by the vehicle according to the information, and congestion loss may be increased [1]. On the expressway in Japan, it was confirmed that such traffic concentration phenomenon occurred actually by providing traffic information on variable message sign boards [2]. Moreover, several methods for reducing traffic concentration phenomenon have also been proposed, and its effect has been evaluated by simulation [3].

Most of the above mentioned research is evaluated in simple road networks such as expressway or corridor. On the other hand, in an actual road network, there are many urban streets with no traffic information, and some drivers use such urban streets to avoid congestion.

First objective of this study is to estimate the socio-economic benefits of link travel time information by VICS WIDE in actual road network and traffic demand.

And second is to check the possibility of occurrence of economic loss due to traffic concentration in the situation where VICS WIDE users spread.

### 3 Overview of VICS WIDE Traffic Information

VICS provides road traffic information with three media, FM multiplex broadcasting, infrared beacon, and radio wave beacon.

VICS WIDE is a new service for FM multiplex broadcasting.

For the more useful DRGS, traffic information of VICS WIDE has been improved as follows.

- Provision of link travel time on ordinary road;  
Although previous VICS has provided only traffic congestion (without link travel time) for ordinary road via FM multiplex broadcasting, VICS WIDE service added link travel time of ordinary road.
- Enhancement of traffic information by taxi probe data;  
We introduced the probe car system by about 5,000 taxis in Tokyo metropolitan area. Probe car system make it possible to provide traffic conditions even in the roads without vehicle detectors.

Figure 1 shows the difference in coverage of link travel time between previous VICS and VICS WIDE in Tokyo Metropolitan area.

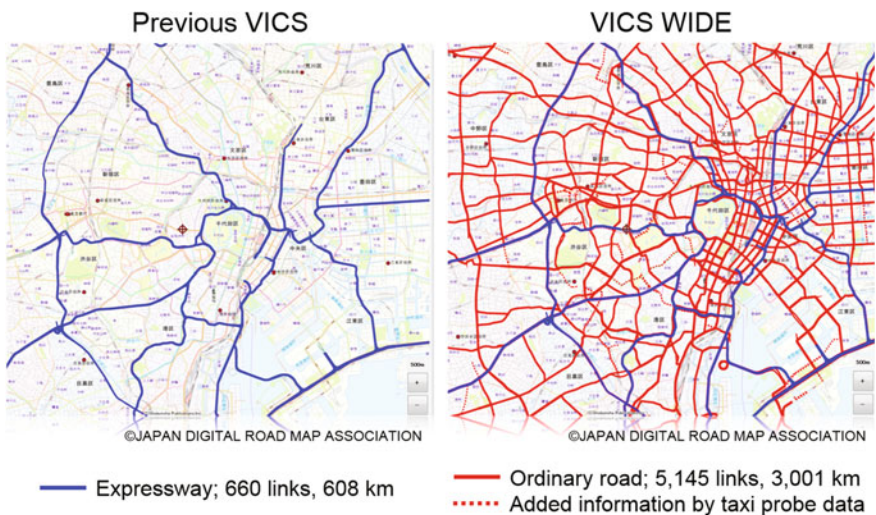


Fig. 1 Overview of coverage of link travel time

## 4 Traffic Simulation for Estimating Socio-Economic Benefits

### 4.1 Framework of Social Benefit

Drivers who refer to previous VICS information or VICS WIDE information select routes avoiding congestion sections on the road network. As a result, these drivers are appropriately allocated to the road section and the traffic congestion of the entire road network will be reduced. Furthermore, also Non VICS users can get benefits as VICS users spread. So VICS system contributes to the reduction of economic cost of traffic congestion like Fig. 2.

In this paper, we estimate the socio-economic benefit by reducing the economic traffic cost by using traffic flow simulation.

### 4.2 Structure of Simulation

In this research, we used “SOUND (a Simulation model On Urban Networks with Dynamic route choice)” that is a macro traffic flow simulator correspond to a large-scale road network developed at the University of Tokyo [4, 5].

Figure 3 shows the structure of simulation. The outlines are as follows.

- Reproduce the traffic flow in the simulation by using input data for one weekday from 4:00 am to 3:59 (see next chapter in detail).
- Traffic simulator output the chosen route of individual vehicle, link traffic volume for every second, and link travel time for every second.

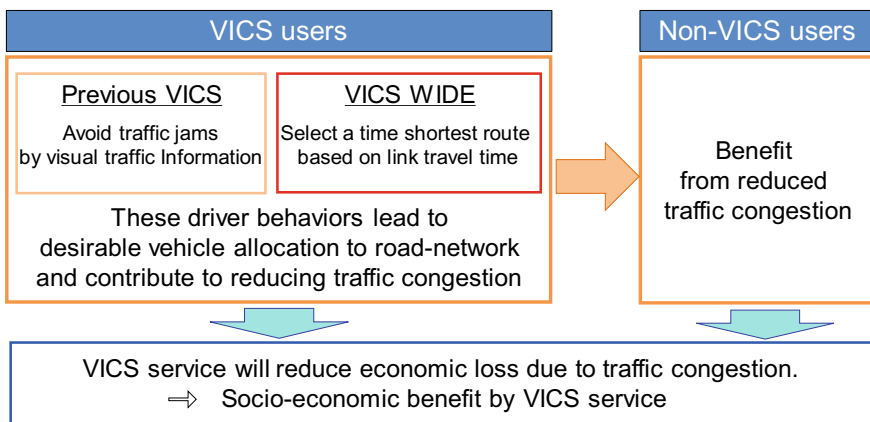


Fig. 2 Framework of social benefit

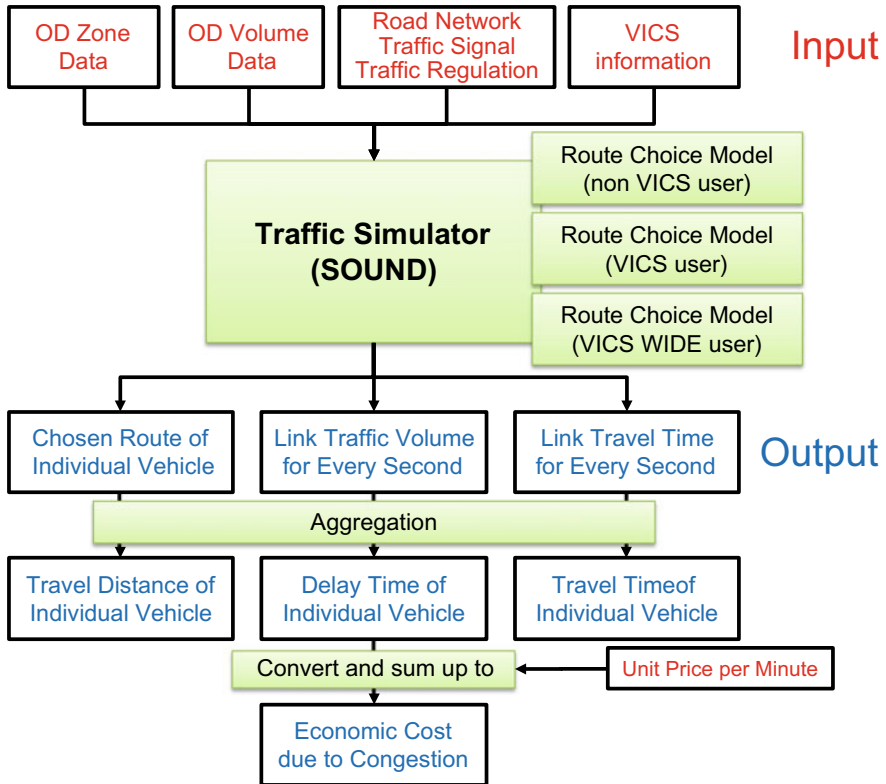
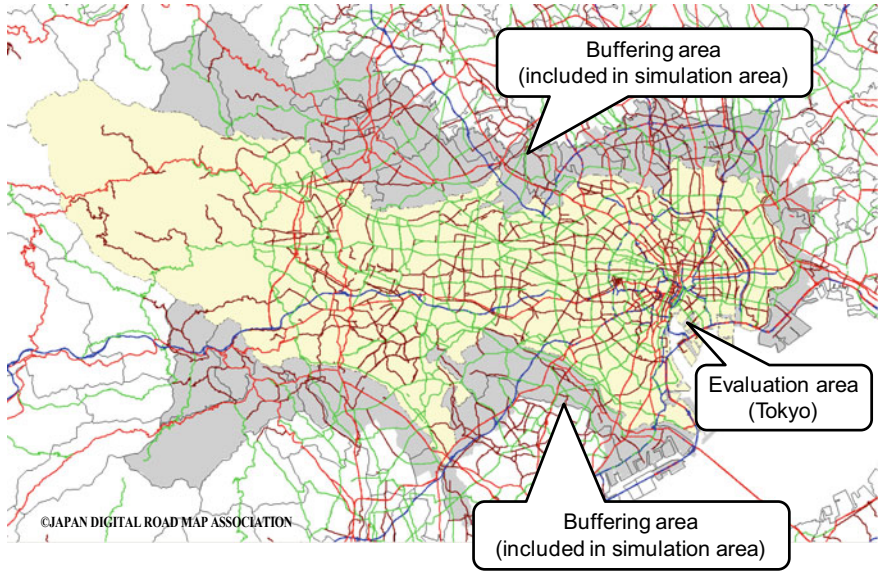


Fig. 3 Structure of simulation

- Calculate the delay time for individual vehicle by tracing chosen route.
- Convert delay time into economic traffic cost of each vehicle by using the “unit price per minute”, and sum the amount.  
The above “unit price per minute” is defined in “cost benefit analysis manual [6]” issued by MLIT (Ministry of Land, Infrastructure and Transport). This value is roughly 40 JPY/minute for general vehicles, and from 45 to 370 JPY/minute for commercial vehicles by type.
- In accordance with the spread scenario of VICS WIDE service, Change the percentage of previous VICS users and/or VICS WIDE users, simulate again, and calculate economic traffic cost again.
- Find the difference between both economic traffic costs and estimate the socio-economic benefit of VICS WIDE.

Simulation scale is as follows.

- Simulation area is Tokyo Metropolis and buffering area; see Fig. 4
- The road network is composed of all roads with a road width of 5.5 m or more. The total length of road network is 14,734 km.



**Fig. 4** Simulation area (Tokyo Metropolis and buffering area)

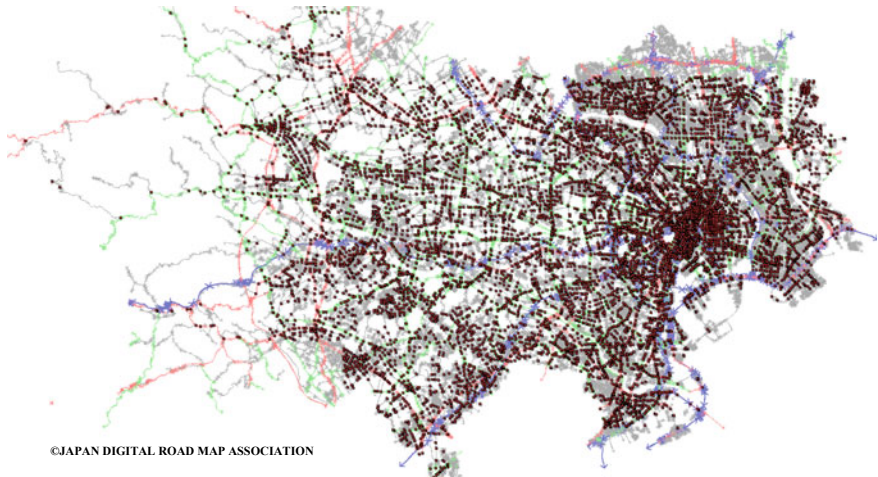


**Fig. 5** Traffic control signals in simulation area

- Approximately 12,000 traffic control signals existing in the above-mentioned road network; see Fig. 5.  
The signal control parameters applied typical static values for all signals.

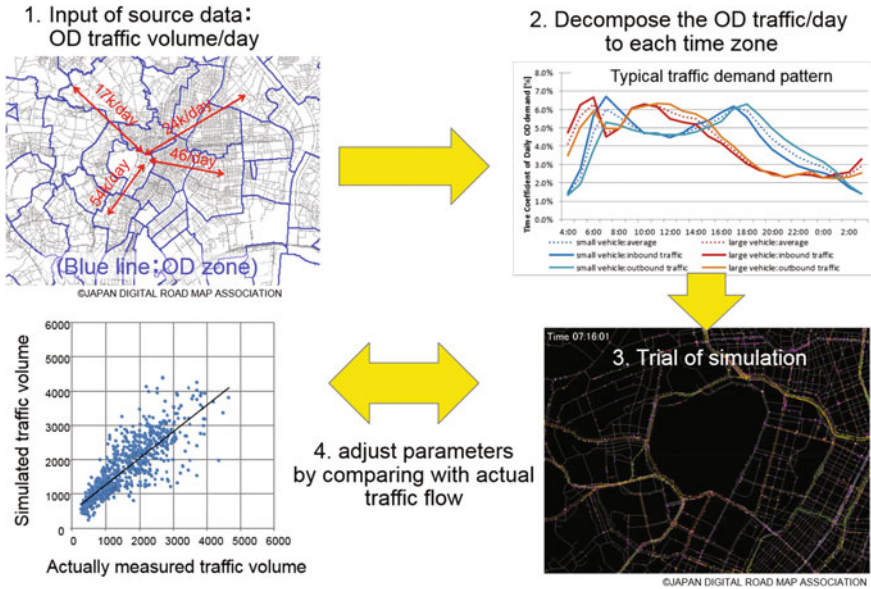


Fig. 6 Reproduction steps of traffic flow

### 4.3 Reproduction of Traffic Flow on Simulation

Reproduction steps of traffic flow is as follows; see Fig. 6.

- 1st step, source data is inputted to the simulation. Source data of traffic flow is “OD (origin destination) traffic volume per day” and “geographical OD zone data”. These data are part of “road traffic census” that is carried out every five years in Japan [7].
- 2nd step, OD traffic volume per day is decomposed to each time zone by referring to the typical traffic demand pattern.
- 3rd step, trial of simulation is done. Each vehicle is generated according to the occurrence probability at origin zone, and moves to destination zone for each. At this time, the classification of VICS user is assigned to each vehicle by using random numbers, and each vehicle selects the route according to the policy of that classification.

The classification of VICS user is shown in Table 1.

- Above process is done from 4:00 AM to 3:59 AM at next day. The reason that 4:00 AM was chosen is because the traffic volume is the smallest in the day. Congestion occurs on roads where vehicles are concentrated, depending on the traffic flow theory. The road capacity and free flow speed is determined by the road structure and road attributes.



**Table 1** Classification of the users

Classification	Description
Non VICS users	<ul style="list-style-type: none"> <li>• In principle, the path is selected without considering the traffic congestion. But some vehicles avoid heavy congestion (assuming use of radio, information board, etc.)</li> <li>• Logit-based route choice model</li> </ul>
Previous VICS users	<ul style="list-style-type: none"> <li>• Select a path based on visual congestion information of VICS information and avoid heavy traffic congestion.</li> <li>• Logit-based route choice model</li> </ul>
VICS WIDE users	<ul style="list-style-type: none"> <li>• Select a time shortest path based on the link travel time and traveling time for each direction at intersection</li> </ul>

**Table 2** Reproducibility of traffic flow

Comparison item	Simulation value	Benchmarks		Reproducibility
		Value	Reference	
Vehicle-kilometers	62.9 million	66.3 million	Road traffic census (2010)	Good
Traffic volume by time zone at representative points	See Fig. 8 Correlation Coefficient 0.82		Road traffic census (2010)	Almost good
Economic traffic cost amount in Tokyo (JPY/year)	0.6 trillion	1.2 trillion	Report by MLIT (2005)	Less than benchmarks

- 4th step, adjust parameters by comparing the simulated traffic volume of each time zone at reprehensive point with actual measured traffic volume and try again until both traffic flow agrees.

Figure 7 shows the example of traffic flow on simulation. Each dot on the road is individual vehicle.

Reproducibility of traffic flow on simulation is shown in Table 2 and Fig. 8

Vehicle-kilometers is good, and traffic volumes by each time zone at representative points are almost good like Fig. 8. However, it must be noted that the total economic cost of congestion is underestimated comparing to the report by MLIT in 2005.

We think that the traffic jam in tsimulation is less than the actual one for some reason. It must be improved in the future.

## 5 Estimation Result of Socio-Economic Benefits

Table 3 shows the test scenario and Fig. 9 shows the simulation result. Reproduced state is scenario 1 and current situation before deploying VICS WIDE is scenario 2.

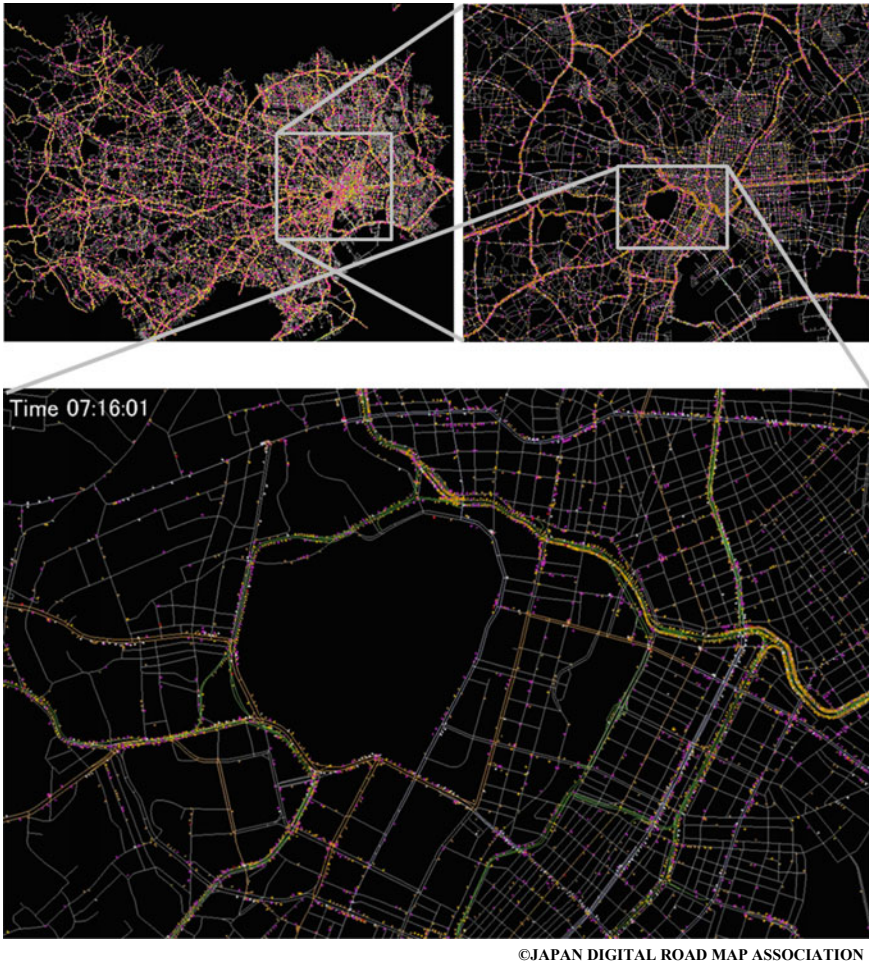
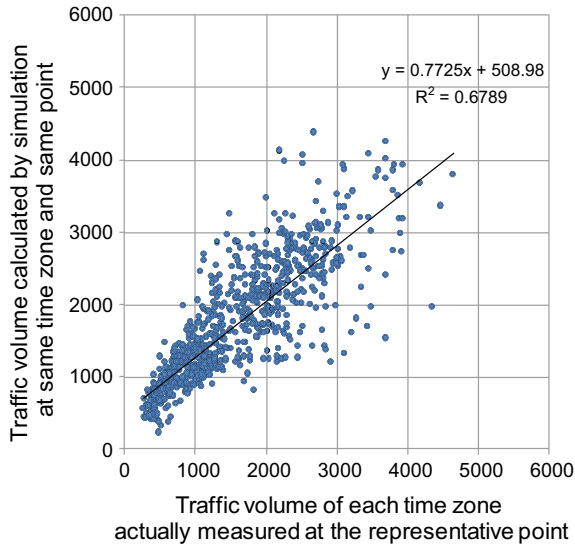


Fig. 7 Overview of simulation

The percentage of previous VICS users in scenario 2 was estimated from the number of past shipments of VICS units and retained motor vehicles. Large-size vehicles rarely have car navigation unit, so all are regarded as non-users of VICS service.

Scenario 4 assumes a time when VICS WIDE is fully popular in the future, and it also serves as an investigation of the occurrence of the traffic concentration phenomenon. Even if the VICS WIDE on-board units are installed in all vehicles, some drivers do not refer to real-time traffic information, so it is estimated that the number of users of VICS WIDE will not exceed 70% over the future.

Figure 9 show that the previous VICS service has reduced the economic cost of traffic congestion by about 12% (scenario 2). By replacing with VICS WIDE, it could



**Fig. 8** Traffic volume of simulation results and actually measured

**Table 3** Test scenario of VICS/VICS WIDE widespread situation

Scenario no.	Description	Non VICS users (%)	Previous VICS users (%)	VICS WIDE users (%)
1	Before deploying VICS System	100	0	0
2	1st year of VICS WIDE (previous VICS deployed)	70	30	0
3	All VICS units are replaced to VICS WIDE	70	0	30
4	Further growth of VICS WIDE	30	0	70

be reduced further by 8% from now (scenario 3), and furthermore, if VICS WIDE gets more popular in the future, we can get 11% reduction (scenario 4).

In this research, traffic concentration did not occur even in scenario 4. This is considered that some vehicles select urban narrow streets without traffic information when avoiding congestion in a complex urban road network, so traffic concentration on unoccupied (guided) roads has been relieved.

Individual user benefit is shown in Fig. 10. This bar graph is the average travel time per one trip for each classification in each scenario. Figure 10 is in good agreement with Fig. 2. That is to say, previous VICS user’s benefit is greater than non-VICS

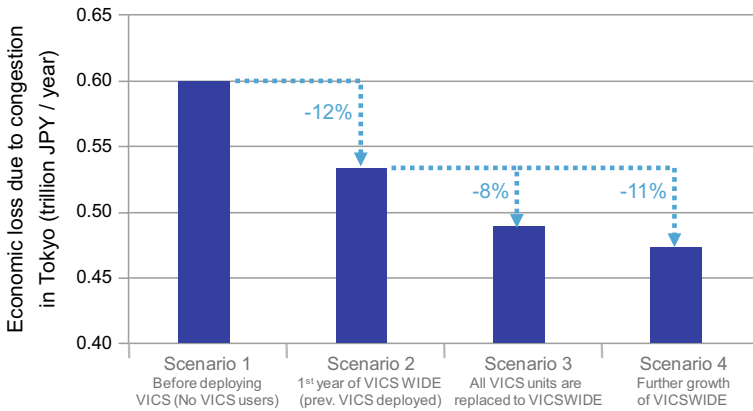


Fig. 9 Estimation result of socio-economic benefits

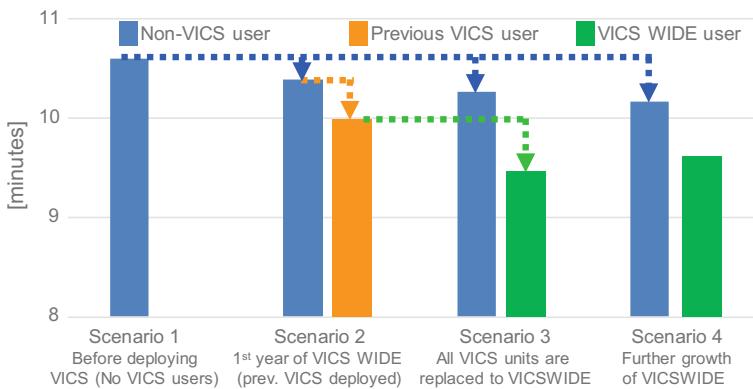


Fig. 10 Average travel time per trip of each classification

user’s benefit (see orange dotted line), VICS WIDE user’s benefit is greater than previous VICS user’s benefit (see green one). Also non-VICS user can get benefit as VICS WIDE user spread (see blue one).

In comparison between scenarios 3 and 4, it is indicated that the benefits of VICS WIDE users are slightly decreased along with the further popularization of VICS WIDE users due to the progress in properly allocating traffic flows.

Figure 11 shows the picture that traffic jam is gradually decreasing as VICS WIDE users increase.



Fig. 11 Example of traffic congestion on simulation

## 6 Conclusion

In April 2015, VICS center added VICS WIDE service aiming at further advancement of VICS service, and traffic information has been improved for more useful DRGS.

We estimated the socio-economic benefits of VICS WIDE service by using traffic flow simulation. The characteristic of this research is that it was done by using traffic simulation with near-reality traffic demand data and road network data.

According to the simulation result, previous VICS service has reduced 12% of economic cost of traffic congestion. Moreover, along with the VICS WIDE service spread, economic traffic cost will be further reduced by about 10%.

Also, congestion loss due to traffic concentration caused by traffic information that was pointed out in the past research did not occur even when the VICS WIDE user reached 70%. This is considered that in a complex urban road network including narrow streets without traffic information, some vehicles select such narrow streets when avoiding congestion, so traffic concentration on unoccupied roads has been relieved.

Analysis of the benefits of individual users confirmed the superiority of VICS WIDE users and previous VICS users, and it was confirmed that non-VICS users also benefit by spreading of VICS user.

## References

1. Mahmassani, H.S., Jayakrishnan, R.: System performance and user response under real-time information in a congested traffic corridor. *Transp. Res. Part A Gen.* **25**, 293–307 (1991)
2. Oguchi, T., Satoh, T., Katakura, M., Shikata, S.: Analysis of traffic congestion and route choice behavior influenced by traffic information. *Int. J. ITS Res.* **1**(1), 75–82 (2003)
3. Chen, Shuwei, Lili, Du: Simulation study of the impact of local real-time traffic information provision strategy in connected vehicle systems. *Int. J. Transp. Sci. Technol.* **6**, 229–239 (2017)
4. Yoshii, T., Kuwahara, M.: SOUND: A traffic simulation model for oversaturated traffic flow on Urban expressways. In: Preprint at 7th World Conference on Transportation Research, Sydney (1995)
5. Oguchi, T., Chikaraishi, M., Iijima, M., Oka, H., Horiguchi, R., Tanabe, J., Mohri, Y.: Advanced simulation model in the region of Tokyo metropolitan urban expressway rings. In: 23rd ITS World Congress, Melbourne (2016)
6. Cost benefit analysis manual: Ministry of Land, Infrastructure and Transport (MLIT) (2008)
7. Road traffic census: Japan Society of Traffic Engineers (JSTE) (2012)

# Explore User Behavior of the Taipei Bikesharing System via Electronic Payment Service Data



Chih-Lin Chung and Shu-Yuan Li

**Abstract** This paper identifies user behavior of the Taipei bikesharing system, YouBike, along with the trip chain between YouBike and Taipei mass rapid transit (MRT). The one-month data from the electronic payment service (EPS) provider contain 1,540,846 YouBike rides and 56,870,619 MRT rides. Data processing techniques and descriptive statistics were applied via SAS<sup>®</sup>. The results show that among the 407,935 YouBikers, 82.97% were casual users (defined as those with 5 or less monthly rides), 14.53% were constant users (6–20 rides), and 2.50% were loyal users (more than 20 rides). 41.35% of the YouBike rides were made by the casual users, 38.61% by the constant users, and 20.04% by the loyal users. 35.90% of the users rode YouBike to or from the MRT stations at least once a month. 23.72% of the YouBike rides complemented MRT by serving as the first- or last-mile feeder mode of MRT. The casual users tended to ride YouBike on the weekends for the leisure purpose, and the loyal and constant users tended to ride YouBike on the weekdays for commuting. YouBike was particularly welcomed by students and general adults. As YouBike has passed its growth peak and is now in the mature phase, it is suggested that the transportation authority provide incentives to encourage existing and potential users.

**Keywords** Bikesharing · Public bike system · Electronic payment service · User behavior

## 1 Introduction

In 2009 Taipei launched its public bike system, also known as YouBike. As a new transportation service, YouBike experienced a difficult introduction stage due to the limited amount of bike stations and complicated rental process. The city government

---

C.-L. Chung (✉) · S.-Y. Li

Department of Transportation Management, Tamkang University, New Taipei City, Taiwan  
e-mail: [cchung@mail.tku.edu.tw](mailto:cchung@mail.tku.edu.tw)

S.-Y. Li

e-mail: [a0985653438@gmail.com](mailto:a0985653438@gmail.com)

© Springer Nature Singapore Pte Ltd. 2019

T. Mine et al. (eds.), *Intelligent Transport Systems for Everyone's Mobility*, [https://doi.org/10.1007/978-981-13-7434-0\\_26](https://doi.org/10.1007/978-981-13-7434-0_26)



**Fig. 1** YouBike station locations and equipment. *Source* compiled from <http://www.youbike.com.tw>

fixed the drawbacks and initiated a revised system three years later. YouBike started to gain its popularity in Taipei since then, and soon spread out all over the country. As of July 2018, YouBike is available in seven local cities; Taipei has 400 YouBike stations and 2.5 million monthly rides while the other six cities have 1,153 stations and 4.8 million monthly rides. The bike, dock, panel, and station locations in Taipei are shown in Fig. 1. The YouBike system is run by the world leading bicycle manufacturer, Giant. Equipped with a three-stage derailleur, comfortable saddle, wheel-driven LED front and tail light, etc., the quality of the bike is superior to regular products on the market. In addition, the patented dock design allows two bikes using one column; this reduces the construction cost and utilizes space more effectively. For the operational performance, each bike is checked out approximately from 4 to 7 times per day in Taipei. Riding YouBike has become not just a travel choice but an urban fashion.

Successful bikesharing and other transportation systems rely, to some degree, on the implementation of electronic payment services (EPS). It enhances the payment efficiency for both service users and providers. Another benefit of EPS is the availability of transaction records regarding every ride. Some cities offer real-time or historical data of bikesharing station status—the number of remaining bikes at the station—for web scraping. Quite a few research [1–3] were in light of such time-series “station-based” big data. Typical station-based analysis includes station performance (with respect to available bikes, available docks, and neighboring land



use), spatial and temporal ridership, etc. Some other cities release their historical bikesharing (ride) transaction data to the public for free downloading. The data usually contain such columns as start time, start station, end time, end station, and the amount of rental fees. An increasing number of research [4–6] have been supported by such “ride-based” big data. Typical ride-based analysis involves spatial and temporal trip distribution, travel duration, estimated travel distance, cost, and so on. If the user identity (in the form of the transportation smart card number) of each ride is accessible, the ride-based analysis can explore more characteristics, including ride frequency and trip chain. We refer this type to the “user-based” or “advanced ride-based” data; it allows all of the ride-based analyses, and can yet report user characteristics.

The principal idea of YouBike as well as many public bike systems in the world is to offer the first- and last-mile service for public transit. Therefore, every mass rapid transit (MRT) station in Taipei has at least one YouBike station nearby. It meanwhile raises the concern that YouBike may replace some short MRT trips. MRT and YouBike are potentially in cooperation. The research objective is thus to verify the characteristics of YouBike trips by various user types in Taipei City. The findings will be helpful for the authorities to position YouBike among the urban transport modes.

## 2 Data Processing

In Taiwan, people can use one smart card such as EasyCard, iPASS, and iCASH for most transport services around the country. The card issuers hold the transaction records in their backend ticketing platforms. Our raw data were purchased from the EasyCard Corporation—the largest local smart card issuer with around 60 million cards in circulation (as of October 2017). That means everyone in the island held 2.6 cards on average. Our data consist of one-month ride transactions in two separate files—one for YouBike and the other for Taipei MRT. All of the transactions occurred in November 2016. Back then, Taipei City had 272 YouBike stations (now 400) and there were 117 MRT stations in the metropolitan area (unchanged since then). The average temperature of the month in Taipei was 22.6 degrees Celsius along with limited rainfall. The decent weather condition kept the YouBike ridership stable in comparison with other months during that period. In other words, the weather factor is not a concern in this study.

The YouBike file originally stored 4,004,750 records. The data columns include the card number, card type (regular, student, elderly, etc.), checkout station, return station, return time, and rental fee. The Taipei MRT file originally stored 57,885,541 records. The data columns include the card number, card type, origin station, destination station, station departure time, and transit fare. Note that due to the data integration gap of the card issuer, neither the YouBike checkout time nor the MRT station arrival time was available in the raw data. However, such information is essential for analyzing transfers between YouBike and MRT. To deal with the issue,

**Table 1** Taipei YouBike progressive rental fees

a. Rental fee (NT\$) from the raw data	b. Rental duration (min)	c. Fees per 30 min	d. Estimated riding time (min) set to be the maximum rental duration
5	<30	NT\$ 5*	30
15, 25, ..., 65, 75	30–240	NT\$ 10	60, 90, ..., 210, 240
95, 115, ..., 215, 235	240–480	NT\$ 20	270, 300, ..., 450, 480
275, 315, ...	>480	NT\$ 40	510, 540, ...

*Note* Starting from April 2018, the first 30-min rental is free of charge given a transfer to or from public transit (MRT or buses). Otherwise a fee of NT\$ 5 applies. During our study period (Nov. 2016), users paid NT\$ 5 for the first 30 min regardless of a transfer or not

we associated the YouBike rental fee with the estimated riding time based on the fee-time lookup table, as shown in the columns (a) and (d) of Table 1. The YouBike checkout time can then be calculated via Eq. (1). Secondly, we collected the travel time of each MRT station pair announced by the MRT Corporation. The MRT arrival time can be calculated via Eq. (2) that set the station dwell time as 5 min.

$$\text{YouBike: checkout time} = \text{return time} - \text{estimated riding time} \quad (1)$$

$$\text{MRT: station arrival time} = \text{station departure time} - \text{travel time} - \text{dwell time} \quad (2)$$

In addition, we assume that every individual consistently uses one card throughout the study period. The YouBike file alone can capture the user frequency and ride characteristics for further marketing strategy making. The YouBike file can link the MRT file through the card number. The joint data reveal the transfer behavior by associating the checkout time and the return time of each bike ride with its upstream or downstream MRT ride, if any. We follow the time span of the city government that defines a transfer as two trips no more than one hour apart. Therefore, when an MRT ride is beyond one-hour earlier or later than its consecutive YouBike ride (or vice versa), they are regarded as two independent trips.

The data cleansing process filtered out the non-Taipei rides, the transactions involved in irregular travel costs, and the outliers with extremely high fees or frequency of use. As a result, 1,540,846 YouBike rides remained, accounting for 89.29% of the Taipei YouBike ridership; 56,870,619 MRT rides remained, accounting for 98.25% of the Taipei MRT ridership.

### 3 Results and Discussion

To identify the YouBike user characteristics, we classified those with 5 or less monthly rides as casual users, those with 6 to 20 monthly rides as constant users, and otherwise loyal users. Among the 407,935 YouBikers, 82.97% were casual users, 14.53% were constant users, and 2.50% were loyal users; in terms of 1,540,846 rides, 41.35% were made by the casual users, 38.61% were by the constant users, and 20.04% were by the loyal users, as shown in Fig. 2 and Table 2. Each user on average rode YouBike for 3.78 times per month. 5 and 21 monthly rides were arbitrarily set as the boundaries of the three user types, they approximately respond to 1 and 5 weekly rides. The city authority may adjust the lower boundary to 4 (or 6) monthly rides, and the upper boundary to 20 (or 22) monthly rides, for example. Table 3 shows the result of the above adjustment. Lower boundary performs a more sensitive impact on the casual users than the upper boundary on the loyal users. Given the adjusted lower boundary, the casual user percentage would decrease (or increase) from 82.97 to 79.00% (or 85.88%), and its ride percentage would decrease (or increase) from 41.35 to 36.09% (or 45.96%). Given the adjusted upper boundary, the loyal user percentage would slightly increase (or decrease) from 2.50 to 2.77% (or 2.26%), and its ride percentage would also slightly increase (or decrease) from 20.04 to 21.47% (or 18.72%).

In terms of the card type, the majority were the regular card holders who accounted for 64.98% of the total YouBikers. However, the student group was the most active users. Such an argument is supported by the following facts. First, according to the statistics in 2017, the number of students at middle school and above accounted for only 11.62% of the total population in Taipei, but the student YouBikers were the second largest among different card types, as shown in Table 4. Second, Table 4

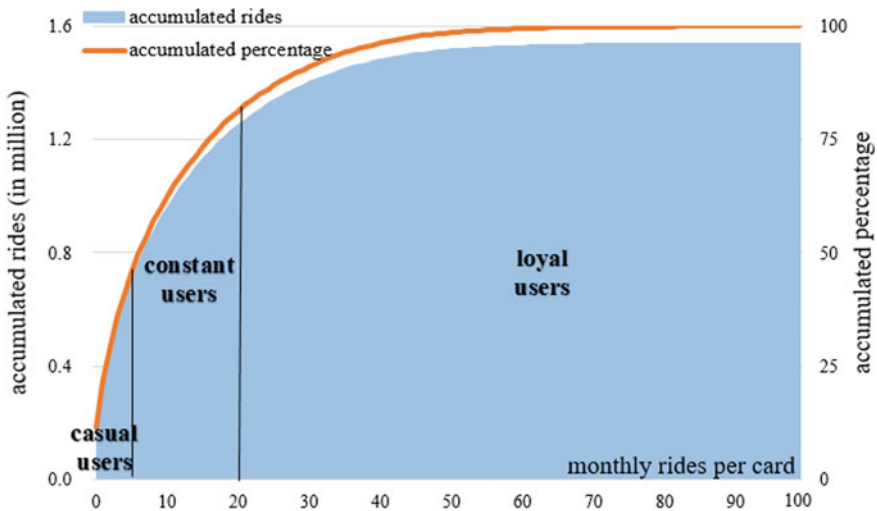


Fig. 2 Accumulated rides and percentage of YouBike rides by user type

**Table 2** Number of users and number of monthly rides by user type

	Casual user ( $\leq 5$ rides)	Constant user (6–20 rides)	Loyal user ( $\geq 21$ rides)	Total
No. of users	338,478 (82.97%)	59,270 (14.53%)	10,187 (2.50%)	407,935 (100%)
No. of monthly rides	637,070 (41.35%)	594,961 (38.61%)	308,815 (20.04%)	1,540,846 (100%)
No. of monthly rides per user	1.88	10.04	30.31	3.78

**Table 3** Sensitivity of the boundaries with respect to the number of users and monthly rides

	Casual user ( $\leq 4$ rides)	Casual user ( $\leq 6$ rides)	Loyal user ( $\geq 20$ rides)	Loyal user ( $\geq 22$ rides)
No. of users	322,271 (79.00%)	350,329 (85.88%)	11,287 (2.77%)	9,217 (2.26%)
No. of monthly rides	556,035 (36.09%)	708,176 (45.96%)	330,815 (21.47%)	288,445 (18.72%)
No. of monthly rides per user	1.73	2.02	29.31	31.29

also presents that the students tended to be more of the loyal or constant users than of the casual users. Third, the official operational report by the YouBike Corporation constantly reveals that 3 out of the most popular 5 YouBike stations are next to universities. On the other hand, the percentage of 65+ year-old usage (0.80%), as expected, was much lower than the percentage of elderly population in Taipei (13.88%). The number of rides by card type and user type in Table 5 presents similar information as Table 4. But interestingly, the monthly rides per card were not much different among the card types, ranging from 3.58 to 3.96, albeit the student card had a relatively greater frequency. Table 4 shows a limited amount of elder YouBikers while Table 5 indicates that once the elderly become YouBikers, they may ride as frequently as, if not more than, the regular card holders.

Risks factors associated with elderly cycling include poor vision, reduced muscle strength, and declining cognition [7]. It is suggested that the authority target the existing regular and student YouBikers to boost their usage. Meanwhile, the authority should try to create new users. An effective way would be the fare integration among public transit. The city government has been implementing a joint monthly pass for buses, MRT, and YouBike since mid-April, 2018. It immediately increased the YouBike ridership in the following months. The monthly pass benefits the ridership of buses and MRT as well. Other promotions in the city include draws of meal coupons for those using YouBike for 11 or more days in the month, and free coffee for YouBikers on Friday morning commuting hours. Although there are safety concerns regarding elderly cycling, the seniors' right to cycling must not be deprived. Some interventions could be taken to prevent elderly cycling accidents (see [7]).

**Table 4** Number of users by card type and user type

	a. Casual user	b. Constant user	c. Loyal user	d. Total
Regular card (column %; row %)	221,550 (65.45%; 83.58%)	37,173 (62.72%; 14.02%)	6,337 (62.21%; 2.39%)	265,060 (64.98%; 100%)
Student card (column %; row %)	107,425 (31.74%; 81.64%)	20,576 (34.72%; 15.64%)	3,589 (35.23%; 2.73%)	131,590 (32.26%; 100%)
Elderly card (column %; row %)	2,688 (0.79%; 82.08%)	525 (0.89%; 16.03%)	62 (0.61%; 1.89%)	3,275 (0.80%; 100%)
Others (column %; row %)	6,815 (2.01%; 85.08%)	996 (1.68%; 12.43%)	199 (1.95%; 2.48%)	8,010 (1.96%; 100%)
Total (column %; row %)	338,478 (100%; 82.97%)	59,270 (100%; 14.53%)	10,187 (100%; 2.50%)	407,935 (100%; 100%)

**Table 5** Number of monthly rides by card type and user type

	a. Casual user	b. Constant user	c. Loyal user	d. Total	e. Monthly rides per card
Regular card (column %; row %)	414,573 (65.07%; 42.36%)	371,815 (62.49%; 37.99%)	192,343 (62.28%; 19.65%)	978,731 (63.52%; 100%)	3.69
Student card (column %; row %)	205,065 (32.19%; 39.35%)	207,888 (34.94%; 39.89%)	108,187 (35.03%; 20.76%)	521,140 (33.82%; 100%)	3.96
Elderly card (column %; row %)	5,038 (0.79%; 40.87%)	5,309 (0.89%; 43.06%)	1,981 (0.64%; 16.07%)	12,328 (0.80%; 100%)	3.76
Others (column %; row %)	12,394 (1.95%; 43.26%)	9,949 (1.67%; 34.73%)	6,304 (2.04%; 22.01%)	28,647 (1.86%; 100%)	3.58
Total (column %; row %)	637,070 (100%; 41.35%)	594,961 (100%; 38.61%)	308,815 (100%; 20.04%)	1,540,846 (100%; 100%)	3.78

Note Column (e) is from column (d) of this table divided by column (d) of Table 4

YouBike in Taipei adopts progressively increasing rental fees, as shown previously in Table 1. Table 6 lists the percentiles of travel cost (rental fees). It is found that (1) regardless of the user type and weekdays or weekends, the majority of rentals were within 30 min, (2) the weekend rentals had a longer duration than the weekday rentals, and (3) for 95- and 99-percentiles of travel cost, the loyal users were the lowest, the constant users were in the middle, and the casual users were the highest.

**Table 6** Travel cost (in NT\$) by user type

Percentile	Casual user		Constant user		Loyal user	
	Weekday	Weekend	Weekday	Weekend	Weekday	Weekend
99	65	75	45	55	35	45
95	35	45	25	25	15	25
75	5	15	5	5	5	5
50	5	5	5	5	5	5

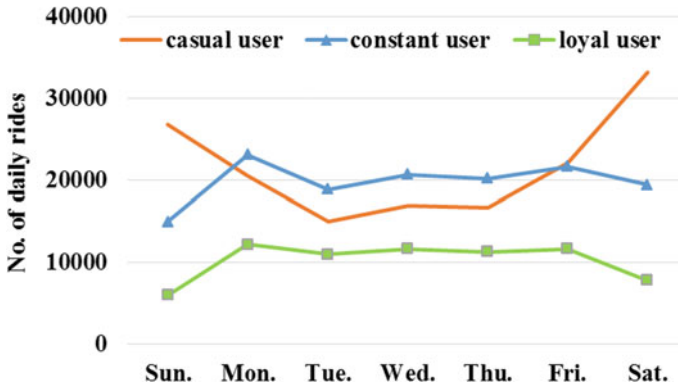


**Fig. 3** No. of rides by user type and day of week

These findings justify the weekday rides for short-distance daily commutes, and the weekend rides for the leisure purpose with longer rental duration in general.

Figure 3 further identifies the characteristics of each user type. The casual users primarily rode YouBike on the weekends, while the other two types were mainly weekday users. Figure 4 shows that the constant and loyal users had different amounts of weekday rides but similar usage patterns throughout the day. On the weekdays, there were noticeable AM (8–9) and PM (18–19) peaks as well as mini noon (12–13) and evening (21–22) peaks. As for the casual users, there were one noticeable PM peak and three mini AM, noon, and night peaks. Figure 5 shows that on the weekends, the casual and constant users presented a PM (17–18) peak, but the loyal users had flat YouBike usage. Overall speaking, the characteristics of the casual users were found quite different from those of the loyal users. The constant users performed somewhere in between. The loyal and constant users tended to be weekday commuters, and the casual users tended to ride YouBike on the weekends.

Another item of interest is the transfer behavior between YouBike and MRT. As shown in Table 7, among the 1,540,846 YouBike rides, 160,415 (10.41%) were the first-mile feeder service of MRT, or YouBike to MRT (Y2M). Proportionally, more rides were by the loyal users (12.44%) and constant users (10.40%) than by the casual users (9.43%). 205,146 rides (13.31%) were the last-mile feeder service of MRT, or MRT to YouBike (M2Y). Proportionally, more rides were generated by the

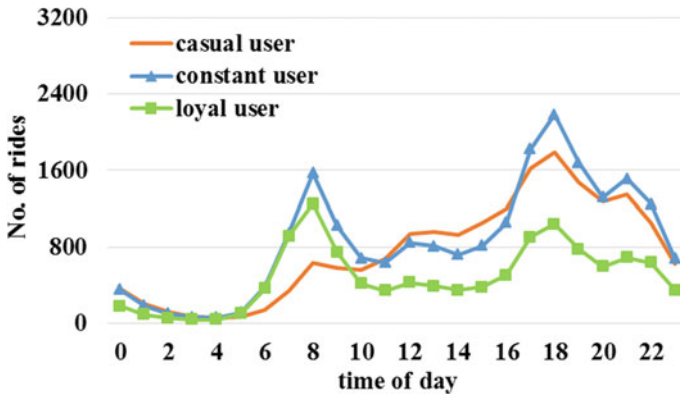


Fig. 4 No. of weekday rides by user type and time of day

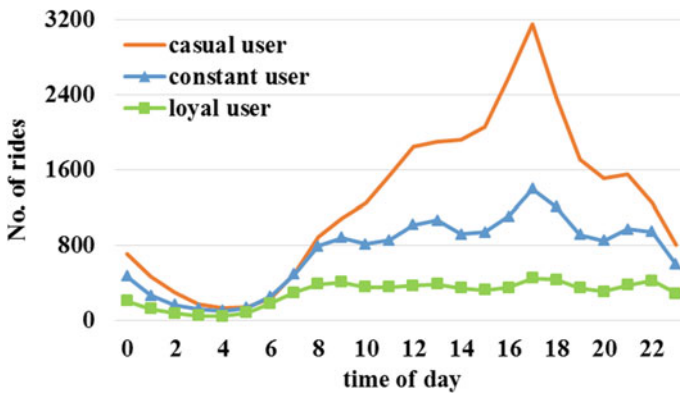


Fig. 5 No. of weekend rides by user type and time of day

constant users (13.72%) and loyal users (13.56%) than by the casual users (12.82%). The results can extend the above argument to be that the loyal and constant users tended to be weekday commuters who made transfers between YouBike and MRT frequently. Besides, it appears that the M2Y rides (205,146) were greater than the Y2M rides (160,415). The M2Y rides are likely in the evening/afternoon when people get off work/school and use YouBike in a relaxed manner for going home, exercising, shopping, or other purposes. Sweating is not a concern for M2Y once they are home. Y2M, on the contrary, are more likely in the morning rush and people may worry about the odor after cycling. Therefore, M2Y more popular than Y2M matches the general understanding.

Aggregately, 23.72% of the YouBike rides were about MRT connection. YouBike in this case enhanced the accessibility of Taipei MRT and to a certain degree accomplished its original purpose. Since 74 out of the 272 YouBike stations were next to the MRT stations, some people would choose YouBike instead of MRT, especially

**Table 7** YouBike monthly rides to or from MRT stations

	Casual user	Constant user	Loyal user	Total
a. No. of rides	637,070	594,961	308,815	1,540,846
b. No. of Y2M rides	60,104	61,883	38,428	160,415
c. Y2M ride ratio (=b/a)	9.43%	10.40%	12.44%	10.41%
d. No. of M2Y rides	81,661	81,621	41,864	205,146
e. M2Y ride ratio (=d/a)	12.82%	13.72%	13.56%	13.31%
f. No. of transfers (=b+d)	141,765	143,504	80,292	365,562
g. Transfer ratio (=f/a)	22.25%	23.12%	26.00%	23.72%

**Table 8** YouBike users to or from MRT stations

	Casual user	Constant user	Loyal user	Total
a. No. of users	338,478	59,270	10,187	407,935
b. No. of Y2M users	53,975	22,964	5,663	82,602
c. Y2M user ratio (=b/a)	15.95%	38.74%	55.59%	20.25%
d. No. of M2Y users	71,724	26,636	5,852	104,212
e. M2Y user ratio (=d/a)	21.19%	44.94%	57.45%	25.55%
f. No. of transfer users	106,427	33,192	6,826	146,445
g. Transfer ratio (=f/a)	31.44%	56.00%	67.01%	35.90%

for short-distance travel. In fact, 133,184 YouBike rides (8.64%) had both ends next to the MRT stations; such travel demand could have been served by Taipei MRT. YouBike in this case is a competitor against Taipei MRT. Fortunately, YouBike trips were more to connect MRT (23.72%) than to replace MRT (8.64%). In addition, the average ridership of Taipei MRT is around 60 million passengers per month. The competing YouBike rides (0.13 million per month) had very limited impacts on the MRT operation.

In terms of the 407,935 users, 82,601 (20.25%) rode YouBike to reach the MRT stations while 104,212 (25.55%) rode YouBike to leave the MRT stations, as shown in Table 8. Aggregately, 146,445 (35.90%) users rode YouBike to or from the MRT stations at least once in the study month. Proportionally, more loyal users (67.01%) treated YouBike as the first- and last-mile mode of MRT, followed by the constant users (56.00%), and the casual users were the lowest (31.44%). Note that one can simultaneously be a Y2M and M2Y user. The row (f) in Table 8 is not a simple addition of rows (b) and (d) as it is in Table 7.

Figure 6 depicts the top 10 bidirectional transfer stations. Y2M and M2Y stations were very similar, indicating an overall symmetric pattern that people had Y2M in the morning and M2Y in the afternoon/evening. Although the three user types resulted in somewhat different ranking of the transfer stations, many transfer stations overlapped with one another. The downtown area did not perform strong YouBike-MRT transfer demand. The possible reason is that both YouBike and MRT have a denser network.



Taking one single mode can reach most downtown places. There is no need to make a transfer in this case. Once out of downtown, transfer demand pops up. Transfers at Zhishan station, for example, ranked no. 2 for the causal and constant users, and no. 1 for the loyal users. The city government is planning to build an east-west light rail transit (LRT) that connects the north-south MRT line at Zhishan station. Travel demand is significant along the LRT line, and currently some are served by YouBike. Another type of transfer occurs next to the university, such as Gongguan station that ranked no. 1 for the causal and constant users, and no. 2 for the loyal users. Since Y2M and M2Y usually happen in different times of day, imbalanced YouBike traffic is expected. More bikes should be evacuated from the Y2M stations and delivered to the M2Y stations. Figure 6 helps identify the stations with bike reallocation of great concern.

## 4 Conclusions

Since its first launch in 2009, YouBike has experienced the introduction stage and growth stage. In the past two years, the daily turnover rate per bike in Taipei was between 7.2 and 4.4, as shown in Fig. 7. It indicates that YouBike, if not heading for the decline stage, is likely in the mature stage after the completion of 400 stations in 2017. This study is a pioneer research that adopted user-based bikesharing data to identify user characteristics. It should be noted that the results based on the EPS big data could be quite different from those based on the conventional surveys. For example, YouBike rides by student users accounted for 34% in this study, but the number was 42% in another study [8] that system sampled 1200 YouBikers. Other noticeable distinctions between these two studies include the percentages of casual, constant, and loyal users, the percentages of YouBike rides as the first- or last-mile feeder service of MRT, and so on. As the advance of ITS, transportation big data have become more accessible. Such big data can capture the characteristics of the population. Future decision-making should thus be based on information derived from big data instead of that from sampled data analysis.

The bikesharing characteristics found in this study enable the administrative and operational authorities to market YouBike in an accurate way. First, the casual users accounted for over 80% of the total YouBikers, but they only rode YouBike for less than twice per month. There is a huge potential of ridership growth in this user type. As the casual users tended to ride YouBike on the weekends for a longer time, more incentives can be considered to encourage their weekday use of YouBike. For example, any card with 5 rentals on weekdays can earn a free weekend YouBike for one hour. Second, the constant and loyal users tended to ride YouBike on the weekdays. The incentive exemplified above can also benefit them. Many of these two user types treated YouBike as the MRT feeder mode. The transportation authority should ensure at a safe and friendly cycling environment not only on the major roads but also minor streets that connect MRT stations.

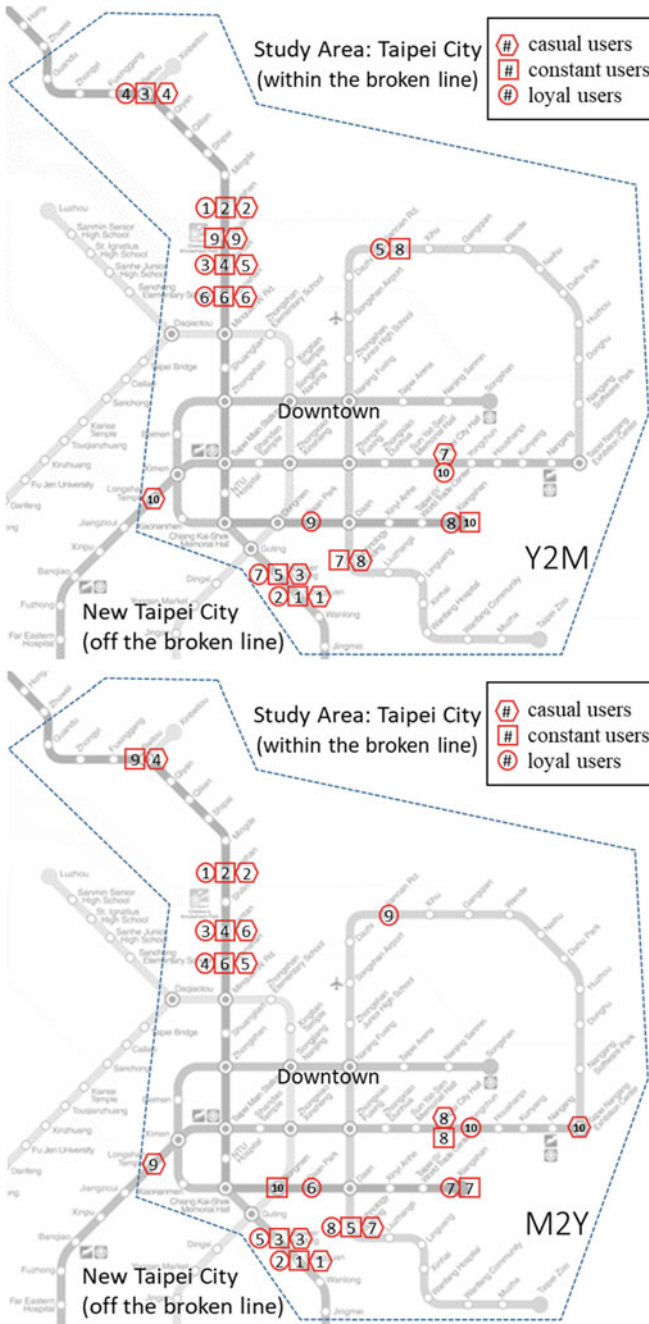


Fig. 6 Top 10 YouBike transfer stations (upper one: Y2M; lower one: M2Y)

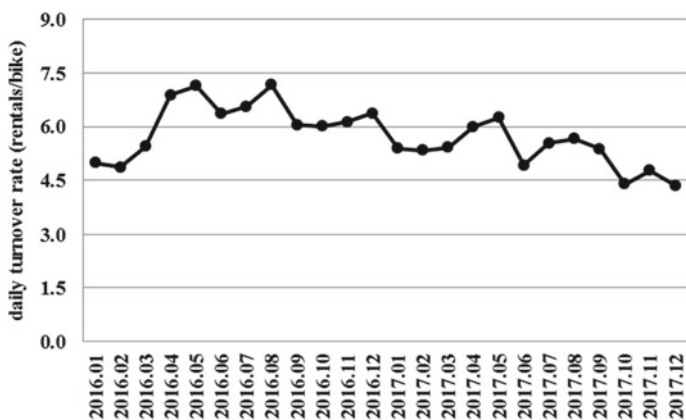


Fig. 7 YouBike daily turnover rate by month

## References

1. Froehlich, J., Neumann, J., Oliver, N.: Sensing and predicting the pulse of the city through shared bicycling. In: Proceedings of the International Joint Conference on Artificial Intelligence, IJCAI 2009, Pasadena, California, USA (2009)
2. Kaltenbrunner, A., Meza, R., Grivolla, J., Codina, J., Banchs, R.: Urban cycles and mobility patterns: exploring and predicting trends in a bicycle-based public transport system. *Pervasive Mob. Comput.* **6**(4), 455–466 (2010)
3. O'Brien, O., Cheshire, J., Batty, M.: Mining bicycle sharing data for generating insights into sustainable transport systems. *J. Transp. Geogr.* **34**(219), 262–273 (2014)
4. Berloco, N., Colonna, P.: Testing and improving urban bicycle performance. *Procedia Soc. Behav. Sci.* **53**, 72–83 (2012)
5. Borgnat, P., Abry, P., Flandrin, P., Rouquier, J.B., Fleury, E.: Shared bicycles in a city: a signal processing and data analysis perspective. *Adv. Complex Syst.* **14**(3), 415–438 (2011)
6. Jensen, P., Rouquier, J.B., Ovtracht, N., Robardet, C.: Characterizing the speed and paths of shared bicycles in Lyon. *Transp. Res. Part D Transp. Environ.* **15**(8), 522–524 (2010)
7. Ikpeze, T.C., Glaun, G., McCalla, D., Elfar, J.C.: Geriatric cyclists: assessing risks, safety, and benefits. *Geriatr. Orthop. Surg. Rehabil.* **9**, 2151458517748742 (2018). <https://doi.org/10.1177/2151458517748742>
8. Taipei City DOT: Annual evaluation of Taipei YouBike operations performance (2017)